

## University of Southampton Research Repository

Copyright © and Moral Rights for this thesis and, where applicable, any accompanying data are retained by the author and/or other copyright owners. A copy can be downloaded for personal non-commercial research or study, without prior permission or charge. This thesis and the accompanying data cannot be reproduced or quoted extensively from without first obtaining permission in writing from the copyright holder/s. The content of the thesis and accompanying research data (where applicable) must not be changed in any way or sold commercially in any format or medium without the formal permission of the copyright holder/s.

When referring to this thesis and any accompanying data, full bibliographic details must be given, e.g.

Thesis: Author (Year of Submission) "Full thesis title", University of Southampton, name of the University Faculty or School or Department, PhD Thesis, pagination.

Data: Author (Year) Title. URI [dataset]



# **University of Southampton**

Faculty of Engineering and Physical Sciences

Chemistry

**The Analysis of Diesel and Related Fuels, New Fuels and Components by Mass Spectrometry and Other Techniques for Propensity for Fouling in Common-rail Diesel Injection Systems**

Volume 1 of 1

by

**Anastarsia Christine Marrie-Louise Carter**

Thesis for the degree of Doctor of Philosophy

September 2020



# University of Southampton

## Abstract

Faculty of Engineering and Physical Sciences

Chemistry

Thesis for the degree of Doctor of Philosophy

The Analysis of Diesel and Related Fuels, New Fuels and Components by Mass Spectrometry and Other Techniques for Propensity for Fouling in Common-rail Diesel Injection Systems

by

Anastarsia Christine Marrie-Louise Carter

Over the last decade, fuel injector deposits in common rail diesel engines have increased in incidence. Concurrently, increasingly strict emission legislation has resulted in multiple changes to both diesel fuel composition and fuel injection systems. Much interest surrounds these deposits due to associated field performance issues.

Novel analytical approaches were developed and applied for the characterisation of deposit components and deposit and non-deposit forming fuels from the field, using multiple chromatography and mass spectrometry techniques. Identification of recognised and currently unrecognised deposit forming components, and a greater understanding of the chemistry of the deposits and the diesel fuel through comparing and contrasting of complimentary data was achieved.

A targeted screening method was developed for known deposit forming component classes and applied to characterise diesel fuels and various FIE deposits. Positive ion electrospray ionisation ultrahigh pressure supercritical fluid chromatography mass spectrometry (ESI UHPSFC-MS) afforded the detection of fatty acid methyl esters (FAMEs), FAME oxidation products, monoacylglycerols and sterol glucosides, while negative ion ESI UHPSFC-MS afforded detection of free fatty acids. Additionally polyisobutylene, polypropylene glycol and additional additives were observed within fuel filter samples. Internal diesel injector deposit (IDID) results were indicative of possible metal carboxylate salt or aged fuel IDIDs.

Analysis protocol flow trees were also devised from this work to assist analysts with characterisation of (IDID) components in fuels (diesels, biodiesels), IDIDs and fuel filter deposits, as well as fuels.

A new species (fatty acid sterol esters) was identified from biodiesel within mineral diesel blends, believed to be unseen previously and currently an unrecognised deposit-forming component.

Further advancement of the analysis method for jet fuel thermal oxidation test (JFTOT) rod deposits and associated diesel fuels, firstly to validate previously unexpected results and to optimise sample preparation methodologies.

A novel positive ion ESI UHPSFC-MS method was developed for the detection and quantitation of the new fiscal fuel marker ACCUTRACE™S10, assisting HMRC to combat fuel laundering, with reported losses of £1.1 billion per annum at present and limiting the damage to vehicles resulting from using adulterated fuel.









# Table of Contents

Table of Contents .....	i
Table of Tables .....	ix
Table of Figures .....	xiii
Research Thesis: Declaration of Authorship .....	xxix
Acknowledgements .....	xxxix
List of Abbreviations .....	xxxiii
Objectives for this PhD .....	xli
<b>Chapter 1 Introduction.....</b>	<b>1</b>
1.1 Petroleum derived fuels .....	1
<b>1.1.1 Diesel.....</b>	<b>3</b>
<b>1.1.2 Fuel legislation .....</b>	<b>12</b>
1.1.3 Recent changes to diesel fuel.....	15
1.1.3.1 Sulfur reduction.....	15
1.1.3.2 Increasing use of biodiesel due to limiting use of fossil fuels in diesel fuel.....	16
1.1.4 Current analytical techniques found in literature for the analysis of fuels .....	19
<b>1.2 Diesel engines .....</b>	<b>22</b>
<b>1.2.1 History.....</b>	<b>22</b>
<b>1.2.2 Operation of a diesel engine .....</b>	<b>23</b>
1.2.3 Fuel injection equipment (FIE) .....	24
1.2.3.1 Indirect injection (IDI).....	25
1.2.3.2 Direct injection (DI) .....	26
1.2.3.3 Common rail fuel injection system.....	27
<b>1.2.4 Evolution of diesel engines to satisfy legislation .....</b>	<b>28</b>
<b>1.3 FIE deposits .....</b>	<b>32</b>
<b>1.3.1 Location of IDIDs.....</b>	<b>33</b>
<b>1.3.2 Composition of IDIDs.....</b>	<b>33</b>
<b>1.3.3 Occurrence and origin of IDIDs .....</b>	<b>35</b>

## Table of Contents

1.3.3.1 Carbonaceous IDIDs .....	37
1.3.3.2 Metal salt IDIDs .....	37
1.3.3.3 Aged fuel IDIDs.....	38
1.3.3.4 Metal carboxylate IDIDs.....	38
1.3.3.5 Polymeric amide IDIDs (Lacquers) .....	41
<b>1.3.4 Problems caused by IDID formation.....</b>	<b>41</b>
<b>1.3.5 Suggested ways to stop IDID/deposit formation.....</b>	<b>42</b>
<b>1.3.6 Challenges of characterisation .....</b>	<b>42</b>
<b>1.3.7 IDID test methods .....</b>	<b>43</b>
1.3.8 Current analytical techniques found in literature for the analysis of IDIDs/deposits.....	44
<b>Chapter 2 Instrumentation.....</b>	<b>49</b>
2.1 Chromatography.....	49
2.2 Chromatographic parameters.....	50
2.3 Gas chromatography (GC).....	54
2.4 Supercritical fluid chromatography (SFC) .....	60
2.4.1 Ultrahigh pressure supercritical fluid chromatography (UHPSFC) .....	61
2.5 Mass spectrometry .....	65
2.5.1 Ion sources.....	66
2.5.1.1 Electron ionisation (EI).....	66
2.5.1.2 Electrospray ionisation (ESI) .....	67
2.5.1.3 Atmospheric pressure photoionisation (APPI) .....	71
2.5.2 Mass analysers.....	75
2.5.2.1 Quadrupole mass analyser .....	75
2.5.2.2 Fourier transform ion cyclotron resonance mass spectrometry (FT-ICR MS).....	80
2.5.3 Tandem MS.....	83
2.5.3.1 Tandem MS (in space) using a triple quadrupole MS.....	83
<b>Chapter 3 Experimental .....</b>	<b>87</b>
3.1 Chemicals.....	87

3.1.1	Reagents.....	87
3.1.2	Samples .....	87
3.1.3	Calibrant standards .....	87
3.2	Sample and calibration standards.....	88
3.2.1	Diesel and Biodiesel .....	88
3.2.2	Deposits.....	88
3.2.2.1	Fuel filters .....	89
3.2.2.2	Fuel injector tip .....	89
3.2.2.3	JFTOT tubes .....	90
3.2.2.4	JFTOT fuels.....	90
3.3	GC-MS.....	92
3.3.1	Polar column .....	92
3.3.2	JFTOT GC method .....	92
3.4	UHPSFC-MS.....	93
3.4.1	UHPSFC chromatographic method .....	93
3.4.2	Positive ion ESI-MS.....	94
3.4.3	Negative ion ESI-MS .....	94
3.5	UHPSFC-MS/MS.....	95
3.6	FT-ICR MS .....	95
3.7	Data processing .....	95
3.7.1	SpectralWorks AnalyzerPro <sup>®</sup> .....	95
<b>Chapter 4 Analysis and comparison of diesel fuels (mineral diesel and biodiesel) and possible deposit forming components using complementary analytical techniques .....</b>		<b>99</b>
4.1	Introduction.....	99
4.1.1	Analytical challenge of diesel and biodiesel fuels in relation to IDIDs/deposits 99	
4.1.2	Comparison of diesel fuels from the field .....	99
4.2	GC-MS Analysis of nine diesel fuels .....	100
4.2.1	Polar column GC-MS analysis.....	101

## Table of Contents

4.2.2	Manual data analysis of polar column GC-MS of nine diesels .....	103
4.2.3	Automated analysis method (including comparison) for polar column GC-MS data using SpectralWorks AnalyzerPro <sup>®</sup> software .....	110
4.2.3.1	SpectralWorks AnalyzerPro <sup>®</sup> .....	110
4.2.4	Automated data analysis of polar column GC-MS of nine diesels .....	112
4.2.5	Summary of polar column GC-MS findings (automated analysis).....	113
4.3	Diesel fuels component screening methodology – UHPSFC-MS and FT-ICR MS analysis.....	114
4.3.1	Fatty acid methyl esters (FAMES) .....	117
4.3.2	Fatty acid methyl ester (FAME) oxidation products .....	123
4.3.3	Free fatty acids (FFAs).....	130
4.3.4	Monoacylglycerols (MAGs).....	135
4.3.5	Sterol glucosides (SGs) .....	140
4.3.6	Diesel fuels analysis summary .....	146
4.4	Detection of fatty acid sterol esters (FASEs) in diesels.....	151
4.4.1	MS/MS data .....	159
4.5	Application of screening method with respect to biodiesel quality.....	162
4.6	Diesel analysis protocol trees .....	163
4.6.1	Analyst flow (diesel).....	163
4.6.2	Diesel flow.....	166
4.7	Conclusions .....	168
4.7.1	GC-MS Analysis .....	168
4.7.2	Diesel fuels component screening methodology .....	168
4.7.3	Fatty acid sterol esters detection method .....	169
4.7.4	Diesel analysis protocol trees .....	170
<b>Chapter 5</b>	<b>Analysis of diesel engine deposits using complimentary analytical techniques.....</b>	<b>173</b>
5.1	Introduction .....	173
5.1.1	The analytical challenge of characterising diesel engine deposits.....	173
5.1.2	Fuel filters .....	173

5.1.3	Fuel injectors .....	175
5.1.4	JFTOT rods and method .....	176
5.1.5	Purpose of this work .....	178
5.2	Analysis of fuel filters from the field .....	179
5.2.1	Fatty acid methyl esters (FAMES).....	180
5.2.2	Fatty acid methyl ester (FAME) oxidation products .....	185
5.2.3	Free fatty acids (FFAs) .....	189
5.2.4	Monoacylglycerols (MAGs) .....	193
5.2.4.1	MS/MS data .....	197
5.2.5	Sterol glucosides (SGs) .....	201
5.2.6	Fatty acid sterol esters (FASEs) .....	206
5.2.7	Other key findings .....	209
5.2.7.1	Polymeric additives <i>e.g.</i> polyisobutylene (PIB) and polypropylene glycol (PPG).....	209
5.2.7.2	Non-ionic emulsifier .....	216
5.2.8	Fuel filter summary .....	219
5.3	Deposit analysis protocol trees .....	225
5.3.1	Analyst flow (deposits).....	225
5.3.2	Deposit flow .....	227
5.4	Analysis of fuel injector tip IDID from the field (work in collaboration with John Langley) .....	229
5.4.1	Direct infusion positive ion ESI FT-ICR MS .....	229
5.4.2	Direct infusion negative ion ESI FT-ICR MS .....	231
5.4.3	Negative ion ESI UHPSFC-MS .....	232
5.4.4	Summary .....	233
5.5	Analysis of JFTOT rods and associated fuels .....	234
5.5.1	Previous work by Patel .....	235
5.5.2	JFTOT rods .....	235
5.5.2.1	FT-ICR MS analysis.....	235
5.5.2.2	Non-polar column GC-MS analysis.....	240

## Table of Contents

5.5.3	Associated fuels .....	244
5.5.3.1	FT-ICR MS analysis .....	244
5.5.3.2	(Non-polar column) GC-MS analysis .....	246
5.5.4	Summary .....	247
5.5.4.1	FT-ICR MS JFTOT rods solvent washing .....	247
5.5.4.2	FT-ICR MS JFTOT rods scraping .....	247
5.5.4.3	(Non-polar column) GC-MS analysis .....	247
5.6	Conclusions .....	248
5.6.1	Fuel filters – Deposit screening method .....	248
5.6.2	Deposit analysis protocol trees.....	248
5.6.3	Fuel injector tip IDID .....	249
5.6.4	JFTOT rods and associated fuels .....	249
<b>Chapter 6</b>	<b>Evaluation of Ultrahigh-Performance Supercritical Fluid Chromatography- Mass Spectrometry (UHPSFC-MS) as an Alternative Approach for the Analysis of ACCUTRACE™ S10 Fuel Marker .....</b>	<b>253</b>
6.1	Introduction .....	253
6.1.1	Fuel markers .....	254
6.1.2	New fuel marker – ACCUTRACE™ S10 .....	256
6.1.2.1	ACCUTRACE™ S10 fuel marker.....	256
6.1.2.2	ACCUTRACE™ S10- <i>d</i> <sub>21</sub> fuel marker internal standard.....	257
6.2	GC-MS .....	258
6.2.1	GC-MS analysis (undertaken in conjunction with Edward Wilmot) .....	261
6.2.1.1	ACCUTRACE™ S10 fuel marker.....	261
6.2.1.2	ACCUTRACE™ S10 fuel marker in a contaminated fuel matrix.....	262
6.2.1.3	ACCUTRACE™ S10- <i>d</i> <sub>21</sub> IS.....	263
6.2.1.4	Fragmentation of ACCUTRACE™ S10 fuel marker and ACCUTRACE™ S10- <i>d</i> <sub>21</sub> IS.....	265
6.2.1.5	GC-MS summary .....	268
6.3	UHPSFC –MS .....	269
6.3.1	UHPSFC-MS analysis .....	270

6.3.1.1	Positive ion APPI UHPSFC-MS (undertaken by John Langley and Julie Herniman).....	270
6.3.1.2	Positive ion ESI UHPSFC-MS .....	272
6.4	Conclusions.....	287
6.5	Acknowledgements .....	288
6.6	Experimental .....	288
6.6.1	Chemicals .....	288
6.6.2	Sample preparation.....	289
6.6.2.1	ACCUTRACE™ S10 stock solution .....	289
6.6.2.2	Internal standard (ACCUTRACE™ S10- <i>d</i> <sub>21</sub> ) stock solution.....	289
6.6.2.3	Calibration solution .....	289
6.6.2.4	Real fuel samples dosed with ACCUTRACE™ S10 fuel marker.....	290
6.6.3	ACCUTRACE™ S10 fuel marker GC-MS method (undertaken in conjunction with Edward Wilmot) (modified Dow method) .....	290
6.6.4	ACCUTRACE™ S10 fuel marker UHPSFC-MS methods .....	290
6.6.4.1	Positive ion APPI UHPSFC-MS (full scan) (undertaken by John Langley and Julie Herniman).....	290
6.6.4.2	Positive ion ESI UHPSFC-MS (full scan and SIR).....	291
6.6.5	Molecular modelling (undertaken by Maria Ashe (current PhD student in Langley Research group)).....	292
<b>Chapter 7</b>	<b>Concluding remarks and future work.....</b>	<b>295</b>
7.1	Concluding remarks.....	295
7.2	Further work.....	299
<b>Appendix A</b>	<b>Conferences, courses and seminars attended .....</b>	<b>303</b>
	Conferences attended: .....	303
	Courses attended:.....	303
	Seminars attended:.....	303
<b>Bibliography</b>	<b>.....</b>	<b>307</b>





## Table of Tables

Table 1-1 Comparison of EN 590:2013 and ASTM D 975 specifications for specific properties of diesel <sup>50-51</sup> .....	8
Table 1-2 - Common diesel additives, their function and examples. Adapted from <sup>55</sup> .....	9
Table 1-3 - Euro Standards and their emission limits for petrol and diesel passenger cars. Data from <sup>71, 78</sup> .....	14
Table 1-4 - Comparison of properties of used cooking oil, biodiesel from used cooking oil and commercial petrodiesel fuel, adapted from <sup>89</sup> .....	17
Table 1-5 – Evolution of diesel engine technology to meet emission limits, adapted from <sup>108, 112-113</sup> . Emission limits data from <sup>71, 78</sup> .....	29
Table 1-6 The relationship between IDID types, precursors/root causes and fuel components. Adapted from <sup>3</sup> .....	35
Table 2-1 Comparison of the properties between liquids, gases and supercritical fluids .....	61
Table 3-1 - Serial dilution of JFTOT fuels.....	91
Table 3-2 - 3 minute gradient elution parameters (2%-40%) .....	94
Table 3-3 - Initial component detection parameters for SpectralWorks AnalyzerPro <sup>®</sup> .....	96
Table 4-1 - Percentage similarities obtained from SpectralWorks AnalyzerPro <sup>®</sup> component database comparison of chromatograms of all nine diesels acquired via GC-MS using a polar column at split ratio 50 and ramp rate of 1 °C /min .....	113
Table 4-2 FAMES summary (nominally isobaric species are in bold and underlined) .....	119
Table 4-3 - Diesel fuels FAMES summary (√=detected, X=not detected, X* = nominal mass detected by positive ion ESI UHPSFC-MS, but monoisotopic mass not detected by positive ion ESI FT-ICR MS) .....	122
Table 4-4 FAME oxidation products summary .....	125
Table 4-5 - Diesel fuels FAMES oxidation products summary (√=detected, X=not detected) ...	129
Table 4-6 FFAs summary .....	131

## Table of Tables

Table 4-7 – Diesel fuels FFAs findings summary (legend: v= detected (observed by UHPSFC-MS and FT-ICR MS), v?= only detected by FT-ICR MS, X = not detected) .....	134
Table 4-8 MAGs Summary (nominally isobaric species <i>m/z</i> in bold and underlined) .....	136
Table 4-9 - Diesel fuels MAGs summary (v=detected, v? = only detected by FT-ICR MS, X* = nominal mass detected by positive ion ESI UHPSFC-MS, but monoisotopic mass not detected by positive ion ESI FT-ICR MS, X=not detected) .....	139
Table 4-10 SGs summary .....	142
Table 4-12 - Diesel fuels SGs summary (v=detected, X=not detected) .....	145
Table 4-13 Diesel fuels analysis summary (V = detected, X* = not detected, however part detected and provides additional information, X = not detected).....	146
Table 4-13 - FASEs summary Masses from literature – Kalo <i>et al.</i> <sup>233</sup> .....	155
Table 4-15 - Diesel fuels FASES summary (v=detected, v*=detected at low abundance, X=not detected) .....	161
Table 5-1 – Fuel filters FAMES summary (v=detected, X=not detected, v? = low abundance detected) .....	184
Table 5-2 – Fuel filters FAMES oxidation products summary (v=detected, X=not detected) ...	188
Table 5-3 – Fuel filters FFAs findings summary (legend: v= detected (by UHPSFC-MS and FT-ICR MS), v?= only detected by FT-ICR MS, X = not detected) .....	192
Table 5-4 – fuel filters MAGs summary (v=detected, X=not detected).....	200
Table 5-5 – Fuel filter SGs and sterol fragment ion summary (v=detected, v*=detected at low abundance( $\sim 10^6$ ), X=not detected) .....	205
Table 5-6 Fuel filters analysis summary.....	219
Table 5-7 - Fuel filters composition summary .....	223
Table 6-1 Author contributions for ACCUTRACE S10 fuel marker work.....	253
Table 6-2 - Ratio of ACCUTRACE™ S10/S10- <i>d</i> <sub>21</sub> IS in methanol .....	282
Table 6-3 - Ratio of ACCUTRACE™ S10/S10- <i>d</i> <sub>21</sub> IS in diesel fuel .....	285

Table 6-4 - Average concentration of ACCUTRACE™ S10 fuel marker in six fuels by positive ion ESI UHPSFC-MS with ACCUTRACE™ S10- $d_{21}$ IS .....	287
Table 6-5 - 3 minute gradient elution parameters (30-40%) .....	291
Table 6-6 - 6 minute gradient elution parameters (2%-5%-40%) .....	292



## Table of Figures

Figure 1-1 - Three stages of crude oil recovery. Adapted from <sup>44-46</sup> .....	2
Figure 1-2 – Simplified fractional distillation process of refining. Adapted from <sup>47</sup> .....	3
Figure 1-3 -Flow chart showing the routes of different products through an oil refinery. Adapted from <sup>45, 47-48</sup> .....	3
Figure 1-4 - Examples of different classes of hydrocarbons found within diesel .....	5
Figure 1-5 - Transesterification reaction scheme. Adapted from <sup>92</sup> .....	18
Figure 1-6 - Diagram showing the operation cycle of a four-stroke diesel engine. Adapted from <sup>46,106</sup> .....	24
Figure 1-7 - Diagram showing Direct injection (DI) and Indirect injection (IDI) fuel injection systems. Adapted from <sup>46</sup> .....	25
Figure 1-8 - Diagram of Common Rail Fuel Injection system. Adapted from <sup>46, 109</sup> .....	27
Figure 1-9 - Diagram showing locations of IDID formation within a fuel injector in a diesel engine .....	33
Figure 1-10 - IDID types and possible causes. Adapted from <sup>3</sup> .....	34
Figure 1-11 - Possible causes of fuel system deposits. Adapted from <sup>86</sup> .....	36
Figure 1-12 -Chemical reaction of a carboxylic acid with water and an alkali metal base .....	39
Figure 1-14 – schematic diagram of the proposed mechanism of metal carboxylate salts. Adapted from <sup>120</sup> .....	40
Figure 1-13 Inverse micelle formation of metal carboxylate.....	40
Figure 2-1 - Schematic showing the theoretical plate model in a chromatographic column.....	52
Figure 2-2 - A van Deemter plot showing all three terms and their relationship with the optimum linear velocity. Adapted from <sup>48, 140-141</sup> .....	53
Figure 2-3 - Schematic diagram of a GC. Adapted from <sup>48</sup> .....	55
Figure 2-4 - Cross section of fused silica open tubular (FSOT) column adapted from <sup>48</sup> .....	57
Figure 2-5 -PEG or Wax structure. Redrawn from <sup>149-150</sup> .....	58

## Table of Figures

Figure 2-6 - dimethyl diphenyl polysiloxane structure. Redrawn from <sup>48</sup> .....	58
Figure 2-7 - Cross section of flame ionisation detector (FID). Adapted from <sup>153</sup> .....	59
Figure 2-8 - Schematic of GC-MS. Adapted from <sup>140, 153</sup> .....	59
Figure 2-9 - Phase diagram of CO <sub>2</sub> . Adapted from <sup>157</sup> .....	60
Figure 2-10 –Schematic showing flow path and components of Waters ACQUITY Ultraperformance Convergence Chromatograph (UPC <sup>2</sup> ) system. Adapted from <sup>161</sup> .....	62
Figure 2-11 -A Van Deemter curve showing a comparison of kinetic performance for both LC and SFC instrumentation using a variety of column particle sizes. Adapted from <sup>156, 159, 162</sup> .....	63
Figure 2-12 - HSS C18 SB column structure .....	63
Figure 2-13 - Simplified schematic of a mass spectrometer. Adapted from <sup>3, 179, 181</sup> .....	65
Figure 2-14 - Electron ionisation source diagram. Adapted from <sup>5, 185-186</sup> .....	66
Figure 2-15 - McLafferty rearrangement.....	67
Figure 2-16 - Schematic of pneumatically assisted Waters Z-Spray ESI source, operating in positive ion ESI. ....	68
Figure 2-17 - Schematic showing ion formation mechanism in ESI. Adapted from <sup>193</sup> .....	69
Figure 2-18 – schematic of the Charged residue model (CRM).....	70
Figure 2-19 – Schematic of the Ion evaporation model (IEM) .....	71
Figure 2-20 A schematic comparing API techniques and their analyte compatibility. Adapted from <sup>202</sup> .....	72
Figure 2-21 - Schematic of APPI Source.....	73
Figure 2-22 – A schematic diagram showing a cylindrical quadrupole mass analyser with stable and unstable trajectories .....	75
Figure 2-23 - Mathieu stability diagram illustrating stability regions for a quadrupole mass analyser. Adapted from <sup>172</sup> .....	78

Figure 2-24 – Combined Stability diagram as a function of U (DC voltage) and V (amplitude of the RF voltage) for ions with different masses ( $m_1 < m_2 < m_3$ ), showing the scan line with offset and gain .....	79
Figure 2-25 - Schematic diagram of cylinder mass analyser cell within a Fourier transform ion cyclotron resonance mass spectrometer with subsequent production of a mass spectrum. The analyser cell is in field of the magnet, which is denoted by B, $I$ is image current. Adapted from <sup>208</sup> .....	81
Figure 2-26 - Ion motion within FT-ICR cell.....	82
Figure 2-27 – Schematic diagram of a triple quadrupole instrument used in tandem MS in space experiments. Adapted from <sup>209</sup> .....	84
Figure 3-1 Chemical structure of L-Arginine .....	88
Figure 3-2 Initial Fuel filter sample preparation .....	89
Figure 3-3 Fuel filter sample preparation for UHPSFC-MS analysis.....	89
Figure 3-4 - Schematic representation of serial dilution of JFTOT fuels.....	91
Figure 4-1 - TICCs of unknown diesel sample D#2 analysed using the following parameters; split ratio 50 and ramp rate 5 °C /min, and split ratio 50 and ramp rate 1 °C /min ... ..	101
Figure 4-2 - TICCs of D#1-D#5 analysed using polar column GC-MS at a split ratio of 50 and a ramp rate of 1 °C /min .....	102
Figure 4-3 - TICCs of D#6 -D#9 analysed using polar column GC-MS at a split ratio of 50 and a ramp rate of 1 °C /min .....	102
Figure 4-4 - TICCs of D#1, D#2 and D#7 analysed using polar column GC-MS at split ratio 50 and ramp rate 1 °C/min. A pale blue box and oval highlight the retention region of FAMES .....	104
Figure 4-5 - TICC and RICCs ( $m/z$ 43, 57, 77, 91, 74 and 87) of D#2 analysed by polar column GC-MS at a split ratio of 50 and a ramp rate of 1 °C /min .....	104
Figure 4-6 - combined mass spectrum of D#1 at $t_R$ 155.4 - 155.8 min analysed using polar column GC-MS at split ratio 50 and ramp rate 1 °C/min.....	105

## Table of Figures

Figure 4-7 – Top - RICCs of C16:0 FAMES ( $m/z$ 74, 87) for (D#1, D#2 and D#7). Bottom - combined mass spectrum of D#1 at $t_R$ 137.0-137.3 min analysed using polar column GC-MS at split ratio 50 and ramp rate 1 °C/min .....	106
Figure 4-8 - RICCs $m/z$ 74 and 87 for D#1, D#2 and D#7 analysed using polar column GC-MS at split ratio 50 and ramp rate 1 °C/min .....	107
Figure 4-9 - Top - RICCs of aliphatic hydrocarbons ( $m/z$ 43, 57) for (D#1, D#2 and D#7). Bottom - combined mass spectrum of D#2 at $t_R$ 117.1-118.5 min analysed using polar column GC-MS at split ratio 50 and ramp rate 1 °C/min .....	108
Figure 4-10 - Top -RICCs of aromatic hydrocarbons ( $m/z$ 77, 91) for (D#1, D#2 and D#7). Bottom - combined mass spectrum of D#2 at $t_R$ 20.91 min. analysed using polar column GC-MS at split ratio 50 and ramp rate 1 °C/min .....	109
Figure 4-11 - Screenshot from SpectralWorks AnalyzerPro® software showing component identification using RICCs for each $m/z$ present under the TICC at each retention time .....	111
Figure 4-12 - Screenshot from SpectralWorks AnalyzerPro® software showing components identified (each indicated by a green lollipop) on TICC .....	111
Figure 4-13 - Screenshot from SpectralWorks AnalyzerPro® software showing comparison of two component databases with percentage confidence calculated as indicated by red box.....	112
Figure 4-14 - Screenshot from SpectralWorks AnalyzerPro® software showing component database showing any components which have also been matched using NIST 2014 mass spectral library.....	112
Figure 4-15 - Positive ion ESI BPICCs of D#1, D#2 and D#7 with retention regions highlighted for compounds of interest .....	117
Figure 4-16 –Positive ion ESI UHPSFC-MS BPICC of D#1 with pale blue box highlighting FAMES region of retention ( $t_R$ 0.55-0.70 min).....	120
Figure 4-17 - Positive ion ESI UHPSFC mass spectrum of D#1 at $t_R$ 0.55-0.70 min, zoomed range $m/z$ 285-319 .....	120
Figure 4-18 - Direct infusion positive ion ESI FT-ICR mass spectrum of D#1 (zoomed $m/z$ 290-330), showing sodiated molecules for FAMES.....	121



Figure 4-19 –Positive ion ESI UHPSFC-MS RICCs of D#1 showing FAMES with pale blue box highlighting FAMES region of retention ( $t_R$ 0.55-0.70 min) .....	121
Figure 4-20 - Direct infusion positive ion ESI FT-ICR mass spectrum of D#5 (zoomed range $m/z$ 325-370), showing sodiated molecules for C18 FAME oxidation products up to the addition of three oxygen atoms .....	126
Figure 4-21 – Positive ion ESI UHPSFC-MS BPICC of D#5 with pale blue box highlighting FAMES and C18 FAME oxidation products region of retention ( $t_R$ 0.50 -0.80 min) .....	127
Figure 4-22 - Positive ion ESI UHPSFC mass spectrum of D#5 at $t_R$ 0.50-0.80 min (zoomed range $m/z$ 300-380), showing ammoniated molecules for C18 FAMES and their respective FAME oxidation products, up to the addition of three oxygen atoms .....	128
Figure 4-23 – Positive ion ESI UHPSFC-MS RICCs of D#5 showing C18:3 FAME and FAME oxidation products.....	128
Figure 4-24 – Negative ion ESI UHPSFC mass spectrum of D#8at $t_R$ 0.85-1.20 min (zoomed range $m/z$ 220-290) .....	132
Figure 4-25 – Negative ion ESI UHPSFC-MS BPICC of D#8 with pale blue box highlighting FFAs region of retention ( $t_R$ 0.85-1.20 min) .....	132
Figure 4-26 - Negative ion ESI UHPSFC-MS RICCs of D#8 showing FFAs (box zoomed to 0.85–1.20 min).....	133
Figure 4-27 - Direct infusion negative ion ESI FT-ICR mass spectrum of D#8 (zoomed range $m/z$ 220-290), showing deprotonated molecules for FFAs. ....	133
Figure 4-28 - Positive ion ESI UHPSFC-MS BPICC of fuel filter D#9 with pale blue box highlighting MAGs region of retention ( $t_R$ 1.20-1.35 min) .....	137
Figure 4-29 - Positive ion ESI UHPSFC mass spectrum of D#9 at $t_R$ 1.20-1.35 min zoomed range $m/z$ 325-390.....	137
Figure 4-30 - Direct infusion positive ion ESI FT-ICR mass spectrum of D#9, (zoomed range $m/z$ 340-390), showing sodiated molecules for MAGs.....	138
Figure 4-31 – Positive ion ESI UHPSFC-MS RICCs of D#9 showing MAGs with pale blue box highlighting MAGs region of retention ( $t_R$ 1.20-1.35 min) .....	138

## Table of Figures

Figure 4-32 - Positive ion ESI UHPSFC-MS BPICC of D#3 with pale blue box highlighting SGs region of retention ( $t_R$ 2.00-2.20 min) .....	143
Figure 4-33 - Positive ion ESI UHPSFC mass spectrum of D#3 at $t_R$ 2.00-2.20 min with pale blue boxes highlighting the $m/z$ values expected for SGs and sterol fragment ions ..	144
Figure 4-34 –Positive ion ESI UHPSFC-MS RICC of D#3 showing SGs and sterol fragment ions with pale blue box highlighting SGs region of retention ( $t_R$ 2.00-2.20 min) .....	144
Figure 4-35 - Positive ion ESI UHPSFC-MS BPICC of D#1 with pale blue box highlighting FASEs region of retention ( $t_R$ 2.00-2.40 min).....	151
Figure 4-36 - Positive ion ESI UHPSFC mass spectrum of D#1 at $t_R$ 2.00-2.40 min with pale blue boxes highlighting the $m/z$ values expected for FASEs and sterol fragment ions ..	152
Figure 4-37 - Positive ion ESI UHPSFC-MS RICC of D#3 showing campesterol fragment ion and its respective FASEs in with pale blue box highlighting FASEs region of retention ( $t_R$ 2.05-2.30 min) .....	153
Figure 4-38 - Product ion mass spectrum of D#1 of precursors nominal $m/z$ 678 (top), 680 (middle) and 682 (bottom) for campesterol esters at $t_R$ 2.28, 2.37 and 2.46 min (TQD) respectively (zoomed over $m/z$ 120-700) CE 10V .....	160
Figure 4-39 - Positive ion ESI UHPSFC-MS BPICC of D#1 (top) and homemade biodiesel (bottom) with pale blue box highlighting FAMES region of retention ( $t_R$ 0.55-0.70 min) ..	162
Figure 4-40 - Negative ion ESI UHPSFC-MS BPICC of homemade biodiesel with pale blue box highlighting FFAs region of retention ( $t_R$ 0.95-1.10 min) .....	162
Figure 4-41 – Analyst flow (diesel) analysis protocol tree.....	165
Figure 4-42 - Diesel flow analysis protocol tree .....	167
Figure 5-1 – Fouled and acceptable fuel filters taken from the field, adapted from <sup>57</sup> .....	174
Figure 5-2 - Biodiesel type contamination on fuel filter, adapted from <sup>253</sup> .....	174
Figure 5-3 - Diagram of Common Rail Fuel Injection system, adapted from <sup>7, 52, 114</sup> .....	174
Figure 5-4 - Diagram of fuel injector.....	176

Figure 5-5 - Schematic of JFTOT testing, adapted from <sup>259</sup> .....	177
Figure 5-6 - JFTOT rod rating system, adapted from <sup>258</sup> .....	178
Figure 5-7 – Positive ion ESI UHPSFC-MS BPICC of fuel filter SS10 with pale blue box highlighting FAMES region of retention ( $t_R$ 0.55-0.70 min) .....	181
Figure 5-8 - Positive ion ESI UHPSFC mass spectrum of fuel filter SS10 at $t_R$ 0.55-0.70 min(A) mass range $m/z$ 120- 1000 (B) zoomed mass range $m/z$ 280-320 .....	181
Figure 5-9 – Positive ion ESI UHPSFC-MS RICCs of SS10 showing FAMES with pale blue box highlighting FAMES region of retention ( $t_R$ 0.55-0.70 min) .....	182
Figure 5-10 - Direct infusion positive ion ESI FT-ICR mass spectrum of SS10 (zoomed $m/z$ 290-330), showing sodiated molecules for FAMES.....	183
Figure 5-11 - Direct infusion positive ion ESI FT-ICR MS data of fuel filter SS4 (zoomed range $m/z$ 310-370), showing sodiated molecules for C18 FAMES and C18 FAME oxidation products up to the addition of three oxygen atoms .....	186
Figure 5-12 – Positive ion ESI UHPSFC-MS BPICC of SS4 with pale blue box highlighting FAMES and C18 FAME oxidation products region of retention ( $t_R$ 0.50 -0.80 min) .....	186
Figure 5-13 - Positive ion ESI UHPSFC mass spectrum of SS4 at $t_R$ 0.50-0.80 min (zoomed range $m/z$ 300-380), showing ammoniated molecules for C18 FAMES and their respective FAME oxidation products, up to the addition of three oxygen atoms.....	187
Figure 5-14 – Positive ion ESI UHPSFC-MS RICCs of SS4 showing C18:2 FAME and FAME oxidation products.....	187
Figure 5-15 - Negative ion ESI UHPSFC-MS BPICC of fuel filter SS10 with pale blue box highlighting FFAs region of retention ( $t_R$ 0.85-1.15 min).....	190
Figure 5-16 – Negative ion ESI UHPSFC mass spectrum of fuel filter SS10 at $t_R$ 0.85-1.15 min (zoomed range $m/z$ 180-300) .....	190
Figure 5-17 - Negative ion ESI UHPSFC-MS RICCs of fuel filter SS10 showing FFAs (box zoomed to 0.85 – 1.15 min) .....	191
Figure 5-18 - Direct infusion negative ion ESI FT-ICR mass spectrum of fuel filter SS10 (zoomed range $m/z$ 180-300), showing deprotonated molecules for FFAs .....	191

## Table of Figures

Figure 5-19 - Positive ion ESI UHPSFC-MS BPICC of fuel filter SS5 with pale blue box highlighting MAGs region of retention ( $t_R$ 1.20-1.35 min) .....	194
Figure 5-20 - Positive ion ESI UHPSFC mass spectrum of fuel filter SS5 at $t_R$ 1.20-1.35 min (zoomed range $m/z$ 325-390) .....	194
Figure 5-21 - Positive ion ESI UHPSFC-MS RICC of fuel filter SS5 showing MAGs with pale blue box highlighting MAGs region of retention ( $t_R$ 1.20-1.35 min) .....	195
Figure 5-22 - Direct infusion positive ion ESI FT-ICR mass spectrum of fuel filter SS5, (zoomed range $m/z$ 340-390), showing sodiated molecules for MAGs .....	196
Figure 5-23 - Direct infusion positive ion ESI FT-ICR mass spectrum of fuel filter SS5, (zoomed range $m/z$ 100 - 1000), showing sodiated molecules for MAGs and MAG dimers .....	196
Figure 5-24 - Direct infusion positive ion ESI FT-ICR mass spectrum of fuel filter SS5, (zoomed range $m/z$ 680-750), showing sodiated molecules for MAG dimers.....	197
Figure 5-25 – Product ion mass spectrum of fuel filter SS5 of precursor nominal $m/z$ 348 MAG C16:0 at $t_R$ 1.11 min (TQD) (zoomed over $m/z$ 120-400) CE 5V .....	198
Figure 5-26 - Product ion mass spectrum of fuel filter SS5 of precursor nominal $m/z$ 374 MAG C18:1 [ $C_{21}H_{40}O_4 + NH_4$ ] <sup>+</sup> at $t_R$ 1.16 min (TQD) (zoomed in over $m/z$ 120-400) CE 5V .....	199
Figure 5-27 - Positive ion ESI UHPSFC-MS BPICC of fuel filter SS2 with pale blue box highlighting SGs region of retention ( $t_R$ 2.00-2.20 min) .....	202
Figure 5-28 - Positive ion ESI UHPSFC mass spectrum of fuel filter SS2 at $t_R$ 2.04-2.14 min (zoomed range $m/z$ 350-625) .....	202
Figure 5-29 - Positive ion ESI UHPSFC-MS RICC of fuel filter SS2 showing SGs and sterol fragment ions with pale blue box highlighting SGs region of retention ( $t_R$ 2.00-2.20 min) .....	203
Figure 5-30 - Direct infusion positive ion ESI FT-ICR mass spectrum of fuel filter SS2 (zoomed range $m/z$ 580-600), showing sodiated molecules for SGs .....	204
Figure 5-31 - Positive ion ESI UHPSFC-MS BPICC of fuel filter SS5 with pale blue box highlighting FASEs region of retention ( $t_R$ 2.20-2.40 min) .....	207

Figure 5-32 – Positive ion ESI UHPSFC mass spectrum of fuel filter SS5 at $t_R$ 2.20-2.40 min ....	207
Figure 5-33 - Positive ion ESI UHPSFC-MS RICCs of fuel filter SS5 with pale blue box highlighting FASEs region of retention ( $t_R$ 1.20-1.35 min).....	208
Figure 5-34 - Direct infusion positive ion ESI FT-ICR mass spectrum of fuel filter SS6 (zoomed range $m/z$ 100-1500), showing two discrete oligomeric series of 56.0626 $m/z$ repeat units (separated by 18.0101 $m/z$ units), highlighted by red and blue arrows ....	209
Figure 5-35 - Positive ion ESI UHPSFC-MS BPICC of fuel filter SS6 with pale blue box highlighting PIBs region of retention ( $t_R$ 2.40-3.00 min) .....	210
Figure 5-36 - Positive ion ESI UHPSFC mass spectrum of fuel filter SS6 at $t_R$ 2.40-3.00 min, showing two discrete series of 56 $m/z$ units difference (separated by 18 $m/z$ units) consistent with two PIB series, highlighted by red and blue arrows .....	211
Figure 5-37 - Positive ion ESI UHPSFC-MS RICCs of fuel filter SS6 showing separation of PIBs ( $t_R$ 1.80-3.00 min).....	211
Figure 5-38 - Direct infusion positive ion ESI FT-ICR mass spectra (A) fuel filter SS6 and (B) fuel filter SS10 (zoomed range $m/z$ 690-960), showing protonated molecules for PIBs .....	212
Figure 5-39 - Direct infusion positive ion ESI FT-ICR mass spectrum of fuel filter SS7 (zoomed in mass range $m/z$ 100-1200), showing a series of 58.0420 $m/z$ units difference consistent with a PPG series, highlighted by purple arrows .....	213
Figure 5-40 - Positive ion ESI UHPSFC-MS BPICC of fuel filter SS7 with pale blue box highlighting PPGs region of retention ( $t_R$ 1.05-1.50 min) .....	214
Figure 5-41 - Positive ion ESI UHPSFC-MS RICCs of fuel filter SS7 showing separation of PPGs ( $t_R$ 1.05-1.50 min).....	214
Figure 5-42 –Positive ion ESI UHPSFC mass spectrum of fuel filter SS7 at $t_R$ 1.05-1.50 min, with pale blue box highlighting PPGs region of with zoomed range $m/z$ 350-1000, showing a series of 58 $m/z$ units difference consistent with a PPG series, highlighted by purple arrows.....	215

## Table of Figures

Figure 5-43 - Direct infusion positive ion ESI FT-ICR mass spectrum of fuel filter SS3 (zoomed range $m/z$ 100-1000), with pale blue box highlighting a sodiated molecule $[C_{24}H_{44}O_6 + Na]^+$ at $m/z$ 451.3044 .....	216
Figure 5-44 - Positive ion ESI UHPSFC-MS BPICC of fuel filter SS3 with pale blue box highlighting compound of interest region of retention ( $t_R$ 1.15-1.35 min).....	217
Figure 5-45 - Positive ion ESI UHPSFC-MS of fuel filter SS3 at $t_R$ 1.15-1.35 min (zoomed range $m/z$ 350-550) .....	217
Figure 5-46 - Positive ion ESI UHPSFC-MS of fuel filter SS3 (A) RICC nominal $m/z$ 446 ammoniated species of interest $[C_{24}H_{44}O_6 + NH_4]^+$ and (B) RICC nominal $m/z$ 451 sodiated species of interest $[C_{24}H_{44}O_6 + Na]^+$ .....	218
Figure 5-47 – Analyst flow (deposit) analysis protocol tree .....	226
Figure 5-48 - Deposit flow analysis protocol tree.....	228
Figure 5-49 - Direct infusion positive ion ESI FT-ICR mass spectrum of fuel injector tip IDID, showing a series of 56.0630 $m/z$ units difference consistent with a PIB series, highlighted by orange arrows .....	230
Figure 5-50 - Direct infusion positive ion ESI FT-ICR mass spectrum of fuel injector tip IDID (zoomed range $m/z$ 260-330) showing sodiated molecules for FFAs .....	231
Figure 5-51 -- Direct infusion negative ion ESI FT-ICR mass spectrum of fuel injector tip IDID (zoomed range $m/z$ 150-700), showing deprotonated molecules for FFAs.....	232
Figure 5-52 – Negative ion ESI UHPSFC-MS (all zoomed to 0.50 – 3.00 min) of fuel injector tip IDID (A) BPICC, (B) RICC nominal $m/z$ 283 $[C_{18}H_{35}O_2 - H]^-$ and (C) RICC nominal $m/z$ 255 $[C_{16}H_{31}O_2 - H]^-$ .....	233
Figure 5-53 – Negative ion ESI UHPSFC-MS (zoomed range $m/z$ 150-600) of fuel injector tip IDID (A) mass spectrum at $t_R$ 0.64 min, (B) mass spectrum at $t_R$ 0.59 min .....	233
Figure 5-54 - Direct infusion positive ion ESI FT-ICR MS and DART-MS for JFTOT rod 3, showing the proposed adipate as sodiated and protonated molecules respectively. Taken from <sup>213</sup> .....	235

Figure 5-55 – Two possible proposed adipate structures ((A) dioctyl adipate and (B) di-2-ethylhexyl adipate) for sodiated molecule $[C_{22}H_{42}O_4 + Na]^+$ at $m/z$ 393.3161 (molecular weight: 370 g/mol) .....	236
Figure 5-56 - mass spectrum of USLD JFTOT methanol:dichloromethane solvent washing analysed by FT-ICR MS.....	237
Figure 5-57 - mass spectrum of B20JFTOT methanol:dichloromethane solvent washing analysed by FT-ICR MS.....	237
Figure 5-58 - Mass spectrum of RF06→B20→RF06 JFTOT methanol:dichloromethane solvent washing analysed by FT-ICR MS.....	238
Figure 5-59 – Comparison of all 3 JFTOT rods methanol:dichloromethane solvent washings analysed by FT-ICR MS.....	238
Figure 5-60 – Glove in methanol:dichloromethane solvent mix (blank) analysed by positive ion ESI FT-ICR MS. Zoomed range $m/z$ 391-399 with a blue box indicating absence of $m/z$ 393.2975.....	240
Figure 5-61 – (A) TICC, RICC nominal $m/z$ 370, RICC nominal $m/z$ 129, RICC nominal $m/z$ 57 and RICC nominal $m/z$ 147 (chromatograms zoomed in 18-20 min). Blue box denotes DEHA expected retention time (B) EI-MS (70 eV) ( $t_R$ 19.18-19.24 min, mass range $m/z$ 20 - 500) of B20 JFTOT rod solvent washing sample analysed using the full scan (non-polar column) GC-MS method .....	241
Figure 5-62 – NIST Library search results for $t_R$ 19.18-19.24 min of RF06→B20→RF06 JFTOT rod solvent washing sample.....	242
Figure 5-63 – (A) TICC, RICC nominal $m/z$ 370, RICC nominal $m/z$ 129, RICC nominal $m/z$ 57 and RICC nominal $m/z$ 147 (chromatograms zoomed in 18-20 min). Blue box denotes DEHA expected retention time (B) EI-MS (70 eV) ( $t_R$ 19.18-19.24 min, mass range $m/z$ 20 - 500) of RF06→B20→RF06 JFTOT rod solvent washing sample .....	242
Figure 5-64 – NIST Library search results for $t_R$ 19.18-19.24 min of B20 JFTOT rod solvent washing sample.....	243
Figure 5-65 –TICC, RICC nominal $m/z$ 370, RICC nominal $m/z$ 129, RICC nominal $m/z$ 57 and RICC nominal $m/z$ 147 (chromatograms zoomed in 18-20 min). Blue box denotes DEHA expected retention time ( $t_R$ 19.18-19.24 min) of ULSD JFTOT rod scraping sample.....	244

## Table of Figures

Figure 5-66 –Mass spectrum of 0.01% SS1 diesel in 6T:4M analysed by direct infusion positive ion ESI FT-ICR MS (mass range: $m/z$ 390– 397).....	245
Figure 5-67 –Mass spectrum of 0.01% SS#2 diesel in 6T:4M analysed by direct infusion positive ion ESI FT-ICR MS (mass range: $m/z$ 391.5 – 395.5).....	245
Figure 5-68 – (A) TICC, RICC nominal $m/z$ 370, RICC nominal $m/z$ 129, RICC nominal $m/z$ 57 and RICC nominal $m/z$ 147 (chromatograms zoomed in 18-20 min). Red box denotes DEHA expected retention time (B) EI-MS (70 eV) ( $t_R$ 19.18-19.24 min, mass range $m/z$ 20 - 500) of SS#2 fuel with split ratio of 1:50.....	246
Figure 6-1 - Chemical structure of Solvent Red 24 fuel dye.....	255
Figure 6-2 - Chemical structure of Quinizarin fuel marker.....	255
Figure 6-3 - Chemical structure of Solvent yellow 124 fuel dye.....	255
Figure 6-4 – Structure of 3-(secbutyl)-4-(decyloxy)phenyl)methanetriyl)tribenzene, ACCUTRACE™ S10 fuel marker .....	257
Figure 6-5 – Isotopically labelled ACCUTRACE™ S10- $d_{21}$ internal standard .....	257
Figure 6-6 - Simplified 5% dimethyl diphenyl polysiloxane structure.....	260
Figure 6-7 - Simplified 50% dimethyl diphenyl polysiloxane structure.....	260
Figure 6-8 – (A) TICC and (B) EI-MS (70 eV) ( $t_R$ 37.07 min, mass range $m/z$ 20 - 555) of 25 ppm ACCUTRACE™ S10 fuel marker in dichloromethane analysed using the modified full scan GC-MS method.....	261
Figure 6-9 –TICC of ACCUTRACE™ S10 fuel marker in contaminated diesel fuel with composition 70:27:3 Diesel, Castrol GTX 5w30 Lubricating oil and Gear Oil 80w90 respectively, analysed using the modified full scan GC-MS method .....	262
Figure 6-10 – TICC of at 2.5 ppm ACCUTRACE™ S10 fuel marker in dichloromethane (S/N = 15) analysed using GC-MS SIR $m/z$ 455 method .....	263
Figure 6-11 – (A) TICC and (B) EI-MS (70 eV) ( $t_R$ 36.44 min, mass range $m/z$ 120 - 650) of ACCUTRACE™ S10- $d_{21}$ IS in dichloromethane.....	264
Figure 6-12 - SIR chromatograms overlaid of molecular species ( $m/z$ 476 and 455 respectively) for GC–MS showing chromatographic separation of ACCUTRACE™ S10- $d_{21}$ IS and	



ACCUTRACE™ S10 fuel marker, respectively (ACCUTRACE™ S10- <i>d</i> <sub>21</sub> IS eluting earliest) .....	265
Figure 6-13 - (A) EI-MS (70 eV) ( <i>t</i> <sub>R</sub> 36.62 min, mass range <i>m/z</i> 100 - 600) for ACCUTRACE™ S10 fuel marker (B) EI-MS (70 eV) ( <i>t</i> <sub>R</sub> 36.34 min, mass range <i>m/z</i> 100 - 600) for ACCUTRACE™ S10- <i>d</i> <sub>21</sub> IS .....	266
Figure 6-14 - EI fragmentation structures for ACCUTRACE™ S10 fuel marker .....	267
Figure 6-16 - EI fragmentation structures for ACCUTRACE™ S10- <i>d</i> <sub>21</sub> internal standard .....	268
Figure 6-17 - A schematic comparing API techniques and their analyte compatibility. Adapted from <sup>201</sup> .....	270
Figure 6-18 –Schematic showing flow path and components of Waters ACQUITY UltraPerformance Convergence Chromatography (UPC <sup>2</sup> ) system. Adapted from <sup>161</sup> .....	271
Figure 6-19 – (A) TICC, (B) RICC ( <i>m/z</i> 555.5) and (C) positive ion APPI MS ( <i>t</i> <sub>R</sub> 0.84 min, zoomed mass range <i>m/z</i> 480 - 640) of ACCUTRACE™ S10 fuel marker in methanol ..	272
Figure 6-20 - (A) TICC,(B) positive ion ESI mass spectrum ( <i>t</i> <sub>R</sub> 2.20 min) and (C) positive ion ESI MS ( <i>t</i> <sub>R</sub> 2.20 min, zoomed mass range <i>m/z</i> 480 - 640) of 500 ppm ACCUTRACE™ S10 fuel marker in methanol .....	274
Figure 6-21 - RICC of 2.5 ppm ACCUTRACE™ S10 fuel marker in methanol analysed using SIR <i>m/z</i> 550.8 method .....	275
Figure 6-22 - Molecular model of ACCUTRACE™ S10 fuel marker electronegativity map <sup>293</sup> . Figure reproduced with permission from ACS.....	276
Figure 6-23 - (A) TICC, (B) positive ion ESI mass spectrum ( <i>t</i> <sub>R</sub> 2.11 min) and (C) positive ion ESI MS ( <i>t</i> <sub>R</sub> 2.11 min, zoomed mass range <i>m/z</i> 480 - 640) of 500 ppm ACCUTRACE™ S10- <i>d</i> <sub>21</sub> IS in methanol .....	277
Figure 6-24 - RICC of 1 ppm ACCUTRACE™ S10- <i>d</i> <sub>21</sub> IS in methanol analysed using SIR <i>m/z</i> 571.9 method .....	278
Figure 6-25 - RICC of 100 ppm ACCUTRACE™ S10 fuel marker and 100 ppm ACCUTRACE™ S10- <i>d</i> <sub>21</sub> IS in methanol showing chromatographic separation of ACCUTRACE™ S10- <i>d</i> <sub>21</sub> IS and ACCUTRACE™ S10 fuel marker, respectively (ACCUTRACE™ S10- <i>d</i> <sub>21</sub> IS eluting earliest) .....	279

## Table of Figures

Figure 6-26 - RICC of ACCUTRACE™ S10 fuel marker standards (A) 1 ppb (B) 5 ppb (C) 10 ppb and (D) 25 ppb analysed using the SIR $m/z$ 550.8 method, demonstrating the LLOD and LLOQ .....	280
Figure 6-27 - Positive ion ESI ACCUTRACE™ S10 fuel marker calibration curve using ACCUTRACE™ S10 fuel marker standards (5, 10, 25, 50, 100, 250, 500, 1000 and 2500 ppb) analysed using the SIR $m/z$ 550.8 method (number of replicates = 6, error bars = $2\sigma$ ) .....	280
Figure 6-28 - RICC of ACCUTRACE™ S10 fuel marker ( $t_R$ 2.34 min) (A) 1 ppb (B) 5 ppb (C) 10 ppb and (D) 25 ppb, each with 500 ppb ACCUTRACE™ S10- $d_{21}$ IS ( $t_R$ 2.24 min) in methanol standards analysed using the SIR $m/z$ 550.8 and 571.9 method, demonstrating the LLOD and LLOQ.....	281
Figure 6-29 - Positive ion ESI ACCUTRACE™ S10 fuel marker and ACCUTRACE™ S10- $d_{21}$ IS calibration curve using ACCUTRACE™ S10 fuel marker standards (5, 10, 25, 50, 100, 250, 500, 1000 and 2500 ppb) each with 500 ppb ACCUTRACE™ S10- $d_{21}$ IS in methanol, analysed using the SIR $m/z$ 550.8 and 571.9 method (number of replicates = 6) .....	283
Figure 6-30 - RICC of ACCUTRACE™ S10 fuel marker ( $t_R$ 2.35 min) (A) 1 ppb (B) 5 ppb (C) 10 ppb (D) 25 ppb (E) 50 ppb and (F) 100 ppb, each with 500 ppb ACCUTRACE™ S10- $d_{21}$ IS ( $t_R$ 2.25 min) in diesel fuel standards analysed using the SIR $m/z$ 550.8 and 571.9 method .....	284
Figure 6-31 - Positive ion ESI ACCUTRACE™ S10 fuel marker and ACCUTRACE™ S10- $d_{21}$ IS calibration curve using ACCUTRACE™ S10 fuel marker standards (5, 10, 25, 50, 100, 250, 500, 1000, 2500, 5000 and 10000 ppb) each with 500 ppb ACCUTRACE™ S10- $d_{21}$ IS in diesel fuel, analysed using the SIR $m/z$ 550.8 and 571.9 method (number of replicates = 6, error bars = $2\sigma$ ) .....	284
Figure 6-32 – (A)BPICC (B) RICC $m/z$ 550.8 and 571.9 (ACCUTRACE™ S10 fuel marker and ACCUTRACE™ S10- $d_{21}$ IS) (C) RICC $m/z$ 571.9(ACCUTRACE™ S10- $d_{21}$ IS) and (D) RICC $m/z$ 550.8 (ACCUTRACE™ S10 fuel marker) of fuel 1 pre-doped with ACCUTRACE™ S10 fuel marker and the addition of 10 ppm ACCUTRACE™ S10- $d_{21}$ IS, analysed using both the full scan and SIR ( $m/z$ 550.8 and 571.9) methods... ..	286





## Research Thesis: Declaration of Authorship

Print name: Anastarsia Christine Marrie-Louise Carter

**Title of thesis: The Analysis of Diesel and Related Fuels, New Fuels and Components by Mass Spectrometry and Other Techniques for Propensity for Fouling in Common-rail Diesel Injection Systems**

I declare that this thesis and the work presented in it are my own and has been generated by me as the result of my own original research.

I confirm that:

1. This work was done wholly or mainly while in candidature for a research degree at this University;
2. Where any part of this thesis has previously been submitted for a degree or any other qualification at this University or any other institution, this has been clearly stated;
3. Where I have consulted the published work of others, this is always clearly attributed;
4. Where I have quoted from the work of others, the source is always given. With the exception of such quotations, this thesis is entirely my own work;
5. I have acknowledged all main sources of help;
6. Where the thesis is based on work done by myself jointly with others, I have made clear exactly what was done by others and what I have contributed myself;
7. Parts of this work have been published as:-

Langley, G. J.; Herniman, J.; Carter, A.; Wilmot, E.; Ashe, M.; Barker, J., Detection and Quantitation of ACCUTRACE S10, a New Fiscal Marker Used in Low-Duty Fuels, Using a Novel Ultrahigh-Performance Supercritical Fluid Chromatography–Mass Spectrometry Approach. *Energy & Fuels* **2018**, *32* (10), 10580-10585.

Barker, J.; Reid, J.; Smith, S. A.; Snape, C.; Scurr, D.; Langley, G.; Patel, K.; Carter, A.; Laphorn, C.; Pullen, F., The Application of New Approaches to the Analysis of Deposits from the Jet Fuel Thermal Oxidation Tester (JFTOT). *SAE International Journal of Fuels and Lubricants* **2017**, *10* (2017-01-2293).

Signature: ..... Date:.....



## Acknowledgements

First and foremost I wish to thank my supervisor Professor John Langley for providing me with the fantastic opportunity to undertake this PhD project. His continuous support, guidance, belief and patience throughout has been invaluable. Thank you for always being there when needed, providing the space to learn and for teaching me so much.

This project was jointly funded by EPSRC and Innospec Inc. (Ellesmere Port, UK). I would like to express a huge amount of gratitude to my industrial supervisors Jim Barker and Jacqueline Reid for their irreplaceable discussions, input, advice and support, particularly around deposits and fuel injectors, and for the supply of samples.

Many thanks to Julie Herniman for her constant support in the lab, both practical guidance and troubleshooting skills on the instrumentation. Thank you for always being there with a smile on your face to help when needed.

Thanks to the Langley group members past and present; Stathis, Ammar, Krina, Ed, Steph, Maria, Dovile, Andreas and Sergio. Thank you for all being wonderful colleagues and great friends during the highs and lows of the PhD.

Thanks to colleagues at the University of Southampton who kindly synthesised homemade biodiesel.

My family, Dad and Chris, and Michael and Jess, thank for believing in me and listening even when you had no clue what I was talking about and your continuous support.

I am especially grateful to my Grandad Reg who throughout his life always encouraged me and was a positive influence of my academic endeavours. Although he may not be here to see the completion of this PhD, he was the biggest advocate of my education and without his belief and encouragement, I wouldn't be where I am today.

Finally, I would like to thank my husband Michael for all his love, support and patience throughout my PhD. Without his belief, encouragement and motivation, I couldn't have completed this. Thank you for letting me pursue my dream even if it meant putting our life plans on hold for a few years.

My heartfelt thanks to you all, this would not have been achieved without you and I am forever grateful.





## List of Abbreviations

2D	Two-dimensional
6T:4M	6:4 toluene:methanol solvent mixture
AC	Alternating Current
ACN	Acetonitrile
AFM	Atomic Force Microscopy
APCI	Atmospheric Pressure Chemical Ionisation
API	Atmospheric Pressure Ionisation
APPI	Atmospheric Pressure Photo Ionisation
ASAP	Atmospheric Solids Analysis Probe
ASTM	American Society of the International Association for Testing and Materials standard test method
B100	100% biodiesel
B7	7% biodiesel, 93% petrodiesel
BDC	Bottom Dead Centre
BHT	Dibutylhydroxytoluene
BPICC	Base Peak Ion Current Chromatogram
CAA	Clean Air Act
CARB	Californian Air Resources Board
CE	Collision Energy
CFPP	Cold Filter Plugging Point
CI	Chemical Ionisation
CID	Collision Induced Dissociation
CO	Carbon Monoxide
CO <sub>2</sub>	Carbon Dioxide
CP	Cloud Point
cm	Centimetre
CRM	Charged Residue Model
Da	Daltons
DAD	Diode Array Detector

## List of Abbreviations

DAG	Diacylglycerol
DART	Direct Analysis in Real Time
DC	Direct Current
DCA	Deposit Control Additive
DCD	Dielectric Current Detector
DCM	Dichloromethane
DEHA	di-2-ethylhexyl adipate
DI	Direct Injection
DLC	Diamond Like Carbon
DOC	Diesel Oxidation Catalyst
DRIFTS	Diffuse Reflectance Infrared Fourier Transform Spectroscopy
EASI	Easy Ambient Sonic-spray Ionisation
ECD	Electron Capture Detector
ECU	Engine Control Unit
ED-XRF	Energy-Dispersive X-ray Fluorescence Spectrometry
EGR	Exhaust Gas Recirculation
EI	Electron Ionisation
ELSD	Evaporative Light Scattering Detector
EM	Electron Multiplier
EN	European standard
ESI	Electrospray Ionisation
eV	Electron Volts
FA	Formic Acid
FAMEs	Fatty Acid Methyl Esters
FASEs	Fatty Acid Sterol Esters
FFAs	Free Fatty Acids
FI	Field Ionisation
FIB-SEM	Focussed Ion Beam -Scanning Electron Microscope
FID	Flame Ionisation Detector
FIE	Fuel Injection Equipment

FSOT	Fused Silica Open Tubular
FT-ICR	Fourier Transform – Ion Cyclotron Resonance
FTIR	Fourier Transform Infrared Spectroscopy
g	Gram
GC	Gas Chromatography
GC x GC	Two-Dimensional Gas Chromatography
h	Hour
HC	Hydrocarbon
HETP	Height Equivalent to a Theoretical Plate
HFRR	High Frequency Reciprocating Rig
HMRC	Her Majesty's Revenue and Customs
HPLC	High Performance Liquid Chromatography
HR	High Resolution
HSS	High-Strength Silica
ICP-AES	Inductively Coupled Plasma – Atomic Emission Spectroscopy
ICP-MS	Inductively Coupled Plasma – Mass Spectrometry
i.d.	Internal Diameter
ID	Isotope Dilution
IDI	Indirect Injection
IDID	Internal Diesel Injector Deposits
ID-ICP-MS	Isotope Dilution - Inductively Coupled Plasma – Mass Spectrometry
IEM	Ion Evaporation Model
IMMS	Ion Mobility Mass Spectrometry
IP	Energy Institute (formally Institute of Petroleum) Standard Test method
IPA	2-propanol
IR	Infrared
IRMS	Isotope Ratio Mass Spectrometry
IS	Internal Standard

## List of Abbreviations

ISM	Internal Solvent Manager
JFTOT	Jet Fuel Thermal Oxidation Test
kg	Kilogram
KV	Kinematic Viscosity
kV	Kilovolts
L	Litre
LC	Liquid Chromatography-Mass Spectrometry
LLOD	Lower Limit of Detection
LLOQ	Lower Limit of Quantitation
m	Metre
MAG	Monoacylglycerol
MALDI	Matrix-Assisted Laser Desorption/Ionisation
MeOH	Methanol
mg	Milligram
min	Minute
mL	Millilitre
mM	Millimolar
mm	Millimetre
mp	Melting Point
MS	Mass Spectrometry
Ms	Milliseconds
MS/MS	Mass Spectrometry/Mass Spectrometry (Tandem MS)
MWD-XRF	Monochromatic Wavelength Dispersive X-ray Fluorescence Spectrometry
$m/z$	Mass/Charge Ratio <i>(Dimensionless, m=mass of ion z=number of charges or charge number)</i>
NFU	National Farming Union
NEDC	New European Driving Cycle
NIR	Near-Infrared Spectroscopy
NIST	National Institute of Standards and Technology
NMR	Nuclear Magnetic Resonance

nm	Nanometre
NO <sub>x</sub>	Nitrogen Oxides
PAH	Polycyclic Aromatic Hydrocarbon
PEG	Polyethylene Glycol
PEMS	Portable Emissions Monitoring System
PIB	Polyisobutylene
PIBSI	Polyisobutylenesuccinimide
PM	Particulate Matter
PP	Pour Point
ppb	Parts per Billion
PPG	Polypropylene glycol
PPL	Pence per Litre
ppm	Parts per Million
ppm wt	Parts per Million by Weight
QQQ	Triple Quadrupole
RDE	Real Driving Emissions
REMPI-ToF-MS	Thermodesorption Resonance-Enhanced Photon Ionisation – Time of Flight – Mass Spectrometry
RF	Radio Frequency
RI	Refractive Index
RICC	Reconstructed Ion Current Chromatogram
RME	Rapeseed Methyl Ester
RR	Ramp Rate
RT	Retention time
RTFO	Renewable Transport Fuel Obligation Order
s	Seconds
scCO <sub>2</sub>	Supercritical Carbon Dioxide
SCR	Selective Catalytic Reduction
SEM/EDAX	Scanning Electron Microscope/Energy Dispersive X-ray analysis

## List of Abbreviations

SEB/BSE	Scanning Electron Microscope with Back Scattered Electrons
SFC	Supercritical Fluid Chromatography
SFCxGC	Supercritical Fluid Chromatography Coupled With Gas Chromatography
SFCxSFC	Two-Dimensional Supercritical Fluid Chromatography
SGs	Sterol Glucosides
SI	Similarity Index
SIR	Selected Ion Recording
s/n	signal to noise ratio
SR	Split Ratio
SRM	Selected Reaction Monitoring
TICC	Total Ion Current Chromatogram
TCD	Thermal Conductivity Detector
TD	Time Domain
TDC	Top Dead Centre
TEM	Transmission Electron Microscopy
TGA	Thermogravimetric Analysis
TICC	Total Ion Current Chromatogram
TLC	Thin Layer Chromatography
ToF-SIMS	Time of Flight Secondary Ion Mass Spectrometry
TPO	Temperature Programmed Oxidation
$t_R$	Retention Time
UCO	Used Cooking Oil
UCOME	Used Cooking Oil Methyl Ester
UHPSFC	Ultra High Pressure Supercritical Fluid Chromatography
UK	United Kingdom
ULSD	Ultra Low Sulfur Diesel

UPC <sup>2</sup> -SQD	Ultra Performance Convergence Chromatography system – Single Quadrupole Detector
UPC <sup>2</sup> -TQD	Ultra Performance Convergence Chromatography system – Triple Quadrupole Detector
USA	United States of America
USEPA	United States Environmental Protection Agency
UV	Ultraviolet
UV-Vis	Ultraviolet-Visible
V	Volts
V <sub>L</sub> -EASI(+)	Venturi Positive Ion Easy Ambient Sonic-spray Ionisation
VAT	Value Added Tax (20%)
WCOT	Wall-Coated Open Tubular
XRF	X-ray Fluorescence
XRD	X-ray Diffraction
μA	Microamp
μg	Microgram
μL	Microlitre
°C	Degrees Celsius





## Objectives for this PhD

### Diesel fuels:

- Study the chemistry and composition of diesel fuels (including biodiesel)
  - To characterise the components within each diesel or biodiesel
  - To identify the differences and variations in diesel fuels
  - To identify recognised deposit precursor components/group of components which may be involved in deposit formation
  - To investigate and attempt to identify other deposit precursors which may be currently unrecognised species involved in deposit formation
- Analyse both deposit-forming fuels and non-deposit forming fuels obtained recently from the field using:
  - Chromatography – GC & UHPSFC
  - Mass spectrometry – EI, ESI & APPI

### Deposits associated with diesel engines and diesel fuels:

- Study the chemistry and composition of deposits associated with diesel engines and diesel fuels
  - To characterise the components within each deposit
  - To identify the differences and variations in each deposit and deposit type
  - To identify any components that are known to currently cause performance issues or are recognised deposit precursors
  - To investigate and attempt to identify other deposit precursors which may be currently unrecognised species involved in deposit formation
  - Relate components back to fuel chemistry and deposit formation
- Analyse deposits associated with diesel engines and diesel fuels obtained recently from the field using:
  - Chromatography – GC & UHPSFC
  - Mass spectrometry – EI & ESI

### Using the results of all sample analysis:

- Further investigation may then be undertaken on species involved in deposit formation to gain a better understanding and increased knowledge of them and the current deposit issue
- Construct diesel analysis protocol trees

## Objectives for this PhD

- Information (*e.g.* types of compounds) provided by each technique
- Suggest methods for diesel analysis for specific IDID types

### **ACCUTRACE™ S10 Fuel Marker:**

- Develop a GC-MS method for the detection and quantitation of ACCUTRACE™ S10 Fuel Marker in low duty fuels for use across widely available instrumentation
- Due to issues with GC-MS method, investigate an alternative analysis technique, ultrahigh-performance supercritical fluid chromatography–mass spectrometry (UHPSFC–MS) to develop method for the detection and quantitation of ACCUTRACE™ S10 Fuel Marker in low duty fuels





## Chapter 1 Introduction

Fuel legislation surrounding emission control has been the main driving force behind recent, and almost simultaneous, major changes, to fuel injection equipment (FIE) and diesel fuel. Diesel engines, particularly the FIE, have evolved in order to meet performance demands as well as legal emissions requirements to obtain near-to-zero emissions. Fuel quality is also very important for engine performance and has also been affected by this legislation. Many fuel additives are added to diesel in order to improve fuel performance.

Over the last decade, deposits have been forming in both fuel filters and fuel injectors in common rail diesel engines. These deposits are known to cause engine problems and sometimes even engine failure, meaning these deposits are of great interest to both the fuel and engine manufacturing industry. Much is still unknown about these recent deposits including the origin and cause of their formation, although much research into this has already been undertaken. It is thought these deposits could result from one or a combination of the recent changes to FIE or the diesel fuel. Internal diesel injector deposits (IDIDs) are the current focus and priority for industry and therefore will be the main type of deposits considered.

A wide variety of analytical techniques have been used previously in the analysis of diesel fuel samples<sup>1-25</sup> and deposit samples from fuel filters and fuel injectors<sup>22, 26-41</sup>.

### 1.1 Petroleum derived fuels

Petroleum (literally meaning “rock oil”), also known as crude oil, is the collective term for the multitude of accumulated hydrocarbon-rich liquors that are obtained from subterranean reservoirs<sup>42-43</sup>. These liquors consist of paraffins, naphthenes and aromatics<sup>43</sup>, however the specific properties and appearance of crude oil are variable and dependent on origin. After the crude oil is recovered using a three-stage recovery process as shown in Figure 1-1<sup>44-46</sup>, it is sold and transported to oil refineries worldwide.

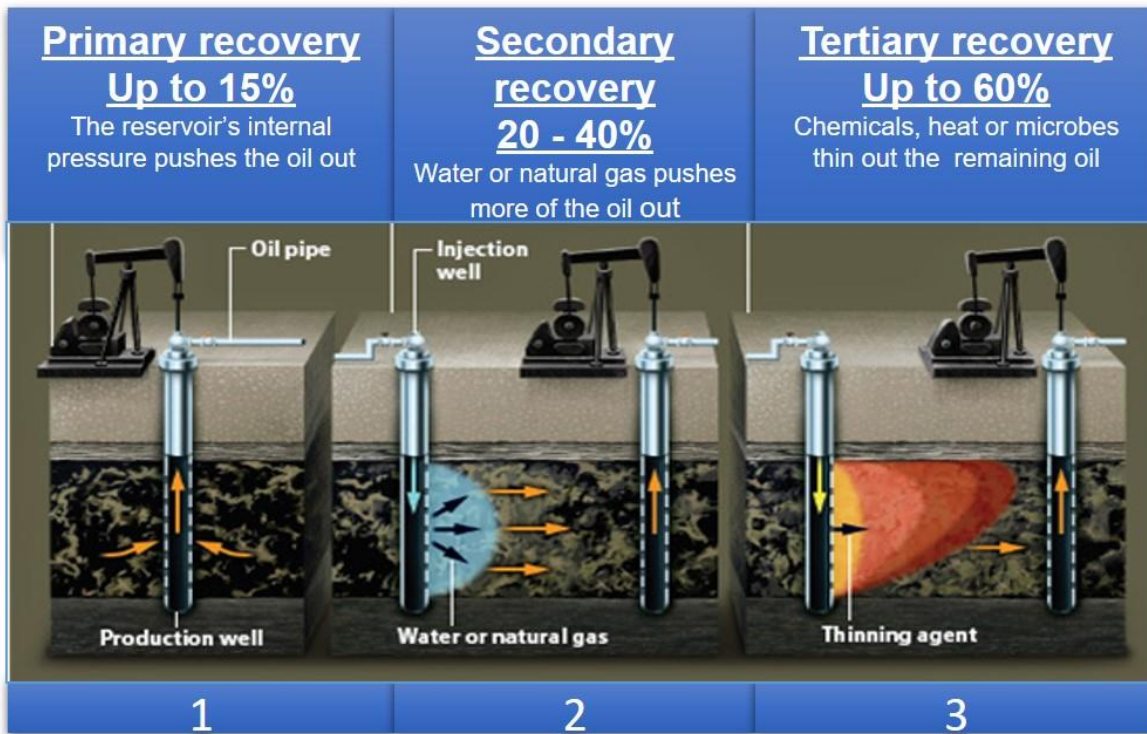


Figure 1-1 - Three stages of crude oil recovery. Adapted from<sup>44-46</sup>

Once at the oil refinery, the crude oil is heated and separated by fractional distillation *via* a series of distillation towers, as shown in Figure 1-2<sup>47</sup>. The different crude fractions then undergo a series of conversion processes in order to convert low value heavy oil into higher value products such as gasoline and diesel. Finally the purification of the resulting products takes place and then the end products are quality tested and ready for sale<sup>47</sup>. The routes of different products through the refinery are shown in Figure 1-3<sup>45, 47-48</sup>.

Many petroleum products are produced, as shown in Figure 1-2 and Figure 1-3, including gasoline, jet fuel and diesel. Petrochemical products are also produced from crude oil by providing petrochemical feedstocks that are often by-products of the refining process. Some examples of petrochemical products include Vaseline (petroleum jelly), butyl rubber for car tyres and wax for candles<sup>47</sup>.

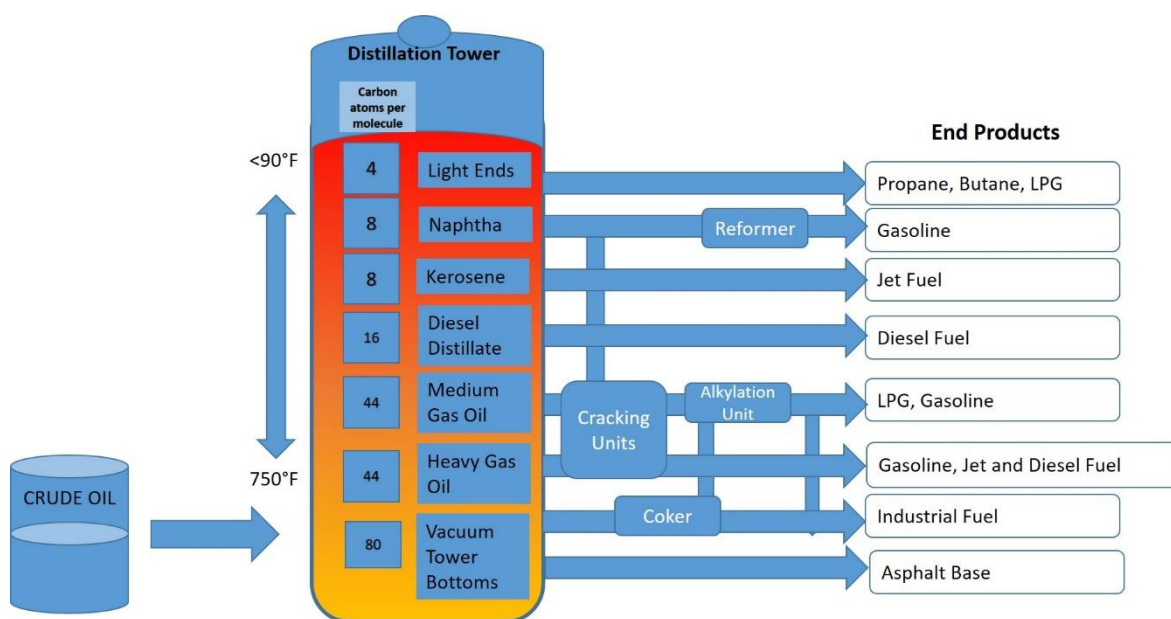


Figure 1-2 – Simplified fractional distillation process of refining. Adapted from<sup>47</sup>

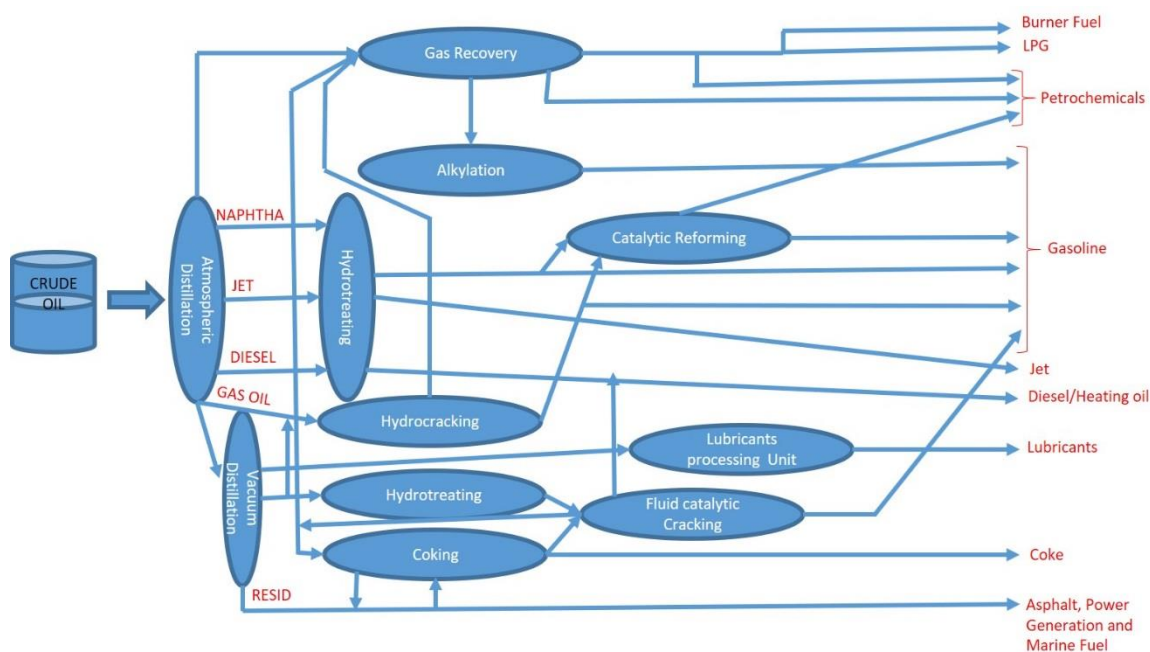


Figure 1-3 -Flow chart showing the routes of different products through an oil refinery. Adapted from<sup>45, 47-48</sup>

### 1.1.1 Diesel

Diesel is a middle distillate fuel, which is a complex blend of hydrocarbon compounds comprising of between 8 and 40 carbon atoms (C8 – C40) with a boiling range from 160 °C – 380 °C<sup>46, 49</sup>. The

## Chapter 1

majority of diesel fuel consists of hydrocarbons of paraffinic, naphthenic and aromatic classes although molecules containing heteroatoms such as sulfur, oxygen and nitrogen are also present. Paraffinic hydrocarbons is a term coined by the petrochemical industry for alkanes, which have the general structural formula  $C_nH_{2n+2}$  ( $n$  = number of carbon atoms) and can be further divided into two subclasses normal paraffins (straight chain alkanes) and isoparaffins (branched chain alkanes). An example formula to illustrate this is  $C_{12}H_{26}$  with n-dodecane and 3,7-dimethyldecane being a normal paraffin and an isoparaffin respectively (as shown in Figure 1-4)<sup>43</sup>.

Naphthenes is another term coined by the petrochemical industry to characterise saturated cyclic hydrocarbons (commonly 5 or 6 membered rings) such as cycloalkanes. A general formula for a naphthenic compound with one ring is  $C_nH_{2n}$ , however multiple rings can be fused resulting in shared carbons. Examples include propylcyclopentane  $C_8H_{16}$  and 2,6-diethyldecahydronaphthalene  $C_{14}H_{26}$  as shown in Figure 1-4<sup>43</sup>.

Aromatics are also hydrocarbon ring structures that contain six carbon atoms joined by double bonds providing aromaticity. The general formula given for a one ring aromatic structure is  $C_nH_{2n-6}$ . As with naphthalenes, multiple ring structures with fused rings are possible and are commonly known as polycyclic aromatics<sup>43</sup>.

Diesel comprises of a mixture of different refinery streams originating from crude oil, with variable blends depending on the specification required<sup>45-46</sup>. Diesel ignites at a relatively low temperature (approximately 350 °C) in comparison to gasoline which ignites at a higher temperature (approximately 500 °C) and requires a spark<sup>46</sup>.

Diesel fuel quality, as well as engine specification are both of great importance with regard to overall performance<sup>41</sup> and therefore diesel fuel specifications are required. The specification of fuel has to take many variables into account and a compromise has to be made between the ideal fuel wanted by engine designers and for fuel injection equipment and what petroleum refiners can produce from the starting crude oil at a reasonable price<sup>40</sup>. The American Society for Testing and Materials (ASTM) controls specification for diesel fuel quality in USA, currently 'ASTM D 975 standard specification for diesel fuel oils'<sup>50</sup> (up to 5% biodiesel) while European committee for standardisation controls diesel fuel quality in UK with specification 'EN 590:2013 - Automotive fuels- Diesel Requirements and test methods'<sup>51</sup> (up to 7% biodiesel). These diesel specifications, and therefore diesel fuel, have undergone significant changes due to legislation and environmental factors<sup>40</sup> as well as the evolution of engine technologies<sup>41, 52</sup> to ensure the diesels are still fit for purpose.



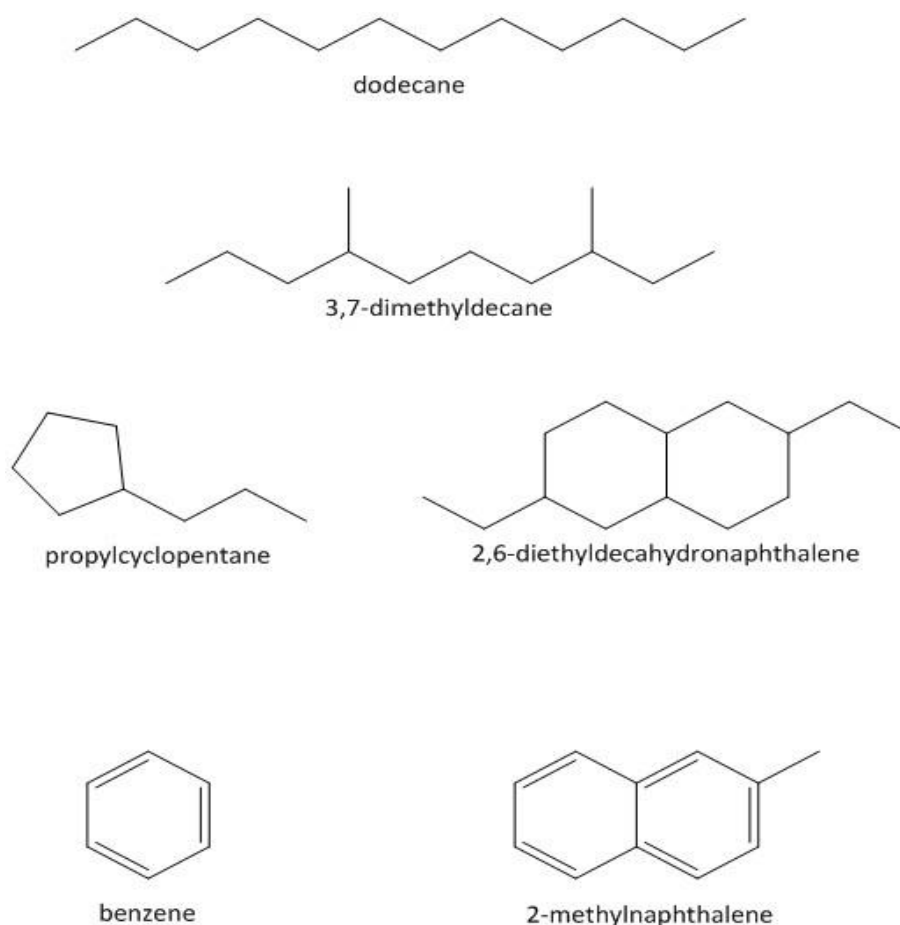


Figure 1-4 - Examples of different classes of hydrocarbons found within diesel

Diesel is subjected to a vast amount of quality testing before it can be released from the refinery and sold to the customer, this ensures it meets specification and results are declared on the certificate of quality.

Some important properties of a diesel fuel including in the specifications are as follows:

### **Cetane number**

Auto ignition, the ability of an air and fuel mixture to spontaneously ignite without an ignition source, is one of the key properties to be considered in a diesel fuel. This can be measured using cetane number that is defined as “a measure of the ignition quality of diesel fuel based on ignition delay (a period of time from fuel injection until start of combustion) in a specific engine”<sup>53</sup>. The higher the cetane number, the shorter the ignition delay which therefore results in a better ignition quality. Cetane index is also used and this is a calculated approximation “based on an empirical relationship with density and volatility parameters”<sup>53</sup>. The cetane number is preferable but a cetane index is acceptable if equipment to determine cetane number is unavailable<sup>53</sup>.

## Chapter 1

A high cetane number is known to improve fuel combustion (by reducing ignition delay) and reduce knocking<sup>54</sup>, which in turn reduces nitrogen oxides (NO<sub>x</sub>) formation, hydrocarbons (HC) and carbon monoxide (CO) emissions. Minimum cetane numbers are stated in diesels specifications<sup>50-51</sup> to meet emission legislation as well as prevent poor performances such as long ignition delay leading to inefficient combustion<sup>53</sup>.

### Density

The density of a diesel fuel, which is the mass per unit volume of diesel fuel at a specific temperature, is related to the amount of carbon in the fuel and therefore the calorific value of the fuel. An increase in a fuel's density also results in a higher energy content in the fuel. This can be problematic as fuel injection is delivered on a volumetric basis, meaning a high-density fuel can cause over-fuelling to occur, resulting in increased smoke and particulate emissions. Modern engine technology compensates for exhaust emission characteristics. A maximum density of 800 kg/m<sup>3</sup> is stated in diesel specifications – as density is reduced it has been shown CO, HC, NO<sub>x</sub> and particulate matter (PM) emissions are reduced<sup>50-51</sup>.

### Viscosity

Viscosity is defined as “a measure of the resistance to flow of a liquid” and the higher the viscosity, the thicker the fuel and greater resistance. The viscosity of a diesel fuel is crucial, too high a viscosity will cause poor fuel atomisation and poor pump function leading to loss of power, whereas too low a viscosity will cause leakages in fuel injection system and hot-start issues<sup>46, 54</sup>. An increase in diesel viscosity has been shown to cause an increase in smoke and PM emissions while reducing NO<sub>x</sub> emissions. A viscosity of 2 – 4 mm<sup>2</sup>/s is acceptable by both ASTM and EN diesel specifications<sup>50-51</sup>.

### Low temperature operability - Cold Filter Plugging Point, Cloud Point and Pour Point

At low temperatures, up to 20% of diesel fuel (mostly heavy paraffinic compounds) will form wax crystals out of solution. Additionally, fatty acid methyl esters (FAMES) now further complicate this as saturated FAMES (commonly used in diesels) have higher melting points, meaning they also solidify out of solution which results in poor cold flow properties. Both of these effects result in operational issues such as clogged fuel filters.

Three properties of diesel are measured to evaluate low temperature performance. Firstly, Cloud Point which is defined as “the temperature at which wax crystals first become visible when fuel is cooled”<sup>53</sup> and Pour Point which is defined as “the temperature at which the amount of wax out of solution is sufficient to gel fuel”<sup>53</sup>. Both cloud point and pour point only look at properties in the diesel and do not show the fuel performance in an engine. Cold Filter Plugging Point is commonly

used to predict low temperature performance of a fuel and is defined as “the lowest temperature at which 20 mL of fuel will pass through a fine wire mesh screen of 45  $\mu\text{m}$  nominal aperture in less than 60 seconds”<sup>53</sup>. The specified values of these three properties on diesel specifications is variable depending on location in the world and seasonality.

### **Lubricity**

Lubricity is defined as “is the ability of a fuel to build-up and to maintain a fluid film that will prevent contact between two solid surfaces”<sup>53</sup> and the fuel injection equipment in particular relies on this diesel property to lubricate and keep the parts moving within the system. To remove sulfur from diesel, hydrotreating occurs and as a result polycyclic aromatic components with sulfur, oxygen and nitrogen content are also removed that are believed to aid lubrication. After the introduction of ultra-low sulfur diesel (ULSD), many issues surrounding lubricity and wear of parts occurred which were overcome with the use of additives. The high frequency reciprocating rig (HFRR) is used as a standardised test for measuring lubricity; it consists of a steel ball moving rapidly against a disk with the fuel being tested between, resulting in a wear scar. The wear scar diameter is measured and diesel specifications state a maximum wear scar diameter, 520  $\mu\text{m}$  in the USA<sup>50</sup> and 460  $\mu\text{m}$  in UK<sup>46, 51, 53</sup>.

### **Sulfur content**

Sulfur within diesel is of great environmental concern due to the conversion of sulfur into  $\text{SO}_x$  therefore the sulfur content within ULSD must be below 10 ppm in the UK and 15 ppm in the USA<sup>50-51</sup>. This is discussed in further detail in section 1.1.2.1.

### **Concentration of water**

Diesel contains small amounts of water and it can absorb water. Dissolved water does not cause issues however free water (even in very low quantities) can damage/corrode and wear FIE very quickly causing damage to fuel lubricated injection pumps<sup>46</sup> and contribute to filter plugging. Water concentration is determined using a Karl Fischer titration<sup>53</sup> and is limited to 200 ppm in UK<sup>51</sup>.

### **Flash point**

The flash point is defined as “the temperature to which the fuel has to be heated to produce a vapour and air mixture that will ignite when a flame is applied”<sup>53</sup>. The Pensky-Martens closed cup method is commonly used; fuel is heated slowly in a closed vessel and opened to a flame periodically until a flash point is reached. It is primarily tested to ensure the fuel is safe for handling and storage, as a fuel could be a fire hazard if it has a flash point that is too low<sup>53</sup>.

**Thermal/oxidative stability**

Long term stability of diesel is a very important quality as it can often be left in storage for a long period before use. Stability of a fuel is determined by both its thermal stability (temperature) and its oxidation stability (availability of oxygen). Oxidative decomposition occurs causing the diesel to degrade resulting in the formation of gums and sediments which are known to block filters or cause deposits to form in FIE and combustion chamber, and to alter diesel colour. This can be accelerated by an increase in temperature and exposure to oxygen *e.g.* recirculation of fuel to a vehicle tank. The presence of biodiesel in a diesel fuel makes it very vulnerable to autoxidation, as it will begin to oxidize as soon as it is produced; antioxidants are often used to negate this issue. Both diesel and biodiesel are subjected to accelerated oxidation stability tests and must meet specification<sup>53</sup>, for an oxidation stability test (ASTM D2247) a maximum of 25 g/m<sup>3</sup> of total solubles (material produced as result of stressing the fuel) in the UK. Additionally if the fuel contains FAMES>2% v/v then a Rancimat test (EN15751) is also undertaken and must have an Induction time of at least 20 hours in the UK<sup>51</sup>.

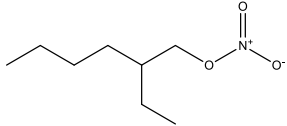
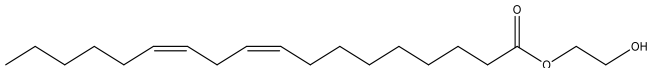
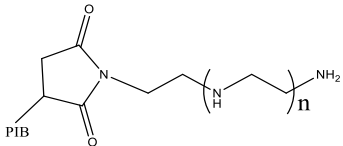
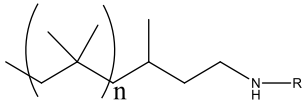
Table 1-1 shows a comparison of some of the key properties of diesel fuel for both EN 590:2013 and ASTM D 975 specifications.

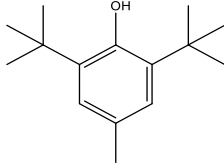
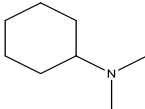
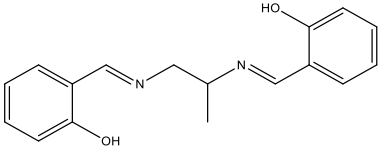
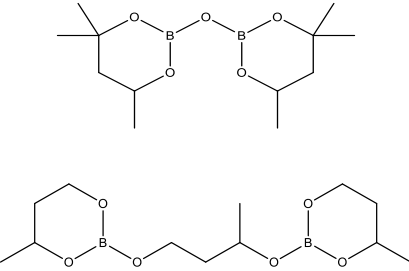
Table 1-1 Comparison of EN 590:2013 and ASTM D 975 specifications for specific properties of diesel<sup>50-51</sup>

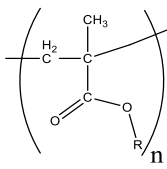
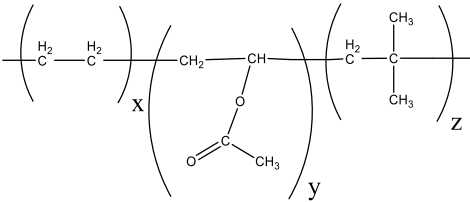
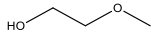
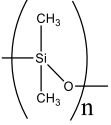
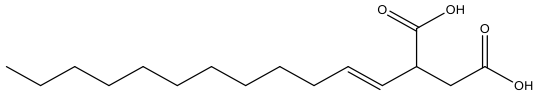
Fuel property	EN 590:2013 specification	ASTM D 975 specification
Cetane number	51 (minimum)	40 (minimum)
Cetane index	46 (minimum)	
Density at 15 °C	820-845 kg/m <sup>3</sup>	800-860 kg/m <sup>3</sup>
Sulfur content	10 ppm (maximum)	15 ppm (maximum)
Flash point	Above 55 °C (minimum)	38-52 °C
Water content	200 ppm (maximum)	
Oxidation stability (*also Rancimat if FAMES>2%)	Total solubles: 25 g/m <sup>3</sup> (maximum), *Induction time: 20 h (minimum)	
Viscosity at 40 °C	2 – 4.5 mm <sup>2</sup> /s	1.3-4.1 mm <sup>2</sup> /s
Cloud point		-20 to 10 °C
Pour point		-35 to -15 °C
Cold filter plugging point Summer Winter	-5 °C (maximum) -15 °C (maximum)	
Lubricity (corrected wear scar diameter at 60 °C)	460 µm (maximum)	520 µm (maximum)

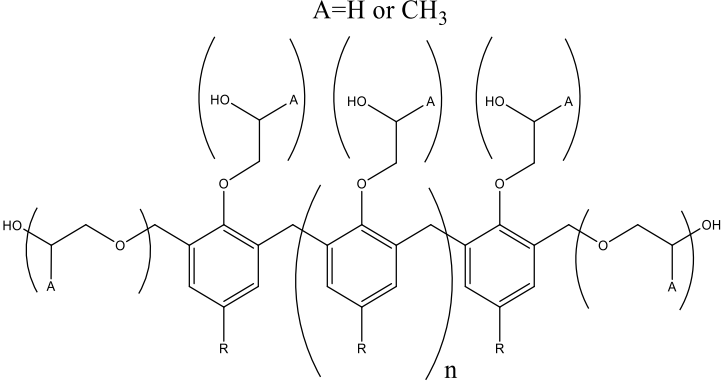
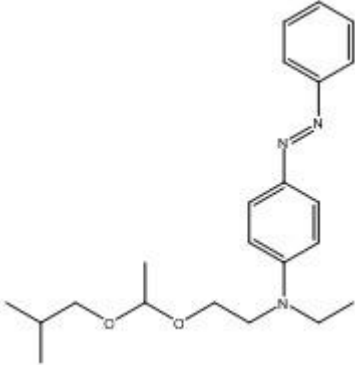
The addition of fuel additives to fuels, in particular diesel, has been undertaken to improve fuel performance<sup>42</sup>. Additives are generally added to fuel at a very low concentration level (approximately <1%) and they are used to meet and maintain specific fuel properties required by specifications<sup>46, 55</sup>. Listed in **Error! Reference source not found.**, below, are the most common types of diesel additives, their function and examples<sup>55</sup>.

Table 1-2 - Common diesel additives, their function and examples. Adapted from<sup>55</sup>

Type of Additive	Function in diesel fuel	Example(s)
Cetane Number Improver	Improves ignition quality by raising cetane number, better starts, reduces white smoke	Nitrates and peroxides <i>e.g.</i> 2-ethylhexyl nitrate <sup>56</sup> 
Lubricity Improvers	Improves lubricity, better injector and pump lubrication	Mono acids, amides, and esters <sup>43</sup> <i>e.g.</i> 2-hydroxy-ethyl linoleate <sup>57</sup> 
Detergents/Dispersants	Clean injectors, better spray patterns	Polyisobutylene-based succinic anhydrides derivatives <sup>58</sup> <i>e.g.</i> mono-succinimides  and polyisobutylene (PIB) amines <sup>59</sup> 

Type of Additive	Function in diesel fuel	Example(s)
Antioxidants	Extend storage life, inhibit oxidation, reduce gum and precipitate formation	Commonly reducing agents, such as hindered phenols, aromatic amines and diamines, or mixtures of aromatic diamines and alkyl phenols <sup>60</sup> <i>e.g.</i> dibutylhydroxytoluene (BHT) <sup>43</sup>  
Stabilizers	Inhibit oxidation and extend storage life	Strongly basic amines <i>e.g.</i> N,N-dimethylcyclohexane amine <sup>43</sup>  
Metal Deactivators	Deactivate copper compounds in fuel, therefore promoting longer storage life	Compounds which can chelate with trace metals <i>e.g.</i> N, N-disalicylidene-1,2-propanediamine <sup>43, 61</sup>  
Biocides	Inhibit bacterial and fungi growth, help prevent fuel filter plugging	Blends of biocides are used; these chemistries are the only diesel biocides approved under the U.S. Military Specification (1988) MIL-S-53021A. <i>E.g.</i> dioxaborinane blend comprised of 2,2-oxybis-(4,4,6-trimethyl-1,3,2-dioxaborinane) + 2,2-(1-methyl-trimethylenedioxy)-bis-(4-methyl- 1,3,2-dioxaborinane) <sup>62</sup>  

Type of Additive	Function in diesel fuel	Example(s)
Pour Point Depressants	Low temperature operability, improve cold-flow properties	Most commonly polymers such as polymethacrylates <i>e.g.</i> poly(methacrylate) <sup>59</sup> 
Cloud Point Depressants (Suppressants)	Reduce temperature at which paraffins solubilize	Also polymers similar to pour point depressants <i>e.g.</i> ethylene vinyl acetate isobutylene terpolymer <sup>63-64</sup> 
De-Icers	Prevent fuel line freezing	Low molecular weight alcohols or glycols <sup>43</sup> <i>e.g.</i> ethylene glycol monomethyl ester <sup>60</sup> 
Anti-Foam Agents	Reduce foaming when filling tanks	Most are organosilicone compounds <sup>43</sup> <i>e.g.</i> polydimethylsiloxane <sup>61</sup> 
Rust Preventors/corrosion inhibitors	Reduce formation of rust in fuel systems and storage tanks	Dibasic acids, phosphate esters or thiophosphates are commonly used. Combinations of inhibitors such as fatty carboxylic acids with an amine or amide <sup>59</sup> . <i>E.g.</i> dodecenyl succinic acid <sup>61</sup> 

Type of Additive	Function in diesel fuel	Example(s)
Demulsifiers/Dehazers	Used to increase the rate of water separation from the fuel	<p>Commonly these are complex mixtures containing “phenolic resins, esters, polyamines, sulfonates or alcohols which have been reacted with ethylene or propylene oxides” <i>e.g.</i> phenolic resin alkoxyate<sup>61</sup></p> 
Dyes	To identify types of diesel for regulatory compliance	<p><i>E.g.</i> Solvent Yellow 124 (Euromarker)</p> 

### 1.1.2 Fuel legislation

Emission standards are “the maximum amount of polluting discharge legally allowed from a single source, mobile or stationary”<sup>65</sup> and this legislation is in place due to environmental concerns and to protect human health<sup>65-66</sup>. The major environmental concerns are that air pollutants can cause climate change, global warming, formation of smog and also reduce air quality<sup>67</sup>. Health conditions such as cancer, cardiovascular, respiratory and neurological diseases have all been found to be linked to toxic air pollutants and poor air quality<sup>67-68</sup>. Engine emission standards are the major regulations surrounding fuels and engines, and were introduced to monitor and reduce vehicle emissions, predominantly from the exhausts of internal combustion engines<sup>69-70</sup>.



Diesel engines have always given out visible emissions due to the soot produced. The first automotive emission legislation occurred in 1946 by the Los Angeles County Air Pollution Control Board (USA) who patrolled to monitor smoke emissions (hydrocarbons (HC)) from diesel engines. Even after this legislation was passed, smog was still present in the Los Angeles basin (USA) that was found to be due to  $\text{NO}_x$ , which are ozone precursors, and in combination with HC cause smog. The first national legislation in the USA was the Clean Air Act (CAA) in 1968. Engine emission standards in Europe were only considered initially during the 1970s and more stringent regulations have been issued subsequently<sup>71-72</sup>.

In Europe, the Euro system has been implemented, with the introduction of the “Euro 1” standard in the early 1990s. Consecutive standards have then followed as the exhaust emission regulations have become increasingly strict, and there are individual standards for both petrol and diesel vehicles, which also differ depending on the category of vehicle. The Euro standards stipulate allowable upper limits of carbon monoxide (CO), HC,  $\text{NO}_x$  and particulate matter (PM) exhaust emissions<sup>71</sup>. There has been approximately a 98% reduction in emissions of CO, HC,  $\text{NO}_x$  and PM from diesel passenger cars since EU emission legislation was introduced (between “Euro 1” and “Euro 6”)<sup>73</sup>. Recently, a particle number (PN) limit of  $6 \times 10^{11}$  particles per km for solid-cored carbonaceous particles with a particle size of  $2.5 \mu\text{m} - 23 \text{nm}$ <sup>74</sup> was introduced for both diesel and petrol engines, “Euro 5” and “Euro 6” respectively (Table 1-3)<sup>75</sup>. The rationale behind this was that PM is an insufficient measure of exposure, only taking mass not number or size of particles into account<sup>76</sup>. Also the solid-cored carbonaceous particles are thought to be more detrimental to human health than larger particles ( $>2.5 \mu\text{m}$ ) as they are found to be associated with numerous health issues including respiratory, cardiovascular, cancer, strokes, low birth weights, and premature deaths<sup>53, 76-77</sup>. All the Euro standards for passenger cars, with their limits, are shown in Table 1-3.

Table 1-3 - Euro Standards and their emission limits for petrol and diesel passenger cars. Data from<sup>71, 78</sup>

Euro standard	New type approvals	All new cars registered	Petrol				PN (#/km)
			CO (g/km)	HC (g/km)	NO <sub>x</sub> (g/km)	PM (g/km)	
Euro 1	01 July 1992	31 December 1992	2.720	0.970	-	-	
Euro 2	01 January 1996	01 January 1997	2.200	0.500	-	-	
Euro 3	01 January 2000	01 January 2001	2.300	0.200	0.150	-	
Euro 4	01 January 2005	01 January 2006	1.000	0.100	0.080	-	
Euro 5	01 September 2009	01 January 2011	1.000	0.100	0.060	0.005 (DI only)	
Euro 6	01 September 2014	01 September 2015	1.000	0.100	0.060	0.005 (DI only)	6x10 <sup>11</sup> (DI only)

Euro standard	New type approvals	All new cars registered	Diesel				PN (#/km)
			CO (g/km)	HC + NO <sub>x</sub> (g/km)	NO <sub>x</sub> (g/km)	PM (g/km)	
Euro 1	01 July 1992	31 December 1992	2.720	0.970	-	0.140	
Euro 2	01 January 1996	01 January 1997	1.000	0.700	-	0.080	
Euro 3	01 January 2000	01 January 2001	0.640	0.560	0.500	0.050	
Euro 4	01 January 2005	01 January 2006	0.500	0.300	0.250	0.025	
Euro 5	01 September 2009	01 January 2011	0.500	0.230	0.180	0.005	6x10 <sup>11</sup>
Euro 6	01 September 2014	01 September 2015	0.500	0.170	0.080	0.005	6x10 <sup>11</sup>

As a result of the Volkswagen 'Dieselgate' scandal and the use of 'defeat devices'<sup>79</sup>, the EU have introduced the Real Driving Emissions (RDE) test. The RDE was implemented from 1<sup>st</sup> September

2017 and is a road test to be undertaken in addition to current laboratory testing. It is hoped the RDE will ensure cars meet emission standards in a larger more varied range of driving conditions, in order to reflect accurate road emissions and reduce the discrepancy between laboratory certification and real-world emissions on the road. The RDE is “performed during vehicle operation using a portable emissions monitoring system (PEMS)”<sup>80</sup>, it “must last from 90 to 120 minutes”<sup>80</sup> and have a route that “must include three segments: urban (< 60 km/h), rural (60-90 km/h) and motorway (> 90 km/h), in that order”<sup>80</sup>, each must cover a distance of at least 16km and each segment represent one third<sup>71, 75, 80</sup>.

In the USA, a similar national engine emission standards system was implemented by the United States Environmental Protection Agency (USEPA). Although, California has even stricter regulations which some other states, known as the Californian Air Resources Board or CARB states, choose to also follow<sup>72, 81</sup>.

### **1.1.3 Recent changes to diesel fuel**

There have recently been some major changes to diesel fuel as well as diesel engines/fuel injection equipment (FIE)<sup>82</sup> (discussed later).

Firstly, a reduction in sulfur to <15 ppm in diesel has occurred due to legislation resulting in increased hydrotreatment of fuels, which are more difficult to refine<sup>82</sup>. Also biodiesel has been blended with diesel in order to meet the “Renewable Transport Fuel Obligations Order” (RTFO) which was first introduced in 2007 but has been recently updated in 2018<sup>83-84</sup>.

Concurrently, since 2008, problematic deposit formation has been observed on fuel injectors in common rail diesel engines. These deposits cause engine performance issues *e.g.* misfiring, stalling, increase in smoke, higher emissions, reduced fuel economy, poor drivability, and/or a severe loss of power.

#### **1.1.3.1 Sulfur reduction**

It is known that high sulfur fuels contributes to acid rain by sulfuric acid (H<sub>2</sub>SO<sub>4</sub>) emissions and sulfates from the fuel contribute to the mass of PM emissions, which are regulated although sulfur emissions are not controlled themselves<sup>40, 52</sup>. Also it has been found that sulfur in fuel can quickly have an adverse effect on the performance of exhaust aftertreatment devices which are intended to “reduce other regulated pollutant emissions”<sup>26, 40, 52, 85</sup>. As a result, diesel is now made with reduced sulfur levels (<15 ppm) and is known as ULSD<sup>85</sup>.

## Chapter 1

In order to achieve less than 15 ppm sulfur in diesel fuel, the process of hydrotreating is used<sup>26, 52, 85</sup>. During this process, sulfur compounds react with the hydrogen gas, producing hydrogen sulfide (H<sub>2</sub>S) gas which is then separated off<sup>52</sup>. Hydrogenation also occurs, during this process, converting unsaturated hydrocarbons to saturated hydrocarbons<sup>40</sup>. Hydrotreating removes excess sulfur, nitrogen, metals and halides from the fuel, however as a consequence concentrations of both aromatic and polar species are reduced<sup>52, 82</sup>. Furthermore “ULSD is less polar than high sulfur grades and so a poorer solvent for any oligomers formed from reactions of any remaining O- and N-containing species”<sup>82</sup>. These consequences of hydrotreating are likely to have a conflicting effect on the propensity of a fuel to form deposits<sup>82</sup>.

Since the desulfurisation of diesel, lubricity has decreased and there has been a “reduction in the solubilising power of the fuel for deposits or their precursors”<sup>31</sup>.

There are numerous test methods used to analyse sulfur levels in diesel fuel in order to ensure the diesel fuel meets specification before release to the customer<sup>86</sup>. Two of the most commonly used methods are energy-dispersive x-ray fluorescence spectrometry (ED-XRF) (ASTM method D 4294) and monochromatic wavelength dispersive x-ray fluorescence spectrometry (MWD-XRF) (ASTM method D 7039)<sup>86</sup>.

### **1.1.3.2 Increasing use of biodiesel due to limiting use of fossil fuels in diesel fuel**

Currently the world is facing two major problems, firstly, fossil fuels are depleting (energy crisis 1970s) as demand for energy increases due to industrialisation and motorisation, and secondly, the deterioration of the environment from pollution<sup>52, 87</sup>. Biofuels have been seen to be a viable solution for both these issues, as they are renewable and largely environmentally friendly. The RTFO<sup>84</sup> was introduced in 2007, by the UK government, in order to preserve fossil fuels and encourage the use of renewable fuels, resulting in greater interest and production of biofuels in the fuel industry. Initially required 2.5% of conventional hydrocarbon road fuel to be made up from renewable fuels, however from April 2018, it now requires 7.25%<sup>83</sup>.

Biodiesel is the most commonly produced biofuel<sup>88</sup> and is used as a renewable alternative to petrodiesel fuel as it has “similar characteristics (Table 1-4) but lower exhaust emissions”<sup>89</sup> and has been widely produced since the 1990s with production increasing steadily year on year<sup>90</sup>.

Table 1-4 - Comparison of properties of used cooking oil, biodiesel from used cooking oil and commercial petrodiesel fuel, adapted from<sup>89</sup>

Property	Used cooking oil	Biodiesel from used cooking oil	Commercial petrodiesel fuel
Kinematic viscosity (mm <sup>2</sup> /s, at 313 K)	36.4	5.3	1.9 – 4.1
Density (kg/L, at 288 K)	0.924	0.897	0.075 – 0.840
Flash point (K)	485	469	340 - 358
Pour point (K)	284	262	254 - 260
Cetane number	49	54	40 - 46
Sulfur content (%)	0.09	0.06	0.35 – 0.55
Water content (%)	0.42	0.04	0.02 – 0.05

Biodiesel is defined as a mixture of monoalkyl esters of long chain (typically C<sub>14</sub> –C<sub>22</sub>) fatty acids (FAMES) which are derived from a renewable lipid feedstock, such as vegetable oil or animal fat, *via* transesterification using short chain alcohols (methanol or preferably ethanol) commonly in the presence of an alkali catalyst, with glycerol as a byproduct<sup>89, 91</sup>.

The first recorded use of vegetable oil as a fuel was in 1900, at Exposition Universelle in Paris, where Rudolph Diesel exhibited an engine running on peanut oil<sup>30</sup>. In 1937, Charles George Chavanne filed a patent for “method of transformation of vegetable oils for use as fuels”, in which the transesterification reaction of palm oil with ethanol using an acid catalyst was outlined<sup>53</sup>.

The transesterification reaction (Figure 1-5)<sup>92</sup> is required to obtain more desirable physical properties, as oils and fats have a higher viscosity and lower volatility than petrodiesel. Firstly, transesterification enables kinematic viscosity (KV) to be decreased as oils normally have a KV a whole order of magnitude higher (see Table 1-4).and a higher KV of fuel can mean poor atomisation which may lead to deposits<sup>53, 89</sup>. Vegetable oils and fats also have a lower volatility than diesel due to their higher molecular weights than diesel; transesterification reduces the molecular weight by splitting these heavy molecules into three lighter molecules. If volatility of a biodiesel is too low, deposit formation may result as oils and fats can stick to cylinder walls or fuel injectors and then

undergo oxidative and thermal polymerization forming a film that gradually gets thicker<sup>93-94</sup>. It is also important that free glycerol is removed after transesterification as this can lead to plugged fuel filters if left in the biodiesel<sup>53</sup>.

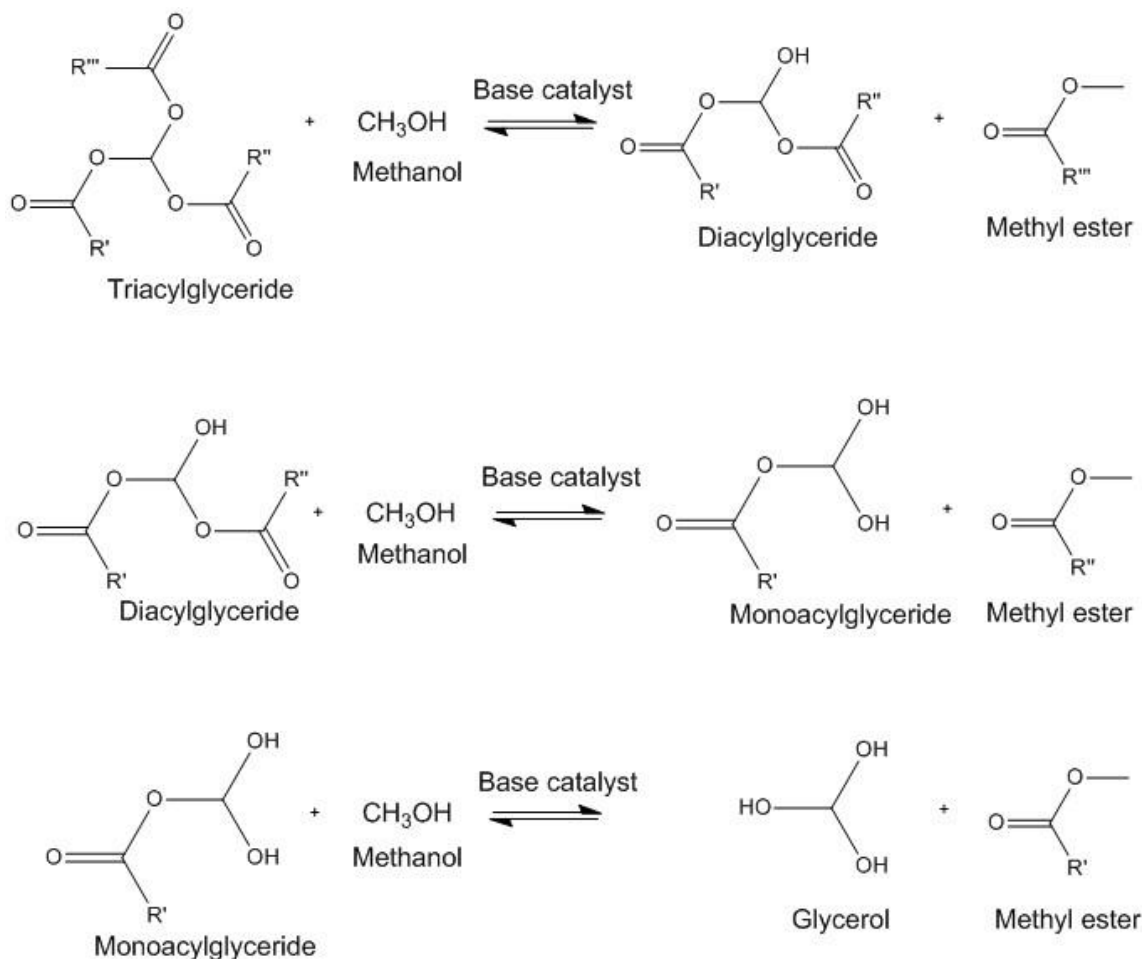


Figure 1-5 - Transesterification reaction scheme. Adapted from<sup>92</sup>

Biodiesels can be made from any fatty acid source, but the most commonly used oil feedstocks were historically rapeseed oil in Europe (including UK), soybean oil in the USA and Palm oil in Asia<sup>53, 95-96</sup>. However, recently the trends in feedstock has shifted to used cooking oil (UCO) being used commonly to produce used cooking oil methyl ester (UCOME). This is now being used globally, particularly in Europe (including UK), and USA. The main reasons for this shift are firstly cost as virgin vegetable oil is 2-3 times more expensive than UCO as a biodiesel feedstock, meaning biodiesel production is 1.5 times more expensive to produce if using virgin feedstocks, therefore the use of UCO significantly reduces this<sup>94</sup>. Another benefit of using UCO as a biodiesel feedstock is that it alleviates concerns surrounding the competition between food crops and energy crops (diversion of agriculture) and which may cause food shortages and increased food prices<sup>97</sup>. The recycling of UCO for biodiesel production is also eliminating problematic waste<sup>98</sup>, which would

often be illegally disposed of into sewers<sup>99</sup> causing problems such as fatberg in London<sup>100</sup> and damage to infrastructure, therefore further polluting the environment<sup>101</sup>. However, theft of UCO has become a prominent issue, as much as 20% is stolen before collectors arrive due to lax security. It is suspected that the thieves then produce biodiesel and illegally sell it on the black market without paying VAT or duty tax<sup>98, 102</sup>. It is estimated that the UK Treasury lose £25 million per year in revenue from the biodiesel black market<sup>102</sup>. Since the introduction of the RTFO in 2007, there has been a large increase in the volume of UCO- derived biodiesel supplied on the UK market and the number of countries supplying UCO have also increased greatly. Between April 2011- April 2012 (4<sup>th</sup> year after RTFO) UCO-derived biodiesel generated was 137 million litres, some of which was exported<sup>102</sup>. Additionally a crop cap was introduced in 2018, which limits the contribution that biodiesels made from crops can make towards the RTFO. A maximum of 4% crop derived biodiesel was allowed in 2018, by 2032 only 2% will be allowed<sup>83</sup>. Therefore the production of UCO derived biodiesel is likely to increase further.

There are many advantages of using biodiesel as either a direct replacement fuel or a blending component into diesel. Firstly it is environmentally friendly, in a number of ways, such as being produced from a renewable source and it is biodegradable and nontoxic<sup>96</sup>. Also biodiesel does not contain sulfur, it does not produce any new carbon dioxide into the atmosphere and it reduces all exhaust emissions except NO<sub>x</sub> which increase slightly<sup>103</sup>; this means it is good at meeting current fuel emissions legislation<sup>96</sup>. Finally it is less flammable than diesel but has similar viscosity, so this facilitates safe use and easy transportation<sup>96</sup>.

However the use of biodiesel as a fuel also has its drawbacks, such as its low fuel stability and its susceptibility to oxidation, both auto- and chemical<sup>96</sup>. FAMES are known to “readily degrade” through auto-oxidation and produce many other products which are detrimental to the fuel in a number of different ways<sup>96</sup>. Fuel blends containing biodiesel are therefore more susceptible to auto-oxidation compared with pure diesel fuel<sup>96</sup>.

Biodiesel is thought to possibly play a role in some deposit formation<sup>85, 104</sup>, however it is important to note other changes to diesel fuel and engines also took place at this time. This will be discussed later in this chapter (1.3) and in chapter 5.

#### **1.1.4 Current analytical techniques found in literature for the analysis of fuels**

Diesel fuels are a very challenging analyte, largely due to them being a complex chemical mixture of compounds including additives. However their analysis is very important for a variety of reasons, including fuel quality and characterisation, and this therefore provides a chemical challenge of obtaining rapid and complete analysis<sup>2</sup>.

## Chapter 1

Chromatography has been widely utilised in the analysis of petroleum fuels and crude oils.

High performance liquid chromatography (HPLC) has numerous applications in the petroleum industry including “hydrocarbon-type separation and determination, as well as separation, identification, and, in some cases, quantitative determination of target compounds in many petrochemical samples”<sup>3</sup>, some examples include IP test methods, IP391 and IP368<sup>3</sup>. Most available HPLC detectors have been used in fuel analysis for both quantification and detection<sup>3</sup>.

Gas chromatography (GC) techniques has also been greatly used in the analysis of fuels, some examples include gas chromatography coupled to a flame ionisation detector (GC-FID)<sup>1</sup>, gas chromatography-field ionisation mass spectrometry (GC-FIMS)<sup>4</sup> and gas chromatography-mass spectrometry (GC-MS)<sup>5</sup>. Cho *et al.*<sup>6</sup> obtained a detailed chemical composition of a diesel sample with the combined use of the complementary methods: two dimension gas chromatography (GCxGC-MS or 2D GC-MS) together with atmospheric pressure photo ionisation (APPI) mass coupled to Fourier transform-ion cyclotron resonance mass spectrometry (FT-ICR MS)<sup>6</sup>. Compounds containing aliphatic alkyl, saturated cyclic ring(s), and one aromatic ring structures were identified with 2D GC-MS whereas compounds with one to three aromatic rings (or 4 benzene rings) were mainly identified by APPI-FT-ICR MS, showing the need for both techniques for a more complete analysis of the composition of the diesel sample<sup>6</sup>.

Since the 1980s, supercritical fluid chromatography (SFC) has been used in the analysis of petroleum compounds<sup>7</sup>. Thiébaud<sup>7</sup> reviewed the application of SFC in the petroleum industry, outlining the major uses and techniques which include “simulated distillation, group-type analysis and related applications including the implementation of multi detection in a so-called “hypernated” system, as well as the hyphenation to GCxGC for improved group-type separation, SFCxGC and first promising SFCxSFC results.”<sup>7</sup>. Other SFC techniques used include SFC coupled to a flame ionisation detector (SFC-FID)<sup>8</sup> and SFC-field ionisation time-of-flight (high resolution) mass spectrometry (SFC-FI-ToF-MS)<sup>7, 9</sup>.

Mass spectrometry as a standalone analysis technique has also been utilised in fuel analysis<sup>2, 10-18, 20, 49, 105</sup>.

The use of negative electrospray ionisation mass spectrometry (ESI-MS) was reported by Rostad<sup>10</sup> for the analysis of polar compounds (at low concentrations) in petroleum products, unique to each fuel, which afforded differentiation and identification of different fuel types and sources<sup>10</sup>. This allowed a quick screen method for samples of hydrocarbons from either a fuel spill or release into the environment<sup>10</sup>.



Hughey *et al.*<sup>11</sup> directly analysed the composition of raw and processed diesel fuel using positive ion ESI coupled to FT-ICR MS. This method afforded selective ionisation of pyridine homologues, known to cause fuel instability and hinder removal of heteroatoms, prior to identification using the high resolving power and accurate mass measurements of FT-ICR MS, which allowed separation of closely spaced, adjacent peaks and provided an accurate mass measurement to within 1 ppm. FT-ICR MS is an advantageous technique meaning it is commonly used for analysis of complex mixtures<sup>11</sup>. Similar work was undertaken by Rodgers *et al.*<sup>12</sup> to monitor the elemental composition of petrochemical fuels that undergo weathering<sup>12</sup>. FT-ICR MS was well suited to this work as it affords separation of nominally isobaric species, therefore allowing individual components of interest to be identified and monitored, which provided a much more detailed picture of changes as they occurred<sup>12</sup>.

Many fuels including gasoline, kerosene, diesel and biodiesel<sup>2, 49</sup> have been analysed by Easy ambient sonic-spray ionisation mass spectrometry (EASI-MS). Alberici *et al.*<sup>2</sup> reviewed the use of EASI-MS in the analysis of fuels and concluded “EASI ( $\pm$ )-MS seems to offer an attractive method for single-shot characterisation and quality control of fuels in general. The method is simple, fast and direct (or nearly direct) and requires minimal or no sample preparation and no pre-separation steps. The coupling of EASI to portable, miniaturised mass spectrometers may also provide an excellent alternative for on-site and *in situ* fuel analysis.”<sup>2</sup>.

Many other techniques have also been previously employed in fuel analysis including atmospheric solid analysis probe mass spectrometry (ASAP-MS)<sup>13-15</sup>, inductively coupled plasma mass spectrometry (ICP-MS)<sup>16-17</sup>, isotope-ratio mass spectrometry (IRMS)<sup>18</sup>, direct analysis in real time mass spectrometry (DART-MS)<sup>20, 105</sup> and ion mobility-mass spectrometry (IMMS)<sup>15</sup>. A number of spectroscopy methods have also been employed including ultraviolet visible (UV-Vis) spectroscopy<sup>21</sup>, nuclear magnetic resonance (NMR) spectroscopy<sup>22-23</sup>, near-Infrared spectroscopy (NIR)<sup>23-25</sup>, infrared spectroscopy (IR)<sup>25</sup> and raman spectroscopy<sup>25</sup>.

## 1.2 Diesel engines

### 1.2.1 History

In 1885, Herbert Akroyd Stuart had an incident whereby some “paraffin oil vaporised and ignited after accidentally spilling into a pot of hot metal”<sup>53</sup> causing a small explosion, while working in his father’s tinsplate factory. This sparked his interest in fuel combustion, which led onto the development of the vaporiser engine. In 1890, Herbert Akroyd Stuart along with Charles Richard Binney were granted a patent entitled “Improvements in Engines Operated by the Explosion of Mixtures of Combustible Vapour of Gas and Air”. This patent outlined the use of a vaporiser to heat liquid fuel, as it enters the combustion chamber of the engine, to aid mixing with compressed air, which results in automatic ignition occurring. This mitigated the risk of pre-ignition, which occurs when a hydrocarbon vapour and air are drawn into the combustion chamber together. An example of this invention was exhibited in 1891 at the Royal Agricultural Show in Doncaster, England and was the first oil engine to run without a spark for ignition. This engine was produced by Richard Hornsby and Sons and sold as the Hornsby-Akroyd oil engine<sup>53</sup>.

However, in 1892, Rudolf Diesel filed a patent claiming that:

“By following his process the efficiency of the internal combustion engine could be improved and hence fuel consumption reduced. By adding fuel at a controlled rate to compressed air the rate of heat released could be controlled and therefore the maximum cylinder temperature could be controlled.”<sup>41</sup>.

And Diesel also claimed that every type of fuel could be used in this process and that this process would increase the efficiency of the engine because the amount of energy wasted as lost heat would be reduced by controlling the maximum cylinder temperature<sup>41</sup>. However Diesel tried running his first prototype engine on pulverised coal but it was not a viable design due to failure of his proposed fuel delivery method so the first successful prototype, in 1894, was run on liquid fuel which required atomisation using compressed gas<sup>30, 41</sup>. Furthermore, Diesel then filed another patent in 1898, “claiming a means of controlling the engine by controlling the fuel injected.”<sup>41</sup> with delivery of fuel relying on the use of compressed gas<sup>30, 41</sup>. Akroyd Stuart and Diesel both worked to similar timescales, however, since the turn of the century it has been known as the diesel engine<sup>53</sup>.

James McKechnie filed a patent in 1910, outlining the use of a high pressure (138 bar – 414 bar) fuel injection system using “an engine driven cam and spring mechanism”<sup>30</sup> to generate the high pressure needed to inject the liquid fuel directly into the combustion chamber<sup>30</sup>. He then filed another patent, approximately two years later, outlining what is now known as the “common rail”

system, although he did not state the pressures used, so pressures from the previous patent are assumed<sup>30</sup>. The common rail system is the introduction of fuel under pressure into a main supply pipe, known as the rail, which then supplies the fuel under pressure into the injector valve for each individual cylinder<sup>30</sup>.

Around the same time, a fuel injection system using electrically operated solenoid valves to activate fuel injectors connected to a fuel accumulator was proposed by the American engineer, Thomas Gaff<sup>30</sup>. Bosch started to also develop a fuel injection system for diesel engine in 1922<sup>46</sup>.

However, neither the common rail nor the Gaff system were adopted straightaway and it took over 50 years for common rail with electronically activated fuel injectors to become the favoured choice<sup>30</sup>.

Further improvements to common rail systems did not occur until the late 1980s when Nippondenso Co. Ltd patented their common rail system with a rail pressure of 1500 bar. Since then many systems have been proposed and today systems are able to produce up to 3000 bar<sup>30</sup>.

Fuel economy, reliability and efficiency are some of the main factors that have allowed diesel engines to be favoured over petrol engines in heavy-duty applications and more recently light duty applications too<sup>30, 40</sup>. However the diesel engine had many perceived negatives, such as it was dirtier, noisier and had a lower power density than a petrol engine<sup>40</sup>. It has taken over a century to develop a precise fuel injection system capable of overcoming many of the negatives mentioned previously<sup>40</sup>.

### **1.2.2 Operation of a diesel engine**

Operation in diesel engines can either be in the form of a two-stroke or four-stroke engine, with four-stroke engines commonly used in motor vehicles, such as cars<sup>46</sup>. A stroke refers to the piston moving the full length of the cylinder or 180° rotation of crankshaft (*i.e.* Top Dead Centre (TDC) to Bottom Dead Centre (BDC) or *vice versa*). Therefore, there is one revolution of the crankshaft (360°) for a complete engine cycle in a two-stroke engine, whereas there are two revolutions of the crankshaft (720°) for a complete engine cycle in a four-stroke engine<sup>54</sup>.

All diesel engines require at least one combustion cylinder, within which fuel and highly compressed air mix and then spontaneously combust. This then drives the piston up and down and this movement is then converted into a rotational movement *via* the connecting rod and onto the crankshaft and flywheel, which then in turn moves the wheels of the vehicle<sup>46</sup>.

## Chapter 1

A four-stroke diesel engine works by compression and heat, and without a source of ignition, unlike a less efficient petrol engine which relies on a spark plug for ignition<sup>106</sup>. The operation cycle of a four-stroke engine is shown in Figure 1-6<sup>46, 106</sup>.

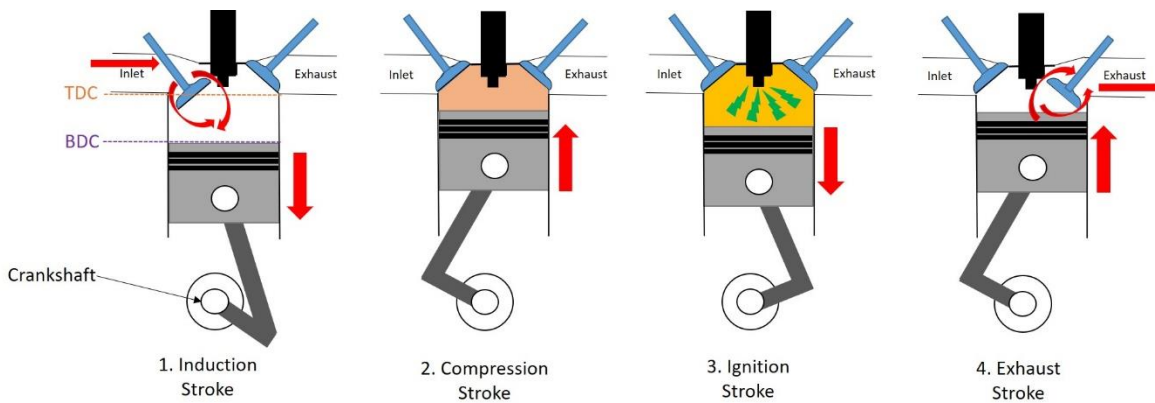


Figure 1-6 - Diagram showing the operation cycle of a four-stroke diesel engine.

Adapted from<sup>46,106</sup>

During the induction stroke, the piston moves in a downward motion to the bottom of the cylinder (BDC) to provide the greatest capacity within the cylinder. Simultaneously the inlet valve is opened to allow air into fill the cylinder. The compression stroke begins when both the inlet and exhaust valves are closed and then the piston moves in an upward motion to compress the air within the cylinder. The degree to which the air is compressed varies and is dependent upon the engine's specific combustion ratio ("between 16:1 and 24:1 in cars and commercial vehicles"<sup>46</sup>). As the combustion occurs, the air is heated up to around 900 °C. As the combustion stroke is reaching its end, the high-pressure fuel is injected *via* the fuel injector into the hot compressed air. The ignition stroke (also known as the working cycle) begins as after a short period of ignition lag (piston slowly moves slightly downwards from top (TDC)). Due to the heat from the compressed air the atomised diesel fuel spontaneously ignites and combusts. As the heat increases in the cylinder due to the fuel combusting, pressure also increases which pushes the piston downwards, meaning chemical energy is converted into kinetic energy. This kinetic energy then drives the crankshaft in a rotational movement. The final step is the exhaust stroke, which begins with the exhaust valve opening just as the piston is approaching the bottom of the cylinder. This allows the gases produced during the ignition stroke to flow out of the cylinder, which is aided by the piston as it moves up to the top of the cylinder to start the operation cycle again<sup>46</sup>.

### 1.2.3 Fuel injection equipment (FIE)

Fuel injection systems are required to deliver the correct volume of fuel at the correct time and pressure, at the correct timing in to the correct position into the combustion cylinder for all

cylinders within a diesel engine<sup>46</sup>. Therefore fuel injection systems have always been of utmost importance in the performance of diesel engines<sup>41</sup>.

As emission regulations have become increasingly strict and customer demand for greater efficiency and improved fuel consumption is ever increasing, so the FIE has had to become far more advanced and precise, to ensure the required amount of fuel is delivered and evenly distributed within the cylinder<sup>41, 46</sup>. As further advancements have occurred and fuel quality has changed, so the FIEs have become increasingly sensitive and intolerant of deposit formation than previous FIEs<sup>27, 30, 41</sup>. Today, high pressure fuel is supplied from the common rail to the fuel injectors, meaning the moving parts within the injector just open and close quickly and accurately to deliver the fuel. In order to achieve this current fuel injectors are much smaller and lighter than their predecessors with reduced clearances between moving parts, which are now between 2-3  $\mu\text{m}$ , meaning they are more susceptible to substandard performance caused by deposits<sup>53, 107</sup>. Also reduced mechanical force of  $\sim 40\text{ N}$  is now used to enable multiple fuel injections to take place per cycle in comparison with the older injectors which used 17600 N for a single injection per cycle, this meant older injectors were not hindered significantly by deposits<sup>27, 107</sup>.

There are two main types of fuel injection systems; indirect injection (IDI) and direct injection (DI), as shown in Figure 1-7<sup>46</sup>. IDI was commonly used in the 1980s and early 1990s due to better exhaust emissions and noise. However due to improvements in DI such as high pressure fuel injection, pre injections and electronic management of the engine, IDI was totally phased out by Euro 3 to make way for DI<sup>46, 108</sup>.

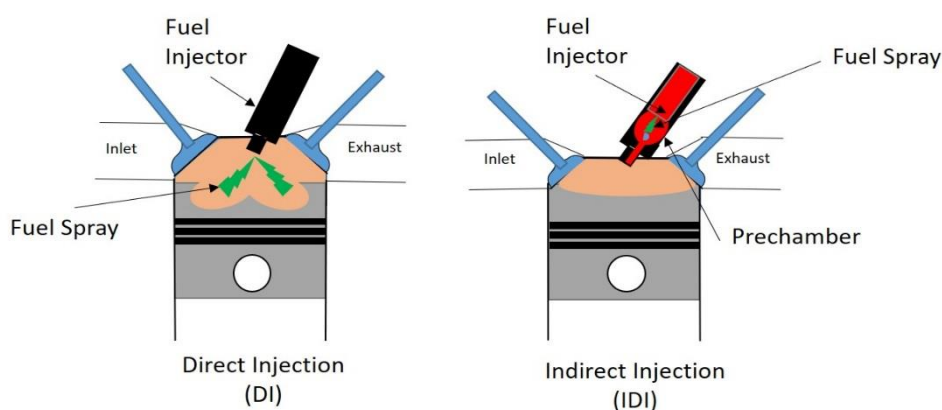


Figure 1-7 - Diagram showing Direct injection (DI) and Indirect injection (IDI) fuel injection systems. Adapted from<sup>46</sup>

### 1.2.3.1 Indirect injection (IDI)

An IDI fuel injection system utilises a divided combustion chamber so the injection and initial combustion of the fuel can be in separate chamber to the main combustion chamber. There are two common types of IDI; Pre-combustion chamber system and Swirl chamber system<sup>46</sup>.

## Chapter 1

In the pre chamber combustion system, there is a hot pre-combustion chamber that is recessed into the cylinder head. Initially fuel is injected at a low pressure (up to 450 bar) through a pintle nozzle into this pre-combustion chamber. The jet of injected fuel is diffused and atomised with the air rapidly, as it hits a special shaped baffle in the centre of pre-combustion chamber. As a result, auto ignition begins within the pre-combustion chamber and the rise in temperature and pressure therefore forces the partly combusted air/fuel mixture through a channel into the main combustion chamber. It then mixes thoroughly with air in main combustion chamber, spreading and completing combustion<sup>46</sup>.

The only major differences between a pre-combustion chamber system and a swirl chamber system is the latter takes almost the entire combustion volume (pre-combustion chamber is only 1/3 of combustion volume) and the air is circulated in the swirl chamber, rather than utilising a baffle<sup>46</sup>.

### **1.2.3.2 Direct injection (DI)**

A DI fuel injection system injects fuel directly into a single, undivided combustion chamber.

The combustion chamber, partly formed by the crown shaped recess in the piston, has fuel directly sprayed into it. During this time, rapid atomisation, heating and vaporisation of the fuel must take place as well as mixing with the air in an even distribution, meaning fuel and air delivery is of utmost importance. Controlled fuel delivery, to evenly distribute fuel, can be achieved through the use of multihole fuel injectors with optimised jet positions for specific combustion chamber design and effective air delivery can be achieved is through air turbulence. (Air turbulence is created through the shape of the intake port creating a swirl of air and the shape of the combustion chamber affecting air flow patterns at point of injection.)

There are two main types of DI; systems that utilise air turbulence to aid air-fuel mixing and systems that control air-fuel mixing by almost only fuel injection control and disregard air turbulence. The latter system relies heavily on the FIE which requires greater optimisation (needle position, degree of atomisation and number of jets) and must operate at very high pressures.

As a result, the DI system affords higher efficiency and a more economical operation than IDI and is now used in all types of commercial vehicles and almost all modern diesel cars<sup>46</sup>.

### 1.2.3.3 Common rail fuel injection system

A common rail fuel injection system, shown in Figure 1-8<sup>46, 109</sup>, is a direct injection (DI) fuel injection system used in both petrol and diesel engines<sup>110</sup>.

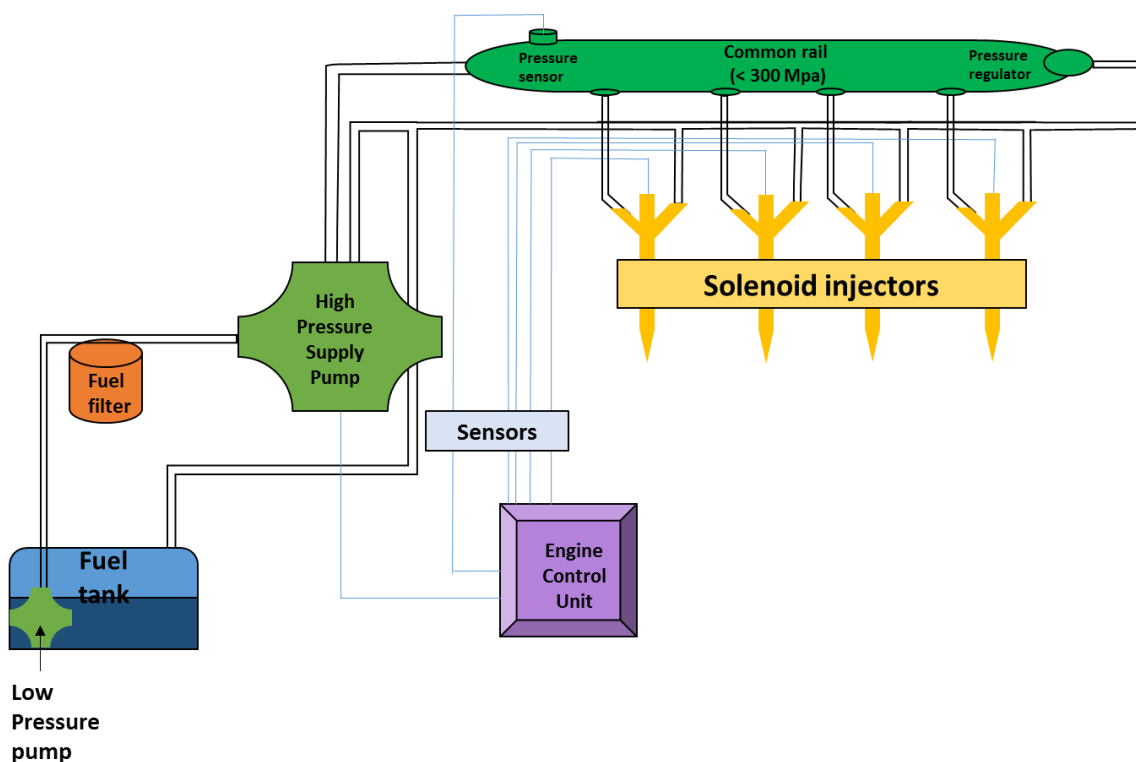


Figure 1-8 - Diagram of Common Rail Fuel Injection system. Adapted from<sup>46, 109</sup>

In a common rail fuel injection system, fuel injection and pressure generation are separated. This advantageously allows much flexibility with injection pressures and timings. The operation of a common rail fuel injection system begins with a reservoir of fuel being stored at high pressure ( $\sim 2000$  bar) in the common rail prior to injection. The common rail is a “pressure-accumulator” which provides fuel for all the multiple fuel injectors and pressure is maintained within it by a high-pressure pump operating continuously. The fuel injectors themselves are piezoelectric injectors and are controlled by the engine control unit (ECU). When the injectors are activated, their hydraulic valve is opened and the fuel is sprayed at the desired constant high pressure in the cylinder (as shown in figure 1-5)<sup>110</sup>. After the fuel injection, the valve closes and the cycle begins all over again<sup>110</sup>. However, in some advanced systems, small injections prior to the main injection may take place and up to 5 injections per cycle can take place. Today common rail fuel injection systems have the ability to reach pressures of 3000 bar, which have resultant temperatures of  $150^\circ\text{C}$  with nozzle temperatures even higher<sup>31, 46, 110</sup>.

The main difference that the common rail system has from other fuel injection systems, is that the fuel injection is at high pressure and injection speed and is not dependent on engine speed and

load<sup>110-111</sup>. It is an advantageous system in comparison to the previously used indirect injection systems as it is “quieter, more fuel efficient, cleaner, and more powerful”<sup>111</sup>.

### 1.2.4 Evolution of diesel engines to satisfy legislation

Diesel engines, particularly the FIE, have had to evolve in order to meet the demand for more power and efficiency, meanwhile increasingly rigorous emissions legislations have been put in place forcing engine manufacturers to engineer systems able to attain near-to-zero emissions<sup>31, 41, 52, 85</sup>. Diesel engine emission control technology comprise of in cylinder control and aftertreatment systems, which have evolved through both improvements as well as implementing new technologies<sup>108</sup>. Table 1-5 shows the evolution of diesel engine emission control technologies over the period from Euro 1- Euro 6.

In Euro 1, mechanically activated exhaust gas regeneration (EGR) were introduced and mechanical fuel injection systems were used, commonly IDI. In addition, oxidation catalysts were used for odour control<sup>108, 112-113</sup>.

During Euro 2, electromechanical fuel injection systems along with electronic fuel timing and metering were slowly introduced, in favour over mechanical systems. The use of turbochargers also became common and cooled EGR systems and fuel injection delay were used for NO<sub>x</sub> emission control<sup>108, 112-113</sup>.

In Euro 3, due to the elimination of a warm up period during New European Driving Cycle (NEDC) testing, cold start became a major focus of emission control. Mechanical FIE was no longer used and DI fuel injection systems were introduced. Electronic controlled individual unit injectors and fuelling rates as well as variable injection aided the DI, which operated at injection pressures of 1500–1700 bar. Diesel oxidation catalysts(DOC) were also installed to control PM<sup>108, 112-113</sup>.

Due to the 50% reduction in NO<sub>x</sub> and PM allowable emissions compared with Euro 3, new technologies were required in Euro 4. A new design of piston was also installed and intercooled turbochargers were used to ensure better fuel-air mixing. High pressure common rail fuel injection systems were introduced with adjustable fuel timing and metering, this along with DOC was used to control PM emissions. NO<sub>x</sub> were controlled using selective catalytic reduction (SCR) technology<sup>108, 112-113</sup>.

In Euro 5, PN emission limit was introduced so improvements were made to current technologies in order to meet even stricter emission limits but no new technologies<sup>108, 112-113</sup>.



In Euro 6 (currently), high pressure (now 2200 bar<sup>113</sup>) common rail fuel injection systems are being utilised and afford wide flexibility, complex injection timing and metering and improved injector design. This is used in combination with a variable geometry turbocharger that can deliver tailored fuel and air volumes to meet specific engine conditions. Aftertreatments have improved significantly, with a multifaceted approach for both NO<sub>x</sub> and PM emissions<sup>108, 112-113</sup>.

Table 1-5 – Evolution of diesel engine technology to meet emission limits, adapted from<sup>108, 112-113</sup>. Emission limits data from<sup>71, 78</sup>

Euro Standard	Technology changes to diesel engines	Emission limits (g/km)
Euro 1	<p><b>Engine-out emissions and air/fuel controls:</b></p> <ul style="list-style-type: none"> <li>• IDI fuel injection</li> <li>• Mechanically activated EGR</li> </ul> <p><b>Aftertreatment systems:</b></p> <ul style="list-style-type: none"> <li>• Oxidation catalysts</li> </ul>	<p><b>CO:2.720</b>  <b>HC + NO<sub>x</sub>:0.970</b>  <b>NO<sub>x</sub>:-</b>  <b>PM:0.140</b></p>
Euro 2	<p><b>Engine-out emissions and air/fuel controls:</b></p> <ul style="list-style-type: none"> <li>• Turbochargers introduced (common in larger light-duty vehicles)</li> <li>• In-line or rotary fuel pump</li> <li>• Fuel injection pressures of 1200 bar</li> <li>• Fuel injection delay for NO<sub>x</sub> control</li> <li>• Cooled ERG</li> <li>• Electronic fuel timing and metering</li> </ul> <p><b>Aftertreatment systems:</b></p> <ul style="list-style-type: none"> <li>• No changes</li> </ul>	<p><b>CO:1.000</b>  <b>HC + NO<sub>x</sub>:0.700</b>  <b>NO<sub>x</sub>:-</b>  <b>PM:0.080</b></p>

Euro Standard	Technology changes to diesel engines	Emission limits (g/km)
Euro 3	<p><b>Engine-out emissions and air/fuel controls:</b></p> <ul style="list-style-type: none"> <li>• DI fuel injection</li> <li>• Injection pressures of 1500–1700 bar</li> <li>• Electronically controlled fuelling rates</li> <li>• Electronic unit injectors</li> <li>• Variable injection</li> </ul> <p><b>Aftertreatment systems:</b></p> <ul style="list-style-type: none"> <li>• DOC (Diesel Oxidation Catalyst)</li> </ul>	<p><b>CO:0.640</b>  <b>HC + NO<sub>x</sub>:0.560</b>  <b>NO<sub>x</sub>:0.500</b>  <b>PM:0.050</b></p>
Euro 4	<p><b>Engine-out emissions and air/fuel controls:</b></p> <ul style="list-style-type: none"> <li>• Electronic unit injectors or common rail fuel injection</li> <li>• Injection pressure of 1700–1900 bar</li> <li>• Variable fuel injection (fuel timing and/or metering)</li> <li>• Piston redesign</li> <li>• Cooled EGR</li> <li>• Turbochargers with intercoolers</li> </ul> <p><b>Aftertreatment systems:</b></p> <ul style="list-style-type: none"> <li>• NO<sub>x</sub> control through vanadium-based, open-loop SCR (Selective Catalytic Reduction) systems</li> <li>• PM control through DOC in some vehicles, with most relying on in-cylinder control</li> </ul>	<p><b>CO:0.500</b>  <b>HC + NO<sub>x</sub>:0.300</b>  <b>NO<sub>x</sub>:0.250</b>  <b>PM:0.025</b></p>

Euro Standard	Technology changes to diesel engines	Emission limits (g/km)
Euro 5	<p><b>Engine-out emissions and air/fuel controls:</b></p> <ul style="list-style-type: none"> <li>• No new engine technologies, only small improvements such as changes in timing strategies</li> </ul> <p><b>Aftertreatment systems:</b></p> <ul style="list-style-type: none"> <li>• NO<sub>x</sub> control through vanadium-based, open-loop SCR systems</li> <li>• Adjustments to SCR system</li> <li>• PM control through DOC in some vehicles, with most relying on in-cylinder control</li> </ul>	<p><b>CO:0.500</b>  <b>HC + NO<sub>x</sub>:0.230</b>  <b>NO<sub>x</sub>:0.180</b>  <b>PM:0.005</b>  <b>PN:6x10<sup>11</sup></b></p>
Euro 6	<p><b>Engine-out emissions and air/fuel controls:</b></p> <ul style="list-style-type: none"> <li>• High-pressure, high-flexibility fuel injection system, with injection pressure greater than 2000 bar</li> <li>• Variable geometry turbocharger</li> <li>• Multimode fuel injector strategies</li> <li>• R&amp;D, advanced combustion, engine calibration</li> <li>• more complex injection timing metering algorithms and fuel injector design</li> <li>• Cooled EGR</li> </ul> <p><b>Aftertreatment systems:</b></p> <ul style="list-style-type: none"> <li>• NO<sub>x</sub> control through zeolite-based, closed-loop SCR system</li> <li>• Ammonia slip catalyst</li> <li>• PM control through DOC and diesel particulate filters (wall-flow)</li> <li>• Lean NO<sub>x</sub> traps</li> </ul>	<p><b>CO:0.500</b>  <b>HC + NO<sub>x</sub>:0.170</b>  <b>NO<sub>x</sub>:0.080</b>  <b>PM:0.005</b>  <b>PN:6x10<sup>11</sup></b></p>

### 1.3 FIE deposits

Since the birth of diesel fuel injection systems, deposit formation has occurred in diesel engines, particularly the FIE in varying locations<sup>31, 85</sup>. These deposits have been of little concern until fairly recently due to the modernisation of FIEs and the emissions regulations being introduced<sup>31</sup>. The FIE is designed in such a way to allow for deposit formation to a small extent, however this allowance causes a variation in emissions which has become a problem in relation to the introduction of increasingly strict emissions regulations<sup>30</sup>. Changes and advancements to both engines and diesel fuels, has been shown to correlate with increased incidence of reported operational problems caused by FIE deposits<sup>31, 85</sup>.

The diesel fuel injector and fuel filter deposits observed since about 2008 are different from those previously seen<sup>31, 52</sup>. There has been substantial interest in these deposits due to both engine manufacturers and fleet operators having increased numbers of reports concerning deposit formation in fuel systems<sup>31</sup>. The reports started in the USA but have spread around the world and still continue today<sup>31</sup>. Initially the reports from the field found deposits on fuel filters but then on injector nozzles and more recently on the internal parts of the injector. In some cases deposits were found in two or all three locations<sup>31</sup>. As a result of these reports, much research has been undertaken regarding the characterisation and the formation of deposits leading to many papers, forums and conference proceedings in this area of research, although no solution or answer has been found to this problem yet<sup>31, 114-116</sup>. The current focus and priority for industry is around the internal diesel injector deposits (IDID) and the existing results are complicated, showing injector deposits cannot to be from a single origin<sup>31, 39</sup>. However these deposits are part of a wider issue involving the whole FIE<sup>39</sup>. It is strongly suspected that the increase in deposits observed recently are caused by one or more recent change(s)<sup>82</sup> including the reduction of sulfur, the introduction of biodiesel and the evolution of FIEs, particularly the increase in injection pressures.

The three main factors that need to be considered in the deposit formation within fuel injectors, are the fuel, the FIE and the legislation which has determined the changes of fuel and the FIE<sup>31, 39</sup>. However, at present, there has been "...no clear correlation between these incidences of severe fouling, and engine type, fuel injection equipment, fuel filter type or fuel supply source"<sup>52</sup>, although engines with high pressure fuel injection equipment, appear to be more susceptible to problems<sup>52</sup>.

Only IDIDs will be discussed in detail below, as they are the key focus of this project.

### 1.3.1 Location of IDIDs

There are two types of diesel injector deposits, “conventional” nozzle coking deposits (injector tip and fuel spray holes) and IDIDs<sup>35</sup>. IDIDs form internally, deep inside the fuel injector body, in areas such as inside the nozzle body, on the nozzle needle, on the piston and on the armature group, as shown in Figure 1-9<sup>35</sup>.

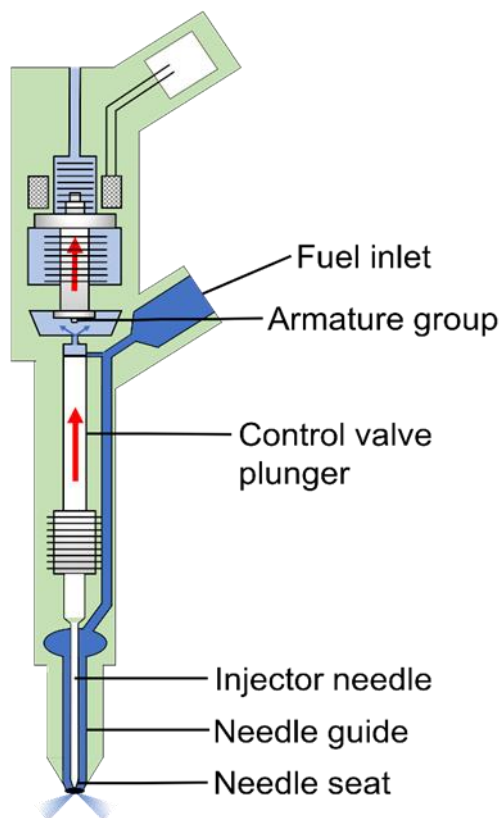


Figure 1-9 - Diagram showing locations of IDID formation within a fuel injector in a diesel engine

### 1.3.2 Composition of IDIDs

There are many types of IDIDs - those found in the field, lack proximity and similarity and are often very complex mixtures of organic and inorganic compounds<sup>117</sup>. As a result they have been characterised into types<sup>31</sup>, although there is still some uncertainty and variation within this<sup>118</sup>, but the key aspects are the same.

Chapter 1

Barker *et al.*<sup>119</sup> described five recognised types of IDID:

1. Carbonaceous: carbon based
2. Metal salt: *e.g.* sodium chloride
3. Aged fuel: associated with biodiesel
4. Metal carboxylate: metal “soaps”
5. Lacquers: thought to be carbonaceous precursors<sup>119</sup>

Berndt *et al.*<sup>28</sup> also categorised IDIDs into 5 different types and suggested possible causes/ deposit precursors, as shown in Figure 1-10<sup>28</sup>.

Lacey *et al.*<sup>120</sup> also investigated different types of deposits and their typical appearance and linked them with deposit precursors and their link to diesel fuel components as shown in Table 1-6.

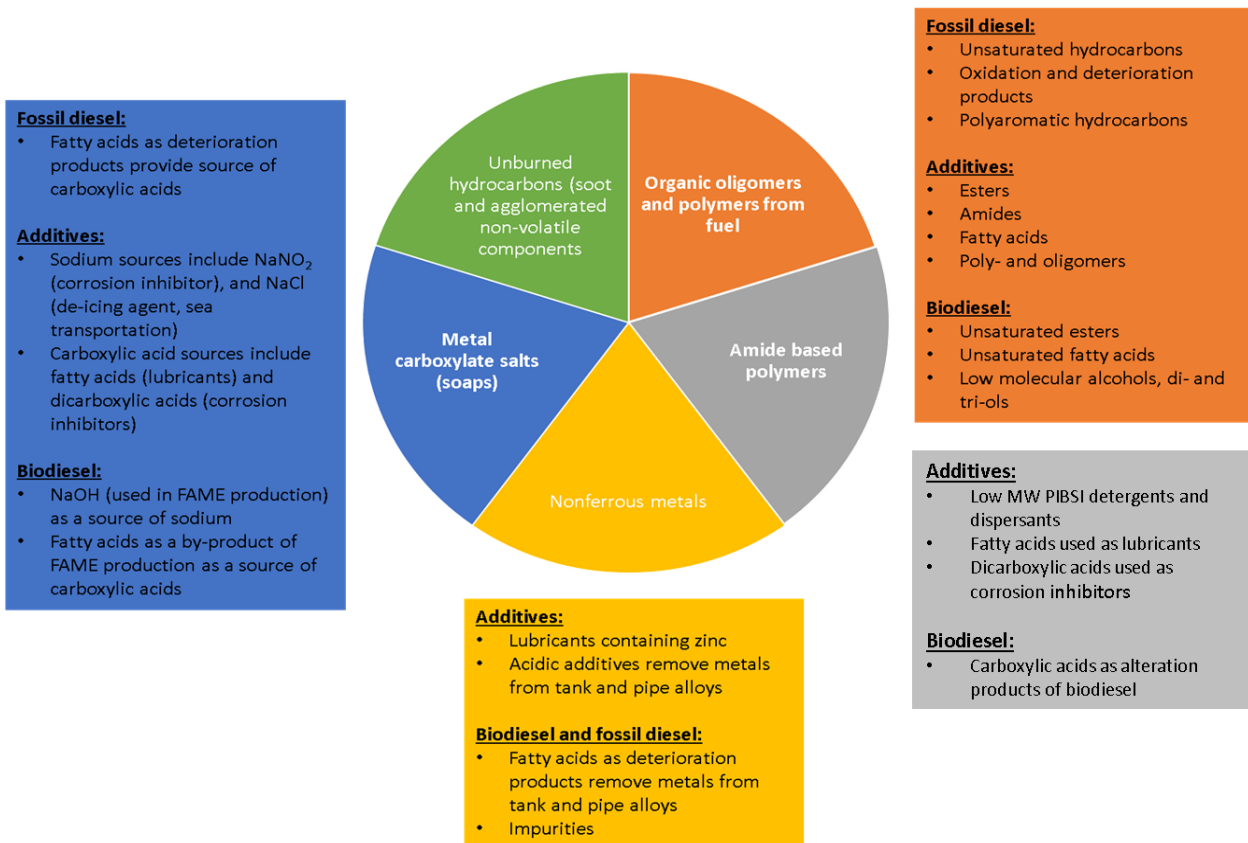
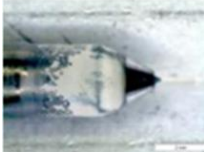
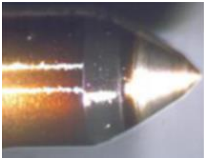
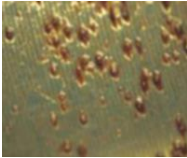



Figure 1-10 - IDID types and possible causes. Adapted from<sup>3</sup>

Table 1-6 The relationship between IDID types, precursors/root causes and fuel components.

Adapted from<sup>3</sup>

Fuel component	Deposit description	Root cause
Trace component	 <p>Metal carboxylate salt</p> <ul style="list-style-type: none"> <li>• Soapy deposit</li> <li>• Soluble in water</li> </ul>	Na>0.2 mg/kg Acidic material, especially alkenyl succinic acids
Additive	 <p>Polymeric amide</p> <ul style="list-style-type: none"> <li>• Very hard</li> <li>• Impervious to solvents</li> </ul>	Degradation of “non-commercial” low molecular weight PIBSI DCA or residual components from PIBSI manufacture
Hydrocarbon or FAME	 <p>Aged fuel</p> <ul style="list-style-type: none"> <li>• Soft, sticky deposits</li> <li>• Soluble in light hydrocarbons</li> </ul>	Poor stability, especially FAME Inappropriate storage High temperatures
Hydrocarbon base	 <p>Pyrolised fuel</p> <ul style="list-style-type: none"> <li>• Fine basic particulate <ul style="list-style-type: none"> <li>• May form coating</li> <li>• May plug filters</li> </ul> </li> </ul>	Poor hydrocarbon stability, high temperatures and cavitation

### 1.3.3 Occurrence and origin of IDIDs

It is not known definitively why IDIDs form, although a number of suggested mechanisms and speculated causes have been given in literature<sup>27, 39, 82, 118</sup>. From these, the explanation is known to be complicated and thought to be of more than one source<sup>39</sup>. The chemistry of a deposit depends upon presence of additive and trace fuel contaminants, the stability of the base fuel hydrocarbons and FAME in the fuel as well as operating conditions of the engine<sup>120</sup>. Overall causes will first be

touched upon then each type of IDID will be considered in turn, and possible root causes, mechanisms and deposit precursors discussed.

It was suggested by Barker *et al.*<sup>52</sup> that “historically deposits have been generated from a number of sources: Bio-contamination, both aerobic and non-aerobic, water contamination, lube oil adulteration, additives, dirt, metals in fuel, and biodiesel degradation”<sup>52</sup>. Many of the suggested causes can be attributed to one or more of the following; incorrect additivation, poor housekeeping, and intended adulteration<sup>30</sup>. Some of the many possible causes, most of which have been seen in field samples are shown in Figure 1-11<sup>85</sup>. However it is worth noting that not all have been reproduced in the laboratory and that they have been seen in combination, although may be reported in isolation due to analysis techniques used for layered samples<sup>31, 85</sup>.

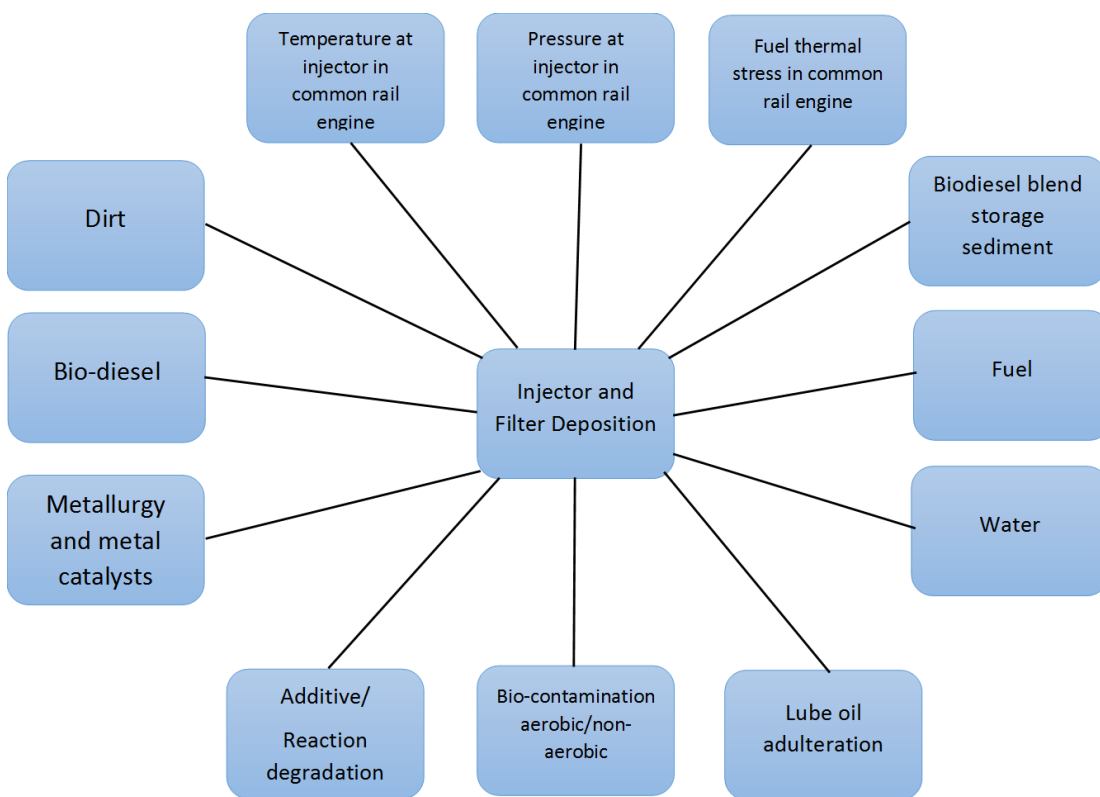


Figure 1-11 - Possible causes of fuel system deposits. Adapted from<sup>86</sup>

It is important to note that changes to engines, particularly the FIE, as a result of the increasingly stringent emission regulations, have culminated in entire fuel injection systems becoming increasingly sensitive and vulnerable to deposit formation. Some suggested causes of this susceptibility include FIEs designs now using a lower force to open fuel injection valves and operating at very high temperatures and pressures, as well as FIEs being manufactured with tighter tolerances between internal components<sup>27, 117</sup>.



Changes to diesel fuel have also occurred including reduced sulfur levels and inclusion of biodiesel, it is thought as a result the fuel has new reaction pathways and a reduced ability to solubilise deposits<sup>117, 120</sup>.

The reduction in sulfur levels, to <15 ppm in ULSD achieved through hydrotreating has resulted in a reduction in lubricity, polarity, solvency of the fuel and reduced corrosion protection due to a loss of O and N<sup>27, 31, 52, 82</sup> as well a reduced solubility for partly soluble components<sup>120</sup>. The effects of these changes must be considered when investigating the cause of recent deposit formation<sup>82</sup>.

There has been an increase in biodiesel levels in fuel, in order to meet the “Renewable Transport Fuel Obligations Order (2007) and (2018)” (RTFO)<sup>82-84</sup>. Biodiesel blends have been shown to have an increased propensity to cause fouling/deposit formation in both fuel injectors and fuel filters<sup>85</sup>. Bio-components are therefore thought to be a contributory factor, due to their less stable components, but not the sole cause in deposit formation<sup>85, 120</sup>. Deposit issues have been reported in ULSD as well as fuels containing biodiesel. Barker *et al.*<sup>52</sup> found that the cause of fouling was independent of whether a biodiesel blend or 100% ULSD was used<sup>52</sup>.

#### **1.3.3.1 Carbonaceous IDIDs**

These IDIDs are carbon based (as the name suggests) and derived from hydrocarbon base fuel<sup>120</sup>. They are thought to be formed as a result of the degradation of diesel fuels with low (thermal and oxidative) stability, this results in precipitation in regions of high pressure in the engine, including the FIE. These fine black surface deposits are more crystalline than soot particles found in the combustion chamber and are composed of a high proportion of carbon<sup>53</sup>. Extended periods of elevated temperature (collapse of cavitation bubbles) and pressure during FIE operation are thought to be the root cause<sup>53, 120</sup>.

#### **1.3.3.2 Metal salt IDIDs**

Metal salt IDIDs are alkali metal salts which are found to precipitate out of fuel onto injector parts<sup>27</sup>. Common examples include chlorides, carbonates and sulfates of both sodium and calcium<sup>27</sup> and there are two major routes by which these are thought to be present in the fuel, either from the refinery or through poor housekeeping of tanks<sup>27</sup>. For example, sodium chloride is used as a drying agent at refineries and is also present in seawater<sup>27, 53</sup>. These deposits highlight a need for greater consideration of cleaning and maintenance of tanks as well as fuel formulation<sup>27</sup>.

The alkali metal salts are thought to be dissolved in water clusters within the fuel, as not all water can be removed at the refinery. After some time, these metal salts will precipitate out of the fuel

onto the metal surface within the fuel injector forming a crystalline structure, this then provides a nucleation site for continual growth of the deposit as more metal salts are available. The deposit can keep growing and eventually cause moving parts to stick within the fuel injector<sup>27</sup>.

### 1.3.3.3 Aged fuel IDIDs

Aged fuel IDIDs are believed to be formed as a result of degradation of fuels containing FAMES (fuel instability). FAME quality has been found to diminish over time in both storage and use, due to the unsaturated bonds within FAMES breaking down to cause an excess of acids as well as polymers and precipitates forming<sup>120</sup>.

These deposits have a similar composition to the residue seen in Rancimat testing (EN 15751) – oxidative stability of FAME added to diesel and storage<sup>53</sup>.

A proposed mechanism for aged fuel IDIDs is that current engine improvements have caused multiple recirculation of fuel in resultant high temperatures and pressures. All of these changes provide a more reactive environment and intensify the oxidation and degradation of unstable fuel components such as FAMES (aging of the fuel), which contributes to the formation of insoluble degradation products<sup>85, 120-121</sup>

The current test procedures (*e.g.* oxidation stability test or Rancimat) used to determine long term storage stability of a fuel, are undertaken at raised temperatures but not increased pressures, meaning therefore they are not completely representative of the conditions the fuel will be exposed to in its lifetime<sup>82</sup>. These tests have been found to be favourable for predicating issues caused by high FAME fuels<sup>121</sup>. Urzędowska and Stępień<sup>121</sup> also state that FAME blended diesel fuel has an increased tendency to create deposits<sup>121</sup>. These deposits have highlighted the importance for the stability of biodiesel batches to be checked initially as well as just before use for blending, as the stability may be reduced after storage<sup>53</sup>.

### 1.3.3.4 Metal carboxylate IDIDs

Metal carboxylates IDIDs are thought to be the most commonly occurring IDID<sup>120</sup> and the one of most current interest<sup>27</sup>. They are commonly referred to as metal “soaps”<sup>119</sup> and are often water soluble and soft and opaque in appearance<sup>120</sup>.

They are the product of an acid-base reaction whereby an alkali metal base (or water) reacts with a carboxylic acid, as shown in Figure 1-12<sup>27</sup>. The alkali metal base is commonly sodium (75% reported cases), others metal include calcium, potassium, iron, tin and zinc<sup>53, 120</sup>. Potential sources of both alkali metal salts and carboxylic acids are abundant in diesels. Sodium hydroxide used in the manufacture of FAME is common<sup>53, 120</sup>. Sources of carboxylic acids include alkenyl succinic acids in corrosion inhibitors<sup>30-31, 34, 122</sup> and fatty acids from lubricity additives as well as production of FAMES<sup>53, 120</sup>.

These deposits can be formed anytime throughout fuel manufacture, storage and delivery,

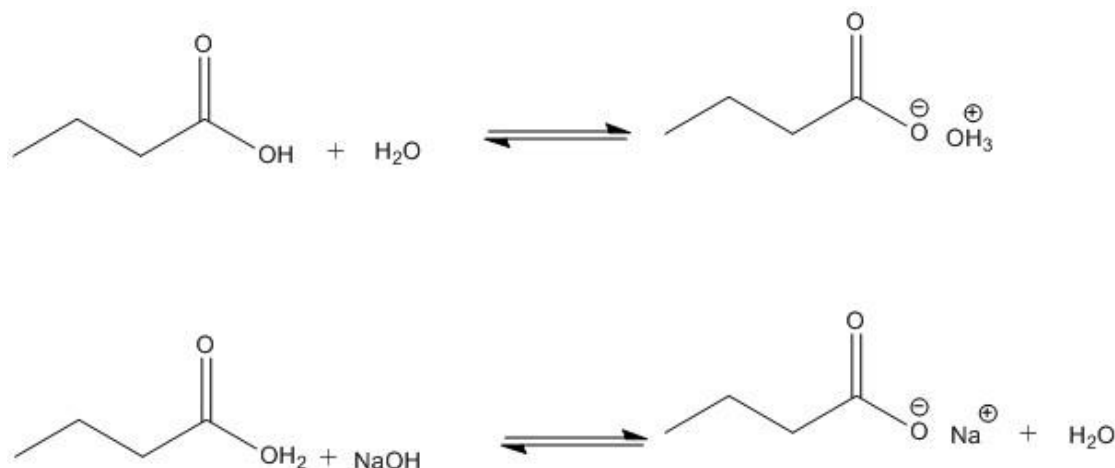


Figure 1-12 -Chemical reaction of a carboxylic acid with water and an alkali metal base

however they only form in specific locations where pressure release and high temperatures are present, and very rarely in areas of low pressure.

The mechanisms of formation and deposition of metal carboxylate IDIDs have been highly investigated and well documented due to the interest around them. Although no actual experimental evidence has been produced, it has been proposed by Lacey *et al.*<sup>120</sup> and Trobaugh *et al.*<sup>27</sup> that after the initial formation through the acid-base reaction, the metal carboxylate salts assemble an inverse micelle (Figure 1-14)<sup>27</sup>, whereby the hydrophilic heads are in the centre of the micelle and the hydrophobic tails protrude from the micelle core<sup>27, 120</sup>. (As an aside, excess water in fuel is not fully solvated and therefore is found in clusters. Hydrocarbons within the fuel are induced to rearrange by the dipole moment of water and as a result the water clusters are surrounded by polar compounds within the fuel in an attempt to solvate and dissolve the water<sup>27</sup>.) The formation of the inverse micelle is due to the hydrophilic effect whereby polar head groups move together to achieve a more energetically favoured environment around the water molecules. Micelles are flexible and can grow and shrink depending upon the number of monomers (metal carboxylates) present. Their stability is affected by temperature and pressure - as heat energy is converted to

Chapter 1

vibrational energy (also vibrations from rough surfaces within injector), this causes metal carboxylates to move and vibrate more and eventually break apart the inverse micelle. The metal carboxylates are insoluble and unstable in the fuel so precipitate on to metal surfaces causing IDIDs<sup>27</sup>. It is important to note the deposit is physically stuck to the metal, although no reactive metallic layer exists<sup>120</sup>. This proposed mechanism is summarised in Figure 1-13<sup>120</sup>.

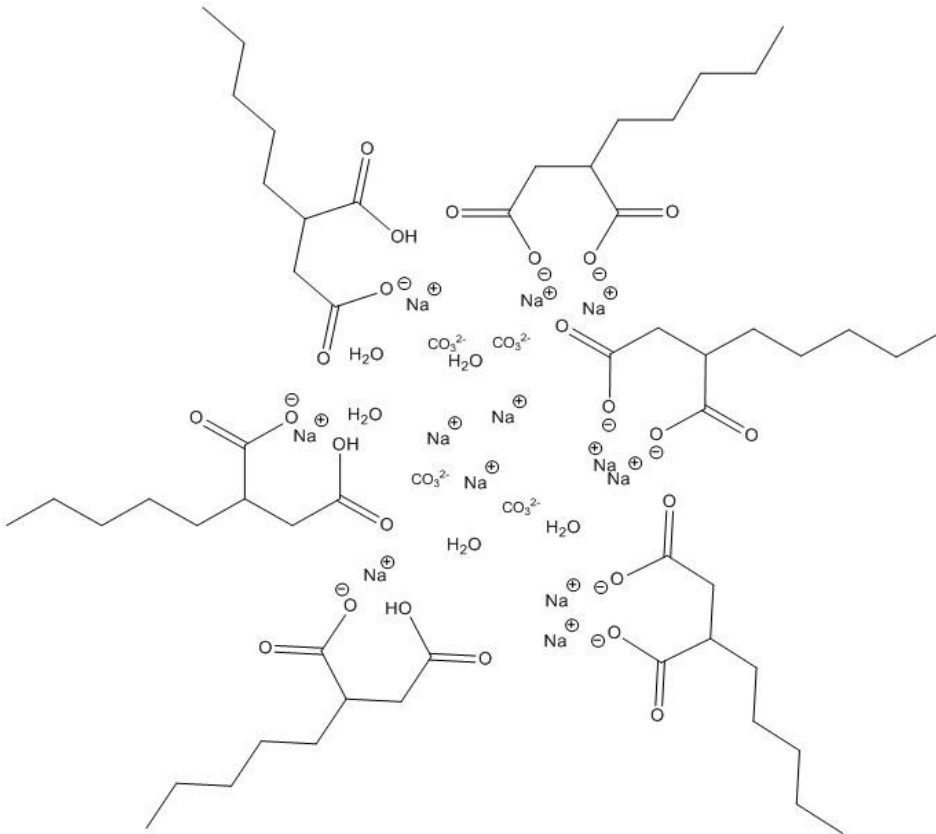


Figure 1-14 Inverse micelle formation of metal carboxylate

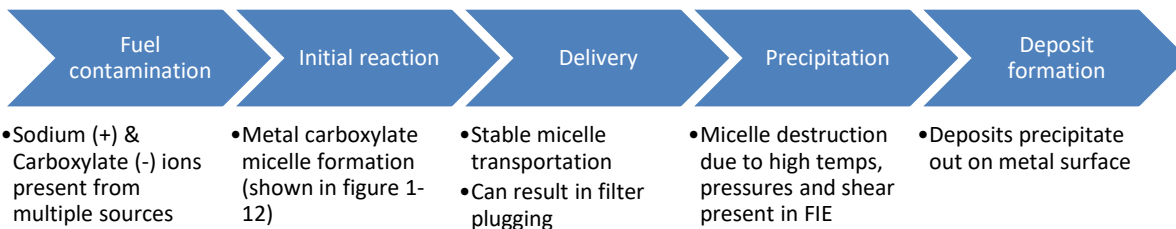


Figure 1-13 – schematic diagram of the proposed mechanism of metal carboxylate salts. Adapted from<sup>120</sup>

### 1.3.3.5 Polymeric amide IDIDs (Lacquers)

Polymeric amide IDIDs are believed to be the second most common IDIDs, after metal carboxylates<sup>120</sup>, and are thought to be precursors to carbonaceous IDIDs<sup>119</sup>. They are observed as a hard, brown, translucent lacquer and when viewed in the field are often found in combination with sodium carboxylate salts<sup>120</sup> or found in layers with carbonaceous IDIDs and metal ion contaminants<sup>38</sup>. Possible amide sources include biofuels and lubricant oils.

Deposit control additives (DCAs) are often added to diesel fuel to prevent deposit build up. The most effective and favoured DCA was polyisobutylenesuccinimide (PIBSI), however PIBSI covers a wide range of chemical structures<sup>123</sup>, so only certain designs and manufacturing conditions produce PIBSIs suitable for deposit removal<sup>38</sup>. Molecular weights for PIBSIs range from 500 to 10,000 Daltons, but more commonly are in the 1,000 to 3,000 Da range<sup>124</sup>. Low molecular weight PIBSIs are known to be a by-product of the synthesis of PIBSIs so typically only polyisobutylenes (PIBs) over 1,000 Da are used in the synthesis of PIBSIs for deposit control additives<sup>123</sup>.

It has been suggested that low molecular weight PIBSIs are precursors to polymeric amide IDIDs(lacquers), however not all engine testing has supported laboratory testing in these claims<sup>53</sup>. It is proposed that the molecular weight of the PIB backbone can affect its solubility in diesel fuel. The hydrophilic PIB back bone, which comes in a variety of molecular weights<sup>53</sup>, is used to give the polar additive stability while the polar head of the additive can attach to the deposit<sup>120</sup>. Lower molecular weight PIBSIs are thought to be less soluble in diesel fuel due to a short PIB back bone, therefore dropping out and forming deposits<sup>38, 120</sup>. As a result of this lower molecular weight PIBSIs are not normally identified as high quality DCAs<sup>38, 120</sup>

Lacey *et al.*<sup>120</sup> found that a majority of normal molecular weight distributed PIBSIs were not found to cause deposits<sup>31</sup> A study by Barker *et al.*<sup>38</sup> showed that (non-commercial) low molecular weight PIBSI caused deposits which resulted in injector sticking during an engine test<sup>38</sup>. "Quality and molecular weight have been shown to be important factors in determining whether a PIBSI will form amide lacquers."<sup>123</sup>.

### 1.3.4 Problems caused by IDID formation

IDIDs are problematic, as they are known to cause sticking of internal injector working parts such as the needle, corrosion of internal components and slower response of fuel injector; this can cause loss of control of fuel injection(including volume of fuel injected, timing of injection and quality of injection) culminating in injector failure. Consequently, engine damage and abnormal engine function can occur, manifesting as misfiring, stalling, rough idling, increase in smoke, higher

emissions, reduced fuel economy, no cold start ability, poor drivability, and/or a severe lack/loss of power<sup>30-31, 35, 85, 117-118</sup>

### 1.3.5 Suggested ways to stop IDID/deposit formation

There are a number of different techniques used to stop or at least reduce deposit formation including coating metal components of FIE to either reduce the propensity for deposit build up or to reduce the wear and tear of parts<sup>41</sup>. Many different materials have been used in coating for both these purposes including a Diamond Like Carbon (DLC), carbides, metal nitrides and oxides<sup>41</sup>.

Some recently suggested solutions to IDID formation include the use of ionic liquids for extraction of trace metals to stop IDIDs caused by trace metals such as sodium<sup>125</sup> and patents have also been issued to try and combat IDID formation<sup>126-127</sup> including the use of 2-ethylhexyl nitrate in combination with one or more detergent additives<sup>128</sup>.

Lacey *et al.*<sup>120</sup> also outlined suggestions for best practice within industry to prevent IDID formation such as ensuring levels of sodium, particularly sodium hydroxide, are as low as possible (0.1 mg/kg). as well as manufacturing fuels which are fit for purpose with sufficient stability without the use of excessive levels of additives, especially alkenyl succinic acids and others that are known deposit precursors. Additionally, maintenance and cleanliness during fuel handling and storage need to be to a high level and include, drainage of water in tank bottoms, ensuring fuels are not exposed to copper, zinc or lead as well as limiting entry of oxygen into the fuel, especially those containing FAMEs. The contaminants from FAME production should also be reduced to limit carryover into fuel<sup>120</sup>. Finally the concentration of LMW PIBSIs should be minimised where possible as they are also known to be a deposit precursor for polymeric amide IDIDs<sup>38, 120</sup>.

### 1.3.6 Challenges of characterisation

From literature it can be seen that one of the main challenges of this research is being able to match up the problems seen in field with the corresponding proposed mechanisms<sup>85</sup>. This can only be achieved with accurate characterisation of both the fuels leading to the deposits and the deposits themselves<sup>85</sup>. Another challenge is finding analytical techniques capable of differentiating between deposits themselves and material that has been attracted to the deposit<sup>41</sup>. This is due to the deposits existing in the field in complex matrices with other materials also present<sup>52</sup>. A common example of this is that deposit control additives in fuel are themselves attracted to the deposits<sup>41</sup>. Removal of deposits from FIE parts is also problematic, particularly when there is only a limited sample or the deposit is insoluble in standard solvents<sup>41</sup>. Physical removal using an implement such as a scraper can also prove difficult, as parts of the implement used or parts of the injector itself

may get removed during the process and become part of the deposit sample which is analysed, giving incorrect/false or inaccurate results<sup>41</sup>. However, deposit removal is a requirement for many analytical techniques used to investigate deposit formation. This also means analysis is often limited by the quantity of deposit obtained<sup>41</sup>. Another problem which can limit characterisation of the FIE deposits is the transportation of deposit around different components in the FIE through much handling during the collection and analysis process<sup>41</sup>. To overcome this, assumptions have to be made as to whether deposits seen on sample are likely to be removed by high pressure and whether they are the cause of operational problems<sup>41</sup>.

Another challenge is ensuring both soluble and insoluble components of the deposit sample are separated and characterised.

The deposits need to be fully understood and characterised, in order for industry test procedures to produce deposits representative of those in the field. This will then allow for the assessment of the propensity of a fuel to form deposits and to determine if a fuel is fit for purpose<sup>40</sup>.

Another challenge in the characterisation of all FIE deposits is the number of variables, including needle type, fuel supply source and fuel housekeeping, which are uncontrolled due to their origins in the field<sup>40</sup>. As a result the amount and composition of deposits from the field are variable, meaning it is hard to make comparisons<sup>40</sup>.

Contamination of samples can also occur and give erroneous results. For example, phthalate peaks have been seen in previous samples but is known to be due to contamination from the plastic bag in which the injector was transported<sup>30</sup>.

Analysis of fuels (both those known to be deposit forming and those not) has also been undertaken, however at present the accepted industry accelerated ageing test (Rancimat – EN 15751) does not correlate with problem fuel found in the field<sup>82</sup>. This therefore means that other, new test methods for this are required in order to accurately study fuels and possibly determine those which are problematic for deposit formation<sup>82</sup>. Additionally chemical characterisation of problem fuels is not straightforward as “dramatic changes in appearance may be accompanied by only subtle changes in composition”<sup>82</sup>.

### **1.3.7 IDID test methods**

Research has expanded over the last ten years due to increased field reports of deposit-associated operational issues<sup>119</sup>.

## Chapter 1

Standard test method/procedures were developed to assess the propensity of a fuel to form deposits on the injector nozzles in the FIE which were to be used in industry testing<sup>30, 40</sup>. In the early 1980s, many companies, individually, began developing test methods which could reproduce deposit problems seen in the field<sup>30</sup>. The first internationally recognised test method was CEC PF26 (used XUD-9 engines) procedure for IDI (common on passenger cars at the time) diesel engine nozzle coking assessment and it was shown to correlate well with field reports<sup>30, 40</sup>. However this method was shown to be unreliable following round robin testing in 1997, so in 1998 a replacement method was proposed by Texaco<sup>129</sup>. This method used an updated engine, XUD-9 A/L and was a ten hour cyclic test rather than the six hour cyclic test used previously<sup>30</sup>. The other key difference in the replacement procedure was that the dynamic injection timing was “adjustable according to a well-defined set of criteria”<sup>30</sup> meaning a specified level of coking will be obtained for each calibration fuel, while the automatic timing was locked<sup>30</sup>. This enabled the engine to be adjusted in line with fuel changes and this method to remain as the industry standard procedure<sup>30</sup>.

Many methods were proposed for heavy duty diesel engine DI injector deposit formation, however the Cummins L10 method became the standard method even though some of those proposed were cheaper and more rapid<sup>30, 40</sup>. These were the only two universally accepted methods until 2008, although the engine technology used in them is now deemed unsuitable for current diesel engines<sup>30, 40</sup>. In response to this, a method for DI (common rail)(DW10) diesel engines nozzle coking test, CEC F-98-08, was approved in 2008, this test relies on doping a reference fuel with zinc<sup>30, 40</sup>. At present there are two CEC tests under development for metal carboxylates IDIDs<sup>28, 130</sup> and for the influence of non-commercial low molecular weight PIBSIs as additives and their propensity to form deposits<sup>123</sup>.

### 1.3.8 Current analytical techniques found in literature for the analysis of IDIDs/deposits

The analytical techniques considered below have been used to investigate all types of diesel fuel system deposits, with a focus particularly on IDIDs.

A variety of mass spectrometry techniques have been used in the analysis of IDIDs, including DART-MS<sup>29</sup>, FT-ICR MS<sup>29, 85</sup>, GC-MS<sup>31, 85</sup> and ESI-MS<sup>85</sup>. Barker *et al.*<sup>39</sup> were the first to use time of flight secondary ion mass spectrometry (ToF-SIMS) for the analysis of FIE deposits<sup>39</sup>. It enabled 3D characterisation of both the surface and inner layers of a deposit, which enabled a better and greater understanding of the structure of the deposits<sup>39</sup>. Lau *et al.*<sup>32</sup> used a similar technique, thermodesorption resonance-enhanced photon ionisation (REMPI)-ToF-MS, to determine the composition of aromatic species in injector ring deposits in common rail fuel injectors, although it can also be used to measure non-aromatic species<sup>32</sup>. Both ToF methods allow analysis of deposits



*in situ* on the injector which is advantageous<sup>32, 39</sup>. A multitude of examples using ToF-SIMS for deposits can also be found in the literature<sup>29, 33, 38</sup>.

Multiple spectroscopy methods are also used including Infrared spectroscopy (IR)<sup>31, 38</sup> and Fourier transform infrared spectroscopy (FTIR)<sup>27, 29</sup>. Schwab *et al.*<sup>34</sup> and Quigley *et al.*<sup>35</sup> used FTIR to analyse IDIDs on problematic injectors, this resulted in detection of sodium salts of low molecular weight alkenyl succinic acids (possibly from corrosion inhibitors) suggesting metal carboxylate salts<sup>34-35</sup>. Raman spectroscopy has been used to analyse FIE deposits in order to produce a “map of ordered and disordered carbonaceous deposits, illustrating some variation across the injector”<sup>36</sup>. ICP-AES was used by Barker *et al.*<sup>85</sup> to determine and quantify multiple trace metal data for both fuels and fuel injector deposit samples from engines in the field in North America which reported operational problems<sup>85</sup>.

Numerous microscopy techniques have been used to analyse FIE deposits in order to gain a better understanding of their structure.

Barker *et al.*<sup>41</sup> used transmission electron microscopy (TEM) to analyse a number of geographically different fuel injector deposits and ascertain the carbon types which were present<sup>41</sup>.

Scanning electron microscopy (SEM) has been used frequently in various forms<sup>27, 29, 31, 38-39</sup>. Barker *et al.*<sup>38</sup> described the use of SEM with energy dispersive x-ray analysis (SEM/EDAX) to identify only metals in FIE deposits. The use of both SEM with back scattered electrons (SEM/BSE) and focused ion-beam SEM (FIB-SEM) in the analysis of fuel injector deposits were reported by Barker *et al.*<sup>36</sup>. SEM/BSE can be used to contrast and identify areas of differing densities and chemical compositions<sup>36</sup>. Heavier elements are known to backscatter electrons more than lighter elements meaning that heavier elements appear brighter than light elements<sup>36</sup>. FIB-SEM works by cutting a series of trenches out of the sample at varying depths, using focussed ion-beam nano machining, that can then be manipulated, while leaving a central section untouched<sup>36</sup>. FIB-SEM allows assessment of structure at differing depths of a deposit, rather than just the top surface which is presented allowing much more detailed structural information to be obtained<sup>36</sup>.

Barker *et al.*<sup>36</sup> also reported the use of atomic force microscopy (AFM) to analyse FIE deposits<sup>36</sup>. AFM allowed the mapping of the FIE deposit surface and measurement of specific features which can then be depicted to scale on the map<sup>36</sup>. It also allowed chemical analysis of the surface to be undertaken. It was complementary to ToF-SIMS and Raman spectroscopy undertaken on the same samples<sup>36</sup>.

## Chapter 1

Other techniques have also been employed to obtain further information to build an overall picture of the deposits, these include profilometry<sup>29</sup>, solid-state NMR spectroscopy<sup>22</sup>, temperature programmed oxidation<sup>41</sup> and hydrolysis<sup>38, 40</sup>.

The use of the Jet Fuel Thermal Oxidation Tester (JFTOT), which is commonly used to test oxidation stability of aviation fuel (ASTM D-341), is becoming increasingly common as a technique to investigate the formation of IDIDs. It enables simulation of diesel fuel passing through an injector, as test fuel is passed over a heated metal rod, which allows for assessment of the fuel for deposit formation and if necessary further characterisation to be undertaken<sup>28-29, 37, 123</sup>.(see chapter 5 for further detail).





## Chapter 2 Instrumentation

This chapter outlines the fundamental principles for the techniques used in this research project. Chromatography and mass spectrometry (MS) have been previously used for the analysis of petrochemical fuels and engine deposits. Both gas chromatography (GC) and supercritical fluid chromatography (SFC) were employed in this project for the separation of components within diesel fuels. The chromatographic techniques were coupled to a MS, whereby a variety of ionisation techniques and mass analysers were implemented to detect and identify the components within the fuels.

### 2.1 Chromatography

Chromatography is a technique that affords the separation of complex mixtures allowing for the identification and quantitation of individual components within a sample. It is defined as “a physical method of separation in which the components to be separated are distributed between two phases, one of which is stationary (stationary phase) while the other (the mobile phase) moves in a definite direction”<sup>131</sup>. Chromatography was initially described at the start of the 20<sup>th</sup> century by William Ramsey<sup>132</sup> separating gases on absorbents and then closely after by Mikhail Tswett<sup>133</sup> separating chlorophylls, however Tswett was believed to be the first to outline the process and use the term chromatography (derived from the Greek to literally mean colour writing), so is often considered as the “father of chromatography”<sup>134</sup>.

Paper chromatography was later introduced and followed by thin layer chromatography (TLC). A TLC plate consists of a glass plate packed with thin layer of powdered silica, to which sample is spotted at the bottom. The TLC plate is then placed into solvent sample –end down and left for solvent to elute up the plate separating the analytes within the sample mixture<sup>135</sup>.

In chromatography, analytes are introduced into the mobile phase, which can consist of a liquid (liquid chromatography (LC)), gas (gas chromatography (GC)) or supercritical fluid (supercritical fluid chromatography (SFC)) and flows through a column which contains the stationary phase. The analytes then become distributed within both phases and interact with the stationary phase. Each analyte has a different affinity for the stationary phase so each will be retained on/ in contact with the column for a different amount of time therefore separating the individual analytes. The greater an analytes affinity for the column the longer it will be retained on the column therefore resulting in a longer retention time. Martin and Synge<sup>136</sup> also found that separations can also be

dependent on the differences in the partition-between two liquid phases of the substances to be separated.

Many stationary phases are manufactured, they can consist of gel, liquid, solid or liquid coated solid support particles<sup>131</sup> and separation can be based on a number of parameters including polarity, boiling point, (size, ionic charge, and binding affinity).

## 2.2 Chromatographic parameters

There are some important parameters which play a major role in the separation of analytes *via* chromatography and are crucial to obtaining symmetrical, narrow peaks with baseline separation.

The first of these is a retention measurement known as the partition ratio (sometimes known as capacity factor) and is calculated using Equation 2.1<sup>48</sup>. Partition ratio is denoted as  $k$  and is a “ratio proportional to the time the compounds spends in the stationary phase relative to the time spent in the mobile phase”<sup>48</sup>. It can be used to obtain a unit less measure of the retention of an individual analytes on the stationary phase and allows direct comparison regardless of other parameters. Retention increases as  $k$  increases, therefore if  $k = 0$ , the analyte is non-retained. A low  $k$  value implies insufficient analyte retention on the column meaning chromatographic separation will not take place, whereas a high  $k$  value implies sufficient analyte retention on the column for chromatographic separation to take place, although if  $k$  is too high, analysis times can be unfavourably long.

$$k = \frac{t_R - t_m}{t_m}$$

**Where:**

$t_R$  = solute retention time

$t_m$  = retention time of non-retained peak

Equation 2.1 – Partition ratio ( $k$ )

After determining the partition ratio of analytes, the separation factor (denoted as  $\alpha$ ) which is a measure of time distance apart between two peaks, can be calculated and evaluated using Equation 2.2. It is always greater than or equal to 1, when equal to 1 retention times are identical so co-elution is occurring<sup>48</sup>.

$$\alpha = \frac{k_2}{k_1}$$

**Where:**  $k_2$  = capacity factor of peak 2

$k_1$  = capacity factor of peak 1

Equation 2.2 - Separation factor ( $\alpha$ )

Resolution (denoted as  $R$ ) of chromatographic peaks is also a measure of peak separation of two analytes at given parameters (mobile phase and chromatographic column) however it also takes peak width into consideration. A major aim of chromatography is to achieve baseline resolved peaks and then separation will also occur as a result. Resolution can be calculated using Equation 2.3. If resolution is calculated to be  $>1.5$  then the two peaks are baseline resolved, no space/baseline is present between the two peaks so minimal separation has occurred. If  $R < 1.5$  then peaks will have some overlap, therefore only partially resolved. Resolution should always be taken into account when evaluating peak separation using  $\alpha$ <sup>48</sup>.

$$R = 1.18 \left( \frac{t_{R2} - t_{R1}}{W_{h1} + W_{h2}} \right)$$

**Where:**  $t_{R1}$  = retention time of peak 1

$t_{R2}$  = retention time of peak 2

$W_{h1}$  = peak width at half height of peak 1 (same time units as  $t_R$ )

$W_{h2}$  = peak width at half height of peak 2 (same time units as  $t_R$ )

Equation 2.3 – Resolution ( $R$ )

Other equations can also be used to calculate  $R$ , however Equation 2.3 is commonly used as it is found to be more convenient and practical because measuring peak width at half height does not take into account any problems associated with peak shape such as fronting and tailing<sup>137</sup>.

Efficiency of a particular column is defined as “relationship between a peak’s retention time and its width”<sup>48</sup>. It can be measured using resolution or by calculating theoretical plates<sup>48</sup>.

The theoretical plate model assumes the column is made up of many separate layers called theoretical plates (Figure 2-1). At each theoretical plate equilibrium of the sample between the

## Chapter 2

stationary and mobile phase can occur. Transfer of sample analytes from plate to plate, through the column, takes place *via* the equilibrated mobile phase.

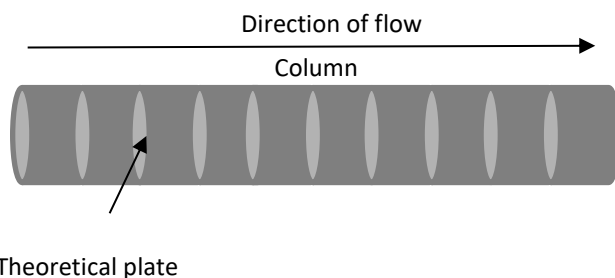


Figure 2-1 - Schematic showing the theoretical plate model in a chromatographic column

There are two equations which can be used to calculate efficiency using theoretical plates; number of theoretical plates ( $N$ )(Equation 2.4) and height equivalent to a theoretical plate ( $H$ , HETP) ( Equation 2.5)<sup>48, 134</sup>.

$$N = 5.545 \left( \frac{t_R}{W_h} \right)^2$$

**Where:**  $t_R$ =retention time of peak

$W_h$ = peak width at half height of peak (same time units as  $t_R$ )

Equation 2.4 - Number of theoretical plates ( $N$ )

$$HETP (H) = \frac{L}{N}$$

**Where:**  $L$ = column length (mm)

$N$ = number of theoretical plates

Equation 2.5 - Height equivalent to a theoretical plate ( $H$ , HETP)

The number of theoretical plates ( $N$ ) can be quoted for a whole column or per metre to allow for easier comparison between columns of different lengths. The higher the number of theoretical plates, the more equilibrations are possible, therefore narrower peaks are produced and baseline resolved separation results<sup>48, 137</sup>.

The smaller the HETP value, the more efficient the column. This is due to the fact that the shorter the theoretical plate, the more theoretical plates able to fit in a specified length of column<sup>48, 138</sup>.



A common phenomenon known as band broadening can be observed during chromatographic separation and is known to reduce separation efficiency. In order to further aid understanding of this phenomenon, J. J. van Deemter<sup>139</sup> developed an equation for packed columns which relates the linear velocity of the mobile phase (cm/s) to HETP. This equation, known as the van Deemter equation, recognises three contributing effects to band broadening is shown below in Equation 2.6<sup>48, 134, 140</sup>.

$$HETP = A + \frac{B}{\bar{u}} + C\bar{u}$$

**Where:** A= eddy diffusion

B= longitudinal molecular diffusion

C= mass transfer

$\bar{u}$ = average linear velocity

Equation 2.6 - Van Deemter equation

The van Deemter equation can also be represented in a graphical form as seen in Figure 2-2<sup>48, 140-141</sup>.

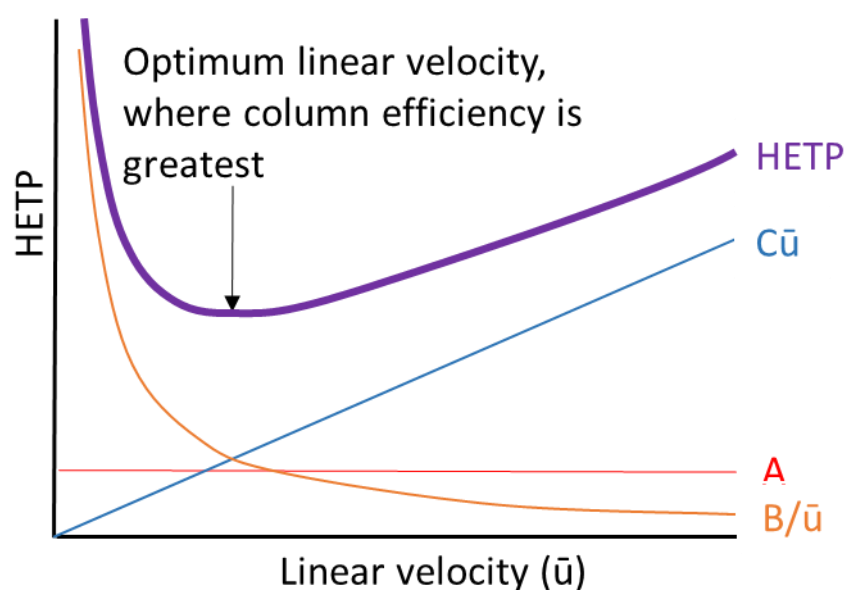


Figure 2-2 - A van Deemter plot showing all three terms and their relationship with the optimum linear velocity. Adapted from<sup>48, 140-141</sup>

The A term within the van Deemter equation is eddy diffusion and relates to the many available pathways which an individual analyte can take as it moves through the column. The particle size and shape of the column packing materials can vary, resulting in different pathways and different

## Chapter 2

distances through the column for the analyte, therefore separating the initial compact band of analytes which enters the column. To minimise the effect of eddy diffusion, columns with evenly distributed homogenous small diameter packing material should be used. The A term is not relevant for open tubular/capillary columns as they do not have packing, so Golay<sup>142</sup> determined a new equation for these types of columns taking this into account<sup>48, 141</sup>.

Longitudinal molecular diffusion is the B term, this relates to the diffusion of the initial high concentration, compact band of analytes which enters the column and is due to the concentration gradients at the edges of the band of analytes, which causes the band to spread out. To minimise the effect of longitudinal molecular diffusion, ensure there is no excess volumes with the system such as in tubing or internal diameter of column and running at higher linear velocities<sup>141</sup>.

Mass transfer is the C term, this relates to the movement of analytes in and out of the pores within the porous stationary phase, and the extent to which they enter the pores. Porous stationary phase is used to provide a greater surface area for interactions between the analyte and the stationary phase to take place. A low analyte concentration in stagnant mobile phase is found within each pore into which analytes can diffuse, some more deeply than others, *e.g.* some do not enter, some slightly enter and some that go deep into the pore. This cause a difference in retention of the same analyte which results in band broadening. To reduce the effect of mass transfer, low linear velocities, smaller diameter packing material and increasing column temperature should be used<sup>48, 141</sup>.

### 2.3 Gas chromatography (GC)

Gas chromatography (GC) is a technique used to separate a mixture of volatile compounds into individual components. The mobile phase and analytes within GC are in a gaseous phase whereas the stationary phase within the GC column can be either liquid or solid<sup>134</sup>. GC was pioneered by Martin and James<sup>143</sup> in 1952 and has continually developed into the modern technique we see today<sup>134</sup>. Samples are vaporised by heating up to ~350-400 °C, meaning they therefore must be volatile, thermally stable and not decompose at high temperatures. As a result, it is estimated that only ~10% of all compounds can be analysed by GC<sup>48</sup>.

Typically, a GC system comprises of an inert carrier gas which is controlled by a two stage regulator and flow control valve, a heated sample inlet, a GC column within a temperature controlled oven, and a detector and data system (Figure 2-3)<sup>48</sup>.

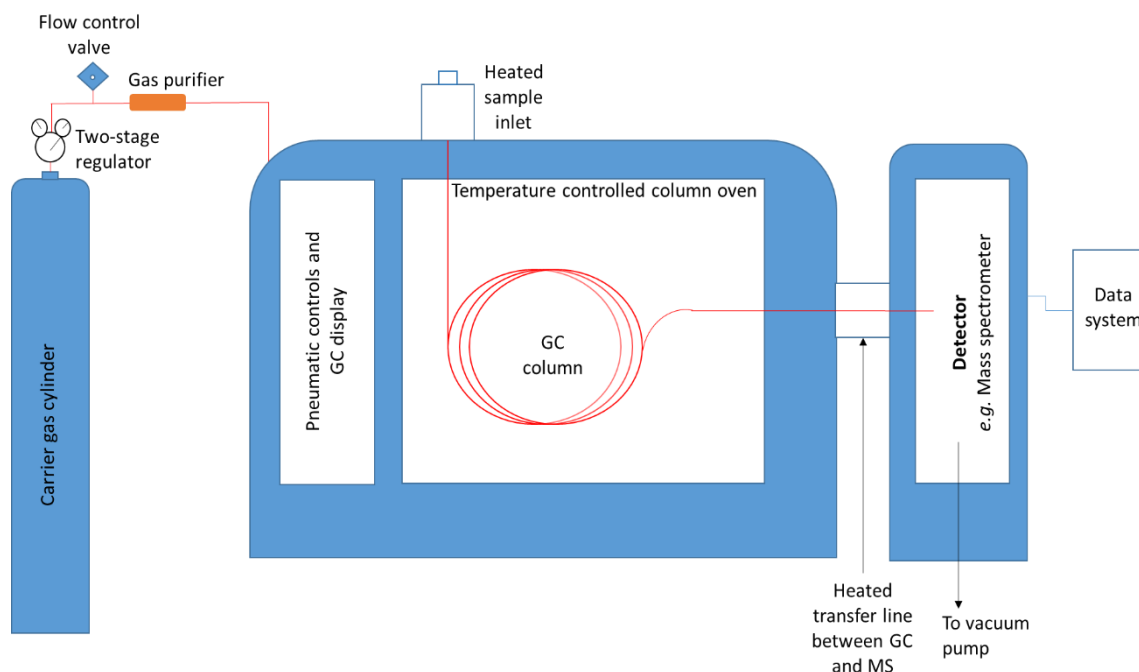


Figure 2-3 - Schematic diagram of a GC. Adapted from<sup>48</sup>

Sample introduction is most commonly undertaken using a syringe, such as with an autosampler. The liquid sample is injected into the heated sample inlet (usually heated to  $\sim 150\text{-}250\text{ }^{\circ}\text{C}$ ), as this occurs, the sample is heated and the volatile sample solutes and solvent are vaporised.

The vaporised components then mix with the inert carrier gas, most commonly nitrogen for stand-alone GC and helium for GC-MS and the sample within the carried gas is transferred to the column<sup>48</sup>. At this point split or splitless injection can occur.

The carrier gas with sample flows into the injector through the column to the detector and its flow is controlled by the flow controller. The carrier gas, acts as the mobile phase, carrying/assisting the vaporised components movement through the column<sup>48</sup>.

For GC, the stationary phases is the film coating within the column and is kept with in a temperature controlled oven which maintains its temperature. GC columns vary in compositions depending on the separation required. The vaporised components in the carrier gas, travel through the column at a rate (retention time) determined by their affinity for the stationary phase as well as the column temperature and composition, separating the individual analytes.

Temperature ramp rate can be altered at this point in order to manipulate the retention time/separation of your analytes. Each component moves through/is retained by the column at a different rate. As each component elutes/leaves the column it then enters the detector and an electrical signal is generated. The magnitude and time of the electrical signal is recorded by the

## Chapter 2

data system to produce a chromatogram. The larger the magnitude of signal, the more of that component present, and therefore the larger the peak area of that component on the chromatogram<sup>48</sup>.

Sample introduction is commonly *via* a split injector, which can operate in two modes; split and splitless. Split mode dilutes the sample with carrier gas, therefore allowing for the manipulation of the amount of sample entering the column, to prevent the column overloading from a high concentration sample. A split ratio is used to quantify the level of splitting and is defined as “the volume of carrier gas entering the column versus the volume leaving *via* the split line” and the column flow is normalized to one when quoting split ratio *e.g.* 1:50, 1 part of sample enters the column for every 50 parts that are discarded. However this can vary slightly from the expected value as it is dependent on many other parameters some of which are out of the control of the operator. So the lower the split ratio, the more sample that enters the column for analysis. This technique reduces the need for sample dilution prior to analysis. Splitless mode is used when analytes are present at trace levels and maximum sensitivity is required<sup>48, 140</sup>.

Temperature programs during acquisitions allows improved separation in number of ways including improved peak shapes, detection limits particularly for late eluting peaks, quicker analysis times and better separation over a vast boiling point range. The temperature of the GC oven and therefore the column temperature, can be programmed using ramp rates and holds. Ramp rate (RR) is “the rate at which the temperature increases during the thermal gradient”<sup>134</sup> and is stated as degrees Celsius per minute *e.g.* 10 °C /min. the temperature of a column can be held at a specific temperature for a specific time and this is often used at the end of an analysis at a high temperature to clean the column, this ensures that the column is regenerated every time used<sup>134, 144</sup>.

The mobile phase, or carrier gas, used in GC must be a chemically inert gas has two functions; to carry the sample through the column (but not interact chemically) and to ensure there is a suitable matrix for the detector to take sample components measurements. The choice of carrier gas used is down to which type of detector is to be used and the most commonly used carrier gases are nitrogen, helium, and hydrogen. The quality of gas used is also very important as low quality gases contain impurities that can chemically attack and damage the stationary phase, so high purity gases are used in combination with gas purifiers. The gas purifiers are in place to reduce gas contamination from hydrocarbons which affects chromatography, and oxygen and moisture which can shorten the column lifetime<sup>134, 145</sup>.

In GC, the stationary phase is within the column and there is a huge variety of GC columns produced, however some column types are more commonly used. There are two main types of columns used in GC; packed and capillary. However capillary columns are estimated to be used in >80% of applications today<sup>146</sup>, so only these will be discussed in detail.

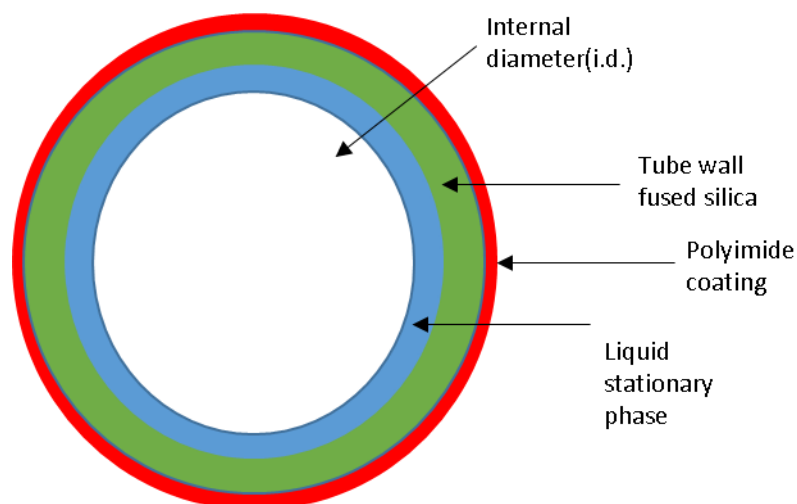


Figure 2-4 - Cross section of fused silica open tubular (FSOT) column adapted from<sup>48</sup>

Capillary columns, as shown in Figure 2-4<sup>48</sup>, consist of fused silica tubing, coated on the outside by most commonly polyimide, which provides physical strength, and the inside walls are treated to minimize chemical interactions and then liquid stationary phase is chemically bound to them. There are numerous types of capillary columns, but only the most common type used today will be discussed; Fused Silica Open Tubular (FSOT) column which is a type of wall-coated open tubular (WCOT). The structure of these FSOT columns allows flexibility meaning they can be wound into coils which can be easily stored and inserted into the temperature controlled GC oven<sup>48, 134</sup>.

Capillary columns are more commonly used due to their better efficiency and higher separation when compared with packed columns<sup>146-148</sup>.

All GC-MS in this project using a polar column was undertaken using the J&W HP-INNOWax column (Agilent Technologies, Santa Clara, CA, USA) which contains a polar stationary phase that consists of polyethylene glycol (PEG) or Wax, as shown in Figure 2-5<sup>149-150</sup>.

All GC-MS in this project using a non-polar column was undertaken using the RTX<sup>®</sup>-5 column (Restek Corporation, Bellefonte, PA, USA) which contains a non-polar dimethyl diphenyl polysiloxane stationary phase, as shown in Figure 2-6<sup>48</sup>. The RTX-5 column can be used in a wide

## Chapter 2

range of applications such as in the analysis of pesticides, essential oils, hydrocarbons and drugs which contributes to this being the most used GC stationary phase<sup>150-151</sup>.

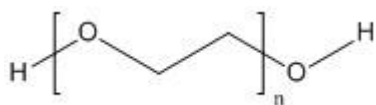


Figure 2-5 -PEG or Wax structure.

Redrawn from<sup>149-150</sup>

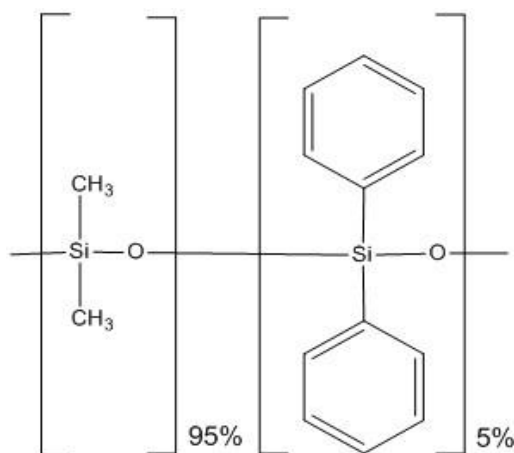


Figure 2-6 - dimethyl diphenyl polysiloxane structure.

Redrawn from<sup>48</sup>

There are many different detectors used with GC including flame ionisation detector (FID), thermal conductivity detector (TCD), electron capture detector (ECD) and mass spectrometry (MS) that are commonly used<sup>48, 134</sup>.

The FID is the most commonly used GC detector<sup>140</sup> and is used to detect compounds containing carbon-hydrogen bonds. Support gases of hydrogen and air are required in a ratio of 10:1 respectively, which then mix and burn just above the flame within the detector. As carbon containing analytes elute from the GC column, they pass through the flame and burn, producing ions. As a result of this electrons are formed. Due to the negative polarising voltage applied between the flame tip electrode and the collector/signal electrode, these electrons cause a current to flow across this gap. Signal is produced by amplifying this current flow<sup>48, 140</sup>. A cross-section of an FID is shown below in Figure 2-7<sup>152</sup>.

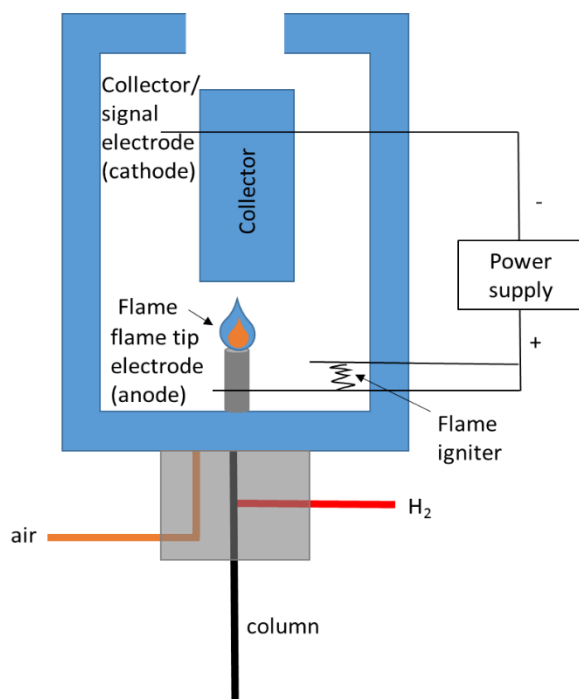


Figure 2-7 - Cross section of flame ionisation detector (FID). Adapted from<sup>153</sup>

For GC-MS, the gas chromatography system is coupled to a mass spectrometer (Figure 2-8)<sup>140, 153</sup>, this allows samples to be separated using chromatography as well as providing chemical information (*e.g.* elemental composition, molecular weight) of analytes and can also be used in quantitation of analytes<sup>134</sup>.

Many different ionisation sources can be used in GC-MS including EI, chemical ionisation (CI) and field ionisation (FI)<sup>134, 140</sup>. An EI source is used in conjunction with a quadrupole mass analyser to acquire data on the GC-MS throughout this project. Mass spectrometry is discussed in greater detail in section 2.5.

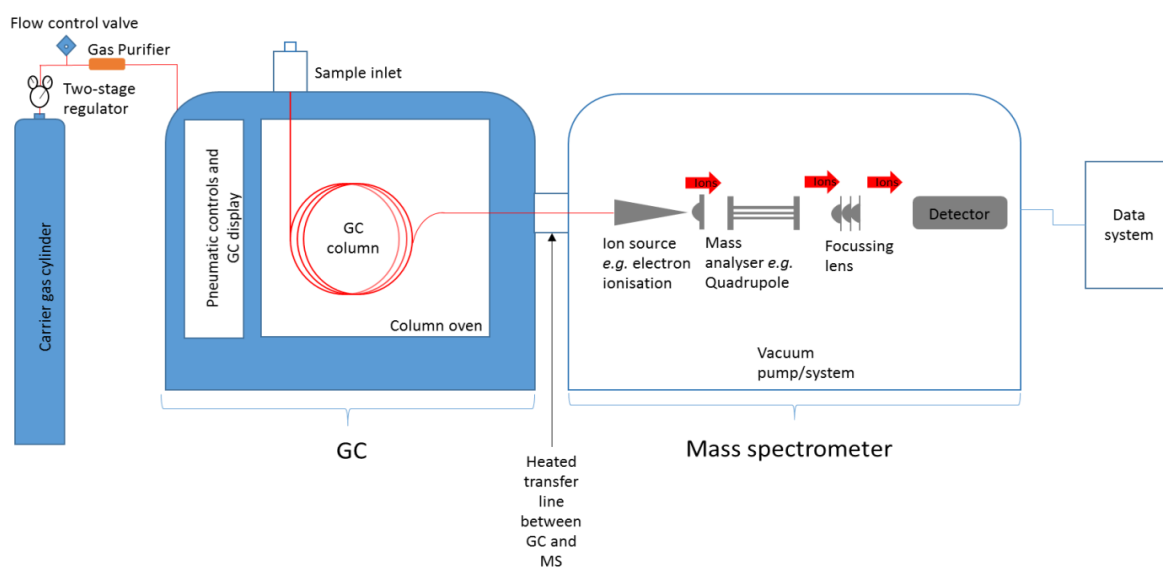


Figure 2-8 - Schematic of GC-MS. Adapted from<sup>140, 153</sup>

## 2.4 Supercritical fluid chromatography (SFC)

Supercritical fluid chromatography (SFC) is a chromatography technique, often considered as an alternative normal phase technique, in which the major component of the mobile phase is a supercritical fluid. A supercritical fluid is a substance that exists at a temperature and pressure above its critical point. It exhibits properties of both a gas and a liquid, such as effuses through solids like a gas and dissolve materials like a liquid<sup>154</sup>. Graphs, known as phase diagrams, are produced to aid understanding of the phases of a substance at different pressures and temperatures, and an example phase diagram for CO<sub>2</sub> is shown in Figure 2-9<sup>155</sup>.

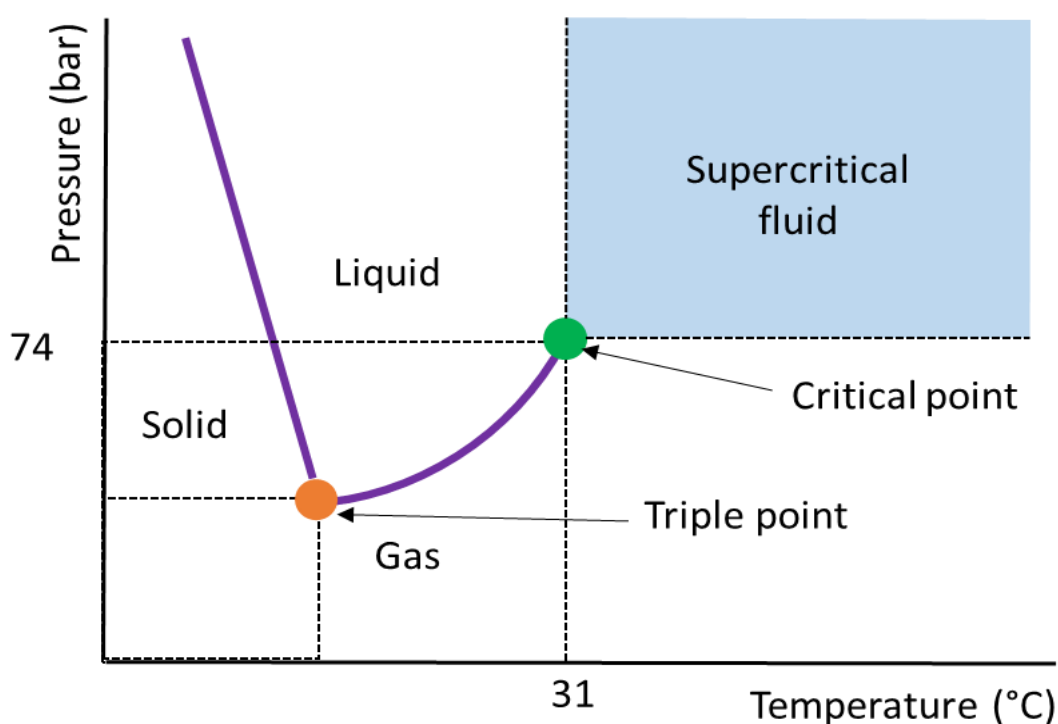


Figure 2-9 - Phase diagram of CO<sub>2</sub>. Adapted from<sup>157</sup>

SFC is often considered an intermediate between HPLC and GC, due to the properties of a supercritical fluid which are between that of a liquid and a gas. It has diffusivity and viscosity typical of a gas but the density and solvating power of a liquid<sup>156</sup>, as shown in Figure 2-9.



Table 2-1 Comparison of the properties between liquids, gases and supercritical fluids

State	Density (g cm <sup>-3</sup> )	Diffusion (cm <sup>2</sup> s <sup>-1</sup> )	Viscosity (g cm <sup>-1</sup> s <sup>-1</sup> )
Gas	10 <sup>-3</sup>	10 <sup>-1</sup>	10 <sup>-4</sup>
<b>Supercritical fluid</b>	<b>10<sup>-1</sup>-1</b>	<b>10<sup>-4</sup>-10<sup>-3</sup></b>	<b>10<sup>-4</sup>-10<sup>-3</sup></b>
Liquid	1	<10 <sup>-5</sup>	10 <sup>-2</sup>

The idea of SFC was first proposed by Jim Lovelock in 1958, although Klesper *et al*<sup>157</sup> was first to demonstrate the use of chlorofluorocarbons as a supercritical fluid to separate metal porphyrins in 1962<sup>158</sup>. However, many early controversies existed around packed column SFC as a technique, particularly around inadequate instrumentation and this resulted in limited growth. In the early 1980s, capillary SFC became popular and was not hindered by the problems surrounding packed column SFC<sup>158</sup>. In the 1990s, Modern packed column SFC emerged mainly due to the advantageous benefits of chiral separations by SFC over HPLC<sup>156, 158</sup>. This resulted in manufacture of commercially available instrumentation that overcame many of the earlier issues and gained increased popularity among chromatographers<sup>156, 158</sup>. In recent years, there has been an SFC revival due to technological advancements (see 2.4.1) but also the acetonitrile shortage in 2008 that drove researchers to find alternatives<sup>156</sup>.

#### 2.4.1 Ultrahigh pressure supercritical fluid chromatography (UHPSFC)

With the new advancements in instrumentation, a modern generation of instruments were made commercially available. The instruments have a novel active back pressure regulation system, (which aids in maintaining the supercritical fluid density), as well as higher upper pressure limits and reduced injection volumes, UV-detector cell volumes and dead volume<sup>159</sup>. The UHPSFC system used in this project was the Waters ACQUITY Ultraperformance Convergence Chromatograph (UPC<sup>2</sup>), as shown in Figure 2-10<sup>160</sup>.

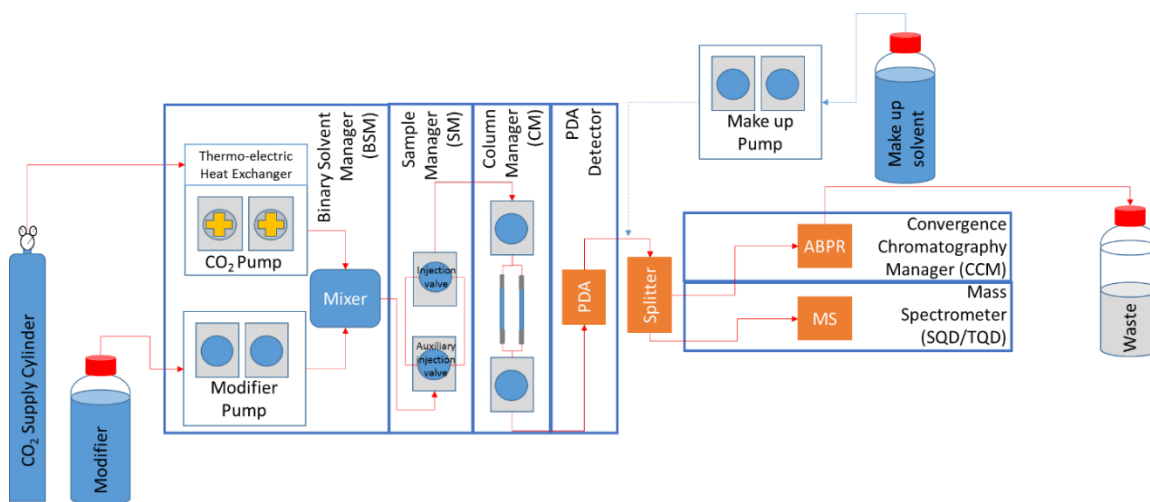


Figure 2-10 –Schematic showing flow path and components of Waters ACQUITY Ultraperformance Convergence Chromatograph (UPC<sup>2</sup>) system. Adapted from<sup>161</sup>

In a similar relationship as HPLC and ultrahigh performance liquid chromatography (UHPLC), the new instruments operate at higher pressures to enable the use of higher flow rates with state-of-the-art sub 2  $\mu\text{m}$  fully porous particle columns that enable ultrahigh pressure supercritical fluid chromatography (UHPSFC) to be achieved<sup>161</sup>.

The introduction of sub 2  $\mu\text{m}$  particles in 2004, were initially only for UHPLC as a means to achieve faster analysis and greater column efficiency<sup>162</sup>. This column technology was then transferred to SFC and exhibited higher efficiency due to the reduction in minimum plate height as shown in Figure 2-11<sup>156, 159, 162</sup>. As a result UHPSFC systems can operate at much higher linear velocity while still maintaining low HETP, meaning a reduction in analysis times can be achieved<sup>156</sup>.

UHPSFC affords high-resolution, efficient and rapid separations and is an orthogonal technique to reversed-phase HPLC with complimentary retention<sup>163</sup>.

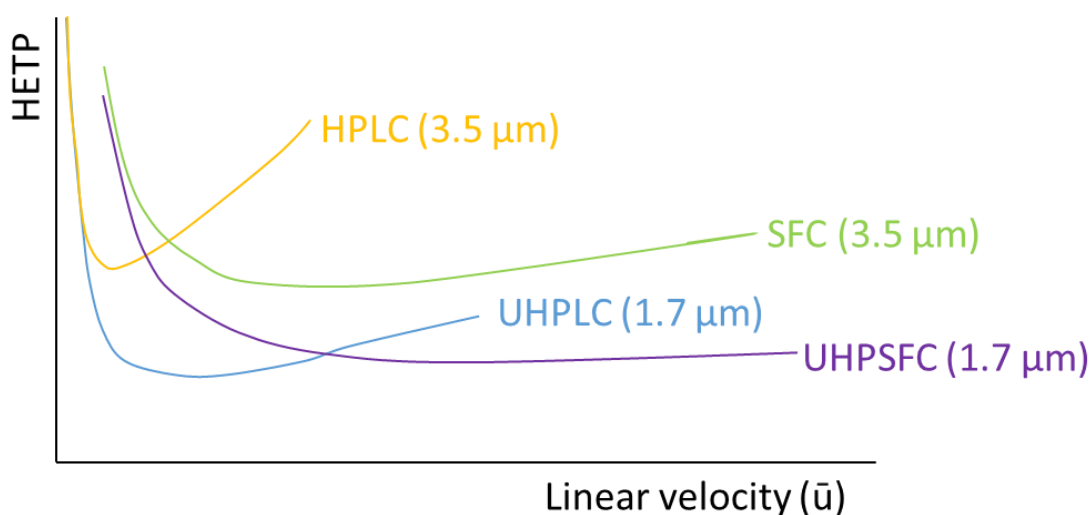


Figure 2-11 -A Van Deemter curve showing a comparison of kinetic performance for both LC and SFC instrumentation using a variety of column particle sizes.

Adapted from<sup>156, 159, 162</sup>

The stationary phases used in UHPSFC are packed columns (the same or as similar to those used in UHPLC), whereby both normal phase and reversed phase HPLC column chemistries can be utilised<sup>164</sup>.

The column used in the UHPSFC-MS in this project was the HSS C18 SB column (1.8 μm). This column is made of high strength silica and has “enhanced retention for basic polar compounds when using low pH mobile phases”<sup>165</sup>. The column structure is shown in Figure 2-12.

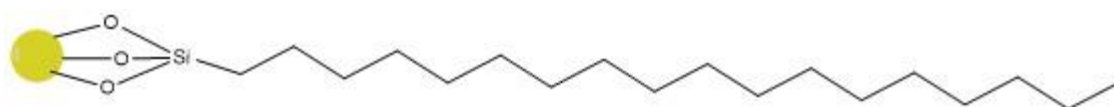


Figure 2-12 - HSS C18 SB column structure

A variety of different substances have been used as the mobile phase for SFC including chlorofluorocarbons, ammonia and light hydrocarbons. However these had many issues including safety and environmental concerns as well as instrumentation damage<sup>156</sup>. Today, supercritical CO<sub>2</sub> (scCO<sub>2</sub>) is the most commonly used mobile phase for multiple reasons<sup>156</sup>. Firstly CO<sub>2</sub> is a supercritical fluid above its relatively low critical point of 31.1 °C and 73.8 bar (Figure 2-9), which can be obtained using conventional instrumentation<sup>166-167</sup>. CO<sub>2</sub> is cheap and easily obtained from the food industry which does not rely on production from other industries, as well as reasonably safe, non-toxic and not flammable. CO<sub>2</sub> is also considered ‘green’ as it is carbon neutral and UHPSFC is considered an eco-friendly technique due to the small volumes of organic solvents used and the reduction in waste<sup>156, 160, 166</sup>. scCO<sub>2</sub> is non-polar and hexane-like affording compatibility

## Chapter 2

with petrochemical fuels such as gasoline, diesel and jet fuel, meaning undiluted fuels can be injected<sup>7, 168</sup>.

SFC also has greater chromatographic selectivity as variable parameters of the mobile phase can be controlled; modifier concentration, additive concentration, temperature, pressure and flow rate. These, in addition to the stationary phase, can be used to optimise chromatographic methods for specific compounds<sup>166</sup>.

The *scCO*<sub>2</sub> mobile phase can be modified using an organic polar co-solvent or modifier (usually 2-40%) that can affect the mobile phase critical point result in chromatographic separations taking place at subcritical conditions. Polar modifiers such as methanol, acetonitrile and ethanol are used and extend SFC to a greater number of application areas<sup>158, 164, 169</sup>. The addition of modifier improves the polarity of the pure *CO*<sub>2</sub>, which has weak polarity when used alone, which in turn increases the solubility of polar analytes in the mobile phase. This is necessary for the elution of polar and high molecular weight analytes. Due to the change in polarity of the mobile phase, the analyte and modifier molecules are in competition for active binding sites (free silanol groups), on the stationary phase within the column. As a result, desorption of polar analytes from the stationary phase is aided, retention time of solutes is reduced and elution order may also be changed<sup>166-167</sup>. The choice of organic modifier is important as the selectivity can be optimised as a result, with alcohols found to be the most universal modifiers, with methanol being the primary choice for polar compounds<sup>156, 166</sup>.

Strong acids and bases can be challenging for modified *scCO*<sub>2</sub> mobile phase, as they will not elute or have poor peak shape. Therefore highly polar additives such as formic acid, citric acid (acidic compounds), trimethylamine, ammonium acetate and ammonium formate (basic compounds), are often mixed or dissolved at low concentrations (usually 0.1 – 2%) into the modifier “to improve peak shape or enable chromatographic elution”<sup>156, 170</sup>. Additives and ammonium salts that have good volatility are preferential when coupled to MS due to compatibility<sup>156, 166</sup>. Two examples of modifiers and additives used in this work are; methanol + 1% formic acid and methanol + 25 mM ammonium acetate.

When UHPSFC is coupled to a mass spectrometer, make-up solvents such as methanol + 1% formic acid and methanol + 50  $\mu$ M ammonium acetate are added prior to the splitter in order to aid ionisation and ensure a stable spray into the mass spectrometer, particularly if <5% modifier is used<sup>156</sup>.

## 2.5 Mass spectrometry

In 1897, J. J. Thomson discovered the electron and as a result of this development, the scientific field of mass spectrometry had its inception between 1911 and 1925<sup>171-172</sup>. The early pioneers of mass spectrometry are considered to be E. Goldstein, J. J. Thomson, F. W. Aston, A. J. Dempster and J. H. E. Mattauach<sup>171-173</sup>.

Mass spectrometry is an analytical technique, defined as the “Study of matter through the formation of gas phase ions that are characterized using mass spectrometers by their mass, charge, structure and/or physio-chemical properties”<sup>174</sup>. A mass spectrometer is an “Instrument that measures the  $m/z$  values (“a dimensionless quantity formed by dividing the ratio of the mass of an ion to the unified atomic mass unit, by its charge number”) and abundances of gas phase ions”<sup>174</sup> to determine the mass of an analyte. It consists of 5 major components; inlet system, ion source, mass analyser, detector and a data system, a simplified schematic of this is shown in Figure 2-13<sup>172-173, 175</sup>.

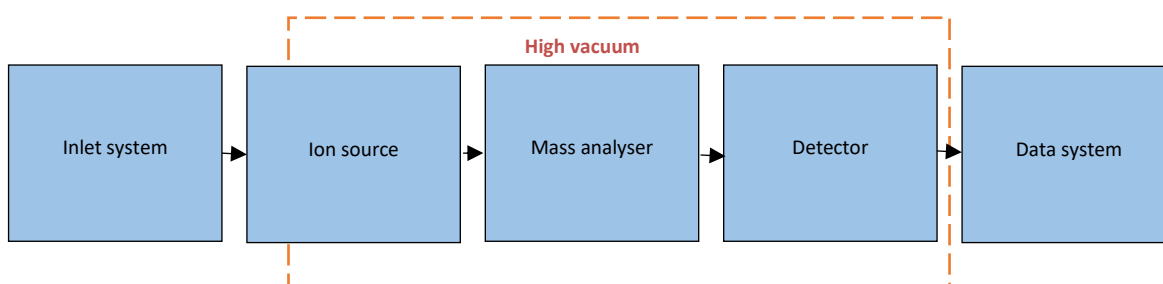


Figure 2-13 - Simplified schematic of a mass spectrometer. Adapted from<sup>3, 179, 181</sup>

The sample is introduced into the mass spectrometer *via* the inlet system such as chromatography techniques such GC or it can be *via* direct infusion using a syringe. Generation of gas-phase ions from the sample occurs in the ion source. There is a large number of different ionisation techniques used in mass spectrometry, some of which require a high vacuum, such as electron ionisation (EI), whilst others require atmospheric pressure ionisation, such as electrospray ionisation (ESI). The gas phase ions then enter the mass analyser, which is under high vacuum, where they are separated out according to  $m/z$ . Some examples of mass analysers include quadrupole, Fourier transform ion cyclotron resonance (FT-ICR), time of flight (ToF) and ion traps (IT). The abundance of the ions of various  $m/z$  values are detected either as they leave the mass analyser by an electron multiplier (EM) in the case of the quadrupole<sup>176</sup> or within the mass analyser cell using detection plates<sup>177</sup>. The detector converts this into electrical signal which can then be processed to produce a mass spectrum<sup>172, 176</sup>.

The following sections focus solely on the mass spectrometry techniques used specifically within this project.

## 2.5.1 Ion sources

### 2.5.1.1 Electron ionisation (EI)

Electron ionisation (EI) is a hard ionisation technique, which was invented by Dempster<sup>178</sup> and then further developed by Bleakney<sup>179</sup> and Nier<sup>180</sup>. This ionisation technique is suitable for gas-phase molecules (and volatile organic molecules) which then interact with energetic electrons to produce molecular ions ( $M^+$ )<sup>172</sup>, as shown in Equation 2.7 below:



Equation 2.7 – Formation of radical cations

Within an EI source (Figure 2-14)<sup>172, 181-182</sup> a wire filament (tungsten or rhenium) is heated using electric current (~3 amps) and electrons are produced. These electrons are accelerated to 70 eV as they cross the source from the filament becoming attracted to the trap anode. Perpendicular to the accelerated electrons, the sample containing neutral analyte molecules (A) is introduced. The gaseous analyte molecules (A) interact with the electron beam resulting in ejection of an electron from the analyte to create a radical ion ( $A^+$ ) and/or fragmentation ( $F^+$  and  $F^+$ ) as a result of energy transfer from an electron to the analyte. The resulting ions are then directed by the repeller electrode into the mass analyser, in this case a quadrupole mass analyser<sup>183</sup>.

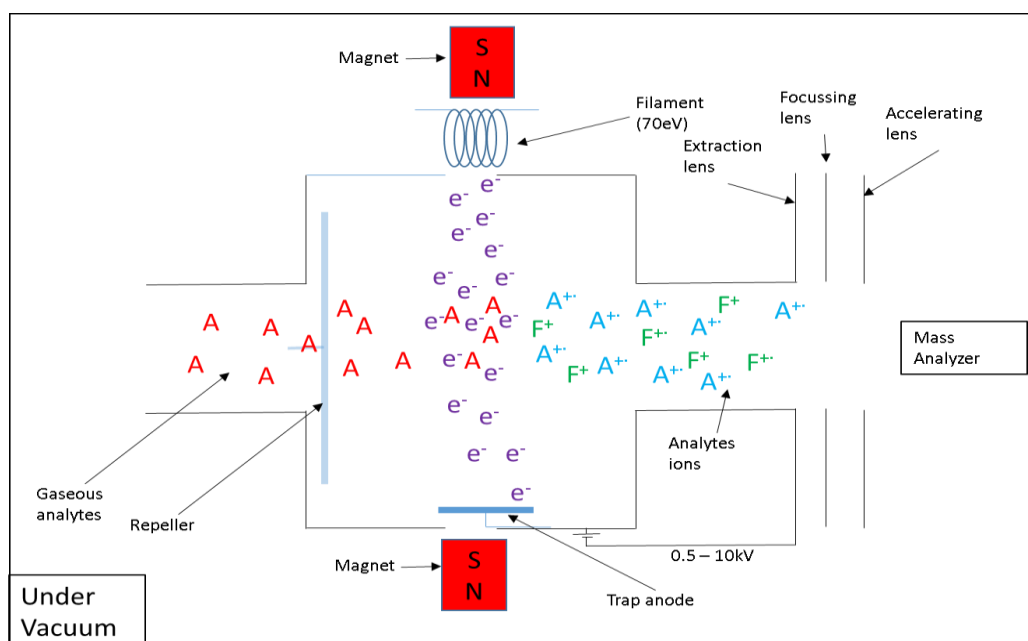


Figure 2-14 - Electron ionisation source diagram. Adapted from<sup>5, 185-186</sup>

EI is a hard ionisation technique and can result in extensive fragmentation of both the molecular ion ( $M^{\bullet+}$  or  $XYZ^{\bullet+}$  below) and fragment ions as shown in Equation 2.8.

**$XYZ^{\bullet+}$ :  $XY^{\bullet+} + Z^{\bullet}$  (cation and radical formed *via* homolytic fission)**

**$XY^{\bullet} + Z^{\bullet+}$  (cation and radical formed *via* homolytic fission)**

**$X^{\bullet} + YZ^{\bullet+}$  (cation and radical formed *via* homolytic fission)**

**$X^{\bullet+} + YZ^{\bullet}$  (cation and radical formed *via* homolytic fission)**

**$XZ^{\bullet+} + Y$  (intermolecular rearrangement leads to loss of a neutral and the formation of a new radical cation)**

Equation 2.8 – EI Fragmentation<sup>184</sup>

McLafferty rearrangement can also take place as shown in Figure 2-15, whereby the  $\gamma$ -Hydrogen is rearranged to an unsaturated group with  $\beta$ -cleavage. As part of the rearrangement, a pair of electrons is supplied. The first of the unpaired electron is donated to the adjacent atom forming a double bond. The second of the unpaired electrons is further transferred to the next atom, resulting in  $\beta$ -cleavage. This rearrangement is commonly seen in compounds containing carbonyl groups such as FAMES.

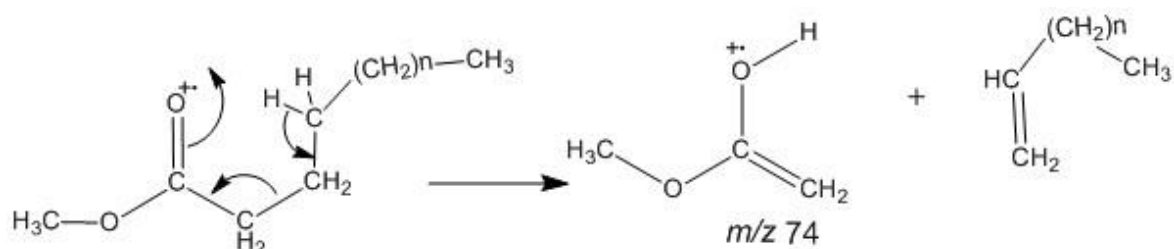


Figure 2-15 - McLafferty rearrangement

### 2.5.1.2 Electrospray ionisation (ESI)

Dole *et al.*<sup>185</sup> initially pioneered the use of spraying a solution through an electrically charged capillary in order to generate gas-phase ions. However Fenn<sup>186</sup> and co-workers further developed this idea into electrospray ionisation (ESI) which interfaces with a mass spectrometer.

ESI is a process whereby ions in a solution are transferred into the gas phase *via* using a high voltage at atmospheric pressure and then move into the high vacuum of the mass

## Chapter 2

spectrometer<sup>187</sup>. A pneumatically-assisted Waters Z-Spray orthogonal ESI source was used in this project and a schematic of such a design (operating in positive ion ESI) is shown in Figure 2-16.

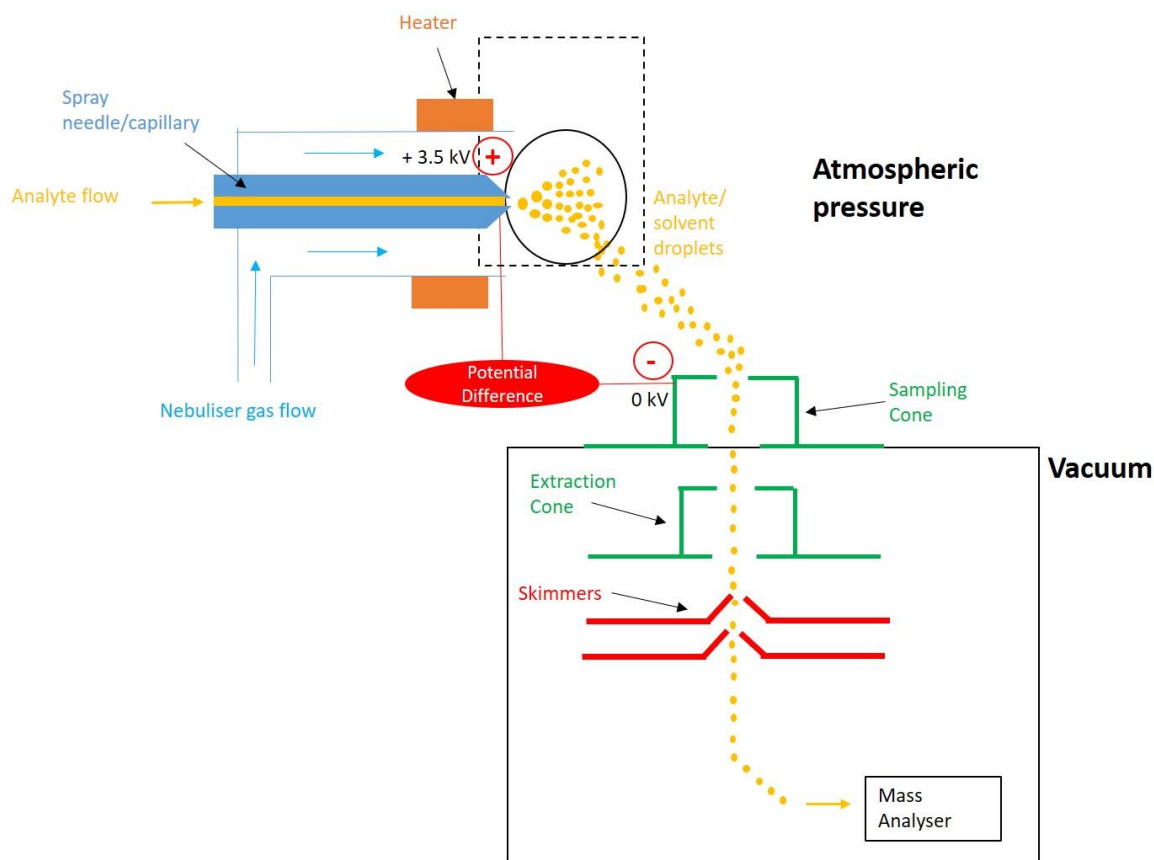


Figure 2-16 - Schematic of pneumatically assisted Waters Z-Spray ESI source, operating in positive ion ESI.

Pneumatically-assisted ESI, often referred to as ESI, uses nitrogen as a coaxial nebuliser gas, which reduces the influence of surface tension therefore making the charging of droplets being more efficient, as well as directing the spray towards the mass analyser. This results in improved nebulisation which enables higher eluent flow rates to be used, which in turn means it can be directly interfaced to a HPLC or UHPSFC<sup>188-189</sup>. Other benefits of ESI include high sensitivity and that it can handle samples with large masses, due to the formation of multiply charged ions<sup>187</sup>. It is also a 'soft' ionisation technique so minimal fragmentation occurs meaning it provides the ability to analyse biological samples, such as proteins and peptides<sup>187</sup>.

ESI is suitable for analytes in solution with medium to high polarity and with either small or large molecular mass<sup>187</sup>.



ESI occurs as a three step process; production of charged droplets at the capillary tip, shrinking of the charged droplets (leading to coulombic fissions), and production of gas phase ions from small/highly charged droplets (Figure 2-17)<sup>190</sup>.

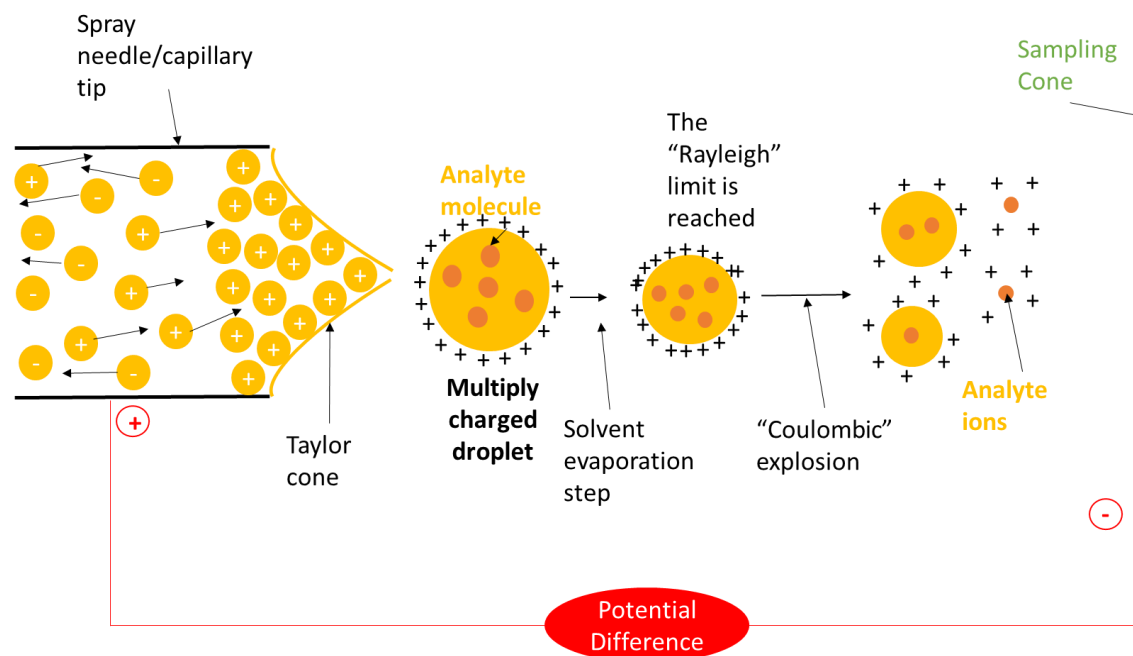


Figure 2-17 - Schematic showing ion formation mechanism in ESI. Adapted from<sup>193</sup>

The charged eluent droplets are produced at the spray needle tip and is sprayed into the desolvation chamber. Both positive and negative ion ESI can be achieved and are dependent on the analyte of interest.. A potential difference (between 2-6 kV) is applied between the capillary, which acts as a positive electrode (anode), and the sampling cone, which acts as the negative electrode (cathode) in positive ion mode. As the eluent solution flows along the capillary, the positive ions found with in it are repelled from the inner walls of the capillary and accumulate as a droplet at the capillary tip. As the charged droplets accumulate at the tip and charge density increases, increased coulombic repulsion forces are also observed. At a point, the eluent surface charge repulsion will be equal to surface tension, and is known as the 'Rayleigh instability limit'. Eventually coulombic repulsions (due to increased charge) will be above the 'Rayleigh instability limit' and, the droplet shape will elongate to form a 'Taylor cone'. As this occurs, a spray of droplets (electrospray) will appear *via* a 'budding' process. This initial step does not occur if using a pneumatically assisted ESI source, as the nebuliser gas flow reduces the influence of the surface tension of the eluent solution.

The sprayed charged droplets will experience solvent evaporation as they move across the desolvation chamber towards the sampling cone. This will result in a reduction in diameter/radius although charge will remain constant. Inert desolvation gas, such as nitrogen, is often pumped into the interface housing to aid solvent evaporation. As the solvent evaporation occurs in the droplet, charge separation at the surface decreases while repulsion of surface charges increases. The Rayleigh instability limit is reached and overcome as the radius of the droplet decreases further until it undergoes a coulombic explosion. This occurs to reduce the coulombic stress found between the surface charges<sup>191</sup>.

There are two proposed mechanisms by which gas phase ions are formed and coulombic stress is further reduced. They are commonly referred to as the charged residue model (CRM) and the ion evaporation model (IEM), shown in Figure 2-18 and Figure 2-19 respectively.

The CRM proposed by Dole<sup>185</sup>, suggests that through continuous and continual coulombic explosions that eventually droplets containing a single ion will be produced and then solvent evaporation of these very small droplets will produce gas phase ions.

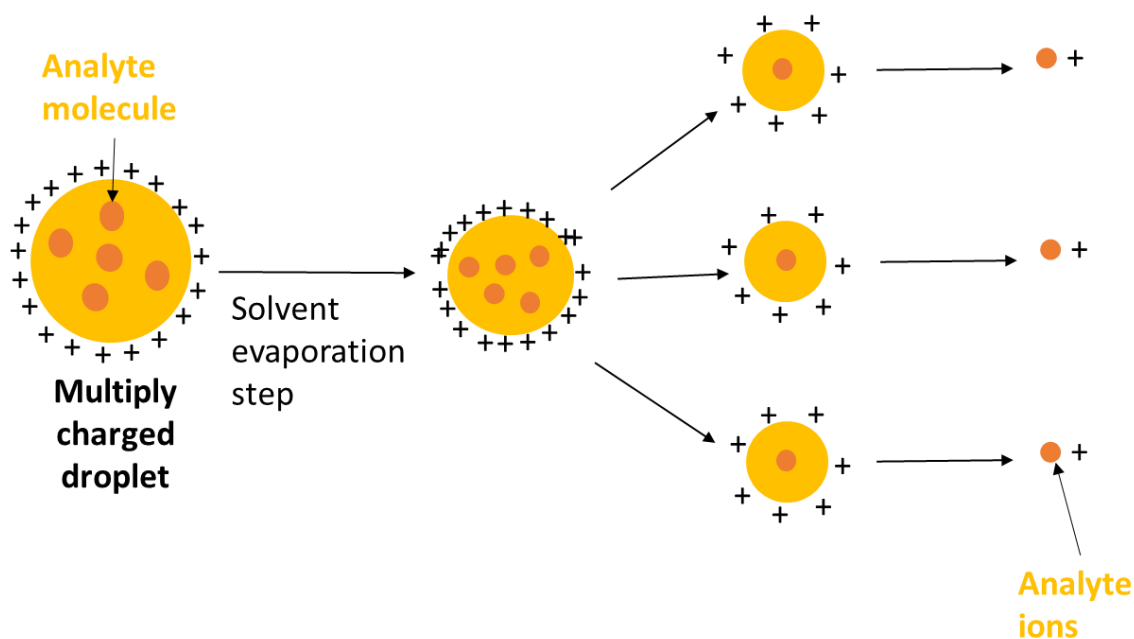


Figure 2-18 – schematic of the Charged residue model (CRM)

The IEM proposed by Iribarne and Thompson<sup>192-193</sup> suggested that “below a droplet radius of 10 nm, an ion is able to ‘evaporate’ from within the droplet”.<sup>188</sup> Ion mobility studies provide evidence which supports this theory over the CRM, therefore meaning that the IEM is the most widely accepted theory at present<sup>172, 188, 194</sup>.

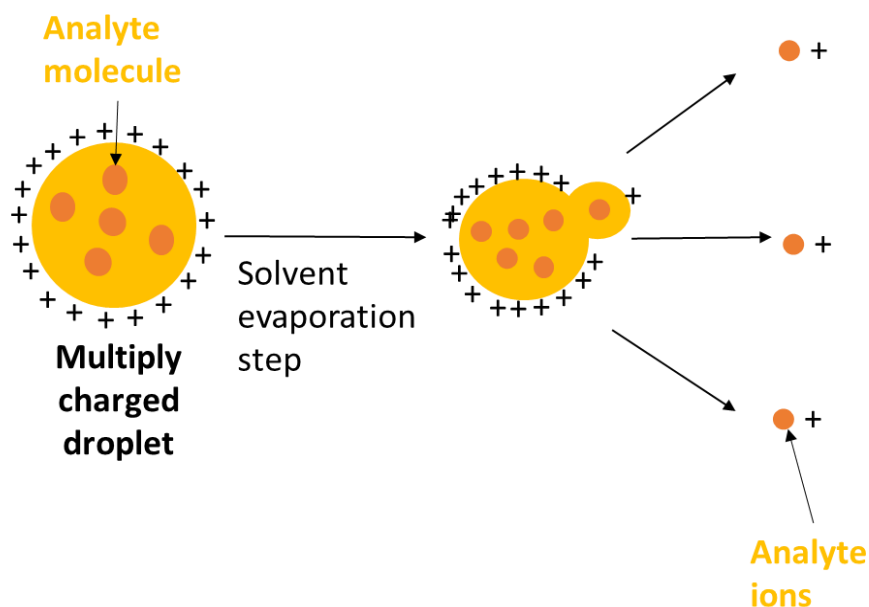


Figure 2-19 – Schematic of the Ion evaporation model (IEM)

Adduct ions which are defined as “an electrically charged species formed by a non-covalent attachment between an ion and a neutral species”<sup>195</sup> are formed by ESI. The typical adduct ions seen commonly in positive ESI are  $[M + H]^+$ ,  $[M + NH_4]^+$ ,  $[M + K]^+$ ,  $[M + Na]^+$ , and  $[M + nH]^{n+}$ , although other less common ones may also be observed. Commonly observed ions in negative ESI include  $[M - H]^-$ ,  $[M - H + Na]^-$ ,  $[M - H + HCO_2]^-$  and  $[M + Cl]^{-196}$ .

### 2.5.1.3 Atmospheric pressure photoionisation (APPI)

Atmospheric pressure photoionisation (APPI) is another soft ionisation technique that was first demonstrated by Robb *et al.*<sup>197</sup> in 2000, coupled with LC-MS, and has been commercially available since 2005<sup>198</sup>.

Great interest has surrounded APPI due the potential of the technique to ionise compounds, particularly non-polar compounds, which cannot be ionised by ESI and APCI. APPI is therefore a complimentary technique to ESI and APCI and as a result, a larger range of compounds can be analysed using atmospheric pressure ionisation (API) techniques<sup>198-199</sup>, as shown in Figure 2-20<sup>200</sup>.

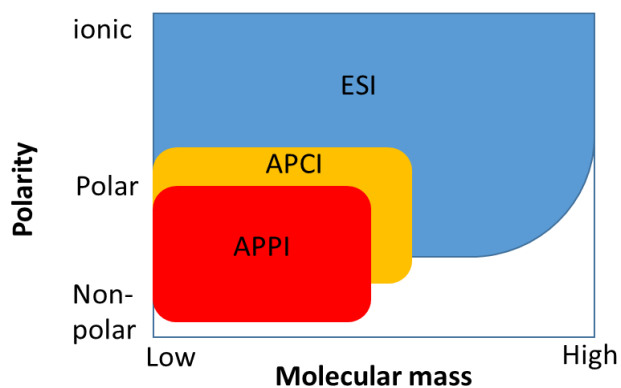


Figure 2-20 A schematic comparing API techniques and their analyte compatibility. Adapted from<sup>202</sup>

Other benefits of APPI include less matrix effects compared to ESI and a wider linear dynamic range.

APPI is a process whereby photons are used to ionise gas phase analytes. The sample is vaporised by heating, the gas phase molecules then react with photons emitted from the lamp. Ionisation then takes place as a result of a series of gas phase reactions are then induced by the emitted photons. A schematic is shown in Figure 2-21 .

The only major difference between the APPI and ESI source is the addition of a discharge lamp emitting photons<sup>199</sup>, in both cases neutral analytes in solution must be vaporised into the gas phase before ionisation can take place.

APPI is suitable for many analytes, particularly neutral and non-polar analytes. Some areas using APPI include drug analysis<sup>198</sup>, lipidomics<sup>201</sup>, and petroleomics<sup>199</sup>.

As in ESI, the sample is introduced into the source *via* a capillary, it is then heated and vaporised into an aerosol, aided by nebuliser gas, and sprayed towards the mass analyser.

An ultraviolet light, commonly a krypton discharge lamp (10.6 eV), emits photons of energy  $h\nu$ . These photons initiate ionisation as they pass through the gas phase analyte molecules, to form molecular ions and protonated molecules which then enter the mass analyser.

A krypton discharge lamp is commonly used as it produces photons of a higher energy than the ionisation potentials of analytes (Ionisation potentials usually 7-10 eV) but lower than that of solvents and atmospheric gases, meaning ionisation is selective and reduces background noise<sup>198-</sup>

<sup>199</sup>.

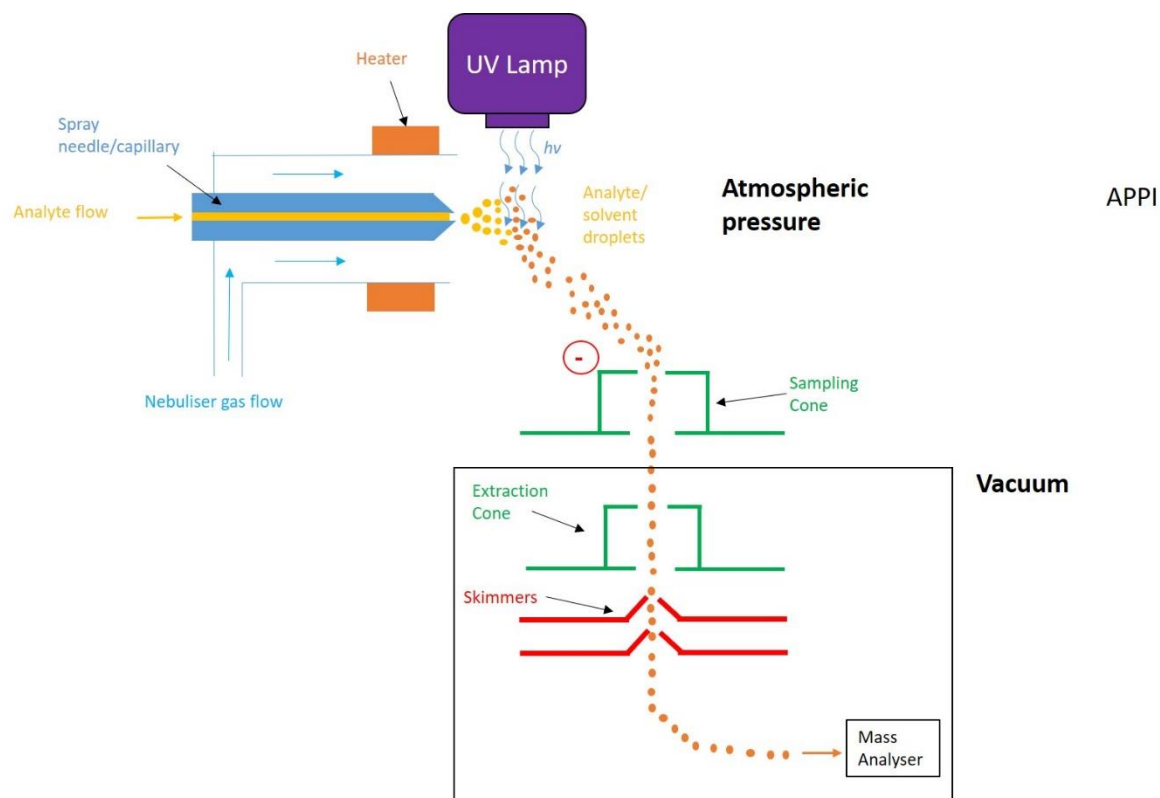
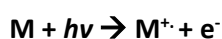


Figure 2-21 - Schematic of APPI Source

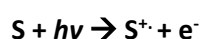
There are two ionisation mechanisms/pathways; Direct APPI and dopant-assisted APPI producing radical cations ( $M^{\cdot+}$ ) and protonated molecules ( $[M + H]^+$ ) in positive ion APPI or deprotonated molecules ( $[M - H]^-$ ) in negative ion APPI. Both ionisation pathways will be discussed for positive ion APPI.

### Direct APPI

Direct APPI occurs if the analyte has a UV chromophore and when the photon is of higher energy than ionisation potential of the analyte, producing radical cations ( $M^{\cdot+}$ ). The analyte initially absorbs the photon and then then ejects an electron, as shown in Equation 2.9<sup>199</sup>. This process allows ionisation of non-polar molecules, however this pathway is known to have low efficiency. This is believed to be partly due to the photon supply becoming depleted due to reactions with solvent molecules if they have an ionisation potential lower than 10 eV (Equation 2.10).



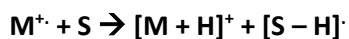
Equation 2.9 – Direct photoionisation of an analyte (M)



Equation 2.10 – Direct photoionisation of a solvent(S)

## Chapter 2

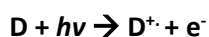
However after photoionisation, further reactions between the radical cation ( $M^+$ ) and the solvent molecules may occur producing protonated molecules ( $[M + H]^+$ ), as shown in Equation 2.11.



Equation 2.11 Abstraction of hydrogen from solvent (S)

### Dopant assisted APPI.

In order to make APPI more efficient, a dopant is commonly employed. The dopant must be a solvent with an ionisation potential lower than  $h\nu$  so it can be ionised directly by the emitted photons. The dopant (D) then forms a dopant molecular ion that will then react further with other molecules present in ion source (Equation 2.12).



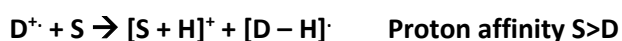
Equation 2.12 – Direct photoionisation of dopant (D)

Charge exchange can occur between the dopant and the analyte molecule if the analyte has an ionisation energy lower than the ionisation energy of the dopant used, forming a molecular ion ( $M^+$ ).



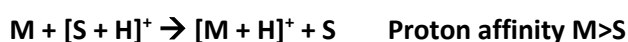
Equation 2.13 – Charge exchange between dopant (D) and analyte (M)

In order to form protonated molecules ( $[M + H]^+$ ), proton transfer must take place. Initially the dopant radical cation must ionise the solvent molecule, which has a higher proton affinity, *via* proton transfer (Equation 2.14).



Equation 2.14 – Proton transfer from dopant (D) to solvent(S)

Ionisation of the analyte can then occur *via* proton transfer, forming protonated molecules, providing the analyte has greater proton affinity than the solvent (Equation 2.15).



Equation 2.15 – Proton transfer from solvent(S) to analyte (M)

Ionisation energies and proton affinities of analyte, solvent and dopant play a determining role in the formation of molecular ions and protonated molecules. Solvents with high proton affinities (*e.g.* methanol) favour proton transfer while charge exchanges is favoured by solvents with low proton affinities (*e.g.* water). A mixture of both molecular ions and protonated molecules is commonly observed in APPI spectra<sup>198-200</sup>.

## 2.5.2 Mass analysers

Once ions are formed, they need to be separated by  $m/z$  using a mass analyser. Several types of mass analysers have been developed, all utilising electrical or magnetic field in a variety of separation principles<sup>172</sup>. Two mass analysers, quadrupole and Fourier transform-ion cyclotron resonance (FT-ICR) have been used in this project and will be discussed in detail below.

### 2.5.2.1 Quadrupole mass analyser

The principle of the quadrupole was first described by Paul and Steinweger<sup>202</sup> in 1953 and then was developed for commercialisation in the 1960s by Story, Shoulders and Finnigan<sup>172, 203</sup>.

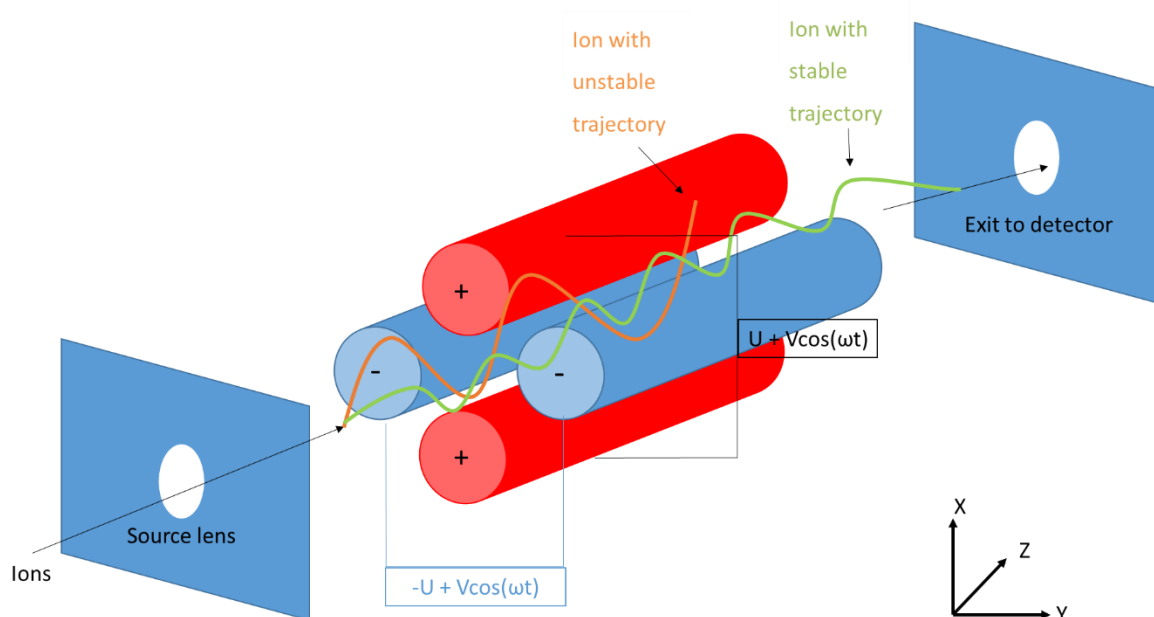


Figure 2-22 – A schematic diagram showing a cylindrical quadrupole mass analyser with stable and unstable trajectories

A quadrupole (Figure 2-22) consists of four perfectly parallel metallic rods, ideally with hyperbolic cross section although commonly cylindrical due to manufacturing practicality and costs<sup>204</sup>. Direct current (DC) voltage is applied on diametric opposite rods and alternating current (AC) voltages

## Chapter 2

(at varying radio frequency (RF) is applied to the other rods at a constant ratio to generate an electric field known as a quadrupolar field. The potential of each rod is denoted as  $+(U + V\cos(\omega t))$  or  $-(U + V\cos(\omega t))$ , for positive (x-axis) and negative (y-axis) rods respectively ( $U$  is DC voltage,  $V$  is the 'amplitude of the RF voltage,  $\omega$  is angular frequency of RF waveform,  $t$  is time domain)<sup>172</sup>. Rods in the x-axis act as a high pass mass filter allowing heavy ions to pass through whereas rods in the y axis act as a low pass mass filter allowing light ions to pass through. Therefore for an ion must remain stable in both axes to enter detector.

In order for an ion to pass through the quadrupole (along the z axis) to the detector it must have a stable trajectory. However a stable trajectory of an ion at a certain  $m/z$  value, through the centre of the rods, is dependent on specific values/magnitude of DC (x axis) and alternating RF (y axis) for a given  $m/z$  value. Therefore ions which do not have a stable trajectory at the particular magnitude of alternating RF and DC of the given scan, will not make it through the quadrupole and will collide with a rod, meaning that unstable ions are filtered out (Figure 2-22).

Repulsion and attraction of ions is constantly occurring as ions move down the quadrupole rods due to the alternating RF voltage switching polarity continuously. As a positive ion travels through the quadrupole, it will be repelled by the rods with positive charge and attracted to rods with negative charge. When the polarity of the rods switches, the ions will change direction, resulting in the ions moving in a spiral motion through the quadrupole due to repeated polarity switching. The trajectory of ion is stable as long as  $x$  or  $y$  is less than  $r_0$  (distance between the rods).

Mathieu derived an ion trajectory equation from Newton's second law of motion to describe ion coordinates along both x and y axis of motion. The equation contains all the variables that affect the electric fields that ions will experience within a quadrupole, and when solved two critical variables for stable trajectories are found, known as  $a$  and  $q$ , as shown in Equation 2.16 and Equation 2.17<sup>204</sup>.



$$a_u = a_x = -a_y = \frac{8zU}{mr_0^2\omega^2}$$

Equation 2.16 –  $a$  and  $q$  derived from Mathieu diagram

$$q_u = q_x = -q_y = \frac{4zV}{mr_0^2\omega^2}$$

Equation 2.17 –  $a$  and  $q$  derived from Mathieu diagram

Where:  $z$ = charge of ion

$U$ = DC voltage

$m$ = mass of ion

$r_0$ = distance between the rods

$\omega$ = angular frequency of RF waveform

$V$ = amplitude of the RF voltage

From Equation 2.16 and Equation 2.17, it can be observed that  $a$  is linked to DC as  $U$  is positive or negative DC and  $q$  is linked to RF as  $V$  is the applied RF potential. The equations for  $a$  and  $q$  can be simplified to Equation 2.18.

$$\frac{a}{q} = \frac{2U}{V}$$

Equation 2.18 – Simplified  $a$  and  $q$  derived from Mathieu diagram

A Mathieu stability diagram can be constructed by plotting  $a$  and  $q$  against each other to demonstrate the stable regions of the  $x$  and  $y$  axis in a quadrupole, as shown in Figure 2-23<sup>172</sup>. An ion must have a stable trajectory in both axes, as highlighted by the four regions circled, in order for it to travel through the quadrupole into the detector. Stability region A is commonly used as the voltages are easily attainable.

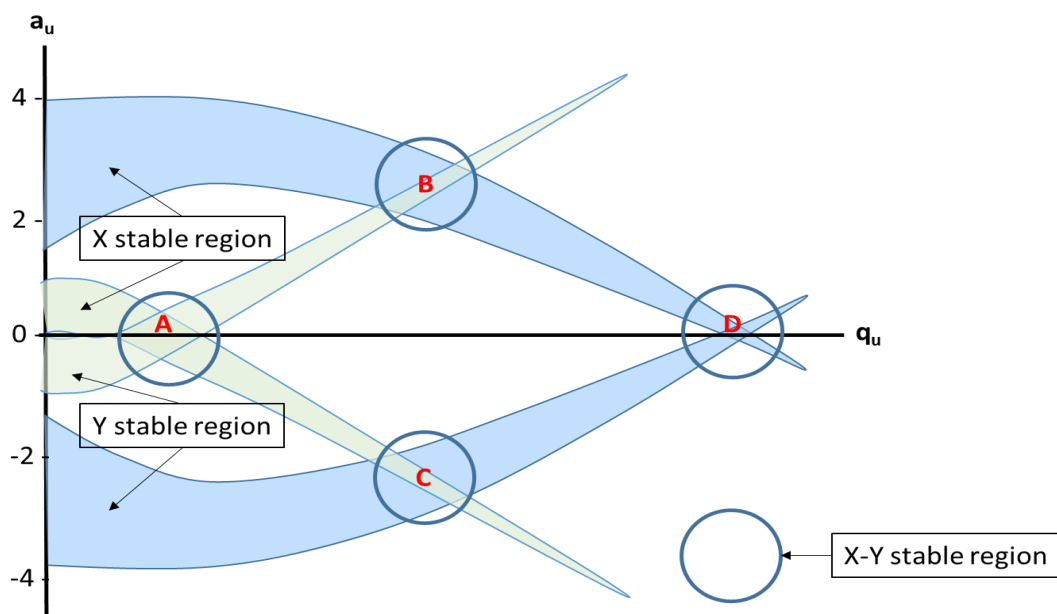


Figure 2-23 - Mathieu stability diagram illustrating stability regions for a quadrupole mass analyser. Adapted from<sup>172</sup>

Figure 2-24 shows a magnified positive region A for three ions with  $m/z$   $m_1$ ,  $m_2$  and  $m_3$ , where  $m_1 < m_2 < m_3$ . A mass scan line is observed which passes just below the tip of each mass stability region. Quadrupoles are commonly operated at unit resolution affording separation of 1 mass unit difference *e.g.*  $m/z$  35 and  $m/z$  36. However by altering the gradient of the mass scan line the resolution can be altered, this is commonly known as gain. Therefore the higher the gain the better the resolution, providing the scan line remains within stability areas for each mass. However sensitivity is reduced as resolution is increased. The offset, which is the magnitude of  $U$  and  $V$  at a fixed ratio, can be altered in order to alter sensitivity. A compromise between resolution and sensitivity must be made.

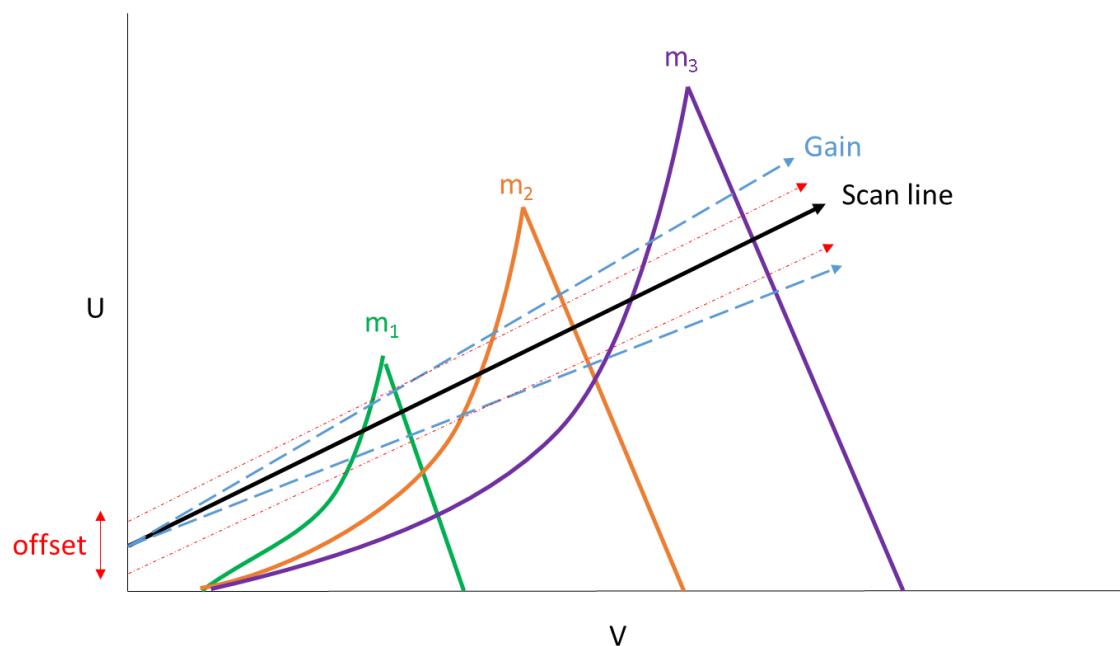


Figure 2-24 – Combined Stability diagram as a function of U (DC voltage) and V (amplitude of the RF voltage) for ions with different masses ( $m_1 < m_2 < m_3$ ), showing the scan line with offset and gain

The quadrupole is a scanning or sequential analyser, as only one  $m/z$  value is measured at a time. A single quadrupole mass analyser has two different scan modes: full scan and selected ion recording (SIR).

When full scan mode is used, DC and alternating RF potentials are ramped at constant ratio from a minimum to a maximum value, as the quadrupole scans from low to high  $m/z$ . The quadrupole scans for a finite time, meaning that ions at each  $m/z$  value only have a stable trajectory at a specific time point within the scan and are only measured for a fraction of time that they are travelling through mass analyser to detector. During full scan operation, ions are scanned one after another stepwise, meaning only ions of one specific  $m/z$  value (e.g.  $m/z$  455) reach the detector at any given moment with ions of all other  $m/z$  values (e.g.  $m/z$  454, 456, etc.), therefore with different trajectories, not reaching the detector. As a result of this only the ion of a given  $m/z$  value being scanned for at a given moment is detected, meaning if a specific  $m/z$  value is of interest it will only be scanned for over a small time window (dwell), meaning only a small fraction of ions with a specific  $m/z$  value will enter the detector with many ions of specific  $m/z$  value lost. Multiple scans are usually undertaken across the full  $m/z$  range and then the intensity of the ions are summed to produce a total ion current chromatogram (TICC).

## Chapter 2

However when operated in SIR, the quadrupole will be set to certain values of  $U/V$  for selected  $m/z$  values only, providing greater selectivity. Due to the quadrupole only scanning for ions of selected  $m/z$  values (e.g.  $m/z$  455), the time window (dwell) for scanning for each  $m/z$  value is much longer meaning a much larger percentage of ions for a given  $m/z$  value reach the detector. This also results in a decrease in noise allowing for an increase in signal from the ions for a given  $m/z$  value (e.g.  $m/z$  455) as no other ions of different  $m/z$  values (e.g.  $m/z$  454, 456, etc.) in the mixture being detected, providing increased sensitivity. Due to the longer dwell time, more points across a chromatographic peak can be collected affording increased accuracy and precision. This will ensure that stable trajectories of the selected  $m/z$  values will only make it through the mass analyser to the detector, resulting in increased sensitivity<sup>175</sup>.

### 2.5.2.2 Fourier transform ion cyclotron resonance mass spectrometry (FT-ICR MS)

Ion cyclotron resonance (ICR) had its inception in 1930s by Lawrence and Edlefsen<sup>205</sup>. However, Fourier transform ion cyclotron resonance mass spectrometry (FT-ICR MS) was not developed until 1974 by Comisarow and Marshall<sup>206</sup>.

FT-ICR MS boasts many advantages including ultrahigh resolving power, as well as high mass accuracy, a wide mass range and the ability to perform  $MS^n$ <sup>200</sup>.

FT-ICR MS is an ion trapping instrument, which consists of four major components; magnet, ultrahigh vacuum system, analyser cell and data system<sup>177</sup>.

Different types of magnets have been used, with superconducting magnets (4.7 – 13 T)<sup>207</sup> being the most common, due to the fact that increasing magnet strength enhances instrumental performance<sup>177</sup>.

The ultrahigh vacuum system uses turbo-molecular pumps to achieve pressures of  $10^9$  -  $10^{10}$  Torr. The ultra-low pressure is required to ensure a long mean free path for the ions and reduce collisions with gas molecules and the higher the vacuum the better the resolution<sup>177</sup>.

The analyser cell was initially designed in a cubic configuration, with many other subsequent designs, however a cylindrical analyser cell is popular as it fits well into the bore of the superconducting magnet. The analyser cell is where the ions are stored, analysed by mass and then detected. Figure 2-25<sup>208</sup> shows a cylindrical analyser cell which consists of two trapping plates on either end of the cylinder, perpendicular to the magnetic field, as well as two detection plates and two excitation plates<sup>177</sup>.

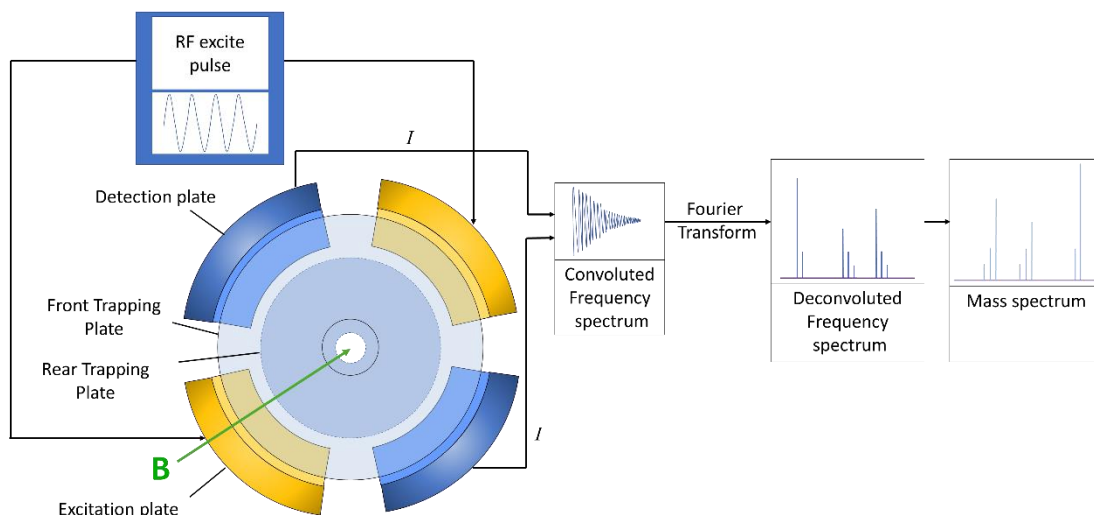


Figure 2-25 - Schematic diagram of cylinder mass analyser cell within a Fourier transform ion cyclotron resonance mass spectrometer with subsequent production of a mass spectrum. The analyser cell is in field of the magnet, which is denoted by  $B$ ,  $I$  is image current. Adapted from<sup>208</sup>

Both magnetic and electric fields are present within the analyser cell and control the motion of the ions present. The ions undergo three types of motion within the analyser cell; cyclotron motion, magnetron motion and trapping motion.

As ions enter the analyser cell through front trapping plate, due to the magnetic field a force is exerted on them, known as the Lorentz force ( $F_L$ ) (Equation 2.19). As a result the ions move in a circular motion, perpendicular to the magnetic field which is known as cyclotron motion.

$$F_L = qv \times B$$

Where  $q$ = total charge of ion

$v$ = velocity

$B$ = magnetic field

(Note:  $q = ze$ , where  $z$ = charge number,  $e$ = elementary electric charge)

Equation 2.19 – Lorentz force

Cyclotron motion is described by cyclotron frequency ( $f_c$ ) which is the frequency at which an ion repeats an orbit and is shown in Equation 2.20.

$$f_c = \frac{zeB}{2\pi m}$$

Equation 2.20 – Cyclotron frequency ( $f_c$ )

Therefore Equation 2.20 shows that cyclotron frequency ( $f_c$ ) is inversely proportional to its mass and proportional to its charge and the strength of the magnetic field, while independent of the ions' initial velocity<sup>200</sup>. FT-ICR MS is able to achieve ultrahigh resolution due to the ion cyclotron frequency not being directly affected by the velocity of the ion<sup>177</sup>.

The measured cyclotron frequency ( $f_c$ ) of an ion is related directly to its mass to charge ratio when in a magnetic field as shown in Equation 2.21. The magnetic field is kept constant so that measured ion cyclotron frequency can be used to determine the mass to charge ratio of an ion.

$$\frac{m}{z} = \frac{eB}{2\pi f_c}$$

Equation 2.21

Magnetron motion (Figure 2-26) is a result of the combination of the magnetic and electric field within the analyser cell that are used for cyclotron and trapping motion. However it is independent of cyclotron and trapping motion as well as  $m/z$ , meaning it has no analytical use. Cyclotron motion (Figure 2-26) is observed as a smaller superimposed circular motion onto magnetron motion, and has a much smaller magnitude than magnetron frequency, moving ions around the cell in a circular motion. A 3D ion trap results which allows ions to be stored in the analyser cell for long periods of time (up to hours).

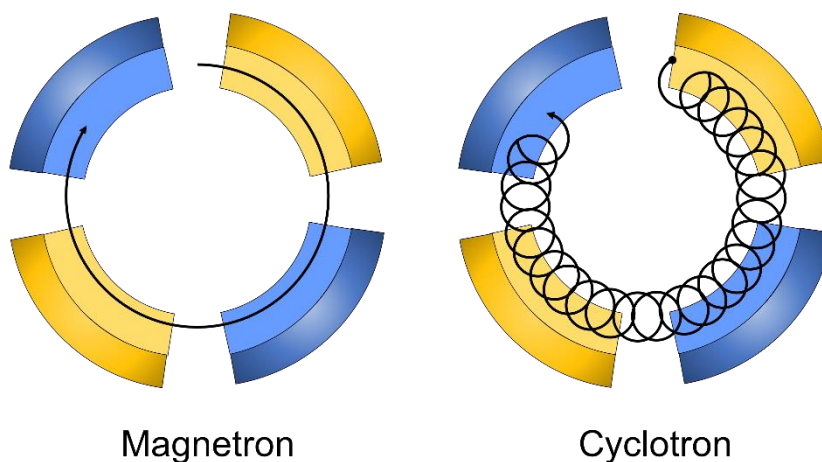


Figure 2-26 - Ion motion within FT-ICR cell

A trapping motion is required to stop rapid loss of the ions from the analyser cell in a radial direction and is achieved using low DC electric potential on trapping plates (both positive voltage for positive ions), which are perpendicular to magnetic field. This results in harmonic oscillation of ions between the two trapping plates along the axis of the magnetic field, therefore trapping the ions.

When ions enter the analyser cell they have low kinetic energy and require excitation in order to be detected. Excitation occurs *via* RF signal being applied to the excitation plates in the analyser cell. For a given  $m/z$ , the excitation frequency of the RF signal will be on-resonance and the same as the cyclotron frequency and will result in excitation to a larger orbit. As a result ions of the same  $m/z$  will be excited together as a packet of ions. Ions in the larger orbit induce an image current ( $I$ ) as they pass the detection plate and detection of the resultant ion frequency signal occurs. This process occurs stepwise, although almost simultaneously for all  $m/z$  values. The complex resultant ion frequency signal spectrum for all  $m/z$  values is amplified and recorded as a function of time, which is known as free induction decay (FID) or as a transient. This raw data FID is then deconvoluted by applying a Fourier transform (FT), converting it to a frequency dependent spectrum, from a time dependent function, from which cyclotron frequency can be converted into  $m/z$  and signal intensity plotted resulting in a mass spectrum<sup>177, 200</sup>.

### 2.5.3 Tandem MS

In soft (low energy) ionisation techniques, generally intact molecular species formed with little or no fragmentation. Tandem MS used induced fragmentation of ions of interest to aid in structural elucidation of unknown compound. It is a combination of 2 or more MS experiments; first to ionise the sample, then select ions of specific  $m/z$  which then undergoes fragmentation and is detected.

#### 2.5.3.1 Tandem MS (in space) using a triple quadrupole MS

Tandem MS in space uses more than one mass analyser so each step is physically separated, as shown in Figure 2-27<sup>209</sup>. A triple quadrupole instrument (QQQ) is commonly used, where three quadrupole mass analysers are placed in series. Two quadrupoles are used as mass analysers denoted as Q1 and Q3, and a third quadrupole (Q2) is used in between as a collision cell (filled with collision gas *e.g.* N<sub>2</sub>, Ar or He), operating in RF only denoted as Q2 (Figure 2-27).

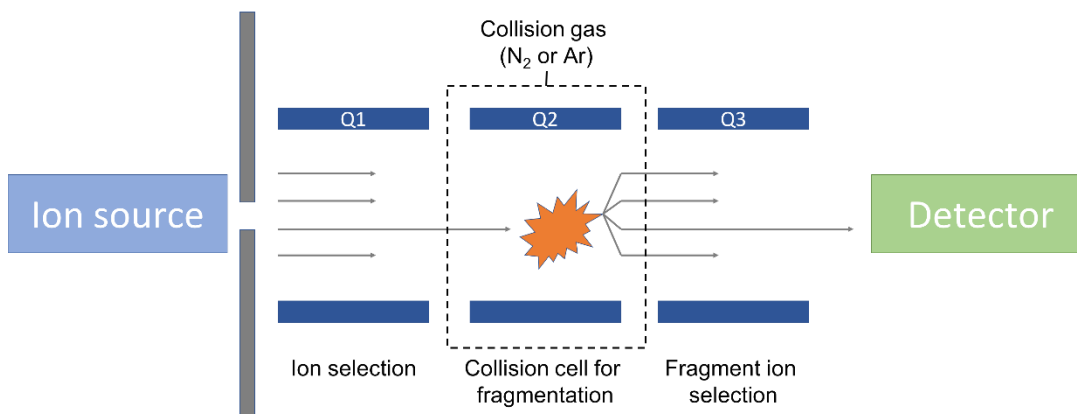


Figure 2-27 – Schematic diagram of a triple quadrupole instrument used in tandem MS in space experiments. Adapted from<sup>209</sup>

There are four major types of experiments that can be undertaken using MS/MS in space; product ion scans, precursor ion scans, neutral loss scans, and selected reaction monitoring (SRM). These will be described in turn using QQQ instrumentation.

A product ion scan is undertaken as follows. A known  $m/z$  value of a specific precursor ion is selected in Q1. Only ions of the selected  $m/z$  then pass into the collision cell, Q2, where they collide with collision gas which produces fragment ions *via* collision induced dissociation (CID). All ions, now known as product ions will exit into Q3 that will then scan over a specified  $m/z$  range.

During a precursor ion scan, Q1 scan over a specified  $m/z$  range, then all ions transfer into Q2 to produce fragment ions *via* CID. Q3 has been set to a specific  $m/z$  value for a chosen product ion. This experiment allows determination of all precursor ions for a given product ion.

A neutral loss scan allows for the determination of neutral losses from precursor ions. Q1 scans over a specified  $m/z$  range, ions then undergo CID in Q2 and then Q3 also scans over a specified  $m/z$  range but has a specific offset in relation to Q1 (*e.g.* -18 if trying determine loss of water).

SRM allows for detection of a specific fragmentation reaction. Q1 is set at a specific  $m/z$  for a precursor ion, these precursor ions undergo CID in Q2 and then Q3 is set for a specific  $m/z$  for a product ion. This experiment therefore results in increased sensitivity, due to spending longer scanning for a specific ion and selectivity as a positive result will only be given if both precursor and product ion are present.







## Chapter 3 Experimental

### 3.1 Chemicals

#### 3.1.1 Reagents

Methanol (MeOH) (LC-MS grade), toluene (HPLC grade), dichloromethane (DCM) (HPLC grade), acetonitrile (ACN) and propan-2-ol (IPA) (LC-MS grade) were purchased from ThermoFisher Scientific (Loughborough, U.K.). Food grade carbon dioxide (CO<sub>2</sub>) was purchased from BOC Special Gases (Manchester, U.K.). Ammonium acetate (NH<sub>4</sub>OAc) and L-Arginine were purchased from Sigma–Aldrich (Gillingham, U.K.) and formic acid (FA) were purchased from Riedel-de Haën (Seelze, Germany).

#### 3.1.2 Samples

A variety of diesel fuel and biodiesel samples (D#1-D#9) were supplied by Innospec Ltd (Ellesmere Port, U.K.). These were all acquired from the field, some of which were known to be deposit causing while others did not cause deposits. Blind analysis was undertaken on these samples to allow experimental bias to be reduced or eliminated.

Homemade biodiesel was synthesised by colleagues at the university and the starting vegetable oil was also obtained.

A variety of fuel filters (SS2-SS4, SS6-SS10) and associated deposits (SS5), as well as a failed fuel injector tip coated with deposits (from a common-rail diesel engine in the field), and three JFTOT tubes with two associated fuels (SS#1 and SS#2) were all supplied by Innospec Ltd (Ellesmere Port, U.K.).

#### 3.1.3 Calibrant standards

Positive and negative ion ESI FT-ICR MS were externally calibrated with 1 µg/mL L-Arginine (Figure 3-1) in methanol, and diluted as necessary.

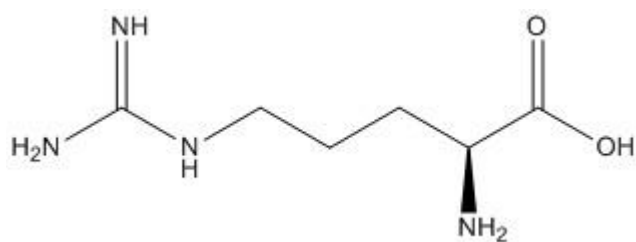


Figure 3-1 Chemical structure of L-Arginine

Positive and negative ESI UHPSFC-MS were externally calibrated with sodium caesium iodide (NaCsI) solution in 50:50 IPA: water, which was available in pre-prepared vials (MS Calibration Solution for atmospheric pressure ionization) obtained from Waters (Manchester, U.K.).

## 3.2 Sample and calibration standards

All sample preparation methodology was developed throughout the project with the optimised methods outlined below.

### 3.2.1 Diesel and Biodiesel

A 100% biodiesel sample (D#1) and a variety of eight commercial diesel fuel samples (D#2-D#9) were used undiluted and analysed by positive and negative ion ESI UHPSFC-MS, as well as polar column GC-MS.

For positive and negative ESI FT-ICR MS analysis, D#1-D#9 were diluted to a 1000 ppm (w/w) solution in a 6:4 toluene: methanol solvent mix, initially. Further dilution then followed until data was obtained with intensity  $10^8$  in the mass spectra. In order to achieve this intensity for each diesel sample, the dilution step varied. Many different toluene:methanol solvent mixes were initially trialled to find the optimum ratio. This sample preparation was used to negate problems associated with space charge effects.

### 3.2.2 Deposits

The sample preparation for the deposit samples was devised but not fully optimised, further investigation would be required.

### 3.2.2.1 Fuel filters

A 1 cm square of each fuel filter (SS2-SS4, SS6-SS10) was put into a vial with ~1 mL methanol. SS5 was a gunk collected from a fuel filter rather than the fuel filter itself and was prepared as follows: glass pipette tip to transfer gunk into a vial with ~1 mL methanol. All shown in Figure 3-2.

1 drop of the infused methanol (shown in Figure 3-3) was taken immediately and diluted into 1 mL methanol for direct infusion positive and negative ion ESI FT-ICR MS analysis.

The addition of formic acid to each sample was also utilised on occasion to force protonation (positive ion ESI) and deprotonation (negative ion ESI) of species, prior to further analysis by direct infusion positive and negative ion ESI FT-ICR MS method.

The 1 cm square of each fuel filter (SS2-SS4, SS6-SS10) put into a vial with ~1 mL methanol, as well as SS5 gunk was left overnight. The undiluted infused methanol was then analysed by positive and negative ion ESI UHPSFC-MS, shown in Figure 3-3

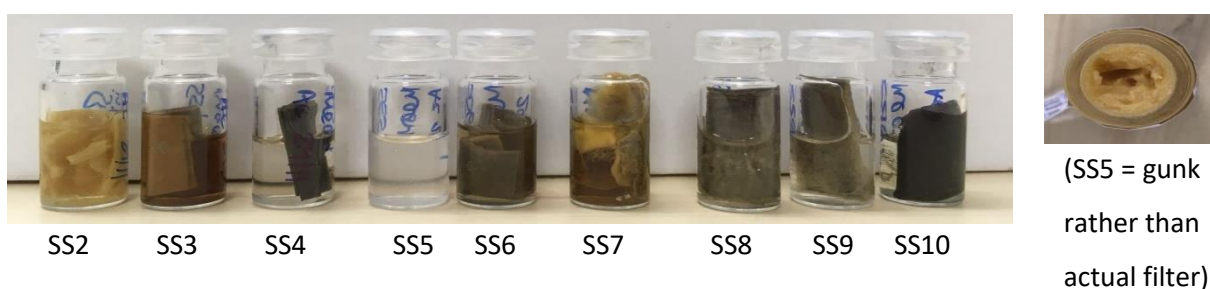


Figure 3-2 Initial Fuel filter sample preparation

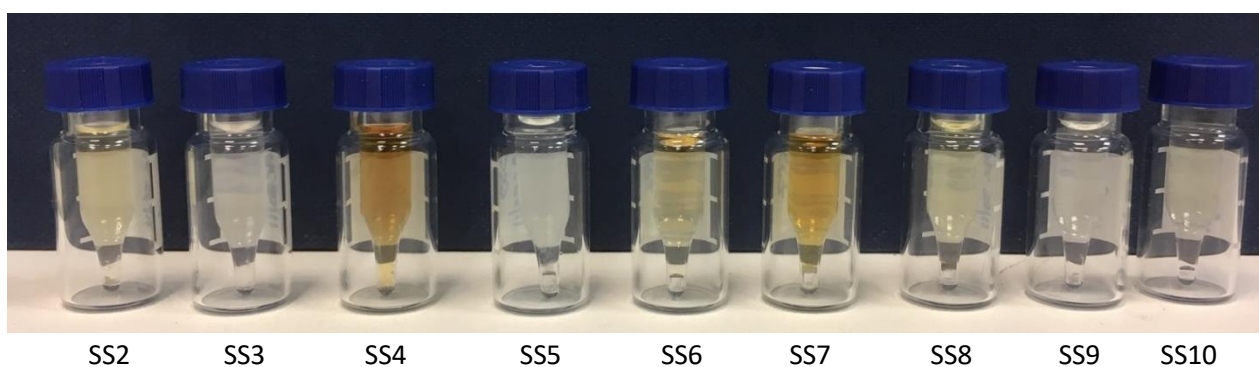


Figure 3-3 Fuel filter sample preparation for UHPSFC-MS analysis

### 3.2.2.2 Fuel injector tip

The failed fuel injector tip was scraped with the tip of a glass Pasteur pipette with 2-3 mm of dichloromethane in the tip. This dichloromethane was washed over the surface of the failed fuel

## Chapter 3

injector tip and returned to pipette several times, resulting in a 'milky solution'. This was added to ~ 0.1 mL MeOH and the milkiness was no longer observed. (N.B. Multiple solvents were attempted before sample miscibility occurred. It is common for deposits to pose challenges with respect to miscibility and removal for analysis).

### **3.2.2.3 JFTOT tubes**

The three JFTOT tubes provided by Innospec; B20, RF06→B20→RF06 and ULSD, were prepared using the associated fuels SS#1 and SS#2. "A volume of fuel was pumped at a fixed rate of 3 mL/min through an initial filter unit containing a 4µm filter paper cut from a diesel fuel filter. The fuel was then passed over a stainless steel test piece heated to 260 °C. The total test time was 2.5 hours and at the end of the test, the metal test piece was cleaned with analytical grade toluene and acetone and dried. Three rods were produced, 1) ULSD, 2) B20 and 3) a composite of ULSD and B20."<sup>29</sup>. This was to provide proof of concept to be demonstrated. The fuel cycles to produce rods were as follows: 150 mins B20 RME fuel (20% RME, 80% diesel), 150 mins ultra low sulphur diesel (ULSD), 450 mins (3 cycles of 150 min) B20, ULSD, B20.

Two sample preparation methods were used for each of the JFTOT tubes; solvent washing of the JFTOT tube first followed by scraping the JFTOT tube.

#### **3.2.2.3.1 Solvent washing method**

Each JFTOT tube was washed with ~5 mL dichloromethane and methanol mix (50:50) into a new individual clean glass beaker. Each of the collected JFTOT tube washings was then analysed by GC-MS (non-polar column) and direct infusion positive ion ESI FT-ICR MS.

#### **3.2.2.3.2 Scraping method**

The lacquered area of each JFTOT tube was scraped using a new clean glass Pasteur pipette, into a new individual clean glass vial. ~5 mL dichloromethane and methanol mix (50:50) was added to each glass vial containing scrapings and then analysed by GC-MS (non-polar column) and direct infusion positive ion ESI FT-ICR MS.

#### **3.2.2.4 JFTOT fuels**

Undiluted fuel samples of SS#1 and SS#2 were analysed by GC-MS (non-polar column).

Serial dilution of each fuel sample (SS#1 and SS#2) into a 60% toluene: 40% methanol solvent mix was required to ensure the concentration was low enough to be analysed by direct infusion positive

ion ESI FT-ICR MS without observing space charge effects. The serial dilution is shown in Table 3-1 and Figure 3-4Error! Reference source not found..

Table 3-1 - Serial dilution of JFTOT fuels

Solution number	Final concentration	Volume of fuel ( $\mu\text{L}$ )	Volume of toluene ( $\mu\text{L}$ )	Volume of methanol ( $\mu\text{L}$ )
0	100% (neat fuel)	1500	0	0
1	1%	15 of solution 0	890	595
2	0.01%	15 of solution 1	890	595
3	0.0001%	15 of solution 2	890	595
4	0.000001%	15 of solution 3	890	595

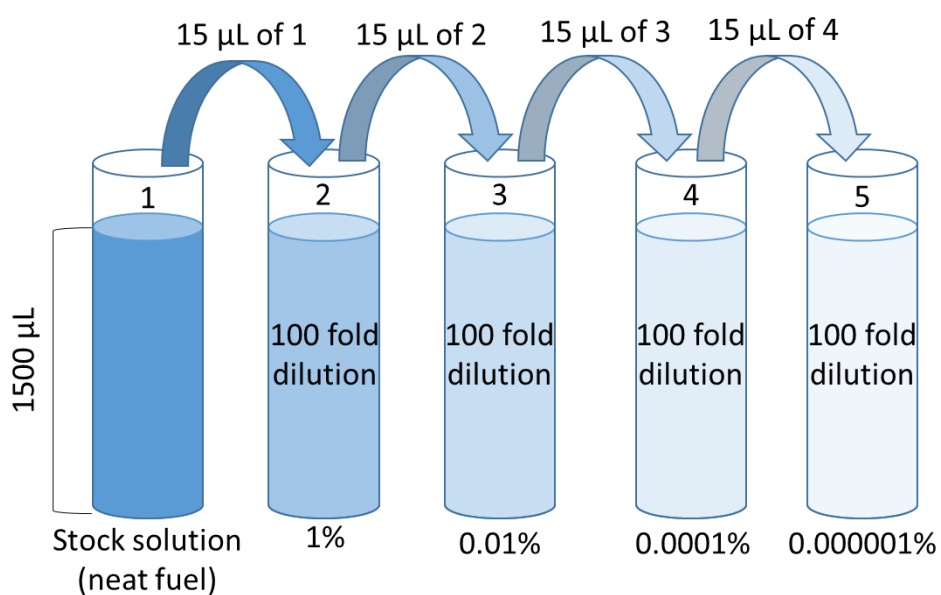


Figure 3-4 - Schematic representation of serial dilution of JFTOT fuels

### 3.3 GC-MS

Method development of GC-MS methods included comparing both polar and non-polar GC columns to optimise chromatographic selectivity, as well as modifying ramp rate and split ratio to optimise chromatographic resolution of compounds present.

#### 3.3.1 Polar column

All analyses were achieved using a ThermoQuest Trace™ GC 2000 coupled to Finnigan Trace MS quadrupole mass spectrometer. A polar HP-INNOWax capillary column (60 m x 0.25 mm i.d., 0.50 µm film thickness) was used. The carrier gas was helium (He) with a flow rate of 1.0 mL/min and 1 µL splitless injections were introduced at 240 °C. The temperature program used was 60 °C for 8 minutes which then increased at 15 °C/min to 240 °C and then held for 16 minutes.

70 eV electron ionisation(EI ) mass spectra were acquired with an ion source temperature of 200 °C and detector voltage of 350 V. Full scan data were acquired,  $m/z$  40 to 500, at a scan rate 2 scans per second and a solvent delay of 5 minutes was used. Xcalibur® software (version 2.0) was used to collect and process data and then the NIST 2014 Mass Spectral Library (version 2.2) was used to compare individual compounds.

After the initial splitless injection, samples were re-analysed using split injection with a split ratio of 50:1. The ramp rate was also modified to 5 °C/min and 1 °C/min and samples reanalysed to achieve improved chromatographic separation.

#### 3.3.2 JFTOT GC method

The non-polar column GC-MS parameters used for the analysis of the JFTOT tubes and associated fuels (SS#1 and SS#2) was found in literature for the detection of adipates by GC-MS<sup>210</sup>. The presence of adipates was suspected from initial positive ion ESI FT-ICR MS data and previous work undertaken by Patel<sup>211</sup>.

All analyses were achieved using a ThermoQuest Trace™ GC 2000 coupled to Finnigan trace MS quadrupole mass spectrometer. A non-polar RTX-5 fused silica capillary column (30 m x 0.25 mm i.d., 0.25 µm film thickness) was used. The carrier gas was helium (He) with a flow rate of 1.5 mL/min and 1 µL split injections with a split ratio of 50:1 were introduced at 280 °C. The temperature program used was 50 °C held for 5 minutes which then increased at 15 °C/min to 280 °C and then held for 5 minutes.



70 eV EI mass spectra were acquired with an ion source temperature of 230 °C and detector voltage of 350 V. Full scan data were acquired,  $m/z$  20 to 500, at a scan rate 2 scans per second and a solvent delay of 5 minutes was used. Xcalibur® software (version 2.0) was used to collect and process data and then the NIST 2014 Mass Spectral Library (version 2.2) was used to compare individual compounds.

### 3.4 UHPSFC-MS

Method development of UHPSFC-MS methods included a column screen of six different columns in combination with different co-solvents to obtain the optimum chromatographic separation. Method run times were also increased (5min and 10min) to create a shallower gradient elution to further separate components. The make up solvent was also optimised to aid ionisation, *e.g.* 1% formic acid was investigated for negative ESI but methanol (50  $\mu$ M ammonium acetate) was found to be superior.

All analyses were undertaken using an Acquity UPC<sup>2</sup> system (Waters, Manchester, U.K.) coupled to a Waters SQD2 (Waters, Manchester, U.K.) single quadrupole mass spectrometer. Tandem MS analyses were undertaken using an Acquity UPC<sup>2</sup> system (Waters, Manchester, U.K.) coupled to a Waters Xevo TQD (Waters, Manchester, U.K.) triple quadrupole mass spectrometer.

#### 3.4.1 UHPSFC chromatographic method

Separations were achieved using an Acquity ultrahigh-performance convergence chromatograph (UPC<sup>2</sup>, Waters, Manchester, U.K.) with a Waters HSS C18 SB packed column, 1.8  $\mu$ m particle size, 3  $\times$  100 mm. The column was held at 40 °C in a column oven, and 2.0  $\mu$ L of each sample was injected. *scCO*<sub>2</sub> with methanol (25 mM ammonium acetate) co-solvent was used for separation at a flow rate of 1.5 mL/min. The *scCO*<sub>2</sub> back pressure of the system was set to 150 bar. A gradient elution was performed using the method in Table 3-2 and a 1 min isocratic pre-run (2% methanol + 25 mM ammonium acetate) was used for column equilibration.

Table 3-2 - 3 minute gradient elution parameters (2%-40%)

Time/min.	Solvent A (CO <sub>2</sub> )/%	Solvent B (methanol + 25 mM ammonium acetate)/%	Curve
0.00	98	2	
2.50	60	40	6
3.00	98	2	6

This chromatographic method will be known as “3min\_C2\_B2\_2\_40%” hereafter.

#### 3.4.2 Positive ion ESI-MS

Positive ion ESI mass spectra were recorded using a single quadrupole mass spectrometer (SQD2) and ESCi multimode ionisation source (Waters, Manchester, U.K.) with the following conditions: capillary voltage, 3.5 kV; cone voltage, 20 V; extractor, 3.0 V; source temperature, 150 °C; cone gas flow 50 L/h, desolvation temperature, 350 °C; desolvation gas flow, 650 L/h (nitrogen); and acquisition and data processing achieved using MassLynx, version 4.1. Mass spectra were acquired between  $m/z$  120 and 1000 at a scan rate of 5 scans/s (scan time of 0.20 s). An internal solvent manager (ISM, Waters, Manchester, U.K.) was used to introduce the make-up solvent, methanol (50 µM ammonium acetate), at a flow rate of 0.5 mL/min. The mass spectrometry full scan method will be known as “ESI POS 120-1000\_3min” hereafter.

#### 3.4.3 Negative ion ESI-MS

Negative ion ESI mass spectra were recorded using a single quadrupole mass spectrometer (SQD2) and ESCi multimode ionisation source (Waters, Manchester, U.K.) with the following conditions: capillary voltage, 3.3 kV; cone voltage, 25 V; extractor, 3.0 V; source temperature, 150 °C; cone gas flow 50 L/h, desolvation temperature, 350 °C; desolvation gas flow, 650 L/h (nitrogen); and acquisition and data processing achieved using MassLynx, version 4.1. Mass spectra were acquired between  $m/z$  80 and 1000 at a scan rate of 5 scans/s (scan time of 0.20 s). An internal solvent manager (ISM, Waters, Manchester, U.K.) was used to introduce the make-up solvent, methanol (50 µM ammonium acetate), at a flow rate of 0.5 mL/min. The mass spectrometry full scan method will be known as “ESI NEG 80-1000\_3min” hereafter.

### 3.5 UHPSFC-MS/MS

Tandem MS analyses were undertaken using an Acquity UPC<sup>2</sup> system (Waters, Manchester, U.K.) coupled to a Waters Xevo TQD (Waters, Manchester, U.K.) triple quadrupole mass spectrometer.

The chromatographic method “3min\_C2\_B2\_2\_40%”(chapter 3.4.1) and positive ion ESI mass spectrometry full scan method “ESI POS 120-1000\_3min”(chapter 3.4.2) were used.

Positive ion ESI tandem mass spectra were recorded using a (Waters Xevo TQD) triple quadrupole mass spectrometer and ESCi multimode ionisation source (Waters, Manchester, U.K.)

Product ion scans were acquired for (all ammoniated molecules  $[M + NH_4]^+$ ) monoacylglycerols (monoglycerides) at  $m/z$  348.3, 372.4, 374.4 and 376.4, and for sterol esters at  $m/z$  678.7, 680.7, 682.7, 692.7, 694.7 and 696.7. To optimise fragmentation in tandem MS experiments, the following collision energies were used: 5, 10, 20, and 30 V.

### 3.6 FT-ICR MS

All high resolution mass spectrometry (HR-MS) analyses were acquired using a Fourier Transform Ion Cyclotron Resonance Mass Spectrometer (FT-ICR MS) (Bruker Daltonics., Coventry, U.K.). A 4.7 Tesla magnet was used. An ESI source was used with an optimised method with TD (Time Domain) of 2M and 64 scans.

The prepared samples were then directly infused, using a 250  $\mu$ L Hamilton syringe, into the FT-ICR MS at a flow rate of 5  $\mu$ L/min. Nebuliser pressure of 1.2 bar, drying temperature 180 °C, drying gas flow rate of 4.0 L/min, end plate offset 500 V and a capillary voltage of -4 kV for positive ion ESI and +4 kV for negative ion ESI. Positive and negative ion ESI-MS were acquired between  $m/z$  150-1500.

Bruker Daltonics Solarix™ (Bruker Daltonics., Coventry, U.K.) was used to operate the FT-ICR MS and to collect data. Bruker Daltonics Compass Data Analysis™ (Bruker Daltonics., Coventry, U.K.) was used to process and calibrate data.

### 3.7 Data processing

#### 3.7.1 SpectralWorks AnalyzerPro®

Polar column GC-MS data files were analysed using SpectralWorks AnalyzerPro® (version 5.3), to enable direct comparison of components within data sets as well as comparison of different data

## Chapter 3

sets. This was achieved using the initial component detection parameters shown in Table 3-3. NIST 2014 Mass Spectral Library (version 2.2) searching parameters were also used with forward and reverse thresholds of 650 and a confidence threshold of 80%.

Table 3-3 - Initial component detection parameters for SpectralWorks AnalyzerPro®

<b>Detection parameter</b>	<b>Value (unitless unless otherwise stated)</b>
Area Threshold	500
Height threshold	0.1%
Width threshold	0.01 min
Signal to noise	5
Scan window	3
Smoothing	3





## **Chapter 4 Analysis and comparison of diesel fuels (mineral diesel and biodiesel) and possible deposit forming components using complementary analytical techniques**

### **4.1 Introduction**

#### **4.1.1 Analytical challenge of diesel and biodiesel fuels in relation to IDIDs/deposits**

Fuel analysis, in this case diesel, is a challenging analyte due to it being a complex chemical mixture. Diesel fuels are commonly found to consist of a variety of compounds including base fuel as well as additives with differing chemistries (polar, non-polar, aliphatic, aromatic, contain S, N, O *etc.*) utilised to alter the fuel chemistry further adding to the analytical problem. However fast, yet thorough fuel analysis is required for fuel quality and characterisation.

Fuels are also ever-changing due to increasingly strict emission legislation, this has led to reduction in sulfur and introduction of biodiesel (engine design is also affected (reduction in fuel injector nozzle diameter) (see 1.1.3 for further detail)). This has resulted in multiple concurrent changes to fuels which results in difficulty determining causes when fuel or engine issues arise, especially as it may be a combination of factors.

The analysis of deposit and non-deposit forming fuels was undertaken using complimentary chromatography and mass spectrometry techniques for characterisation with a hypothesis that the chemistry and components seen in fuels is similar to that seen in fuel injector deposits (IDIDs) and also that precursors to IDIDs may be observed within the fuels.

#### **4.1.2 Comparison of diesel fuels from the field**

Innospec Ltd (Ellesmere Port, U.K.). provided nine diesel fuel samples for analysis (D#1 was commercial B100 biodiesel, D#2-D#9 were unknown diesel fuels); some of these fuels are known to cause deposits in fuel injectors although this information was not provided for this project. Comparisons of datasets were undertaken to see if any similarities or differences in the fuels could be attributed to deposit formation or precursors.

## 4.2 GC-MS Analysis of nine diesel fuels

Gas chromatography-mass spectrometry (GC-MS) analysis provides the separation power of GC coupled with the identifying power of MS<sup>134</sup>. GC-MS has been commonly used for the analysis of diesels and biodiesels historically up to the present day, with ASTM<sup>212-213</sup> and Energy Institute IP<sup>214</sup> test methods utilising the technique. (This also means the instrumentation is readily available in industry, however it may be legacy.)

GC-MS analysis of diesel fuel requires little to no sample preparation and is suitable for low molecular weight, volatile, non-thermally labile compounds<sup>134</sup>, such as some of the base fuel hydrocarbons (C<sub>8</sub>-C<sub>40</sub>)<sup>212</sup> and fatty acid methyl esters (FAMES)<sup>213, 215</sup> present within diesel fuel.

Fatty acid methyl esters (FAMES) are the key component of refined (transesterified) biodiesel, it is a renewable fuel that is commonly blended with mineral diesel, as previously discussed in detail in chapter 1.

MS acts as a universal detector as it is not compound or element specific, but measures mass to charge ratio. Electron ionisation (EI) is utilised to ionise the molecule into the ion source. Electrons at 70eV, the industry standard for electron energy, bombard analyte molecules inducing initial ionisation as well as fragmentation simultaneously due to the kinetic energy of the bombarding electrons having a higher energy than the ionization energy of the analyte. An abundance of fragment ions is produced that provide structural information. 70eV EI mass spectra are reproducible and comparable, with compounds having characteristic fragmentation, resulting in libraries such as the NIST mass spectral database being created. This allows matching of experimental mass spectra to library mass spectra affording rapid compound identification.

GC-MS is one current industry proposed solution to fuel analysis related to the deposit issue. Barker *et al.*<sup>85</sup> previously used Zebron ZBwax polar column GC-MS to analyse ULSD samples. Additionally Dolores *et al.*<sup>216</sup> also utilised GC-MS for analysis of internal diesel injector deposits (IDIDs), as well as further derivatisation steps to convert observed carboxylic salts (from C12 succinic acids, C16 and C18 fatty acids with sodium) by other analytical techniques into methyl esters for GC-MS detection<sup>31, 216</sup>.

Therefore, polar column (INNOwax) GC-MS (3.3.1) was utilised to analyse nine diesel fuel samples from the field, in order to characterise fuels and correlate compounds and deposit formation. The GC-MS TICCs were initially processed manually using NIST library searching for compound identification and compared for similarities and differences. A computational processing method



was also employed to provide rapid comparison and identify differences not seen manually and provide a percentage similarity between fuels.

#### 4.2.1 Polar column GC-MS analysis

Nine diesel fuels (D#1-D#9) were initially analysed using an optimised polar column GC-MS method, at split ratio 50 and ramp rate 5 °C /min, split ratio 50 and ramp rate 1 °C /min. Figure 4-1 shows total ion current chromatograms (TICCs) of D#2 (unknown diesel fuel) analysed by polar column GC-MS. Two different ramp rates are shown (5 °C /min and 1 °C /min) as they are both required. A method with a ramp rate of 1 °C /min has a runtime of 190 minutes that is very impractical, especially if it is to be used in industry, as it would not be economically viable. However, the data acquired at a ramp rate of 5 °C /min generally provides the separation required, although certain regions lack enough separation for the data analysis being undertaken using the NIST 2014 mass spectral library search, meaning the ramp rate of 1 °C /min method data is then required for areas of poor separation.

Total ion current chromatograms (TICCs) show the intensity of the sum of all ions present at a given retention time.

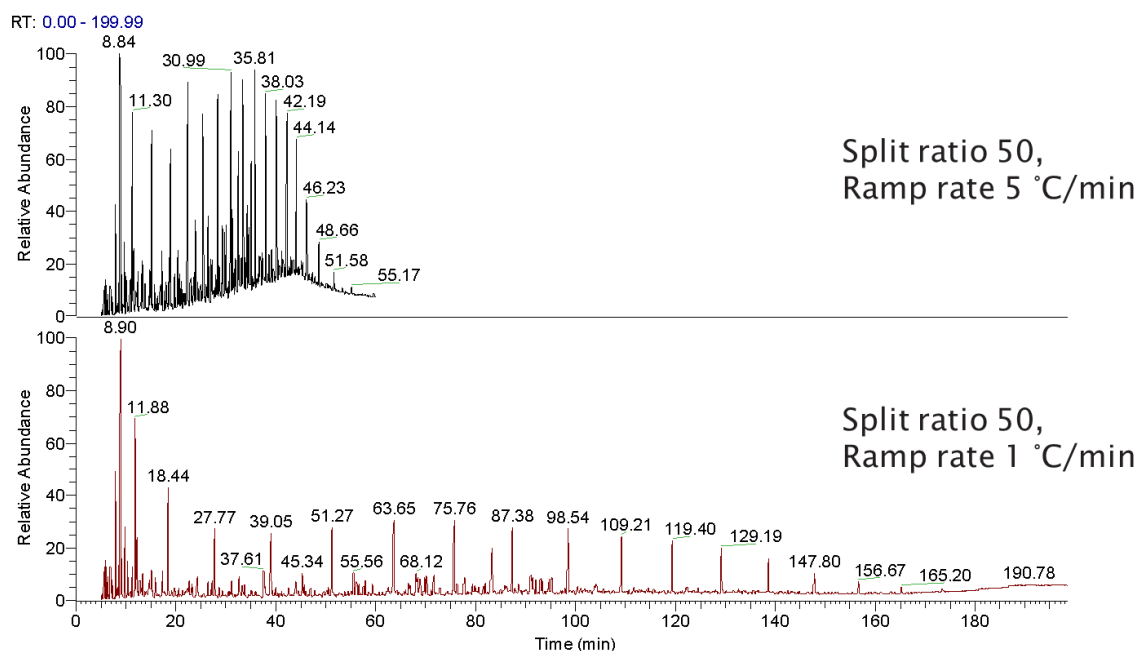


Figure 4-1 - TICCs of unknown diesel sample D#2 analysed using the following parameters; split ratio 50 and ramp rate 5 °C /min, and split ratio 50 and ramp rate 1 °C /min

The GC-MS TICCs of all nine diesel fuels are shown in Figure 4-2 and Figure 4-3.

## Chapter 4

In Figure 4-2 and Figure 4-3 a non-uniform baseline is observed in D#2 and D#7 and overloaded peaks are observed in D#1 and D#9.

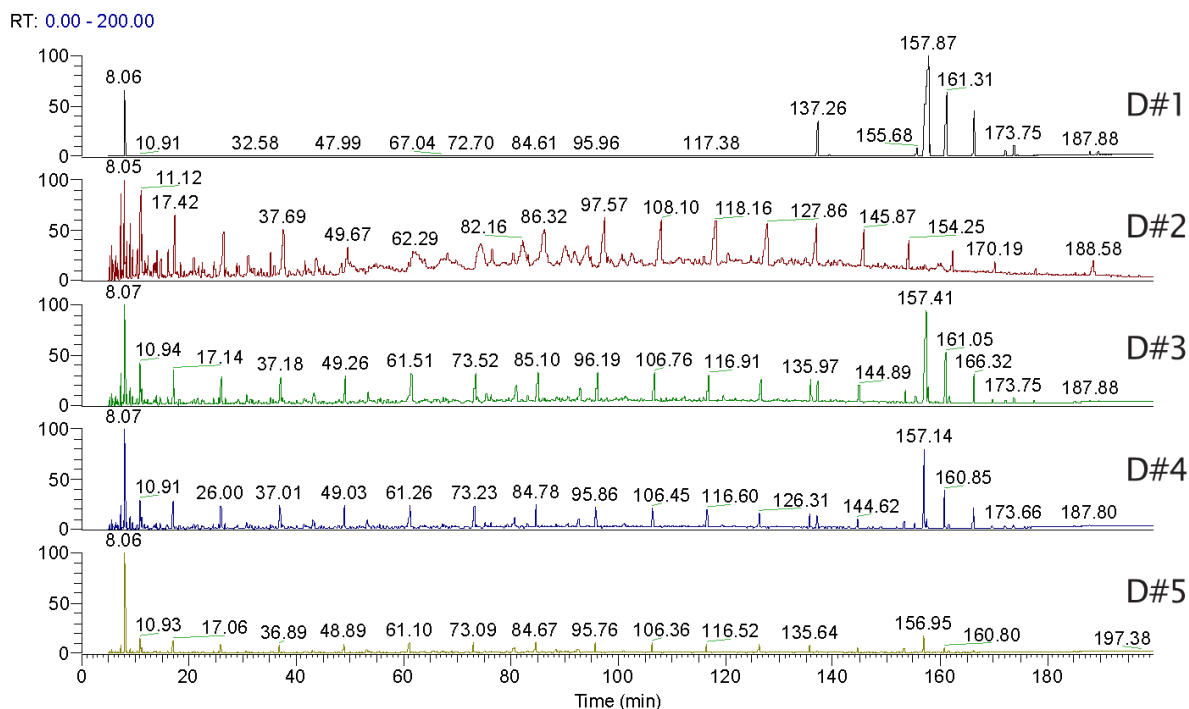


Figure 4-2 - TICCs of D#1-D#5 analysed using polar column GC-MS at a split ratio of 50 and a ramp rate of 1 °C /min

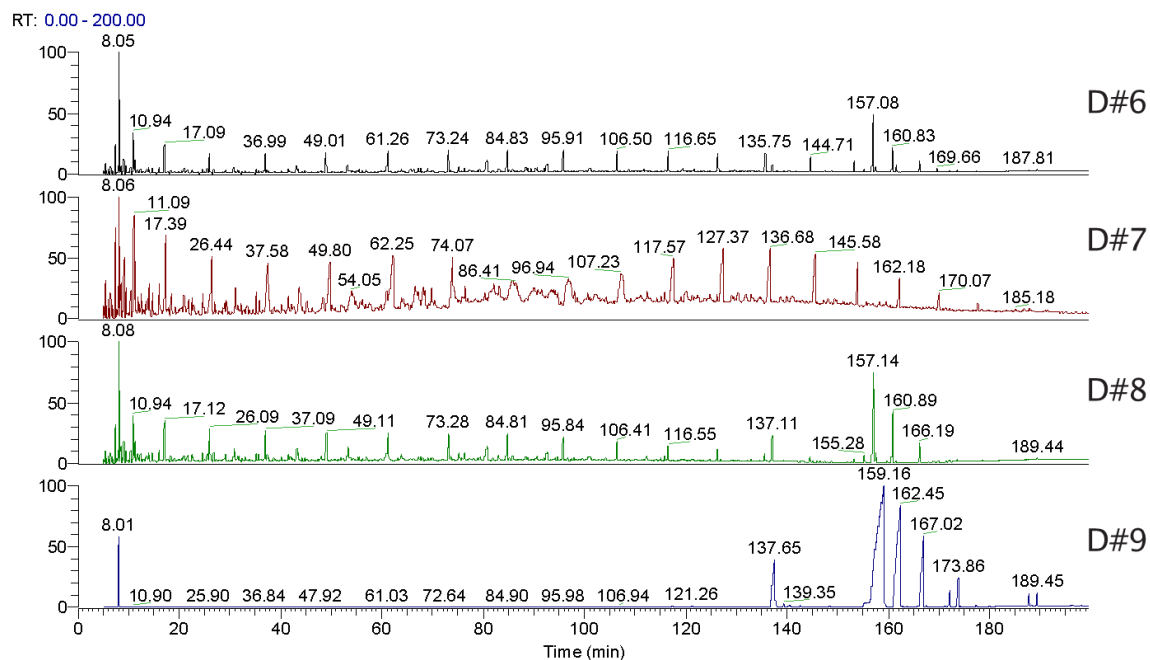


Figure 4-3 - TICCs of D#6 -D#9 analysed using polar column GC-MS at a split ratio of 50 and a ramp rate of 1 °C /min

TICCs of D#1, 3, 4, 6, 8, and 9 look similar with a higher relative abundance of late eluting peaks (FAMEs). TICCs of D#5 has a lower relative abundance of late eluting peaks (FAMEs). TICCs of D#2 and D#7 do not appear to have late eluting peaks (FAMEs) present. All diesel TICCs appear to have repeating peaks (aliphatic and aromatic hydrocarbons) throughout the acquisitions at varying abundances, so it is quite difficult to differentiate visually without more detailed analysis.

#### 4.2.2 Manual data analysis of polar column GC-MS of nine diesels

Data acquired at split ratio 50 and ramp rate of 1 °C /min was analysed initially as it had the best separation between peaks. This allowed easy peak selection and background subtraction for NIST 2014 Mass Spectral Library searching for compound identification. After an initial thorough NIST library search of peaks present, a rapid analysis method was created using reconstructed ion current chromatograms (RICCs) for three compound classes; aliphatic hydrocarbons, aromatic hydrocarbons and FAMEs.

An RICC is chromatogram extracted from acquired full scan mass spectra for one or more  $m/z$  values, commonly shown as signal intensity as a function of time or scan number. This allows compounds of interest to be examined in isolation, resolution of possible coeluting compounds and observation of low level analytes that may not be observed immediately in the TICCs.

The analysis method uses RICCs for  $m/z$  74 and 87 corresponding to FAMEs, RICCs for  $m/z$  43 and 57 corresponding to aliphatic hydrocarbons and RICCs for  $m/z$  77 and 91 corresponding to aromatic hydrocarbons. Also, the peak (in background subtracted data) will only be assigned to a specific compound if the 2014 Mass Spectral Library search (forward searching) gives a similarity index (SI) value of over 850<sup>217</sup>.

Figure 4-5 shows the FAMEs elution between 135-180 min, with the elution order as follows, although some overlap is observed; first aromatic hydrocarbons, then aliphatic hydrocarbons and finally FAMEs.

To simplify data comparison initially, three of the unknown fuels (D#1, D#2 and D#7) are used as to illustrate findings. D#1 was chosen as was known to be 100% commercial biodiesel (B100), meaning it could also act as a FAMEs standard. D#2 and D#7 were chosen as their biodiesel blend level appeared to be low and different from the others. Also, all three should provide current compounds likely to be seen in the field and be a random selection providing a comparison.

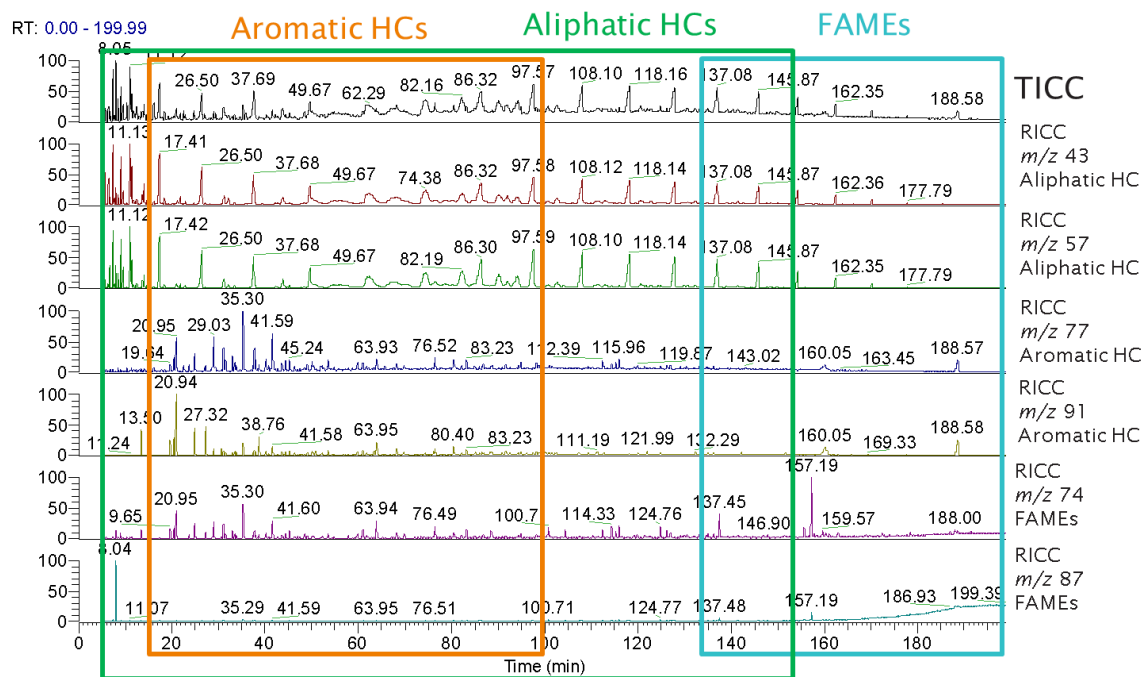


Figure 4-5 - TIC and RICs ( $m/z$  43, 57, 77, 91, 74 and 87) of D#2 analysed by polar column GC-MS at a split ratio of 50 and a ramp rate of 1 °C /min

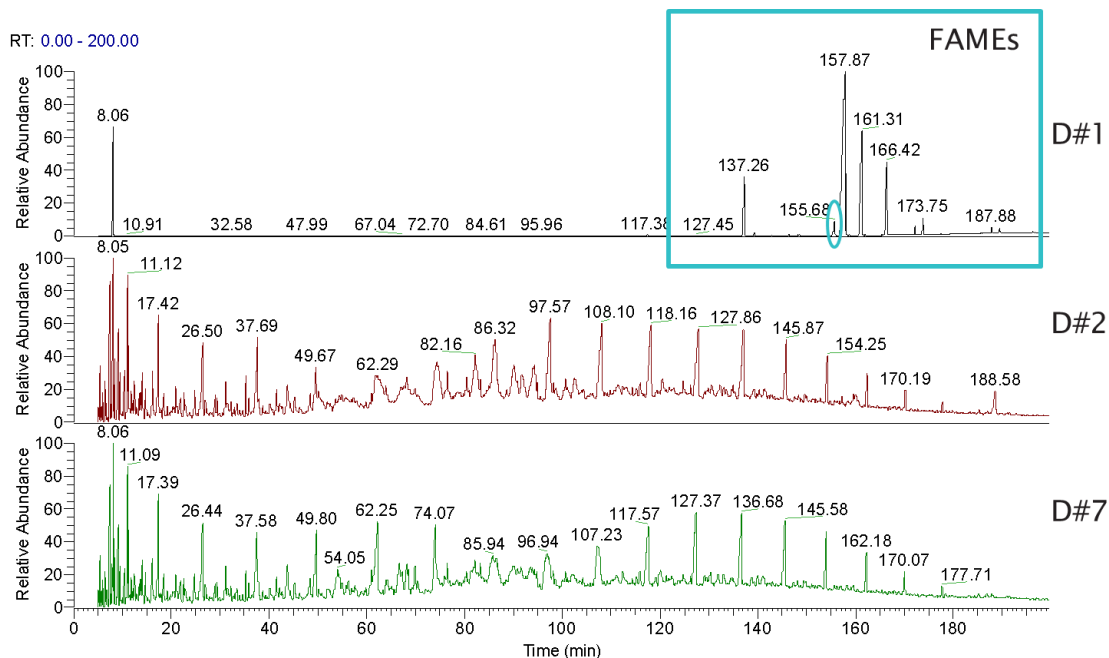


Figure 4-4 - TICs of D#1, D#2 and D#7 analysed using polar column GC-MS at split ratio 50 and ramp rate 1 °C/min. A pale blue box and oval highlight the retention region of FAMES

Figure 4-4 shows TICs of D#1, D#2 and D#7 analysed using polar column GC-MS at split ratio 50 and ramp rate 1 °C/min with a pale blue box highlighting the FAMES retention region. The blue oval within the FAMES region of interest highlights the FAME C18:0 peak at  $t_R$  155.4 -155.8 min,

the mass spectrum of which is shown in Figure 4-6. This figure shows that a molecular ion ( $M^+$ ) is present at  $m/z$  298 as well as a base peak  $m/z$  74 and large peak at  $m/z$  87. (This was the basis for the FAMES RICC method).

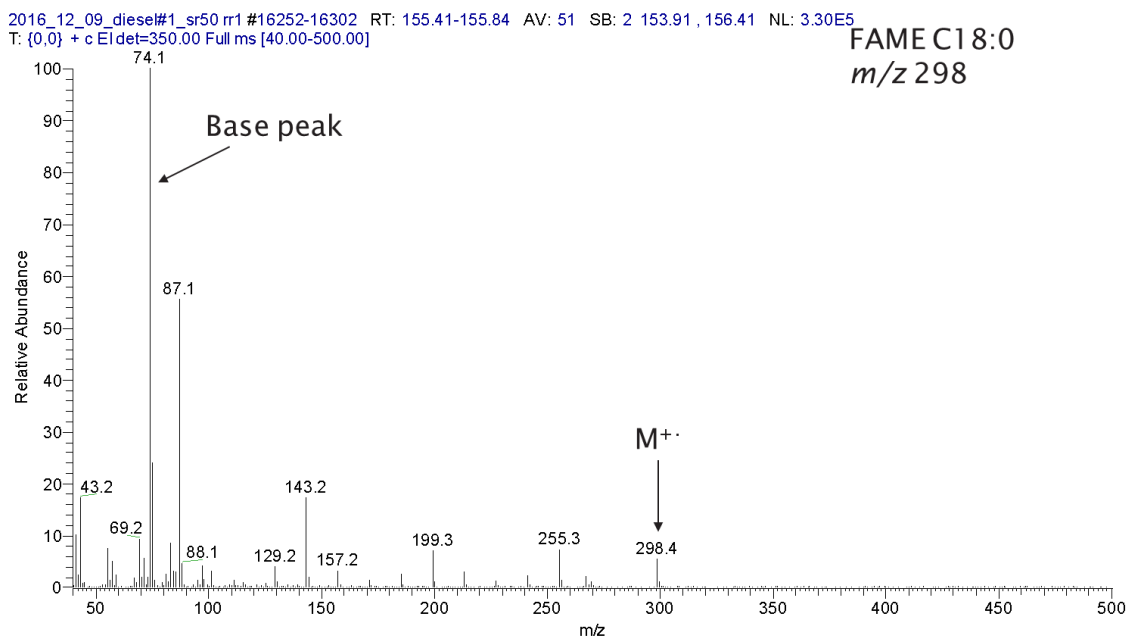
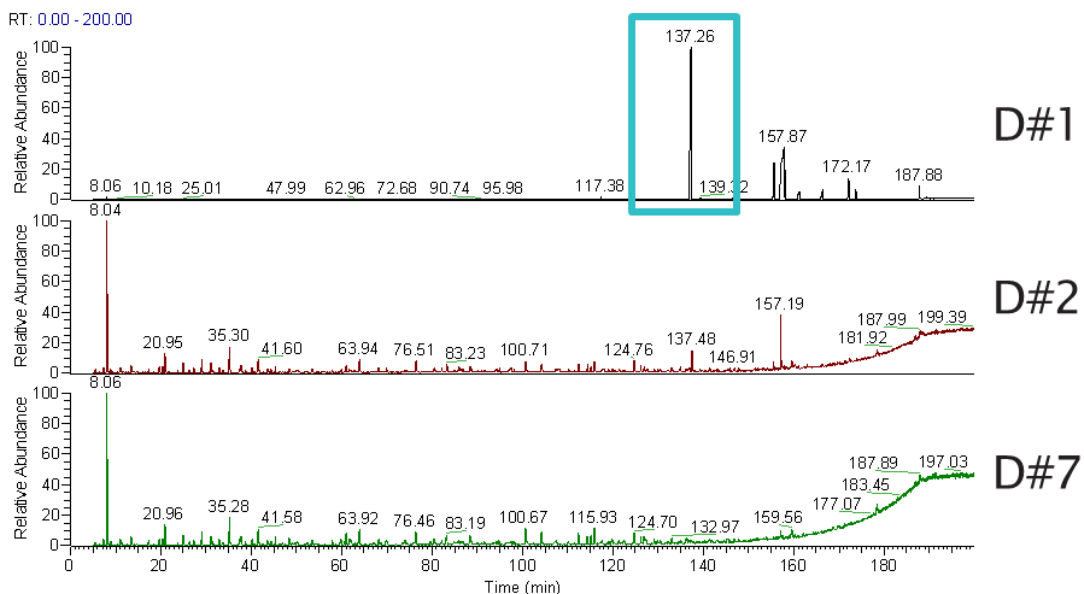


Figure 4-6 - combined mass spectrum of D#1 at  $t_R$  155.4 - 155.8 min analysed using polar column GC-MS at split ratio 50 and ramp rate 1 °C/min

Utilising the FAMES RICCs method, Figure 4-7 shows RICCs of FAMES ( $m/z$  74 and 87) for D#1, D#2 and D#7, with a pale blue rectangle highlighting FAME C16:0 abundant in D#1. The corresponding mass spectrum of D#1 at  $t_R$  137.0- 137.3 min is also shown, again ovals highlighting the base peak  $m/z$  74 and 87 as well as a small molecular ion at  $m/z$  270. Library matching mass spectra for each chromatographic peak in a diesel matrix allows for quick compound identification. The NIST library search results are shown outlining a match for FAME C16:0 with an SI of 937.

## Chapter 4



2016\_12\_09\_dies#1\_sr50\_rr1\_#14181-14240 RT: 136.85-137.35 AV: 60 SB: 2 153.91, 156.41 NL: 9.63E5  
T: (0,0) +c EI de=350.00 Full ms [40.00-500.00]

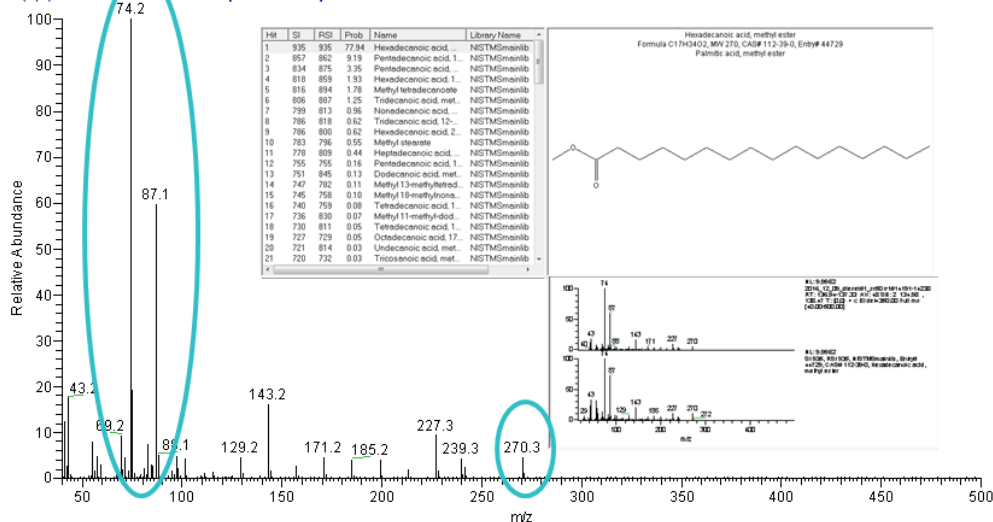


Figure 4-7 – Top - RICCs of C16:0 FAMES ( $m/z$  74, 87) for (D#1, D#2 and D#7).  
Bottom - combined mass spectrum of D#1 at  $t_R$  137.0-137.3 min analysed using polar column GC-MS at split ratio 50 and ramp rate 1 °C/min

Figure 4-8 summarises the use of the FAMES RICCs method for D#1, D#2 and D#7 in the FAME region of interest. It demonstrates, particularly in D#1, how differentiation and identification of different FAMES (carbon number: number of double bonds) was achieved utilising polar column GC-MS. This allows different feedstocks of biodiesel to be identified by different ratios of FAMES species present, as have different fatty acid, therefore FAME compositions dependent on oil type e.g. coconut, rapeseed, soybean<sup>218</sup>.

Base peaks for aliphatic hydrocarbons were found to be  $m/z$  43 and 57, and bases peaks for aromatic hydrocarbons were found to be  $m/z$  77 and 91.

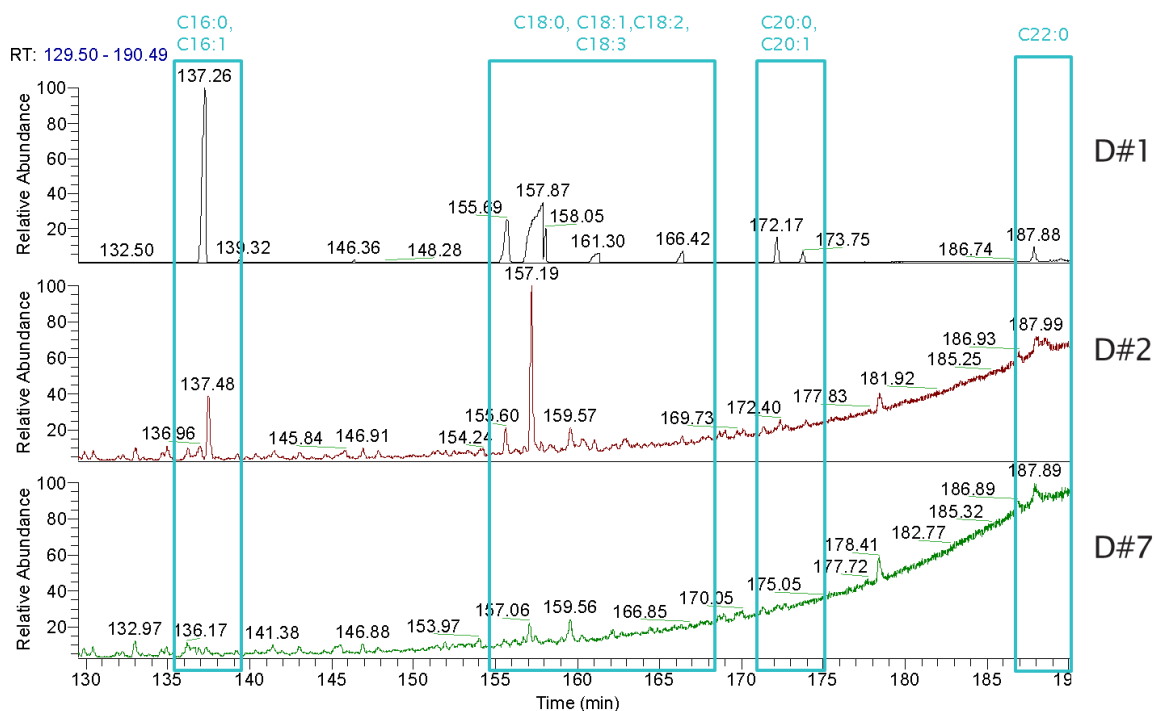


Figure 4-8 - RICCs  $m/z$  74 and 87 for D#1, D#2 and D#7 analysed using polar column GC-MS at split ratio 50 and ramp rate 1 °C/min

Figure 4-9 shows the utilisation of RICCs of aliphatic hydrocarbons ( $m/z$  43 and 57) for D#1, D#2 and D#7, with a pale blue rectangle highlighting an aliphatic hydrocarbon abundant in D#2 at 118.14 min. The corresponding mass spectrum of D#2 at  $t_R$  117.1- 118.5 min is also shown, again ovals highlighting base peak  $m/z$  57 and an abundant ion at  $m/z$  43, as well as a small molecular ion at  $m/z$  282. The NIST library search results are shown outlining a match for eicosane with an SI of 897.

# Chapter 4

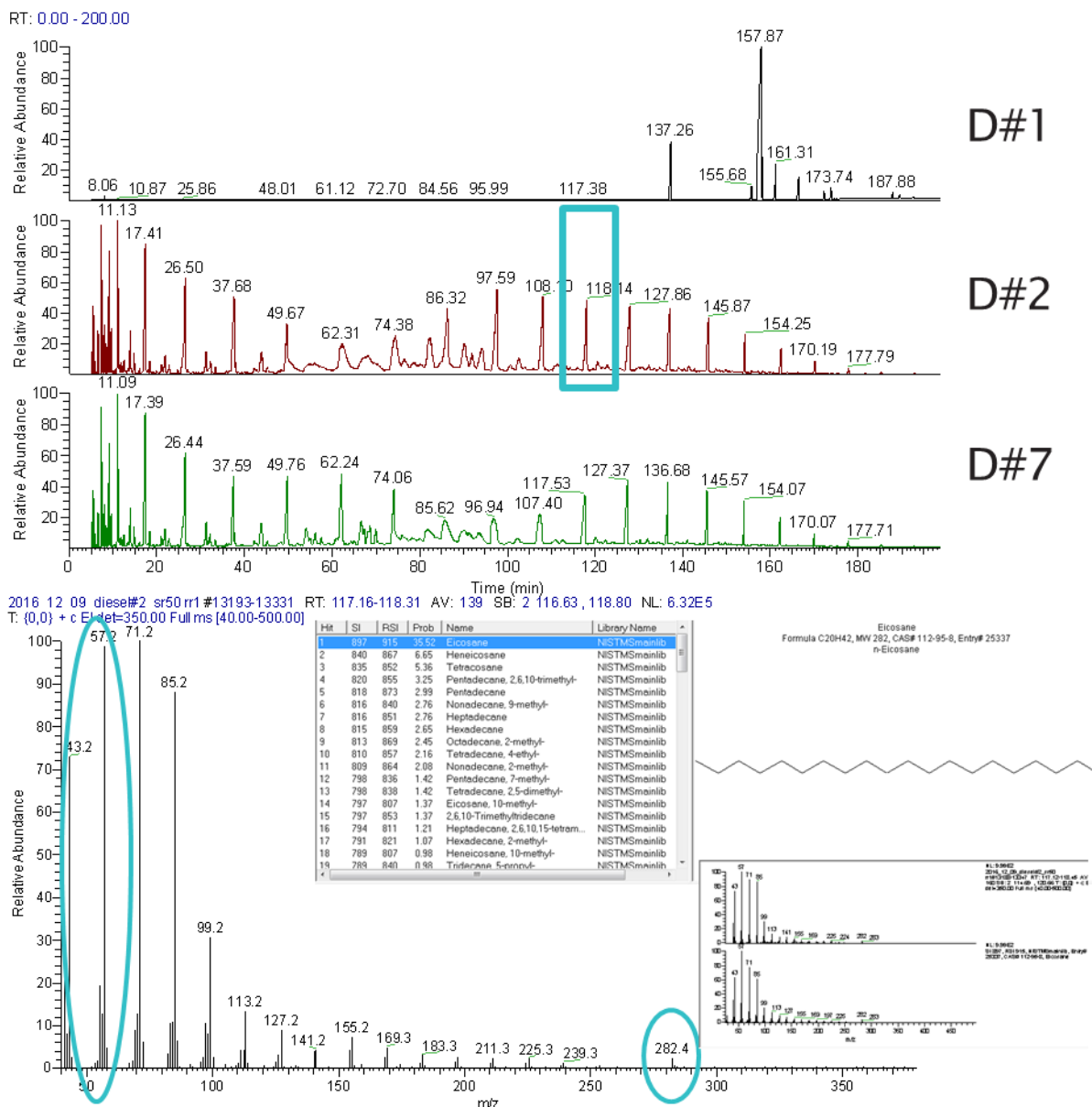


Figure 4-9 - Top - RICCs of aliphatic hydrocarbons ( $m/z$  43, 57) for (D#1, D#2 and D#7). Bottom - combined mass spectrum of D#2 at  $t_R$  117.1-118.5 min analysed using polar column GC-MS at split ratio 50 and ramp rate 1 °C/min

Figure 4-10 shows the utilisation of RICCs of aromatic hydrocarbons ( $m/z$  77 and 91) for D#1, D#2 and D#7, with a pale blue rectangle highlighting an aromatic hydrocarbon abundant in D#2 at  $t_R$  20.94 min. The corresponding mass spectrum of D#2 at  $t_R$  20.91 min is also shown, again ovals highlighting base peak  $m/z$  91 and an abundant ion at  $m/z$  77, as well as a molecular ion at  $m/z$  106. The NIST library search results are shown outlining a match for ethylbenzene with an SI of 906.



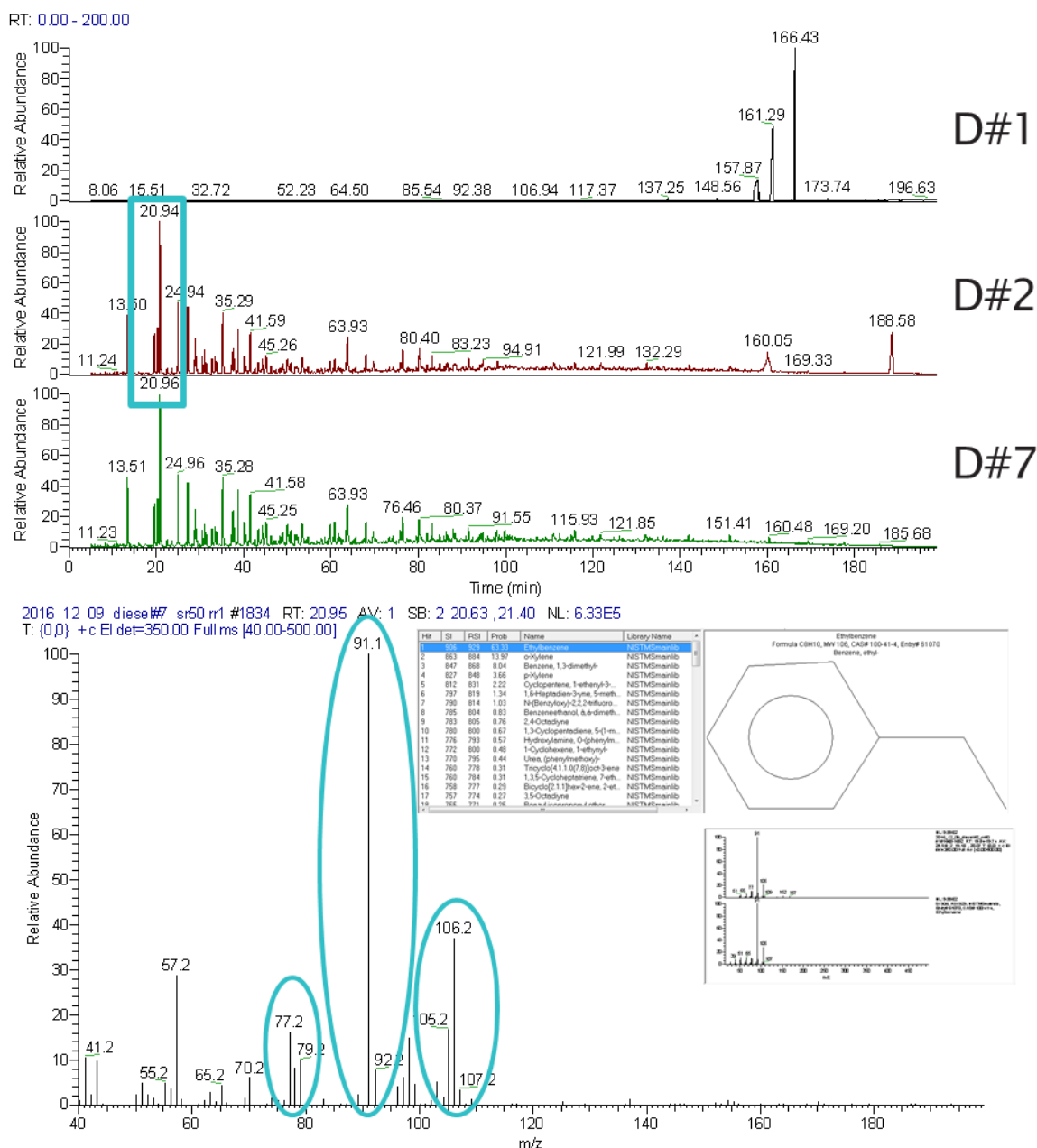


Figure 4-10 - Top -RICCs of aromatic hydrocarbons ( $m/z$  77, 91) for (D#1, D#2 and D#7). Bottom -combined mass spectrum of D#2 at  $t_R$  20.91 min. analysed using polar column GC-MS at split ratio 50 and ramp rate 1 °C/min

D#1 (commercial biodiesel) contains only FAMES *i.e.* B100. FAMES C16:1,0 , C18:3,2,1,0 , C20:1,0 and C22:0 are all observed in D#1.

FAMES are not observed in TICCs in D#2 and D#7 but can possibly be observed using the FAMES RICCs method ( $m/z$  74 and 87) and are shown at a very low abundance.

D#2 and D#7 are similar with varying abundances of aliphatic (RICCs  $m/z$  43 and 57) and aromatic (RICCs  $m/z$  77 and 91) base fuel hydrocarbon compounds and appear different from D#1.

Only base fuel hydrocarbons and FAMEs in diesels are observed by polar column GC-MS, so some compounds and additives could be missed. Although other compounds may be observed *via* derivatisation prior to GC-MS analysis.

#### **4.2.3 Automated analysis method (including comparison) for polar column GC-MS data using SpectralWorks AnalyzerPro<sup>®</sup> software**

Using the manual analysis method, the deposit forming and non-deposit forming diesels still looked similar with the only major difference being FAMEs content and varying abundance of base fuel hydrocarbons. This suggests identification of subtle differences may be key for determining a correlation between components within fuels and deposit formation.

The use of an automated analysis processing method for polar column GC-MS TICCs affords quick identification of peaks/components and possibly compounds, if linked to a library, within diesel samples. Detected peaks/identified compounds can be cross checked and compared with peaks and compounds present in other diesel samples. Numerical similarity values can also be calculated between diesel fuels as a percentage, which allows for easy comparison of diesels.

These additional tools provided by an automated analysis processing method mean subtle differences may be emphasized.

##### **4.2.3.1 SpectralWorks AnalyzerPro<sup>®</sup>**

SpectralWorks AnalyzerPro<sup>®</sup> is a “productivity software application” which provides rapid analysis of data sets<sup>219</sup>. It can provide direct sample to sample comparison and mass spectral library searching.

SpectralWorks AnalyzerPro<sup>®</sup> software works in the following way for each GC-MS chromatogram and analysis takes place as described.

Initially component identification is undertaken using RICCs for each  $m/z$  present under the TICC at each retention time (Figure 4-11).

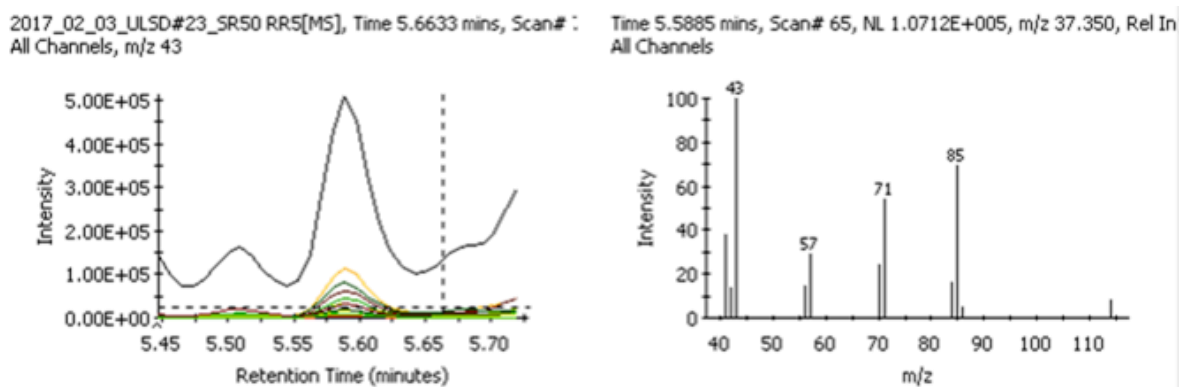


Figure 4-11 - Screenshot from SpectralWorks AnalyzerPro® software showing component identification using RICCs for each  $m/z$  present under the TICC at each retention time

From this, individual components are identified which correspond to compounds present in the sample (Figure 4-12).

2017\_02\_03\_ULSD#23\_SR50 RR5[MS], Time 27.7733 mins, Scan#  
All Channels, TIC

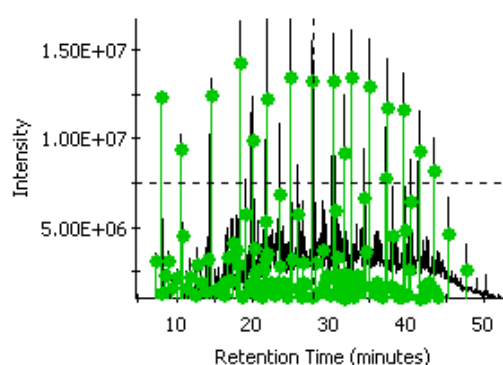


Figure 4-12 - Screenshot from SpectralWorks AnalyzerPro® software showing components identified (each indicated by a green lollipop) on TICC

A component database can then be created for an individual diesel sample which consists of its own specific set of components identified using both retention time and mass to charge ratio ( $m/z$ ). For EI MS data, the identified components are then subjected to a NIST 2014 Mass Spectral Library search to see if particular compounds can be matched to the mass spectrum of each individual component (Figure 4-14).

Summary Report																				
RT	Scan	Start RT	End RT	Area	Area %	Total %	Height	Width	Purity	Base Peak	Ions	Confidence	Forward	Reverse	Target Component	Confidence %	Forward			
2	5.5885	65	5.5333	5.6390	925448	1.25	0.04	396944	0.1057	62.87	43	11	89.48%	905	879	Heptane, 2,4-dimethyl-	88.60	886	886	2213-23
3	5.7202	80	5.6470	5.7970	200683	0.27	0.01	65023	0.1500	13.73	43	4	99.53%	1000	993	2017_02_01_ULSD#23 1%RME_SR50_RRS_0001				
4	5.9394	105	5.8280	6.0352	1157135	1.56	0.05	333291	0.2072	37.97	97	9	92.36%	934	903	Cyclohexane, 1,3-dimethyl-	86.80	868	868	591-21-
5	6.4298	161	6.3452	6.4918	2367350	3.20	0.09	612063	0.1465	58.86	43	12	89.96%	883	947	Heptane, 2,3-dimethyl-	88.10	881	881	3074-71
6	6.6665	188	6.6073	6.7730	960901	1.30	0.04	267230	0.1657	21.39	57	10	95.59%	941	1000	Octane, 3-methyl-	85.30	853	853	2216-33
7	6.8768	212	6.7847	7.0137	3138308	4.24	0.13	716309	0.2290	62.31	69	15	93.08%	925	949	2017_02_01_ULSD#23 1%RME_SR50_RRS_0002	81.08	809	815	3073-66
8	7.2803	258	7.1788	7.3325	861666	1.16	0.03	279564	0.1537	21.35	69	4	99.35%	1000	984	Cyclohexane, 1,3,5-trimethyl-	80.50	805	805	1839-63
9	7.3324	264	7.1977	7.4969	1997023	2.70	0.08	421375	0.2992	9.60	83	4	99.45%	999	993	Cyclohexane, ethyl-	87.90	879	879	1678-91
10	7.3676	268	7.2660	7.5144	13859045	18.72	0.55	3183099	0.2485	70.73	43	25	98.87%	984	1000	Nonane	93.20	932	932	111-84-
11	7.6114	296	7.5175	7.6411	602281	0.81	0.02	201024	0.1236	31.24	71	6	94.82%	947	955	Heptane, 3,3,4-trimethyl-	81.82	799	863	20278-8
12	7.7082	307	7.6494	7.7982	1608216	2.17	0.06	480497	0.1488	34.38	71	13	96.84%	956	1000	2017_02_01_ULSD#23 1%RME_SR50_RRS_0003				

Figure 4-14 - Screenshot from SpectralWorks AnalyzerPro® software showing component database showing any components which have also been matched using NIST 2014 mass spectral library

Two components databases for two diesels can then be compared to each other and a percentage similarity/confidence calculated (Figure 4-13).

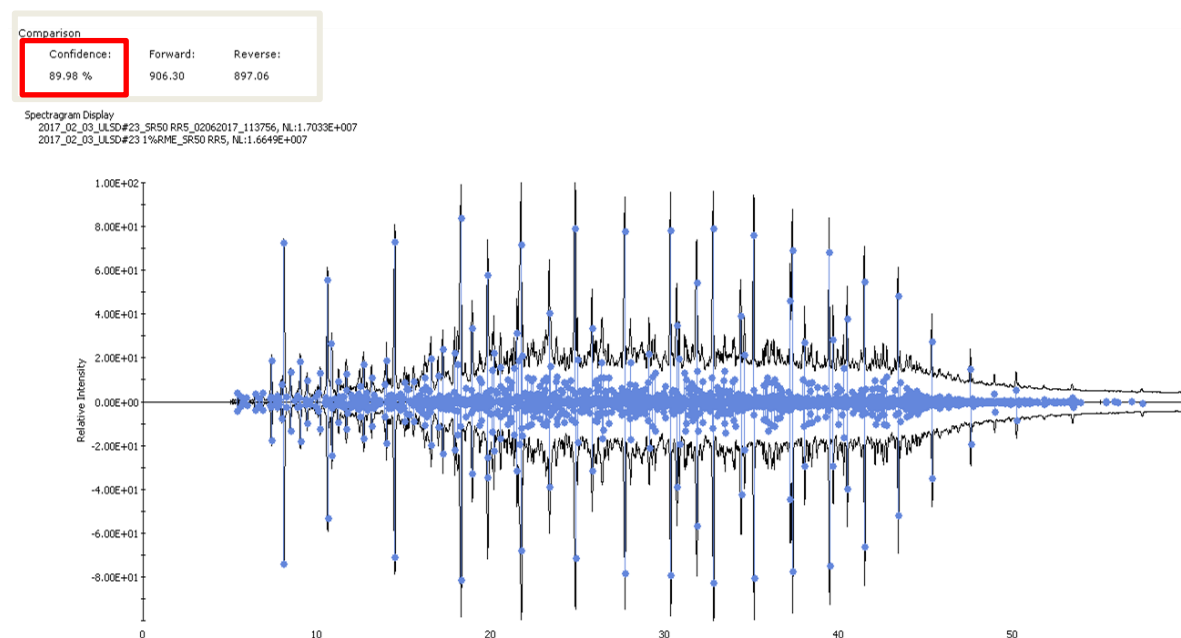


Figure 4-13 - Screenshot from SpectralWorks AnalyzerPro® software showing comparison of two component databases with percentage confidence calculated as indicated by red box

#### 4.2.4 Automated data analysis of polar column GC-MS of nine diesels

Polar column GC-MS data files of the nine diesel samples (D#1-D#9) (Figure 4-2 and Figure 4-3) from one continuous analysis (to reduce issues around retention time drift) were analysed using SpectralWorks AnalyzerPro® in order to identify components present and therefore collate individual component databases, similar to a fingerprint as unique, for each diesel. This enabled direct comparisons to be made between any two fuels in order to obtain a percentage similarity

for each chromatogram when compared to another in the data set (**Error! Reference source not found.**).

**Error! Reference source not found.** shows the heat mapped percentage similarities obtained for pairs of diesel component databases using SpectralWorks AnalyzerPro®, with green being most similar and red the least similar. 100% matches are observed when a diesel is compared with itself and is shown in green. Any big differences observed show a diesel is very different to all the other diesels, at least in base fuel and FAMES composition (as detected by GC-MS).

Table 4-1 - Percentage similarities obtained from SpectralWorks AnalyzerPro® component database comparison of chromatograms of all nine diesels acquired via GC-MS using a polar column at split ratio 50 and ramp rate of 1 °C /min

Chromatogram comparison (% Similarity)									
	D#1	D#2	D#3	D#4	D#5	D#6	D#7	D#8	D#9
D#1	100	20	54	53	78	52	21	35	52
D#2	21	100	43	42	61	42	78	2	40
D#3	39	34	100	65	89	63	35	47	5
D#4	38	33	65	100	89	63	33	79	6
D#5	49	39	75	75	100	74	40	57	74
D#6	38	33	64	63	89	100	34	46	63
D#7	21	77	44	43	62	43	100	30	40
D#8	31	5	57	84	82	55	29	100	3
D#9	39	28	13	13	89	63	29	8	100

Percentage similarities appear to be quite varied between diesels, suggesting differences are present. D#2 and D#7 only ~30-40% similar with other fuels except with each other, also D#1 also only 20-50% similarity to other fuels. It appears that either the absence or presence (high abundance) of FAMES is resulting in these differences. Low percentage similarities (<20%) can be seen with pairs of anomalies for some comparisons of two particular fuels highlighted with black boxes. It is unknown why these anomalies have occurred in D#9 although percentage similarity was very variable in the eight diesels when compared with D#9 showing many pairs of anomalies. D#9 was observed to have an abundance of FAMES, however further investigation is needed to determine the root cause.

#### 4.2.5 Summary of polar column GC-MS findings (automated analysis)

SpectralWorks AnalyzerPro® provides a rapid screening method that creates component databases for each diesel, which can then be compared to another diesel component database

providing percentage similarity. These percentage similarities highlight differences and similarities seen between pairs of diesels, however FAMEs seem to play a part in influencing percentage similarity.

Overall, GC-MS (EI) using a polar column afforded detection of base fuel hydrocarbons (aliphatic and aromatic) and FAMEs in diesel fuels. However, diesel samples still appear very similar and some compounds and additives could be missed, therefore multiple analytical techniques are required for diesel analysis.

### **4.3 Diesel fuels component screening methodology – UHPSFC-MS and FT-ICR MS analysis**

As with the SpectralWorks AnalyzerPro<sup>®</sup> approach, the concept of a quick screening methodology appeared a logical way to characterise diesels, observing similarities and differences. However, instead of an untargeted approach as illustrated previously by polar column GC-MS (section 4.2), a targeted approach screening for known deposit forming compounds was believed to be a better approach. This methodology would differentiate the fuels by the presence of deposit forming compounds in the hope of linking fuels with a propensity to form deposits.

Firstly, known deposit forming compounds (with well documented masses) were chosen from literature for the screening method, then for each compound or class of compound chosen an appropriate analysis technique identified. The analytical technique chosen may also show other compounds not just the targeted deposit forming compound of interest.

The following deposit-forming compounds were highlighted:

- Fatty acid methyl esters (FAMEs)
- Fatty acid methyl ester (FAME) oxidation products
- Free fatty acids (FFAs)
- Sterol glucosides (SGs)
- Monoacylglycerols (MAGs)

Polar column GC-MS (EI) only allows detection of FAMEs and hydrocarbons meaning other chromatographic methods as well as different MS ionisation techniques are needed to observe the deposit forming compounds of interest for the proposed screening method.

Chromatography is advantageous for diesel analysis as it separates complex mixtures. An alternative chromatographic method, ultra-high performance supercritical fluid chromatography-mass spectrometry (UHPSFC-MS) (discussed previously in chapter 2.4) was used as it has many favourable properties for diesel and biodiesel analysis including the compatibility of undiluted petrochemical fuels with  $scCO_2$  due to its hexane-like, non-polar properties. UHPSFC-MS has been used previously for both diesel<sup>7</sup> and biodiesel<sup>92, 168, 220</sup> analysis (discussed in greater detail in 1.1.4).

Positive electrospray ionisation (ESI) was used, this technique is a selective atmospheric pressure ionisation technique that ionises compounds of a much wider range of molecular weight species than EI, and of medium to high polarity (basic compounds with site of protonation *e.g.* amines), therefore rendering non-polar base fuel hydrocarbons invisible, meaning other compounds can be more easily observed<sup>221-222</sup>. Negative ESI was used to ionise acidic compounds with a site of deprotonation *e.g.* carboxylic acids. ESI is also a soft ionisation technique resulting in no or very little fragmentation.

Atmospheric pressure ionisation (API) techniques have been commonly used in the analysis of crude oils<sup>222</sup> (especially APPI)<sup>199, 221</sup>, diesels (ESI and APCI<sup>223</sup>, APPI<sup>6</sup>) as well as biodiesels<sup>224</sup>, lipids<sup>201, 225</sup>, and vegetable oils<sup>226</sup>.

Similarities and differences were observed in the nine diesels by positive ion ESI UHPSFC-MS compared with the diesels looking very similar by polar column GC-MS.

However, direct infusion Fourier transform-ion cyclotron resonance mass spectrometry (FT-ICR MS) was also utilised due to its advantages over low resolution quadrupole mass spectrometry (used in UHPSFC-MS); high mass accuracy and high resolving power. As a result of this, identification using molecular formulae for elemental compositions can be calculated (using monoisotopic masses) from the measured accurate mass of the species. This also allows separation of nominally isobaric species (same nominal  $m/z$ , different chemical formulae) observed by low resolution mass spectrometry.

Nine diesel fuel samples (D#1-D#9) were prepared as outlined in 3.2.1 for respective methods. Undiluted diesels (D#1-D#9) were analysed using the described positive and negative ion ESI UHPSFC-MS methods. The diluted 6:4 toluene: methanol solvent mix for each sample was analysed using the described direct infusion positive and negative ion ESI FT-ICR MS method.

One example of each known deposit-forming compound found to be present within the diesel fuels is shown in detail, comparing and contrasting a variety of both positive and negative ion ESI UHPSFC-MS and FT-ICR MS data. The key findings of each diesel fuel sample will be discussed with

## Chapter 4

similarities between diesel fuel samples outlined and the diesels grouped by compounds present. However, only the screened deposit forming components have been highlighted below, further analysis in greater detail still needs to be undertaken and may uncover further components of interest as minor components or at trace levels.

UHPSFC-MS data is shown as base peak ion current chromatograms (BPICCs) throughout this project. A BPICC only shows the intensity of the most intense peak at a given retention time, compared with a TICC that shows the intensity of the sum of all ions present at a given retention time. BPICCs were utilised in this project as they produce chromatograms with less noise than TICCs, that are easier to take in and understand.

Confirmation that the chromatographic peaks in UHPSFC-MS data are most likely related to a compound of interest and their associated nominal  $m/z$  values (commonly  $[M + NH_4]^+$  and  $[M + H]^+$  or  $[M + Na]^+$  in positive ion ESI data) is achieved using RICCs (similar to GC-MS). Peaks should have a matching specific retention time with the associated nominal  $m/z$  values for the compound of interest.

### Key method information: Positive ion ESI methods

Compounds are observed most abundantly as ammoniated molecules  $[M + NH_4]^+$  using the positive ion ESI UHPSFC-MS method in this project. Protonated and sodiated molecules are also observed but at a much lower abundance as ammonium acetate is used as an additive in the modifier and make-up solvent to force ammoniation.

The chromatographic separation of the UHPSFC-MS method affords both separation of the compounds by chain length as well as by degree of saturation. The longer the carbon chain, the longer the retention on the column (longer elution time) *e.g.* FAME C18 has a longer elution time compared to FAME C16. Also the greater the degree of saturation, the longer the retention on the column (longer elution time) *e.g.* FAME C18:0 has a longer elution time than FAME C18:3. This is illustrated in the RICCs shown in Figure 4-19.

Compounds are most abundantly observed as sodiated molecules  $[M + Na]^+$  when using direct infusion positive ion ESI FT-ICR MS. Protonated molecules  $[M + H]^+$  are also observed, however due to excess sodium ions in the FT-ICR MS sodiated molecules are often preferentially observed.

### Key method information: Negative ion ESI methods

Compounds are most abundantly observed as deprotonated molecules  $[M - H]^-$  using both direct infusion negative ion ESI FT-ICR MS and negative ion ESI UHPSFC-MS.



### 4.3.1 Fatty acid methyl esters (FAMES)

FAMES have previously been linked to both fuel filter blocking and IDIDs, see chapter 1. Diesel blends containing biodiesel (FAMES) have an increased likelihood to form deposits or fouling in fuel filters and fuel injectors<sup>85, 227</sup>, however deposit issues have also been reported in mineral diesel fuels<sup>52</sup>. Therefore bio-components are believed to play some contributing role to deposit formation due to their unstable nature, but are not the sole cause of deposit formation<sup>85, 120</sup>.

As FAMES, have been highlighted as a deposit forming compound and have known well documented masses and structures in literature<sup>168</sup>, but the role they play within deposit formation is not fully understood, they provided a good starting point to develop the diesel fuel component screening method.

FAMES were previously detected by polar column GC MS (section 4.2), providing complimentary data for additional comparison. However, the diesels looked similar and were difficult to differentiate by polar column GC-MS (EI) meaning an alternative analysis technique such as UHPSFC-ESI MS was needed.

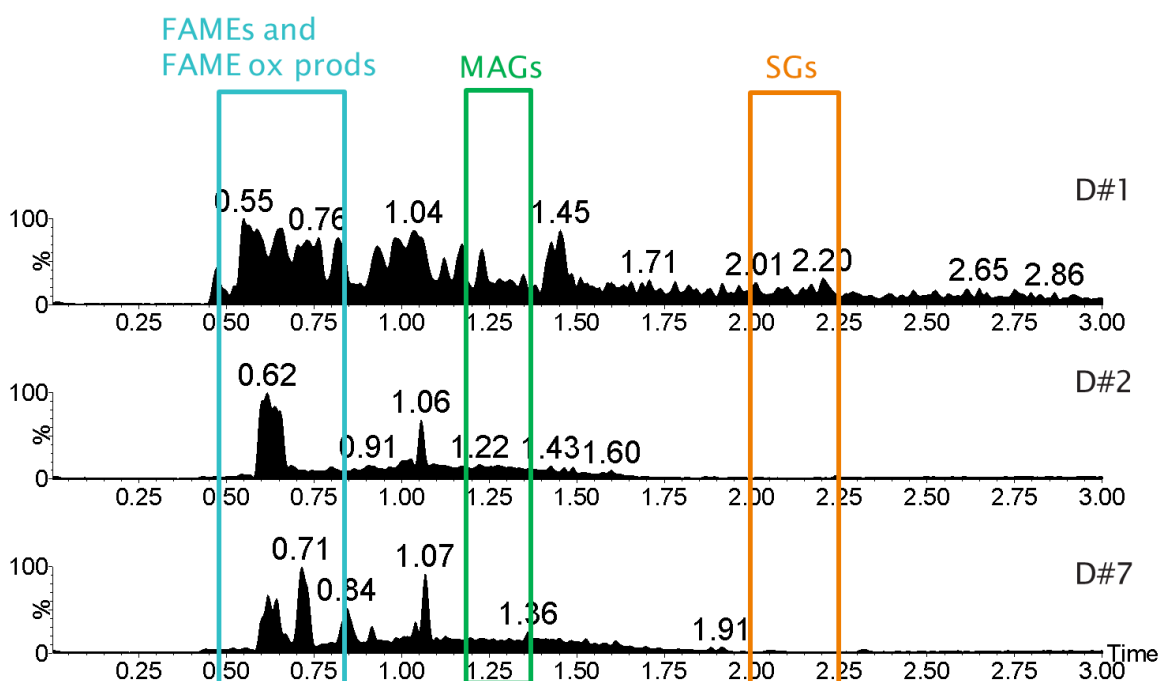


Figure 4-15 - Positive ion ESI BPICCs of D#1, D#2 and D#7 with retention regions highlighted for compounds of interest

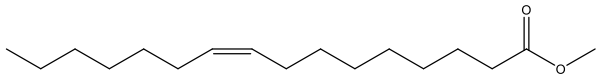
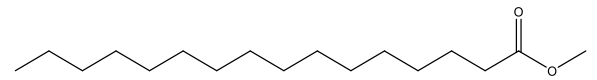
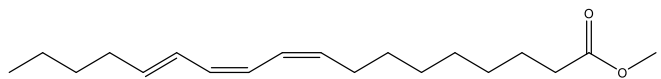
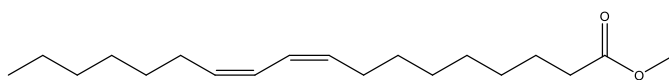
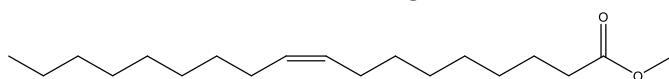
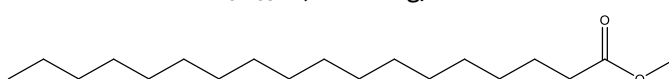
## Chapter 4

Figure 4-15 demonstrates visual differences and similarities observed in positive ion ESI UHPSFC-MS BPICCs of D#1, D#2 and D#7. The screening compound regions of retention are highlighted, however free fatty acids are not included in this figure, as they are observed by negative ion ESI UHPSFC-MS in this screening method.

Table 4-2 shows a summary of FAMEs to be screened for, their respective molecular formulae and structures, adducts that can be present and their associated masses. Nominally isobaric species are in bold and underlined. FAME and fatty acid shorthand nomenclature is as follows; CY:Z where Y is the number of C, carbon atoms, in the fatty acid chain and Z is the number of double bonds (therefore degree of saturation).

Nominally isobaric species are observed with both  $[C_{16}:0 + Na]^+$  and  $[C_{18}:3 + H]^+$  at nominal  $m/z$  293, with only 0.0024  $m/z$  units difference (observed) between the monoisotopic masses of the two species. Separation of these species ( $[C_{16}:0 + Na]^+$  at  $m/z$  293.2456 and  $[C_{18}:3 + H]^+$  at  $m/z$  293.2480) can be achieved by FT-ICR MS, as well as complimentary adduct ions (e.g.  $[C_{16}:0 + H]^+$  at  $m/z$  271.2636 and  $[C_{18}:3 + Na]^+$  at  $m/z$  315.2295) being observed to provide confirmation of compounds present. Additionally, observation of  $[C_{16}:0 + NH_4]^+$  at nominal  $m/z$  288 and  $[C_{18}:3 + NH_4]^+$  at nominal  $m/z$  310 in positive ion ESI UHPSFC-MS data would also aid confirmation.

Table 4-2 FAMES summary (nominally isobaric species are in bold and underlined)

FAMES (Carbon number: number of double bonds)	Molecular formula, exact mass and structure	Expected $m/z$ (nominal for UHPSFC-MS, monoisotopic (4 dp) for FT-ICR MS)		
		$[M + H]^+$	$[M + NH_4]^+$	$[M + Na]^+$
C16:1	$C_{17}H_{32}O_2$ , 268.24 g/mol 	269.2475	286 ( $t_R$ :0.58 min)	291.2301
C16:0	$C_{17}H_{34}O_2$ , 270.26 g/mol 	271.2636	288 ( $t_R$ :0.60 min)	<b><u>293.2456</u></b>
C18:3	$C_{19}H_{32}O_2$ , 292.24 g/mol 	<b><u>293.2480</u></b>	310 ( $t_R$ :0.60 min)	315.2295
C18:2	$C_{19}H_{34}O_2$ , 294.26 g/mol 	295.2636	312 ( $t_R$ :0.62 min)	317.2451
C18:1	$C_{19}H_{36}O_2$ , 296.27 g/mol 	297.2791	314 ( $t_R$ :0.64 min)	319.2608
C18:0	$C_{19}H_{38}O_2$ , 298.29 g/mol 	299.2945	316 ( $t_R$ :0.68 min)	321.2765

D#1 is used as the example to illustrate the presence of FAMES within biodiesel, as it (commercial B100) can act as a FAMES standard as it is 100% biodiesel, meaning the assignment of the FAMES can be given with reasonable confidence. FAMES were also observed in diesel fuels but at a lower level so D#1 was the best example for this.

## Chapter 4

FAMES were found to elute at  $t_R$  0.55-0.70 min as shown in Figure 4-16 (positive ion ESI UHPSFC-MS base peak ion current chromatogram (BPICC) of D#1). The corresponding positive ion ESI UHPSFC mass spectrum shown in Figure 4-17, shows ammoniated molecules  $[M + NH_4]^+$  observed at nominal  $m/z$  286-316 that are consistent with compounds of nominal mass 268-298 g/mol, is in agreement with nominal masses of FAMES from literature<sup>168</sup>.

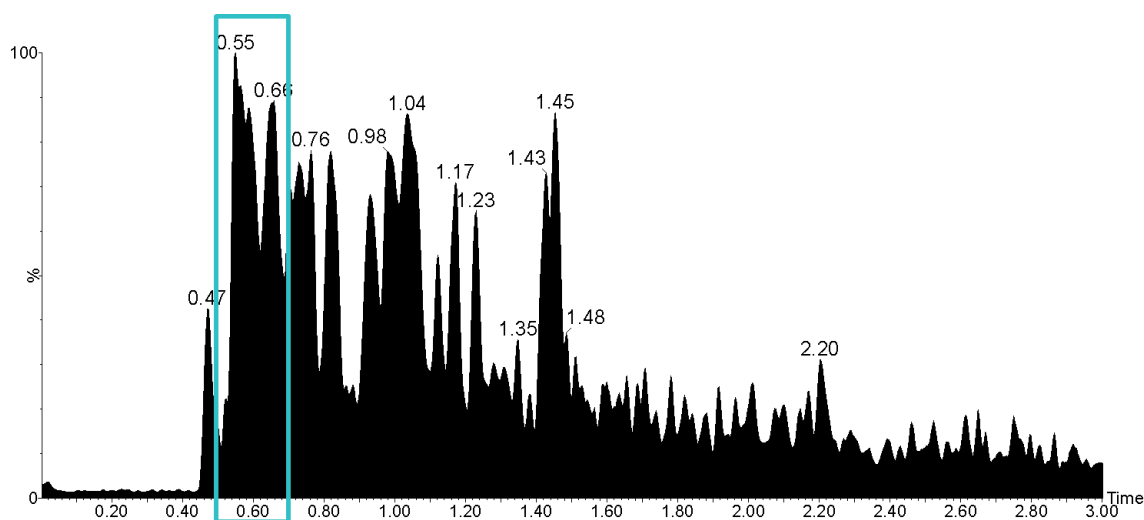


Figure 4-16 –Positive ion ESI UHPSFC-MS BPICC of D#1 with pale blue box highlighting FAMES region of retention ( $t_R$  0.55-0.70 min)

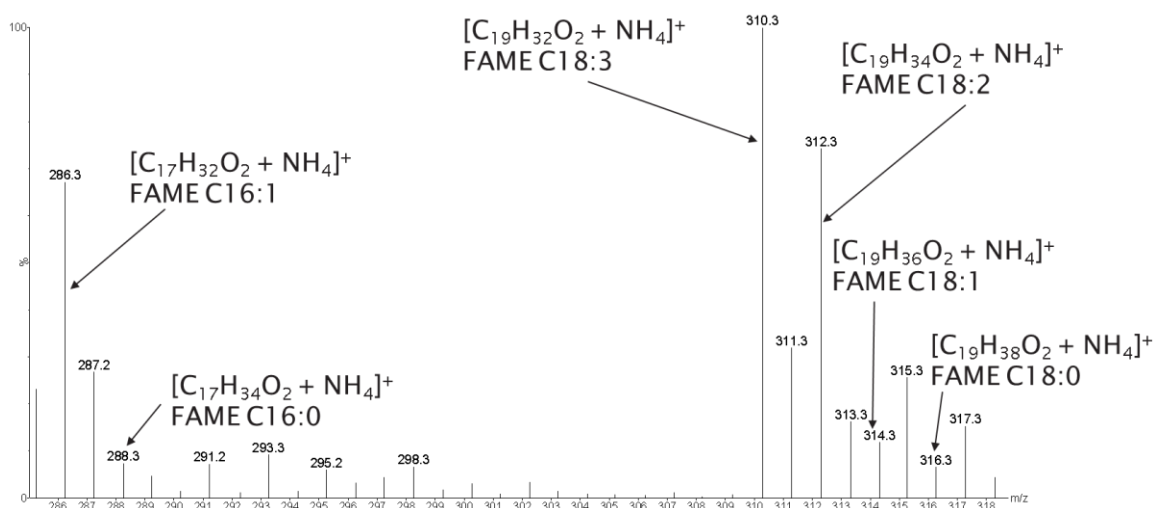


Figure 4-17 - Positive ion ESI UHPSFC mass spectrum of D#1 at  $t_R$  0.55-0.70 min, zoomed range  $m/z$  285-319

RICCs of associated  $m/z$  values for FAMES ( $[M + NH_4]^+$  as shown in Table 4-2) were used as shown in Figure 4-19. The peaks observed are highly consistent with C16:1, C16:0, C18:3, C18:2, C18:1 and C18:0 FAMES.

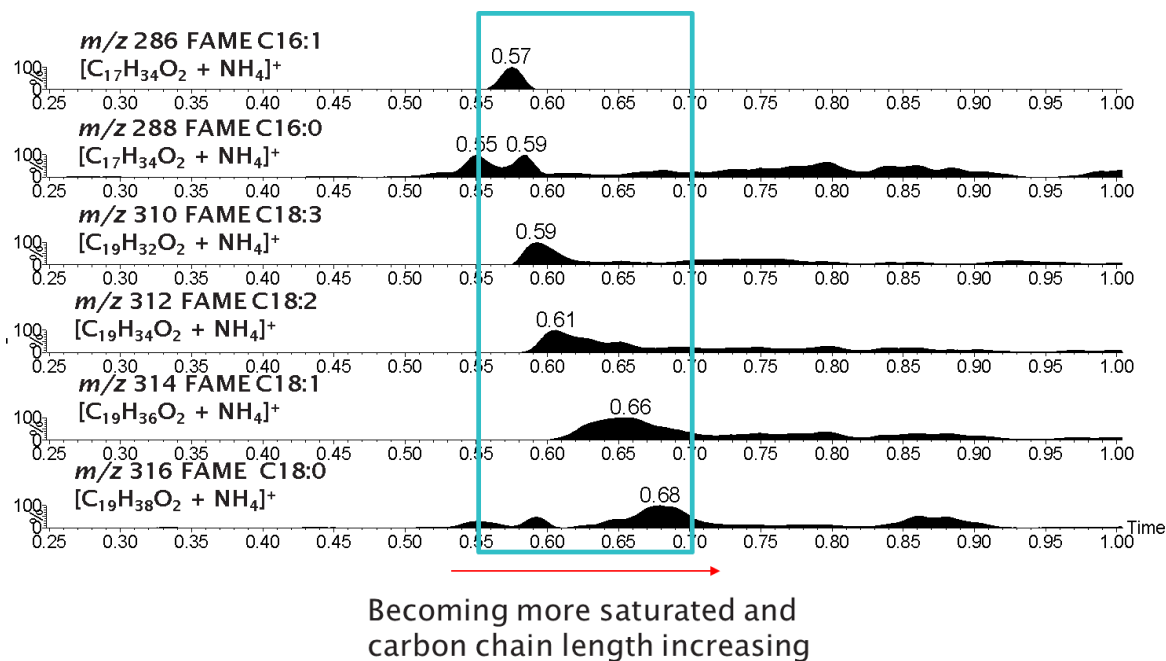


Figure 4-19 –Positive ion ESI UHPSFC-MS RICCs of D#1 showing FAMES with pale blue box highlighting FAMES region of retention (t<sub>r</sub> 0.55-0.70 min)

Figure 4-18 shows sodiated molecules observed for FAMES C16:1, C16:0, C18:3, C18:2, C18:1 and C18:0 when using direct infusion positive ion ESI FT-ICR MS (Table 4-2). This is in agreement with proposed FAMES observed in the positive ion ESI UHPSFC-MS data for D#1 with the sodium adducts further confirming presence of FAME species with accurate mass measurements providing formulae, increasing confidence in compound assignments.

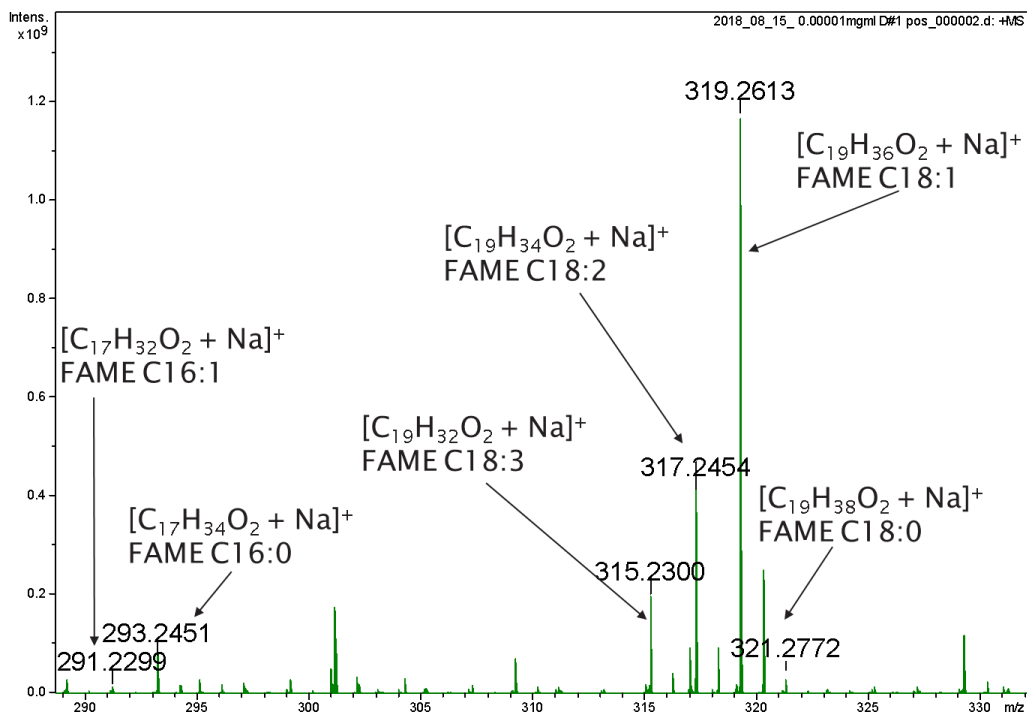


Figure 4-18 - Direct infusion positive ion ESI FT-ICR mass spectrum of D#1 (zoomed m/z 290-330), showing sodiated molecules for FAMES

## Chapter 4

Table 4-3 shows a summary of the FAMES detected in nine diesel fuel analysed. The symbol X\* has been utilised for results when the nominal  $m/z$  was initially detected by positive ion ESI UHPSFC-MS in RICCs, however the presence of the compound by monoisotopic mass was not detected by direct infusion positive ion ESI FT-ICR MS.

Table 4-3 - Diesel fuels FAMES summary (✓=detected, X=not detected, X\* = nominal mass detected by positive ion ESI UHPSFC-MS, but monoisotopic mass not detected by positive ion ESI FT-ICR MS)

	FAMES (carbon number: number of double bonds)						
		C16:1	C16:0	C18:3	C18:2	C18:1	C18:0
Diesels	D#1	✓	✓	✓	✓	✓	✓
	D#2	✓	✓	✓	✓	✓	✓
	D#3	✓	✓	✓	✓	✓	✓
	D#4	X*	X	✓	✓	✓	✓
	D#5	✓	✓	✓	✓	✓	✓
	D#6	X*	X	✓	✓	✓	X*
	D#7	X	X	✓	✓	✓	X
	D#8	X*	X	✓	✓	✓	✓
	D#9	X*	X	✓	✓	✓	✓

FAMES were observed to be detected in all nine fuels during analysis, with all diesels containing FAMES C18:3, C18:2, and C18:1.

The major differences observed were all FAMES in the screening method were detected in D#1, D#2, D#3 and D#5. C16 FAMES were not detected in D#4, D#6, D#7, D#8 and D#9 and FAME C18:0 were not detected in D#6 and D#7.

As FAMES are present in all nine diesels it suggests that for deposit formation it is not simply the presence of FAMES that is deposit forming but other factors or compounds and likely to be a complex combination.

These results can be used to split the diesel into 3 groups;

- D#1, D#2, D#3 and D#5
- D#4(?), D#8 and D#9
- D#6 and D#7 (D#4 could also go in here possibly)

These differences and similarities could link specific fuels to deposit formation but further information would be required.

FAMES were observed in D#2 and D#7 with ease using the screening method suggesting this is an improved technique compared with polar column GC-MS. The selectivity of ESI rendered the non-polar base fuel hydrocarbons invisible, providing improved observation of polar species such as FAMES. Positive ion ESI UHPSFC-MS was mostly sufficient, however it cannot separate the nominally isobaric species. Different adducts are present to aid this and positive ion ESI FT-ICR MS was used to confirm the assignment and obtain molecular formulae for increased confidence of assignment.

#### 4.3.2 Fatty acid methyl ester (FAME) oxidation products

FAMES within biodiesel are known to have low stability and are very susceptible to auto oxidation<sup>96</sup>. Auto oxidation is the spontaneous oxidation process over a period of time and is thought to take place *via* a radical pathway<sup>228</sup>. During auto-oxidation, the FAMES in biodiesel reacts with air producing FAME oxidation products including hydroperoxides, aldehydes and alcohols<sup>229-230</sup>.

FAME oxidation products have been linked to filter fouling/blocking as well as both aged fuel IDIDs and metal salt IDIDs<sup>85, 120-121</sup>. Oxidative stress has been found to cause the formation of insolubles and deposits causing filter plugging, injector blockage and component failure<sup>231</sup>.

Table 4-4 shows a summary of the FAMES and FAME oxidation products, their respective molecular formulae, adducts that can be present and their associated masses<sup>96, 232</sup>. Each FAME has a designated colour, dependent on number of double bonds, that match the coloured arrows in Figure 4-20 and Figure 4-22. It should be noted that only C18 FAME oxidation products were

## Chapter 4

screened for in this project as they are the most commonly occurring due to abundance of C18 FAMES in fuels from feedstocks prior to oxidation<sup>92</sup>.



Table 4-4 FAME oxidation products summary

FAMEs (carbon number: number of double bonds)	Molecular formula	Expected $m/z$ (nominal for UHPSFC-MS, monoisotopic for FT-ICR MS)								
		$[M + H]^+$	$[M + NH_4]^+$	$[M + Na]^+$	$[(M + O) + NH_4]^+$	$[(M + O) + Na]^+$	$[(M + 2O) + NH_4]^+$	$[(M + 2O) + Na]^+$	$[(M + 3O) + NH_4]^+$	$[(M + 3O) + Na]^+$
C18:3	$C_{19}H_{32}O_2$	293.2480	310	315.2297	326	331.2249	342	347.2197	358	363.2147
C18:2	$C_{19}H_{34}O_2$	295.2632	312	317.2456	328	333.2400	344	349.2354	360	365.2307
C18:1	$C_{19}H_{36}O_2$	297.2794	314	319.2618	330	335.2560	346	351.2506	362	367.2460

D#5 is used as the example to illustrate FAME oxidation products in diesel fuels (to demonstrate components can be observed at respective biodiesel blending levels *i.e.* B7, and allow the petrodiesel matrix complexity to also be observed). The diesel samples showed that multiple species have the same nominal mass, as the FAME oxidation products. In the positive ion ESI UHPSFC-MS data, multiple peaks at various retention times are observed for these species in RICCs. This makes it difficult to assign peaks with confidence even if expected retention time is known. Whereas direct infusion positive ion ESI FT-ICR MS provides separation of nominally isobaric species due to accurate mass measurements, providing molecular formulae.

Therefore, direct infusion positive ion ESI FT-ICR MS is the preferred technique for FAME oxidation products and will be shown first with positive ion ESI UHPSFC-MS discussed afterwards. However, it should be noted that positive ion ESI FT-ICR MS will only show one species at a given  $m/z$  and not show structural isomer information, although it can be used in conjunction with chromatographic separation in the positive ion ESI FT-ICR MS method.

Figure 4-20 shows ions consistent with the respective FAME oxidation products up to the addition of three addition oxygen atoms were also observed in agreement with Table 4-4.

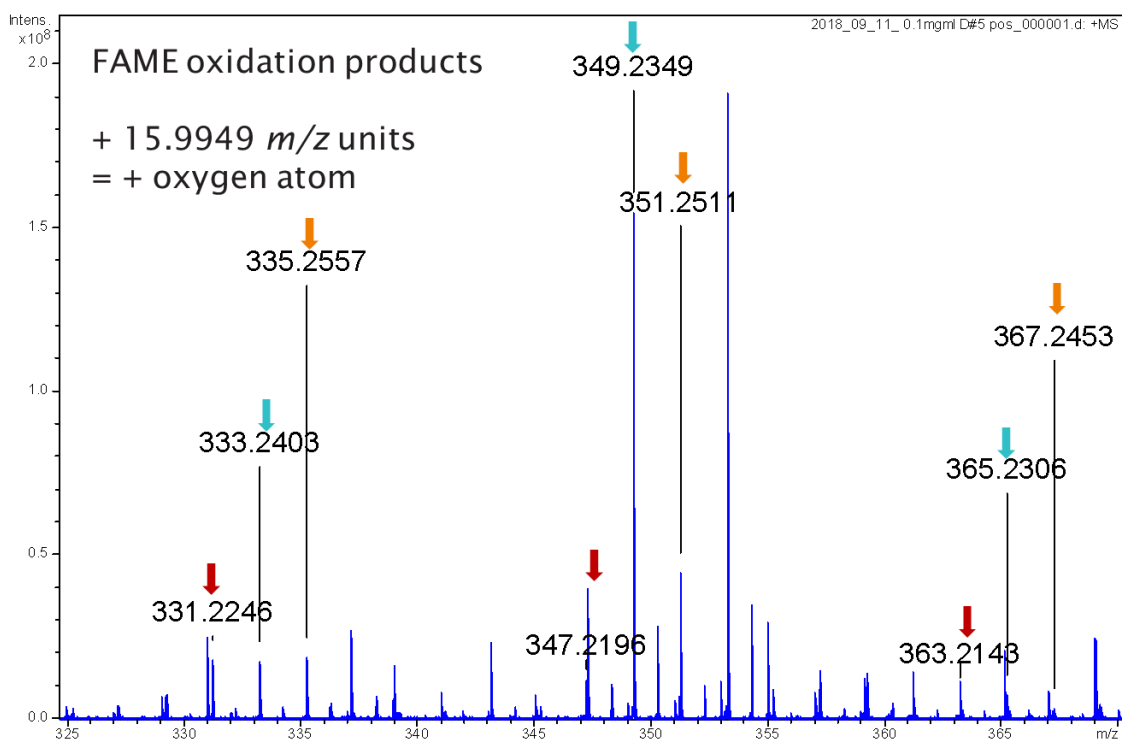


Figure 4-20 - Direct infusion positive ion ESI FT-ICR mass spectrum of D#5 (zoomed range  $m/z$  325-370), showing sodiated molecules for C18 FAME oxidation products up to the addition of three oxygen atoms

The presence of FAME oxidation products is further supported by the absence of a FAME C18:0 oxidation series as saturated species do not undergo auto oxidation readily due to no double bonds being present.

FAMES and FAME oxidation products were found to elute between  $t_R$  0.50-0.80 min as shown in Figure 4-21. The corresponding positive ion ESI UHPSFC mass spectrum shown in Figure 4-22, shows ammoniated molecules  $[M + NH_4]^+$  observed at nominal  $m/z$  310-360, which are consistent with compounds of nominal mass 293-343 g/mol, which is in agreement with FAMES and FAME oxidation product nominal masses as shown in Table 4-4.

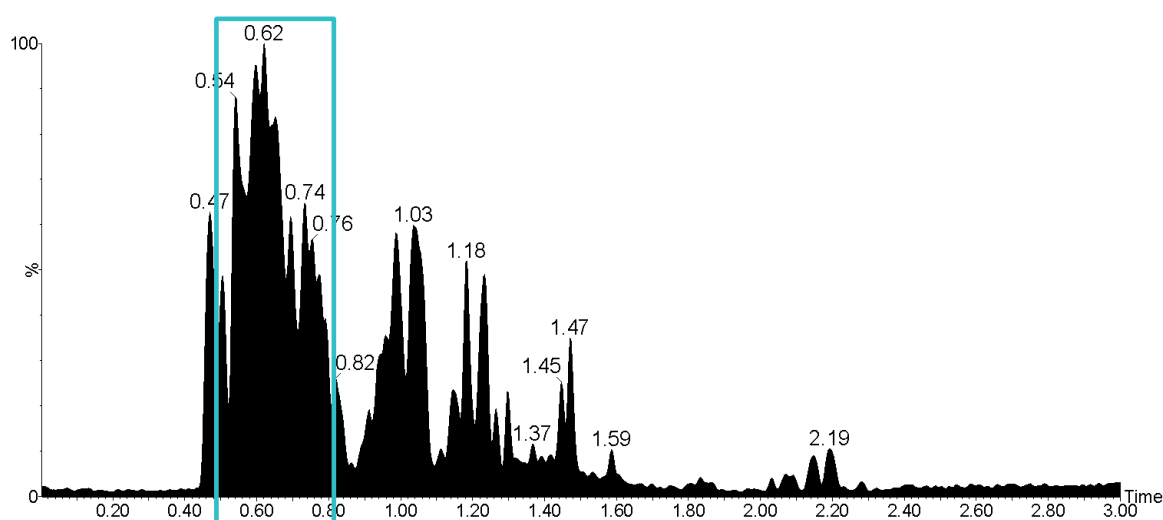


Figure 4-21 – Positive ion ESI UHPSFC-MS BPICC of D#5 with pale blue box

highlighting FAMES and C18 FAME oxidation products region of retention ( $t_R$  0.50 - 0.80 min)

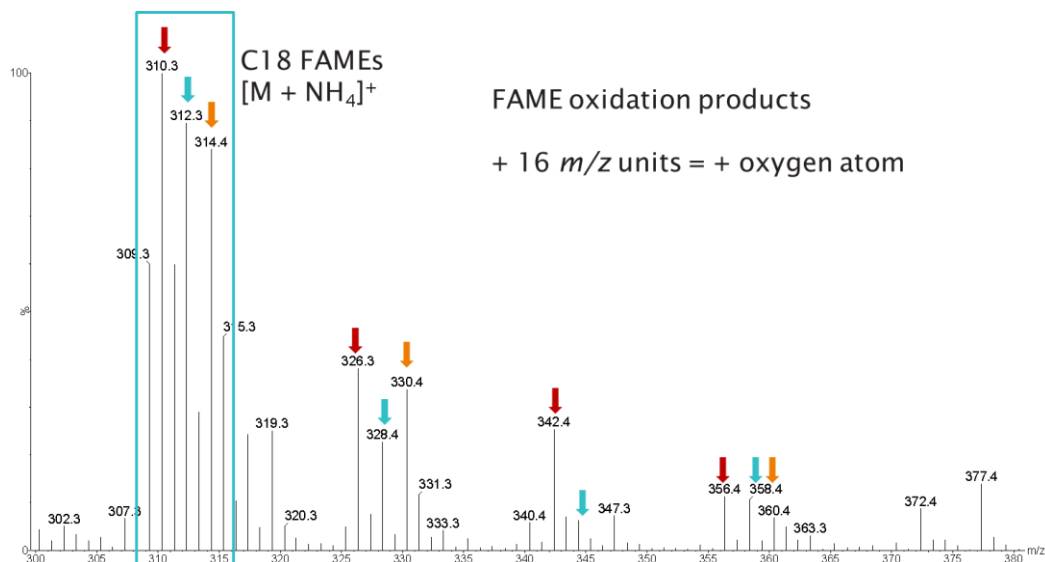


Figure 4-22 - Positive ion ESI UHPSFC mass spectrum of D#5 at  $t_R$  0.50-0.80 min (zoomed range  $m/z$  300-380), showing ammoniated molecules for C18 FAMES and their respective FAME oxidation products, up to the addition of three oxygen atoms

RICCs for nominal  $m/z$  associated with FAME C18:3 and associated FAME oxidation products (in this case  $[M + NH_4]^+$  as shown in Table 4-4) is shown in Figure 4-23, to confirm the assignment.

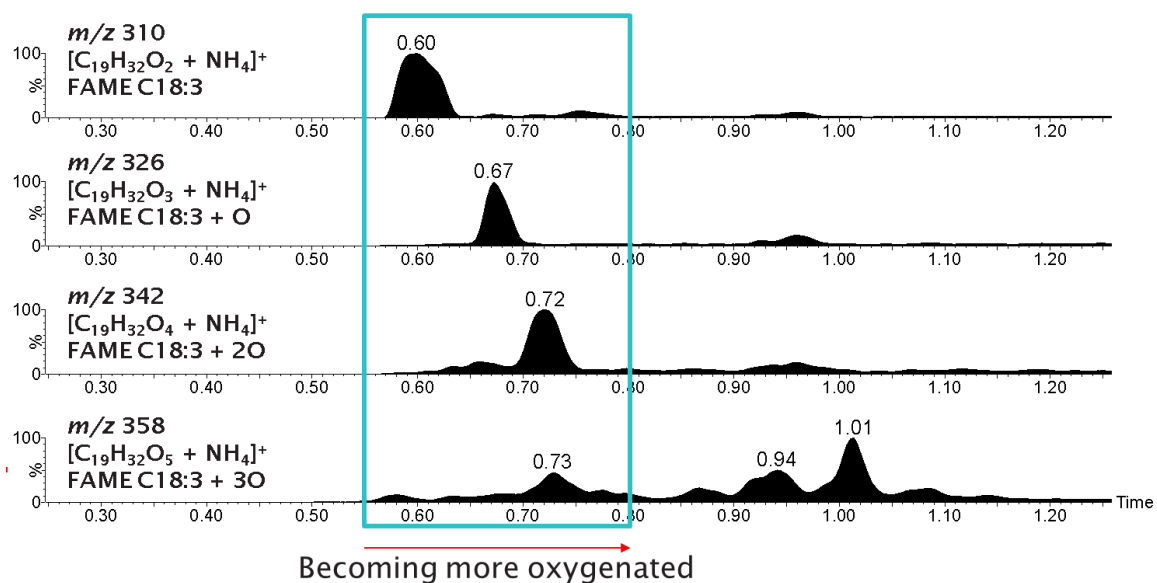


Figure 4-23 – Positive ion ESI UHPSFC-MS RICCs of D#5 showing C18:3 FAME and FAME oxidation products

Table 4-5 - Diesel fuels FAMES oxidation products summary (√=detected, X=not detected)

Diesels	FAME oxidation products (carbon number: number of double bond)		
	C18:3	C18:2	C18:1
D#1	√ +10, +20,+30	√ +10, +20,+30	√ +10, +20,+30
D#2	√ +10	√ +10, +20	√ +10, +20
D#3	√ +10, +20,+30	√ +10, +20	√ +10, +20,+30
D#4	√ +10, +20,+30	√ +20,+30	√ +30
D#5	√ +10, +20,+30	√ +10, +20,+30	√ +10, +20,+30
D#6	X	X	X
D#7	√ +10	√ +10, +20	√ +10, +20,+30
D#8	X	X	X
D#9	√ +30	√ +20	√ +20

C18 FAME oxidation products were only detected in D#1, 2, 3, 4, 5, 7 and 9 during analysis. C18 FAME oxidation products were not detected in D#6 and D#8 suggesting that D#6 and D#8 fuels contain unoxidized FAMES only (both only contained C18:3,C18:2 and C18:1 FAMES initially).

## Chapter 4

These results can be split into 5 groups;

- D#1, D#3 and D#5
- D#2 and D#7
- D#4
- D#9
- D#6 and D#8 (none detected)

FAME oxidation products show that diesels have been oxidised, suggesting poor storage, old fuel, *etc.* The difference in abundances of FAME oxidation products as well as the number of oxygen atoms observed corresponds to the different extent of oxidation each fuel has undergone.

Both techniques used were suitable for FAME oxidation products analysis however positive ion ESI FT-ICR MS was able to confirm the assignment and a molecular formula.

These findings of multiply oxygenated auto oxidation products are in agreement with work presented by Wicking<sup>96</sup> however FAME species containing only up to 3 oxygen atoms have been observed in this diesel screening method.

### 4.3.3 Free fatty acids (FFAs)

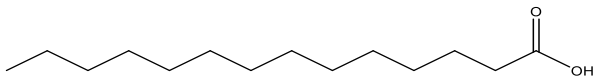
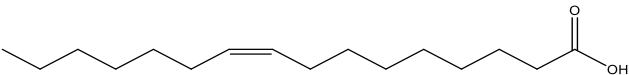
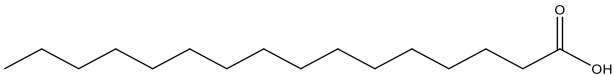
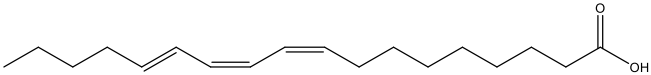
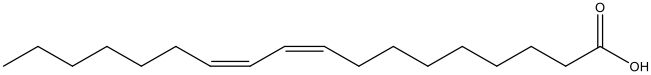
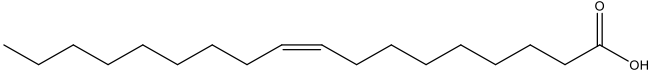
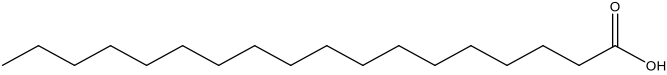
A free fatty acid (FFA) is commonly used as a lubricity additives/friction modifier within diesel fuel or can be observed as a byproduct of FAME production in biodiesel<sup>53, 61, 120</sup>.

FFAs are well known as a contributing compound for metal carboxylates deposits both in fuel filter and fuel injector IDIDs<sup>27, 120</sup>. Barker *et al.*<sup>227</sup> reported that monoacid lubricity improver additives in combination with sodium hydroxide were found to cause “severe fuel filter fouling” resulting from the formation and agglomeration of a sodium carboxylate deposit.

Table 4-6 shows a summary of the FFAs, their respective molecular formulae and structure, the adduct that can be present for each and their associated masses<sup>233</sup>.

A note of caution for this method, FFA C16:0 is found in methanol so if a strong signal for FFA C16:0 is observed and it is different to the blank then it is likely to be present. However, it is worth being aware a signal may be seen that is a false positive arising from C16:0 being present in the methanol.

Table 4-6 FFAs summary

		<i>m/z</i> (nominal for UHPSFC-MS, monoisotopic for FT-ICR MS)
FFA (Carbon number:number of double bonds)	Molecular formula, exact mass and structure	[M - H]-
C14:0	C <sub>14</sub> H <sub>28</sub> O <sub>2</sub> , 228.21 g/mol 	227.2022 ( <i>t<sub>R</sub></i> :0.96 min)
C16:1	C <sub>16</sub> H <sub>30</sub> O <sub>2</sub> , 254.22 g/mol 	253.2180 ( <i>t<sub>R</sub></i> :1.02 min)
C16:0	C <sub>16</sub> H <sub>32</sub> O <sub>2</sub> , 256.24 g/mol 	255.2337 ( <i>t<sub>R</sub></i> :1.05 min)
C18:3	C <sub>18</sub> H <sub>30</sub> O <sub>2</sub> , 278.22 g/mol 	277.2182 ( <i>t<sub>R</sub></i> :1.03 min)
C18:2	C <sub>18</sub> H <sub>32</sub> O <sub>2</sub> , 280.24 g/mol 	279.2339 ( <i>t<sub>R</sub></i> :1.04 min)
C18:1	C <sub>18</sub> H <sub>34</sub> O <sub>2</sub> , 282.26 g/mol 	281.2496 ( <i>t<sub>R</sub></i> :1.09 min)
C18:0	C <sub>18</sub> H <sub>36</sub> O <sub>2</sub> , 284.27 g/mol 	283.2652 ( <i>t<sub>R</sub></i> :1.14 min)

FFAs can also be observed using positive ion ESI MS<sup>233</sup>. At present only negative ion ESI methods are included in detail in the screening method for FFAs as they appear to be more abundant as deprotonated molecules, however positive ion ESI data should still be considered as it could provide further confidence in FFA assignment.

D#8 will be used as the example to illustrate FFAs within diesel fuels.

## Chapter 4

FFAs were found to elute at  $t_R$  0.85 – 1.20 min as shown in Figure 4-25. The corresponding negative ion ESI UHPSFC mass spectrum shown in Figure 4-24, shows deprotonated molecules  $[M - H]^-$  observed at nominal  $m/z$  values matching those in Table 4-6. RICCs of associated  $m/z$  values for FFAs (in this case  $[M - H]^-$  as shown in Table 4-6) were used for compound confirmation as shown in Figure 4-26, and the peaks observed suggest the presence of C14:0, C16:1, C16:0, C18:3, C18:2, C18:1 and C18:0 FFAs. Additionally, chromatographic separation of the negative ion ESI UHPSFC-MS method provides both separation of the FFAs by chain length as well as by degree of saturation.

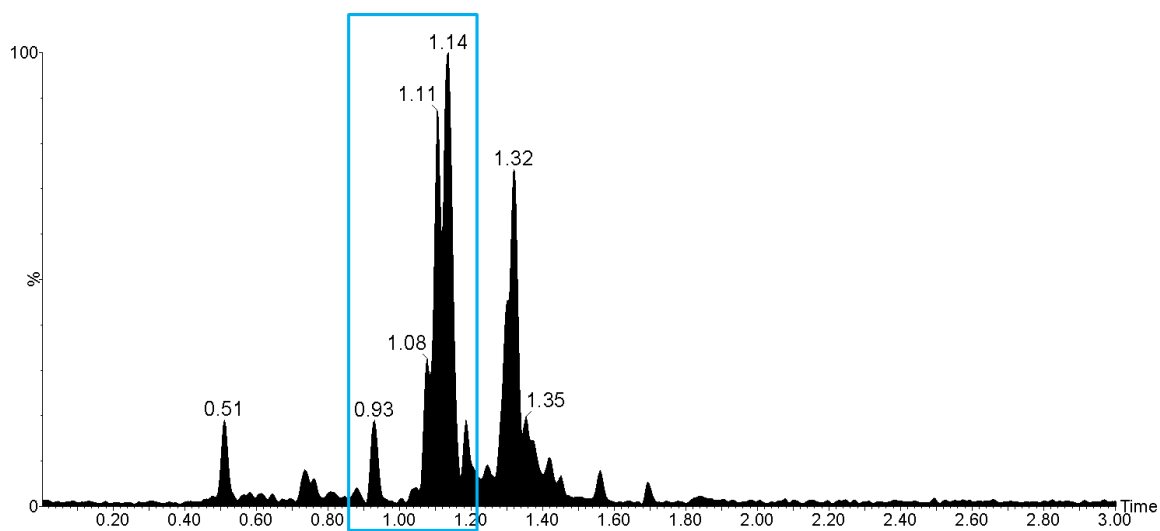


Figure 4-25 – Negative ion ESI UHPSFC-MS BPICC of D#8 with pale blue box highlighting FFAs region of retention ( $t_R$  0.85-1.20 min)

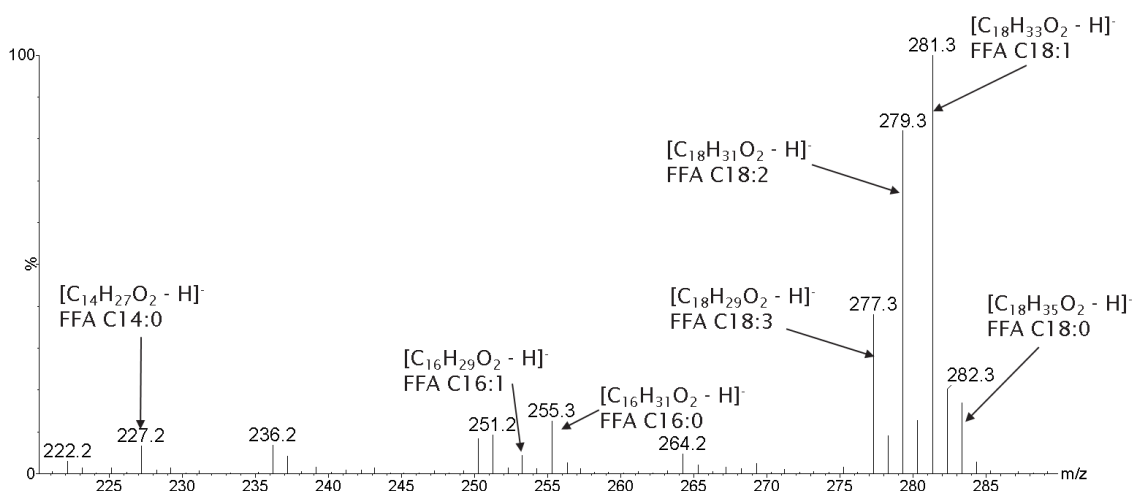


Figure 4-24 – Negative ion ESI UHPSFC mass spectrum of D#8 at  $t_R$  0.85-1.20 min (zoomed range  $m/z$  220-290)



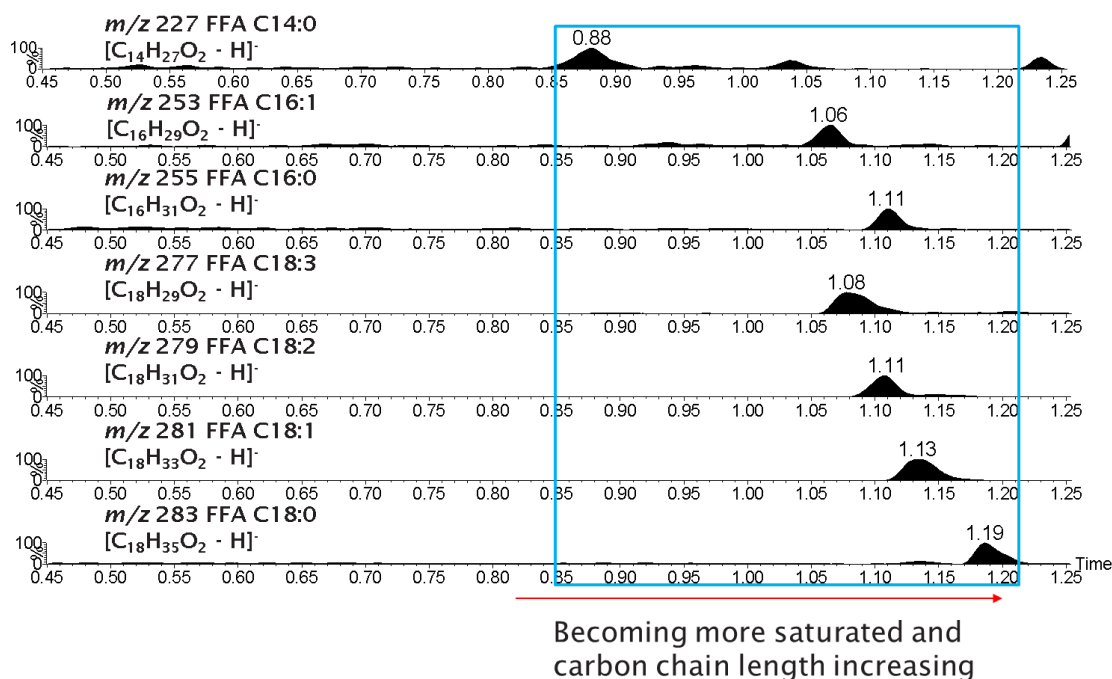


Figure 4-26 - Negative ion ESI UHPSFC-MS RICCs of D#8 showing FFAs (box zoomed to 0.85–1.20 min)

FFAs were also observed as deprotonated molecules  $[M - H]^-$  in D#8 ( $m/z$  values in Table 4-6) using direct infusion negative ion ESI FT-ICR MS as shown in Figure 4-27.

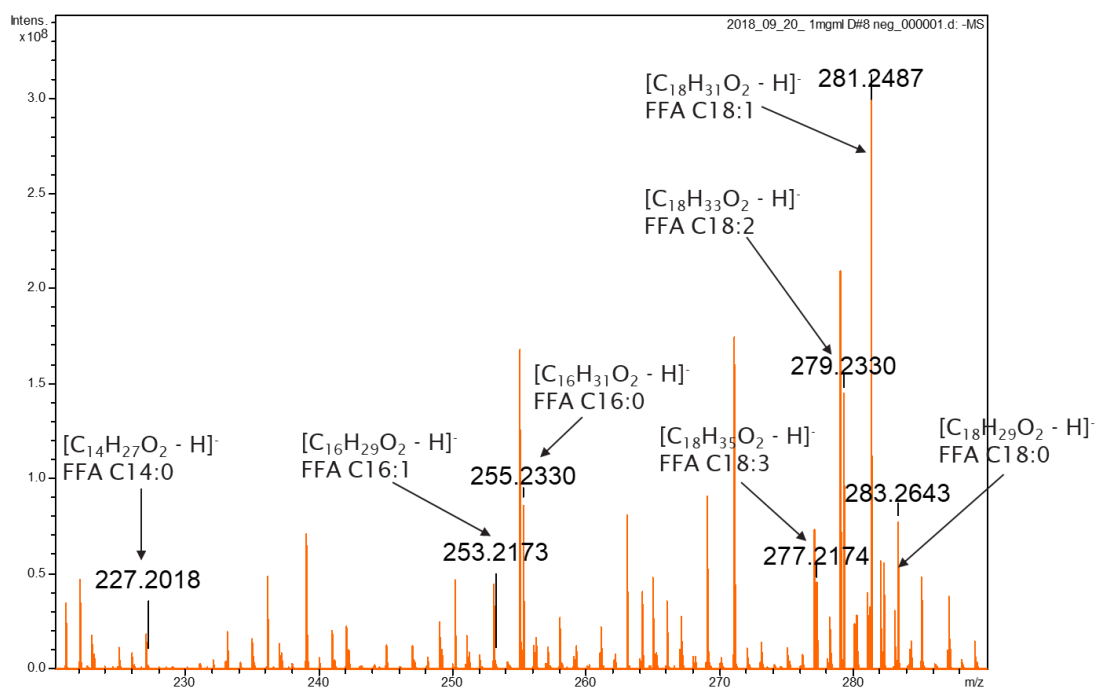


Figure 4-27 - Direct infusion negative ion ESI FT-ICR mass spectrum of D#8 (zoomed range  $m/z$  220-290), showing deprotonated molecules for FFAs.

Chapter 4

The accurate mass data provides further confidence that C14:0, C16:1, C16:0, C18:3, C18:2, C18:1 and C18:0 FFAs were detected in D#8 in agreement with negative ion ESI UHPSFC-MS.

Table 4-7 shows a summary of the FFAs detected within nine diesel fuel analysed and is a culmination of results from negative ion ESI UHPSFC-MS and direct infusion negative ion ESI FT-ICR MS. FFAs have been denoted as detected when observed by both techniques, whereas tentative assignment has been given if FFAs have only been detected by direct infusion negative ion ESI FT-ICR MS.

Table 4-7 – Diesel fuels FFAs findings summary (legend: √= detected (observed by UHPSFC-MS and FT-ICR MS), √?= only detected by FT-ICR MS, X = not detected)

		FFAs (carbon number: number of double bonds)						
		C14:0	C16:1	C16:0	C18:3	C18:2	C18:1	C18:0
Diesels	D#1	√	X	√	√	√	√	√
	D#2	√?	X	√?	X	√	√	√?
	D#3	√	√	√	√	√	√	√
	D#4	√	√	√	√	√	√	√
	D#5	√	√?	√	√	√	√	√
	D#6	√	√?	√	√	√	√	√
	D#7	X	X	√?	√?	√	√	X
	D#8	√	√	√	√	√	√	√
	D#9	X	√	√	√	√	√	√

FFAs were detected in all nine diesel samples during analysis.

The major differences are D#2 and D#7 only have confirmed assignments for FFAs C18:1 and C18:2. FFA C16:1 is only confirmed to be present in D#3, 4, 8 and 9 with tentative assignments for D#5 and D#6.

The key similarities are FFAs C18:2 and C18:1 are detected in all nine diesels. FFAs C18:0, C18:3 and C16:3 are detected in all diesels except D#2 and D#7.

These results can be used to split the diesel into 5 groups:

- D#3, 4 and 8
- D#5 and D#6 (possibly with D#3, 4 and 8 but has tentative assignments)
- D#2 and D#7
- D#1
- D#9

These results suggest that the FFAs in the diesels originate either from FAME production as a byproduct as this is in agreement with FAME results. However the FFAs could also originate from the addition of lubricity additives to the diesels at blending<sup>234</sup>, although D#1 (B100) does not contain FFA C16:1 that some of the other fuels contain. This may suggest a combination of origins, more information about the fuel blending/additive package is required to determine this.

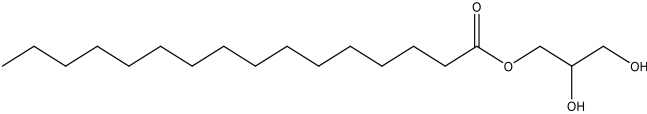
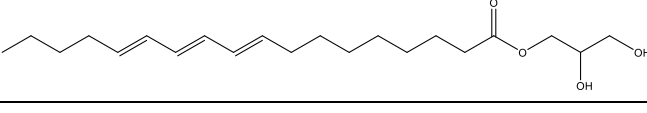
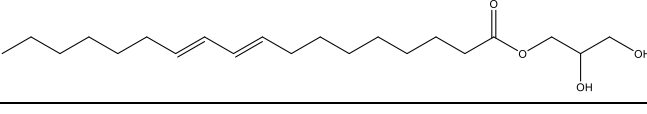
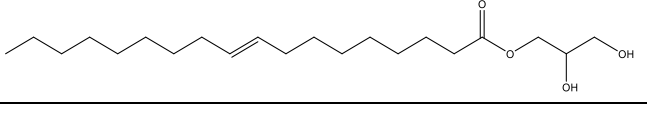
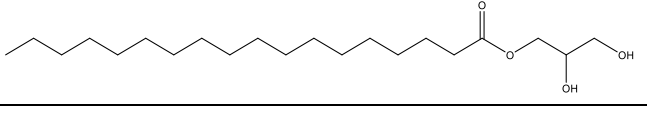
#### 4.3.4 Monoacylglycerols (MAGs)

Monoacylglycerols (MAGs) consist of a glycerol linked *via* an ester bond to a fatty acid<sup>235</sup>. MAGs are present as minor constituents or contaminants, within biodiesel as a byproduct of incomplete transesterification<sup>236</sup> (further detail in chapter 1).

Saturated MAGs have been found to plug fuel filters due to the low solubility of MAGs in biodiesel leading to the formation of solid precipitates in cold weather<sup>237-239</sup>.

Table 4-8 shows a summary of the MAGs, their respective molecular formulae and structures, adducts that can be present and their associated masses<sup>233</sup> with nominally isobaric species  $m/z$  in bold and underlined.

Table 4-8 MAGs Summary (nominally isobaric species  $m/z$  in bold and underlined)

MAGs (Carbon number: number of double bonds)	Molecular formula, exact mass and structure	Expected $m/z$ (nominal for SFC, monoisotopic (4 dp) for FT)		
		$[M + H]^+$	$[M + NH_4]^+$	$[M + Na]^+$
C16:0	$C_{19}H_{38}O_4$ , 330.28 g/mol 	331.2843	348 ( $t_R$ : 1.25 min)	<b><u>353.2662</u></b>
C18:3	$C_{21}H_{36}O_4$ , 352.26 g/mol 	<b><u>353.2686</u></b>	370 ( $t_R$ : 1.23 min)	375.2506
C18:2	$C_{21}H_{38}O_4$ , 354.28 g/mol 	355.2843	372 ( $t_R$ : 1.25 min)	377.2662
C18:1	$C_{21}H_{40}O_4$ , 356.29 g/mol 	357.2999	374 ( $t_R$ : 1.28 min)	379.2819
C18:0	$C_{21}H_{42}O_4$ , 358.31 g/mol 	359.3156	376 ( $t_R$ : 1.31 min)	381.2975

D#3 will be used as the example to illustrate MAGs within diesels.

MAGs were found to elute at  $t_R$  1.20-1.35 min as shown in Figure 4-28. The corresponding positive ion ESI UHPSFC mass spectrum shown in Figure 4-29, shows a mixture of protonated  $[M + H]^+$  and ammoniated  $[M + NH_4]^+$  molecules with nominal masses in agreement with MAGs nominal masses in Table 4-8.

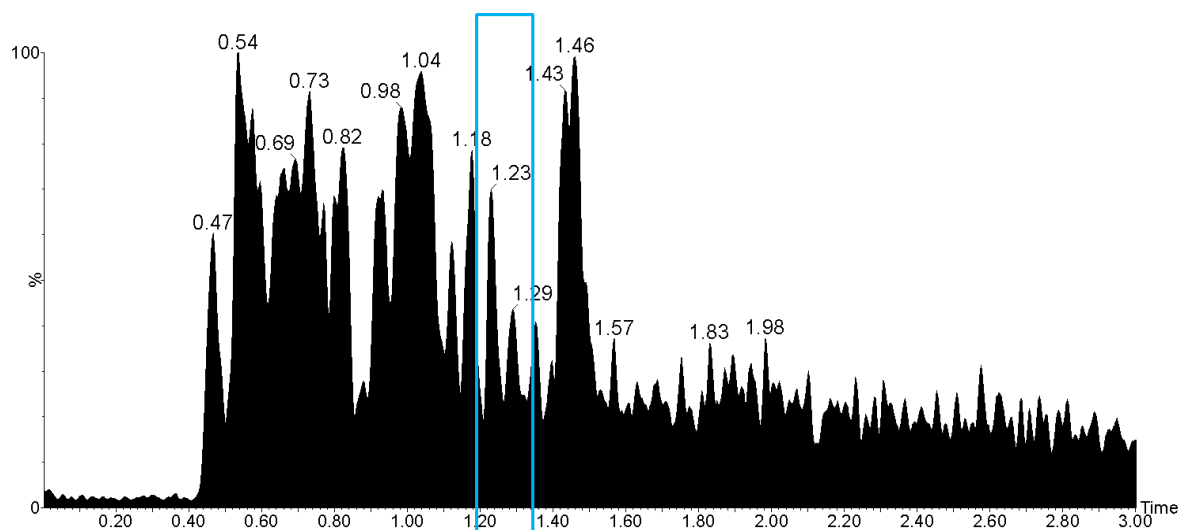


Figure 4-28 - Positive ion ESI UHPSFC-MS BPICC of fuel filter D#9 with pale blue box highlighting MAGs region of retention ( $t_R$  1.20-1.35 min)

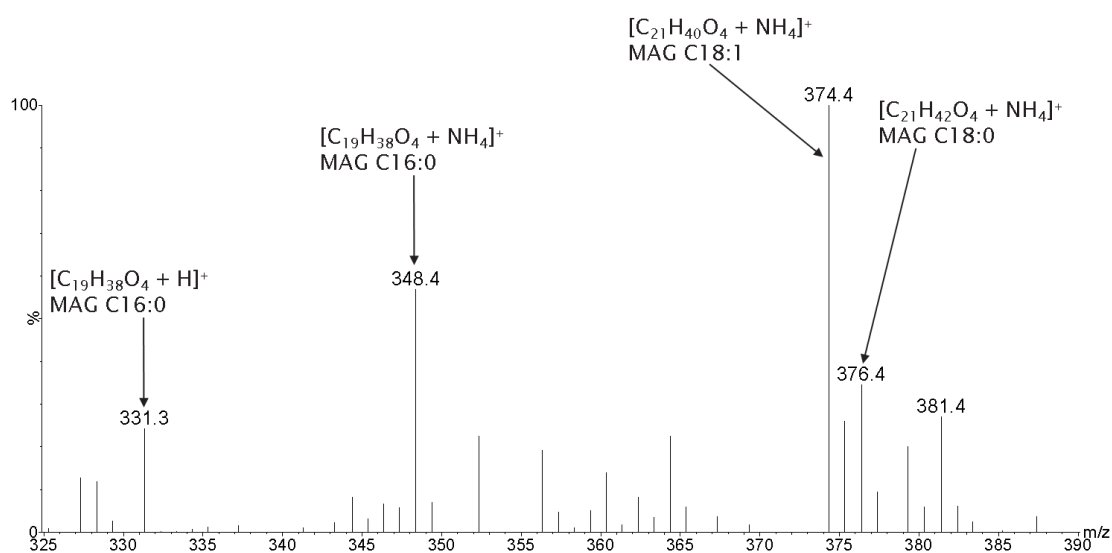


Figure 4-29 - Positive ion ESI UHPSFC mass spectrum of D#9 at  $t_R$  1.20-1.35 min zoomed range  $m/z$  325-390

RICCs of associated  $m/z$  values for MAGs ( $[M + NH_4]^+$  as shown in Table 4-8) were used as shown in Figure 4-31 which suggests that the respective peaks are related to MAGs C16:0, C18:3, C18:2, C18:1 and C18:0, and is in agreement with those observed in the direct infusion positive ion ESI FT-ICR MS data.

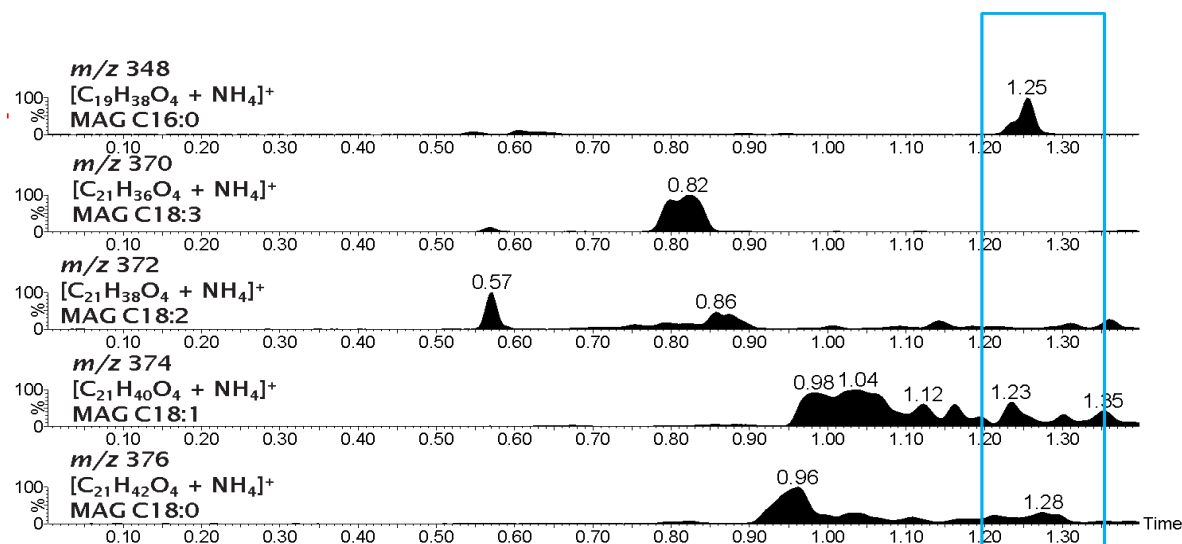


Figure 4-31 – Positive ion ESI UHPSFC-MS RICCs of D#9 showing MAGs with pale blue box highlighting MAGs region of retention ( $t_R$  1.20-1.35 min)

For additional confirmation and to aid separation of nominally isobaric species, MAGs are observed as sodiated molecules  $[M + Na]^+$  using direct infusion positive ion ESI FT-ICR MS, (Figure 4-30). Saturated MAGs are dominating the mass spectra and these has previously been found to be problematic blocking fuel filters, with clear detection afforded by this methodology.

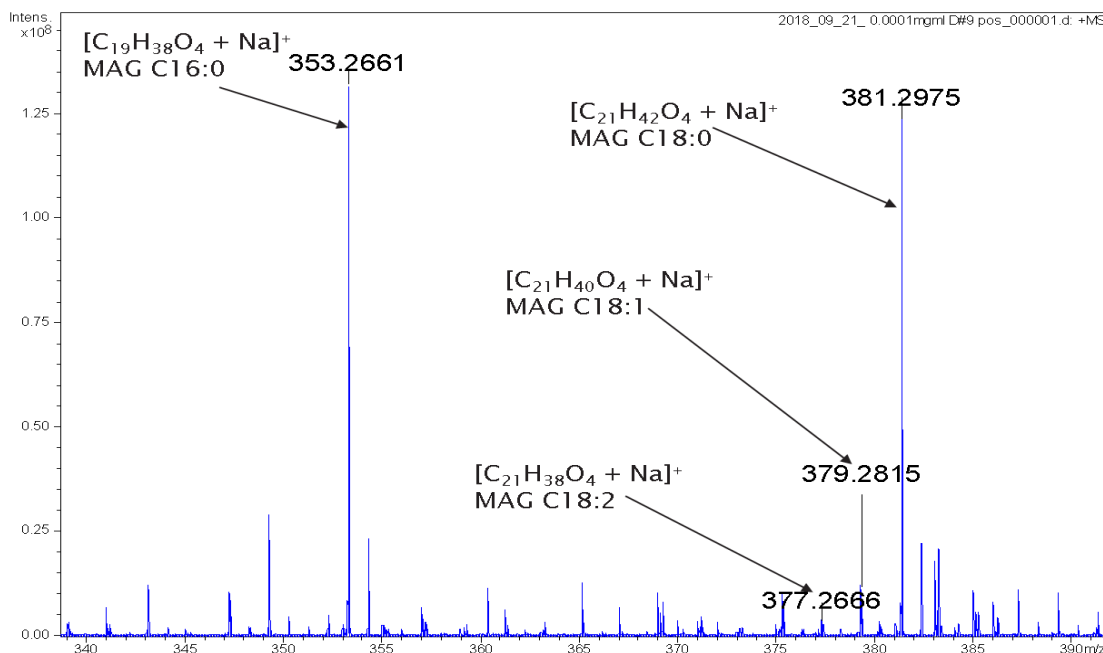


Figure 4-30 - Direct infusion positive ion ESI FT-ICR mass spectrum of D#9, (zoomed range  $m/z$  340-390), showing sodiated molecules for MAGs

As observed previously with FAMES in 4.3.1, nominally isobaric species are also observed between MAGs  $[C16:0 + Na]^+$  and  $[C18:3 + H]^+$ , however for  $[MAG C16:0 + Na]^+$  and  $[MAG C18:3 + H]^+$  it is at

nominal  $m/z$  353 as shown in Table 4-8. Observation of complimentary adducts and FT-ICR MS analysis allow for separation of isobaric species.

To further confirm the assignment of MAGs, MS/MS was undertaken on SS5 fuel filter sample, in 5.3.5.1.

Table 4-9 shows a summary of the MAGs detected within the nine diesel fuels analysed. MAGs have been denoted as detected when observed by both techniques, whereas tentative assignment has been given if MAGs have only been detected by direct infusion positive ion ESI FT-ICR MS. The symbol X\* has been utilised for results when the nominal  $m/z$  was initially detected by positive ion ESI UHPSFC-MS in RICCs, however the presence of the compound by monoisotopic mass not detected by direct infusion positive ion ESI FT-ICR MS.

Table 4-9 - Diesel fuels MAGs summary (√=detected, √? = only detected by FT-ICR MS, X\* = nominal mass detected by positive ion ESI UHPSFC-MS, but monoisotopic mass not detected by positive ion ESI FT-ICR MS, X=not detected)

		<b>MAGs (carbon number: number of double bonds)</b>				
		<b>C16:0</b>	<b>C18:3</b>	<b>C18:2</b>	<b>C18:1</b>	<b>C18:0</b>
<b>Diesels</b>	<b>D#1</b>	√	X	X	√	√
	<b>D#2</b>	√?	X	√?	√?	√?
	<b>D#3</b>	√	X	√?	√?	√
	<b>D#4</b>	√	X	√?	√?	√
	<b>D#5</b>	√	X	√?	√?	√
	<b>D#6</b>	√	X	√?	√?	√
	<b>D#7</b>	√?	X	X	√?	√?
	<b>D#8</b>	X*	X	X	X	X*
	<b>D#9</b>	√	X	√?	√	√

## Chapter 4

MAGs were detected in D#1, 3, 4, 5, 6 and 9 only, with tentative observations by FT-ICR MS only in D#2 and D#7 (suggesting possibly MAGs absent) and MAGs were not detected in D#8 during analysis.

These results can be used to split the diesel into 5 groups;

- D#3, 4, 5 and D#6
- D#1 and D#9
- D#2 and D#7 (most likely absent)
- D#8 (absent)

Unsaturated MAGs C16:0 and C18:0 were most commonly detected. MAG C18:1 was detected in D#1 and D#9 with tentative assignments by FT-ICR MS in all other diesels with the exception of D#8. MAGs C18:3 were not detected with MAGs C18:2 most likely not detected or only detected by FT-ICR MS, possibly due to low levels near limit of detection (LOD).

The presence of MAGs in diesels suggested the biodiesel blend was a result of an incomplete transesterification, while no detection of MAGs in D#8 suggests the biodiesel blend was a result of a complete transesterification reaction.

Vegetable oils are known to contain a much lower level of saturated components than animal fats. However as the uses of UCO and waste animal fats has increased to reduce the cost of biodiesel, meaning more saturated components are present in biodiesel<sup>240</sup>. As aforementioned saturated MAGs are known to be problematic and block fuel filters<sup>237-239</sup>. A method was therefore required to detect saturated MAGS in fuels so remediation could take place. This is also an example of fuel composition being linked back to fuel feedstock.

### 4.3.5 Sterol glucosides (SGs)

Sterol glucosides (SGs) consists of a sterol linked at the hydroxyl group (by a glycosidic bond) to a sugar<sup>241</sup>. SGs are present as minor constituents, also known as contaminants, within biodiesel<sup>236</sup>.

SGs naturally exist in the acylated form (with a fatty acid attached) in vegetable oil and are converted to SGs during transesterification. The loss of the fatty acid chain reduces the solubility of SGs in biodiesel<sup>242</sup>. Cold temperatures and concentration exacerbate the precipitation of SGs, forming large complex agglomerates with MAGs or DAGs in biodiesel and biodiesel blends, resulting in solid residues that can clog fuel filters<sup>237-238</sup>.



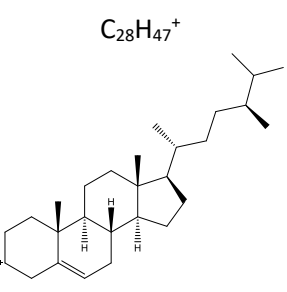
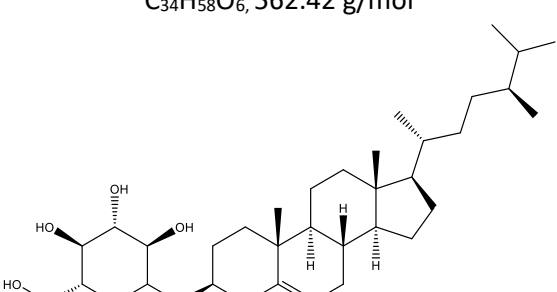
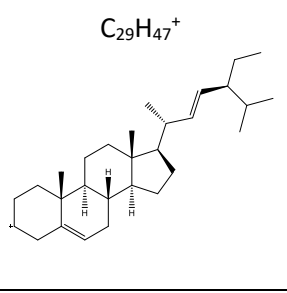
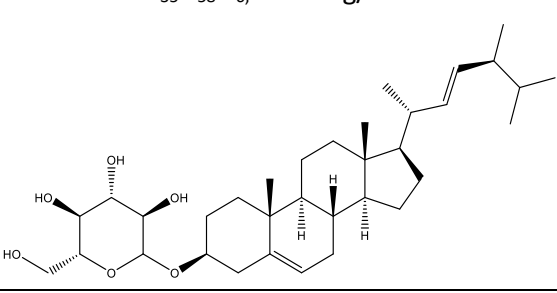
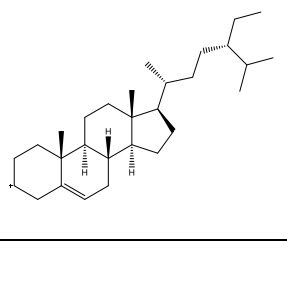
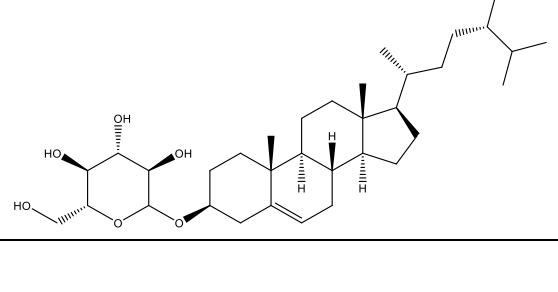
SGs can cause biodiesel to appear hazy at room temperature due to SGs high MP (*e.g.* 240 °C for  $\beta$ -sitosterol glucoside) that results in limited solubility even at low concentrations (10-90 ppm). Processing is used to reduce SG content to stop related issues, however, low levels can still settle in the bottom of fuel storage tanks and build up over time<sup>242</sup>.

SGs have been identified as a species known to cause filtration problems with filter blocking known to occur above the cloud point(CP) (chapter 1) of a given fuel<sup>243</sup>. Industry tests CP and CFPP (chapter 1) used to evaluate cold flow properties of a fuel did not predict the tendency for the formation of the solid precipitates from the biodiesel blends, meaning a new test was developed; cold soak filtration test (ASTM D7501)<sup>32</sup>.

This part of the diesel fuel component screening methodology was developed from previous work by Patel<sup>211</sup> also in relation to diesel and IDID deposit formation.

Table 4-10 shows a summary of the SGs, their respective molecular formulae and structures, adducts that can be present and their associated masses<sup>211, 244-245</sup>.

Table 4-10 SGs summary

<i>m/z</i> (nominal for UHPSFC-MS, monoisotopic for FT-ICR MS)					
Sterol glucosides	Molecular formula and structure of sterol fragment ion	[M + H - sugar] <sup>+</sup> sterol fragment	Molecular formula, exact mass and structure of sterol glucoside	[M + NH <sub>4</sub> ] <sup>+</sup> sterol glucoside	[M + Na] <sup>+</sup> sterol glucoside
Campesterol glucoside	$C_{28}H_{47}^+$ 	383.3672	$C_{34}H_{58}O_6$ , 562.42 g/mol 	580 (tr:2.08 min)	585.4119
Stigmasterol glucoside	$C_{29}H_{47}^+$ 	395.3672	$C_{35}H_{58}O_6$ , 574.42 g/mol 	592 (tr:2.07 min)	597.4126
$\beta$ -sitosterol glucoside	$C_{29}H_{49}^+$ 	397.3829	$C_{35}H_{60}O_6$ , 576.44 g/mol 	594 (tr:2.10 min)	599.4282

D#3 is used as the example to illustrate the absence of SGs for the nine diesel samples although SGs have been observed previously in biodiesel blend (unknown diesels) samples by Patel<sup>211</sup>. However, in this case, only the sterol fragment ions were observed in the diesels.

Sterol fragment ions (with the absence of SGs) were found to elute at  $t_R$  2.00-2.20 min as shown in Figure 4-32. The corresponding positive ion ESI UHPSFC mass spectrum (Figure 4-33) shows sterol fragment ions, corresponding to the protonated molecules  $[M + H - \text{sugar}]^+$  are observed at nominal  $m/z$  380-400. However, there is an absence of ammoniated molecules for SGs at nominal  $m/z$  580-600 in full scan data. SGs may be present below the LLOD, one way to increase the LLOD and sensitivity of the method would be to use selected ion recording for  $m/z$  values for the SGs to confirm their absence.

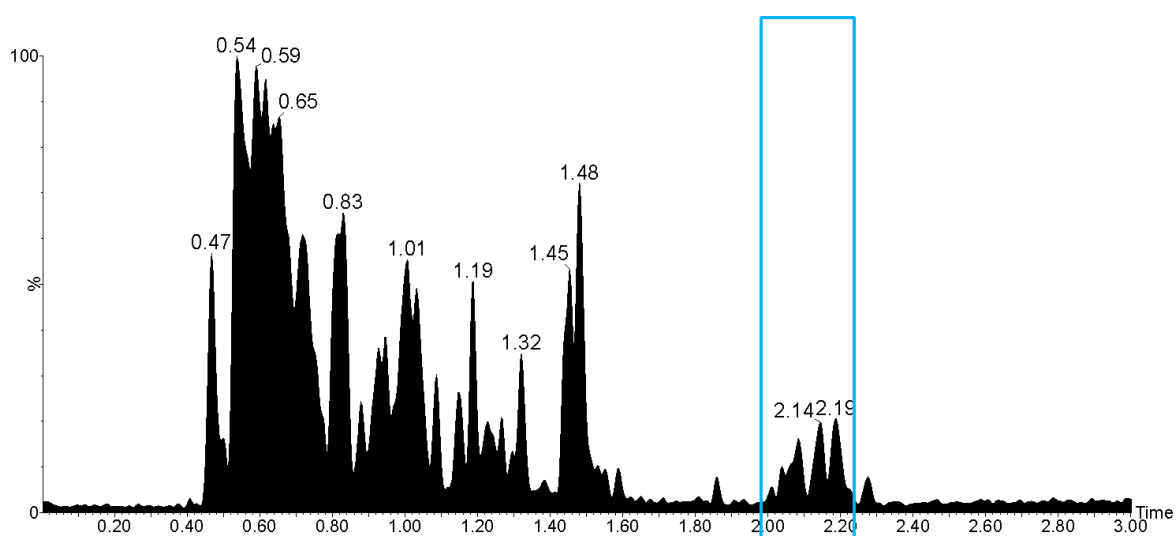


Figure 4-32 - Positive ion ESI UHPSFC-MS BPICC of D#3 with pale blue box highlighting SGs region of retention ( $t_R$  2.00-2.20 min)

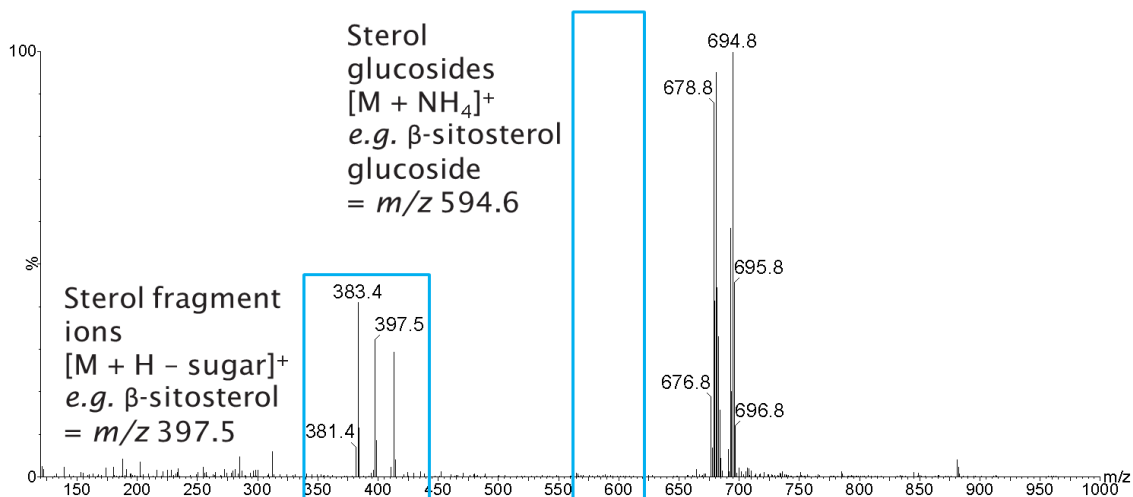


Figure 4-33 - Positive ion ESI UHPSFC mass spectrum of D#3 at  $t_R$  2.00-2.20 min with pale blue boxes highlighting the  $m/z$  values expected for SGs and sterol fragment ions

RICCs (Figure 4-34) also confirm that SGs are not present in D#3 as the chromatographic peaks for the sterol fragment ion  $[M + H - \text{sugar}]^+$  and the SG  $[M + \text{NH}_4]^+$  should be at the same retention time (e.g. for campesterol glucoside  $m/z$  383  $[M + H - \text{sugar}]^+$  and  $m/z$  580  $[M + \text{NH}_4]^+$ ). However, no SG peaks are observed at the retention time of interest (2.00-2.20 min) that match with sterol fragment ion, this suggests the absence of SGs (or below LLOD in full scan) in D#3. SGs and sterol fragment ions were also not observed by direct infusion positive ion ESI FT-ICR MS.

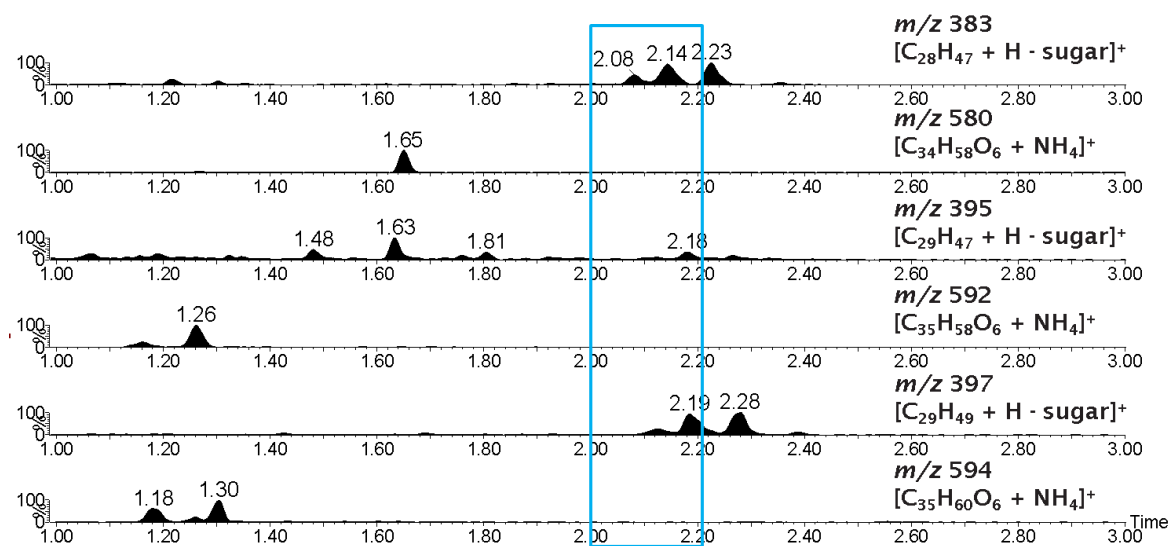


Figure 4-34 –Positive ion ESI UHPSFC-MS RICCs of D#3 showing SGs and sterol fragment ions with pale blue box highlighting SGs region of retention ( $t_R$  2.00-2.20 min)

Table 4-11 shows a summary of the SGs detected within nine diesel fuels analysed.

Table 4-11 - Diesel fuels SGs summary (✓=detected, X=not detected)

	SGs						
		Campesterol glucoside		Stigmasterol glucoside		β-sitosterol glucoside	
		Sterol Fragment ion	SG	Sterol Fragment ion	SG	Sterol Fragment ion	SG
Diesels	D#1	✓	X	✓	X	✓	X
	D#2	X	X	X	X	X	X
	D#3	✓	X	X	X	✓	X
	D#4	✓	X	X	X	✓	X
	D#5	✓	X	X	X	✓	X
	D#6	✓	X	X	X	✓	X
	D#7	X	X	X	X	X	X
	D#8	✓	X	X	X	✓	X
	D#9	✓	X	X	X	✓	X

SGs were not detected in all nine diesels during analysis, as no SG ions were observed relating to relevant sterol fragment ions. This may suggest that processing has taken place to remove SGs to reduce related issues or that SGs are at such low levels they are not detected.

However sterol fragment ions were observed in D#1, 3, 4, 5, 6, 8 and 9, although the stigmasterol fragment ion was only observed in D#1.

The presence of these sterol fragment ions is linked to another plant sterol species and is further discussed in 4.4.

### 4.3.6 Diesel fuels analysis summary

Table 4-12 is a summary of all findings from diesel fuels analysis undertaken using the screening methods outlined in 4.3.

Table 4-12 Diesel fuels analysis summary (√ = detected, X\* = not detected, however part detected and provides additional information, X = not detected)

Diesel fuels									
Compound	D#1	D#2	D#3	D#4	D#5	D#6	D#7	D#8	D#9
FAMES	√	√	√	√	√	√	√	√	√
	<ul style="list-style-type: none"> <li>• C16:1,</li> <li>  C16:0</li> <li>• C18:3,</li> <li>  C18:2,</li> <li>  C18:1,</li> <li>  C18:0</li> <li>• C14:0 (low abundance)</li> </ul>	<ul style="list-style-type: none"> <li>• C16:1</li> <li>• C18:3,</li> <li>  C18:2,</li> <li>  C18:1,</li> <li>  C18:0</li> </ul>	<ul style="list-style-type: none"> <li>• C16:1</li> <li>• C18:3,</li> <li>  C18:2,</li> <li>  C18:1,</li> <li>  C18:0</li> </ul>	<ul style="list-style-type: none"> <li>• C18:3,</li> <li>  C18:2,</li> <li>  C18:1,</li> <li>  C18:0</li> </ul>	<ul style="list-style-type: none"> <li>• C16:1 present,</li> <li>  C18:3,</li> <li>  C18:2,</li> <li>  C18:1</li> </ul>	<ul style="list-style-type: none"> <li>• C18:3,</li> <li>  C18:2,</li> <li>  C18:1</li> </ul>	<ul style="list-style-type: none"> <li>• C18:3,</li> <li>  C18:2,</li> <li>  C18:1,</li> <li>  C18:0</li> </ul>	<ul style="list-style-type: none"> <li>• C18:3,</li> <li>  C18:2,</li> <li>  C18:1,</li> <li>  C18:0</li> </ul>	<ul style="list-style-type: none"> <li>• C18:3,</li> <li>  C18:2,</li> <li>  C18:1,</li> <li>  C18:0</li> </ul>

Diesel fuels

Compound	D#1	D#2	D#3	D#4	D#5	D#6	D#7	D#8	D#9
FAME oxidation products	<p>✓</p> <ul style="list-style-type: none"> <li>• C18:3 (+10,+20,+30)</li> <li>• C18:2 (+10,+20,+30)</li> <li>• C18:1 (+10,+20,+30)</li> </ul>	<p>✓</p> <ul style="list-style-type: none"> <li>• C18:3 (+10)</li> <li>• C18:2 (+10,+20)</li> <li>• C18:1 (+10,+20)</li> </ul>	<p>✓</p> <ul style="list-style-type: none"> <li>• C18:3 (+10,+20,+30)</li> <li>• C18:2 (+10,+20)</li> <li>• C18:1 (+10,+20,+30)</li> </ul>	<p>✓</p> <ul style="list-style-type: none"> <li>• C18:3 (+10,+20,+30)</li> <li>• C18:2 (+20,+30)</li> <li>• C18:1 (+30)</li> </ul>	<p>✓</p> <ul style="list-style-type: none"> <li>• C18:3 (+10,+20,+30)</li> <li>• C18:2 (+10,+20,+30)</li> <li>• C18:1 (+10,+20,+30)</li> </ul>	<p>X</p>	<p>✓</p> <ul style="list-style-type: none"> <li>• C18:3 (+10)</li> <li>• C18:2 (+10,+20)</li> <li>• C18:1 (+10,+20,+30)</li> </ul>	<p>X</p>	<p>✓</p> <ul style="list-style-type: none"> <li>• C18:3 (+30)</li> <li>• C18:2 (+20)</li> <li>• C18:1 (+20)</li> </ul>

## Diesel fuels

Compound	D#1	D#2	D#3	D#4	D#5	D#6	D#7	D#8	D#9
FFAs	✓ • C14:0 • C16:0 • C18:3, C18:2, C18:1, C18:0.	✓ • C18:2 and C18:1 • C14:0, C18:0 (observed by FT only)	✓ • C14:0 • C16:1, C16:0 • C18:3, C18:2, C18:1, C18:0	✓ • C14:0 • C16:1, C16:0 • C18:3, C18:2, C18:1, C18:0 C18:0.	✓ • C14:0 • C16:0 • C18:3, C18:2, C18:1, C18:0 • low abunda nce C16:1 (by FT only)	✓ • C14:0 • C16:0 • C18:3, C18:2, C18:1, C18:0 • low abund ance C16:1 (by FT only)	✓ • C18:2 and C18:1 • C18:3 (by FT only)	✓ • C14:0 • C16:1, C16:0 • C18:3, C18:2, C18:1, C18:0 C18:0	✓ • C16:1, C16:0 • C18:3, C18:2, C18:1, C18:0
Sterol glucosides	X* (sterol fragment ions:	X	X*	X*	X*	X*	X	X*	X*



Diesel fuels

Compound	D#1	D#2	D#3	D#4	D#5	D#6	D#7	D#8	D#9
	Camp, Stig, β-sito)		(sterol fragment ions: Camp, β-sito)	(sterol fragment ions: Camp, β-sito)	(sterol fragment ions: Camp, β-sito)	(sterol fragment ions: Camp, β-sito)		(sterol fragment ions: Camp, β-sito)	sterol fragment ions: Camp, β-sito)
MAGs	<p>✓</p> <ul style="list-style-type: none"> <li>• C16:0</li> <li>• C18:1 and C18:0</li> </ul>	<p>✓</p> <ul style="list-style-type: none"> <li>• C16:0</li> <li>• C18:2, C18:1 and C18:0 by FT only</li> </ul>	<p>✓</p> <ul style="list-style-type: none"> <li>• C16:0</li> <li>• C18:1 and C18:0</li> <li>• C18:2 by FT only</li> </ul>	<p>✓</p> <ul style="list-style-type: none"> <li>• C16:0</li> <li>• C18:0</li> <li>• C18:2 and C18:1 by FT only</li> </ul>	<p>✓</p> <ul style="list-style-type: none"> <li>• C16:0</li> <li>• C18:0</li> <li>• C18:2 and C18:1 by FT only</li> </ul>	<p>✓</p> <ul style="list-style-type: none"> <li>• C16:0</li> <li>• C18:0</li> <li>• C18:2 and C18:1 by FT only</li> </ul>	<p>✓</p> <ul style="list-style-type: none"> <li>• C16:0</li> <li>• (C18:3, C18:2)</li> <li>• C18:1 and C18:0 by FT only)</li> </ul>	<p>✓</p> <ul style="list-style-type: none"> <li>• C16:0 and C18:0. Only by SQD – possibly should be in FT data</li> </ul>	<p>✓</p> <ul style="list-style-type: none"> <li>• C16:0</li> <li>• C18:1 and C18:0</li> <li>• C18:2 by FT only</li> </ul>

## Chapter 4

A screening methodology has been developed for five known deposit forming compounds; FAMES, FAME oxidation products, FFAs, SGs, and MAGs.

The similarities and differences afforded by positive and negative ion UHPSFC-MS and FT-ICR MS allow grouping of fuels by a specific deposit forming compound or a combination of deposit forming compounds.

The following common trends were observed in the five deposit forming compound groupings for analysis of nine unknown diesel fuels:

- D#2 and D#7 occurred three times (FAME oxidation products, FFAs and MAGs)
- D#4 and D#8 occurred three times (FAMES, MAGs and (SGs))
- D#1, D#3, D#4, D#5, D#6 and D#9 occurred twice (MAGs and SGs) with D#1, D#3 and D#5 occurred four times (FAMES, FAME oxidation products, (MAGs and SGs))

SGs were absent in all nine diesels however sterol fragment ions were observed in D#1, 3, 4, 5, 6, 8 and 9, with the stigmasterol fragment ion present in D#1 only. The absence of SGs is suggestive that biodiesel have been processed to remove SGs to reduce related issues or that SGs are at such low levels they are not detected. Additional ions were observed at  $\sim m/z$  670-700 believed to be related to the sterol fragments so further work is required to investigate this.

#### 4.4 Detection of fatty acid sterol esters (FASEs) in diesels

In 4.3.5, sterol glucosides (SGs) were found to be absent in the nine diesel fuel samples, however the detection of the sterol fragment ion was indicative that a sterol related compound was present in all of the fuels except D#2 and D#7.

The possibility of the presence of another plant sterol species was investigated in conjunction with considering a series of chromatographic peaks are present at  $t_R$  2.00-2.40 min (Figure 4-35) and the related positive ion ESI UHPSFC mass spectrum shown in Figure 4-36.

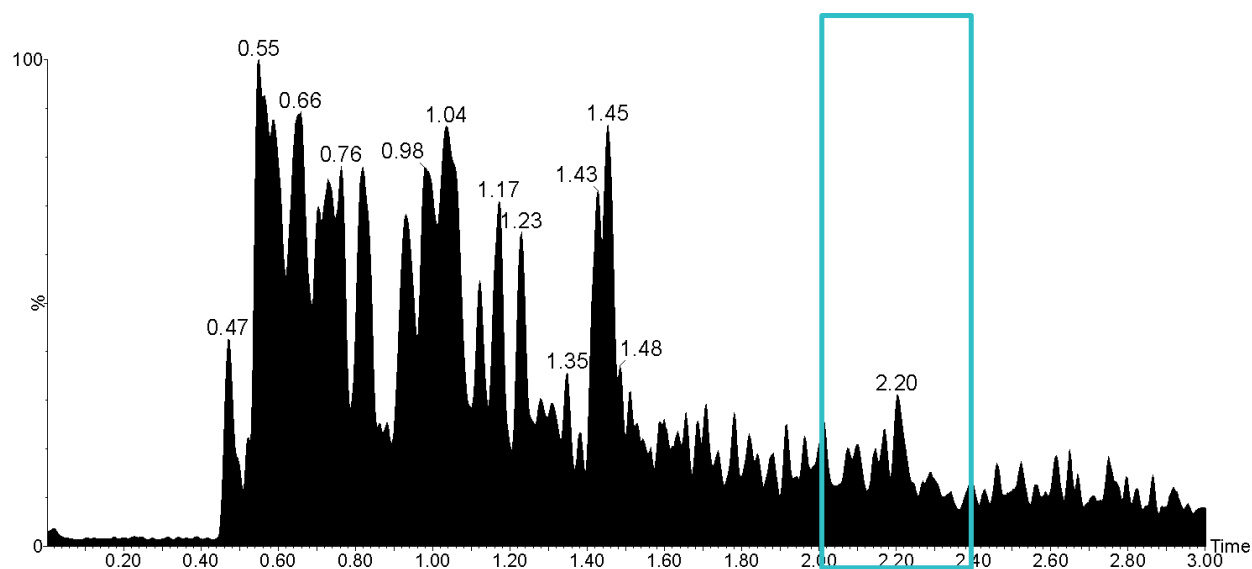


Figure 4-35 - Positive ion ESI UHPSFC-MS BPICC of D#1 with pale blue box highlighting FASEs region of retention ( $t_R$  2.00-2.40 min)

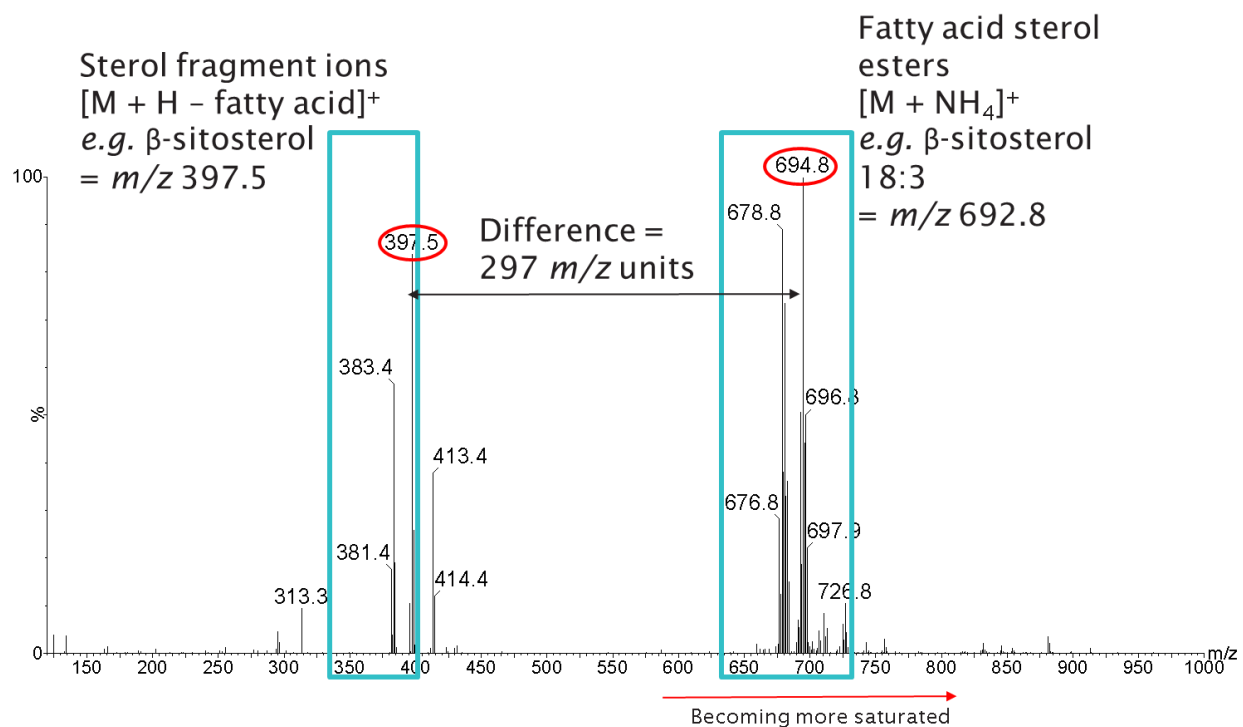


Figure 4-36 - Positive ion ESI UHPSFC mass spectrum of D#1 at  $t_R$  2.00-2.40 min with pale blue boxes highlighting the  $m/z$  values expected for FASEs and sterol fragment ions

Three major sterol containing compound classes are found in plants; SGs, acylated SGs and fatty acid sterol esters (FASEs)<sup>245</sup>. It was therefore thought likely that this unknown species could be either FASEs or acylated SGs. However, the  $m/z$  of acylated SGs would be much larger than that observed. Therefore, FASEs were determined from the  $m/z$  values in the positive ion ESI UHPSFC-MS mass spectrum of D#1 at  $t_R$  2.00-2.40 min and from literature. The losses observed between the sterol fragment ions and the unknown ions ( $m/z$  670-700) was equivalent to the loss of a fatty acid chain (*e.g.*  $m/z$  694 -  $m/z$  397 =  $m/z$  297) further suggesting a fatty acid sterol ester (FASE). The masses observed were also in agreement with previous analysis of FASEs by Kalo *et al.*<sup>233</sup>.

RICCs (Figure 4-37) also confirm that FASEs are likely to be present in D#1 as the chromatographic peaks for the sterol fragment ion (*e.g.* campesterol glucoside  $m/z$  383  $[M + H - \text{fatty acid}]^+$  and related FASEs  $m/z$  678, 680 and 682  $[M + \text{NH}_4]^+$ ) are at corresponding retention times with chromatographic separation based on degree of saturation of the fatty acid chain.

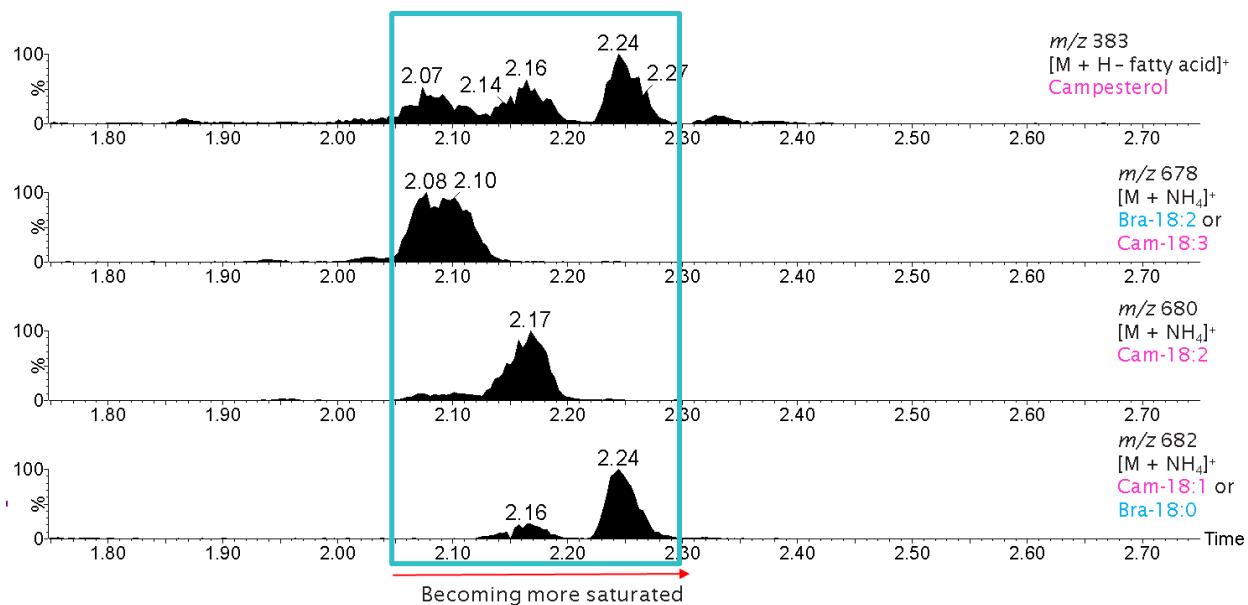


Figure 4-37 - Positive ion ESI UHPSFC-MS RICCS of D#3 showing campesterol fragment ion and its respective FASEs in with pale blue box highlighting FASEs region of retention ( $t_R$  2.05-2.30 min)

Plank and Lorbeer<sup>246-247</sup> were pioneers in the 1990s, analysing FASEs in vegetable oil methyl esters (biodiesels) developing an online LC-GC technique. Verleyen *et al.*<sup>248</sup> also used GC-FID to analyse sterols and FASEs in vegetable oil.

Extensive work was undertaken by Kalo *et al.*<sup>233</sup> using normal phase liquid chromatography – positive ion electrospray tandem mass spectrometry to characterise lipid species in rapeseed oil (MAGs, DAGs and triacylglycerides, FASEs, sterols and FFAs) including MS fragmentation.

Wewer *et al.*<sup>245</sup> developed a quantification method for sterols, FASEs, SGs and acylated SGs using mass spectrometry.

Hailat and Helleur<sup>249</sup> also used electrospray mass spectrometry to detect FASEs in lipid extracts from margarine and corn kernels, with further identification demonstrated through structural elucidation utilising ESI-quadrupole ion trap MS<sup>n</sup>.

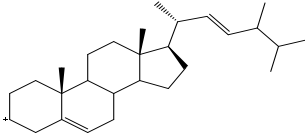
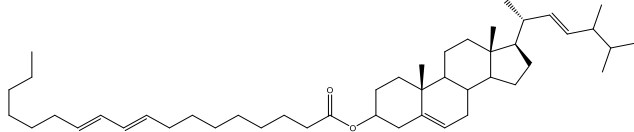
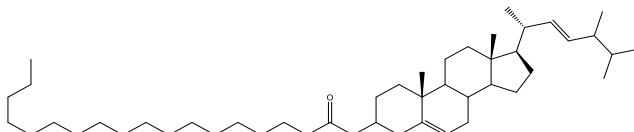
The observation of FASEs in diesel/biodiesel fuel blends is of great significance in the field. As prior to this work, in literature, FASEs have only been analysed in pure biodiesel and vegetable oils and not in fuel blends therefore this is novel work. Additionally FASEs are not stated in the literature to have been investigated or found to cause filter blocking or IDIDs.

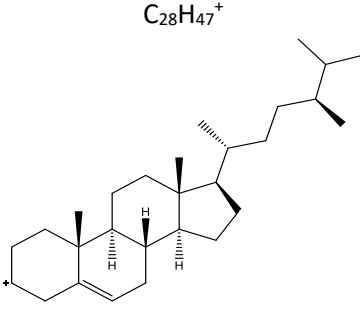
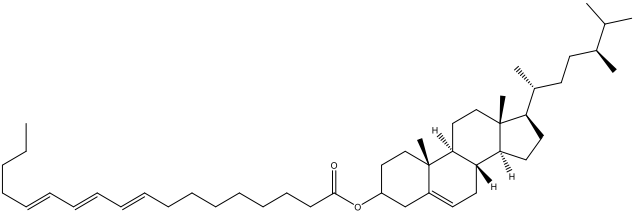
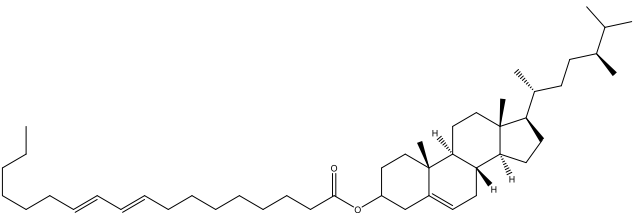
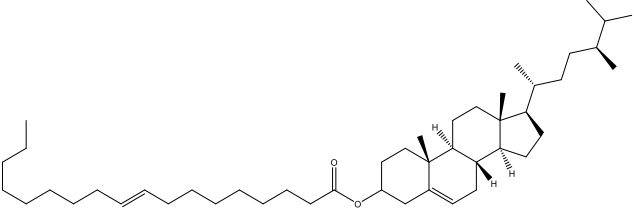
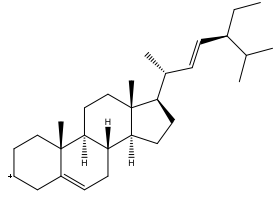
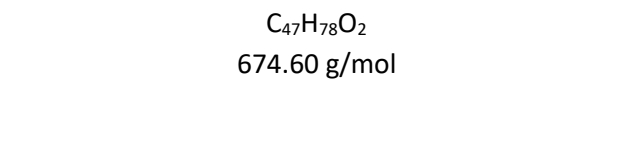
## Chapter 4

Based upon knowledge that SGs and FFAs are deposit forming compounds, and that acylated SGs become less soluble in biodiesel upon loss of the fatty acid chain during transesterification. FASEs may also be a concern as a possible deposit forming precursor or component and further research is required. Work by Feld and Oberender<sup>250</sup> discussed FASEs as possible contaminants of biodiesel that may form deposits after seed crystals of SGs have initially accumulated in fuel filters.

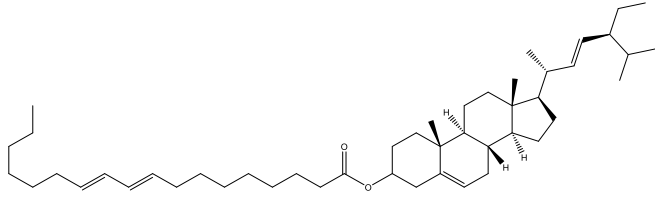
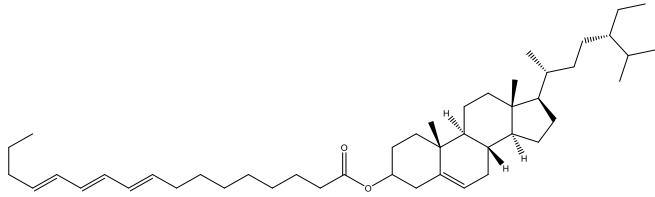
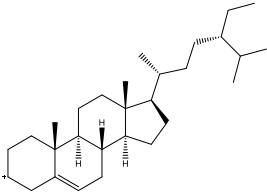
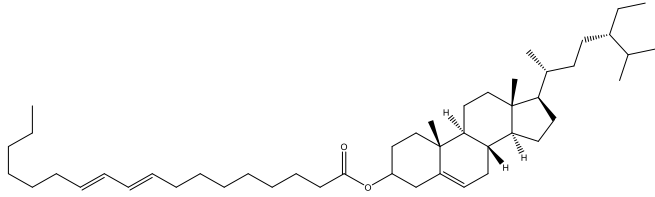
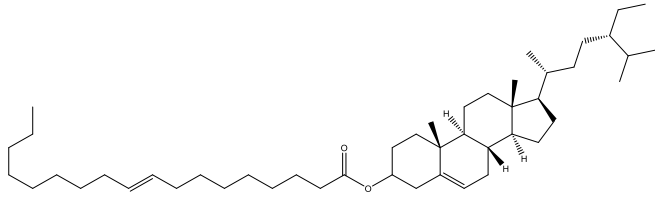
FASEs and sterol fragment ions are only observed by positive ion ESI UHPSFC-MS method and not seen by positive ion ESI FT-ICR MS analysis most likely due to FASEs present at low concentration and ion suppression. It is of note that Kalo *et al.*<sup>233</sup>, Wewer *et al.*<sup>245</sup> and Hailiat and Helleur<sup>249</sup> observed FASEs as ammonium adducts. Previous work by Hailiat<sup>249</sup> states that non-polar nature of SEs resist ESI so the addition of the ammonium acetate facilitates the ionisation as ammonium adducts. Ammonium formate was utilised as an additive in both the modifier and cosolvent in positive ion ESI UHPSFC-MS whereas ammonium adducts are not produced in the direct infusion FT-ICR MS method as the additive was not used in this way, this may also explain why FASEs were absent by positive ion ESI FT-ICR MS. Table 4-13 shows a summary of the FASEs, their respective molecular formulae and structures, adducts that can be present and their associated masses<sup>233</sup>.

Table 4-13 - FASEs summary Masses from literature – Kalo *et al.*<sup>233</sup>

<i>m/z</i> (nominal for UHPSFC-MS)					
Fatty acid sterol esters	Sub compounds (degree of saturation)	Molecular formula and structure of sterol fragment ion	[M + H – fatty acid] <sup>+</sup> sterol fragment ion	Molecular formula, exact mass and structure of sterol ester	[M + NH <sub>4</sub> ] <sup>+</sup> sterol ester
Brassicasterol ester	18:2	$C_{28}H_{45}^+$ 	381	$C_{46}H_{76}O_2$ 660.58 g/mol 	678 ( <i>t<sub>R</sub></i> :2.09 min)
	18:0		381	$C_{46}H_{80}O_2$ 664.62 g/mol 	682 ( <i>t<sub>R</sub></i> :2.16 min)

Campesterol ester	18:3	$C_{28}H_{47}^+$ 	383	$C_{46}H_{76}O_2$ 660.58 g/mol 	678 ( $t_R$ :2.09 min)
	18:2		383	$C_{46}H_{78}O_2$ 662.60 g/mol 	680 ( $t_R$ :2.17 min)
	18:1		383	$C_{46}H_{80}O_2$ 664.62 g/mol 	682 ( $t_R$ :2.24 min)
Stigmasterol ester	18:2	$C_{29}H_{47}^+$ 	395	$C_{47}H_{78}O_2$ 674.60 g/mol 	692 ( $t_R$ :2.14 min)



					
β-sitosterol ester	18:3		397	$C_{47}H_{78}O_2$ 674.60 g/mol 	692 ( $t_R$ :2.14 min)
	18:2	$C_{29}H_{49}^+$ 	397	$C_{47}H_{80}O_2$ 676.62 g/mol 	692 ( $t_R$ :2.20 min)
	18:1		397	$C_{47}H_{82}O_2$ 678.63 g/mol 	696 ( $t_R$ :2.29 min)



#### 4.4.1 MS/MS data

Tandem MS (MS/MS) was undertaken on D#1 to further fully characterise the suspected FASEs species within D#1. Positive ion ESI UHPSFC MS/MS QQQ was used (further details in 2.5.3.1 and 3.5).

The masses for the ammoniated molecules  $[M + \text{NH}_4]^+$  of interest, in this case,  $m/z$  678, 680, 682, 692, 694 and 696 as shown in Table 4-13, were individually isolated and then fragmented in the collision cell. Four different collision energies were considered; 5, 10, 20 and 30 V, with 10 V being considered the best. The resulting product ions were then detected as shown in the example for campesterol esters (Figure 4-38).

The product ion scan for  $m/z$  678 (Figure 4-38) shows that precursor ion  $m/z$  678 has two product ions related to it;  $m/z$  381 and  $m/z$  383. From Table 4-13,  $m/z$  381 and  $m/z$  678 suggest Brassicasterol ester 18:2 while  $m/z$  383 and  $m/z$  678 suggest Campesterol ester 18:3 are present. As aforementioned, the loss of 297 and 295  $m/z$  units respectively is the loss of fatty acid chains differing by a double bond. This confirms that the sterol fragment ions are product ions of the precursor ions observed, in this case  $m/z$  678.

The product ion scan for  $m/z$  680 (Figure 4-38) shows that precursor ion  $m/z$  680 has one product ion related to it;  $m/z$  383. From Table 4-13,  $m/z$  383 and  $m/z$  680 suggest Campesterol ester 18:2 is present with the loss of 297  $m/z$  units is the loss of fatty acid chain.

The product ion scan for  $m/z$  682 (Figure 4-38) shows that precursor ion  $m/z$  682 has one product ion related to it;  $m/z$  383. From Table 4-13,  $m/z$  383 and  $m/z$  682 suggest Campesterol ester 18:1 is present with the loss of 299  $m/z$  units is the loss of fatty acid chain.

## Chapter 4

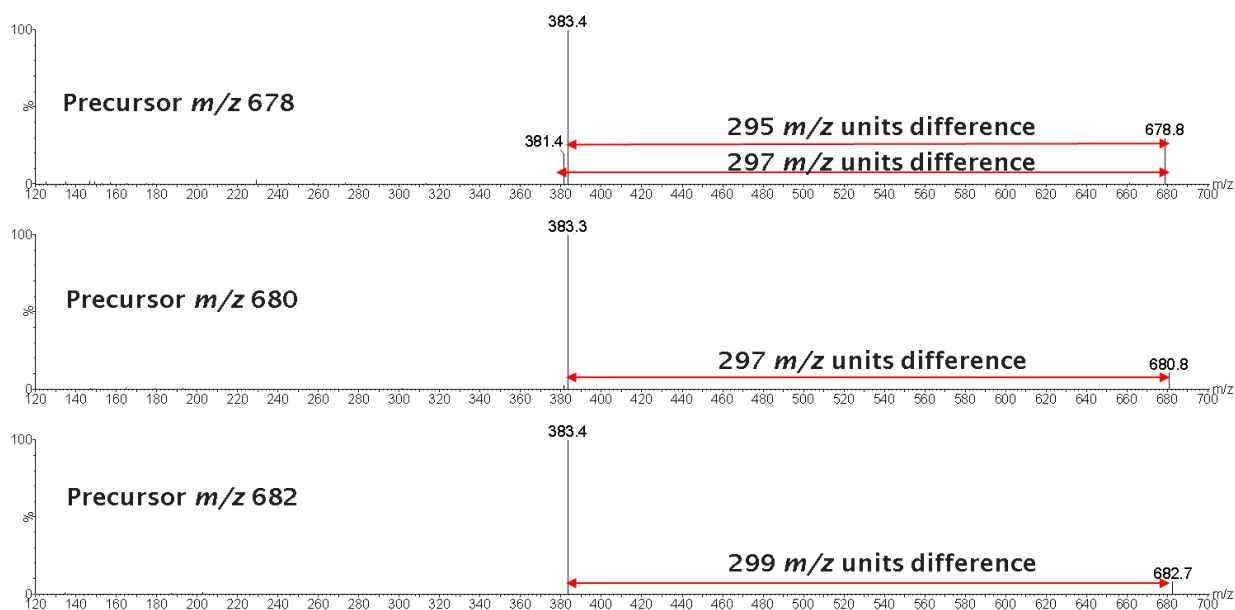


Figure 4-38 - Product ion mass spectrum of D#1 of precursors nominal  $m/z$  678 (top), 680 (middle) and 682 (bottom) for campesterol esters at  $t_R$  2.28, 2.37 and 2.46 min (TQD) respectively (zoomed over  $m/z$  120-700) CE 10V

Table 4-14 shows a summary of the FASEs detected within nine diesel fuels analysed. The symbol  $v^*$  has been utilised for results when compound detected at low abundance (FASE at  $1-5 \times 10^6$  with sterol fragment ion present at  $10^5$ ).

Table 4-14 - Diesel fuels FASES summary (√=detected, √\*=detected at low abundance, X=not detected)

		FASEs								
		Brassicasterol ester		Campesterol ester			Stigmast erol ester	β-sitosterol ester		
		18:2	18:0	18:3	18:2	18:1	18:2	18:3	18:2	18:1
Diesels	D#1	√	√	√	√	√	X	√*	√	√
	D#2	X	X	X	X	X	X	X	X	X
	D#3	√	√	√	√	√	√*	√	√	√
	D#4	√	√	√	√	√	X	√*	√	√
	D#5	√	√*	√	√	√	X	√	√	√
	D#6	√	√*	√	√	√	X	√	√	√
	D#7	X	X	X	X	X	X	X	X	X
	D#8	√	√*	√	√	√	X	√	√	√
	D#9	√	√*	√	√	√	X	√*	√	√

FASEs were detected in D#1, 3, 4, 5, 6, 8 and 9 during analysis. FASEs were not detected in D#2 and D#7.

Stigmasterol ester 18:2 was not detected in all fuels with the exception of D#3 but that is at low abundance. Campesterol esters and β-sitosterol esters were the most abundant FASEs in the diesel samples.

The presence of FASEs in diesels is believed to be linked to biodiesel and feedstocks so may suggest poor transesterification.

The FASEs in this work were observed during screening of diesels/biodiesel blended diesels from the field. However, from literature FASEs have been not been reported to have been detected in

biodiesel/diesel blends or fuels containing any petrodiesel quantity before and are not known/not reported to be a deposit forming compound at present. Therefore, this work is novel and of great significance.

### 4.5 Application of screening method with respect to biodiesel quality

An example application for the diesel fuels components screening method is to determine biodiesel quality, in this particular case, the degree to which transesterification had taken place. Characterisation of homemade biodiesel and neat vegetable oils is of current interest as used cooking oils are being used to make used cooking methyl esters (UCOME) in addition to people trying to run vehicles on untransesterified oils.

Homemade biodiesel was synthesised by colleagues at the University of Southampton and compared to commercial biodiesel B100 (D#1). The starting vegetable oil and the homemade biodiesel were analysed with both positive and negative ion ESI UHPSFC-MS.

The absence of FAMES (shown in Figure 4-39) in the homemade biodiesel compared with D#1 and the presence of FFAs (shown in Figure 4-40) in the homemade biodiesel shows failed transesterification.

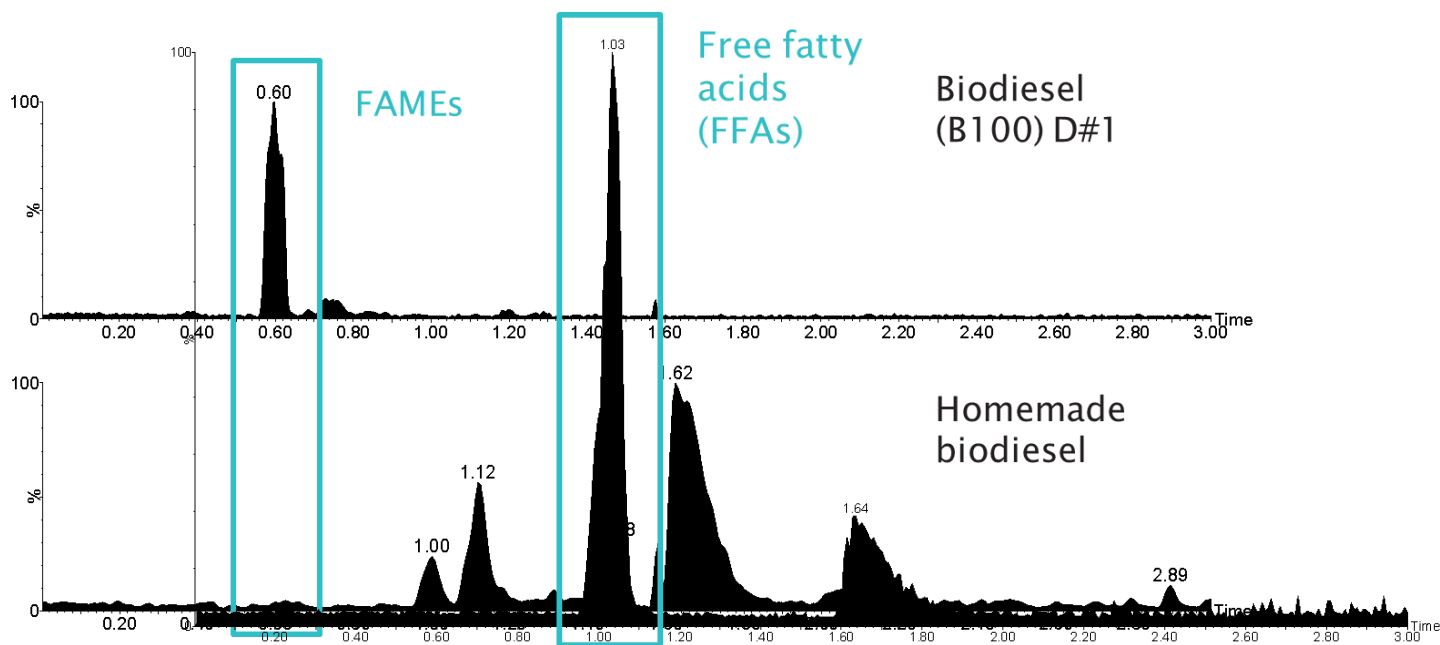


Figure 4-39 - Figure 4-40 - Negative ion ESI UHPSFC-MS BPICC of homemade biodiesel with pale blue box highlighting FFA region of retention ( $t_R$  0.95-1.10 min)

This screening methodology allows for the relative abundance of the fatty acid composition profile observed to then be related back to biodiesel feedstocks. Each feedstock has a unique

fatty acid composition, for instance rapeseed is most abundant in C18:1 whereas soybean is most abundant in C18:2<sup>96</sup>. This allows for the identification and differentiation of biodiesel feedstocks from diesel blends and biodiesel fuels, demonstrating an additional way in which this screening methodology and the data can be utilised. To relate this to actual relative amounts in fuels, reference standards of known concentration would also need to be analysed in a similar fuel matrix, however due to the complexity of fuel samples often due to the sheer number of other components present, it may prove difficult to determine accurately. Another applicability example for my screening methodology is fuel industry quality control testing for specific components in routine testing.

## 4.6 Diesel analysis protocol trees

Diesel analysis protocol trees have been designed as reference tools to aid in the understanding of diesel fuels' chemistry in both their practical analysis and characterisation respectively. This is a culmination of the analysis techniques used throughout this project in order to characterise diesels, highlighting similarities and differences, and determine any links between fuels and their propensity to form deposits. Both analysis protocol trees are visual representation of the analysis to help to link compounds to specific analysis techniques.

Diesel analysis protocol trees have been devised as both an analyst flow providing a practical experimental process, and as a diesel flow format providing a thought process for diesel analysis.

### 4.6.1 Analyst flow (diesel)

The analyst flow (diesel) analysis protocol tree, as shown in Figure 4-41, should be considered as the practical laboratory experimental process. This is a proposed flow protocol for an analyst to consult when faced with a sample of an unknown diesel/biodiesel sample X that requires characterisation of compounds present.

The analyst flow (diesel) analysis protocol tree clearly and concisely answers the following:

- What do specific analytical techniques tell me about diesel X?
  - What components can be detected?
  - Which technique should be used for a specific component?

The characterisation approach can be undertaken in two ways; targeted or untargeted.

## Chapter 4

An untargeted approach is initially undertaken utilising direct infusion positive and negative ion ESI using a low concentration sample. This untargeted screen will be data rich and this can be gleaned to inform concentration as well as further experimentation.

The targeted approach is commonly used if a specific compound is suspected (*e.g.* if biodiesel is thought to be problematic, analyse for FAMES, MAGs, etc.) or information from the initial untargeted screen suggests presence of specific compounds.

The data from the targeted analysis for a specific compound (targeted component screen) can then also be used to inform other experiments and what is actually present – data will be rich even if the expected compound is absent *e.g.* if using ESI to screen for FAMES, MAGs will also be observed if present.

It should be noted each targeted component screen is still untargeted for that technique (ionisation and chromatographic parameters) but could be further optimised for a specific compound to be further targeted (selected ion recording (SIR) for specific  $m/z$  values, further optimise chromatography).

Some compounds of interest can be identified using multiple analysis techniques, however if there is a preferred technique it is indicated in Figure 4-41, with the compound underlined and in bold in the preferred characterisation method.

If specific compounds were of great interest, full characterisation/structural elucidation could be undertaken using tandem MS – such as FASEs in D#1 as an example (discussed in 4.4.1).



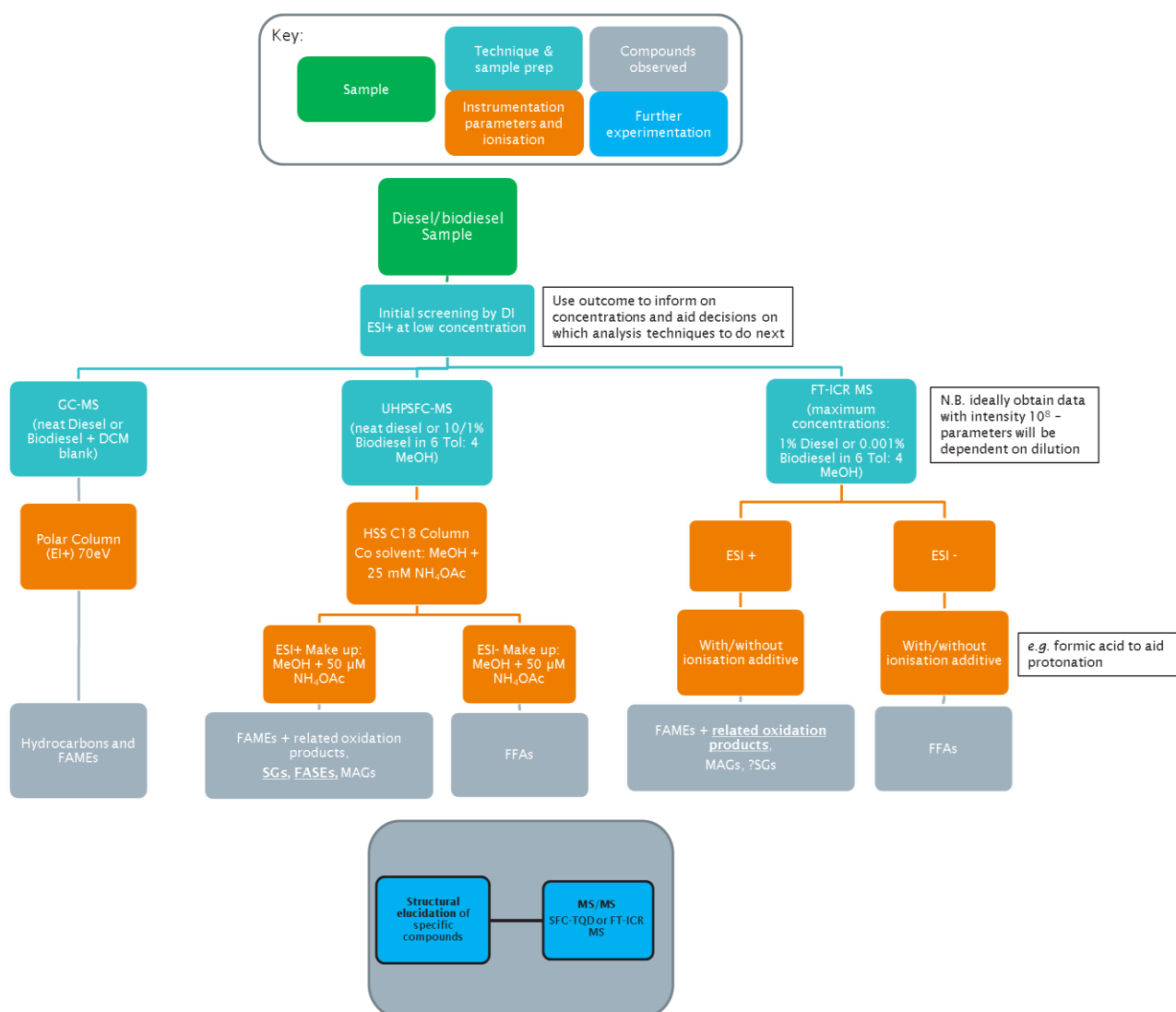


Figure 4-41 – Analyst flow (diesel) analysis protocol tree

(Compounds that are in bold and underlined indicate the preferred method for characterisation)

#### 4.6.2 Diesel flow

The diesel flow analysis protocol tree, as shown in Figure 4-42, should be considered as more of a thought experiment/protocol. This flow is proposed for consultation as a visual reference tool when faced with an unknown diesel/biodiesel sample that requires characterisation of compounds present.

Initially the fuel sample should be inspected and any additional information about the sample obtained. This can provide valuable information that can aid in the characterisation and provide early indications as to the types of components possibly present.

An untargeted approach is initially undertaken utilising direct infusion positive and negative ion ESI using a low concentration sample. This untargeted screen will be data rich and used to inform further experimentation, it may show specific compounds are present.

The targeted approach is then commonly used if a specific compound is suspected.

However, numerous questions must be asked prior to analysis. These should include:

- Which technique will give confirmation of the compound of interest?
  - Need to think about chromatography, ionisation and chemistry of sample

The data from the targeted component screen for a specific compound scan is also data rich and can be used to inform other experiments and what is present in the sample. Data will be rich even if the expected compound is absent, meaning compounds may be observed even if not those initially targeted *e.g.* if using ESI to screen for FAMES, MAGs will also be observed if present.

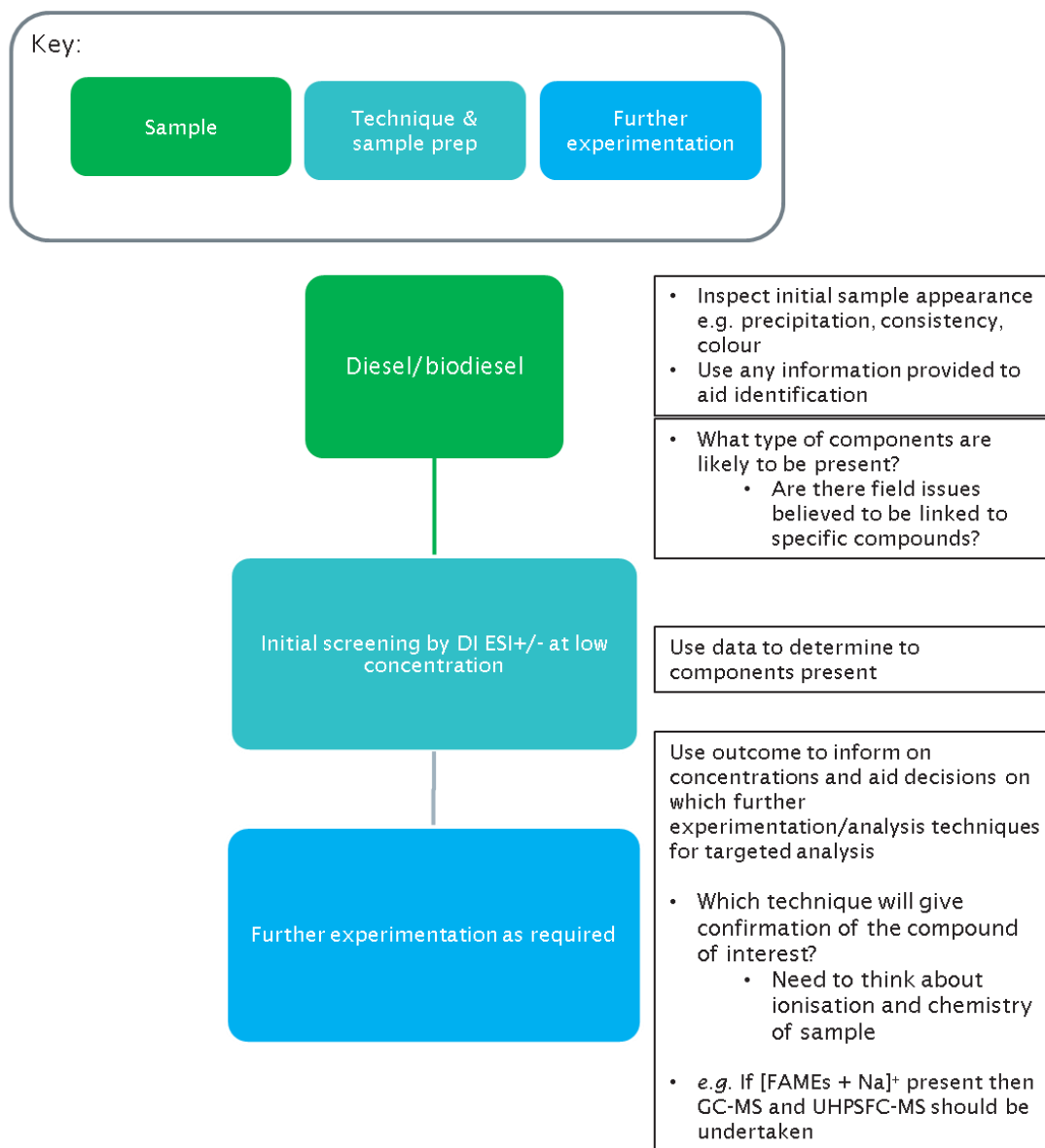


Figure 4-42 - Diesel flow analysis protocol tree

## 4.7 Conclusions

### 4.7.1 GC-MS Analysis

The optimised polar column GC-MS method provided chromatographic separation and detection of base fuel hydrocarbons and FAMEs in diesel and biodiesel fuels. EI provided characteristic fragmentation in mass spectra that allowed structural information to be obtained. The following ions were used (manually) in RICCs, as they are known to be characteristic for the compounds of interest;  $m/z$  43 and 57 (aliphatic hydrocarbons),  $m/z$  74 and 87 (FAMEs), and  $m/z$  77 and 91 (aromatic hydrocarbons). Slight differences such as different ion ratios within the fragmentation patterns also afforded the differentiation and identification of different FAMEs (carbon number :number of double bonds). Each FAME species was chromatographically separated (retention time different) which aided confirmation of compound identification.

However, the nine diesel fuels analysed by polar column GC-MS looked very similar as the only differences that were observed are varying abundances of base fuel hydrocarbons and FAMEs or absence of these compounds. This therefore makes it difficult to differentiate the fuels or link fuels with a propensity to form deposits.

SpectralWorks AnalyzerPro<sup>®</sup> was employed as an automated processing methodology for fast compound identification (or components if library match not made) and used to compare component libraries of two diesels to achieve a percentage similarity between two diesels. This software enables direct diesel to diesel comparison and highlights any significant differences or similarities. Varied percentage similarities between diesels suggests differences are present, particularly observed in D#1 , D#2 and D#7.

### 4.7.2 Diesel fuels component screening methodology

A rapid screening methodology for five known deposit forming component classes (FAMEs, FAME oxidation products, MAGs, FFAs, and SGs) has been developed and applied to characterise diesel fuels, affording many similarities and differences to be seen within deposit and non-deposit forming diesel fuels from the field.

Positive ion ESI UHPSFC-MS afforded detection of FAMEs, FAME oxidation products and MAGs, while negative ion ESI UHPSFC-MS afforded detection of FFAs with chromatographic separation by fatty acid chain length and degree of unsaturation being achieved.

SGs were not detected by either positive ion ESI techniques, however sterol fragment ions were detected by positive ion ESI UHPSFC-MS in a number of the diesels, found to relate to fatty acid sterol esters (FASEs).

Positive ion and negative ion ESI FT-ICR MS aided in the resolution of nominally isobaric species and further confirmed assignments by providing molecular formulae.

These analytical techniques allowed problematic compounds to be detected; both recognised deposit precursor components/group of components and other currently unrecognised species that may be involved in deposit formation which then add to the knowledge and understanding of the current deposit issues. Additionally, the analysis of fuels allowed for the identification of components that may be precursors to IDIDs as well as compounds that do not make it to the fuel injector.

This screening methodology and the individual methods within it have multiple applications including (not exhaustive) the characterisation of unknown fuels, the characterisation of deposit forming fuels under investigation, fuels to be checked for these specific classes of compounds. Another is a biodiesel screen, as exemplified in section 4.5, which afforded the characterisation of vegetable oil and homemade biodiesel with these methods demonstrating its use with vegetable oil type matrices, in the age of upcoming used cooking oil methyl esters (UCOMEs).

#### **4.7.3 Fatty acid sterol esters detection method**

A novel positive ion ESI UHPSFC-MS detection method for fatty acid sterol esters (FASEs) in biodiesel and fuels (diesel/biodiesel) has also been developed as part of the screening method, also affording chromatographic separation based on the degree of saturation of the fatty acid chain.

FASEs were fully characterised using positive ion ESI UHPSFC MS/MS QQQ as FASEs and sterol fragment ions are only detected by positive ion ESI UHPSFC-MS method as  $[M + \text{NH}_4]^+$  and  $[M + \text{H} - \text{Fatty acid}]^+$  respectively, and not seen by positive ion ESI FT-ICR MS.

FASEs were detected for the first time in diesel/biodiesel fuel blends, preceding this FASEs have only been reported to have been analysed in pure biodiesel and vegetable oils. Also FASEs at present have not been investigated or found to cause filter blocking or IDIDs Therefore this novel work is of great importance.

#### 4.7.4 Diesel analysis protocol trees

As a result of the screening method, structured visual representations were constructed linking analytical techniques to compounds, aiding understanding and suggesting methodologies for analysis for an end user in industry.

Two diesel analysis protocol trees were devised (analyst flow (diesel) and diesel flow) to consolidate methodologies and provide visualisation (flow chart) of analytical techniques linked to the compounds detected by them respectively.

These diesel analysis protocol trees were created as a tool to assist analysts and the fuel industry with characterisation of fuels (diesels, biodiesels), specifically identifying known deposit forming compounds and possibly enabling links to be made between fuel components and their propensity to form deposits.

The diesel analysis protocol trees provide a reference tool to aid both practical analysis and the analysis thought process of diesels.

The analyst flow (diesel) analysis protocol tree affords guidance suggesting analytical approaches to be utilised for an unknown diesel/biodiesel sample X. Initially using an untargeted screen, followed by various techniques for different targeted analysis (specific compound of interest), in a similar way to test methods already used in industry *i.e.* follow method protocol for a given method for compound X. This leads to rapid analysis of samples as targeted analysis for the particular compound of interest can be undertaken rather than running standard techniques in the hope of observing the compound X.

The diesel flow analysis protocol tree informs thought processes (a logical flow to chart) to improve future understanding and characterisation of diesels.







## Chapter 5 Analysis of diesel engine deposits using complimentary analytical techniques

### 5.1 Introduction

Multiple analytical approaches, used previously for the analysis of diesel fuels (Chapter 4), were also used to analyse and characterise deposits from various locations within the fuel injection equipment (FIE) and some associated fuels.

The analytical challenges posed by diesel engine deposits are outlined below along with a brief introduction to each deposit type encountered in this chapter.

#### 5.1.1 The analytical challenge of characterising diesel engine deposits

Numerous analytical techniques have previously been employed in the complex study of diesel engine deposits (discussed in further detail in 1.3.8).

However problematic deposit formation known to cause engine performance issues, is still occurring even after much research<sup>31, 39</sup>. Therefore, characterisation of these deposits is of utmost importance, as it will lead to increased understanding and knowledge of deposits and their formation, possibly resulting in remediation chemistries.

However, the current deposit problem is very complex with multiple issues particularly around characterisation (1.3).

#### 5.1.2 Fuel filters

A fuel filter is comprised of a filtration medium (either a paper, cloth or felt filter<sup>53</sup>) pleated into a cartridge (Figure 5-1)<sup>52</sup>. The folding into a concertina type structure results in an increased surface area for filtration and provides reasonable particulate capacity to maximise life-time between filter changes<sup>46</sup>. The large surface area also means the filter is less likely to block or clog with particulate matter or biodiesel type contamination that would result in restricted flow in the fuel line and reduced engine performance<sup>46, 53</sup> (Figure 5-1 and Figure 5-2<sup>51</sup>).

Fuel filters are located on the fuel line after the fuel tank. They are sited before the fuel is pumped to high pressure into the common rail of the fuel injection system that supplies fuel to

the fuel injectors, as shown in Figure 5-3<sup>1, 46, 109</sup>. Fuel filters are designed to be compatible with specific FIEs<sup>46</sup> and some vehicles have two fuel filters installed for even better protection for the FIE<sup>53</sup>.

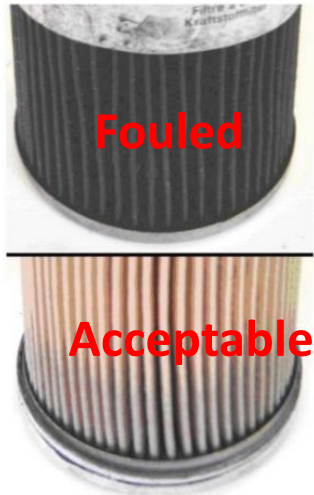


Figure 5-1 – Fouled and acceptable fuel filters taken from the field, adapted from<sup>57</sup>

Associated residue/gunk from biodiesel contamination



Figure 5-2 - Biodiesel type contamination on fuel filter, adapted from<sup>253</sup>

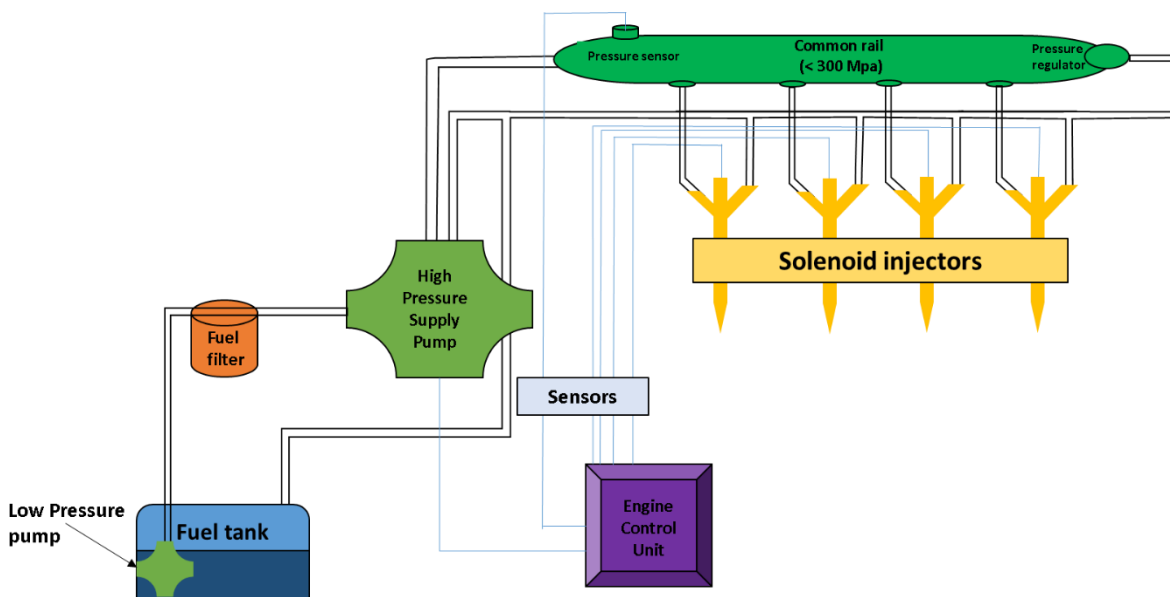


Figure 5-3 - Diagram of Common Rail Fuel Injection system, adapted from<sup>7, 52, 114</sup>

A fuel filter is used to filter out and remove particulate contaminants (>5-10  $\mu\text{m}$ ) within the fuel, such as dirt and rust particles, to ensure good fuel purity prior to it entering the high precision FIE

in a common rail diesel engine<sup>46, 53-54</sup>. The FIE has tight tolerances that are extremely sensitive to contamination and can ultimately result in wear, damage or blockage leading to failure in either pumps or fuel injectors<sup>46, 53-54</sup>.

Water can also cause corrosion so it is also removed by the fuel filter due to the different surface tensions of water and diesel<sup>46, 54</sup>, 72.8 mN/m and 30.9 mN/m at 20 °C respectively<sup>252-253</sup>. The water molecules amalgamate on the filter and are then collected in the water accumulation chamber below the filter<sup>46</sup>.

The main objectives for analysing fuel filters and their associated deposits was as follows:

- To characterise the components within each deposit
- To identify the differences and variations in each deposit and deposit type
- To identify any components that are known to currently cause performance issues or are recognised deposit precursors
- To investigate and attempt to identify other deposit precursors which may be currently unrecognised species involved in deposit formation
- Relate components back to fuel chemistry and deposit formation

The analysis of the fuel filters and their associated deposits was undertaken as the fuel filter is located prior to the FIE, and more specifically the fuel injectors. The hypothesis was that the chemistry and components seen in fuel filter deposits may be similar to that seen in fuel injector deposits (IDIDs) and also that precursors to IDIDs may be observed within the fuel filter deposits.

### **5.1.3 Fuel injectors**

A fuel injector is shown in Figure 5-4 and consists of a nozzle and a solenoid valve that can switch quickly and controls the opening and closing of the nozzle. Each combustion cylinder of the engine has an individual fuel injector within the cylinder head, resulting in an individual injection cycle for each cylinder. The fuel injector injects the exact volume of diesel required directly into the combustion chamber at a constant pressure (from the common rail) and at an exact time, all of which are calculated by the electronic engine control unit, resulting in a high precision fuel injection system which can be manipulated in line with engine operating status. Subsequently

diesel engines using these systems afford overall high engine performance, particularly in terms of fuel efficiency, as well low engine noise and low emissions<sup>46</sup>.

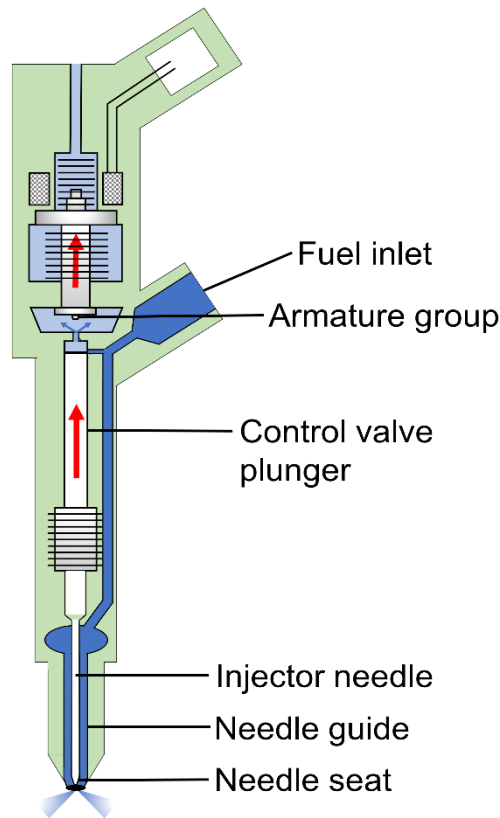


Figure 5-4 - Diagram of fuel injector

The operation of fuel injectors within a common rail diesel engine is outlined in 1.2.3.3.

As outlined in the project objectives and chapter 1, deposits, particularly internal diesel injector deposits (IDIDs) have been found to occur on fuel injectors within common rail diesel engines. There is still much to be understood around IDIDs, so analysis of fuel injectors with IDIDs in addition to fuels believed to be deposit forming should aid in gaining a greater understanding of IDIDs.

#### 5.1.4 JFTOT rods and method

The Jet Fuel Thermal Oxidation Tester (JFTOT) is commonly used to test aviation turbine fuel (AVTUR)(ASTM D3241 – Thermal Oxidation Stability of Aviation Turbine Fuels<sup>254</sup>) is used to measure/study the thermal oxidation of a fuel at a high temperature by simulating conditions experienced within an engine<sup>28, 255</sup>. All fuels are subjected to the air when in use, particularly within the engine. The oxygen in the air causes the fuel to oxidise and form materials that deposit on the

engine parts. The thermal stability of a fuel is “a measure of the amount of heat fuel can be exposed to before it oxidizes”<sup>256</sup>.

However it is becoming increasingly common that the JFTOT test can be used with diesel samples rather than AVTUR to simulate the deposit formation seen on fuel injectors in diesel engines in the laboratory<sup>28, 123</sup>. This is one current industry proposed solution and links possible problematic fuels to deposit formation<sup>28-29</sup>. Innospec used the JFTOT test in this way to prepare the samples for analysis in this work.

During the test, deposit formation is facilitated through aerating and heating the fuel and then a JFTOT rod (metal surface) is used to collect deposits. Fuel pumped at a fixed rate is pressurised, aerated and heated up to 275 °C). This heated fuel then passes through a stainless steel filter where deposition of degradation products may occur. A schematic is shown in Figure 5-5<sup>257</sup>.

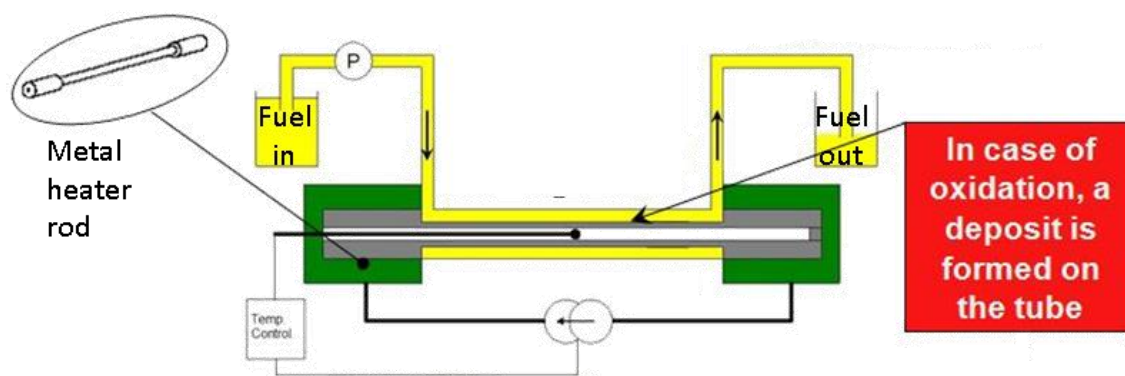


Figure 5-5 - Schematic of JFTOT testing, adapted from<sup>259</sup>

A metal heater rod, known as a JFTOT rod, is used in the test and the amount of deposits on the JFTOT rod is rated after testing. The JFTOT rod rating is undertaken visually after each test by examining the JFTOT rod and comparing to a visual match chart (Figure 5-6<sup>256</sup>). The JFTOT rod ratings are between 0 and 4, with 3 and above as a failing test result (Figure 5-6). The JFTOT rod rating is then used as part of an assessment of the thermal oxidative stability of the fuel<sup>256</sup>.

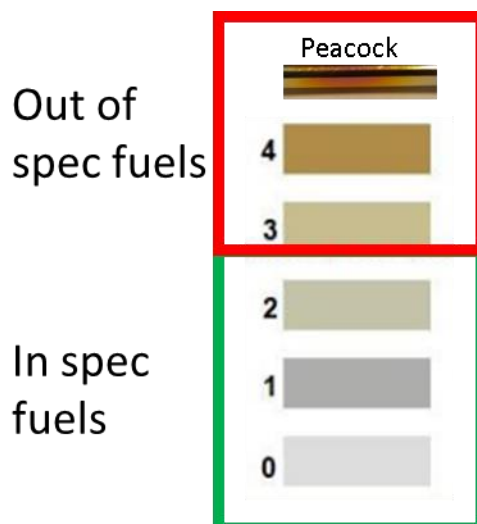


Figure 5-6 - JFTOT rod rating system, adapted from<sup>258</sup>

The JFTOT rods and associated fuels in this project were analysed to:

- Characterise species in both the fuels and the deposits on the JFTOT rods
- Compare and contrast the fuel with the deposits on its associated JFTOT rod
- Compare and contrast the species present in the deposits on the different JFTOT rods
- Investigate two sample preparation methods to find the optimum deposit removal method by comparing species present, to further develop the laboratory analysis method

Additionally this JFTOT rod work was undertaken to replicate work undertaken by Patel<sup>29, 211</sup> to validate results and further improve and develop the analysis method.

#### 5.1.5 Purpose of this work

The various deposit samples discussed in this chapter were all analysed using the same complimentary chromatography and mass spectrometry techniques for characterisation of the fuels discussed previously. This demonstrates the versatility of this analytical approach to be used for all deposit related samples (fuels, filters, deposits and laboratory synthesised deposits), meaning that all samples relating to deposit issues within the field can be analysed following the entire flow through the FIE. As a result, comparisons can be made between different areas of an FIE to further understand the chemistry taking place and compounds present. These analytical techniques also allow problematic compounds to be identified that then add to the knowledge and understanding of the current deposit issues.

The analysis of fuel filters allows for the identification of components which may be precursors to IDIDs as well as compounds which do not make it to the fuel injector, due to their position in the FIE. Their analysis also adds to knowledge surrounding the ongoing fuel filter deposit/blocking issues which are also present in the field and of interest to the fuel industry<sup>52</sup>. Eight fuel filters and a fuel filter residue (gunk) were analysed in this work, which provided a greater and more comprehensive insight into the different types of compounds present in fuel filters.

Additionally, the analysis of the fuel injector tip IDID from the field provided an example of the key issue that was the motivation and justification for this project and demonstrates the issues surrounding analysis of these samples, particularly sample preparation.

The analysis of JFTOT rods and associated fuels were also included in this body of work as they are an example of deposits artificially synthesised within petrochemical lab environment from fuel thought to be problematic or as a means of determining whether a fuel is deposit forming. As both deposits on JFTOT rods and the associated fuels were analysed, it allowed for links to be made between them. Again, as multiple rods and fuels were analysed a more comprehensive depiction of the deposit issue could be achieved.

## 5.2 Analysis of fuel filters from the field

Eight fuel filter samples (SS2-SS4, SS6-SS10) and the associated residue (gunk) collected from a fuel filter (SS5) were prepared as outlined in 3.2.2.4.

The diesel screening methodology (further detail in chapter 4) utilised previously for the analysis of fuels, both diesels and biodiesels, was used to demonstrate the method scope with fuel filter samples initially. This allowed the development of a deposit screening methodology, affording direct comparison between diesels and deposit samples. GC-MS was not utilised for analysis of the fuel filter samples, as the other analytical approaches demonstrated in chapter 4 were found to glean much richer sample information as initial screening methods (rather than detection of FAMES and hydrocarbons only).

The compounds (observed and discussed in detail in chapter 4) included in the screening methodology:

- Fatty acid methyl esters (FAMES)
- Fatty acid methyl ester (FAME) oxidation products
- Free fatty acids (FFAs)

## Chapter 5

- Sterol glucosides (SGs)
- Monoacylglycerols (MAGs)
- Fatty acid sterol esters (FASEs)

One example of each compound found to be present within the fuel filters will be shown in detail, comparing and contrasting both positive and negative ion ESI UHPSFC-MS and FT-ICR MS data.

The key findings/highlights of each fuel filter sample will be discussed with similarities between fuel filter samples outlined and the filters grouped by compounds present. However, only the major components or those easily recognisable (listed above) have been highlighted below, further analysis in greater detail still needs to be undertaken and may uncover further components of interest as minor components or at trace levels.

### 5.2.1 Fatty acid methyl esters (FAMES)

The SS10 fuel filter is used as the example to illustrate the presence of FAMES within fuel filter samples.

Table 4-2 (page 119) shows a summary of FAMES to be screened for, their respective molecular formulae and structures, adducts that can be present and their associated masses. Nominally isobaric species are in bold and underlined.

Figure 5-7 shows a positive ion ESI UHPSFC-MS base peak ion current chromatogram (BPICC) of the SS10 fuel filter, with the pale blue box highlighting chromatographic peaks within the region of retention found for FAMES ( $t_R$  0.55-0.70 min). The corresponding positive ion ESI UHPSFC-MS mass spectrum shown in Figure 5-8, shows ammoniated molecules  $[M + NH_4]^+$  observed at nominal  $m/z$  286-316, consistent with FAMES nominal masses.



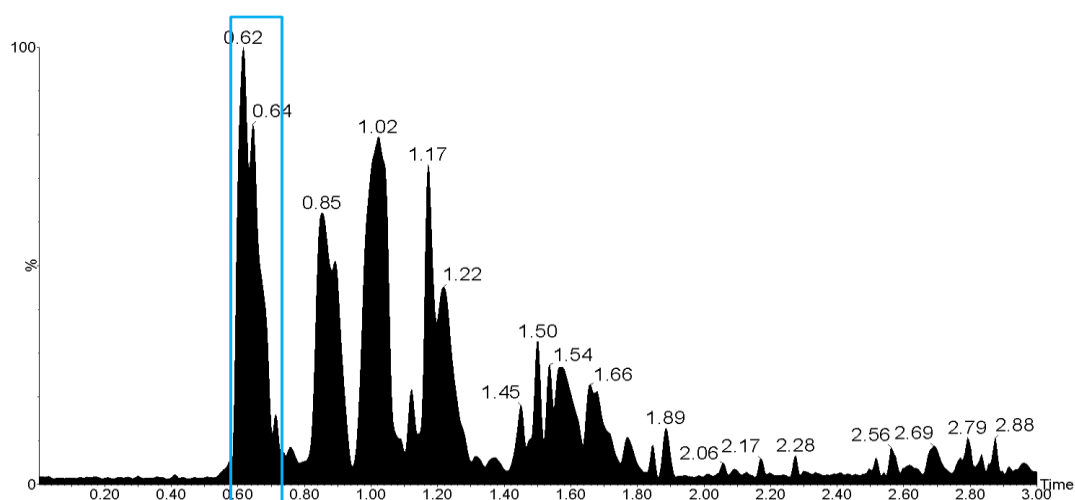


Figure 5-7 – Positive ion ESI UHPSFC-MS BPICC of fuel filter SS10 with pale blue box highlighting FAMEs region of retention ( $t_R$  0.55-0.70 min)

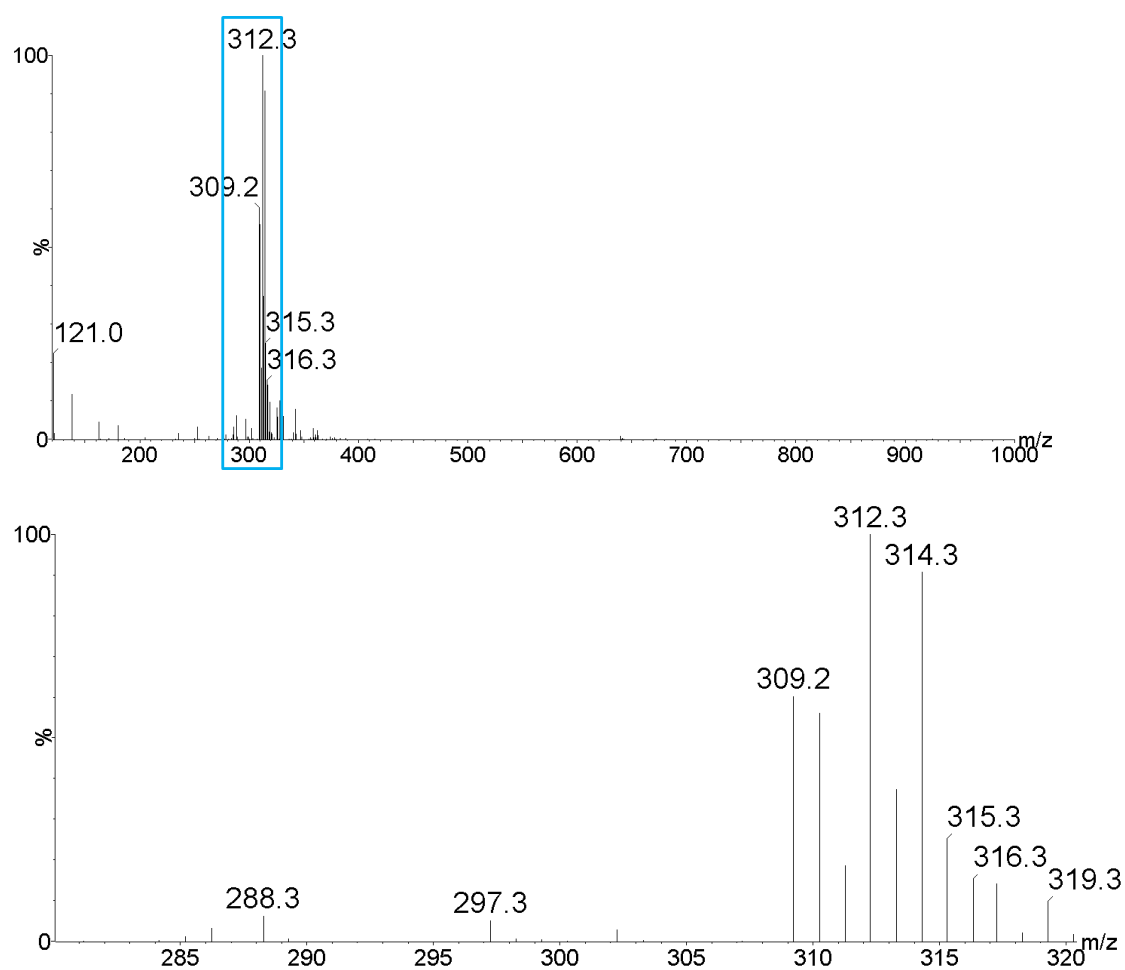


Figure 5-8 - Positive ion ESI UHPSFC mass spectrum of fuel filter SS10 at  $t_R$  0.55-0.70 min(A) mass range  $m/z$  120- 1000 (B) zoomed mass range  $m/z$  280-320

## Chapter 5

RICCs for FAMES and their associated nominal  $m/z$  values (in this case  $[M + \text{NH}_4]^+$  as shown in Table 4-2) is shown in Figure 5-9, suggesting that the respective peaks are related to the C16:1, C16:0, C18:3, C18:2, C18:1 and C18:0 FAMES.

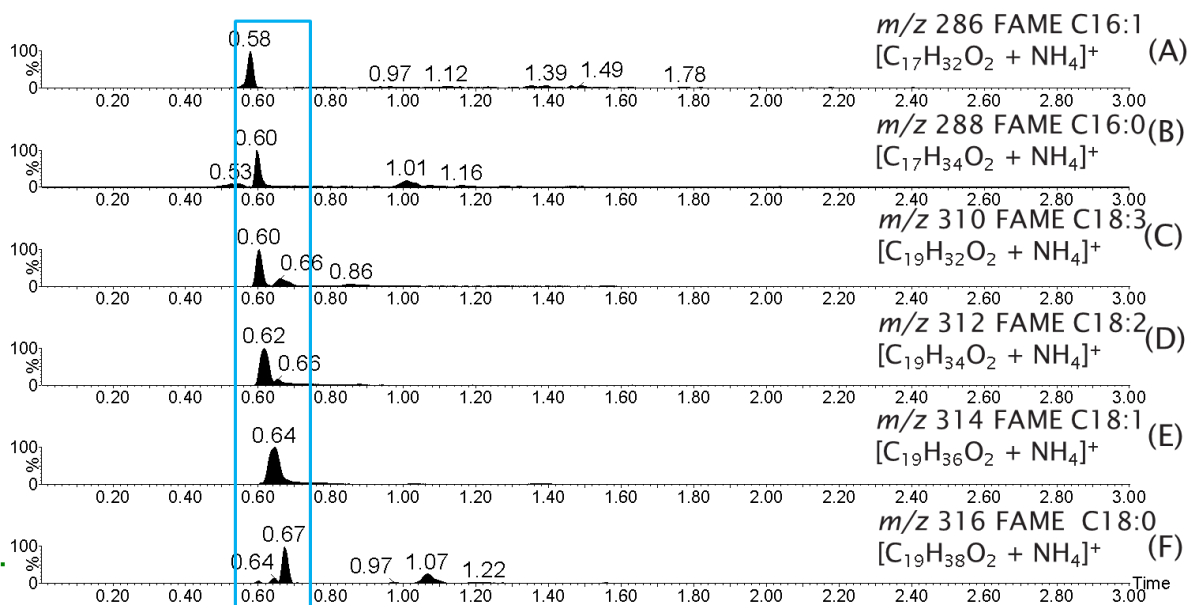


Figure 5-9 – Positive ion ESI UHPSFC-MS RICCs of SS10 showing FAMES with pale blue box highlighting FAMES region of retention ( $t_R$  0.55-0.70 min)

As D#1 (commercial B100) has been previously analysed (chapter 4) and essentially acted as a FAMES standard, the assignment of the FAMES can be given with reasonable confidence.

Figure 5-10 shows sodiated molecules observed for FAMES C16:1, C16:0, C18:3, C18:2, C18:1 and C18:0 when using direct infusion positive ion ESI FT-ICR MS (Table 4-2). This is in agreement with proposed FAMES observed in the positive ion ESI UHPSFC-MS data for SS10, with the sodium adducts further confirming presence of FAME species with accurate mass measurements providing formulae increasing confidence in compound assignments.

Nominally isobaric species are observed with both  $[\text{C16:0} + \text{Na}]^+$  and  $[\text{C18:3} + \text{H}]^+$  at nominal  $m/z$  293. An attempt to resolve this in the fuel filter samples was *via* forced protonation of the FAMES to enhance the signal for the protonated molecule, using the addition of formic acid. However, cationisation was still prevalent and therefore forced cationisation (*e.g.* use of ammonium acetate) is a better route.

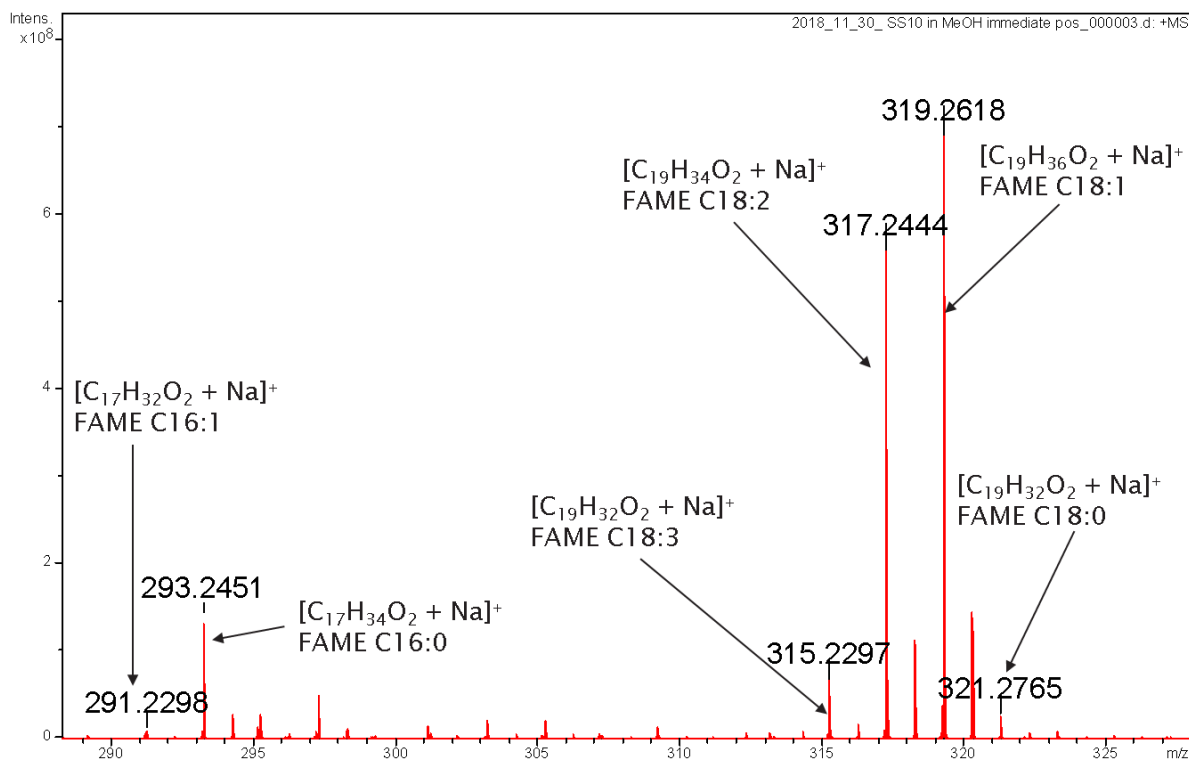


Figure 5-10 - Direct infusion positive ion ESI FT-ICR mass spectrum of SS10 (zoomed  $m/z$  290-330), showing sodiated molecules for FAMES

Table 5-1 shows a summary of the FAMES detected within the fuel filters analysed. The symbol  $\nabla$  has been utilised for results when low abundance ( $10^6$ ) detected.

Table 5-1 – Fuel filters FAMES summary (√=detected, X=not detected, √? = low abundance detected)

	FAMES (carbon number: number of double bonds)						
		C16:1	C16:0	C18:3	C18:2	C18:1	C18:0
Fuel filters	SS2	√	√	√	√	√	√?
	SS3	X	X	X	X	X	X
	SS4	√?	√?	√?	√?	√?	X
	SS5	√	√	√	√	√	√?
	SS6	X	X	X	X	X	X
	SS7	X	X	X	X	X	X
	SS8	X	X	X	X	X	X
	SS9	X	X	X	X	X	X
	SS10	√	√	√	√	√	√?

The major differences between the fuel filters were all FAMES were detected in fuel filter SS4 at trace level except for FAME C18:0. Also FAME C18:0 is only detected approximately an order of magnitude less in fuel filter SS10.

The key similarities are that fuel filters SS2 and SS5 both have low abundance ( $\sim 10^6$ ) of 18:0 detected but all other FAMES detected are the same. In addition, fuel filters SS2, SS5 and SS10 all have C16:1, C16:0, C18:3, C18:2, C18:1 detected.

The FAMES not detected in some of the fuel filter samples suggests that some of the fuels were neat mineral diesel B0 meaning no FAMES were present.

These results agree with previous GC-MS work by Barker *et al.*<sup>52</sup> but demonstrated the use of different analytical techniques to analyse fuel filters. Positive ion ESI was utilised as a selective ionisation technique rendering the base fuel hydrocarbons invisible affording improved detection

of polar components within deposits. The use of FT-ICR MS allowed separation of nominally isobaric species and confirmation of FAMES from generated molecular formulae from accurate mass measurements.

FAMES have previously been linked to both fuel filter blocking and IDIDs as aforementioned in chapter 1 and chapter 4. Diesel blends containing biodiesel (FAMES) have an increased likelihood to form deposits or fouling in fuel filters (and fuel injectors)<sup>85, 227</sup>, however deposit issues have also been reported in mineral diesel fuels<sup>52</sup>. Therefore bio-components are believed to play some contributing role to deposit formation due to their unstable nature, but are not the sole cause of deposit formation<sup>85, 120</sup>. FAMES are also observed in aged fuel IDIDs (chapter 1 and chapter 4) so is it possible their presence in fuel filters (if not all filtered out at this stage) suggests that they could be precursor compounds to aged fuel IDIDs.

Other factors to consider when analysing deposits for FAMES include whether the solubility or the age of the biodiesel within the fuel effects whether it plays a role in if it is filtered out and blocks the filter. Additionally, does the quantity of the biodiesel blended into the fuel affect this.

### 5.2.2 Fatty acid methyl ester (FAME) oxidation products

The SS4 fuel filter will be used as the example to illustrate FAME oxidation products within fuel filter samples.

Table 4-4 (page 125) shows a summary of the FAMES and FAME oxidation products, their respective molecular formulae, adducts that can be present and their associated masses<sup>96, 232</sup>. Each FAME has a designated colour, dependent on number of double bonds, which match the coloured arrows in Figure 5-11 and Figure 5-13.

Figure 5-11 shows ions consistent with the respective FAME oxidation products up to the addition of three addition oxygen atoms were also observed, in agreement with Table 4-4.

Chapter 5

FAMES and FAME oxidation products were found to elute between  $t_R$  0.50-0.80 min as shown in Figure 5-12. The corresponding positive ion ESI UHPSFC mass spectrum shown in Figure 5-13 shows ammoniated molecules  $[M + NH_4]^+$  in agreement with FAMES and FAME oxidation product nominal masses as shown in Table 4-4.

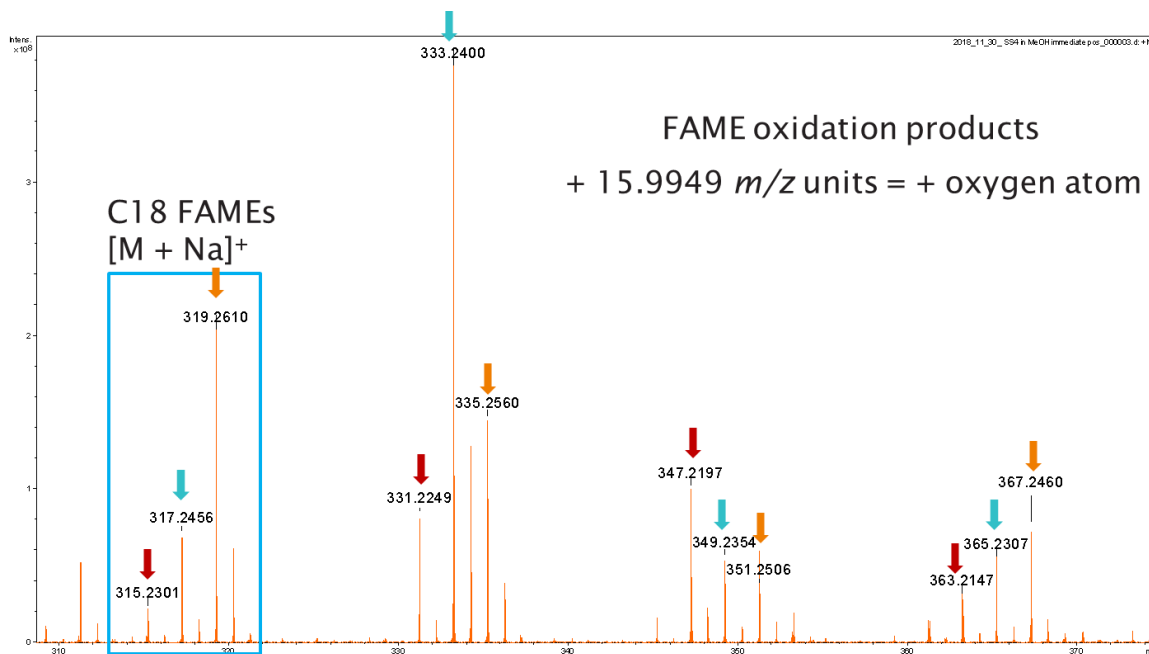


Figure 5-11 - Direct infusion positive ion ESI FT-ICR MS data of fuel filter SS4 (zoomed range  $m/z$  310-370), showing sodiated molecules for C18 FAMES and C18 FAME oxidation products up to the addition of three oxygen atoms

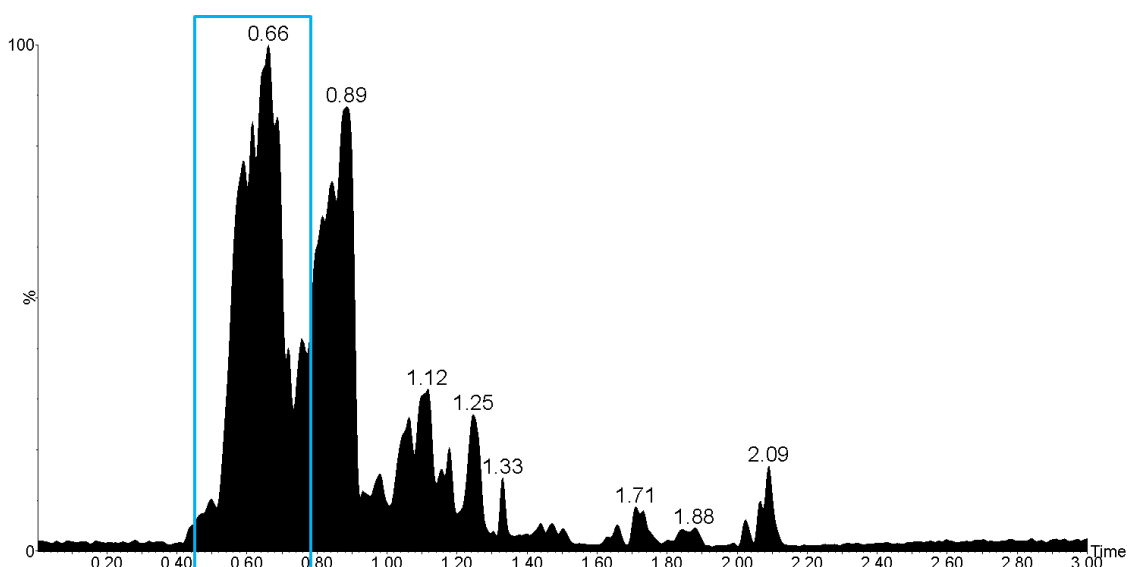


Figure 5-12 – Positive ion ESI UHPSFC-MS BPICC of SS4 with pale blue box highlighting FAMES and C18 FAME oxidation products region of retention ( $t_R$  0.50 -0.80 min)

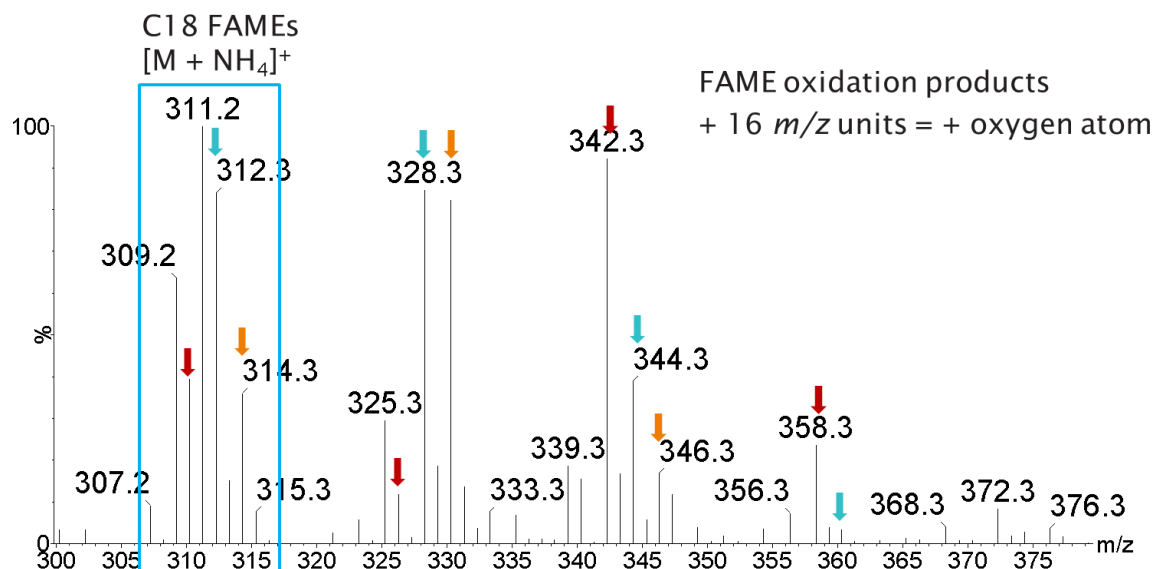


Figure 5-13 - Positive ion ESI UHPSFC mass spectrum of SS4 at *t<sub>R</sub>* 0.50-0.80 min (zoomed range *m/z* 300-380), showing ammoniated molecules for C18 FAMES and their respective FAME oxidation products, up to the addition of three oxygen atoms.

RICCs for nominal *m/z* associated with FAME C18:2 and associated FAME oxidation products (in this case [M + NH<sub>4</sub>]<sup>+</sup> as shown in Table 4-4) is shown in Figure 5-14, to confirm the assignment.

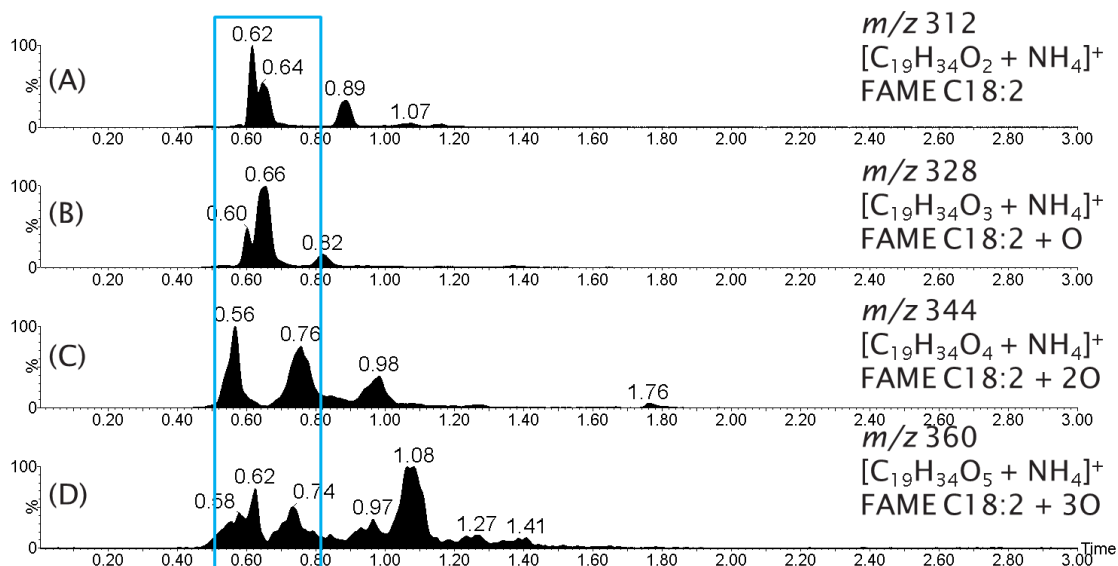


Figure 5-14 – Positive ion ESI UHPSFC-MS RICCs of SS4 showing C18:2 FAME and FAME oxidation products

Table 5-2 shows a summary of the FAME oxidation products detected within the fuel filters analysed.

Table 5-2 – Fuel filters FAMEs oxidation products summary (√=detected, X=not detected)

	<b>FAME oxidation products (carbon number: number of double bond)</b>			
		<b>C18:3</b>	<b>C18:2</b>	<b>C18:1</b>
<b>Fuel filters</b>	<b>SS2</b>	√ +10, +20,+30	√ +10, +20,+30	√ +10, +20,+30
	<b>SS3</b>	X	X	X
	<b>SS4</b>	√ +10, +20,+30	√ +10, +20,+30	√ +10, +20,+30
	<b>SS5</b>	√ +10, +20	√ +10, +20	√ +10, +20
	<b>SS6</b>	X	X	X
	<b>SS7</b>	X	X	X
	<b>SS8</b>	X	X	X
	<b>SS9</b>	X	X	X
	<b>SS10</b>	√ +10 (Low abundance+20,+30 (~10 <sup>6</sup> ))	√ +10 (Low abundance+20,+30 (~10 <sup>6</sup> ))	√ +10 (Low abundance+20,+30 (~10 <sup>6</sup> ))

This is in agreement with the FAME observations previously. The main differences are fuel filter SS10 was only detected to have FAME oxidation products with the addition of one oxygen atom, whereas fuel filter SS5 was observed to have FAME oxidation products up to the addition of two oxygens.



The major similarities are FAME containing fuel filters have FAME oxidation products detected at C18:3, C18:2 and C18:1 with varying additions of oxygen. Data for fuel filters SS2 and SS4 showed the presence of FAMES with up to three additional oxygen atoms.

The presence of FAME oxidation products suggests that the fuels passing through SS2, SS4, SS5 and SS10 have oxidised. The difference in abundances of FAME oxidation products detected corresponds to the different extent of oxidation each fuel will have undergone. The trace levels of FAMES in SS4 could suggest that almost all FAMES have oxidized to FAME oxidation products in SS4.

FAME oxidation products have been linked to filter fouling/blocking as well as both aged fuel IDIDs and metal salt IDIDs<sup>85, 120-121</sup>. Oxidative stress has been found to cause the formation of insolubles and deposits causing filter plugging, injector blockage and component failure<sup>231</sup>.

### 5.2.3 Free fatty acids (FFAs)

The SS10 fuel filter will be used as the example to illustrate FFAs within fuel filter samples.

Table 4-6 (page 131) shows a summary of the FFAs, their respective molecular formulae, exact mass and structure, the adduct that can be present for each and their associated masses<sup>233</sup>.

FFAs were found to elute at  $t_R$  0.85 – 1.20 min as shown in Figure 5-15. The corresponding negative ion ESI UHPSFC mass spectrum shown in Figure 5-16, shows deprotonated molecules  $[M - H]^-$  observed at nominal  $m/z$  values matching those in Table 4-6. RICCs of associated  $m/z$  values for FFAs (in this case  $[M - H]^-$  as shown in Table 4-6) as shown in Figure 5-17, are consistent with C14:0, C16:1, C16:0, C18:3, C18:2, C18:1 and C18:0 FFAs.

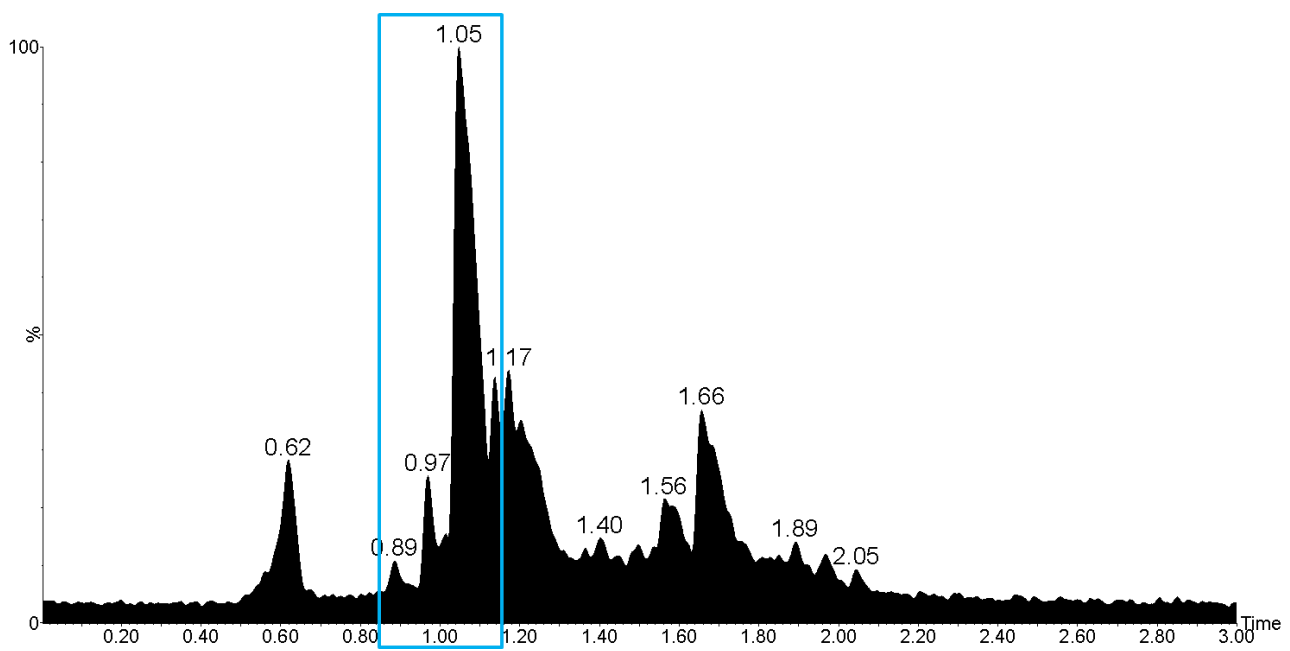


Figure 5-15 - Negative ion ESI UHPSFC-MS BPICC of fuel filter SS10 with pale blue box highlighting FFAs region of retention ( $t_R$  0.85-1.15 min)

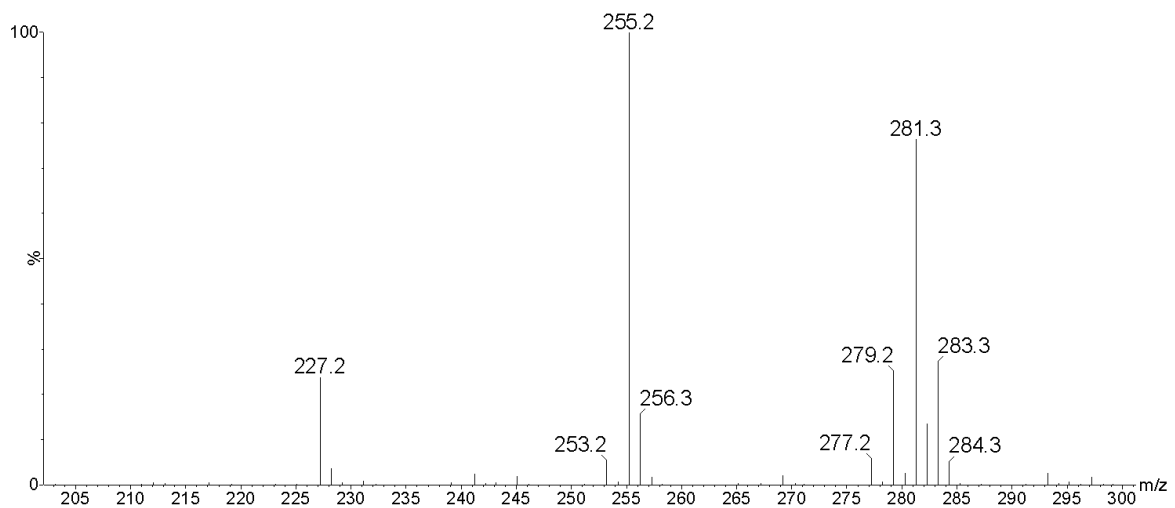


Figure 5-16 – Negative ion ESI UHPSFC mass spectrum of fuel filter SS10 at  $t_R$  0.85-1.15 min (zoomed range  $m/z$  180-300)

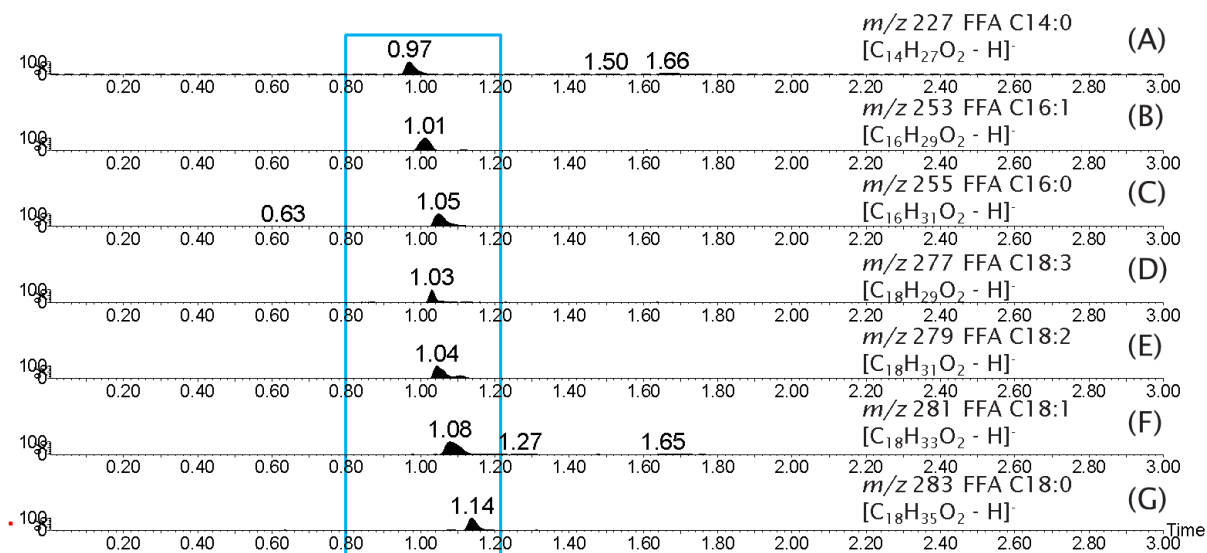


Figure 5-17 - Negative ion ESI UHPSFC-MS RICCs of fuel filter SS10 showing FFAs (box zoomed to 0.85 – 1.15 min)

FFAs were also observed as deprotonated molecules  $[M - H]^-$  in fuel filter SS10 ( $m/z$  values in Table 4-6) using direct infusion negative ion ESI FT-ICR MS as shown in Figure 5-18.

The accurate mass data provides further confidence that C14:0, C16:1, C16:0, C18:3, C18:2, C18:1 and C18:0 FFAs were observed in SS10 in agreement with negative ion ESI UHPSFC-MS.

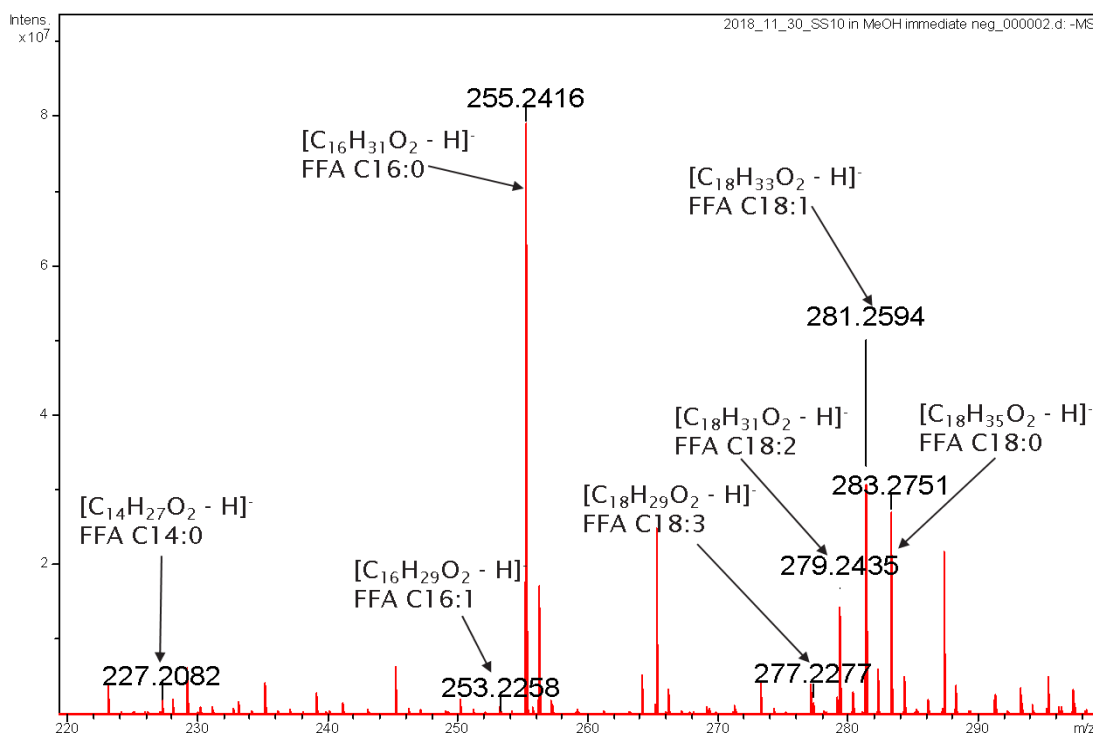


Figure 5-18 - Direct infusion negative ion ESI FT-ICR mass spectrum of fuel filter SS10 (zoomed range  $m/z$  180-300), showing deprotonated molecules for FFAs

Table 5-3 shows a summary of the FFAs detected within fuel filters analysed and is a culmination of results from negative ion ESI UHPSFC-MS and direct infusion negative ion ESI FT-ICR MS. FFAs have been denoted as present when detected by both techniques, whereas tentative assignment has been given if FFAs have only been detected by direct infusion negative ion ESI FT-ICR MS.

Table 5-3 – Fuel filters FFAs findings summary (legend: √= detected (by UHPSFC-MS and FT-ICR MS), √?= only detected by FT-ICR MS, X = not detected)

		FFAs (carbon number: number of double bonds)						
		C14:0	C16:1	C16:0	C18:3	C18:2	C18:1	C18:0
Fuel filters	SS2	√?	x	√	√	√	√	√
	SS3	x	x	√	√	√	√	√
	SS4	√?	x	√	√?	√	√	√
	SS5	x	x	√	X	√	√	√
	SS6	x	x	√	X	x	√	√
	SS7	x	x	x	X	x	x	x
	SS8	x	x	√	√	√	√	√
	SS9	x	√	√	X	√	√	√
	SS10	x	√	√	X	√	√	√

**FFAs were detected to be present in all fuel filters samples with the exception of SS7 during analysis.**

The major differences are FFA C16:1 only seems to be present in fuel filters SS9 and SS10 and FFA C14:0 is possibly present in SS2 and SS4 however at very low levels.

The key similarities are all fuel filters with FFAs present contain FFA C18:1 and FFA C18:0, and all except SS6 contains FFA C18:2. Fuel filters SS9 and SS10 contain the same composition of FFAs, both containing FFAs C18:2,1,0 and C16:1,0.

As the presence of FFAs are observed on the majority of fuel filters analysed including those that were found to not contain FAMES, it is suggestive that the source may be from monoacid lubricity additives, particularly as only some FFA species are observed. If FFAs were only observed in SS2, SS4, SS5 and SS10, then that would suggest FAME production as only FAMES were only observed in these fuel filters. However, fuel filters SS9 and SS10 contain the same composition of FFAs; also suggesting that in this case, the source is not from FAME production.

FFAs are well known as a contributing compound for metal carboxylates deposits both in fuel filter and fuel injector IDIDs<sup>27, 120</sup>(further detail chapter 1 and 4). Is the presence of FFAs on the fuel filter suggestive that metal carboxylate IDIDs may form in the FIE?

Barker *et al.*<sup>227</sup> reported that monoacid lubricity improver additives in combination with sodium hydroxide were found to cause “severe fuel filter fouling” resulting from the formation and agglomeration of a sodium carboxylate deposit.

#### 5.2.4 Monoacylglycerols (MAGs)

The SS5 fuel filter will be used as the example to illustrate MAGs within fuel filter samples.

Table 4-8 (page 136 shows a summary of the MAGs, their respective molecular formulae, exact mass and structures, adducts that can be present and their associated masses<sup>233</sup> with nominally isobaric species  $m/z$  in bold and underlined.

MAGs were found to elute at  $t_R$  1.20-1.35 min as shown in Figure 4-28. The corresponding positive ion ESI UHPSFC mass spectrum shown in Figure 5-19, shows a mixture of protonated  $[M + H]^+$  and ammoniated  $[M + NH_4]^+$  molecules with nominal masses in agreement with MAGs nominal masses in Table 4-8.

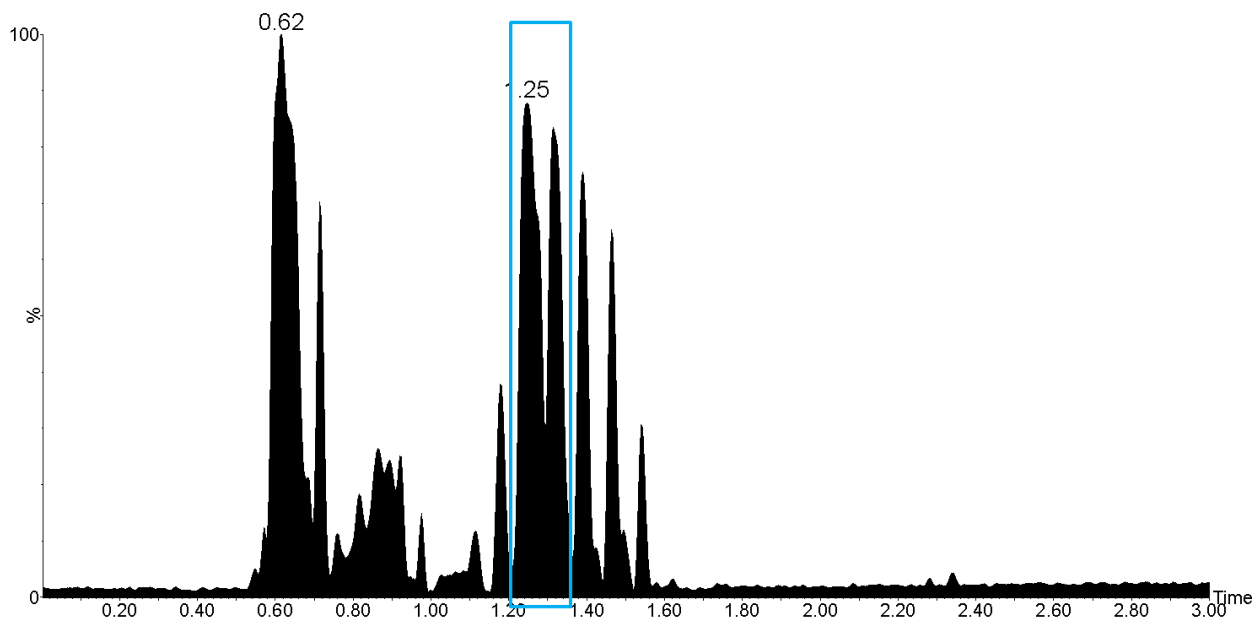


Figure 5-19 - Positive ion ESI UHPSFC-MS BPICC of fuel filter SS5 with pale blue box highlighting MAGs region of retention ( $t_R$  1.20-1.35 min)

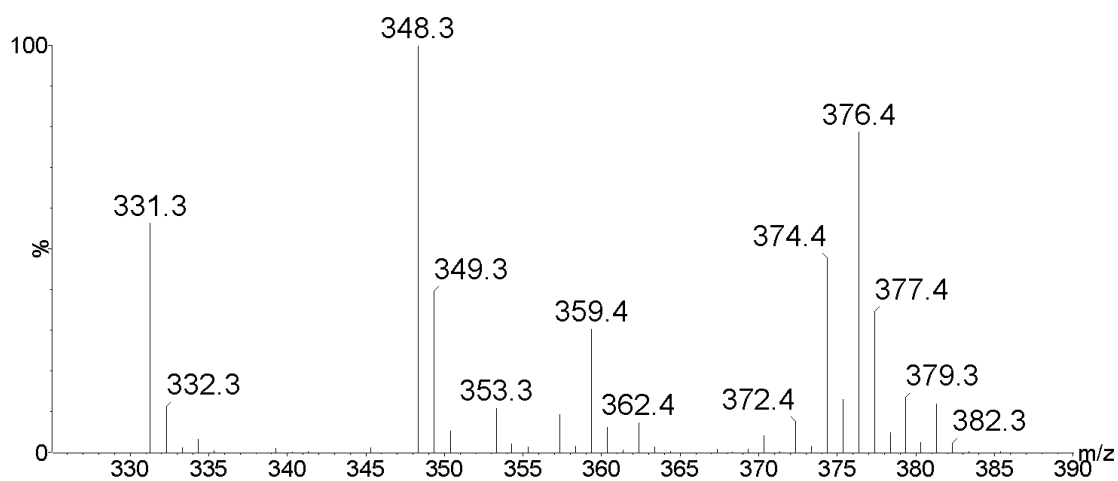


Figure 5-20 - Positive ion ESI UHPSFC mass spectrum of fuel filter SS5 at  $t_R$  1.20-1.35 min (zoomed range  $m/z$  325-390)

RICCs of associated  $m/z$  values for MAGs ( $[M + NH_4]^+$  as shown in Table 4-8) were used as shown in Figure 5-21 which suggests that the respective peaks are related to MAGs C16:0, C18:3, C18:2, C18:1 and C18:0.

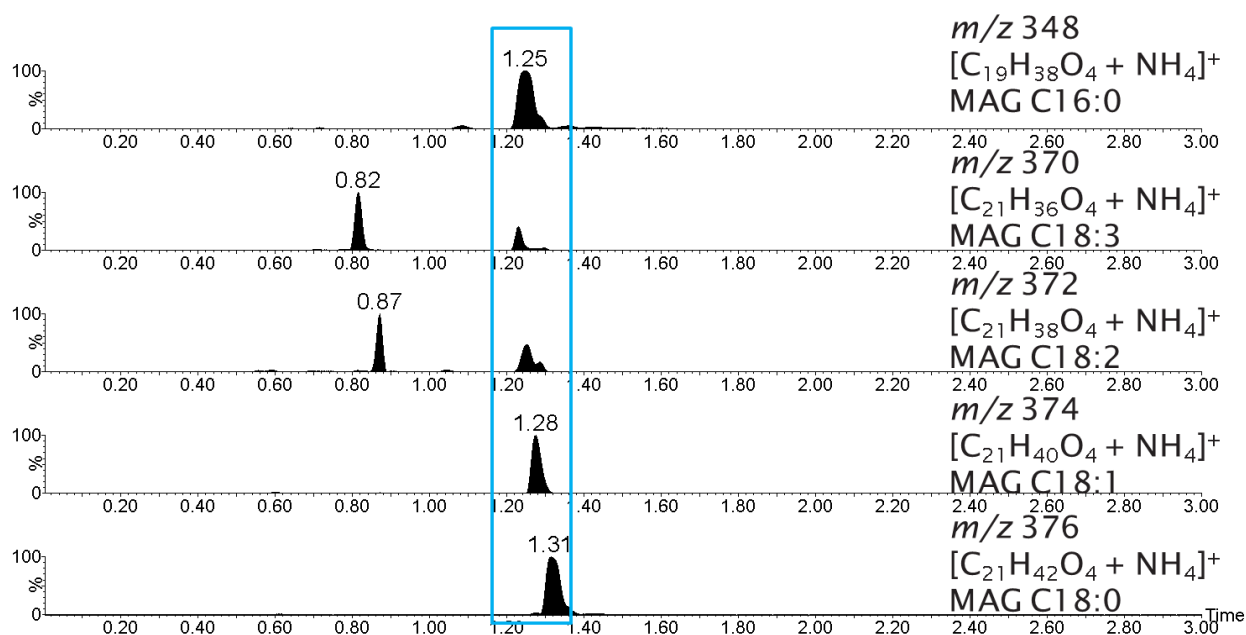


Figure 5-21 - Positive ion ESI UHPSFC-MS RICCs of fuel filter SS5 showing MAGs with pale blue box highlighting MAGs region of retention ( $t_R$  1.20-1.35 min)

MAGs are observed as sodiated molecules  $[M + Na]^+$  using direct infusion positive ion ESI FT-ICR MS, (Figure 5-22, Figure 5-23 and Figure 5-24 Figure 4-30).

Dimeric MAG species are also observed as sodiated molecules  $[2M + Na]^+$  (Figure 5-22) and are most likely artefacts formed during the ESI process, rather than present in the fuel filter sample. Dimers often suggests a component is present at a high concentration, therefore dilution is required.

To further confirm the assignment of MAGs, MS/MS was undertaken on SS5 fuel filter sample, in 5.3.5.1.

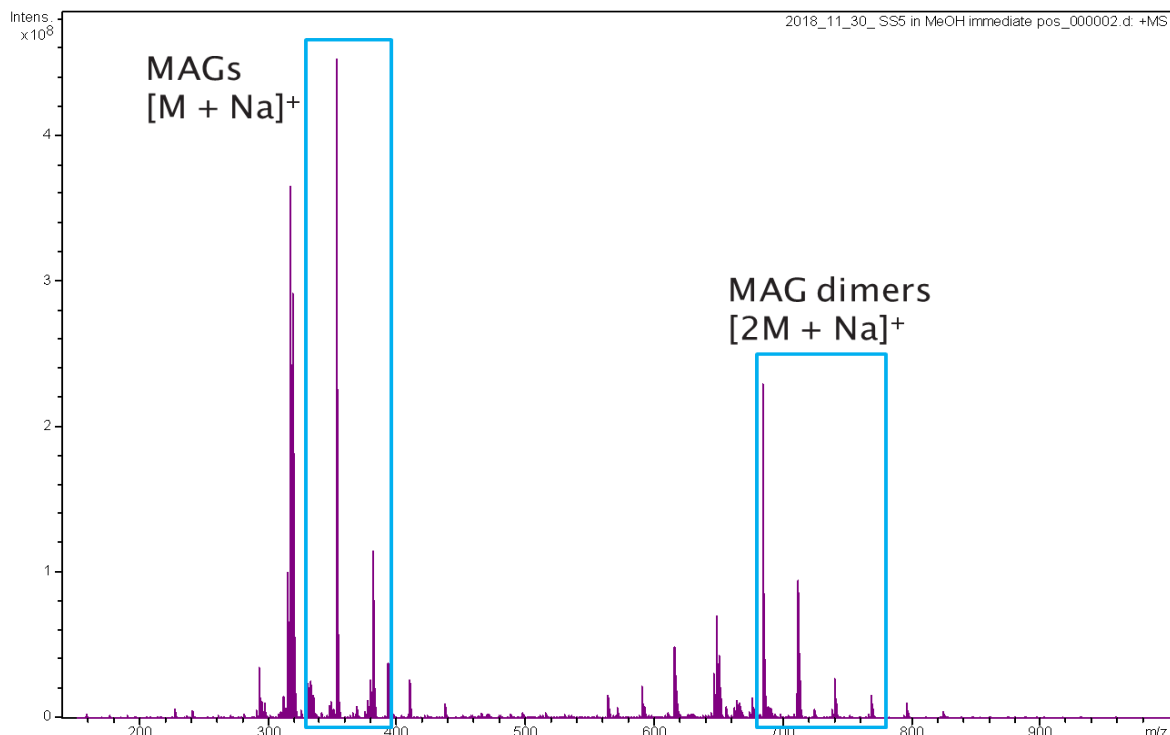


Figure 5-23 - Direct infusion positive ion ESI FT-ICR mass spectrum of fuel filter SS5, (zoomed range  $m/z$  100 - 1000), showing sodiated molecules for MAGs and MAG dimers

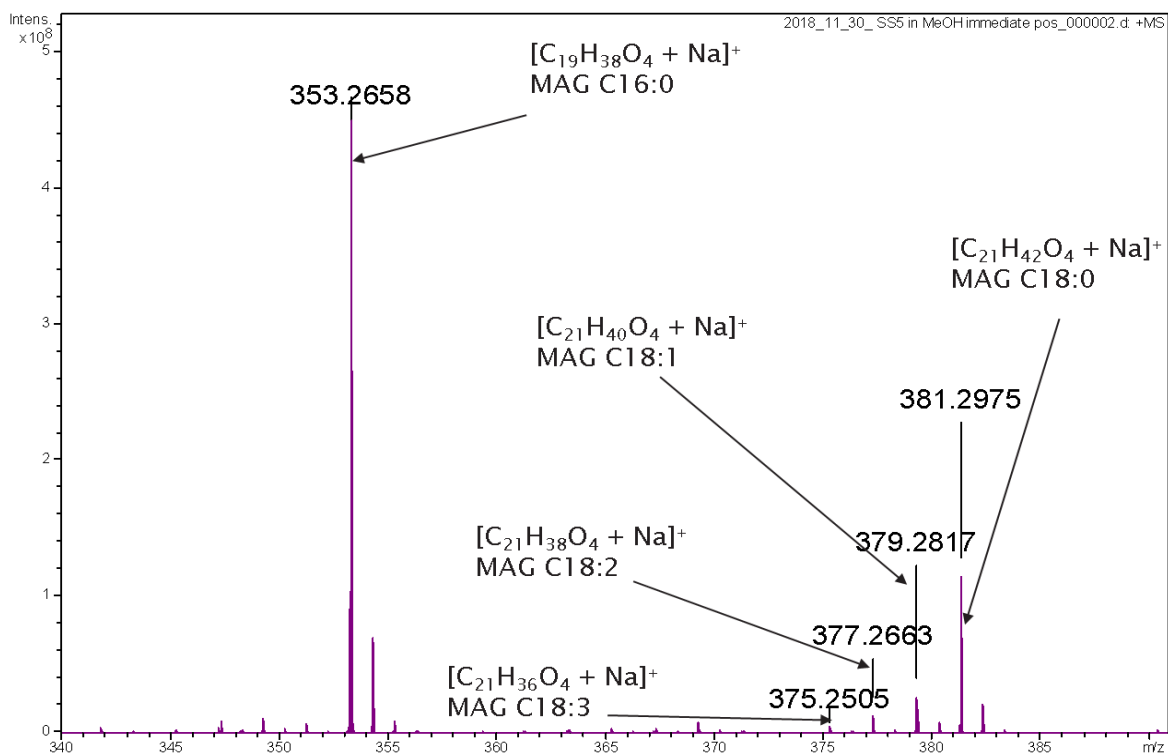


Figure 5-22 - Direct infusion positive ion ESI FT-ICR mass spectrum of fuel filter SS5, (zoomed range  $m/z$  340-390), showing sodiated molecules for MAGs



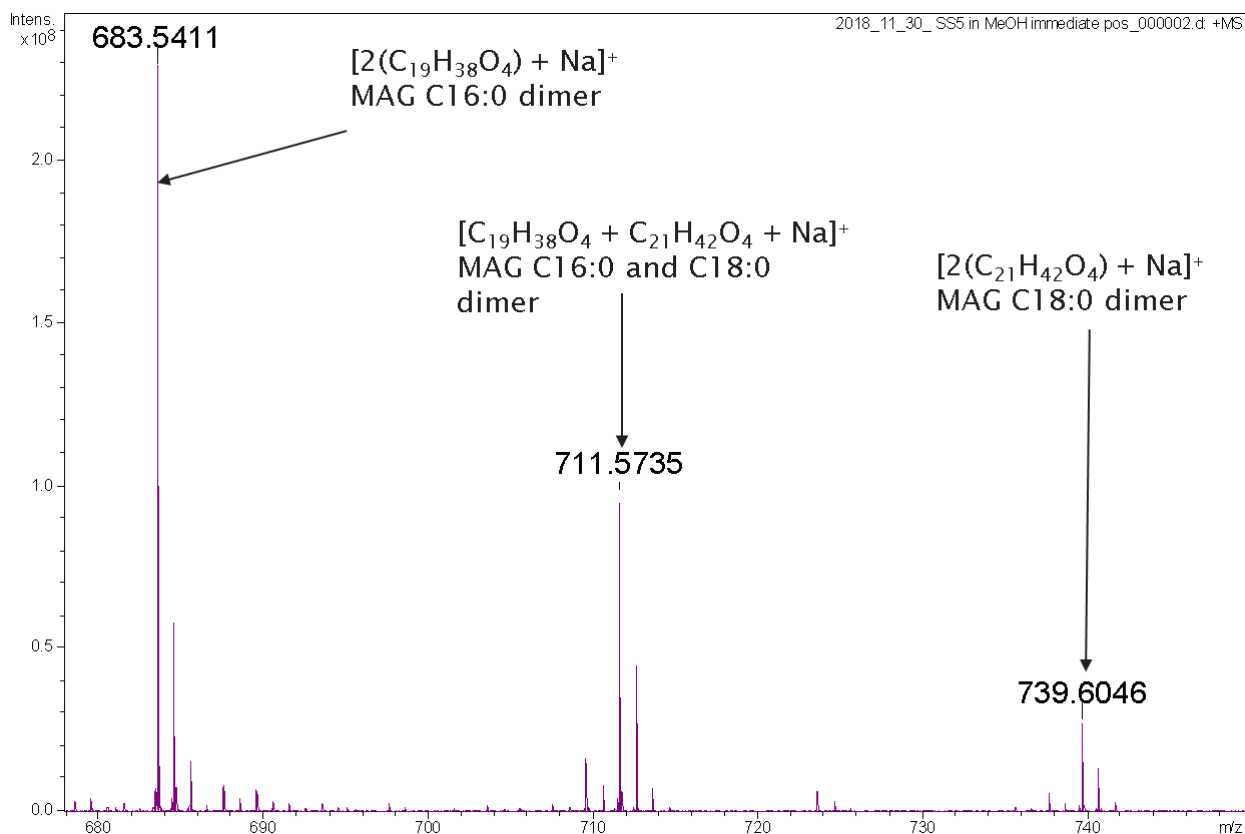


Figure 5-24 - Direct infusion positive ion ESI FT-ICR mass spectrum of fuel filter SS5, (zoomed range  $m/z$  680-750), showing sodiated molecules for MAG dimers

#### 5.2.4.1 MS/MS data

Alongside accurate mass measurements obtained using positive ion ESI FT-ICR MS, tandem MS (MS/MS) was undertaken on SS5 to further fully characterise the suspected MAG species within the sample. UHPSFC ESI+ MS/MS QQQ was used (3.5 and 2.5.3.1).

The masses for the ammoniated molecules  $[M + NH_4]^+$  of interest, in this case,  $m/z$  348, 370, 372, 374, 376 as shown in Figure 4-31, were individually isolated and then fragmented in the collision cell. The resulting product ions were then detected, see Figure 5-25 and Figure 5-26.

Three different collision energies were considered; 5, 10 and 20 V, with 5 V being considered optimal for fragmentation to produce product ions. Two examples, MAG C16:0 (Figure 5-25) and MAG C18:1 (Figure 5-26) will be discussed in detail.

The product ion scan for  $m/z$  348 (Figure 5-25) is consistent with the precursor ion for MAG C16:0 ammoniated molecules at  $m/z$  348  $[C_{19}H_{38}O_4 + NH_4]^+$ . It has four product ions related to it;  $m/z$  331,  $m/z$  313,  $m/z$  257 and  $m/z$  239.

## Chapter 5

$m/z$  331 is consistent with MAG C16:0 protonated molecules  $[C_{19}H_{38}O_4 + H]^+$ , while the loss of 18  $m/z$  units resulting in  $m/z$  313 ( $[C_{19}H_{36}O_3 + H]^+$ ), is consistent with the loss of  $H_2O$  from MAG C16:0.

Additionally a neutral loss of 92  $m/z$  units believed to correspond to loss of glycerol is observed from  $m/z$  331 resulting in the dehydrated fatty acid chain at  $m/z$  239 ( $[FFA - H_2O + H]^+ = [C_{16}H_{30}O + H]^+$ ).

$m/z$  257 is believed to be the protonated fatty acid chain ( $[FFA + H]^+ = [C_{16}H_{32}O_2 + H]^+$ ), in this case, FFA C16:0.

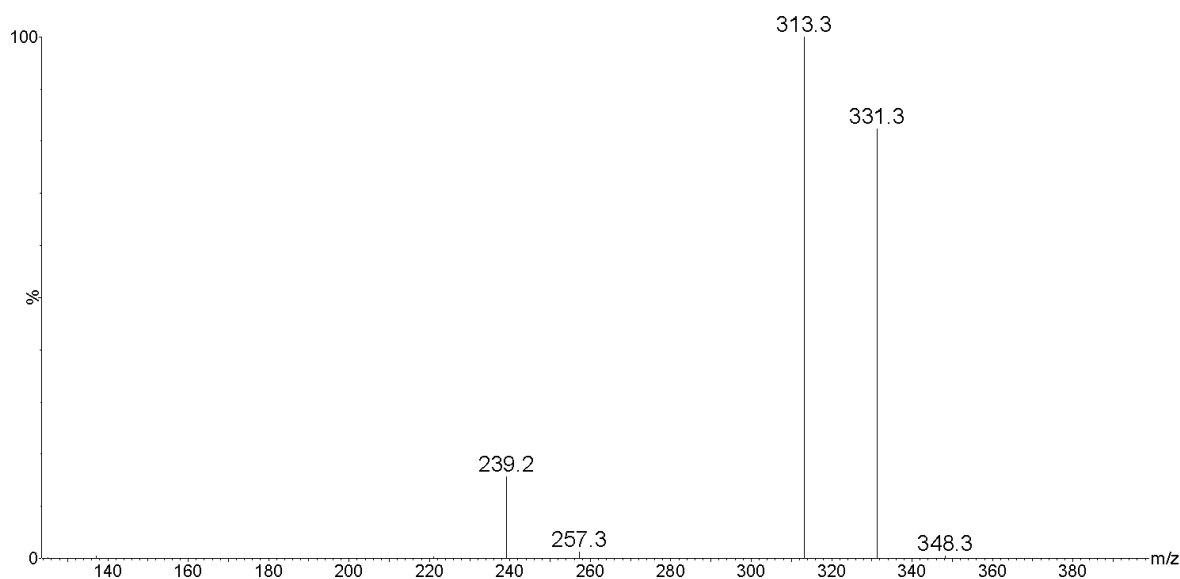


Figure 5-25 – Product ion mass spectrum of fuel filter SS5 of precursor nominal  $m/z$  348 MAG C16:0 at  $t_R$  1.11 min (TQD) (zoomed over  $m/z$  120-400) CE 5V

The product ion scan for  $m/z$  374 (Figure 5-26) is consistent with the precursor ion for MAG C18:1 ammoniated molecules at  $m/z$  374  $[C_{21}H_{40}O_4 + NH_4]^+$ . It has four key product ions related to it;  $m/z$  357,  $m/z$  339,  $m/z$  283 and  $m/z$  265.

$m/z$  357 is consistent with MAG C18:1 protonated molecules  $[C_{21}H_{40}O_4 + H]^+$ , while the loss of 18  $m/z$  units resulting in  $m/z$  339 ( $[C_{21}H_{38}O_3 + H]^+$ ) is consistent with the loss of  $H_2O$  from MAG C18:1.

Additionally a neutral loss of 92  $m/z$  units believed to correspond to loss of glycerol is observed from  $m/z$  357 resulting in the dehydrated fatty acid chain at  $m/z$  265 ( $[FFA - H_2O + H]^+ = [C_{18}H_{32}O + H]^+$ ).

$m/z$  283 is believed to be the protonated fatty acid chain ( $[FFA + H]^+ = [C_{18}H_{34}O_2 + H]^+$ ), in this case, FFA C18:1.

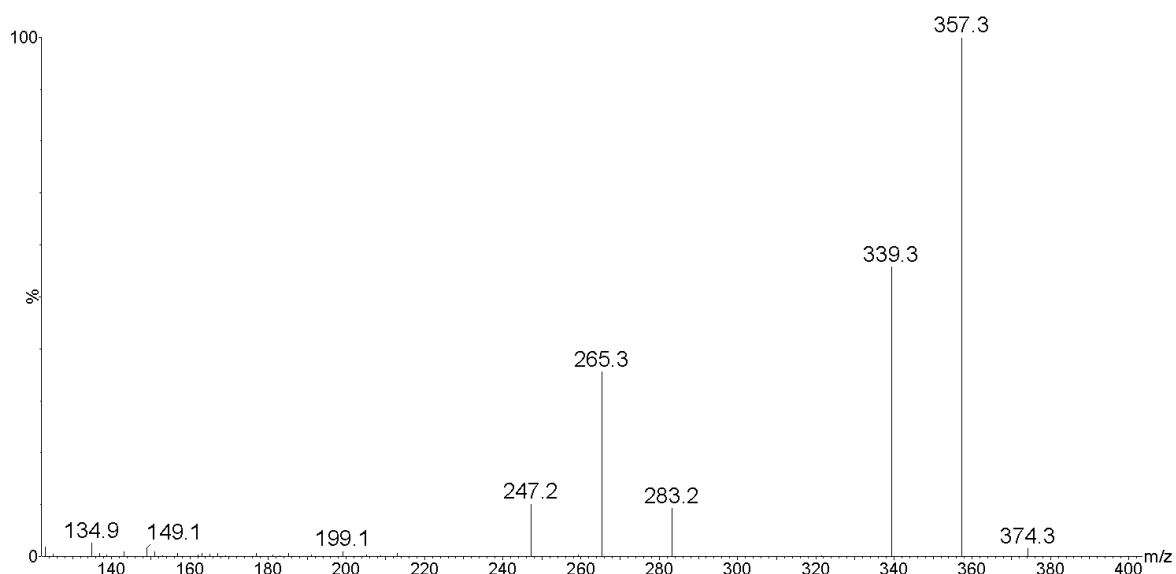


Figure 5-26 - Product ion mass spectrum of fuel filter SS5 of precursor nominal  $m/z$  374 MAG C18:1  $[C_{21}H_{40}O_4 + NH_4]^+$  at  $t_R$  1.16 min (TQD) (zoomed in over  $m/z$  120-400) CE 5V

MS/MS data was found to be in agreement with Gao *et al.*<sup>258</sup> and Gil *et al.*<sup>259</sup> who undertook structural elucidation of MAGs.

Table 5-4 shows a summary of the MAGs present within the fuel filters analysed. MAGs have been denoted as present when detected by both techniques, whereas tentative assignment has been given if MAGs have only been detected by direct infusion positive ion ESI FT-ICR MS. The symbol X\* has been utilised for results when the nominal  $m/z$  was initially detected by positive ion ESI UHPSFC-MS in RICCs, however the presence of the compound by monoisotopic mass not detected by direct infusion positive ion ESI FT-ICR MS.

Table 5-4 – fuel filters MAGs summary (✓=detected, X=not detected)

	<b>MAGs (carbon number: number of double bonds)</b>					
		<b>C16:0</b>	<b>C18:3</b>	<b>C18:2</b>	<b>C18:1</b>	<b>C18:0</b>
<b>Fuel filters</b>	<b>SS2</b>	✓	✓	✓	✓	✓
	<b>SS3</b>	X	X	X	X	X
	<b>SS4</b>	X	X	X	X	X
	<b>SS5</b>	✓	✓	✓	✓	✓
	<b>SS6</b>	X	X	X	X	X
	<b>SS7</b>	X	X	X	X	X
	<b>SS8</b>	X	X	X	X	X
	<b>SS9</b>	X	X	X	X	X
	<b>SS10</b>	✓ (low abundance (10 <sup>6</sup> ))	X	✓ (low abundance (10 <sup>6</sup> ))	✓ (low abundance (10 <sup>6</sup> ))	✓ (low abundance (10 <sup>6</sup> ))

MAGs were only detected in SS2, SS5 and SS10 (low abundance) fuel filter samples during analysis. This is in agreement with the FAME observations previously discussed with the exception of fuel filter SS4.

The major differences observed were all MAGs were only detected at low level in fuel filter SS10, with the complete absence of MAG C18:3.

The key similarities are that fuel filters SS2 and SS5 both have all MAGs present with dimers. In addition, C16:1, C16:0, C18:3, C18:2, C18:1 were detected in fuel filters SS2, SS5 and SS10.

The detection of MAGs in fuel filters SS2, SS5 and SS10 suggests the biodiesel blended into the related fuels was a result of an incomplete transesterification reaction. No detection of MAGs in

fuel filter SS4 suggests the biodiesel blended into the fuel passing through SS4 is likely to be a result of complete transesterification.

In 1996, creamy pastes found to contain MAGs and DAGs were extracted from plugged filters from buses in Iowa. In agreement with these previous findings, the associated gunk from fuel filter SS5(3.2.2.1) analysed in this work was observed to be a creamy paste and found to contain a high abundance of MAGs from a plugged fuel filter providing further evidence that MAGs seems to be linked to this.

In the USA, it was reported in winters 2004-2006 that ferry boats fueled by B20 blends were experiencing issues with solid precipitates plugging filters and the solid residues were found to be mainly composed of saturated MAGs<sup>239</sup>. Along with SGs, saturated MAGs have been found to form solid precipitates in cold weather due to low solubility of MAGs in biodiesel<sup>237</sup>.

MAGs are amphiphilic and may react with any water present in the fuel, with alcohol 'head' of the chain being hydrophilic and more soluble in water while the carbon chain 'tail' is hydrophobic, therefore more soluble in the non-polar petrodiesel. Biodiesel blends result in decreased solubility and accelerated precipitation. Industry tests cloud point (CP), pour point (PP) and cold filter plugging point (CFPP) (chapter 1) are used to evaluate cold flow properties of a fuel to predict the tendency for the formation of the solid precipitates from the biodiesel blends<sup>32</sup>. At temperatures even above the CP (temperature at which crystals become visible), precipitates can settle in storage tanks and during and after fuel transfer causing restricted flow and blockages (PP temperature)<sup>260</sup>.

### 5.2.5 Sterol glucosides (SGs)

The SS2 fuel filter will be used as the example to illustrate SGs within fuel filter samples.

Table 4-10 (page 142) shows a summary of the SGs, their respective molecular formulae and structures, adducts that can be present and their associated masses<sup>211, 244-245</sup>.

Figure 5-27 shows a positive ion ESI UHPSFC-MS BPICC of the SS2 fuel filter, with the pale blue box highlighting chromatographic peaks within the region of retention found for SGs ( $t_R$  2.00 – 2.20 min).

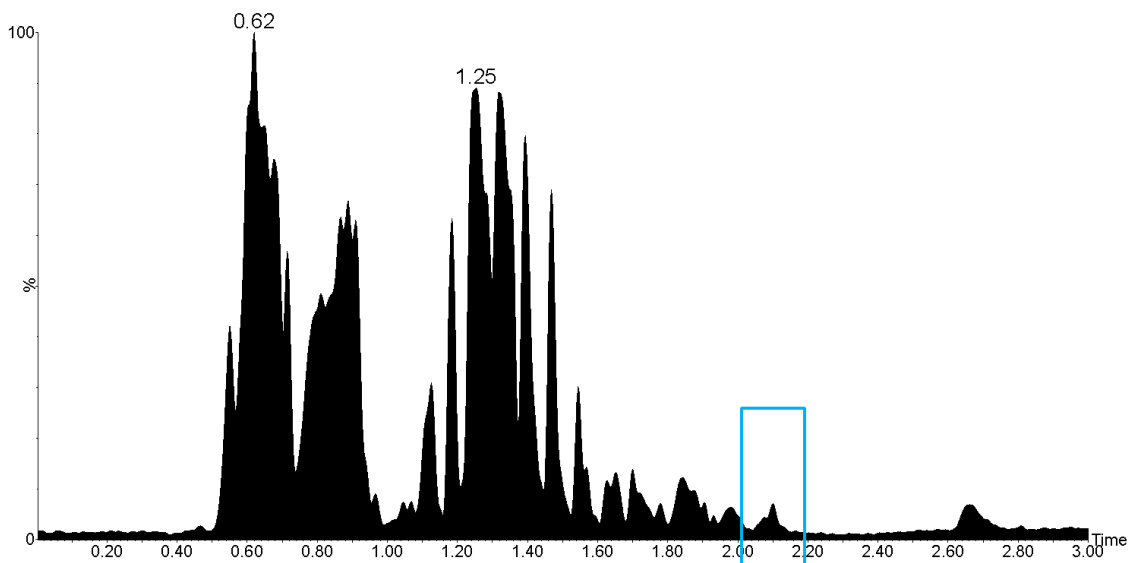


Figure 5-27 - Positive ion ESI UHPSFC-MS BPICC of fuel filter SS2 with pale blue box highlighting SGs region of retention ( $t_R$  2.00-2.20 min)

Figure 5-28 shows ammoniated molecules  $[M + NH_4]^+$  observed at nominal  $m/z$  580-600, which are consistent with compounds of nominal mass 557-577 g/mol. Sterol fragment ions, corresponding to the protonated molecules  $[M + H - \text{sugar}]^+$  are also observed at nominal  $m/z$  380-400.

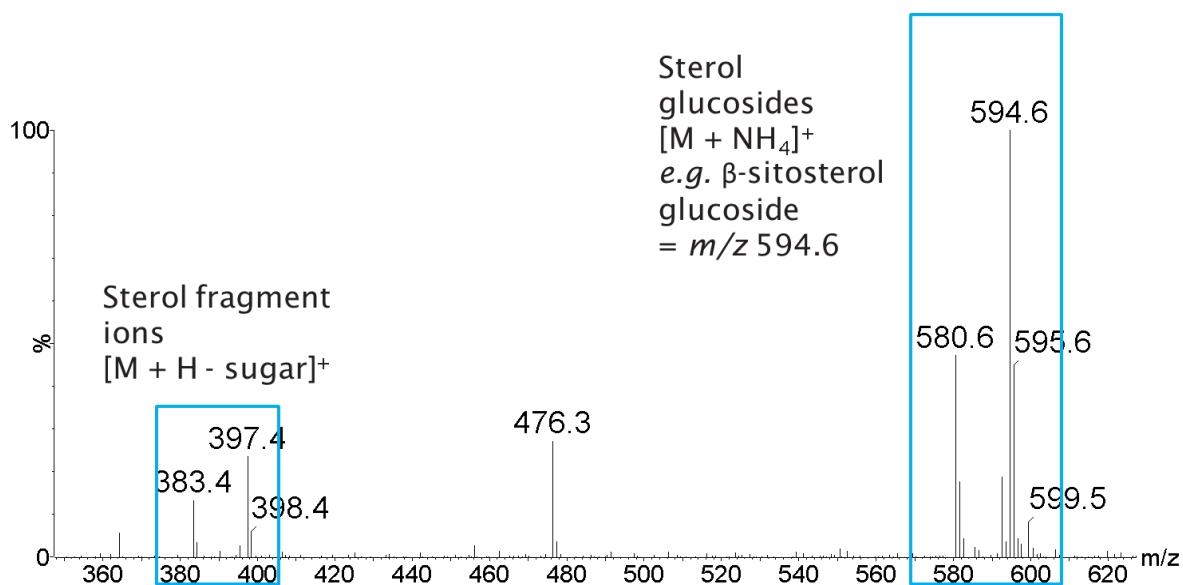


Figure 5-28 - Positive ion ESI UHPSFC mass spectrum of fuel filter SS2 at  $t_R$  2.04-2.14 min (zoomed range  $m/z$  350-625)

Confirmation that the chromatographic peaks in this region are most likely related to SGs and their associated nominal  $m/z$  values (in this case  $[M + NH_4]^+$  and  $[M + H - \text{sugar}]^+$  as shown in Table 4-10) is achieved using RICCs. Figure 5-29 shows RICCs and allows alignments/matchings of sterol fragment ions to the associated SG to be achieved (e.g. for campesteryl glucoside  $m/z$  383  $[M + H - \text{sugar}]^+$  and  $m/z$  580  $[M + NH_4]^+$ ). This suggests that the respective peaks are related to SGs and is in agreement with previous findings of Patel<sup>211</sup>, adding to the confidence in the assignment.

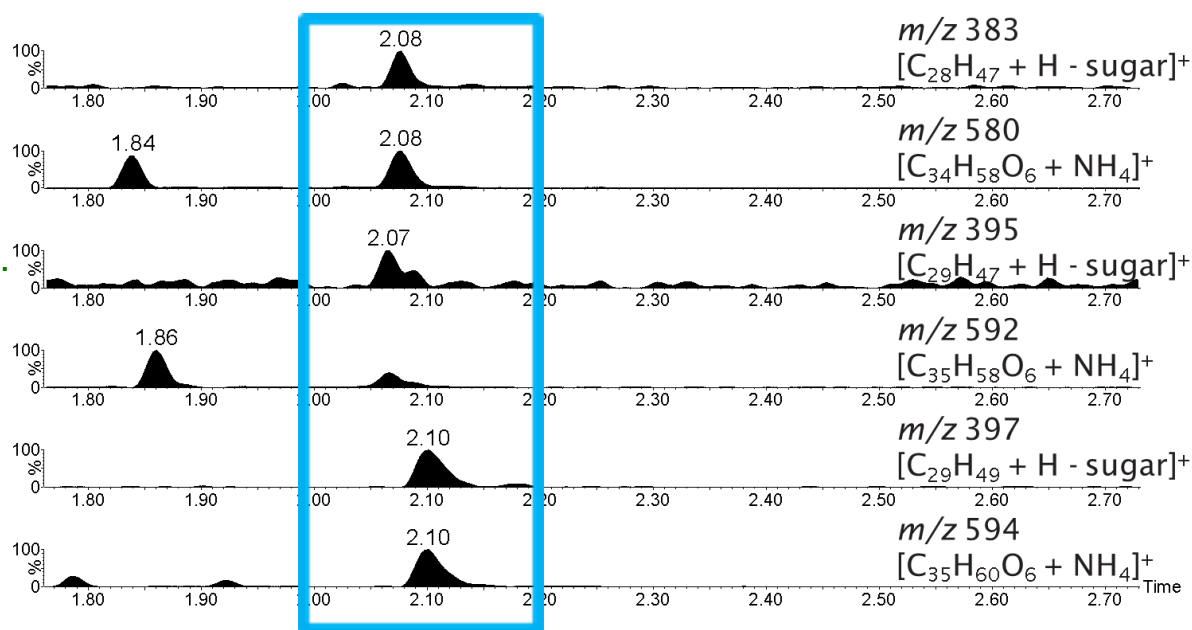


Figure 5-29 - Positive ion ESI UHPSFC-MS RICCs of fuel filter SS2 showing SGs and sterol fragment ions with pale blue box highlighting SGs region of retention ( $t_R$  2.00-2.20 min)

SGs were not easily observed by direct infusion positive ion ESI FT-ICR MS but found to be present at low abundance as the sodiated molecules  $[M + Na]^+$ , as shown in Figure 5-30. However, the sterol fragment ions were not observed as protonated molecules  $[M + H - \text{sugar}]^+$  as previously observed by positive ion ESI UHPSFC-MS, most likely due to the low abundance and possible ion suppression.

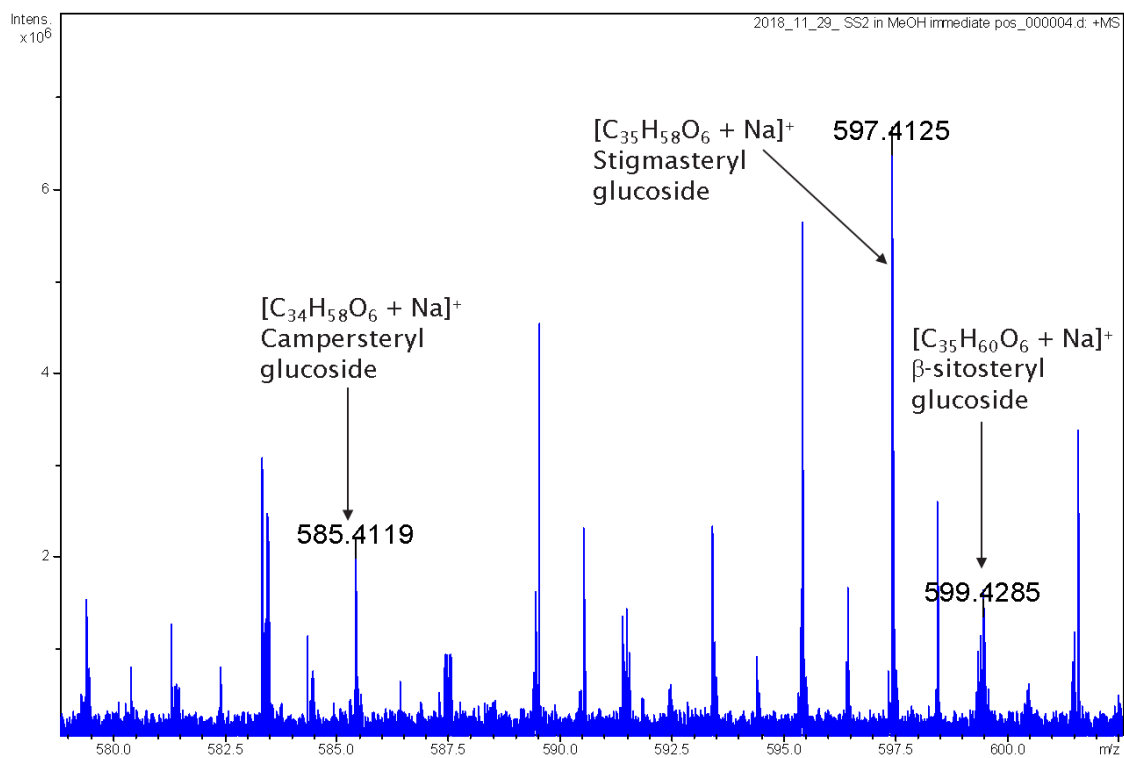


Figure 5-30 - Direct infusion positive ion ESI FT-ICR mass spectrum of fuel filter SS2 (zoomed range  $m/z$  580-600), showing sodiated molecules for SGs

Table 5-5 shows a summary of the SGs and sterol fragment ions detected within the fuel filters analysed.



Table 5-5 – Fuel filter SGs and sterol fragment ion summary (√=detected, √\*=detected at low abundance( $\sim 10^6$ ), X=not detected)

	SGs						
		Campesterol glucoside		Stigmasterol glucoside		β-sitosterol glucoside	
		Sterol Frag ion	SG	Sterol Frag ion	SG	Sterol Frag ion	SG
Fuel filters	SS2	√	√	√*	√*	√	√
	SS3	X	X	X	X	X	X
	SS4	√	√	√*	√*	√	√
	SS5	√*	√*	√*	√*	√*	√*
	SS6	X	X	X	X	X	X
	SS7	X	X	X	X	X	X
	SS8	X	X	X	X	X	X
	SS9	X	X	X	X	X	X
	SS10	X	X	X	X	X	X

SGs were detected in SS2 and SS4 fuel filters and at very low abundance in SS5 fuel filter samples possibly due to presence of fatty acid sterol esters (FASEs) (5.2.6).

The presence of SGs is in agreement with the observation of FAMES in fuel filters; however, there are no SGs present in fuel filter SS10.

It was much easier to detect SGs by positive ion ESI UHPSFC-MS compared to direct infusion positive ion ESI FT-ICR MS due to ion suppression.

### 5.2.6 Fatty acid sterol esters (FASEs)

Fatty acid sterol esters (FASEs) consists of a sterol linked at the hydroxyl group (*via* an ester bond) to a fatty acid. FASEs are naturally occurring in vegetable oils and biodiesel feedstocks and are therefore found as minor constituents/contaminants within biodiesel<sup>236, 249</sup>.

This FASEs method was based upon a novel positive ion UHPSFC-MS detection method outlined in 4.4, demonstrates the novel detection of FASEs in diesel fuel blends as prior to this FASEs have only been analysed in pure biodiesel and vegetable oils. FASEs are also not stated in the literature to have been investigated or found to cause filter blocking or IDIDs. However, knowledge that SGs and FFAs are deposit forming compounds suggests FASEs may also be a possible deposit forming precursor or component with work by Feld and Oberender<sup>250</sup> showing FASEs from biodiesel forming deposits after SGs have initially accumulated in fuel filters. Further research is required surrounding their role in biodiesel blends and forming deposits.

The FASEs are only observed by positive ion ESI UHPSFC-MS and they were not apparent by direct infusion positive ion ESI FT-ICR MS due to ion suppression.

The SS5 fuel filter will be used as the example to illustrate detection and identification of FASEs within fuel filter samples.

FASEs are observed most abundantly as ammoniated molecules  $[M + NH_4]^+$  in this project. Related sterol fragment ions are also observed but as protonated molecules  $[M + H - \text{fatty acid}]^+$  using positive ion ESI UHPSFC-MS.

Figure 5-31 shows a positive ion ESI UHPSFC-MS BPICC of the SS5 fuel filter, with the pale blue box highlighting chromatographic peaks within the region of retention found for FASEs ( $t_R$  2.20 – 2.40 min). However, within the BPICC of SS5, the FASE peaks were not initially apparent and may have been passed by if not using this screen method due to low levels of compounds present.

The corresponding mass spectrum, Figure 5-32, shows ammoniated molecules  $[M + NH_4]^+$  observed at nominal  $m/z$  678-696, which are consistent with compounds of nominal mass 660-678 g/mol. Fragment ions  $[M + H - \text{fatty acid}]^+$  are also observed at nominal  $m/z$  381-397, which are consistent with compounds of nominal mass 380-396 g/mol. Both of which are in agreement with FASEs nominal masses as shown in Table 4-13 (page 161).

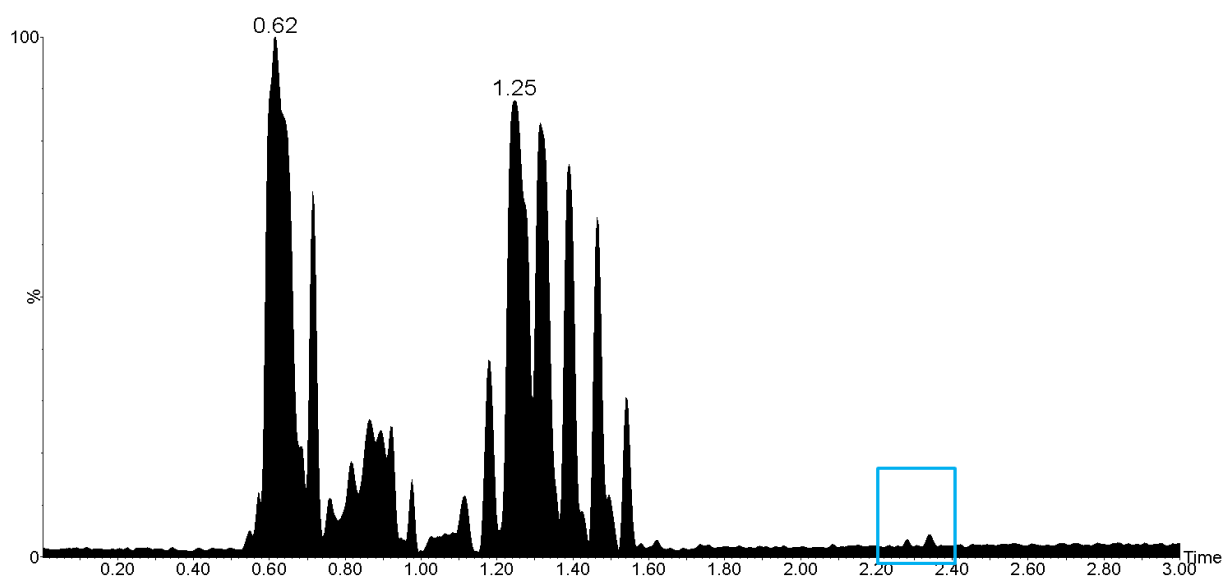


Figure 5-31 - Positive ion ESI UHPSFC-MS BPICC of fuel filter SS5 with pale blue box highlighting FASEs region of retention ( $t_R$  2.20-2.40 min)

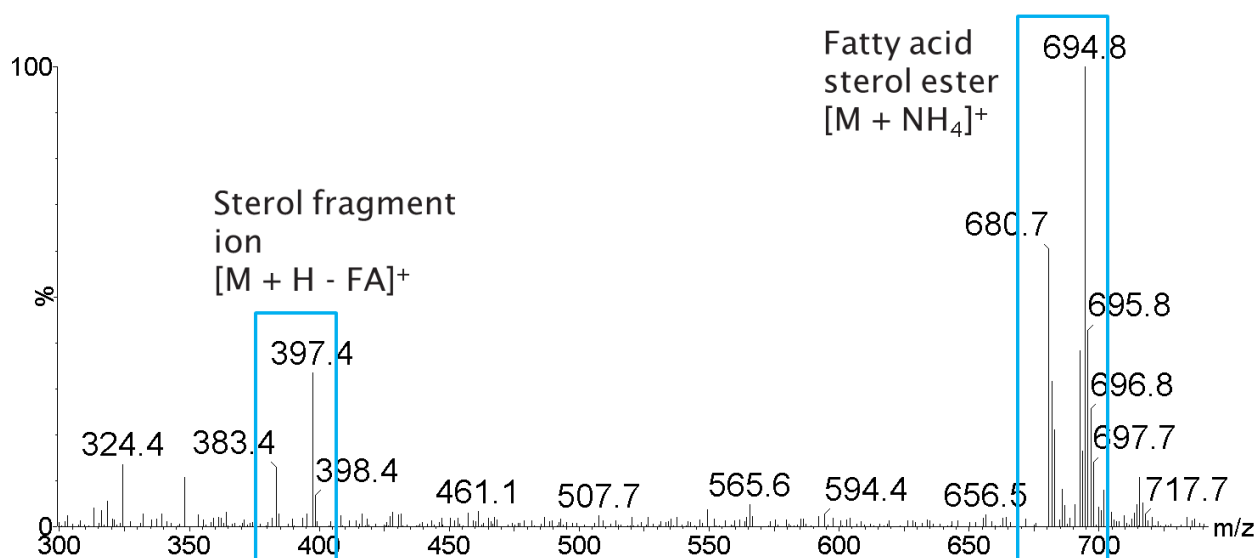


Figure 5-32 – Positive ion ESI UHPSFC mass spectrum of fuel filter SS5 at  $t_R$  2.20-2.40 min

Confirmation that the chromatographic peaks in this region are most likely related to FASEs and associated fragment as shown in Table 4-13). Figure 5-33 shows that the RICCs of the sterol fragments to the associated FASE to be achieved (e.g. for Campesterol ester  $m/z$  383  $[M + H - \text{fatty acid}]^+$  and  $m/z$  679  $[M + \text{NH}_4]^+$  for C18:3,  $m/z$  681  $[M + \text{NH}_4]^+$  for C18:2, or  $m/z$  683  $[M + \text{NH}_4]^+$  for C18:1). This suggests that the respective peaks are related to FASEs and is in agreement

## Chapter 5

with previous findings in chapter 4 and  $m/z$  values provided in literature so there can be confidence in the assignment.

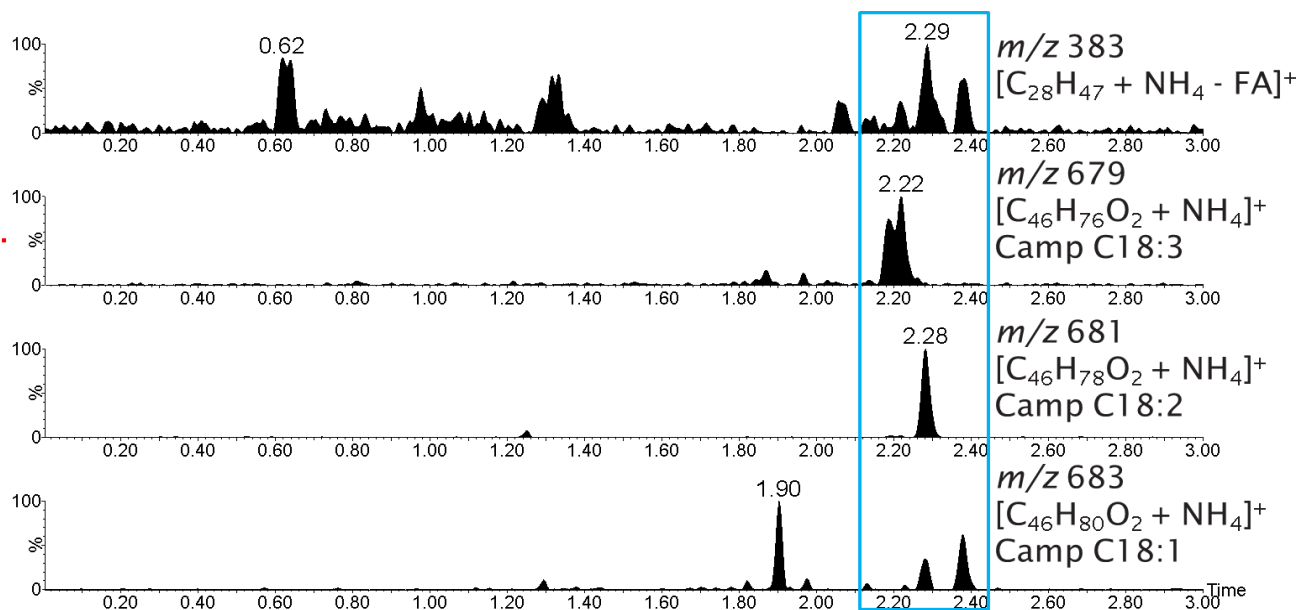


Figure 5-33 - Positive ion ESI UHPSFC-MS RICCs of fuel filter SS5 with pale blue box highlighting FASEs region of retention ( $t_R$  1.20-1.35 min)

Table 4-13 (page 161) shows a summary of the FASEs and related sterol fragments with their respective molecular formulae and their associated masses.  $m/z$  values taken from Kalo *et al.*<sup>233</sup>.

Campesterol ester C18:3, C18:2 and C18:1 and  $\beta$ -sitosterol ester C18:3, C18:2 and C18:1 only were observed to be present in the fuel filter SS5 (associated gunk). No fatty acid brassicasterol ester or stigmasterol esters were found to be present using the full scan method, however they may be below the limit of detection (LOD). SIR analysis could be undertaken for the specific masses to improve sensitivity to ensure the FASEs are absent.

It may be possible that a poor source of biodiesel was used in fuel passing through SS5 causing the plugged fuel filter and associated residue, or it may be more related to an accumulation issue which may explain why it was only observed in one fuel filter in the gunk but in multiple fuel samples in chapter 4.

FASEs are not stated in the literature to cause filter blocking or IDIDs, however this work shows that a plugged fuel filter associated residue (SS5) was found to contain FASEs for the first time. This is ground-breaking research that will add to knowledge and understanding of plugged fuel filters initially and strongly suggests that research is required surrounding their role in biodiesel blends and forming engine deposits.

## 5.2.7 Other key findings

### 5.2.7.1 Polymeric additives e.g. polyisobutylene (PIB) and polypropylene glycol (PPG)

Many additives, including multiple polymeric additives are added to diesel to enhance specific properties of the fuel and therefore the overall performance of the fuel. This is outlined in more detail in 1.1.1 and Table 1.2.

#### 5.2.7.1.1 Polyisobutylene (PIB) series

Polyisobutylene succinimides (PIBSIs) are commonly added to fuels as deposit control additives (DCAs) to prevent the build-up of deposits on fuel injectors and with the FIE (1.3.3).

SS6 fuel filter will be used as the example to illustrate the detection and interpretation of PIBs within fuel filter samples.

Two discrete oligomeric series of 56.0626  $m/z$  units difference starting in the  $m/z$  range 297.2175-1026.0297 and  $m/z$  315.2279-1267.3386 inclusive, are observed as protonated molecules  $[M + H]^+$  in the direct infusion positive ion ESI FT-ICR MS data (Figure 5-34) highlighted by red and blue arrows. The two series are separated by 18.0101  $m/z$  units consistent with a  $H_2O$  difference (e.g.  $m/z$  521.4676 and  $m/z$  539.4777,  $[C_{32}H_{60}N_2O_3 + H]^+$  and  $[C_{32}H_{62}N_2O_4 + H]^+$  respectively). These series of 56.0626  $m/z$  units difference confirm a formula  $(C_4H_8)$  that is consistent with a PIB series.

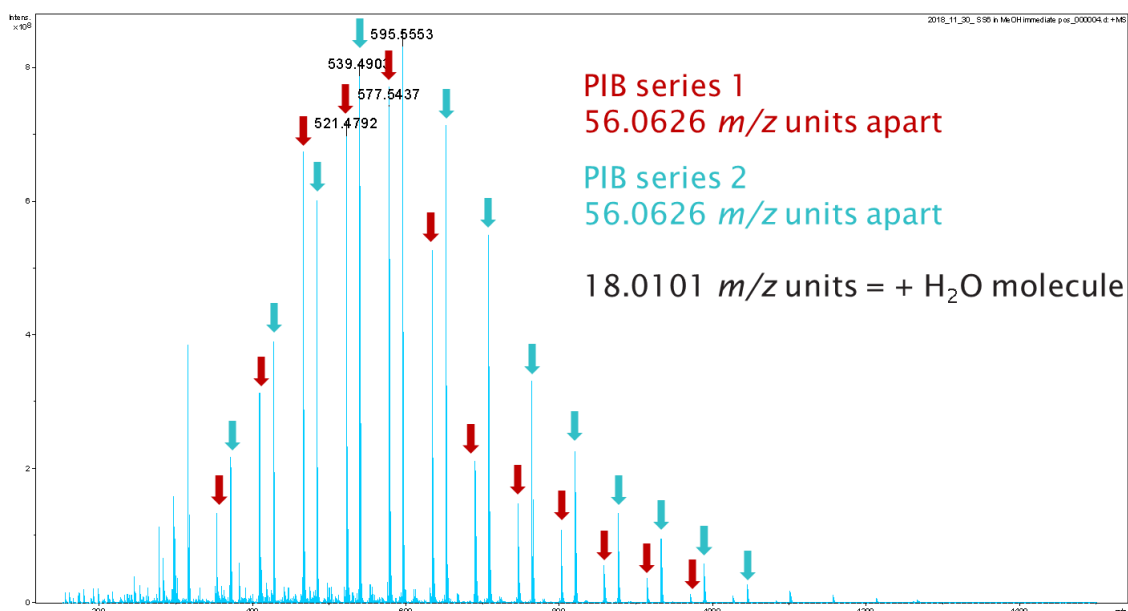


Figure 5-34 - Direct infusion positive ion ESI FT-ICR mass spectrum of fuel filter SS6 (zoomed range  $m/z$  100-1500), showing two discrete oligomeric series of 56.0626  $m/z$  repeat units (separated by 18.0101  $m/z$  units), highlighted by red and blue arrows

## Chapter 5

PIBs are observed as protonated molecules  $[M + H]^+$  in the positive ion ESI UHPSFC-MS data. Figure 5-35 shows a positive ion ESI UHPSFC-MS BPICC of the SS6 fuel filter, with the pale blue box highlighting chromatographic peaks within the region of retention found for PIBs ( $t_R$  2.40-3.00 min). The corresponding positive ion ESI UHPSFC mass spectrum shown in Figure 5-36, shows two series of protonated molecules  $[M + H]^+$  of 56  $m/z$  units difference observed at nominal  $m/z$  297-577 and  $m/z$  315-427 inclusive, highlighted by red and blue arrows. These two series are separated by 18  $m/z$  units consistent with a  $H_2O$  difference and are consistent with those observed in the direct infusion positive ion ESI FT-ICR MS data. However, a much smaller mass range of PIBs is observed by positive ion ESI UHPSFC-MS compared with direct infusion positive ion ESI FT-ICR MS, meaning the latter is the preferred method for this component of the screening method. Figure 5-37 shows the RICCs for the oligomeric PIB series 1 observed by positive ion ESI UHPSFC-MS demonstrating the separation of the PIB species.

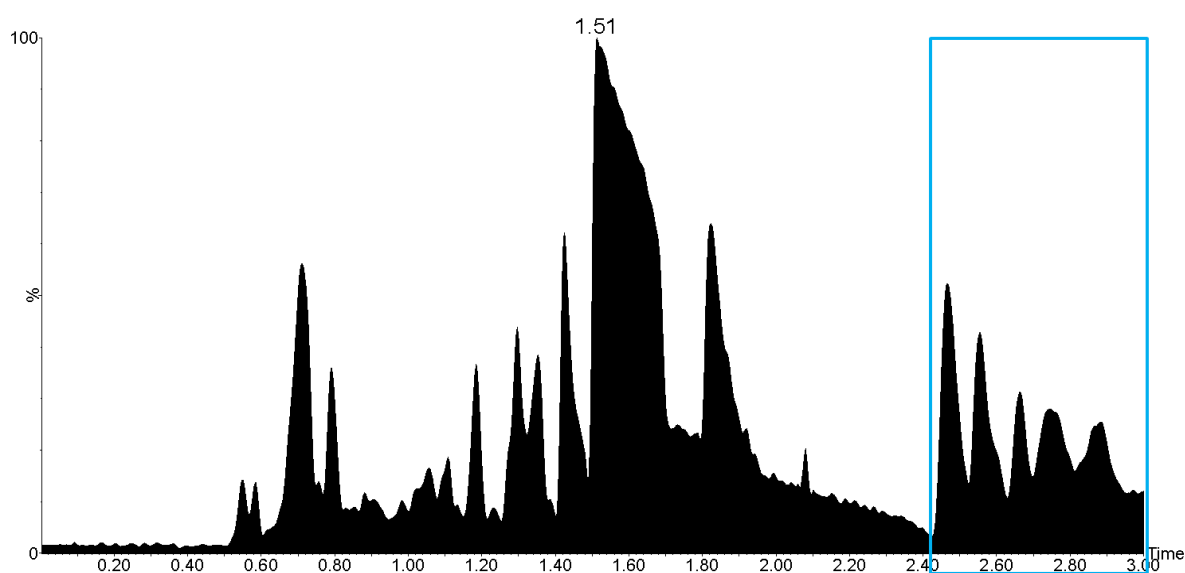


Figure 5-35 - Positive ion ESI UHPSFC-MS BPICC of fuel filter SS6 with pale blue box highlighting PIBs region of retention ( $t_R$  2.40-3.00 min)

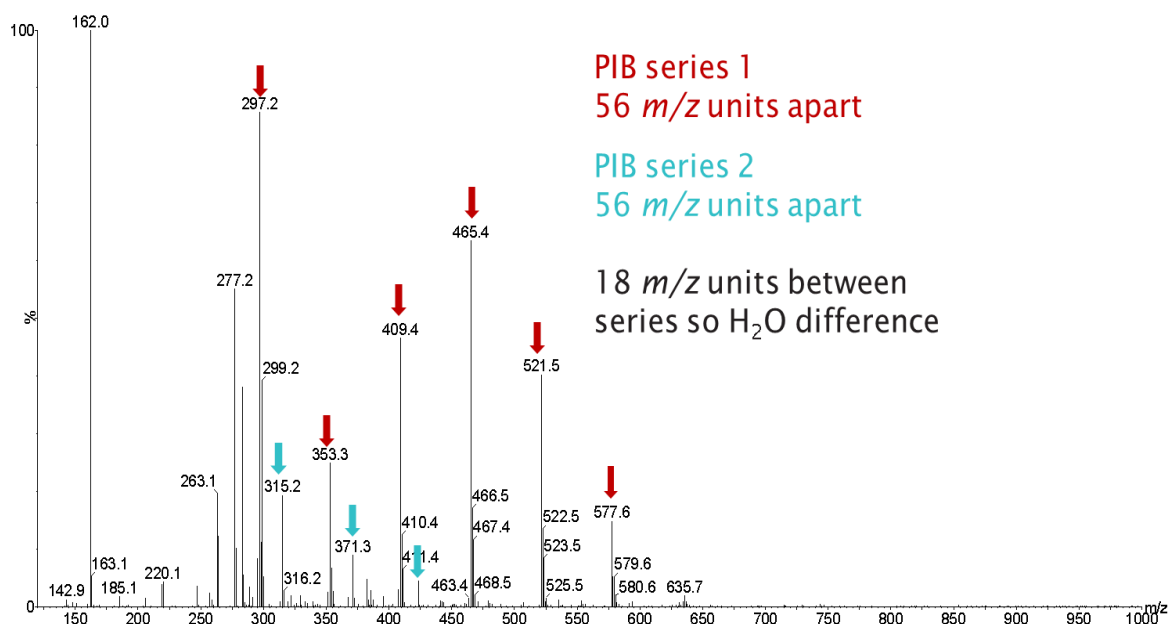


Figure 5-36 - Positive ion ESI UHPSFC mass spectrum of fuel filter SS6 at  $t_R$  2.40-3.00 min, showing two discrete series of 56  $m/z$  units difference (separated by 18  $m/z$  units) consistent with two PIB series, highlighted by red and blue arrows

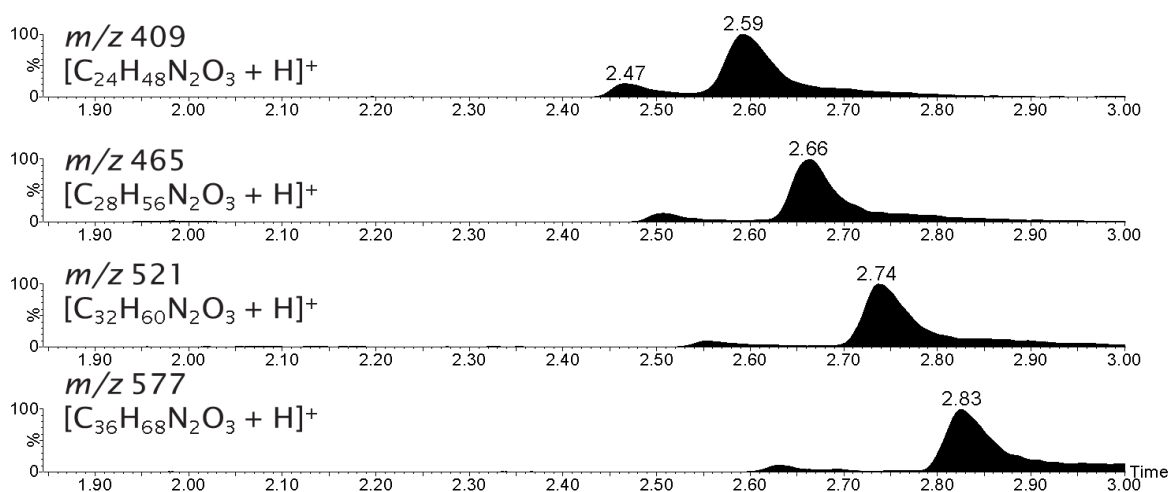


Figure 5-37 - Positive ion ESI UHPSFC-MS RICCs of fuel filter SS6 showing separation of PIBs ( $t_R$  1.80-3.00 min)

## Chapter 5

PIBs were only observed to be present in SS6 and SS10 fuel filter samples during analysis. The same two different PIB series, 18  $m/z$  units apart are observed in both however at much lower abundance in SS10, shown in Figure 5-38. This suggests both fuels have been doped with the same PIBSI DCAs, however at different concentrations. Ion intensity observed in SS6 is approximately an order of magnitude higher than SS10, however the two different PIB series appear to be doped at differing concentrations within each fuel filter adding further complexity.

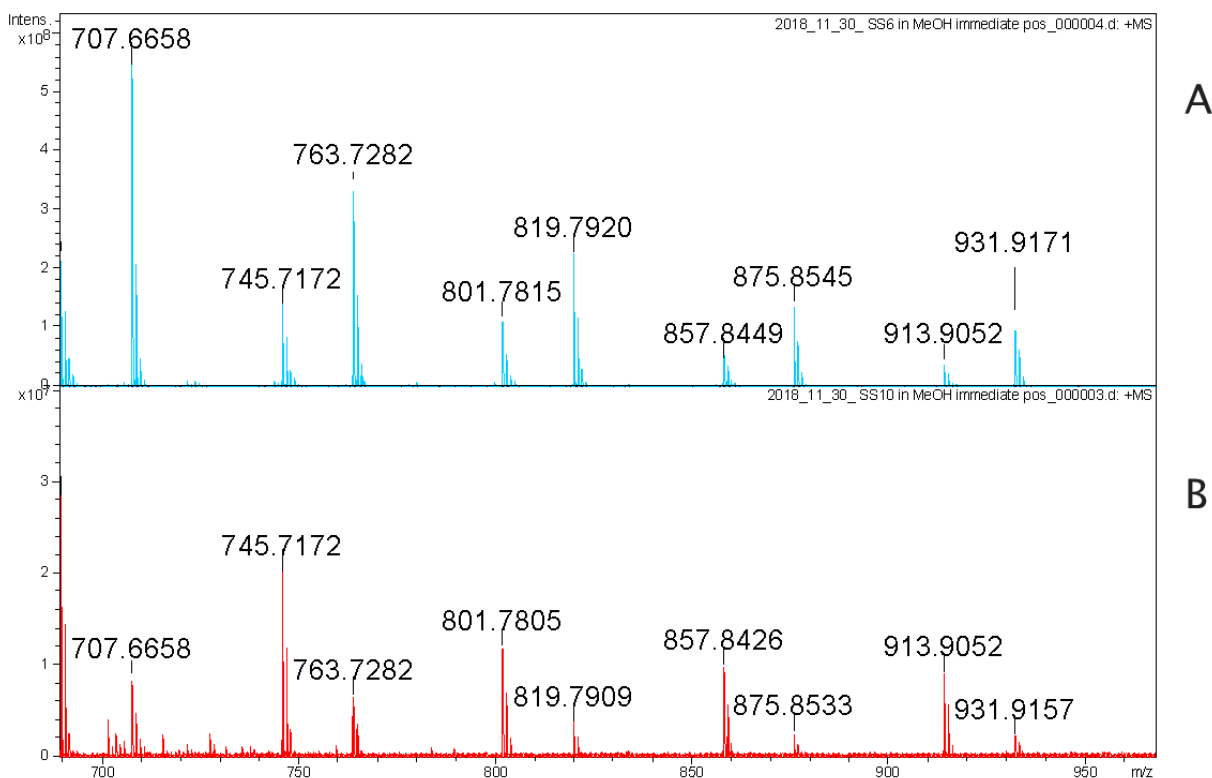


Figure 5-38 - Direct infusion positive ion ESI FT-ICR mass spectra (A) fuel filter SS6 and (B) fuel filter SS10 (zoomed range  $m/z$  690-960), showing protonated molecules for PIBs

As discussed in further detail in 1.3.3, “non-commercial” low molecular weight PIBSIs (<1000 Da) are believed to cause IDIDs, as they have a short polyisobutylene (PIB) backbone that is less soluble in diesel fuel and as a result drops out of solution forming deposits. Therefore, it was proposed that low molecular weight PIBSIs are precursors to polymeric amide IDIDs<sup>38, 123</sup>. These proposed PIB series indicate the presence of PIB based DCAs on these filters which is not surprising considering the mitigation task they undertake in fuel. Other sources suggest that commercial PIBSIs do not contain sufficient “Non-commercial” low molecular PIBSI fraction to cause problems<sup>37, 261</sup>, and indeed commercial DCA with doped “Non-commercial” low molecular weight PIBSI has been shown to be non-deposit forming.



### 5.2.7.1.2 Polypropylene glycol (PPG) series

Another additive used in diesel fuel as a de-icing additive<sup>43</sup> is low molecular weight polypropylene glycol (PPG) (also discussed in section 1.1.1 and Table 1.2).

The SS7 fuel filter will be used as the example to illustrate PPGs within fuel filter samples as they were only found to present in this fuel filter.

A oligomeric series of 58.0420  $m/z$  units difference starting at  $m/z$  621.4197-1085.7544 inclusive, is observed as sodiated molecules  $[M + Na]^+$  in the direct infusion positive ion ESI FT-ICR MS data (Figure 5-39) highlighted by purple arrows. This series of 58.0420  $m/z$  units difference ( $C_3H_6O$ ) is consistent with a PPG series. Below  $m/z$  621, an abundance of ions, possibly consistent with hydrocarbons, are present meaning it is not possible to assign the PPG series at any lower  $m/z$  values with confidence, also ion suppression may result.

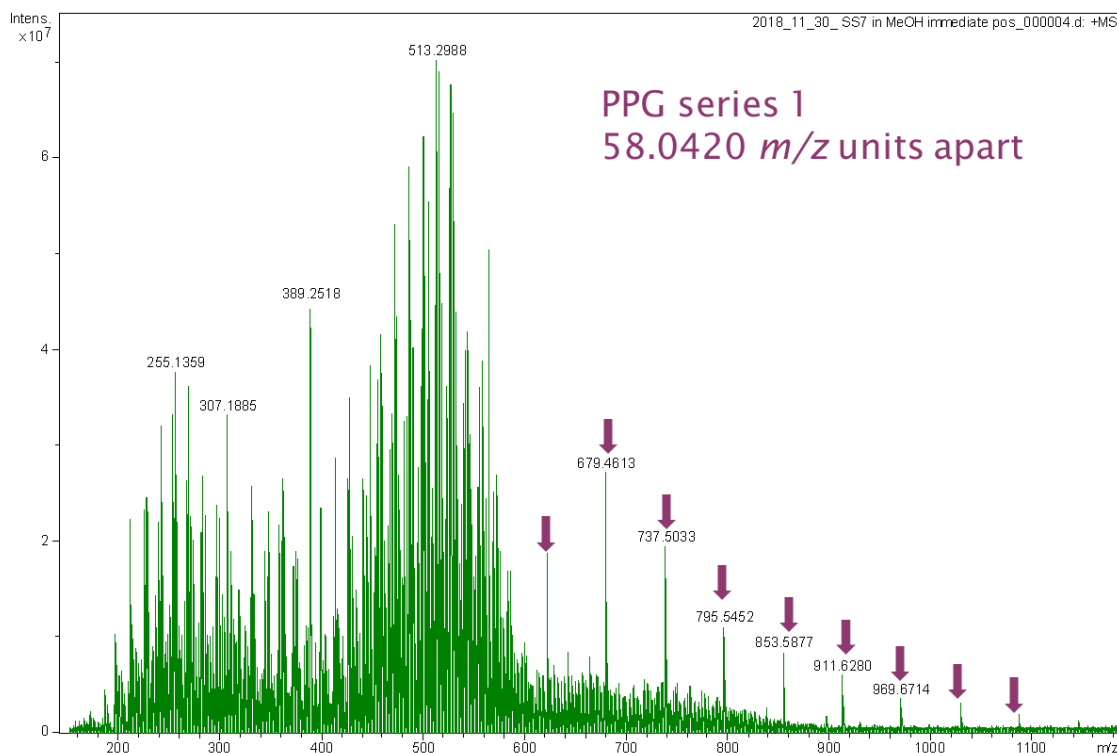


Figure 5-39 - Direct infusion positive ion ESI FT-ICR mass spectrum of fuel filter SS7 (zoomed in mass range  $m/z$  100-1200), showing a series of 58.0420  $m/z$  units difference consistent with a PPG series, highlighted by purple arrows

Figure 5-40 shows a positive ion ESI UHPSFC-MS BPICC of the SS7 fuel filter, with the pale blue box highlighting chromatographic peaks within the region of retention found for PPGs ( $t_R$  1.05-1.50 min).

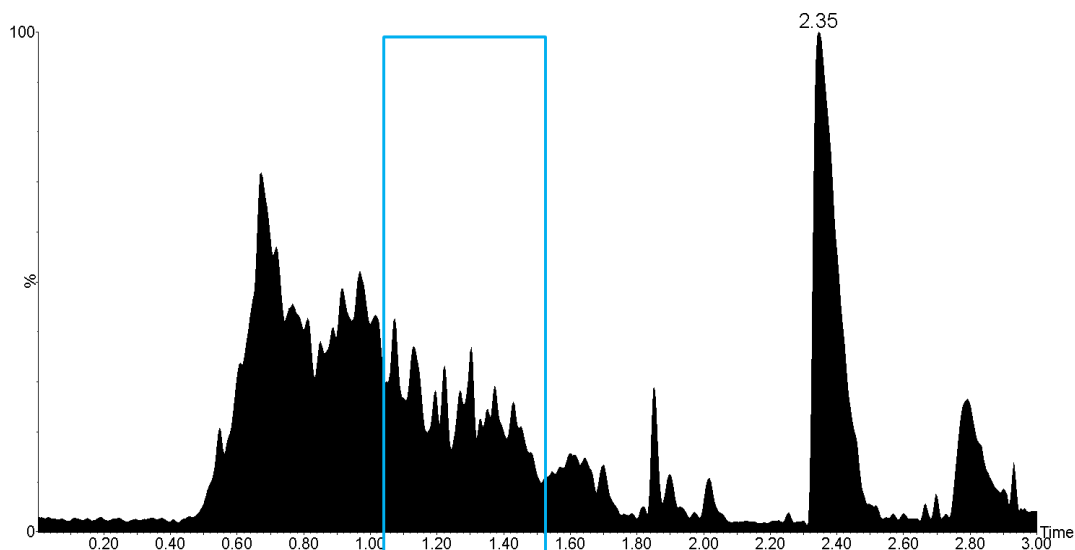


Figure 5-40 - Positive ion ESI UHPSFC-MS BPICC of fuel filter SS7 with pale blue box highlighting PPGs region of retention ( $t_R$  1.05-1.50 min)

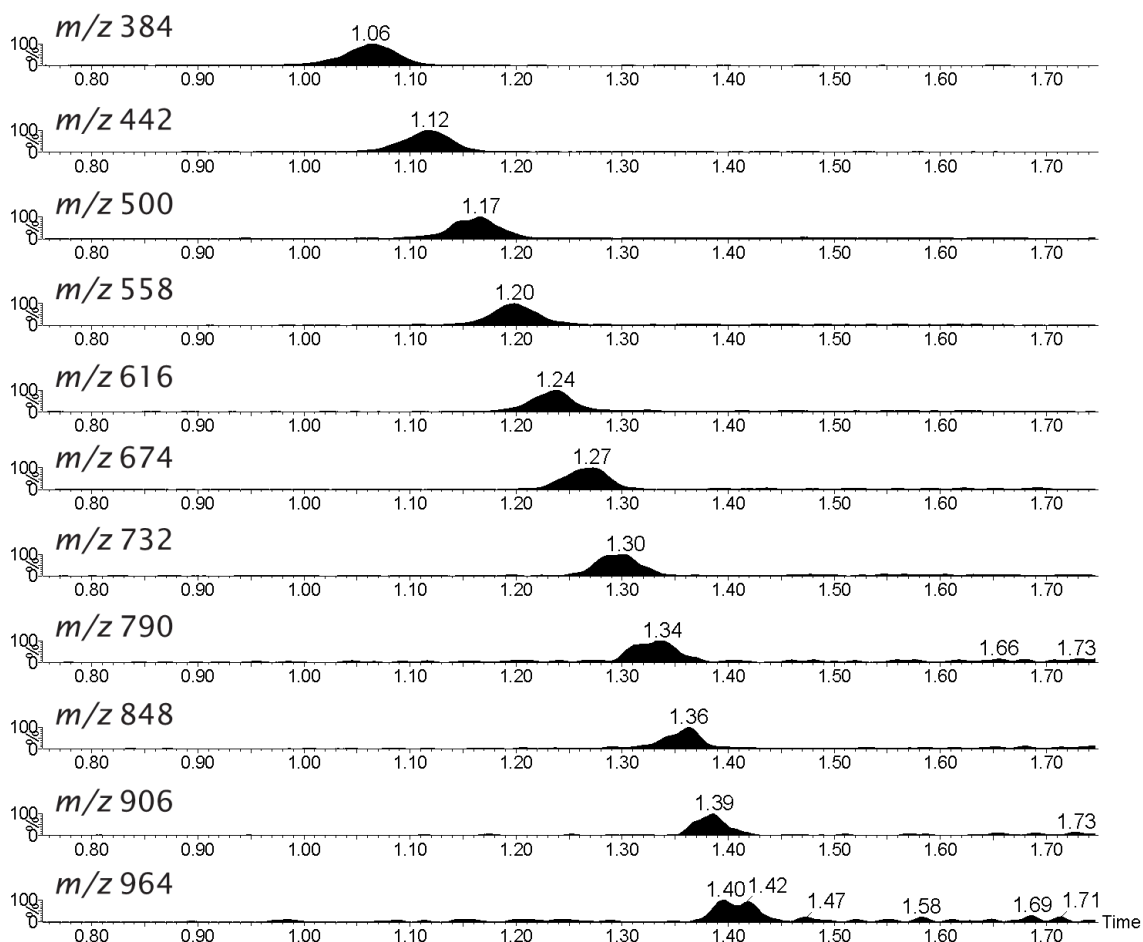


Figure 5-41 - Positive ion ESI UHPSFC-MS RICCs of fuel filter SS7 showing separation of PPGs ( $t_R$  1.05-1.50 min)

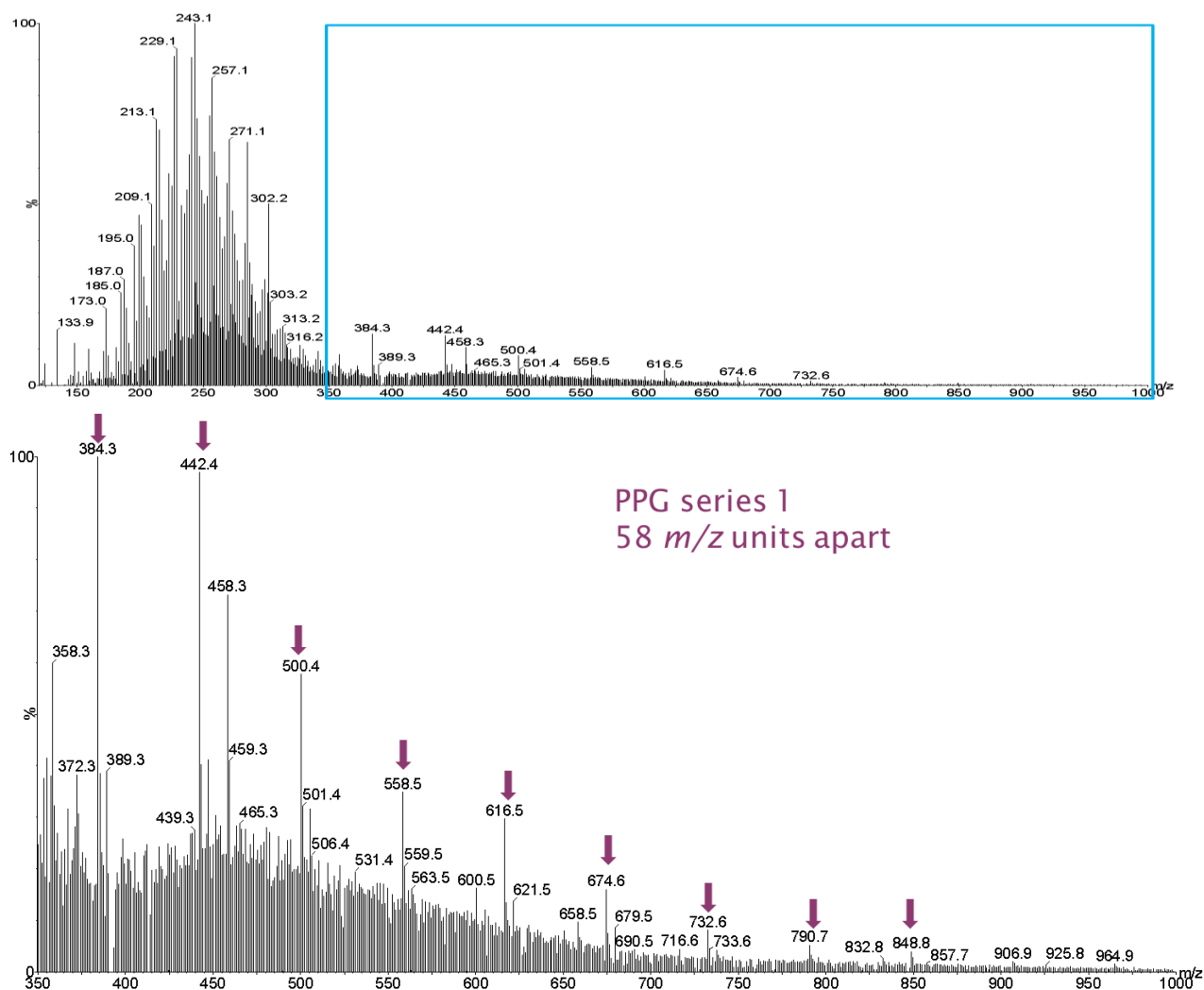


Figure 5-42 –Positive ion ESI UHPSFC mass spectrum of fuel filter SS7 at  $t_R$  1.05-1.50 min, with pale blue box highlighting PPGs region of with zoomed range  $m/z$  350-1000, showing a series of 58  $m/z$  units difference consistent with a PPG series, highlighted by purple arrows

The RICCs and corresponding positive ion ESI UHPSFC-MS mass spectrum shown in Figure 5-41 and Figure 5-42 respectively, shows a series of ammoniated molecules  $[M + NH_4]^+$  of 58  $m/z$  units difference observed at nominal  $m/z$  384-964 inclusive, highlighted by purple arrows. As observed in direct infusion positive ion ESI FT-ICR MS below  $m/z$  350, an abundance of ions, possibly consistent with hydrocarbons, are present meaning it is not possible to assign the PPG series at any lower  $m/z$  values with confidence, also ion suppression may result. The PPG series observed is consistent with that in the direct infusion positive ion ESI FT-ICR MS data, however different mass ranges of the PPG series are observed by positive ion ESI UHPSFC-MS compared with direct infusion positive ion ESI FT-ICR MS. Additionally to this chromatographic separation of PPG species by positive ion ESI UHPSFC-MS, meaning that both methods are complementary for this component of the screening method.

## Chapter 5

PPGs were only observed to be present in SS7 fuel filter samples during analysis. The origin of this PPG observable on a fuel filter still needs to be considered fully. Additionally more fuels would require deicer than only the fuel filter observed to have PPG present.

As with FASES, PPGs are not currently stated in the literature as known causes of filter blocking or IDIDs. Further research is required surrounding their role in diesel blends/additivation and forming engine deposits.

### 5.2.7.2 Non-ionic emulsifier

$m/z$  451.3044 is observed in direct infusion positive ion ESI FT-ICR MS data (Figure 5-43), this is believed to be a sodiated molecule  $[C_{24}H_{44}O_6 + Na]^+$ . This molecular formula is believed to correspond to sorbitan monooleate, which is a non-ionic emulsifier/ common surfactant used in diesel to aid homogenisation.

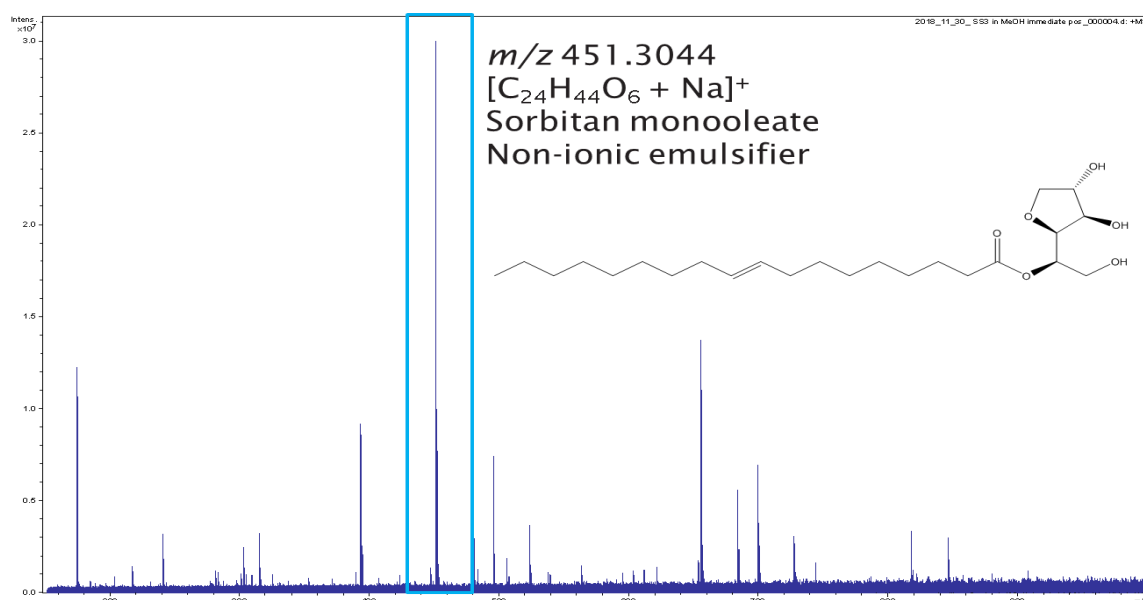


Figure 5-43 - Direct infusion positive ion ESI FT-ICR mass spectrum of fuel filter SS3 (zoomed range  $m/z$  100-1000), with pale blue box highlighting a sodiated molecule  $[C_{24}H_{44}O_6 + Na]^+$  at  $m/z$  451.3044

Figure 5-44 shows a positive ion ESI UHPSFC-MS BPICC of the SS3 fuel filter, with the pale blue box highlighting chromatographic peaks within the region of retention for ammoniated species of interest at nominal  $m/z$  446 ( $t_R$  1.15-1.35 min).

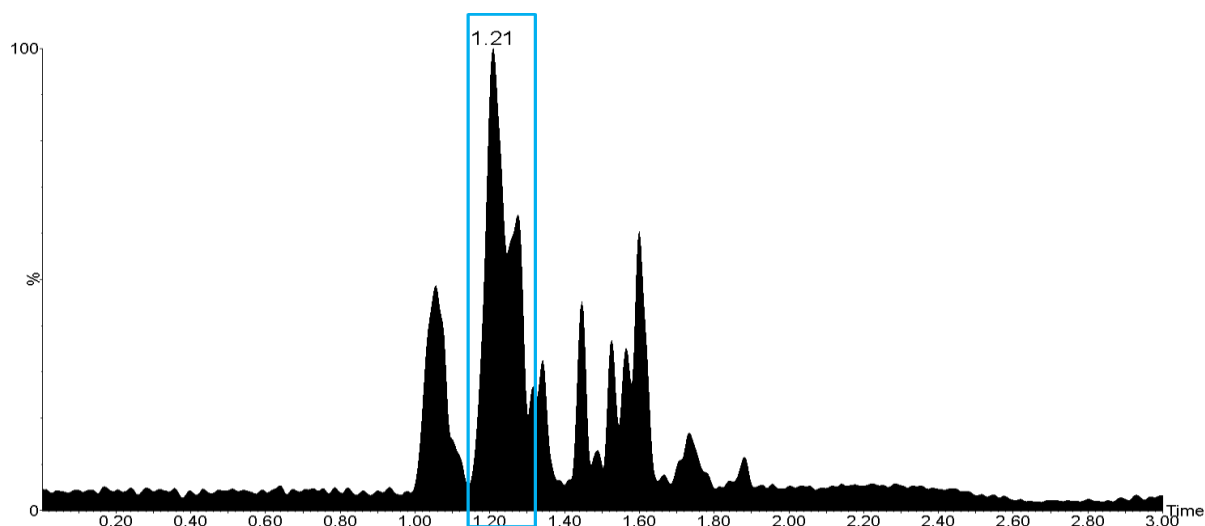


Figure 5-44 - Positive ion ESI UHPSFC-MS BPICC of fuel filter SS3 with pale blue box highlighting compound of interest region of retention ( $t_R$  1.15-1.35 min)

The corresponding positive ion ESI UHPSFC-MS mass spectrum shown in Figure 5-45 shows nominal  $m/z$  446 and 451 observed as ammoniated molecule  $[M + NH_4]^+$  and sodiated molecule  $[M + Na]^+$  respectively. Confirmation that the chromatographic peaks in this region are most likely related to  $C_{24}H_{44}O_6$  and their associated nominal  $m/z$  (in this case  $[M + NH_4]^+$  and  $[M + Na]^+$ ) is achieved using RICCs. Data shown in Figure 5-46, which suggests that the respective peaks are related to the  $C_{24}H_{44}O_6$ , which agrees with those observed in the direct infusion positive ion ESI FT-ICR MS data.

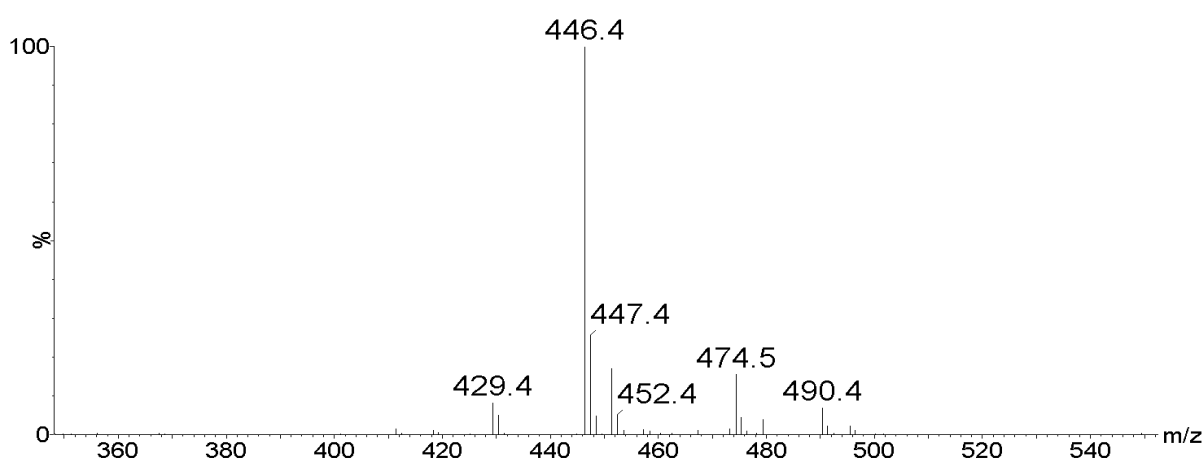


Figure 5-45 - Positive ion ESI UHPSFC-MS of fuel filter SS3 at  $t_R$  1.15-1.35 min (zoomed range  $m/z$  350-550)

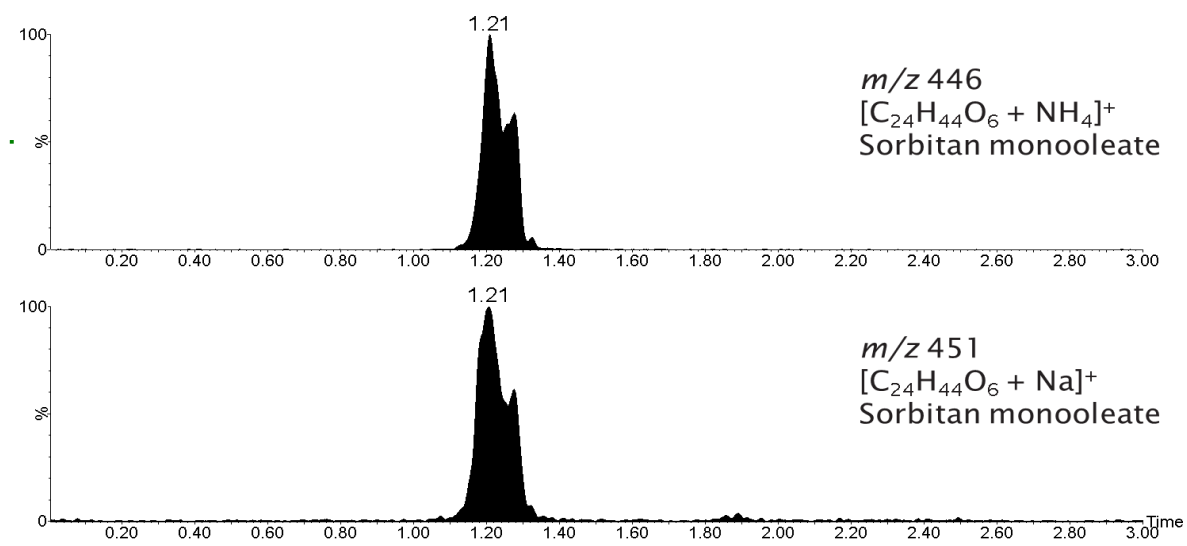


Figure 5-46 - Positive ion ESI UHPSFC-MS of fuel filter SS3 (A) RICC nominal  $m/z$  446 ammoniated species of interest  $[C_{24}H_{44}O_6 + NH_4]^+$  and (B) RICC nominal  $m/z$  451 sodiated species of interest  $[C_{24}H_{44}O_6 + Na]^+$

This illustrates that these two analysis techniques used for targeted analysis do not just highlight the compounds of interest listed in the screening method but can also show other additives or compounds present.

This compound was only observed to be present in SS3 fuel filter and the origin of this still needs to be considered fully.

**5.2.8 Fuel filter summary**

Table 5-6 is a summary of all findings from fuel filter analysis undertaken using the screening methods outlined in section 5.2.

Table 5-6 Fuel filters analysis summary

Fuel filters									
Compound	SS2	SS3	SS4	SS5 (gunk)	SS6	SS7	SS8	SS9	SS10
FAMES	√ (C16:1 and C16:0, C18:3, C18:2, C18:1. traces 18:0),		√ (C16:1 and C16:0, C18:3, C18:2, C18:1. traces)	√ (C16:1 and C16:0, C18:3, C18:2, C18:1, traces 18:0.)					√ (C16:1 and C16:0, C18:3, C18:2, C18:1, 18:0),
FAME oxidation products	√ (C18:3, C18:2, C18:1 only (+1 O,+2 O,+3O))		√ (C18:3, C18:2, C18:1 only (+1 O,+2 O,+3O))	√ (C18:3, C18:2, C18:1 only (+1 O and +2 O))					√ (C18:3, C18:2, C18:1 only (+1 O)(+2O & +3O low abundance))
FFAs	√	√	√	√	√	X	√	√	√

## Fuel filters

Compound	SS2	SS3	SS4	SS5 (gunk)	SS6	SS7	SS8	SS9	SS10
	(?C14:0, C16:0, C18:3, C18:2, C18:1.and 18:0),	(C16:0, C18:3, C18:2, C18:1.and 18:0),	(?C14:0, C16:0, ?C18:3, C18:2, C18:1.and 18:0),	(C16:0, C18:2, C18:1.and 18:0),	(C16:0, C18:1.and 18:0),		(C16:0, C18:3, C18:2, C18:1.and 18:0)	(C16:1, C16:0, C18:2, C18:1.and 18:0)	(C16:1, C16:0, C18:2, C18:1.and 18:0)
SGs	√ (Campesterol glucoside, β-sitosterol glucoside and low abundance of Stigmasterol glucoside)		√ (Campesterol glucoside, β-sitosterol glucoside and very low abundance of Stigmasterol glucoside)	√ (All very low abundance of campesterol glucoside, β-sitosterol glucoside and Stigmasterol glucoside)					
MAGs	√	√		√					√



Fuel filters

Compound	SS2	SS3	SS4	SS5 (gunk)	SS6	SS7	SS8	SS9	SS10
	(C16:0, C18:3, C18:2, C18:1, C18:0. Dimers at <i>m/z</i> 683, 711, 739)	(C16:0 and C18:0.)		(C16:0, C18:3, C18:2, C18:1, C18:0. Dimers at <i>m/z</i> 683, 711, 739)					(C16:0, C18:2, C18:1, C18:0.(low abundance))
FASEs				√ (Campesterol ester C18:3, C18:2 and C18:1and β- sitosterol ester C18:3, C18:2 and C18:1)					
PIBs					√ (2 series, 18 <i>m/z</i> units apart)				√ (2 series, 18 <i>m/z</i> units apart)
PPGs						√			

Fuel filters

Compound	SS2	SS3	SS4	SS5 (gunk)	SS6	SS7	SS8	SS9	SS10
						(1 series)			
Other		<p>✓                      (Sorbitol monooleate?                      (additive - emulsifier))</p>							

From the analysis of the fuel filters (and associated residue), the composition information shown in Table 5-7 was determined for each fuel filter.

Table 5-7 - Fuel filters composition summary

Fuel filter	Composition
<b>SS2</b>	FAMEs, FAME ox prods, FFAs, SGs and MAGs
<b>SS3</b>	FFA and MAGs – solid residues like those found in literature. Also possible emulsifier observed
<b>SS4</b>	similar to SS2 but no MAGs but biodiesel related
<b>SS5</b>	similar to SS2 but addition of FASEs but biodiesel related
<b>SS6</b>	FFA and PIB –aged fuel/metal carboxylate IDIDs and polymeric amide lacquer components
<b>SS7</b>	FFA and PPG – aged fuel/metal carboxylate IDIDs
<b>SS8</b>	FFA - aged fuel/metal carboxylate IDIDs, similar to SS9
<b>SS9</b>	FFA - aged fuel/metal carboxylate IDIDs, similar to SS8
<b>SS10</b>	FAMEs, FAME ox prods, FFA, MAG and PIB

In this work only the fuel filters and a single fuel injector tip IDID were analysed, however it would have been useful to have the entire flow of the FIE (fuel, fuel filter and fuel injector IDID/deposit) sampled to be able to link together the findings to answer the questions outlined above.

Complementarity of the approaches and the information obtained can be observed in this chapter Agreement between the two analytical techniques utilised in this methodology (FT-ICR-MS and UHPSFC-MS) can be observed for FAMEs, FAMEs oxidation products, FFAs, MAGs, PIBs and PPGs. For example FAMEs C18 species dominate the mass spectra, although the relative ion intensities vary between techniques but this may be due to looking at different cationised species. C16:0 and C18:1 FFAs dominate both FT-ICR-MS and UHPSFC-MS mass spectra with similar relative ion

## Chapter 5

intensities. Saturated MAGs C16:0 and C18:0 dominate all mass spectra again at similar relative ion intensities. PIBs and PPGs mass spectra have respective similar mass spectra for both techniques however a larger  $m/z$  range can be observed in one technique over the other.

### 5.3 Deposit analysis protocol trees

In a similar manner to the diesel analysis protocol trees (chapter 4.6), deposit analysis protocol trees have been developed both as an analyst flow (deposit) and a deposit flow format. These have been designed as an accessible reference tool to aid in the understanding of the deposits, both in their practical analysis and characterisation respectively. This is a consolidation of the analysis techniques used throughout this project to tackle the deposit issue, by linking specific known deposit forming compounds (possibly deposits) to specific analysis techniques.

As discussed in 1.3.6 and throughout this chapter, sample preparation of the deposits is of high importance but can be challenging and is very dependent on the deposit. Commonly (including analysis methods used in this project), the deposit components must be infused into solvent for analysis either by soaking or washing the sample. A variety of solvents may have to be used, as it will be dependent on the solubility of the deposit components in a specific solvent. This may require working through a series of different solvent and solvent mixtures until deposit components are observed when the infused solvent is analysed by direct infusion ESI.

#### 5.3.1 Analyst flow (deposits)

The analyst flow (deposits), as shown in Figure 5-47, should be considered as the practical laboratory experimental process. This is a proposed flow protocol for an analyst to consult when faced with an unknown deposit sample X that requires characterisation of deposit types and/or compounds present.

The characterisation approach can be undertaken in the same way as the analyst flow (diesels) as discussed in 4.6.1. (Polar column) GC-MS is omitted from Figure 5-47 as positive ion ESI UHPSFC-MS afforded detection of FAMES, however (polar column) GC-MS could be used if detection of hydrocarbons was required.

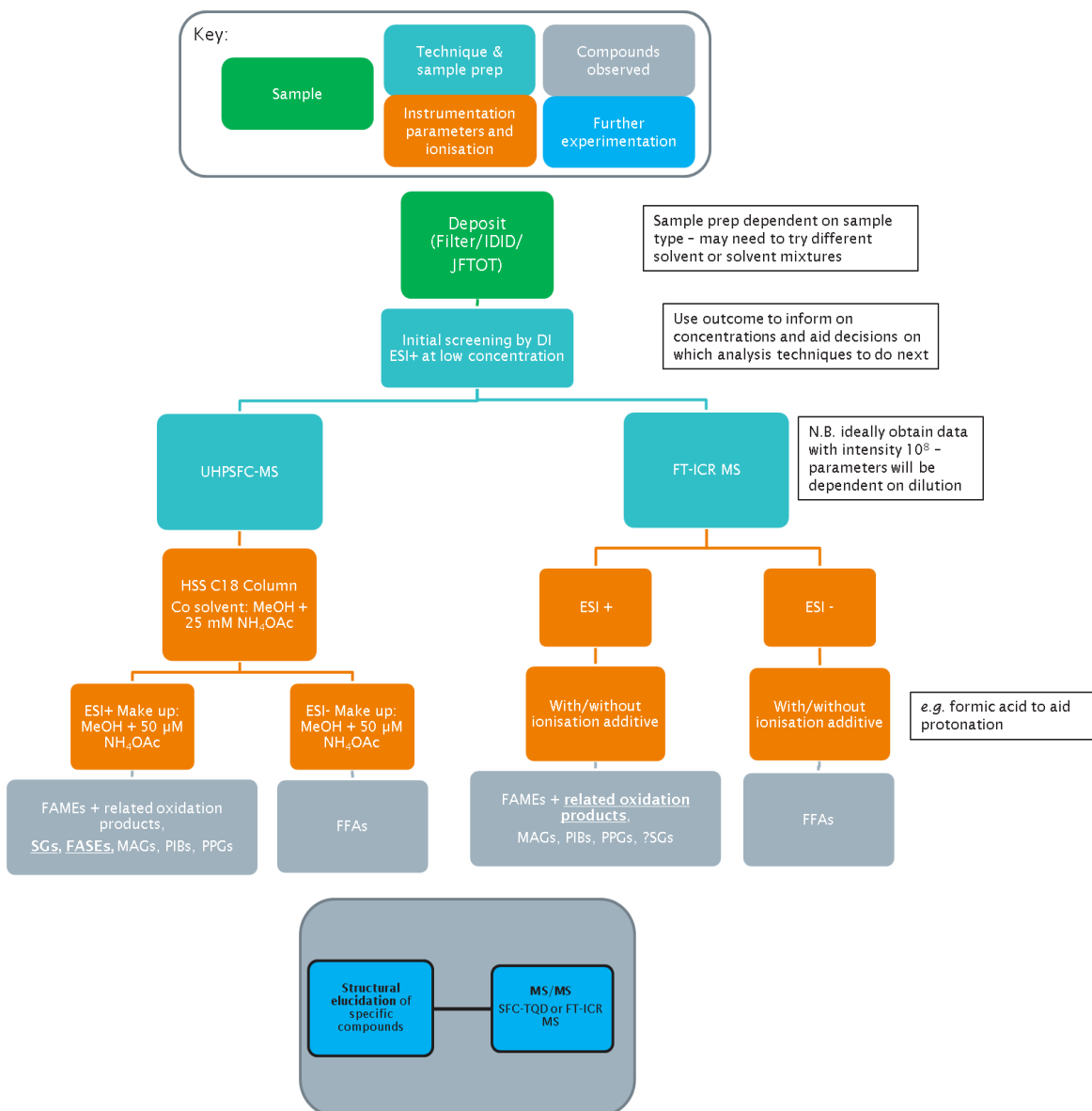


Figure 5-47 – Analyst flow (deposit) analysis protocol tree

(Compounds that are in bold and underlined indicate the preferred method for characterisation)

### 5.3.2 Deposit flow

The deposit flow analysis protocol tree, as shown in Figure 5-48, as with the diesel flow analysis protocol tree is a thought experiment/protocol. This flow is proposed for consultation when faced with a sample of an unknown deposit X that requires characterisation of deposit types and/or compounds present.

The analysis is similar to the diesel flow analysis protocol tree in 4.6.2. Differences and additions are highlighted below.

Initially the deposit sample should be inspected and any additional information about the sample obtained. This can provide valuable information that can aid in the characterisation and provide early indications as to deposit type or the types of components possibly present.

Additional questions must be asked prior to analysis. These should include:

- Which components are present within the type of the deposit believed to be present?
  - Which technique would detect these?

Some examples of expected components that may be linked to specific IDIDs include:

- Aged fuel IDIDs = FAMES and related oxidation products
- Metal carboxylate IDIDs = FFAs

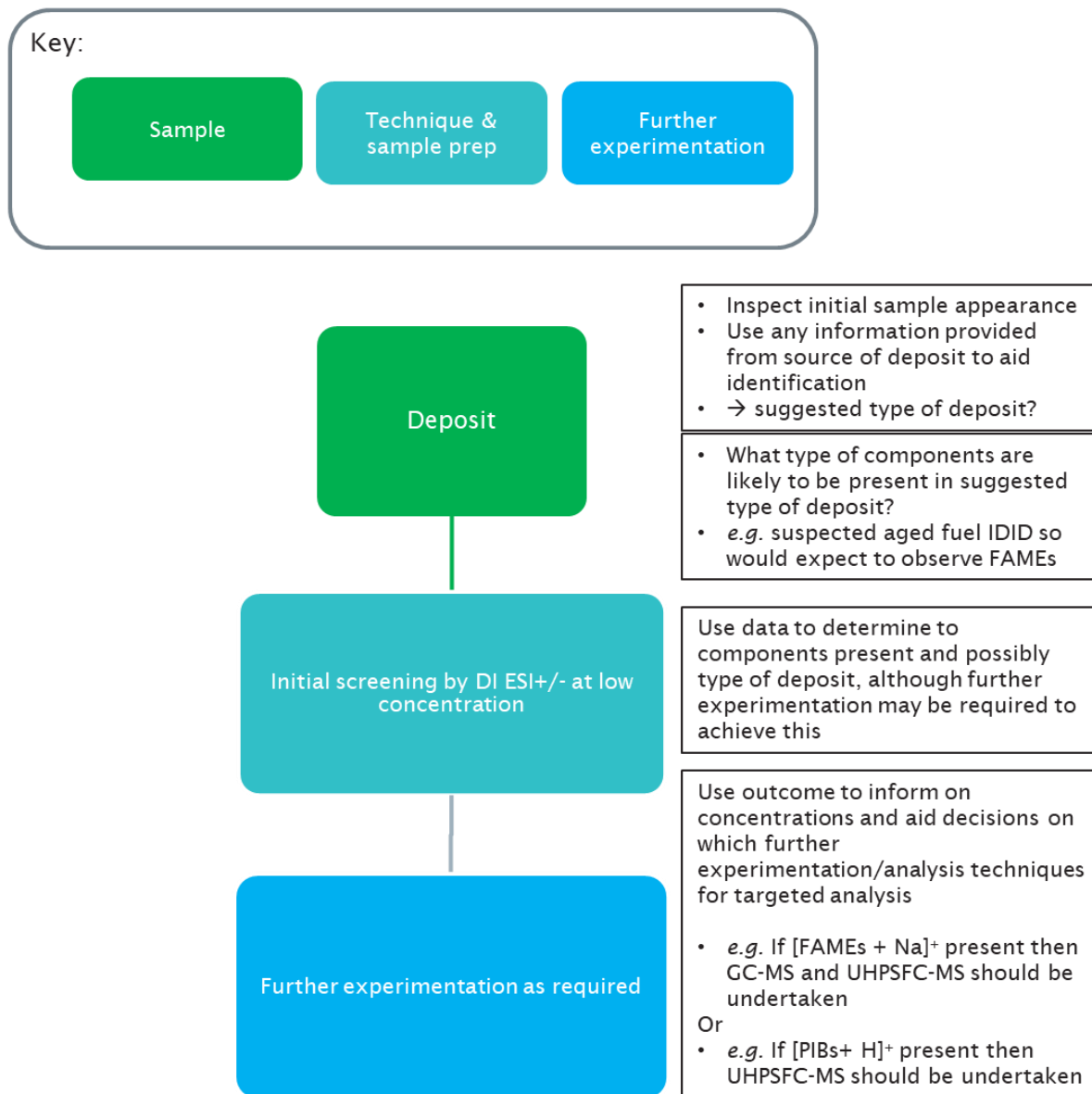


Figure 5-48 - Deposit flow analysis protocol tree



## 5.4 Analysis of fuel injector tip IDID from the field (work in collaboration with John Langley)

The deposit screening methodology (further detail in 5.2) utilised previously for the analysis of fuel filter samples, was now used to demonstrate the method scope with a failed common rail fuel injector with IDID. This allowed further development of the deposit screening methodology.

A variety of sample preparation methods were employed in order to achieve dissolution of the IDID from the fuel injector, as this was found to be problematic due to the unknown chemical composition. Many different solvents and solvent mixtures were attempted, and the optimised sample preparation is outlined in 3.2.2.3.

The resulting infused methanol:dichloromethane scraping solvent mix was analysed using the described direct infusion positive and negative ion ESI FT-ICR MS and negative ion ESI UHPSFC-MS methods.

### 5.4.1 Direct infusion positive ion ESI FT-ICR MS

An oligomeric distribution with  $m/z$  difference of 56.0630, starting at  $m/z$  409.3446 up to  $m/z$  1250.2812, is observed in the direct infusion positive ion ESI FT-ICR MS data (Figure 5-49) highlighted by orange arrows.  $m/z$  521.2691 and  $m/z$  577.5328 with corresponding molecular formulae  $[C_{32}H_{60}N_2O_3 + H]^+$  and  $[C_{36}H_{68}N_2O_3 + H]^+$  respectively, are observed in the oligomeric distribution separated by 56.0630  $m/z$  units difference that is shown to correspond to  $C_4H_8$ . This is consistent of a polyisobutylene (PIB) series as outlined in 5.2.7. This observed PIB series may suggest “non-commercial” low molecular weight PIBSI used as deposit control additive (DCA) in the fuel that has been attracted to the IDID or is present on the injector tip. This PIB series is also observed in SS6 and SS10 fuel filter samples (5.2.7).

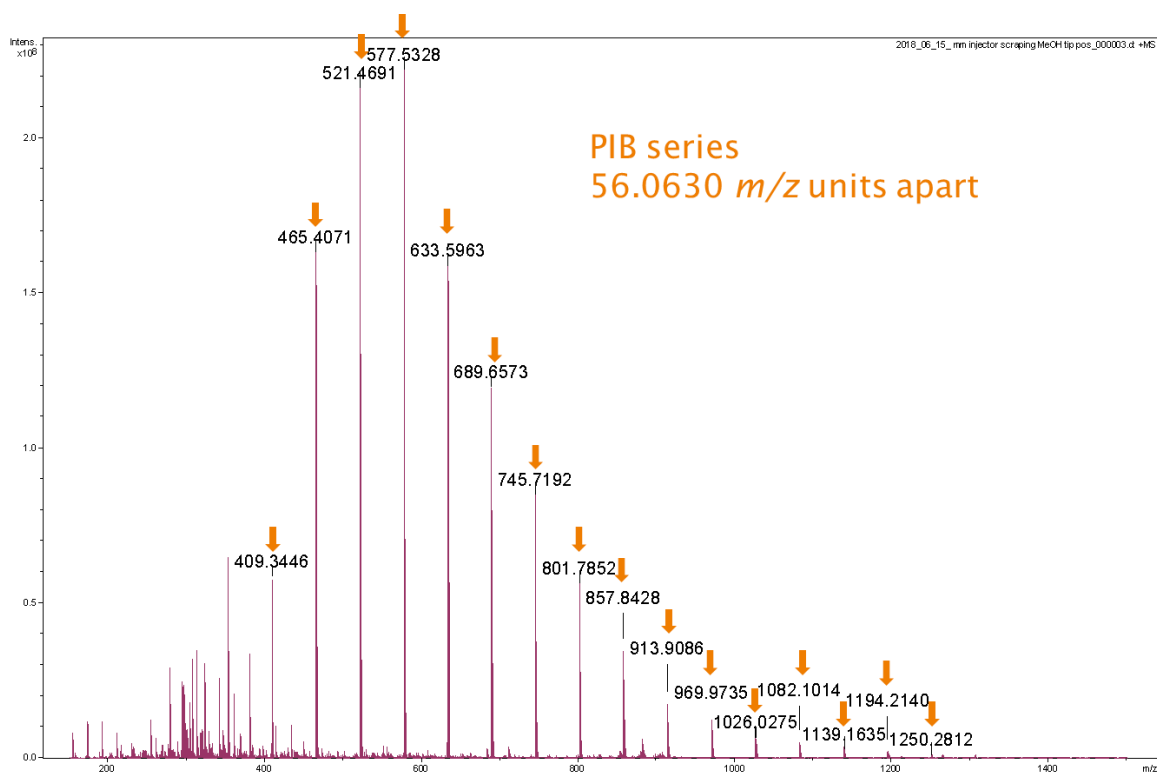


Figure 5-49 - Direct infusion positive ion ESI FT-ICR mass spectrum of fuel injector tip IDID, showing a series of 56.0630  $m/z$  units difference consistent with a PIB series, highlighted by orange arrows

$m/z$  279.2295 and 307.2613 are also observed (Figure 5-50) and are believed to be sodiated molecules with corresponding molecular formulae  $[C_{16}H_{32}O_2 + Na]^+$  and  $[C_{18}H_{36}O_2 + Na]^+$  respectively. These molecular formulae are believed to be the sodiated molecules of the saturated FFAs of C16:0 ( $C_{16}H_{32}O_2$ ) and C18:0 ( $C_{18}H_{36}O_2$ ) with the source of the sodium ion being from the ESI-MS/ionisation process (sodium within MS system to form cationised molecule) or as sodium carboxylate salts with the sodium being present in the IDID. There is no way to distinguish between both these suggested assignments. The source of these FFAs is either from hydrogenated biodiesel (due to the lack of unsaturated fatty acids) or from monoacid lubricity improver additives. In combination with sodium hydroxide, monoacid lubricity improver additives have been found to form sodium carboxylate deposits causing fuel filter fouling<sup>227</sup>.

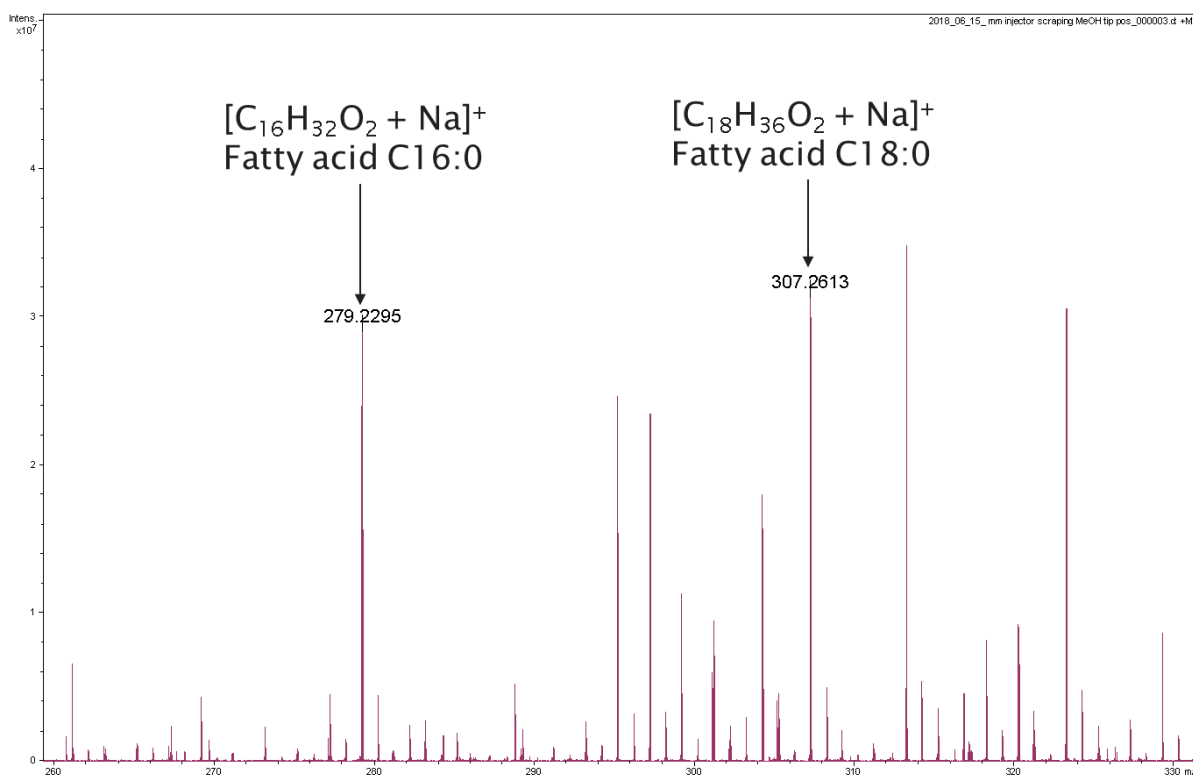


Figure 5-50 - Direct infusion positive ion ESI FT-ICR mass spectrum of fuel injector tip IDID (zoomed range  $m/z$  260-330) showing sodiated molecules for FFAs

#### 5.4.2 Direct infusion negative ion ESI FT-ICR MS

$m/z$  255.2334 and 283.2653 are observed in the direct infusion negative ion ESI FT-ICR MS data (Figure 5-51), these are believed to be deprotonated molecules  $[C_{16}H_{31}O_2 - H]^-$  and  $[C_{18}H_{35}O_2 - H]^-$  respectively. These molecular formulae correspond to the same saturated FFAs of C16:0 ( $C_{16}H_{32}O_2$ ) and C18:0 ( $C_{18}H_{36}O_2$ ) observed as sodiated molecules in the direct infusion positive ion ESI FT-ICR MS data.

Dimeric species correspond to the same saturated FFAs of C16:0 ( $C_{16}H_{32}O_2$ ) and C18:0 ( $C_{18}H_{36}O_2$ ) are also observed as deprotonated molecules.  $[2(C_{16}H_{32}O_2) - H]^-$ ,  $[(C_{16}H_{32}O_2 + C_{18}H_{36}O_2) - H]^-$  and  $[2(C_{18}H_{36}O_2) - H]^-$  are observed at  $m/z$  511.4744, 536.5026 and 567.5339 respectively. These are most likely formed in the ESI process, and present because the sample is at a high concentration, dilution of sample would remedy this.

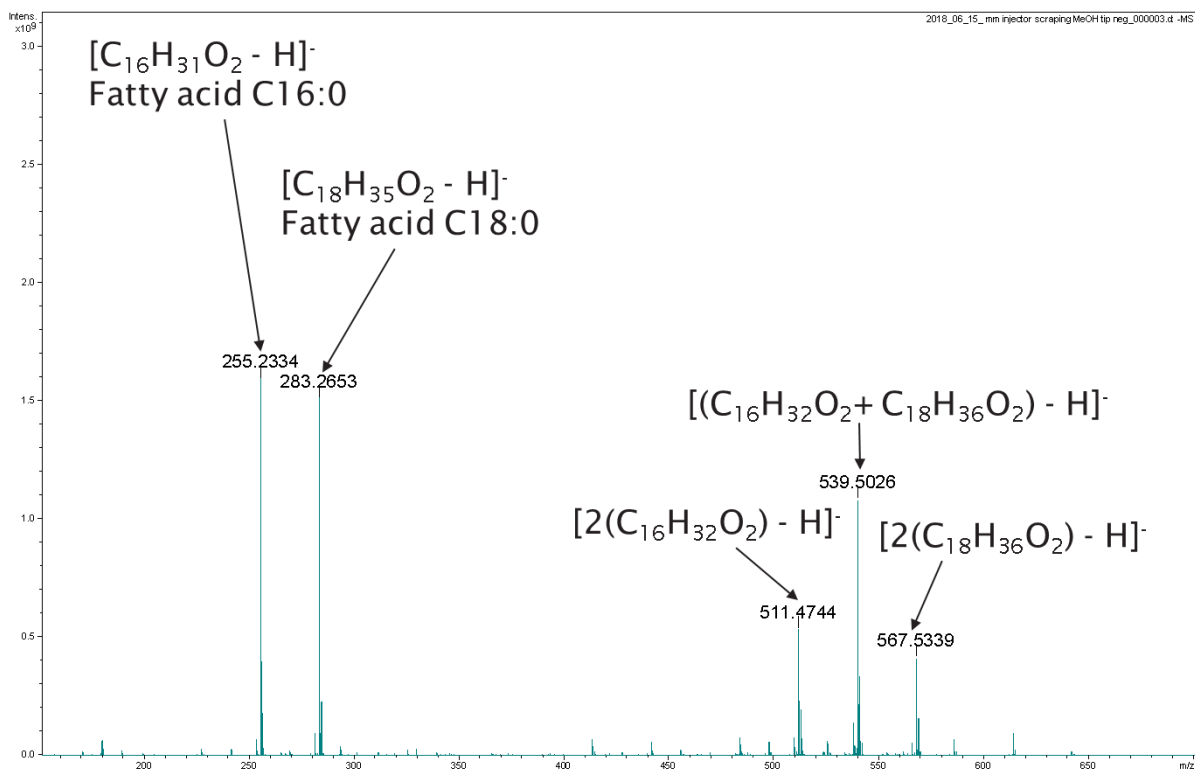


Figure 5-51 -- Direct infusion negative ion ESI FT-ICR mass spectrum of fuel injector tip IDID (zoomed range  $m/z$  150-700), showing deprotonated molecules for FFAs

#### 5.4.3 Negative ion ESI UHPSFC-MS

Two chromatographic peaks can be observed in the BPICC of the negative ion ESI UHPSFC-MS (Figure 5-52(A)) with corresponding mass spectra (Figure 5-53) showing deprotonated molecules observed at nominal  $m/z$  255 and 283 respectively. This is consistent with compounds of nominal relative molecular mass of 256 and 284 respectively. Confirmation that the two chromatographic peaks are related to nominal  $m/z$  255 and 283 is achieved using RICCs (Figure 5-52(B) and (C)) and is highly suggestive that they are related to the saturated FFAs C16:0 and C18:0 also observed in the direct infusion negative ion ESI FT-ICR MS.

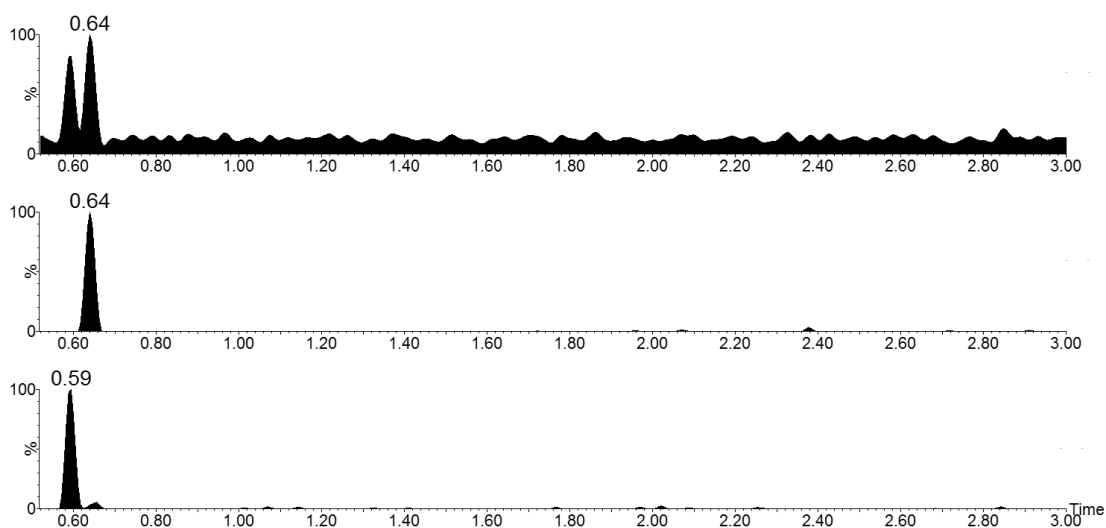


Figure 5-52 – Negative ion ESI UHPSFC-MS (all zoomed to 0.50 – 3.00 min) of fuel injector tip IDID (A) BPICC, (B) RICC nominal  $m/z$  283 [ $C_{18}H_{35}O_2 - H$ ]<sup>-</sup> and (C) RICC nominal  $m/z$  255 [ $C_{16}H_{31}O_2 - H$ ]<sup>-</sup>

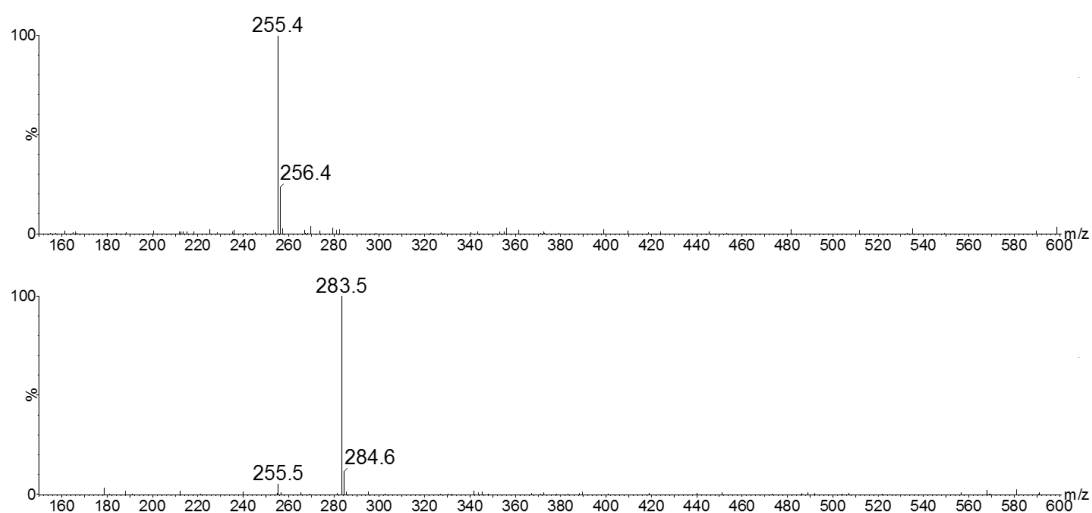


Figure 5-53 – Negative ion ESI UHPSFC-MS (zoomed range  $m/z$  150-600) of fuel injector tip IDID (A) mass spectrum at  $t_R$  0.64 min, (B) mass spectrum at  $t_R$  0.59 min

#### 5.4.4 Summary

Positive ion ESI FT-ICR MS data shows data consistent with the presence of a PIB series, as an oligomeric series was observed with 56.0630  $m/z$  units difference starting at  $m/z$  409.3446 up to  $m/z$  1250.2812. The presence of PIB suggests that “non-commercial” low molecular weight PIBSI used as deposit control additive (DCA) in the fuel that has been attracted to the IDID or is present on the injector tip.

Both positive and negative ion ESI FT-ICR MS and UHPSFC-MS data suggests the presence of C16:0 & C18:0 FFAs, that suggests either metal carboxylate salt IDID. The source of these saturated FFAs is either from hydrogenated biodiesel (due to the lack of unsaturated fatty acids) or from monoacid lubricity improver additives.

This is most likely to be in agreement with work by Lacey *et al.*<sup>120</sup>, which stated that polymeric amides are often found in combination with sodium carboxylate salts<sup>120</sup>(outlined further in 1.3.3.5).

## 5.5 Analysis of JFTOT rods and associated fuels

**Some of the work in this section is published in: Barker, J.; Reid, J.; Smith, S. A.; Snape, C.; Scurr, D.; Langley, G.; Patel, K.; Carter, A.; Laphorn, C.; Pullen, F., . The Application of New Approaches to the Analysis of Deposits from the Jet Fuel Thermal Oxidation Tester (JFTOT). *SAE International Journal of Fuels and Lubricants*, 2017, 10(3), 741-755.**

Some of the work contained in this section around JFTOT rods and their associated fuels is based upon initial work by Patel<sup>211</sup>.

A JFTOT instrument was adapted to assess deposit formation in two diesel fuels (B20, USLD) and a composite mix of both, and three JFTOT rods (B20, ULSD and RF06→B20→RF06) were produced by Innospec, as outlined in chapter 3.2.2.1. These JFTOT rods along with the associated fuels (SS#1 and SS#2) were prepared for analysis as outlined in chapter 3.2.2.1. Two sample preparation methods were used to allow for comparison for removal of deposits from the JFTOT rods.

The infused methanol:dichloromethane solvent mix resulting for each JFTOT rod prepared by each preparation method (solvent washing and scraping) was analysed using positive ion ESI FT-ICR MS and non-polar column GC-MS.

### 5.5.1 Previous work by Patel

Initial work<sup>211</sup> analysing JFTOT rods was first undertaken by Patel, using surface analysis techniques and mass spectrometry. Direct analysis in real time mass spectrometry (DART-MS) and positive ion ESI FT-ICR MS data showed the presence of an adipate in JFTOT rods when the deposits were extracted using a solvent washing method (Figure 5-54). This adipate was observed as a sodiated molecule at  $m/z$  393.3161 [ $C_{22}H_{42}O_4 + Na$ ]<sup>+</sup> in positive ion ESI FT-ICR MS data and the corresponding protonated molecule at  $m/z$  371 in DART-MS data, as shown in Figure 5-54<sup>211</sup>. From tandem MS experiments, the adipate was believed to correspond to either dioctyl adipate or di-2-ethylhexyl adipate (DEHA), as shown in Figure 5-55.

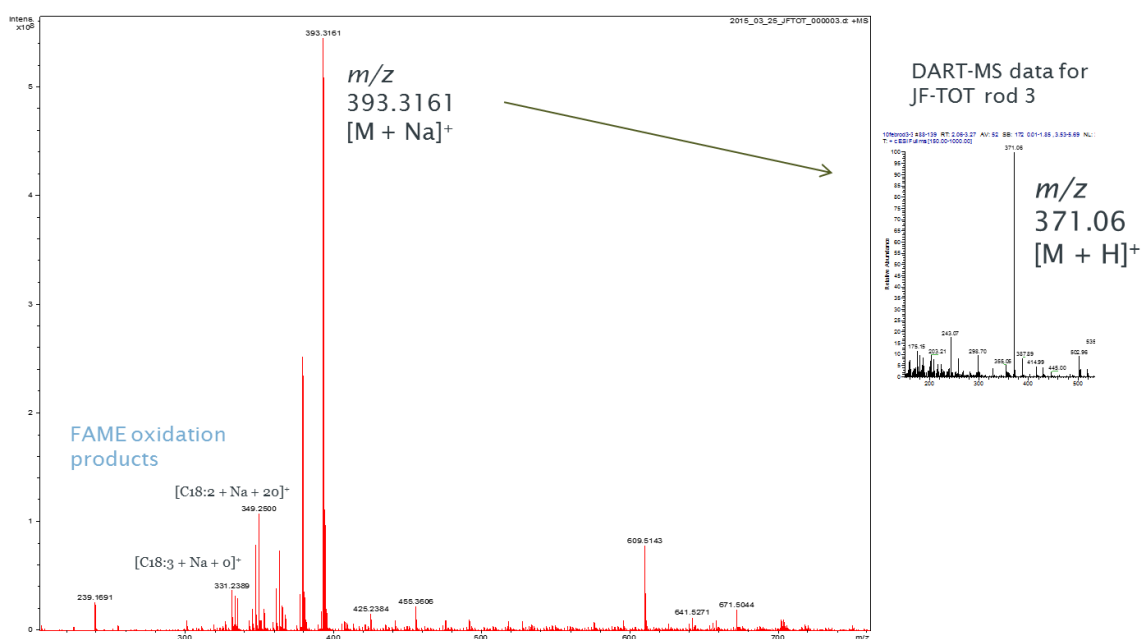


Figure 5-54 - Direct infusion positive ion ESI FT-ICR MS and DART-MS for JFTOT rod 3, showing the proposed adipate as sodiated and protonated molecules respectively. Taken from<sup>213</sup>

### 5.5.2 JFTOT rods

#### 5.5.2.1 FT-ICR MS analysis

Direct infusion positive ion ESI FT-ICR MS was used as in previous work undertaken by Patel/shown in publication to analyse all samples (JFTOT rods and associated fuels). The work shown below was undertaken to validate the results reported by Patel<sup>211</sup> and further optimise the analysis method.

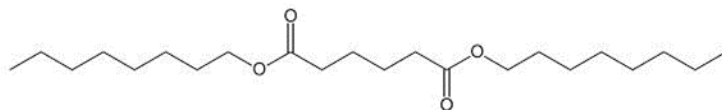
### 5.5.2.1.1 Solvent washing method

Initially, blanks of the methanol:dichloromethane solvent mix and methanol:dichloromethane solvent mix from the glassware (glass blank) were obtained, in order to know which ions were present before samples were introduced. \* will be used to denote peaks found in blank in all other data and # will be used to denote peaks found in glass blank in all other data.

The infused methanol:dichloromethane solvent mix samples obtained by solvent washing were analysed using direct infusion positive ion ESI FT-ICR MS and two distinct ions ( $m/z$  393.2968 and 763.6031) were observed in all three JFTOT rod samples (Figure 5-56, Figure 5-57, Figure 5-58 and Figure 5-59).

The observation of  $m/z$  393.3161 was also reported in JFTOT rod work by Patel<sup>211</sup> and is thought to correspond to  $[C_{22}H_{42}O_4 + Na]^+$ , (molecular weight of 370 g/mol). From previous work by Patel<sup>211</sup>, it is most likely that it could correspond to two possible adipates, dioctyl adipate or di-2-ethylhexyl adipate (DEHA), that are structural isomers with the same chemical formula and molecular weight (Figure 5-55).

(A) Dioctyl adipate ( $C_{22}H_{42}O_4$ ) molecular weight : 370.57 g/mol



(B) Di-2-ethylhexyl adipate ( $C_{22}H_{42}O_4$ ) molecular weight : 370.57 g/mol

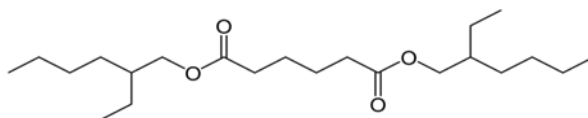


Figure 5-55 – Two possible proposed adipate structures ((A) dioctyl adipate and (B) di-2-ethylhexyl adipate) for sodiated molecule  $[C_{22}H_{42}O_4 + Na]^+$  at  $m/z$  393.3161 (molecular weight: 370 g/mol)

$m/z$  763.6031 was observed and corresponds to the sodiated dimer of the proposed adipate species  $[2(C_{22}H_{42}O_4) + Na]^+$ . This is most likely formed during the ESI process, suggesting the compound is present within a sample at a high concentration.

The observation of FAME 18:1 on JFTOT rods (likely origin from the rapeseed methyl ester (RME) in B20 biodiesel) is in agreement with previous work by Patel<sup>211</sup>.



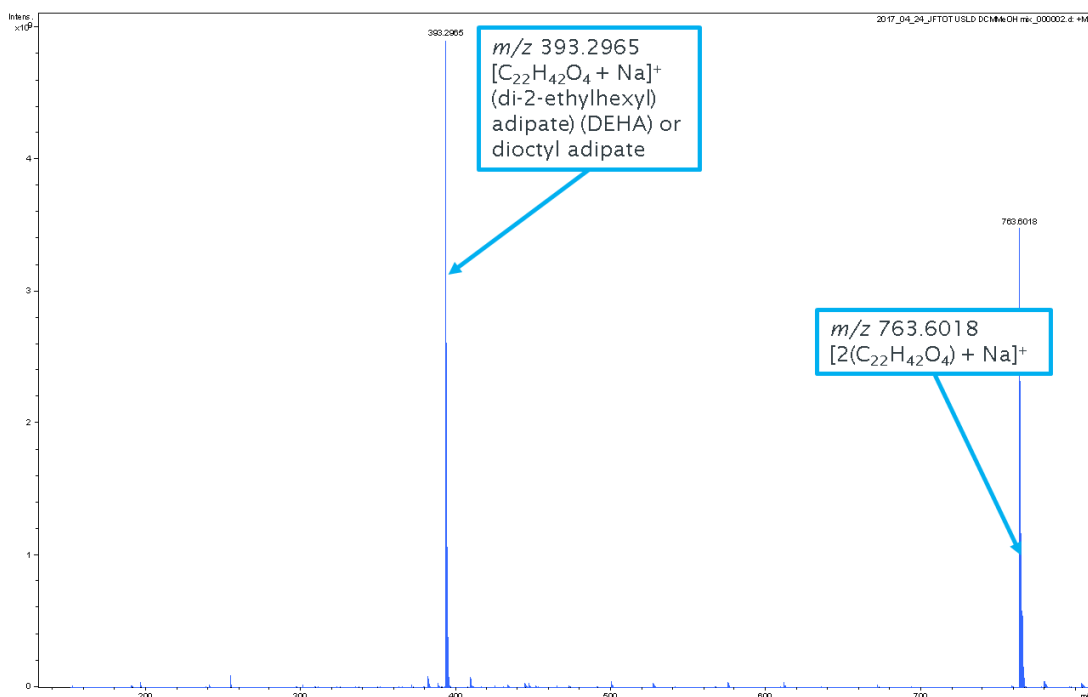


Figure 5-56 - mass spectrum of USLD JFTOT methanol:dichloromethane solvent washing analysed by FT-ICR MS

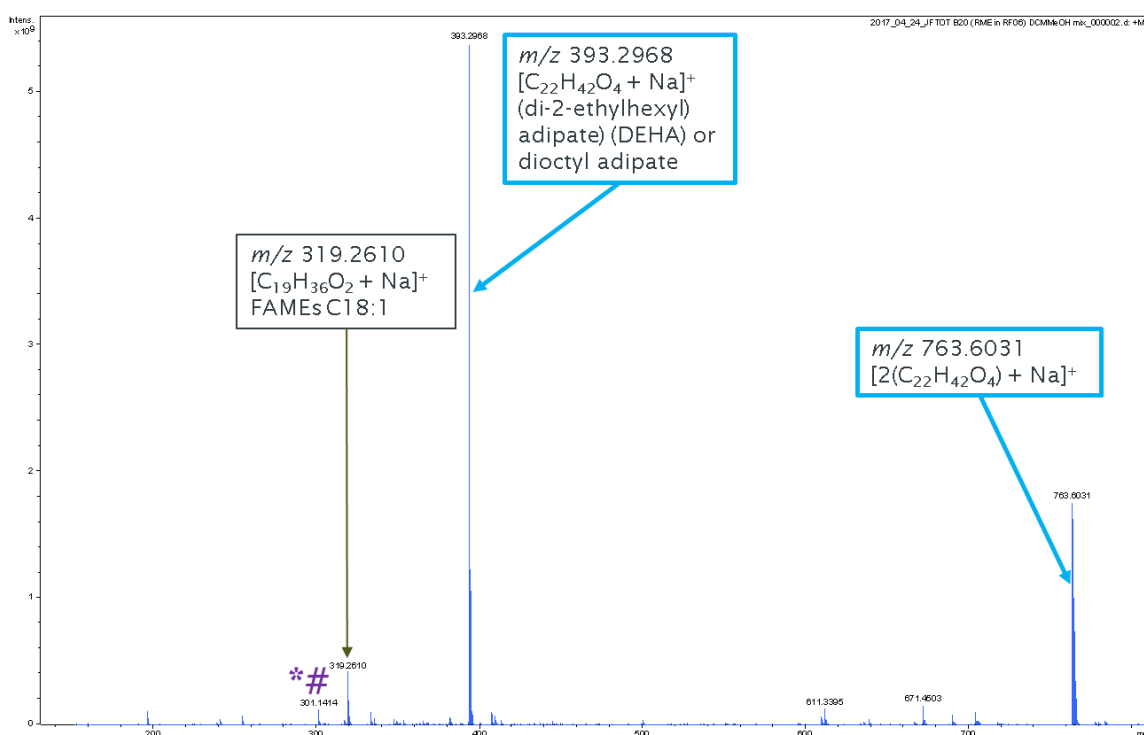


Figure 5-57 - mass spectrum of B20JFTOT methanol:dichloromethane solvent washing analysed by FT-ICR MS

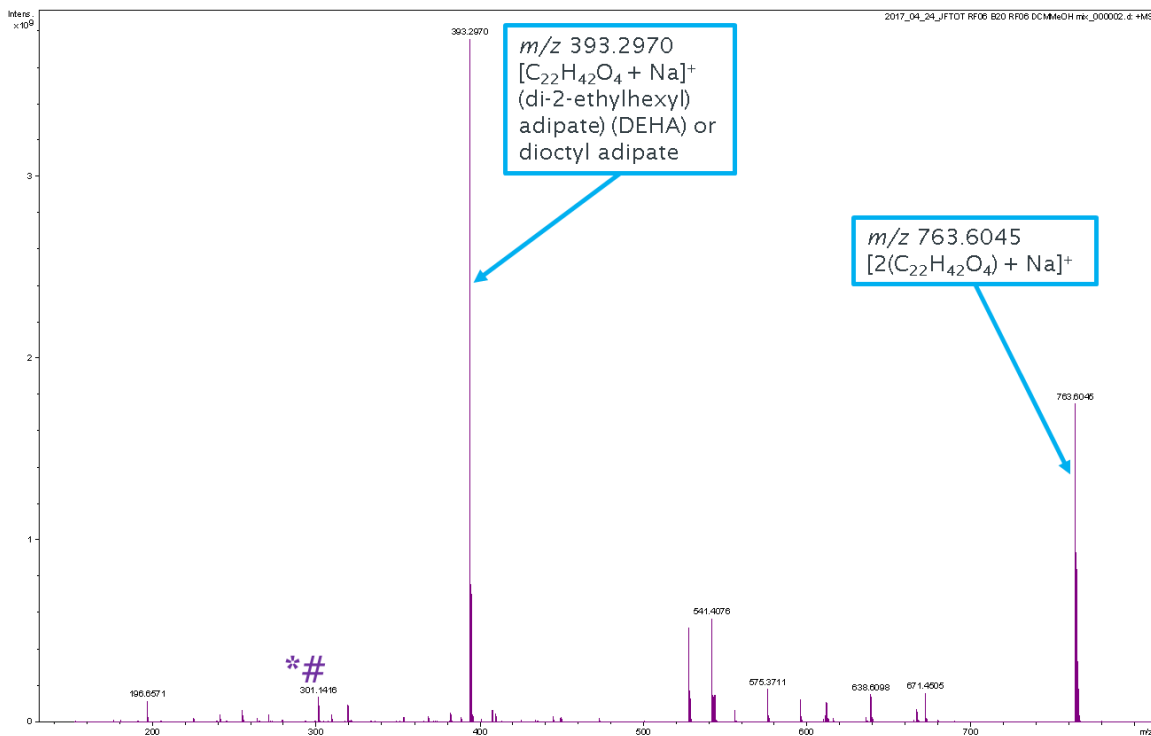


Figure 5-58 - Mass spectrum of RF06→B20→RF06 JFTOT methanol:dichloromethane solvent washing analysed by FT-ICR MS

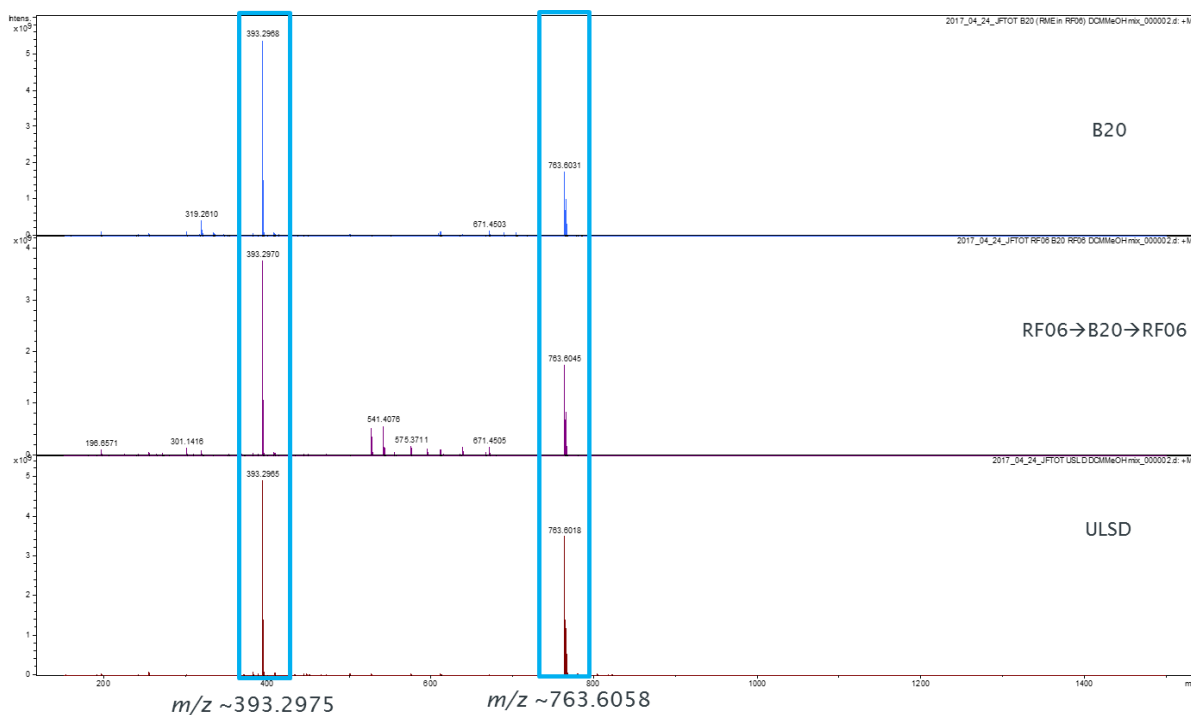


Figure 5-59 – Comparison of all 3 JFTOT rods methanol:dichloromethane solvent washings analysed by FT-ICR MS

In Figure 5-58, additional ions were observed between  $m/z$  500 -700 at relatively low abundance in comparison to the proposed adipate ions. On further inspection of these ions, they were present at low levels (<2.5% in B20 and <1% ULSD) in either or both of the other JFTOT rods (ULSD or B20). As this is the composite JFTOT rod, it has been exposed to both fuels at an elevated temperature and pressure for a prolonged length of time (~three times longer than the other two rods). These compounds may be present at low levels in B20 and ULSD and their concentrations increased in the composite partly due to the increase in fuel volume (three-fold increase) but also possibly due to the increased temperature and pressure the JFTOT rod undergoes (3x test due to 3 fuel tested).

As the suspected adipate ( $m/z$  393.2975) was observed in all three JFTOT rod solvent washing samples (at similar ion intensities), in agreement with previous work by Patel<sup>211</sup>, the source/origin of the adipate was investigated. Adipates are frequently used in polyvinyl chloride (PVC) products as plasticisers to soften and improve flexibility. Such items include PVC tubing, PVC films and PVC gloves. A review was undertaken to ascertain whether any PVC might be present during the entirety of the production of the JFTOT rods and their analysis and determine what this source may be. Many possible sources were suggested including lids on fuel sampling bottles, gloves used during fuel sampling, production and analysis, PVC tubing within JFTOT system, and both pre and post production JFTOT storage containers. Innospec also undertook investigations to try to determine whether the source of adipate was introduced during the sampling process, prior to analysis at Southampton.

One possible source that could be easily verified was the gloves used during the analysis of the JFTOT rods and associated fuels. The finger of an unused glove was submersed in a methanol:dichloromethane solvent mix for 10 mins and the resulting infused solvent was analysed by positive ion ESI FT-ICR MS. The resulting mass spectrum (Figure 5-60) indicates the absence of  $m/z$  393.2975 suggesting the gloves used during analysis sample preparation are not the source of the proposed adipate.

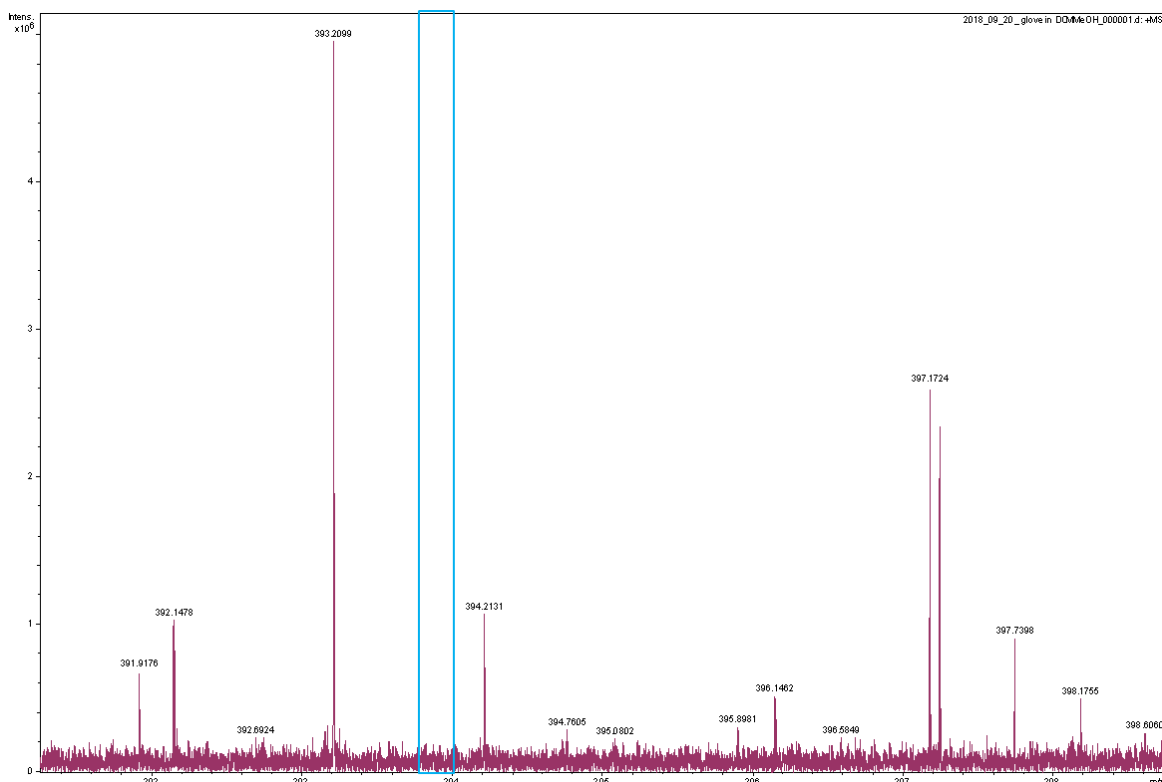


Figure 5-60 – Glove in methanol:dichloromethane solvent mix (blank) analysed by positive ion ESI FT-ICR MS. Zoomed range  $m/z$  391-399 with a blue box indicating absence of  $m/z$  393.2975

Another avenue of investigation that should be considered is has adipate been observed in JFTOT rods following AVTUR testing rather than diesel. Soft ionisation MS techniques are rarely used to analyse AVTUR samples so it may not have been observed.

#### 5.5.2.1.2 Scraping method

No adipates were observed in JFTOT rod scraping samples analysed by direct infusion positive ion ESI FT-ICR MS. The scrapings of the JFTOT rods were taken from the same rods post solvent washing, meaning components were expected to be present at low trace levels and the background was abundant. This insinuates that either solvent washing effectively removes the deposit or scraping was an ineffective sample preparation method.

Further work would need to be undertaken to explore the sample preparation methods further as only one set of JFTOT rods were provided meaning it was difficult to make a fair comparison of the two sample preparation methods.

#### 5.5.2.2 Non-polar column GC-MS analysis

To further confirm the presence of the adipate on the JFTOT rod samples, a complementary analytical technique was used. A (non-polar column) GC-MS method described by Cao<sup>210</sup> reported

the detection and quantification of numerous different phthalates and adipates including di-2-ethylhexyl adipate (DEHA) ( $C_{22}H_{42}O_4$ , MW 370 g/mol). DEHA was the adipate of interest, as it is one of the two possible proposed adipate structures (Figure 5-55) believed to be observed in direct infusion positive ion ESI FT-ICR MS data acquired by Patel<sup>211</sup>.

The infused methanol:dichloromethane solvent mix samples of both solvent washing and scraping, as well as undiluted samples of both fuels were analysed using the Cao (non-polar column) GC-MS method for the detection of adipates<sup>210</sup>.

### 5.5.2.2.1 Solvent washing method

The TICC along with the following chromatograms were examined; RICC of expected molecular ion at nominal  $m/z$  370, as well as nominal  $m/z$  mass 129 as a quantification ion with nominal  $m/z$  57 and 147 as qualifier ions, with DEHA was expected to elute at  $t_R \sim 20$  min, as described by Cao<sup>210</sup>.

A peak was observed at  $t_R$  19.19-19.24 in the B20 JFTOT rod solvent washing sample with an associated mass spectrum that was believed to correspond to DEHA. The top three results of the

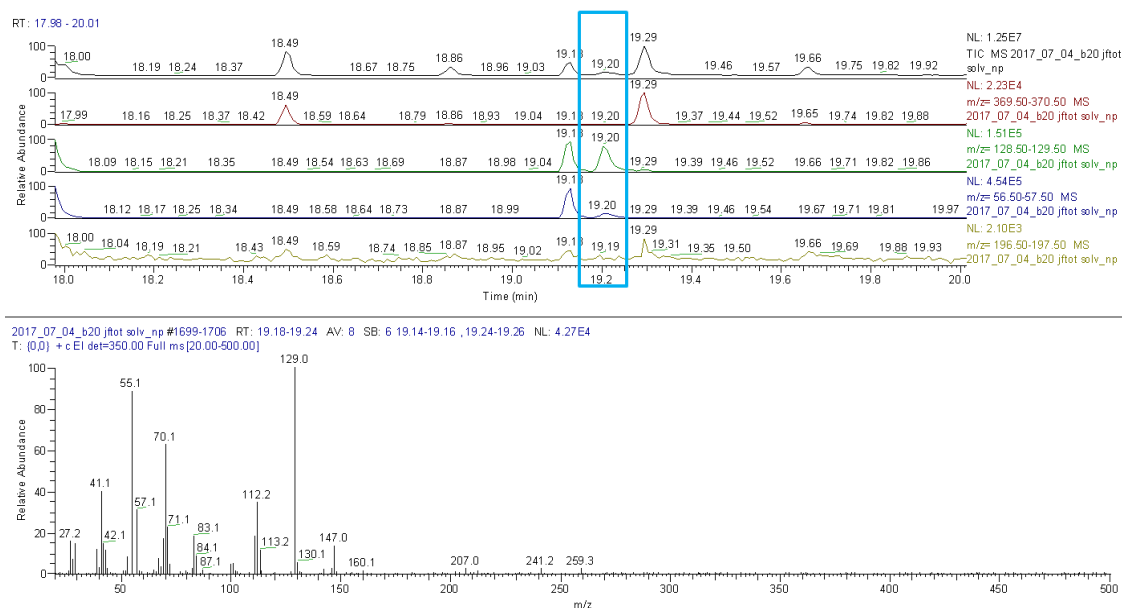


Figure 5-61 – (A) TICC, RICC nominal  $m/z$  370, RICC nominal  $m/z$  129, RICC nominal  $m/z$  57 and RICC nominal  $m/z$  147 (chromatograms zoomed in 18-20 min). Blue box denotes DEHA expected retention time (B) EI-MS (70 eV) ( $t_R$  19.18-19.24 min, mass range  $m/z$  20 - 500) of B20 JFTOT rod solvent washing sample analysed using the full scan (non-polar column) GC-MS method

NIST library search were all adipate structures with molecular weight 370 g/mol and had an upper similarity index (SI) of  $\sim 800$ .

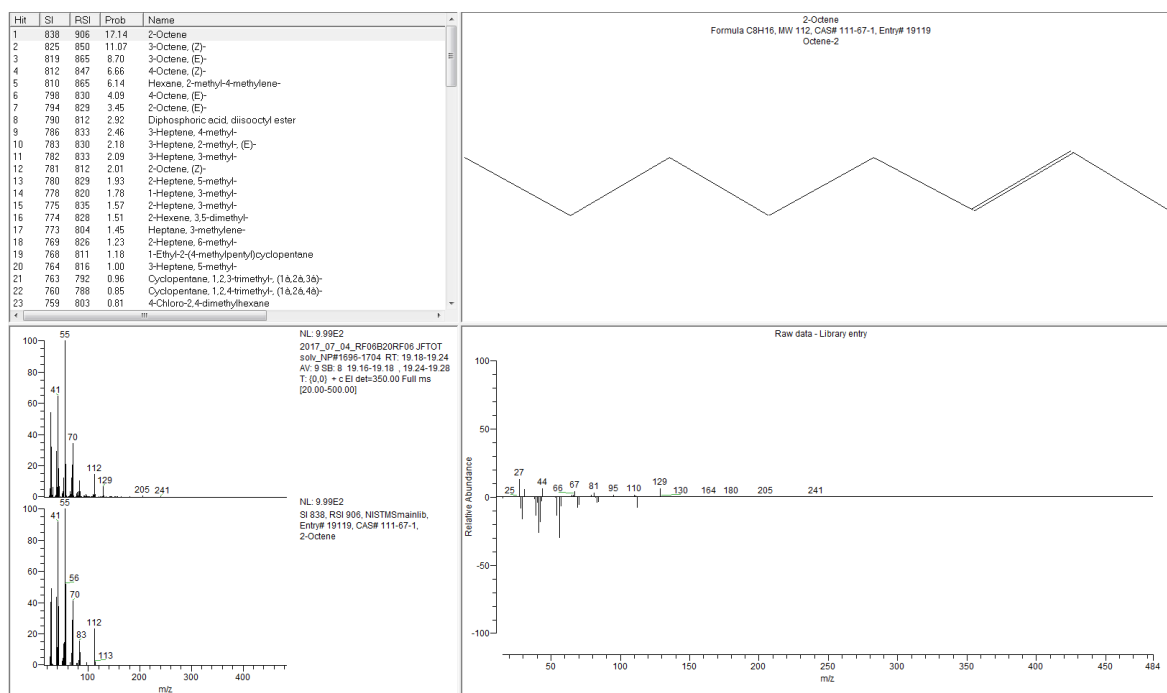


Figure 5-62 – NIST Library search results for  $t_R$  19.18-19.24 min of RF06 to B20 to RF06 JFTOT rod solvent washing sample

A similar peak was observed at  $t_R$  19.19-19.24 in the ULSD JFTOT rod solvent washing sample with an associated mass spectrum that was believed to correspond to DEHA. Again, a NIST library search was undertaken with the top three results all being adipate structures with molecular weight 370 g/mol and had an upper similarity index (SI) of ~891.

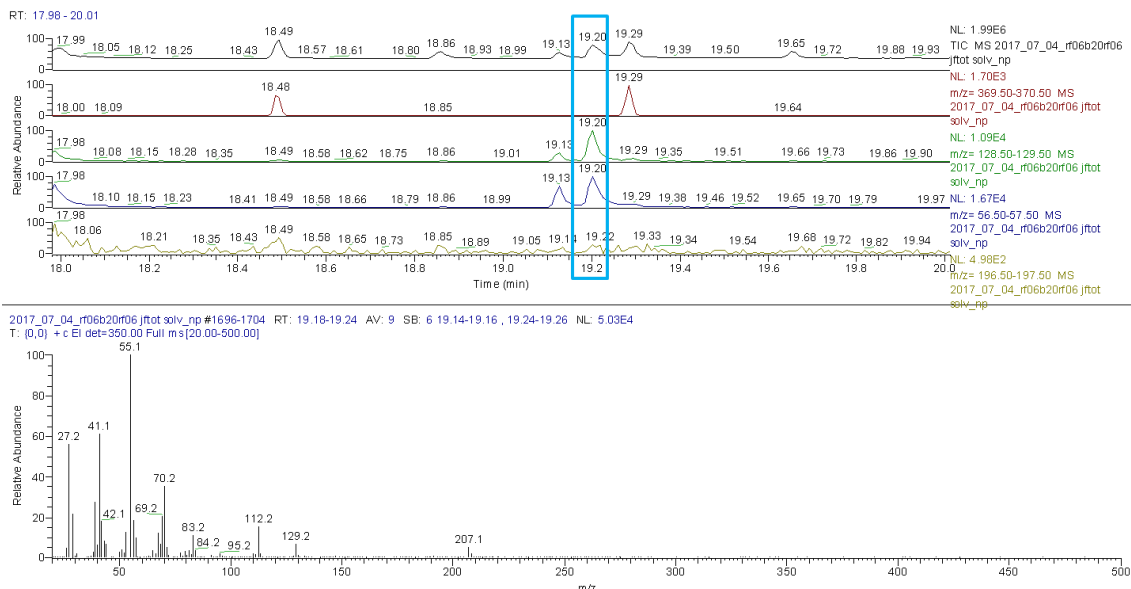


Figure 5-63 – (A) TIC, RIC, and RICC chromatograms zoomed in 18-20 min. Blue box denotes DEHA expected retention time (B) EI-MS (70 eV) ( $t_R$  19.18-19.24 min, mass range  $m/z$  20 - 500) of RF06 to B20 to RF06 JFTOT rod solvent washing sample

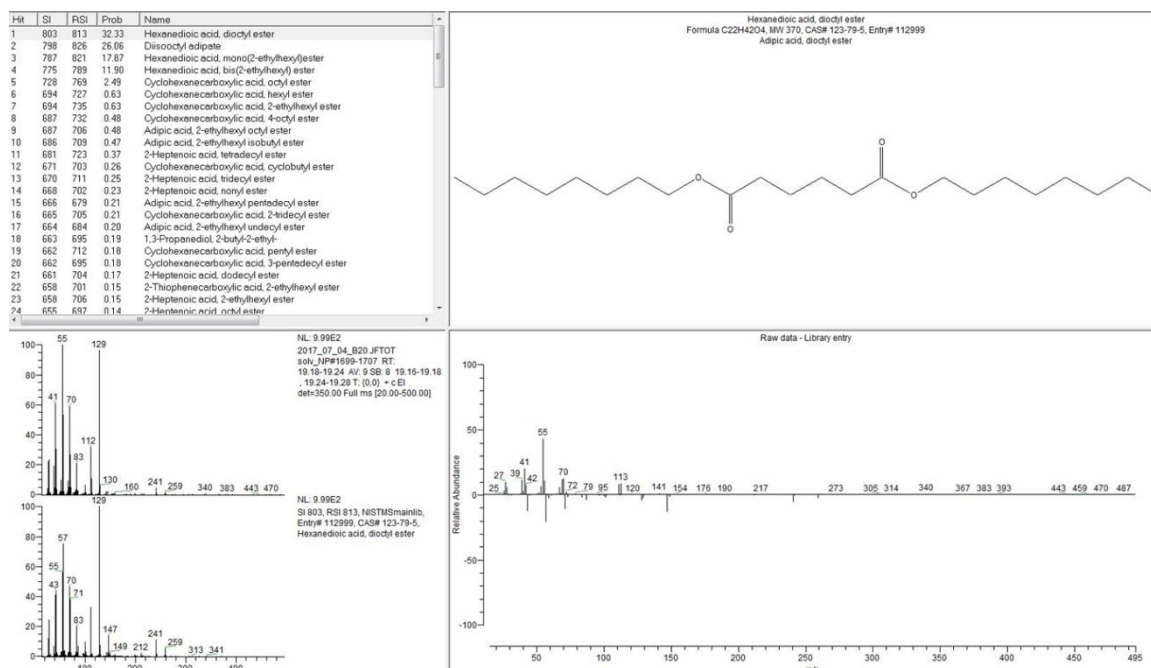


Figure 5-64 – NIST Library search results for  $t_R$  19.18-19.24 min of B20 JFTOT rod solvent washing sample

A peak was observed at  $t_R$  19.20 in the RF06→B20→RF06 JFTOT rod solvent washing sample, however the associated mass spectrum did not correspond to DEHA (Figure 5-63). A NIST library search suggested it corresponded to 2-octene (Figure 5-62).

The apparent absence of DEHA in the (non-polar column) GC-MS data for RF06→B20→RF06 JFTOT rod solvent washing sample may be because  $m/z$  393.2970 was the least abundant. In the solvent washing sample DEHA intensity was  $4 \times 10^9$  compared to at least  $5 \times 10^9$  (at least ~20% more abundant) in both the B20 and ULSD JFTOT rod solvent washing samples. This lower abundance may mean that the concentration below the LLOD using the full scan (non-polar column) GC-MS method.

### 5.5.2.2 Scraping method

No DEHA peaks were observed in the three scraping samples by (non-polar column) GC-MS analysis (Figure 5-65), this is in agreement with the absence of  $m/z$  393.2975 (adipate) in the direct infusion positive ion ESI FT-ICR MS data.

RT: 17.98 - 20.01

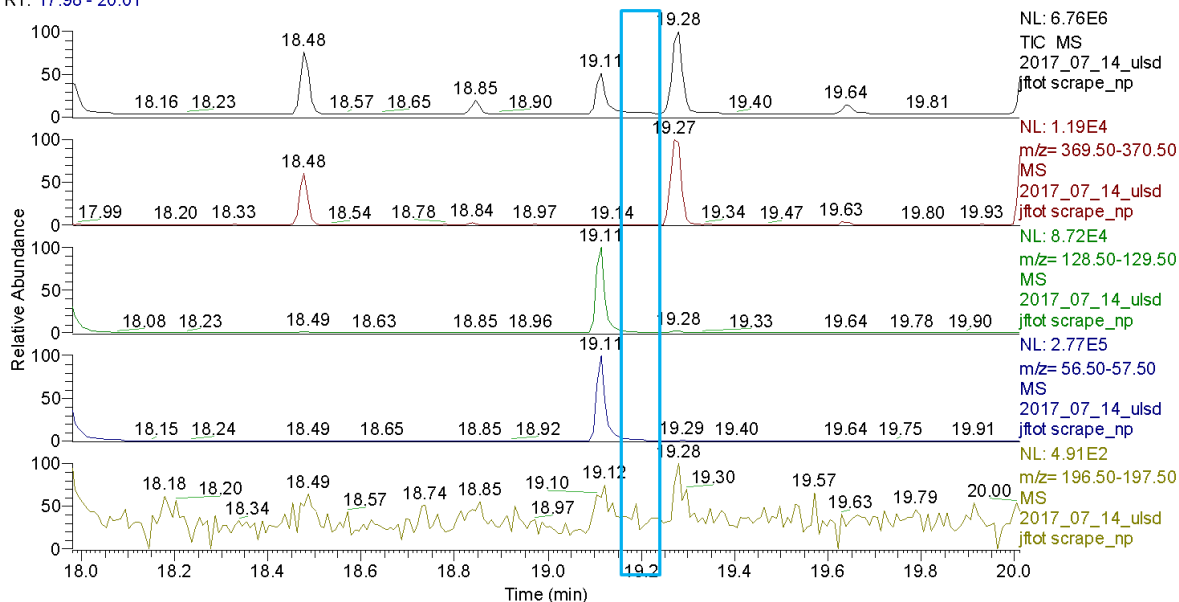


Figure 5-65 –TICC, RICC nominal  $m/z$  370, RICC nominal  $m/z$  129, RICC nominal  $m/z$  57 and RICC nominal  $m/z$  147 (chromatograms zoomed in 18-20 min). Blue box denotes DEHA expected retention time ( $t_r$  19.18-19.24 min) of ULSD JFTOT rod scraping sample

### 5.5.3 Associated fuels

#### 5.5.3.1 FT-ICR MS analysis

Both associated fuels (SS#1 and SS#2) were also analysed by direct infusion positive ion ESI FT-ICR MS.

In 0.01% SS#1 fuel (Figure 5-66),  $m/z$  393.2981 was observed at an intensity of  $1 \times 10^6$  with  $s/n$  of 41, whereas in 0.01% SS#2 fuel (Figure 5-67),  $m/z$  393.2983 was observed at an intensity of  $3 \times 10^5$  with  $s/n$  of 11. The proposed adipate was observed at  $\sim 4 \times 10^9$  in the three JFTOT rods so in comparison the intensities observed in the diesels are very low. Taking the  $s/n$  ratio into account, where LLOD is 3 and lower limit of quantification (LLOQ) is 10, SS#2 diesel is very close to the LLOQ and LLOD.



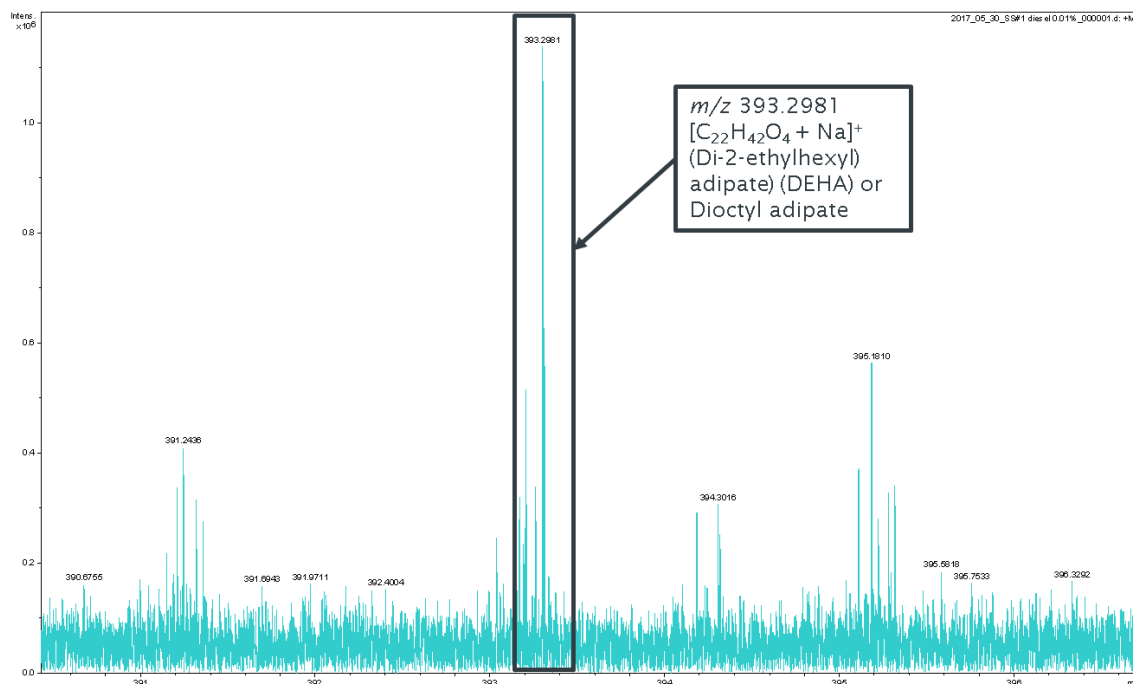


Figure 5-66 –Mass spectrum of 0.01% SS1 diesel in 6T:4M analysed by direct infusion positive ion ESI FT-ICR MS (mass range:  $m/z$  390– 397)

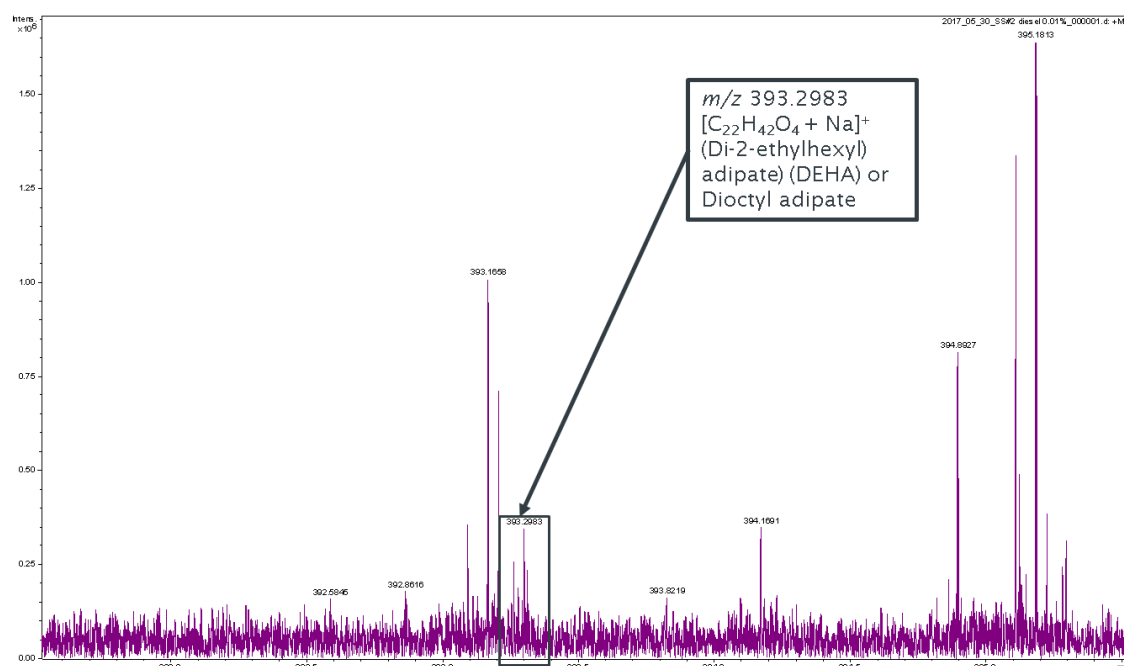


Figure 5-67 –Mass spectrum of 0.01% SS#2 diesel in 6T:4M analysed by direct infusion positive ion ESI FT-ICR MS (mass range:  $m/z$  391.5 – 395.5)

As the proposed adipates were observed at low levels only, a complementary analytical technique in this case (non-polar column) GC-MS, was utilised to determine if adipate was actually present in the fuels or as contamination or carryover.

## 5.5.3.2 (Non-polar column) GC-MS analysis

No DEHA peaks were observed in the two fuel samples by GC-MS (non-polar column) analysis (Figure 5-68); this disagrees with the direct infusion positive ion ESI FT-ICR MS data, where  $m/z \sim 393.2982$  at low abundance was observed. It should be noted the undiluted fuels were initially analysed with no split ratio, however this resulted in overloading of the column. The undiluted fuels were subsequently analysed with a split ratio of 1:50 in order to rectify the overloading, with the acquired data showing an absence of DEHA. The use of a split ratio is discussed in chapter 2.3. However, the use of a split ratio may have resulted in the loss of the DEHA components in the part of the sample that was discarded rather than entering the column for analysis, if present at very low concentration.

One possibility could be that the adipate is present in the fuel, but below the LOD and is then being concentrated onto the JFTOT rod during the test.

Full scan mass spectra across a specified mass range was also acquired for all (non-polar column) GC-MS analysis as a wider, more general analysis of samples was required in the first instant, and not just detection of the DEHA (although that was of interest) as there may have been other compound present of interest.

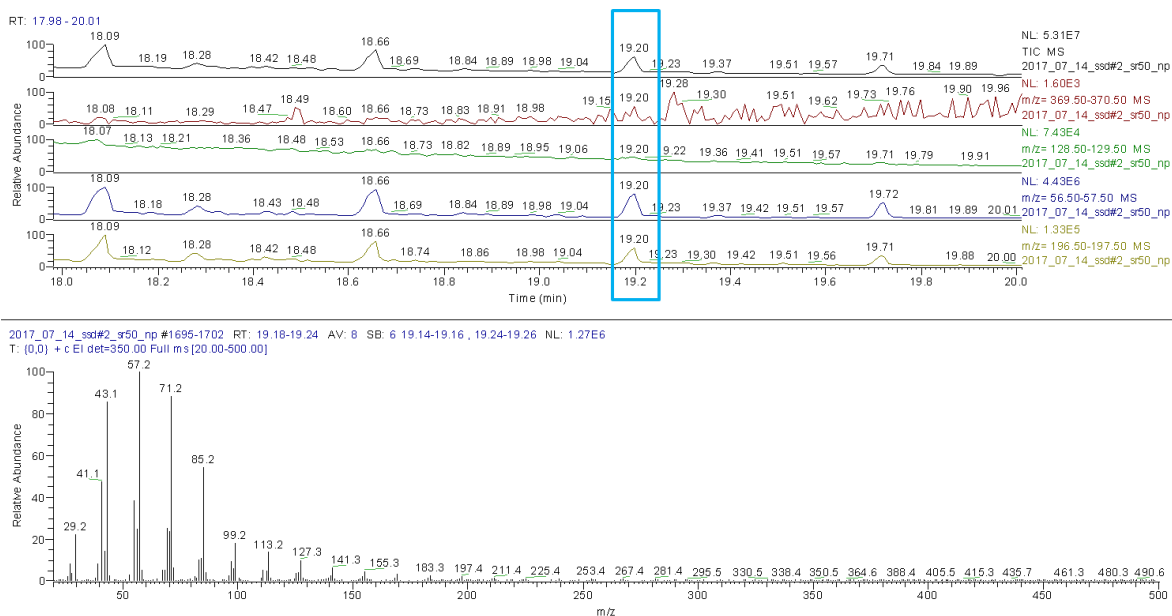


Figure 5-68 – (A) TIC, RIC nominal  $m/z$  370, RIC nominal  $m/z$  129, RIC nominal  $m/z$  57 and RIC nominal  $m/z$  147 (chromatograms zoomed in 18-20 min). Red box denotes DEHA expected retention time (B) EI-MS (70 eV) ( $t_R$  19.18-19.24 min, mass range  $m/z$  20 - 500) of SS#2 fuel with split ratio of 1:50

#### 5.5.4 Summary

This work was undertaken to validate previous results and optimise JFTOT rod deposit analysis methodology further.

##### 5.5.4.1 FT-ICR MS JFTOT rods solvent washing

$m/z$  ~393.297 with a proposed assignment ( $[\text{C}_{22}\text{H}_{42}\text{O}_4 + \text{Na}]^+$  (Di-2-ethylhexyl)adipate) (DEHA) or dioctyl adipate) was found to be present in all three JFTOT rod solvent washing samples analysed by direct infusion positive ion ESI FT-ICR MS.

This proposed adipate has an unknown origin as was not found to be present in solvent blank, glass blank, or glove.

However, adipate was believed to be present at low intensity in both of the fuel samples, further work was required to confirm this due to the trace levels observed.

$m/z$  319.2610 was also observed in all B20 and RF06→B20→RF06 JFTOT rod solvent washing samples, this is believed to correspond to sodiated FAME 18:1  $[\text{C}_{19}\text{H}_{36}\text{O}_2 + \text{Na}]^+$  and thought to originate from the B20 biodiesel component

##### 5.5.4.2 FT-ICR MS JFTOT rods scraping

No adipates observed with the most abundant ions in the mass spectra corresponding to the blanks so very low/trace level sample ions present. This suggests that either solvent washing effectively removes the deposit or scraping was ineffective.

##### 5.5.4.3 (Non-polar column) GC-MS analysis

The (non-polar column) GC-MS analysis method afforded the detection of adipates (DEHA) at nominal  $m/z$  370 at RT ~19.2 min in two out of three JFTOT rod solvent washing samples (B20 and ULSD).

DEHA/adipate was **not** detected in the RF06→B20→RF06 JFTOT rod solvent washing sample and in either fuel sample (SS#1 and SS#2) by (non-polar column) GC-MS.

This was potentially due to low levels of adipate present (split ratio) as it is observed in these samples when analysed by direct infusion positive ion ESI FT-ICR MS.

## 5.6 Conclusions

New analytical approaches (chromatography and mass spectrometry) were developed and applied for the analysis of fuel filter deposits, internal diesel injector deposits (IDIDs) and JFTOT rods and associated rods.

### 5.6.1 Fuel filters – Deposit screening method

A rapid screening methodology previously applied to successfully characterise diesel fuels, for five known deposit forming component classes (FAMEs, FAME oxidation products, MAGs, FFAs, and SGs) in addition to novel FASEs, was further developed through its utilisation in engine deposit analysis, particularly fuel filters.

As with diesel fuels, positive ion ESI UHPSFC-MS afforded detection of FAMEs, FAME oxidation products, MAGs, SGs and FASEs while negative ion ESI UHPSFC-MS afforded detection of FFAs.

Additionally PIBs, PPGs and a possible emulsifier were also detected by positive ion ESI UHPSFC-MS.

FASEs were identified in a plugged fuel filter associated residue (SS5), which has not previously been reported in literature and FASEs are not stated in the literature to cause filter blocking or IDIDs.

Positive ion and negative ion ESI FT-ICR MS aided in the resolution of nominally isobaric species and further confirmed assignments by providing molecular formulae.

The compounds observed enabled conclusions to be made about the fuel entering the filter and if plugged what might be a contributing factor.

These analytical techniques allowed problematic compounds to be detected; both recognised deposit precursor components/group of components and other currently unrecognised species that may be involved in deposit formation which then add to the knowledge and understanding of the current deposit issues.

### 5.6.2 Deposit analysis protocol trees

Two deposit analysis protocol trees were developed (analyst flow (deposit) and deposit flow) from the diesel analysis protocol trees to consolidate methodologies and provide visualisation (flow chart) of linking compounds detected to specific analytical techniques.

These deposit analysis protocol trees were devised as a tool to assist analysts and the fuel industry with characterisation of (IDIDs) components in IDIDs and fuel filter deposits, specifically identifying known deposit forming compounds and possibly enabling links to be made between fuel components and their propensity to form deposits.

In a similar way to the diesel analysis protocol trees, the deposit analysis protocol trees provide a reference tool to aid both practical analysis and the analysis thought process of deposit samples.

The analyst flow (deposits) analysis protocol tree offers guidance suggesting analytical approaches to be utilised for an unknown deposit sample X.

The deposit flow analysis protocol tree advises thought processes (logical flow to follow) to improve future understanding and characterisation of deposits.

### 5.6.3 Fuel injector tip IDID

The deposit screening methodology was successfully used for the analysis of an IDID sample.

Positive ion ESI infusion FT-ICR MS data shows PIBs present, this suggests “non-commercial” low molecular weight PIBSI used as deposit control additive (DCA) in the fuel that has been attracted to the IDID or is present on the injector tip.

Both positive and negative ion ESI FT-ICR MS and UHPSFC-MS data suggests the presence of C16:0 & C18:0 FFAs, that suggests either metal carboxylate salt IDIDs or aged fuel IDIDs. The source of these saturated FFAs is either from hydrogenated biodiesel or from monoacid lubricity improver additives.

### 5.6.4 JFTOT rods and associated fuels

Further advancement of the analysis method for JFTOT rod deposits and associated fuels was undertaken, firstly to validate previously unexpected results and to optimise sample preparation methodologies.

Adipate was observed in all three JFTOT rods solvent washing samples analysed by direct infusion positive ion ESI FT-ICR MS and found to be present at low intensity in both of the fuel samples. (non-polar column) GC-MS method was required to confirm this due to the trace levels observed.

A (non-polar column) GC-MS analysis method afforded the detection of adipates in two out of three JFTOT rod solvent washing samples (B20 and ULSD). However adipate was **not** detected in the RF06→B20→RF06 JFTOT rod solvent washing sample and in either fuel sample (SS#1 and SS#2) by

## Chapter 5

(non-polar column) GC-MS. This was thought to be potentially due to low levels of adipate present (split ratio) as it is observed in these samples when analysed by direct infusion positive ion ESI FT-ICR MS.

There is still not a clear origin/source of the adipates following investigation by both Innospec and at Southampton, but as the same proposed adipate was observed on, two occasions independently with two samples prepared separately but identically, it is highly likely it is present in the sample, meaning its origin of source is of importance.

Scraping of the JFTOT tubes was undertaken post solvent washing and analysed by direct infusion positive ion FT-ICR MS with no adipates observed.

Solvent washing was the optimum JFTOT rod sample preparation method in this work due to abundance/intensity of ions, however the results were not definitive as it was not direct fair comparison so further work is required







## Chapter 6 Evaluation of Ultrahigh-Performance Supercritical Fluid Chromatography-Mass Spectrometry (UHPSFC-MS) as an Alternative Approach for the Analysis of ACCUTRACE™ S10 Fuel Marker

The work in this chapter is published in: Langley, G. J.; Herniman, J.; Carter, A.; Wilmot, E.; Ashe, M.; Barker, J., Detection and Quantitation of ACCUTRACE S10, a New Fiscal Marker Used in Low-Duty Fuels, Using a Novel Ultrahigh-Performance Supercritical Fluid Chromatography–Mass Spectrometry Approach. *Energy & Fuels* 2018, 32 (10), 10580-10585.

Table 6-1 Author contributions for ACCUTRACE S10 fuel marker work

Author name	Contribution/role
A. Carter	All UHPSFC-ESI+ MS method development and analysis including quantitation and real fuel samples. Also collaborated with E Wilmot on GC-MS analysis.
G. J. Langley	UHPSFC-APPI+ MS analysis.
J. Herniman	UHPSFC-APPI+ MS analysis.
E. Wilmot	Initial GC-MS method development and then collaboration with A Carter for further GC-MS analysis.
M. Ashe	Molecular modelling of ACCUTRACE S10 molecule.
J. Barker	Provided all samples from Innospec Ltd.

### 6.1 Introduction

The major aim of this work was to investigate ultrahigh-performance supercritical fluid chromatography–mass spectrometry (UHPSFC–MS) as a surrogate analytical solution for the

detection and quantitation of ACCUTRACE™ S10 fuel marker in low-duty fuels. At present, all other proposed detection and quantitation methods for ACCUTRACE™ S10 fuel marker use either GC-MS or 2D GC-MS. However issues with the GC-MS method are observed as the diesel fuel matrix is directly injected into the GC-MS, which results in the ion source quickly becoming contaminated resulting in a decrease in instrument sensitivity and frequent ion source cleaning. Also 2D GC-MS, which is not widely available in industry, must be used to detect ACCUTRACE™ S10 fuel marker at tank dilution level (25 ppb = 1%). Therefore, legacy GC-MS is unable to deliver a solution and as a result there is the need for an alternative method.

### 6.1.1 Fuel markers

Fuel markers are molecular markers (chemicals or dyes) which are used to identify different grades and types of petroleum products for both security and fiscal reasons<sup>262</sup>.

Fuel markers allow lower tax/government subsidised fuels (gasolines, middle distillates and petroleum products) to be distinguished from more expensive “normal” road transport fuel, which is in order to combat tax evasion<sup>262-264</sup>. In most countries, some fuels are taxed at different rates depending on their purpose<sup>265</sup> *e.g.* fuels have lower tax or government subsidised in order to support industrial sectors such as agriculture and mining, with its main purpose being to fuel off-road vehicles and equipment/machinery and also to provide affordable heating for the population<sup>262-263, 266</sup>. In the United Kingdom (UK), “marked” diesel excise duty is charged at 11.14 pence per litre (PPL) instead of the full rate on “normal” diesel of 57.95 PPL<sup>267</sup>.

In the UK, some diesel fuel is government subsidised and until recently it was commonly known as “red diesel” due to the use of solvent red 24 (Figure 6-1), a red dye used to mark it for easy visual identification, and a fuel marker Quinizarin (Figure 6-2) was also used to aid identification<sup>268</sup>.

All subsidised fuels mentioned above also contain Solvent Yellow 124 (Figure 6-3), also known as “Euromarker”; this is a yellow azo dye which is used in the European Union to mark subsidised fuels in addition to individual countries’ fiscal markers<sup>268-269</sup>.

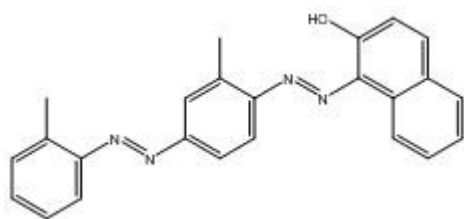


Figure 6-1 - Chemical structure of  
Solvent Red 24 fuel dye

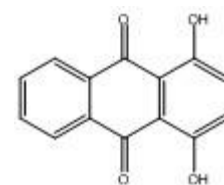


Figure 6-2 - Chemical structure  
of Quinizarin fuel  
marker

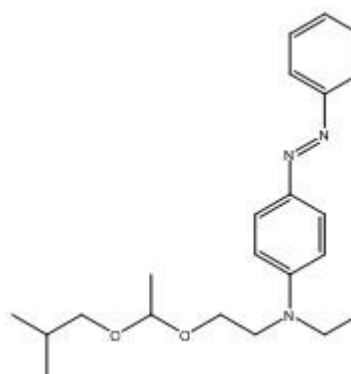


Figure 6-3 - Chemical structure  
of Solvent yellow  
124 fuel dye

The fuel industry generally analyse the fuel markers rather than the dyes in fuels<sup>269</sup> e.g. quinizarin content in marked diesel<sup>270</sup>. IP 298, an ultraviolet-visible (UV-Vis) spectrophotometric method *via* extraction is used for the determination of quinizarin in fuel. Quinizarin is extracted out of the diesel/gas oil *via* numerous steps using butanol, sodium hydroxide and hydrochloric acid into cyclohexane and then the cyclohexane extract is analysed using a ultraviolet-visible (UV-Vis) spectrophotometer to obtain an absorption spectrum<sup>270-271</sup>. Quinizarin is ultraviolet (UV) active and has a characteristic absorption spectrum with five peaks at 463, 476, 487, 508 and 521 nm. Quinizarin is quantified by comparing the height of the peak at 521 nm in relation to a cyclohexane blank<sup>271</sup>.

Numerous detection techniques are found in literature, for both marked fuel and previously marked fuel where the illegal removal of dye and marker has been attempted<sup>263-264, 272-279</sup>.

Due to the vast difference in fuel prices, as a result of government subsidy/lower taxes, fuel laundering to evade fuel taxation has become prevalent. Fuel laundering commonly consists of obtaining lower taxed fuel, removing the visible dyes and fuel markers and then either selling on the fuel at the higher taxed road transport price, in order to make money or illegally using the fuel for applications of higher taxed fuels. Fuel laundering can take place using a multitude of physical and chemical techniques<sup>265</sup>. The consequences of fuel laundering are immense, as governments will experience massive losses in tax revenue. For example, in the UK, £1.1 billion is loss every year and the adulterated fuel can cause adverse effects to customers' vehicles<sup>263-264, 280-281</sup>. Worldwide this loss is more than \$100 billion per annum<sup>282-283</sup>. There are also other ways in which fuel tax evasion takes places, such as through dilution of the higher taxed road transport fuel with hydrocarbons or the rebated fuels, smuggling illegal fuel into the country, and using rebated fuels for purposes specifically requiring higher taxed road transport fuels, such as fuelling a roadworthy car<sup>264</sup>.

Fuel marker detection methods are required to detect fuel markers within a very complex matrix in tampered fuel due to the addition of extra components (*e.g.* hydrocarbon mixtures) by fuel launderers in order to mask the presence of the marker. The extra components are generally added as they mask the fuel marker by either eluting at similar time chromatographically and/or may have similar ions in a mass spectrum<sup>284</sup>.

In an attempt to counter the issues around fuel laundering, a new fuel marker was developed to replace UV-Vis fuel markers such as quinizarin<sup>285</sup>.

### **6.1.2 New fuel marker – ACCUTRACE™ S10**

#### **6.1.2.1 ACCUTRACE™ S10 fuel marker**

ACCUTRACE™ S10 fuel marker is produced by Dow Chemical Company and was introduced for use, at a treat rate of 2.5 ppm, on 1<sup>st</sup> April 2015 in the UK and Ireland<sup>214, 280</sup>. The active marker in ACCUTRACE™ S10 fuel Marker is ((3-(secbutyl)-4-(decyloxy)phenyl)methanetriyl)tribenzene), which is shown in Figure 6-4<sup>214</sup>. It comes in a powder form and a 20% active marker liquid form.

ACCUTRACE™ S10 fuel marker, was introduced in both the UK and Ireland in order to “boost both countries’ fight against illegal fuel laundering”<sup>267</sup>. Many claims have been made relating to the ACCUTRACE™ S10 fuel marker, including it being “significantly more effective than the current markers, and highly resistant to known laundering techniques”<sup>267</sup>. Also the ACCUTRACE™ S10 fuel marker is “so difficult to remove that the very process requires the destruction of the fuel in which it is contained.” and “that it can still be detected in fuel lines and tanks for up to four or five fuel cycles”<sup>286</sup>. Dow Chemical Company state that with low ppm treat rates (desired treat rate = 2.5

ppm), it is cost effective fuel marker, compatible with other fuel dyes such as Euomarker and that it contains “no known ozone-depleting additives”<sup>281</sup>. The National farming union (NFU) also say “the move to a more resistant dye could also help to reduce fuel thefts from farms”<sup>280</sup>.

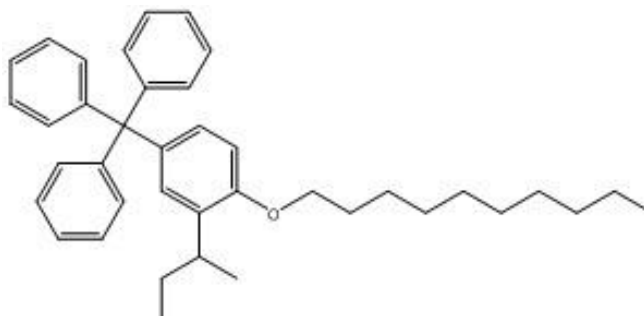


Figure 6-4 – Structure of 3-(secbutyl)-4-(decyloxy)phenylmethanetriyl)tri benzene, ACCUTRACE™ S10 fuel marker  
(Molecular weight = 532 g/mol)

#### 6.1.2.2 ACCUTRACE™ S10-*d*<sub>21</sub> fuel marker internal standard

Dow Chemical Company also developed an isotopically labelled variant of the ACCUTRACE™ S10 fuel marker to be used as an internal standard (IS), known as ACCUTRACE™ S10-*d*<sub>21</sub> IS (Figure 6-5). The ACCUTRACE™ S10-*d*<sub>21</sub> IS molecule had all twenty one hydrogen atoms replace with deuterium atoms on the decyl ether chain and is therefore a stable isotope labelled analogue of the analyte.

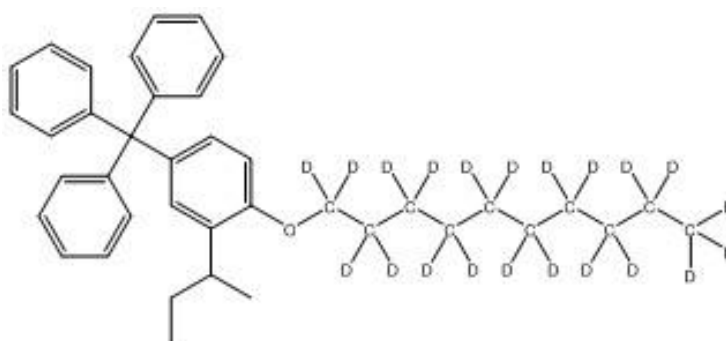


Figure 6-5 – Isotopically labelled ACCUTRACE™ S10-*d*<sub>21</sub> internal standard  
(Molecular weight = 553 g/mol)

An IS is used to aid quantification of an analyte by adding a known concentration of IS to every sample that will be analysed<sup>131</sup>. A calibration curve is then plotted using the ratio of the analyte signal (peak area or height) to the IS signal (peak area or height) as a function of the analyte

concentration of the standards analysed. The use of a known concentration of an IS is known as standard addition and is used to alleviate matrix effects which are hard to predict and control. These matrix effects result from components within the matrix coeluting with the analyte, which effect ionisation of the analyte *e.g.* ion suppression and/or ion enhancement<sup>287</sup>.

An IS should be a very similar compound to the analyte of interest, with near identical chemical properties. There are two types of IS; stable isotope labelled analogue of the analyte, that is D, <sup>13</sup>C or <sup>15</sup>N labelled, or a structural analogue, that is either an isomer, homologue or a compound related structurally to the analyte<sup>288</sup>. Other properties to consider when choosing an IS include<sup>288</sup>:

- it is not naturally occurring in sample
- it should not interfere with sample components
- it is pure
- it is chemically stable
- it is compatible with the detector of choice at similar concentration range to analyte

A stable isotope labelled analogue of the analyte of interest, such as ACCUTRACE™ S10-*d*<sub>21</sub>, is used to correct matrix effects and should in theory have equal response characteristics to the analyte of interest. Ideally a deuterated internal standard should have the same retention time as the analyte of interest. However the mass difference between the analyte of interest and the deuterated internal standard must be large enough that the mass spectrometer can distinguish between the two compounds. Extraction efficiency from the matrix and ionisation response should also be the same, meaning that the internal standard would experience the same ionisation conditions as the analyte. Therefore any effects due to sample preparation, matrix extraction and matrix effects can be corrected for. If the internal standard does not co-elute with the analyte of interest then complete compensation cannot be achieved<sup>287-288</sup>.

It should be noted that ACCUTRACE™ S10 fuel marker and ACCUTRACE™S10 fuel marker IS (S10-*d*<sub>21</sub>) cannot be detected using IP 298 as they are not UV active at the wavelengths used in this method. The ACCUTRACE™ S10 fuel marker and ACCUTRACE™S10 fuel marker IS (S10-*d*<sub>21</sub>) were designed with electron ionisation (EI) as the favoured ionisation technique therefore resulting in GC-MS being the proposed method of detection and quantification <sup>214, 289-290</sup>.

## 6.2 GC-MS

Dow Chemical Company<sup>290</sup> proposed a method to detect and quantify ACCUTRACE™ S10 fuel marker within a contaminated diesel fuel matrix consisting of a 70:27:3 diesel/lubricating oil/gear oil mixture *via* gas chromatography (GC) using heart-cut and refocusing techniques (The Energy

Institute have also created an IP test method (IP PM EU) using the same technique)<sup>214</sup>. The Dow method is able to identify ACCUTRACE™ S10 fuel marker over the range of 50 µg/L to 500 µg/L (2%-20% of fuel treat rate)<sup>290</sup>.

The GC method utilises a high temperature Agilent DB17-HT capillary column (30 m x 0.25 mm inner diameter, 0.15 µm film thickness) with a final high temperature of the oven programme at 365 °C<sup>290</sup>.

No sample preparation is required for the Dow method, meaning the contaminated diesel fuel matrix is injected directly into the GC injection port. Due to the high concentration of diesel fuel matrix entering the ion source, it can quickly become contaminated resulting in a decrease in instrument sensitivity. This means frequent ion source cleaning is required to ensure instrument sensitivity is maintained.

To circumvent the ion source contamination issues observed with the original GC-MS Dow method, it was suggested<sup>289</sup> to use conventional two-dimensional (2D) heart cutting GC-MS. This method incorporates a capillary flow Deans switch that prevents ion source contamination using a heart-cutting technique. Heart-cutting allows only a small selected time window of the chromatogram, the peak of interest, to be transferred to the mass spectrometer, diverting the sample before and after the selected time window to the flame ionisation detector (FID) or to waste. This results in the detector only being exposed to a small amount of diesel during each analysis which minimises contamination of the ion source. Improved sensitivity (S/N ratio) is also achieved, due to less contamination in the fuel matrix reaching the ion source. This method allows for a longer operational time using the same calibration curve and reduced ion source cleaning. The capillary flow Deans switch also reduces analysis time by using a back flush, resulting in reduced high temperature bake out time at the end of each acquisition. The FID can profile diesel samples allowing the analyst to observe any additional oils that may have been added to the diesel<sup>289</sup>.

Using the original Dow GC-MS method, ACCUTRACE™ S10 fuel Marker could not be detected at tank dilutions (1% of original tank dosing= 25 ppb). However Dow Chemical Company<sup>290</sup> reported that a lower limit of detection (LLOD) of ≤1 ppb for the ACCUTRACE™ S10 fuel marker in gasoline was obtained, using a 2D GC-MS method with a DB-1HT pre-column and a DB-17HT column<sup>290</sup>.

It should also be noted that any test method issued within the petrochemical industry (*via* ASTM and the Energy Institute) must be transferable across a range of widely available analytical instrumentation.

However, the DB17-HT capillary column, used in both methods, is unlikely to be commonly available in most laboratories, whereas a column such as an RTX-5 fused silica capillary column (30m x

## Chapter 6

0.25mm i.d., 0.25 $\mu$ m film thickness) or equivalent is likely to be more commonplace within a laboratory inventory.

Both these capillary columns have diphenyl dimethyl polysiloxane stationary phases, however the RTX-5 contains 5% diphenyl (Figure 6-6)<sup>48</sup>, whereas the DB-17HT contains 50% diphenyl (Figure 6-7)<sup>48</sup>, thus the DB-17HT has an increased selectivity to polar compounds due to higher phenyl content.

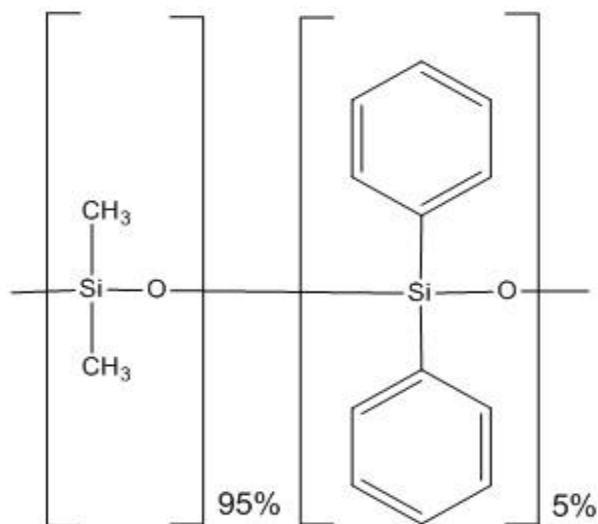


Figure 6-6 - Simplified 5% dimethyl diphenyl polysiloxane structure. (RTX-5 column)  
Redrawn from<sup>51</sup>

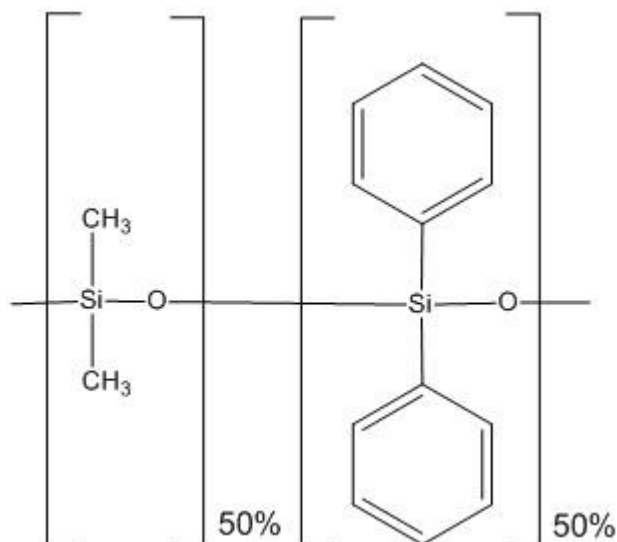


Figure 6-7 - Simplified 50% dimethyl diphenyl polysiloxane structure. (DB-17HT column)  
Redrawn from<sup>51</sup>

2D GC-MS instrumentation is also a limited capability in the petrochemical industry, with legacy GC-MS instrumentation being commonplace.

To investigate whether the Dow GC-MS method is “transferable across a range of widely available analytical instrumentation”, the Dow GC-MS method was adapted for use with the more widely available RTX-5 column and the final temperature of the oven programme was lowered to 320 °C, to be within the recommended temperature range of the column. This modified method was utilised with legacy GC-MS instrumentation, a Trace GC 2000 with auto-sampler and single quadrupole mass spectrometer, again in order to mimic widely available instrumentation within industry.



## 6.2.1 GC-MS analysis (undertaken in conjunction with Edward Wilmot)

### 6.2.1.1 ACCUTRACE™ S10 fuel marker

Using the modified GC-MS method, the ACCUTRACE™ S10 fuel marker (25 ppm) was identified in the resulting total ion current chromatogram (TICC) at  $t_R$  37.07 min with a mass spectrum (Figure 6-8) showing the characteristic intense molecular ion at nominal  $m/z$  532 (~45%) and base peak ion at nominal  $m/z$  455, which results from the loss of a phenyl group (Fragmentation further discussed in chapter 6.2.1.4.)

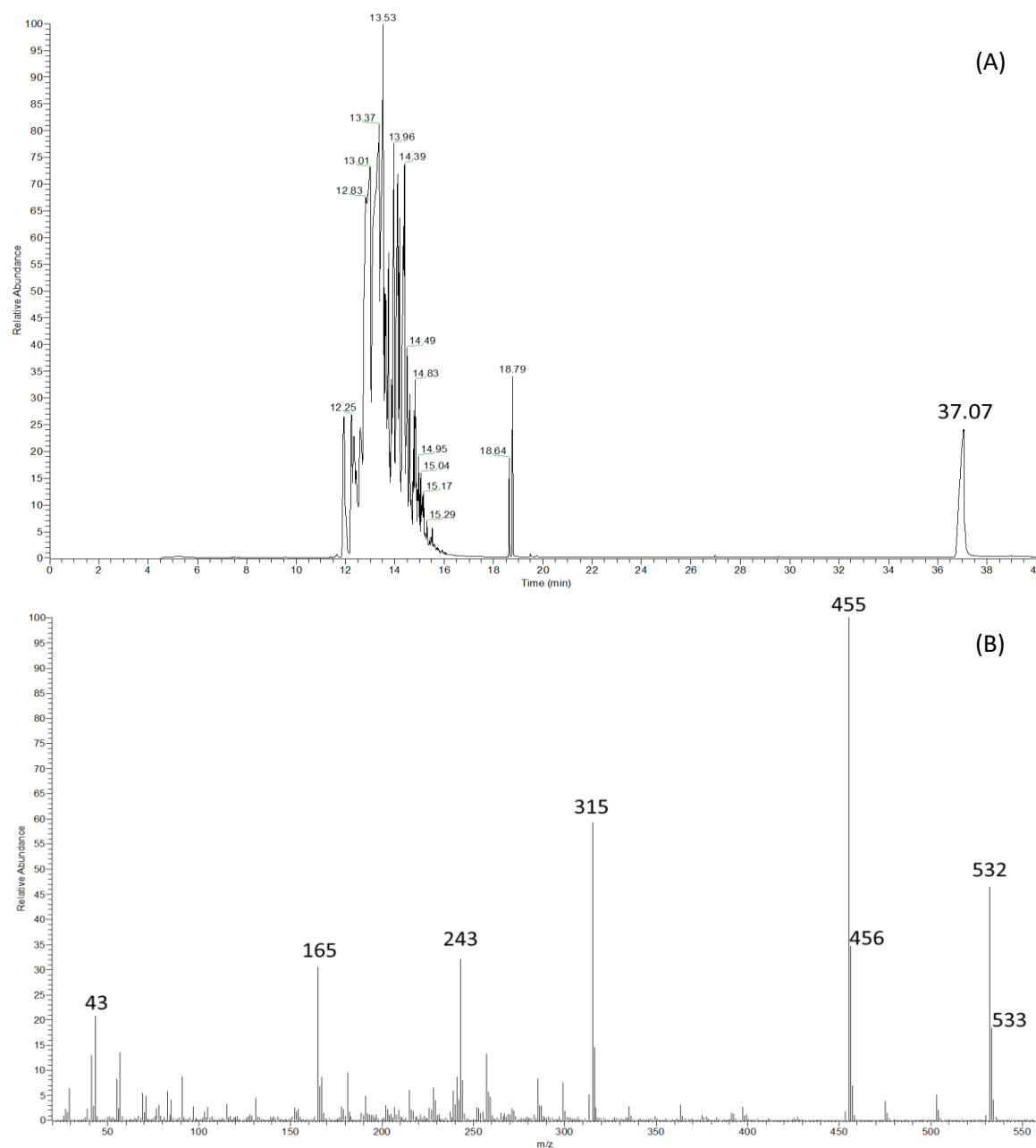


Figure 6-8 – (A) TICC and (B) EI-MS (70 eV) ( $t_R$  37.07 min, mass range  $m/z$  20 - 555) of 25 ppm ACCUTRACE™ S10 fuel marker in dichloromethane analysed using the modified full scan GC-MS method

### 6.2.1.2 ACCUTRACE™ S10 fuel marker in a contaminated fuel matrix

The proposed Dow GC-MS method<sup>290</sup> also states that it was for the detection and quantification of ACCUTRACE™ S10 fuel marker within a contaminated diesel fuel matrix consisting of a 70:27:3 diesel/lubricating oil/gear oil mixture.

ACCUTRACE™ S10 fuel marker was spiked into this contaminated diesel fuel matrix and analysed using the full scan GC-MS method. A large unresolved hump eluting was observed (Figure 6-9).

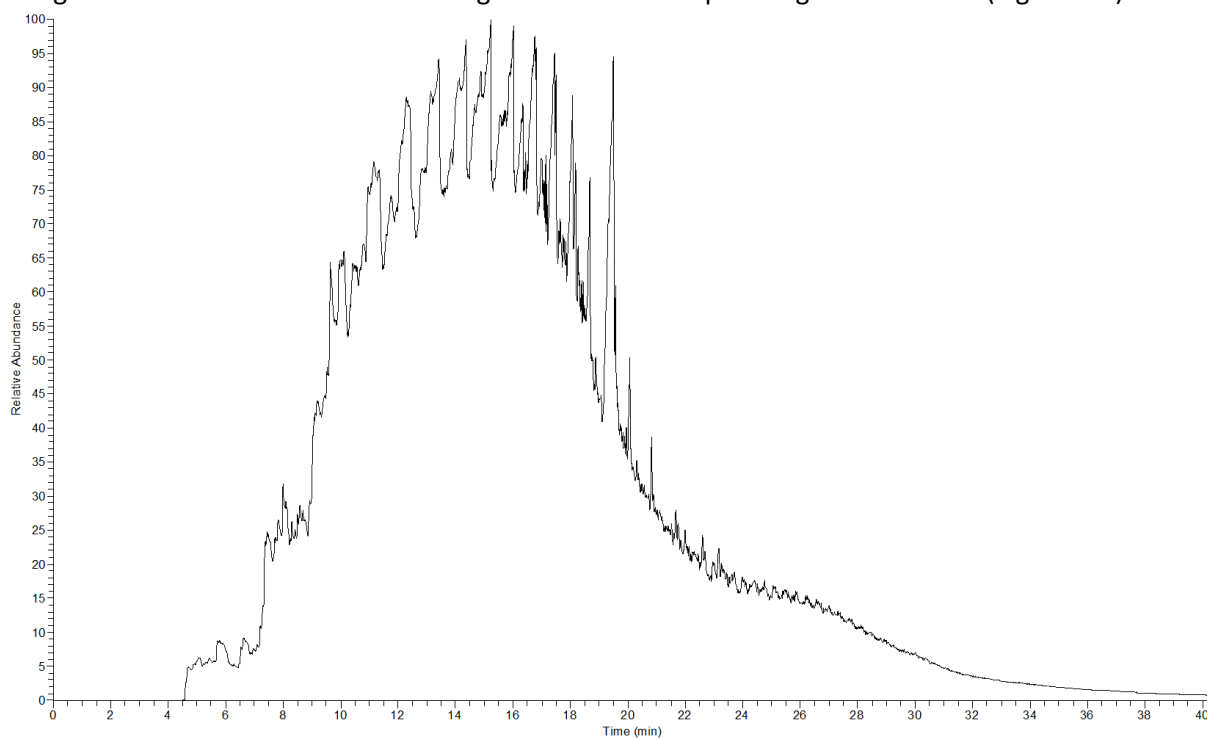


Figure 6-9 –TIC of ACCUTRACE™ S10 fuel marker in contaminated diesel fuel with composition 70:27:3 Diesel, Castrol GTX 5w30 Lubricating oil and Gear Oil 80w90 respectively, analysed using the modified full scan GC-MS method

Due to the complexity and nature of the contaminated diesel fuel matrix, long acquisition times for GC are required. Diesel is known to elute up to approximately 26 min whereas lubricating oil elutes between 16-38 min and gear oil elutes between 10-40 min, both of which are within the region of the ACCUTRACE™ S10 fuel marker retention time of 37.07 min.

Single ion recording (SIR) operation of a quadrupole mass analyser (discussed more in detail in chapter 2.5.2.1) can be used to overcome these issues by improving the sensitivity and selectivity of the method.

A GC-MS SIR method utilising both the base peak ion at nominal  $m/z$  455 and the molecular ion at nominal  $m/z$  532 was used. Due to the relatively high  $m/z$  of ACCUTRACE™ S10 fuel marker ions, the detection and quantitation is improved as they are distinct from the fuel matrix. This GC-MS

SIR method was required, not only for the increased sensitivity, but to allow for identification of the fuel marker with limited interference from the lubricating oil and gear oil.

The base peak at nominal  $m/z$  455 was utilised for quantification due to no interferences, this negated the use of the intense molecular ion at nominal  $m/z$  532 due to interferences observed within a contaminated fuel matrix, as stated by the proposed Dow method<sup>290</sup>. The ACCUTRACE™ S10 fuel marker could only be detected and quantified at doping level (2.5 ppm)(Figure 6-10), at  $t_R$  36.66 min with a S/N ratio of 15, immediately following cleaning of the ion source and replicate detection was unachievable without extensive daily cleaning of the ion source. Also ACCUTRACE™ S10 fuel marker was unable to be detected at tank dilutions level (25 ppb = 1%) by this method.

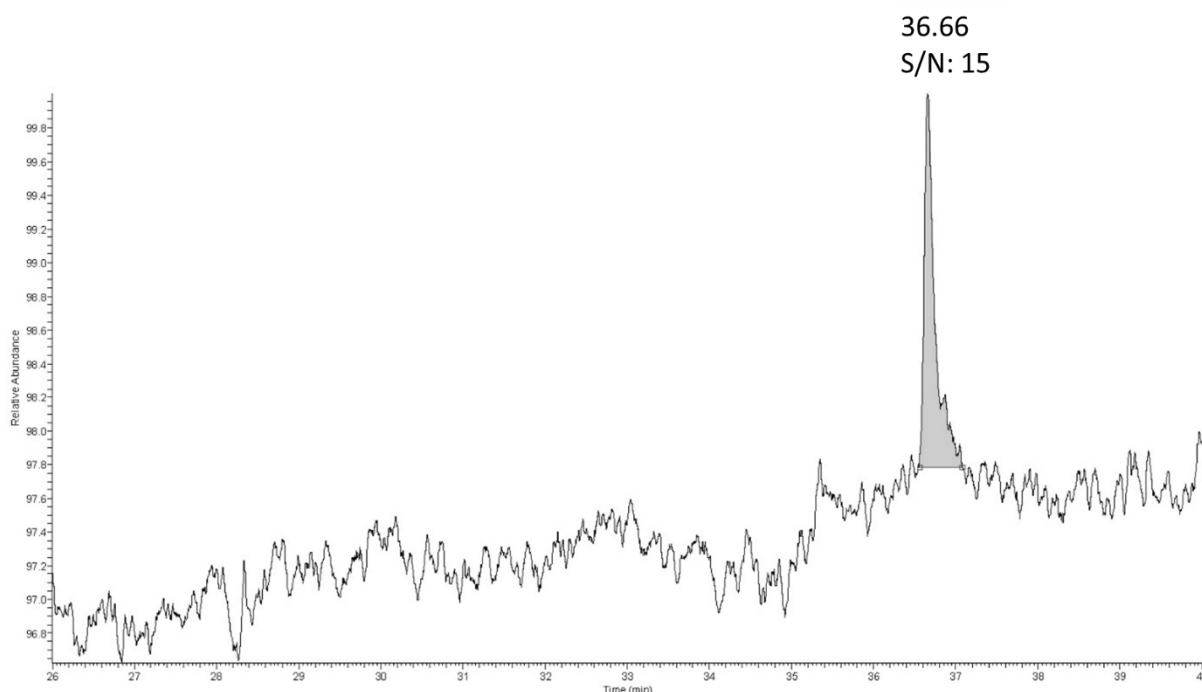


Figure 6-10 – TICC of at 2.5 ppm ACCUTRACE™ S10 fuel marker in dichloromethane (S/N = 15) analysed using GC-MS SIR  $m/z$  455 method

These results validate and necessitate the use of 2D GC-MS for the detection and quantitation of ACCUTRACE™ S10 fuel marker, particularly at low levels. However, this instrumentation and expertise is not readily available in the fuel industry, meaning another approach is required.

### 6.2.1.3 ACCUTRACE™ S10- $d_{21}$ IS

Dow Chemical Company also produced an ACCUTRACE™ S10- $d_{21}$  IS for quantitation (previously mentioned in 6.1.2.2). To investigate the behaviour of ACCUTRACE™ S10- $d_{21}$  IS, it was analysed using the same full scan method as ACCUTRACE™ S10 fuel marker. A peak is observed at  $t_R$  36.44 min. from the TICC (Figure 6-11), which is similar to the retention time of ACCUTRACE™ S10 fuel marker at  $t_R$  37.07 min.

## Chapter 6

The electron ionization mass spectrum (EI-MS) (Figure 6-11) for the ACCUTRACE™ S10- $d_{21}$  IS peak displayed a similar pattern of ions when compared to the ACCUTRACE™ S10 fuel marker. Although a 21  $m/z$  units increase is observed as expected, due to the replacement of twenty one hydrogen atoms with deuterium atoms, giving a molecular ion of nominal  $m/z$  553 and base peak ion of nominal  $m/z$  476.

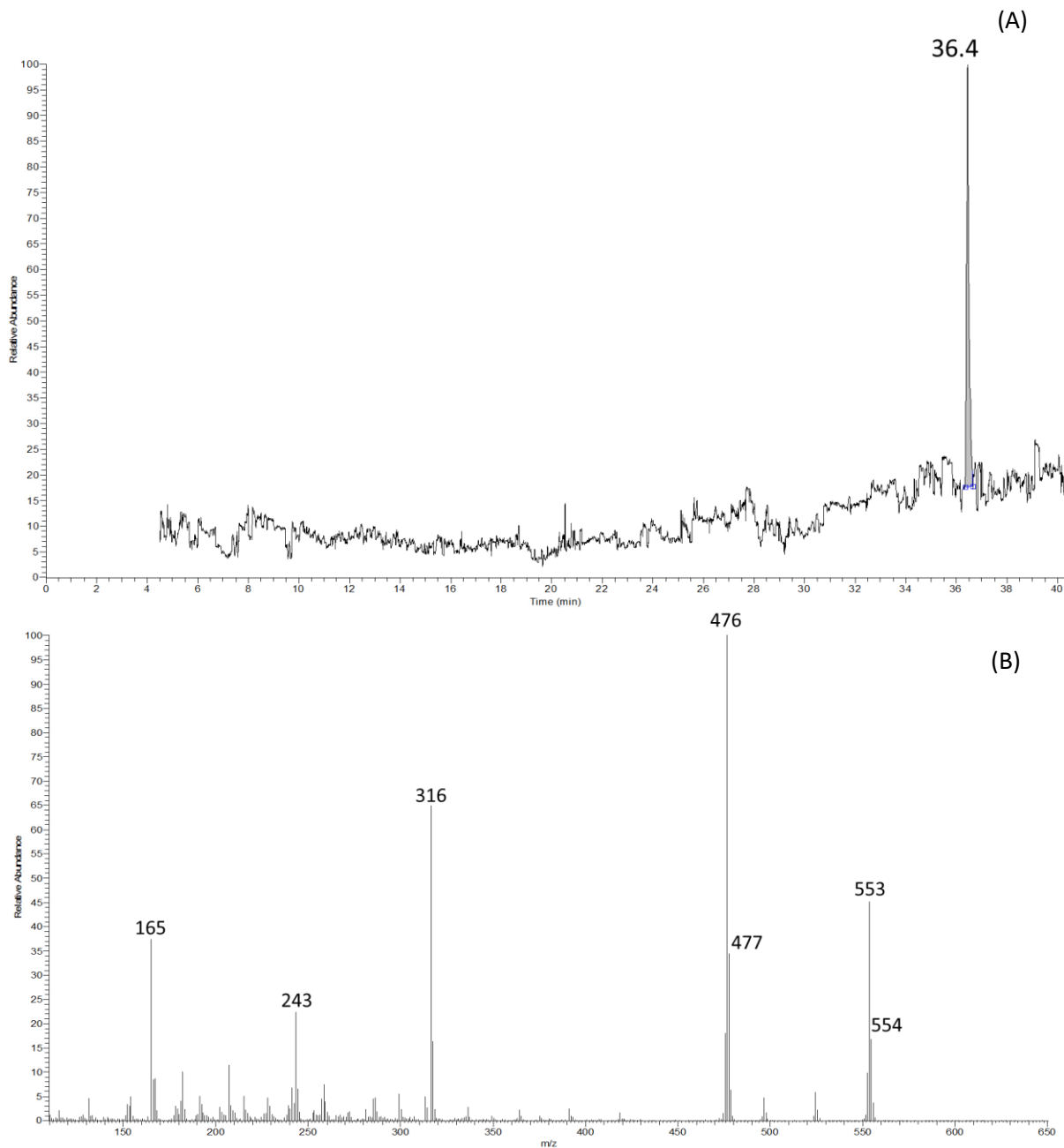


Figure 6-11 – (A) TIC and (B) EI-MS (70 eV) ( $t_R$  36.44 min, mass range  $m/z$  120 - 650) of ACCUTRACE™ S10- $d_{21}$  IS in dichloromethane

As discussed previously (6.1.2.2), a deuterated internal standard would normally be expected to co-elute with the analyte of interest. However, this was not the case for ACCUTRACE™ S10 fuel marker and ACCUTRACE™ S10- $d_{21}$  IS, where they are observed to chromatographically separate by GC-MS

(Figure 6-12) with ACCUTRACE™ S10- $d_{21}$  IS eluting first. This separation may result from the high number of deuterium atoms within ACCUTRACE™ S10- $d_{21}$  IS and may result from the deuterium isotope effect. “The deuterium isotope effect is thought to be caused by changes in lipophilicity of the molecule when hydrogen is replaced by deuterium.”<sup>287</sup>. It is common practice, for between three and five deuterium atoms to be used in an isotopically labelled internal standard so the twenty one deuterium atoms used in ACCUTRACE™ S10- $d_{21}$  IS may be jeopardising its use as an internal standard. Therefore it should be treated as a structural homologue internal standard for ACCUTRACE™ S10 fuel marker quantitation.

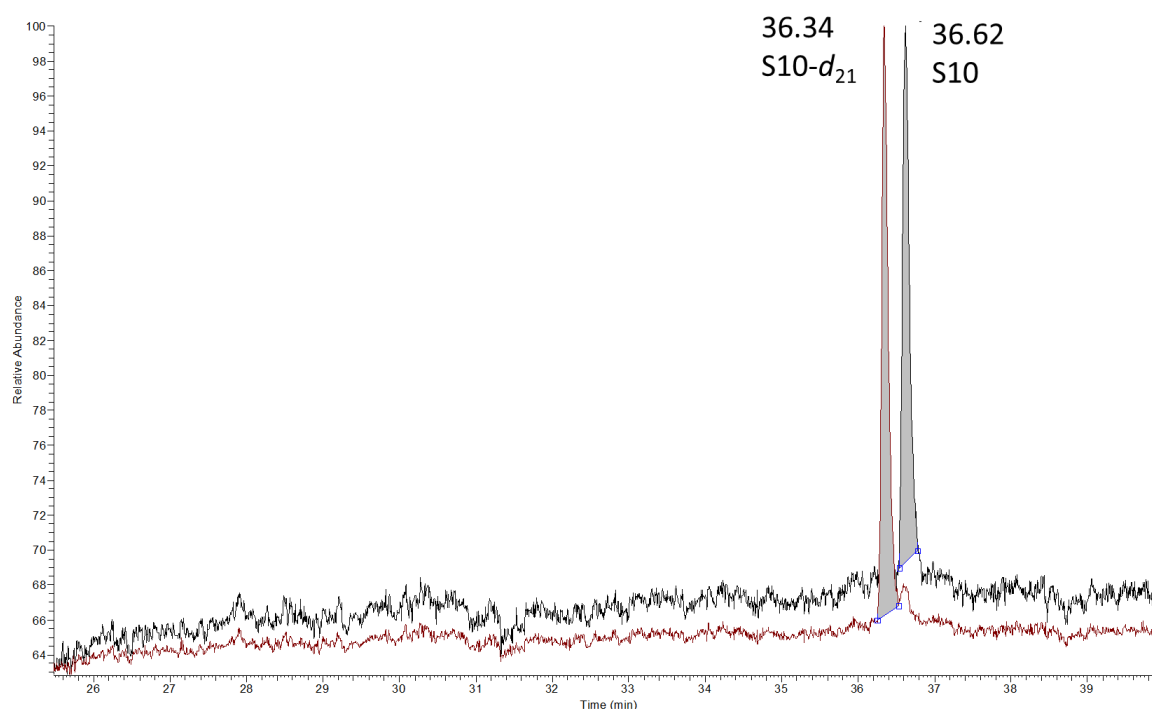


Figure 6-12 - SIR chromatograms overlaid of molecular species ( $m/z$  476 and 455 respectively) for GC-MS showing chromatographic separation of ACCUTRACE™ S10- $d_{21}$  IS and ACCUTRACE™ S10 fuel marker, respectively (ACCUTRACE™ S10- $d_{21}$  IS eluting earliest)

#### 6.2.1.4 Fragmentation of ACCUTRACE™ S10 fuel marker and ACCUTRACE™ S10- $d_{21}$ IS

A loss of 77  $m/z$  units corresponding to the loss of a phenyl group, can be observed for both the ACCUTRACE™ S10 fuel marker and S10- $d_{21}$  (Figure 6-13), with the resulting structures of both shown in **Error! Reference source not found.** and Figure 6-15. It should be noted that the 21  $m/z$  unit increase/difference in S10- $d_{21}$  IS remains after this fragmentation event.

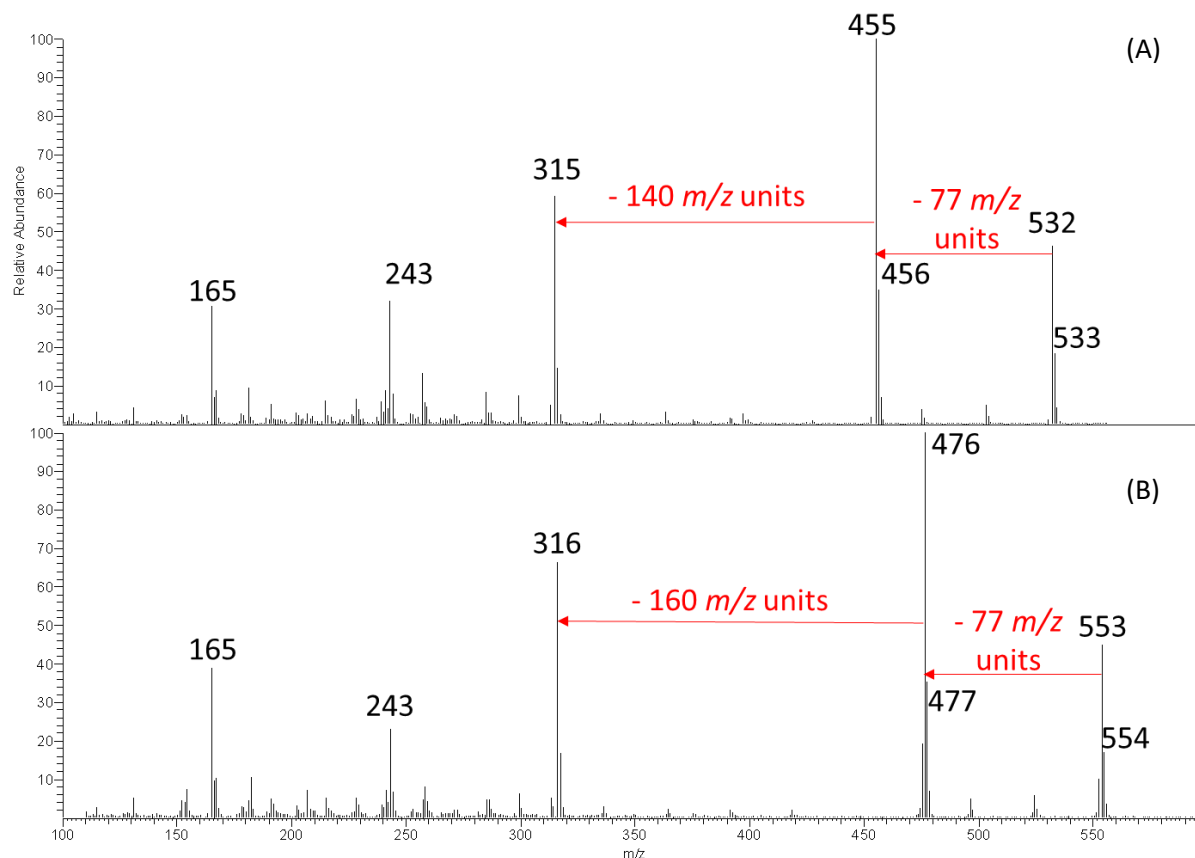


Figure 6-13 - (A) EI-MS (70 eV) ( $t_R$  36.62 min, mass range  $m/z$  100 - 600) for ACCUTRACE™ S10 fuel marker (B) EI-MS (70 eV) ( $t_R$  36.34 min, mass range  $m/z$  100 - 600) for ACCUTRACE™ S10- $d_{21}$  IS

In the ACCUTRACE™ S10 fuel marker mass spectrum (Figure 6-13), loss of 140  $m/z$  units can also be observed, corresponding to the loss of the straight chain decyl group. In the ACCUTRACE™ S10- $d_{21}$  IS mass spectrum, loss of 160  $m/z$  units is observed which has a difference of 20  $m/z$  units from the ACCUTRACE™ S10 fuel marker loss of 140  $m/z$  units. This suggests the loss of 160  $m/z$  units corresponds to the deuterated part of the ACCUTRACE™ S10- $d_{21}$  IS molecule and is believed to be the same fragmentation event as the loss of 140  $m/z$  units in the ACCUTRACE™ S10 fuel marker with the additional mass loss due to deuteration. Therefore it is thought to be the loss of a deuterated straight chain decyl group. Losses of 141 and 161  $m/z$  units were expected to be lost from ACCUTRACE™ S10 fuel marker and S10- $d_{21}$  IS respectively for this ionisation event as 21 hydrogen/deuterium atoms are present on the decyl chain. However the losses of 140 and 160  $m/z$  units observed can be explained due to the remaining fragment ion rearranging to an alcohol. The alcohol fragment ion is observed as  $m/z$  315 and 316 for ACCUTRACE™ S10 fuel marker and S10- $d_{21}$  IS respectively further confirming this theory. The difference of 1  $m/z$  unit is due to a deuterium atom on newly formed hydroxyl group in the ACCUTRACE™ S10- $d_{21}$  IS compared with a hydrogen in the

same location in the ACCUTRACE™ S10 fuel marker. A trityl ion is also observed in both mass spectra at  $m/z$  243, showing no deuteration present in this part of the molecules.

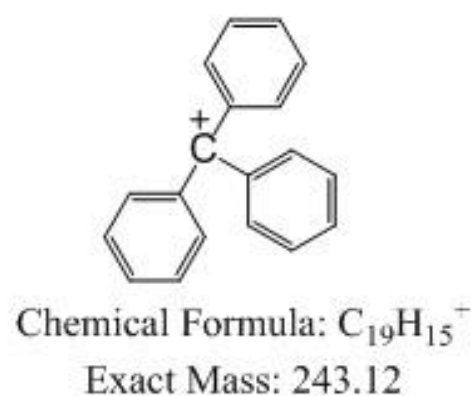
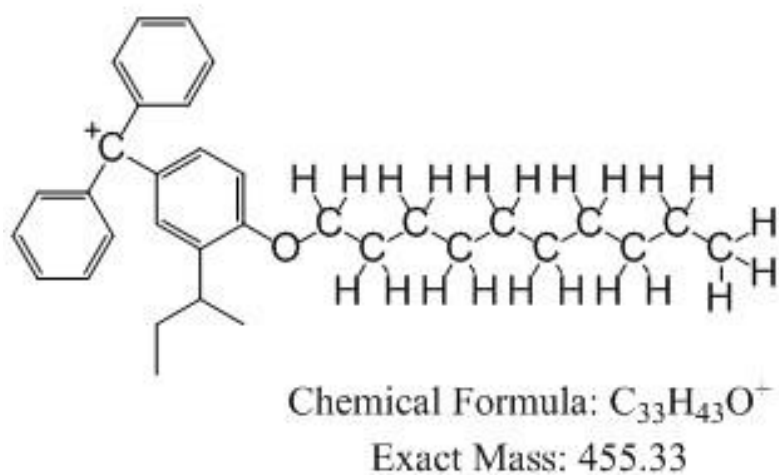
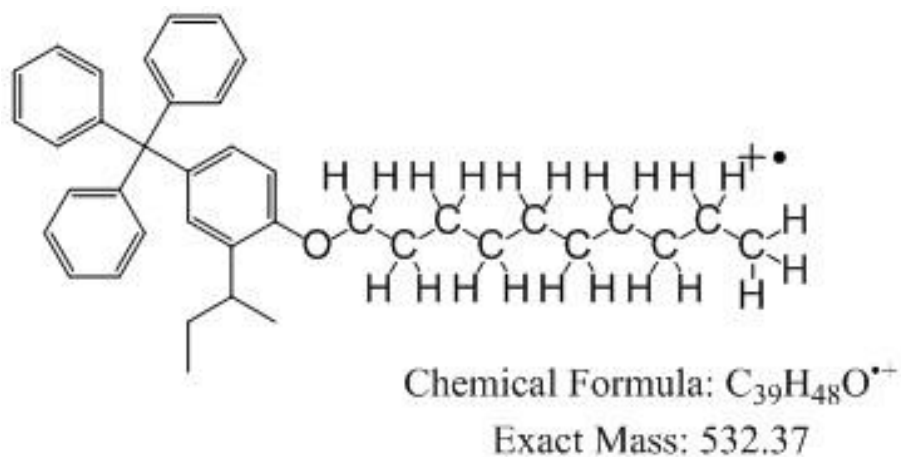


Figure 6-14 - EI fragmentation structures for ACCUTRACE™ S10 fuel marker

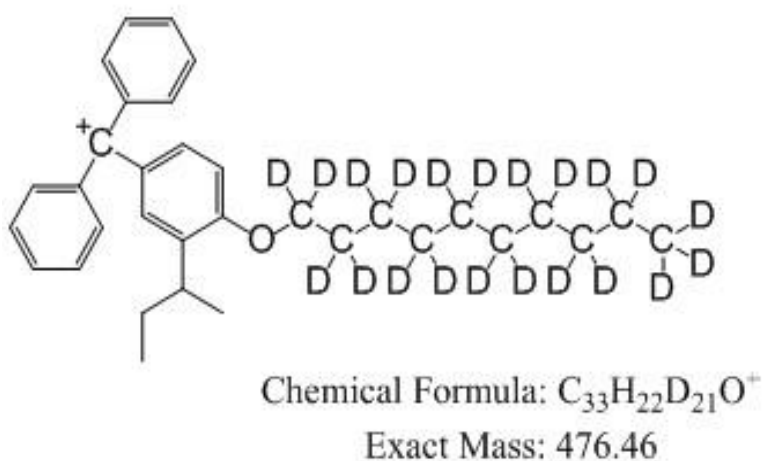
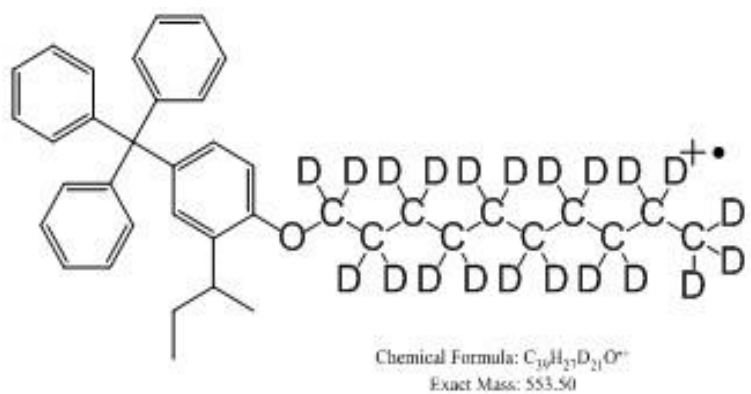


Figure 6-15 - EI fragmentation structures for ACCUTRACE™ S10- $d_{21}$  internal standard

#### 6.2.1.5 GC-MS summary

ACCUTRACE™ S10 fuel marker could only be detected and quantified at 2.5 ppm immediately following cleaning of the ion source and was unable to be detected at tank dilutions level when using legacy GC-MS systems with the modified Dow GC-MS method. Other limitations of this



method included rapidly deteriorating sensitivity and performance due to repeat fuel injections that result in an ion source change every 6 analyses and a lower limit of quantitation (LLOQ) of ~2 ppm.

Modern 2D GC-MS systems, with the use of capillary flow Deans switch, such as those used in the Agilent<sup>289</sup> method, are required to overcome these issues and provide a robust analytical solution. As previously explained, this method prevents ion source contamination using a heart-cutting technique, whereby only the peaks of interest, ACCUTRACE™ S10 fuel marker and the ACCUTRACE™ S10-*d*<sub>21</sub> IS, reach the detector with the rest of the sample going to waste. However, 2D GC-MS is not readily available in industry meaning that this method is not widely applicable and a different approach is required.

Currently all proposed detection methods for ACCUTRACE™ S10 fuel marker utilise GC-MS. For detection at tank dilution levels 2D GC-MS is required, however there is current industry shortage of 2D GC-MS capability. The GC-MS method is unsuitable when utilised with legacy GC-MS instrumentation, which is commonplace in industry as it is not fit-for purpose and a solution is unable to be achieved. As a result, an alternative method was required, so ultra-high performance supercritical fluid chromatography-mass spectrometry (UHPSFC-MS) was investigated as an alternate analytical solution.

### 6.3 UHPSFC –MS

Due to the issues aforementioned with the GC-MS method, ultra-high performance supercritical fluid chromatography-mass spectrometry (UHPSFC-MS) was investigated as an alternative analytical solution.

As discussed previously in chapter 2.4, UHPSFC-MS has many properties that make it particularly suitable as an alternative analysis technique for the detection and quantitation of ACCUTRACE™ S10 fuel marker. The non-polar and hexane-like properties of *sc*CO<sub>2</sub> make it compatible with direct introduction of undiluted refined petrochemical fuels, such as diesel, gasoline and aviation turbine fuel (AVTUR), into the solvent stream<sup>7, 92</sup>. Similarly to the GC-MS method, this means no sample preparation is required, however fuel matrix issues and problems associated with ion source degradation seen in the GC-MS method are not experienced with UHPSFC-MS.

### 6.3.1 UHPSFC-MS analysis

#### 6.3.1.1 Positive ion APPI UHPSFC-MS (undertaken by John Langley and Julie Herniman)

The ACCUTRACE™ S10 fuel marker was originally designed with EI as the preferred ionisation technique, however due to the aromaticity within the structure it is also a good candidate for analysis using atmospheric pressure photoionisation (APPI).

APPI is an atmospheric pressure ionisation (API) technique (discussed in chapter 2.5.1.3) that selectively ionises aromatic compounds with moderate to low polarity and non-polar compounds<sup>291-292</sup>, as shown graphically in Figure 6-16<sup>200</sup>. APPI can ionise species that are “not accessible by ESI or APCI”<sup>291</sup>. Dopant assisted APPI was utilised in this project, with toluene as the dopant, to achieve more efficient ionisation<sup>199</sup>. Advantageously, the UHPSFC-MS system (Waters ACQUITY UPC<sup>2</sup>) allows for easy APPI dopant introduction using make up solvent system, making the system readily amenable for dopant assisted APPI (Figure 6-17<sup>160</sup>)(greater discussion in chapter 2.4).

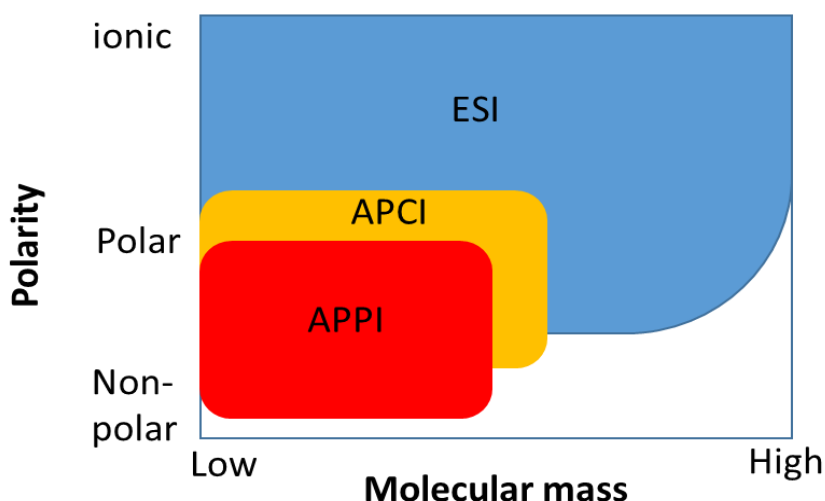


Figure 6-16 - A schematic comparing API techniques and their analyte compatibility.

Adapted from<sup>201</sup>

Within literature, Kauppila *et al.*<sup>199</sup> reports that APPI is commonly used in petroleomics for fuel related compounds due to highly complex crude oil samples containing “thousands or tens of thousands of components with highly different properties, such as completely nonpolar PAHs, polar acids and bases, or metal complexes”. APPI was also utilised for the analysis of non-polar aromatic hydrocarbons within complex petrochemical mixtures<sup>291</sup> and for the determination of PAHs<sup>292</sup>.

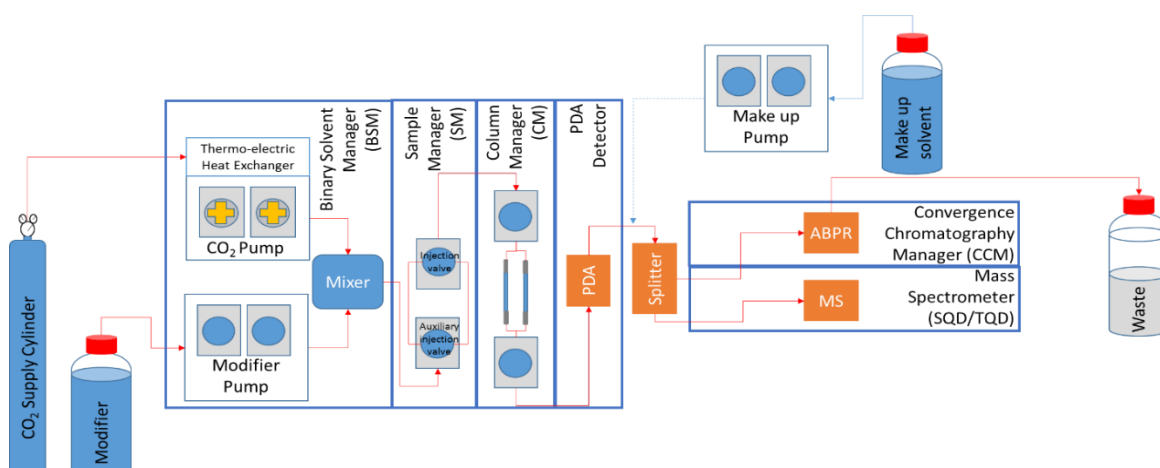


Figure 6-17 –Schematic showing flow path and components of Waters ACQUITY

UltraPerformance Convergence Chromatography (UPC<sup>2</sup>) system. Adapted from<sup>161</sup>

The ACCUTRACE™ S10 fuel marker contains aromaticity and is similar in structure to some compounds within petrochemical mixtures, suggesting it would be well suited for ionisation by APPI.

UHPSFC-APPI MS was utilised in the initial analysis of 2.5 ppm standard solution of ACCUTRACE™ S10 fuel marker. A signal was observed in TICC and reconstructed ion current chromatogram (RICC) at  $t_R$  0.84 mins (Figure 6-18) with this peak expected to correspond to a radical cation/molecular ion as dopant assisted APPI was utilised.

However protonated molecules  $[S10 + H]^+$  at nominal  $m/z$  533, potassiated molecules  $[S10 + K]^+$  at nominal  $m/z$  571 and very abundant sodiated molecules protonated  $[S10 + Na]^+$  at nominal  $m/z$  555 were clearly visible in the atmospheric pressure photoionization mass spectrum (Figure 6-18). The presence of cationised molecules, particularly the intense sodiated molecules, suggested photoionisation of the molecule was not occurring; rather the ion was formed *via* an ion evaporation process.

As a result of these findings, positive ion electrospray ionisation (ESI) was investigated as protonated and cationised molecules are easily generated using this technique.

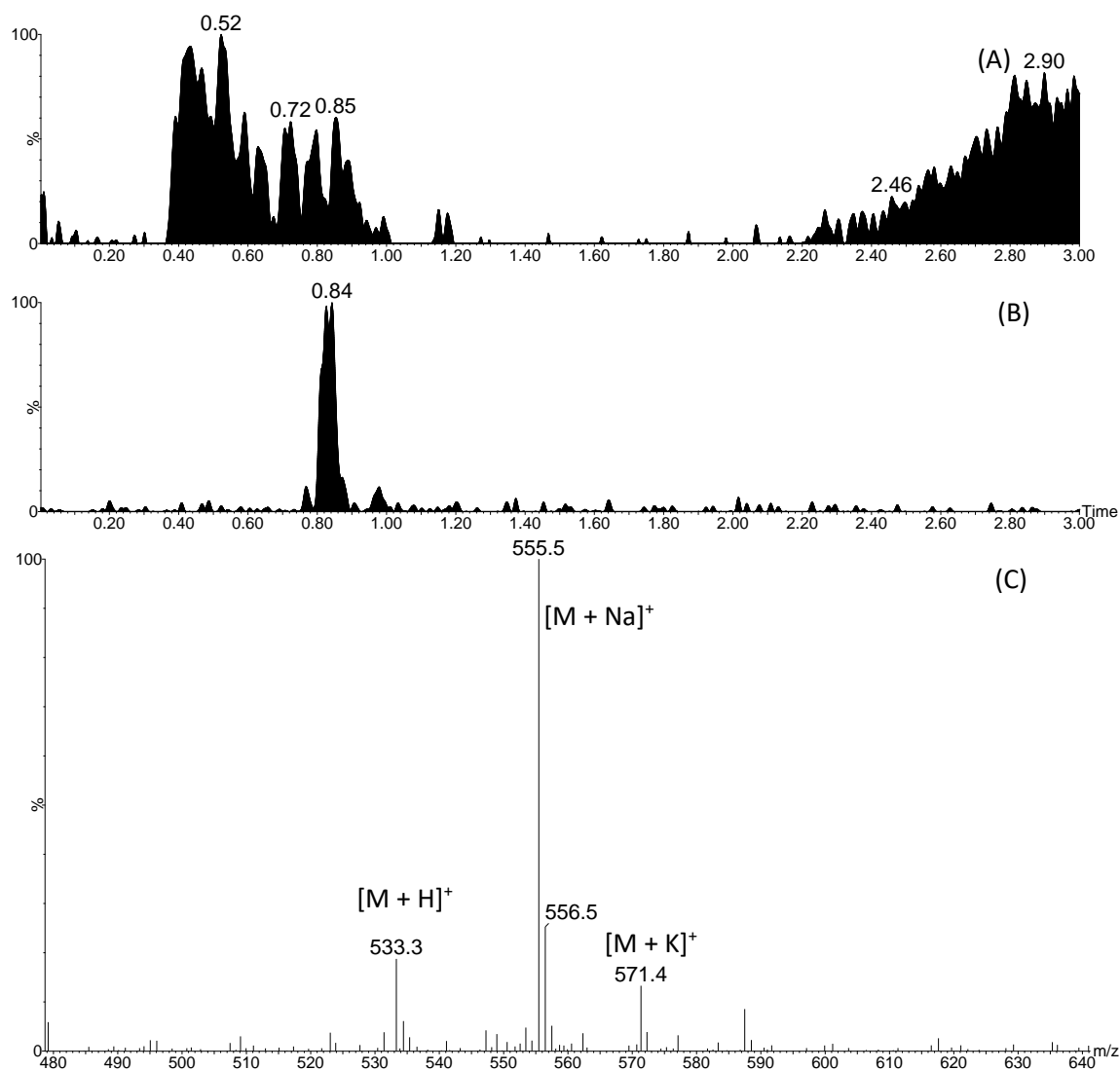


Figure 6-18 – (A) TICC, (B) RICC ( $m/z$  555.5) and (C) positive ion APPI MS ( $t_R$  0.84 min, zoomed mass range  $m/z$  480 - 640) of ACCUTRACE™ S10 fuel marker in methanol

### 6.3.1.2 Positive ion ESI UHPSFC-MS

#### 6.3.1.2.1 ACCUTRACE™ S10 fuel marker

The ionisation of ACCUTRACE™ S10 fuel marker by positive ion ESI was unexpected due to the non-polar structure of the compound. Basic sites are required for ionisation using positive ion ESI, however there were no obvious basic sites for ionisation in the ACCUTRACE™ S10 fuel marker molecule.

ESI is an API technique (discussed in greater detail in 2.5.1.2) which selectively ionises with negative ion ESI ionising acidic compounds and positive ion ESI ionising basic compounds<sup>291</sup>. This can be advantageous as other compounds remain invisible, such as base fuel hydrocarbons in this case, meaning ionised compounds are more easily observed and complexity can be reduced.

A positive ion ESI UHPSFC-MS method was developed and fully optimised. Ammonium acetate was required in both, as an additive (25 mM) in the methanol modifier for chromatography as well as in the methanol make-up solvent (50  $\mu$ M) which encourages the formation of ammoniated molecules preferentially.

A 500 ppm solution of ACCUTRACE™ S10 fuel marker in methanol was analysed using positive ion ESI UHPSFC-MS in full scan mode. The ACCUTRACE™ S10 fuel marker was observed in the resulting chromatograms at  $t_R$  2.20 mins with  $[S10 + H]^+$  at nominal  $m/z$  533,  $[S10 + NH_4]^+$  at nominal  $m/z$  550 and  $[S10 + Na]^+$  at nominal  $m/z$  555 clearly visible in the ESI mass spectrum (Figure 6-19).

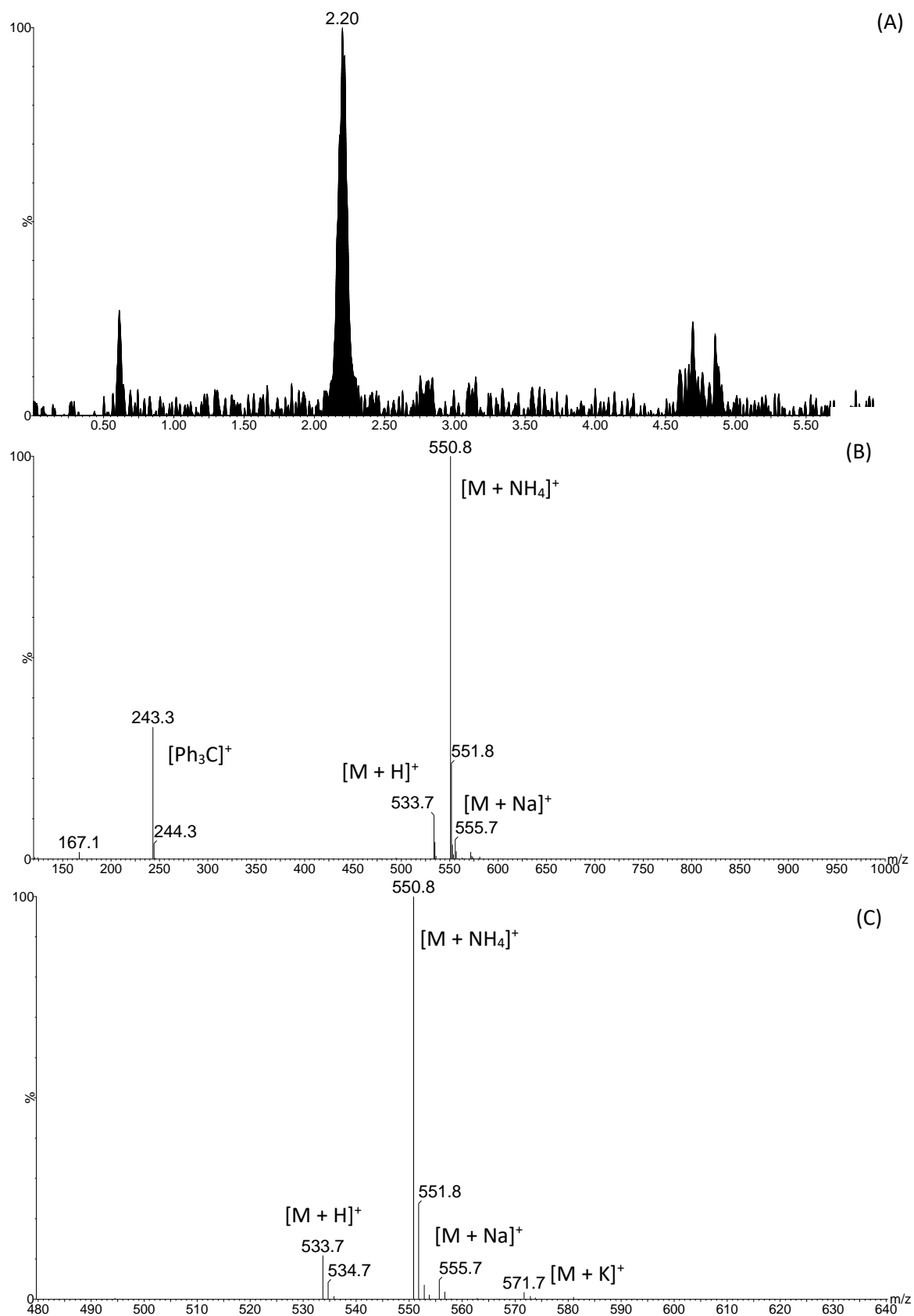


Figure 6-19 - (A) TIC, (B) positive ion ESI mass spectrum (t<sub>R</sub> 2.20 min) and (C) positive ion ESI MS (t<sub>R</sub> 2.20 min, zoomed mass range m/z 480 - 640) of 500 ppm ACCUTRACE™ S10 fuel marker in methanol

As with the GC-MS method, an SIR method was developed for the same reasons mentioned in chapters 2.5.2.1. The use of SIR was advantageous as it provides increased sensitivity, meaning the LOD and LOQ would be lower using an SIR method. The most abundant ACCUTRACE™ S10 fuel marker adduct was the ammoniated form  $[S10 + NH_4]^+$ , so an SIR method for the ion  $m/z$  550.8 was created.

2.5 ppm ACCUTRACE™ S10 fuel marker in methanol was analysed with the SIR  $m/z$  550.8 method to observe the response at doping level. A retention time of 2.31 min was observed and the RICC for the ammoniated molecule  $m/z$  550.8 gives a S/N ratio of 1468 (Figure 6-20).

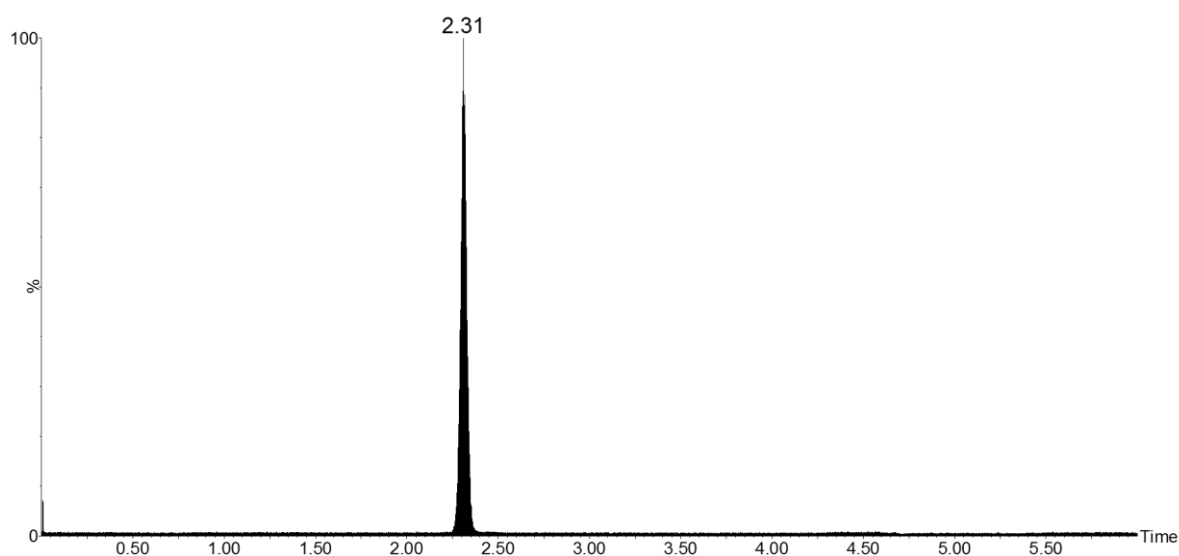


Figure 6-20 - RICC of 2.5 ppm ACCUTRACE™ S10 fuel marker in methanol analysed using SIR  $m/z$  550.8 method

#### 6.3.1.2.2 Molecular modelling of ACCUTRACE™ S10 fuel marker (undertaken by Maria Ashe)

As mentioned previously, ACCUTRACE™ S10 fuel marker has no obvious basic sites for ionisation by positive ion ESI, however it can be observed to unexpectedly ionise by positive ion ESI. Molecular modelling was utilised to determine likely ionisation sites in the ACCUTRACE™ S10 fuel marker molecule. The molecular modelling allows an electron density of a molecule to be generated showing the expected electronegativity of a molecule and therefore the location where ionisation is most likely to occur.

The decyl ether oxygen is the only heteroatom present within the ACCUTRACE™ S10 fuel marker molecule. As observed in Figure 6-21<sup>293</sup>, the greatest electronegativity is present at the ether oxygen atom, however due to the shape of the ACCUTRACE™ S10 fuel marker molecule it is inaccessible. It should be noted that there are highly electronegative regions within the aromatic

rings of the molecule. The ionisation is believed to be related to the oxygen cation being attracted to this highly electronegative region within the aromatic rings in the molecule.

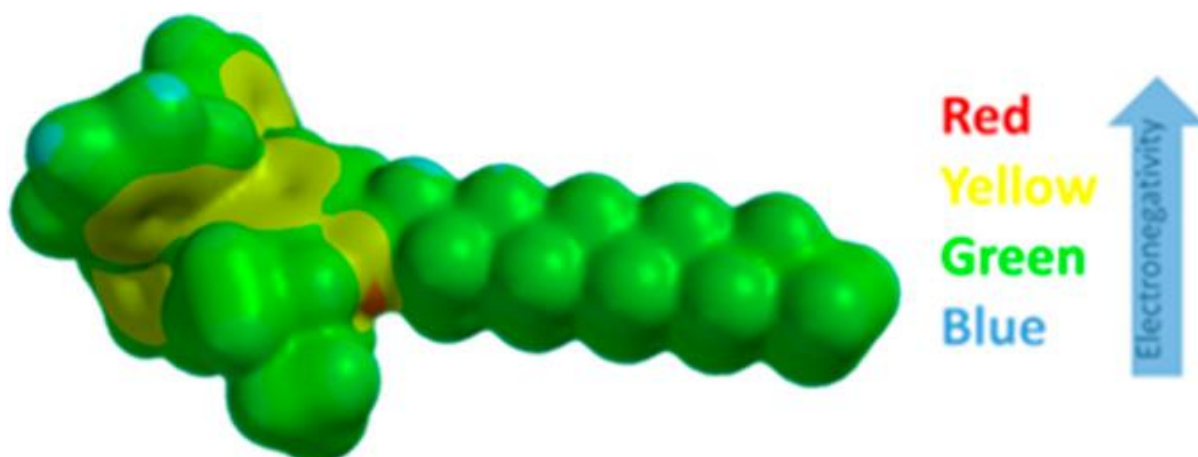


Figure 6-21 - Molecular model of ACCUTRACE™ S10 fuel marker electronegativity map<sup>293</sup>. Figure reproduced with permission from ACS

#### 6.3.1.2.3 ACCUTRACE™ S10-*d*<sub>21</sub> internal standard

The same approach was used to observe the behaviour of the ACCUTRACE™ S10-*d*<sub>21</sub> IS by positive ion ESI. Initially 500 ppm ACCUTRACE™ S10-*d*<sub>21</sub> IS solution in methanol was analysed using the same positive ion ESI UHPSFC-MS full scan parameters used for ACCUTRACE™ S10 fuel marker previously. The resulting chromatogram and the positive ion ESI MS acquired at the peak *t*<sub>R</sub> 2.11 minutes are shown in Figure 6-22.



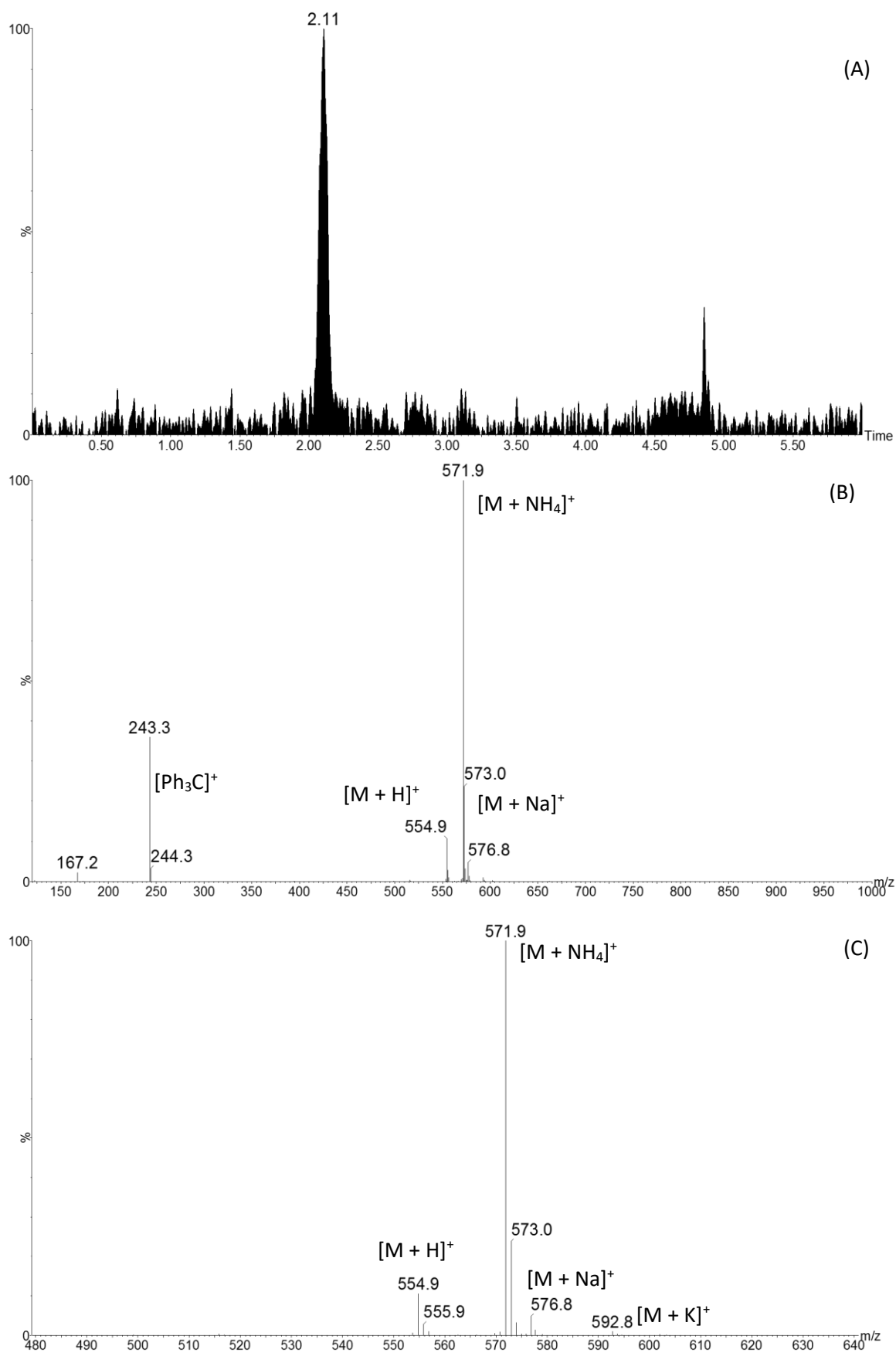


Figure 6-22 - (A) TIC, (B) positive ion ESI mass spectrum ( $t_R$  2.11 min) and (C) positive ion ESI MS ( $t_R$  2.11 min, zoomed mass range  $m/z$  480 - 640) of 500 ppm ACCUTRACE™ S10- $d_{21}$  IS in methanol

## Chapter 6

As with the ACCUTRACE™ S10 fuel marker, the most abundant ACCUTRACE™ S10-*d*<sub>21</sub> IS adduct was the ammoniated form [S10-*d*<sub>21</sub> + NH<sub>4</sub>]<sup>+</sup>, so again an SIR method was created for the ammonium adduct, this time using *m/z* 571.9.

1 ppm ACCUTRACE™ S10-*d*<sub>21</sub> IS in methanol was analysed using the SIR *m/z* 571.9 method to observe the response at a level approximate to that used in conjunction with ACCUTRACE™ S10 fuel marker for quantitation at doping level. A retention time of 2.13 min was observed and the RICC for the ammoniated molecule *m/z* 571.9 gives a S/N ratio of 1094 (Figure 6-23).

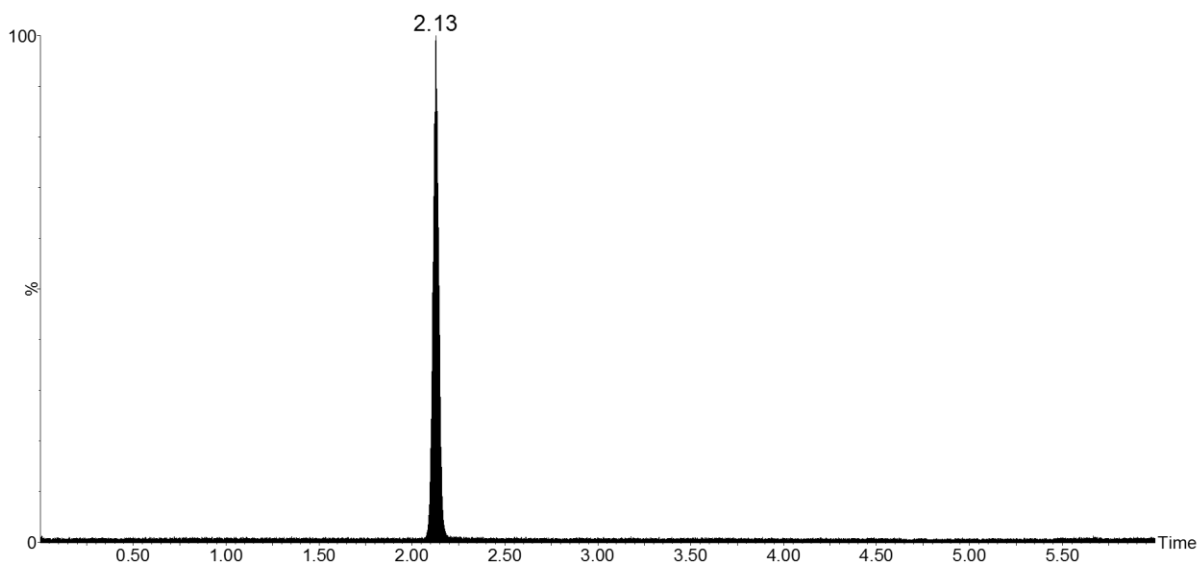


Figure 6-23 - RICC of 1 ppm ACCUTRACE™ S10-*d*<sub>21</sub> IS in methanol analysed using SIR *m/z* 571.9 method

### 6.3.1.2.4 ACCUTRACE™ S10 fuel marker and ACCUTRACE™ S10-*d*<sub>21</sub> IS

ACCUTRACE™ S10 fuel marker and ACCUTRACE™ S10-*d*<sub>21</sub> IS were then combined in a methanol solution and a new SIR method was created to analyse both ACCUTRACE™ S10 fuel marker and ACCUTRACE™ S10-*d*<sub>21</sub> IS together. An SIR method for *m/z* 550.8 and 571.9 was created. 100 ppm ACCUTRACE™ S10 fuel marker and 100 ppm ACCUTRACE™ S10-*d*<sub>21</sub> IS in methanol was then analysed using this SIR method and the acquired RICC is shown in Figure 6-24. ACCUTRACE™ S10-*d*<sub>21</sub> IS has a retention time of 2.10 min and elutes first, with ACCUTRACE™ S10 fuel marker eluting at 2.20 min, meaning chromatographic separation is achieved.

The chromatographic separation observed between ACCUTRACE™ S10 fuel marker and ACCUTRACE™ S10-*d*<sub>21</sub> IS was unexpected as coelution is generally expected between an analyte and a deuterated internal standard (discussed in greater detail in 6.1.2.2 and 6.2.1.3). This is believed to occur due to the high number of deuterium atoms present in ACCUTRACE™ S10-*d*<sub>21</sub> IS. This results in ACCUTRACE™ S10-*d*<sub>21</sub> IS being treated as a structural analogue internal standard

rather than a homologue/isotopologue when used for ACCUTRACE™ S10 fuel marker quantitation.

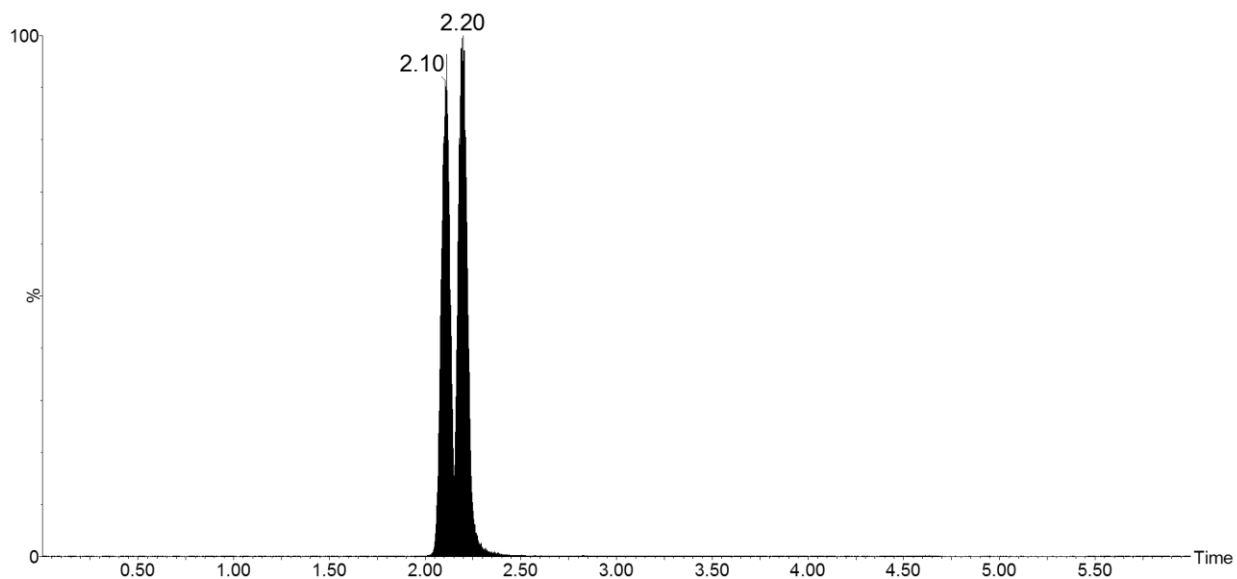


Figure 6-24 - RICC of 100 ppm ACCUTRACE™ S10 fuel marker and 100 ppm ACCUTRACE™ S10- $d_{21}$  IS in methanol showing chromatographic separation of ACCUTRACE™ S10- $d_{21}$  IS and ACCUTRACE™ S10 fuel marker, respectively (ACCUTRACE™ S10- $d_{21}$  IS eluting earliest)

### 6.3.1.2.5 Calibration

#### 6.3.1.2.5.1 ACCUTRACE™ S10 fuel marker in methanol

All ACCUTRACE™ S10 fuel marker calibration standards were analysed using the SIR method for  $m/z$  550.8, an lower limit of detection (LLOD) of 5 ppb and lower limit of quantitation (LLOQ) of 10 ppb was determined (Figure 6-25), which is below tank dilution level (25 ppb = 1%).

An ACCUTRACE™ S10 fuel marker calibration curve was plotted as shown in Figure 6-26. A linear trend line with an  $R^2$  value 0.9932 suggests all standards are within one linear dynamic range. However, further dilution of the higher concentration standards would improve the precision of the measurements.

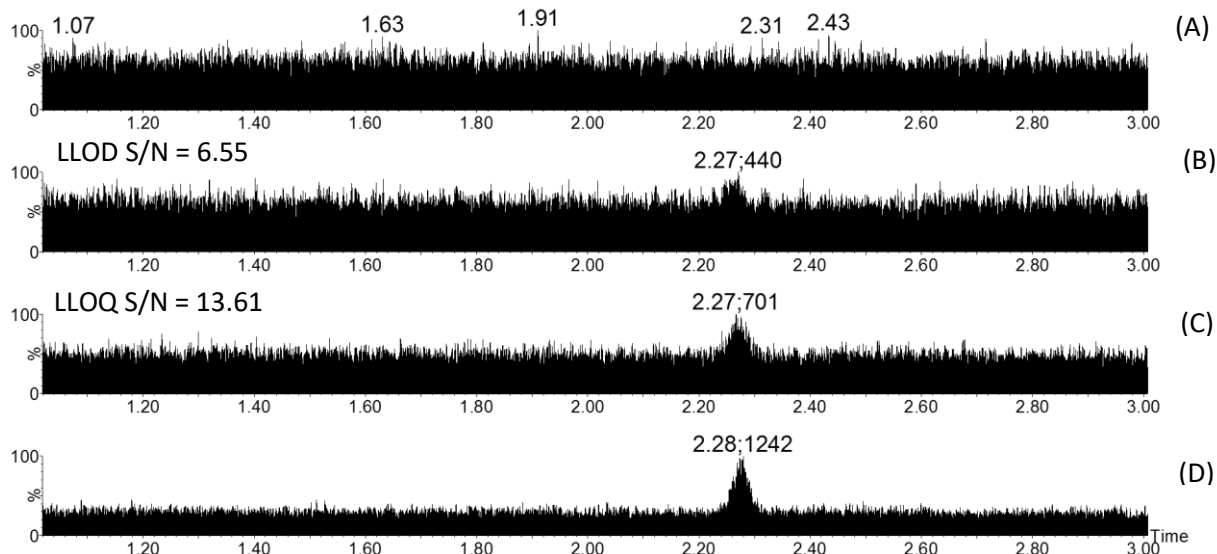


Figure 6-25 - RICCs of ACCUTRACE™ S10 fuel marker standards (A) 1 ppb (B) 5 ppb (C) 10 ppb and (D) 25 ppb analysed using the SIR  $m/z$  550.8 method, demonstrating the LLOD and LLOQ

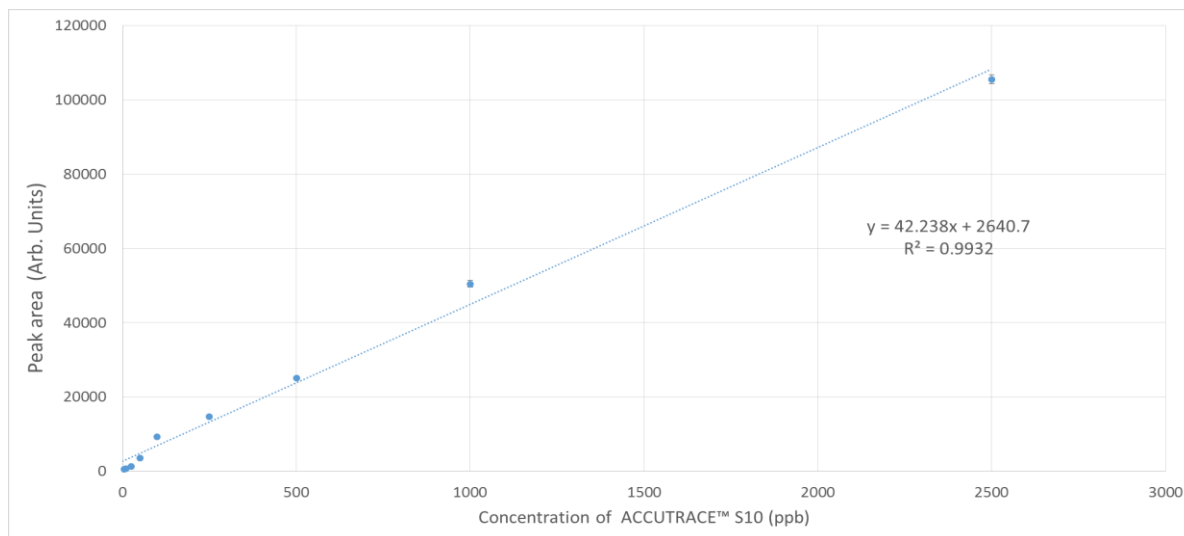


Figure 6-26 - Positive ion ESI ACCUTRACE™ S10 fuel marker calibration curve using ACCUTRACE™ S10 fuel marker standards (5, 10, 25, 50, 100, 250, 500, 1000 and 2500 ppb) analysed using the SIR  $m/z$  550.8 method (number of replicates = 6, error bars =  $2\sigma$ )

6.3.1.2.5.2 ACCUTRACE™ S10 fuel marker and ACCUTRACE™ S10-*d*<sub>21</sub> IS in methanol

All ACCUTRACE™ S10 fuel marker and ACCUTRACE™ S10-*d*<sub>21</sub> IS calibration standards were analysed using the SIR method for *m/z* 550.8 and 571.9. An LLOD of 5 ppb and LLOQ of 10 ppb was determined (Figure 6-27), which is below tank dilution level (25 ppb = 1%).

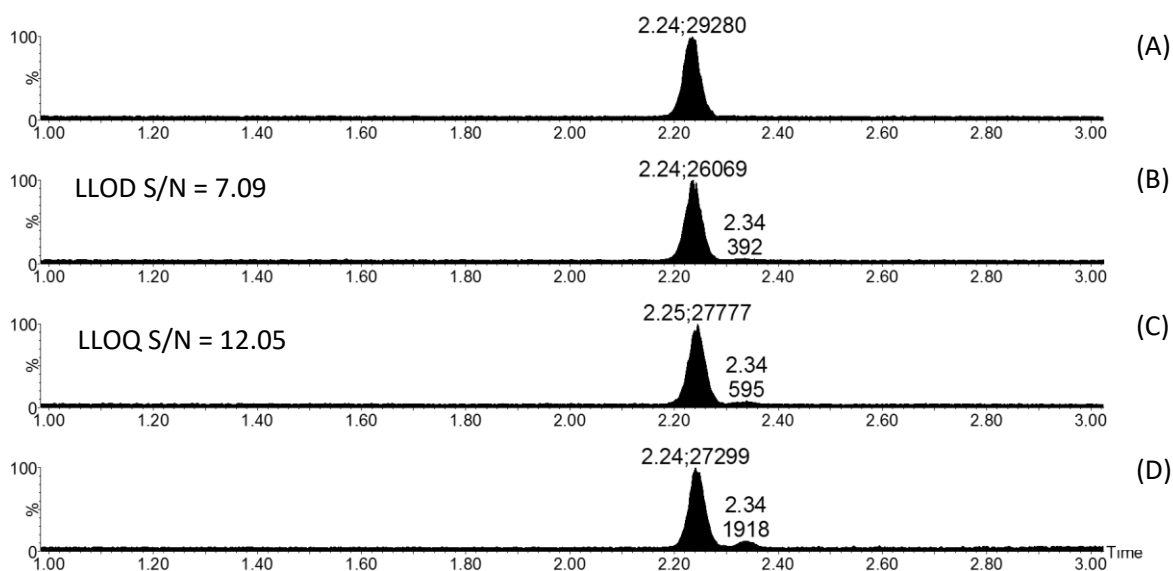


Figure 6-27 - RICCs of ACCUTRACE™ S10 fuel marker ( $t_R$  2.34 min) (A) 1 ppb (B) 5 ppb (C) 10 ppb and (D) 25 ppb, each with 500 ppb ACCUTRACE™ S10-*d*<sub>21</sub> IS ( $t_R$  2.24 min) in methanol standards analysed using the SIR *m/z* 550.8 and 571.9 method, demonstrating the LLOD and LLOQ

The individual peak areas ACCUTRACE™ S10 fuel marker and ACCUTRACE™ S10-*d*<sub>21</sub> IS were used to calculate a ratio, as shown in Table 6-2, which was then plotted to create a calibration curve (Figure 6-28), as ionisation response is 1:1. A linear trend line with an  $R^2$  value 0.9987 suggests all standards are within one linear dynamic range up to 2500 ppb and further dilution of the higher concentration standards would improve the precision of the measurements. Higher concentration calibration standards up to 10000 ppb were analysed (data not shown), with standards at 10000 ppb found to be outside the linear dynamic range, suggesting the upper limit of quantification (ULOQ) is reached between 5000 and 10000 ppb although further work using a greater number of calibration standards in this range would be required to determine an exact ULOQ.

Table 6-2 - Ratio of ACCUTRACE™ S10/S10- $d_{21}$  IS in methanol

Concentration of ACCUTRACE S10 fuel marker (ppb)	Ratio of S10/S10- $d_{21}$ (Concentration of S10 - $d_{21}$ = 500 ppb)		Error (Standard deviation) (number of replicates =6)
	Calculated	Measured	
5	0.01	0.013	$4 \times 10^{-4}$
10	0.02	0.020	0.001
25	0.05	0.063	0.001
50	0.1	0.123	0.006
100	0.2	0.281	0.004
250	0.5	0.658	0.023
500	1	1.197	0.154
1000	2	2.078	0.089
2500	5	5.211	0.105

x

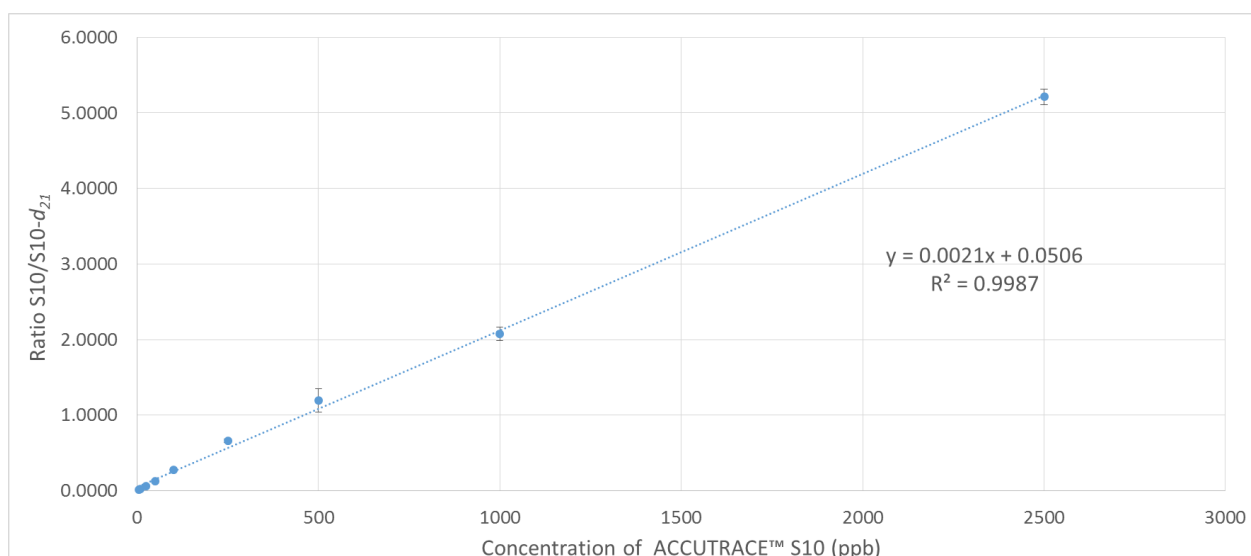


Figure 6-28 - Positive ion ESI ACCUTRACE™ S10 fuel marker and ACCUTRACE™ S10-*d*<sub>21</sub> IS calibration curve using ACCUTRACE™ S10 fuel marker standards (5, 10, 25, 50, 100, 250, 500, 1000 and 2500 ppb) each with 500 ppb ACCUTRACE™ S10-*d*<sub>21</sub> IS in methanol, analysed using the SIR *m/z* 550.8 and 571.9 method (number of replicates = 6)

#### 6.3.1.2.5.3 ACCUTRACE™ S10 fuel marker and ACCUTRACE™ S10-*d*<sub>21</sub> IS in diesel fuel

A calibration curve was also required in the fuel matrix to ensure the method was transferrable. All ACCUTRACE™ S10 fuel marker and ACCUTRACE™ S10-*d*<sub>21</sub> IS in diesel fuel calibration standards were analysed using the SIR method for *m/z* 550.8 and 571.9. An LLOD of 50 ppb and LLOQ of 100 ppb was determined (Figure 6-29) which is approximately 10 times higher than that of ACCUTRACE™ S10 fuel marker and ACCUTRACE™ S10-*d*<sub>21</sub> IS standards in methanol only. This increase is caused by the fuel matrix as other compounds found within the fuel are observed eluting with the same *m/z* throughout SIR acquisition, rather than a single peak observed within methanol only standards. At present, the LLOD and LLOQ is above tank dilution level (25 ppb = 1%) but the use of selected reaction monitoring (SRM) could further improve this. The determination of the exact LLOD and LLOQ, using a greater number of calibration standards within the range of interest is also required.

Again, the individual peak areas ACCUTRACE™ S10 fuel marker and ACCUTRACE™ S10-*d*<sub>21</sub> IS were used to calculate a ratio, as shown in Table 6-3, which was then plotted to create a calibration curve (Figure 6-30). To ensure the doping level, 2.5 ppm, of ACCUTRACE™ S10 fuel marker was in the mid-range of the calibration curve, a greater range of calibration standards were used. This was to make sure that the concentration of ACCUTRACE™ S10 fuel marker in them will still be able to be

determined even if fuels are doped higher than the doping level, which may happen to ensure the fuel is correctly doped.

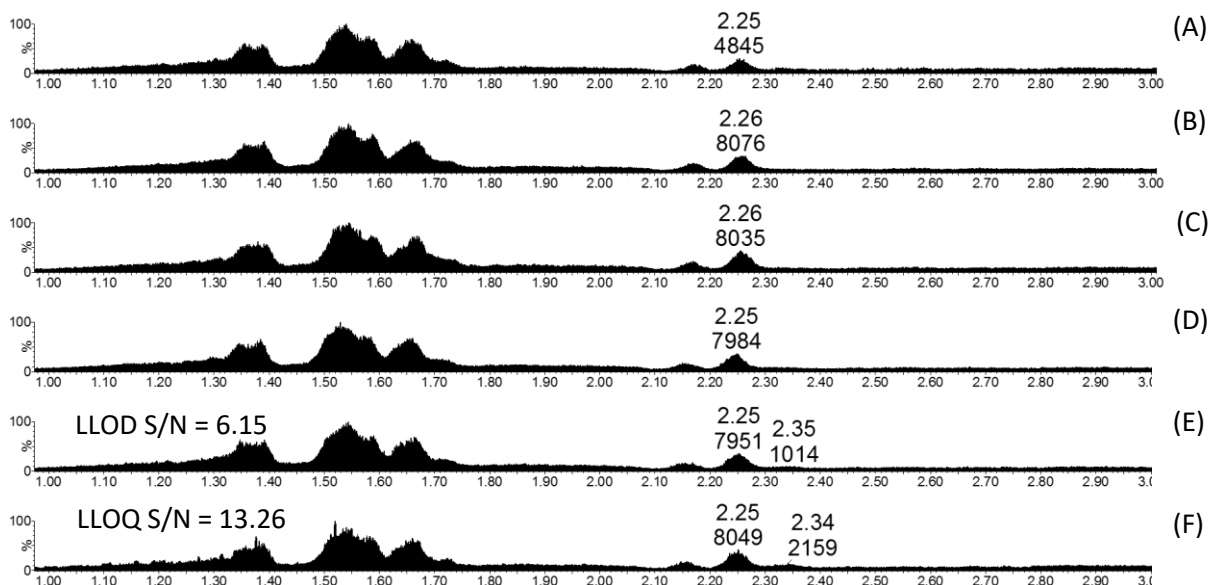


Figure 6-29 - RICCs of ACCUTRACE™ S10 fuel marker ( $t_R$  2.35 min) (A) 1 ppb (B) 5 ppb (C) 10 ppb (D) 25 ppb (E) 50 ppb and (F) 100 ppb, each with 500 ppb ACCUTRACE™ S10- $d_{21}$  IS ( $t_R$  2.25 min) in diesel fuel standards analysed using the SIR  $m/z$  550.8 and 571.9 method

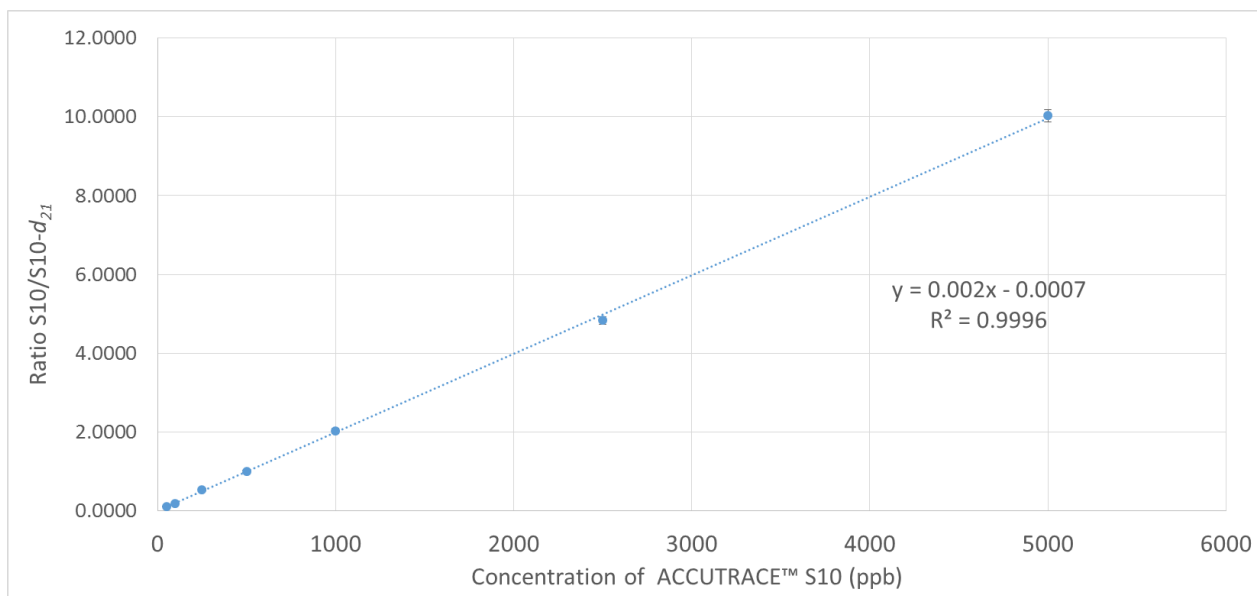


Figure 6-30 - Positive ion ESI ACCUTRACE™ S10 fuel marker and ACCUTRACE™ S10- $d_{21}$  IS calibration curve using ACCUTRACE™ S10 fuel marker standards (5, 10, 25, 50, 100, 250, 500, 1000, 2500, 5000 and 10000 ppb) each with 500 ppb ACCUTRACE™ S10- $d_{21}$  IS in diesel fuel, analysed using the SIR  $m/z$  550.8 and 571.9 method (number of replicates = 6, error bars =  $2\sigma$ )



Table 6-3 - Ratio of ACCUTRACE™ S10/S10- $d_{21}$  IS in diesel fuel

Concentration of ACCUTRACE S10 fuel marker (ppb)	Ratio of S10/S10- $d_{21}$ (Concentration of S10 - $d_{21}$ = 500 ppb)		Error (Standard deviation) (number of replicates =6)
	Calculated	Measured	
50	0.1	0.109	0.005
100	0.2	0.194	0.009
250	0.5	0.543	0.028
500	1	0.994	0.028
1000	2	2.023	0.070
2500	5	4.837	0.097
5000	10	10.028	0.161

A linear trend line with an  $R^2$  value 0.9996 suggests all standards are within one linear dynamic range up to 5000 ppb and further dilution of the higher concentration standards would improve the precision of the measurements. It should be noted that standards at 10000 ppb were found to be outside the linear dynamic range, suggesting the ULOQ is reached between 5000 and 10000 ppb although further work using a greater number of calibration standards in this range would be required to determine an exact ULOQ.

#### 6.3.1.2.6 S10 in fuel samples

Six pre-doped fuels with ACCUTRACE™ S10 fuel marker were also spiked with 10 ppm ACCUTRACE™ S10- $d_{21}$  IS and each fuel then screened using the same parameters as previous, both full scan and SIR (for  $m/z$  550.8 and 571.9) methods, allowing for acquisition of both full scan and SIR data. The data acquired for fuel 1 is shown in Figure 6-31. ACCUTRACE™ S10 fuel marker and ACCUTRACE™ S10- $d_{21}$  IS cannot be observed in the full scan base peak ion current chromatogram (BPICC) whereas in using the SIR method they can both be clearly observed. Additionally, the base fuel components within the doped fuels are not ionised by ESI due to the lack of basic functional groups and therefore are rendered invisible.

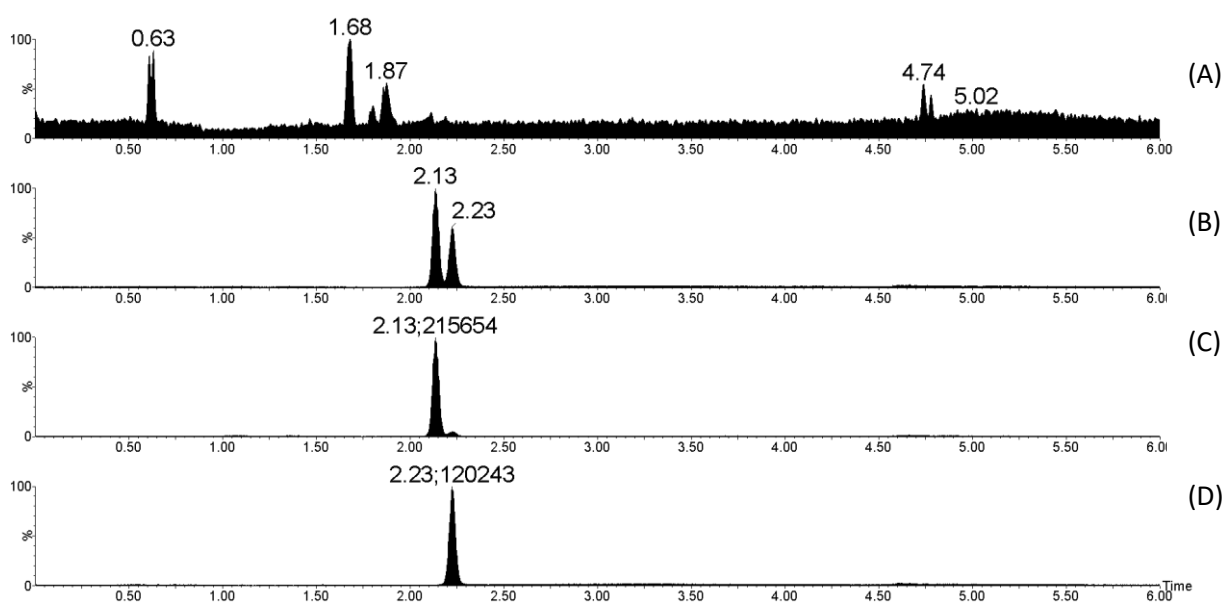


Figure 6-31 – (A)BPICC (B) RICC  $m/z$  550.8 and 571.9 (ACCUTRACE™ S10 fuel marker and ACCUTRACE™ S10- $d_{21}$  IS) (C) RICC  $m/z$  571.9(ACCUTRACE™ S10- $d_{21}$  IS) and (D) RICC  $m/z$  550.8 (ACCUTRACE™ S10 fuel marker) of fuel 1 pre-doped with ACCUTRACE™ S10 fuel marker and the addition of 10 ppm ACCUTRACE™ S10- $d_{21}$  IS, analysed using both the full scan and SIR ( $m/z$  550.8 and 571.9) methods

Again, the use of SIR provided increased sensitivity allowing detection of the ACCUTRACE™ S10 fuel marker and ACCUTRACE™ S10- $d_{21}$  IS. The peak areas were then used with the ratio calculation and calibration curve to calculate the concentration of ACCUTRACE™ S10 fuel marker in each fuel (Table 6-4).

This screening demonstrated that the UHPSFC-MS method can be utilised with real fuel sample matrices for both detection and quantitation of ACCUTRACE™ S10 fuel marker.

Table 6-4 - Average concentration of ACCUTRACE™ S10 fuel marker in six fuels by positive ion ESI UHPSFC-MS with ACCUTRACE™ S10-*d*<sub>21</sub> IS

Fuel	Average Conc. S10 / ppm
1	5.57
2	5.26
3	5.76
4	5.69
5	4.68
6	5.71

## 6.4 Conclusions

Legacy GC-MS instrumentation was utilised with the Dow modified GC-MS method (40 min) to detect and quantify ACCUTRACE™ S10 fuel marker at 2.5 ppm immediately following cleaning of the ion source and ACCUTRACE™ S10 fuel marker was unable to be detected at tank dilutions level (25 ppb = 1%). The sensitivity and performance of the instrument rapidly deteriorated due to repeat fuel injections that result in an ion source changes every 6 analyses and a limit of quantitation (LOQ) of ~2 ppm. Modern 2D GC-MS systems, with the use of capillary flow Deans switch, can be used to overcome these issues and provide a robust analytical solution although 2D GC-MS is not readily available in industry so it not widely applicable.

A rapid and robust method was successfully developed on UHPSFC-MS to detect and quantify S10 fuel marker in fuel samples, with a limit of detection of 50 ppb (required quantitative level was 2.5 ppm) and a runtime of 8 minutes (~5 times faster than GC-MS). UHPSFC-MS is completely compatible with neat fuel injections containing S10 and the addition of the internal standard is sufficient to quantify S10 present with little or no source cleaning issues. Good separation and resolution of ACCUTRACE™ S10 fuel marker and ACCUTRACE™ S10-*d*<sub>21</sub> IS was obtained using a developed UHPSFC-SIR method. Six fuel samples containing S10 fuel marker were also analysed and the concentration of ACCUTRACE™ S10 fuel marker successfully determined.

## Chapter 6

Unexpected ionisation was observed by positive ion ESI due to the lack of obvious basic sites present in the ACCUTRACE™ S10 fuel marker. Positive ion APPI was expected to be favoured due to aromaticity of ACCUTRACE™ S10 fuel marker structure. The selectivity of positive ion ESI reduced the complexity of the data for detecting ACCUTRACE™ S10 fuel marker and ACCUTRACE™ S10- $d_{21}$  IS in doped fuels due to the lack of basic functional groups within base fuel components, meaning they are not ionised by ESI and not observed.

Unexpected chromatographic separation of ACCUTRACE™ S10 fuel marker and ACCUTRACE™ S10- $d_{21}$  IS was observed, this is believed to be related to the high number of deuterium atoms within the ACCUTRACE™ S10- $d_{21}$  IS molecule. Therefore the ACCUTRACE™ S10- $d_{21}$  IS should be regarded as a structural analogue rather than homologue/isotopologue.

### 6.5 Acknowledgements

I would like to thank Edward Wilmot for his initial GC-MS method development and then further collaboration with me on GC-MS analysis. Huge thanks also goes to John Langley and Julie Herniman for undertaking the UHPSFC-APPI+ MS analysis and to Maria Ashe for the molecular modelling. Also thanks to Jim Barker at Innospec Ltd for providing the samples for analysis.

### 6.6 Experimental

As the methods and materials for this project are standalone from the rest of the PhD, they are described below rather than in the experimental chapter

#### 6.6.1 Chemicals

Methanol [(LC-MS) grade] and dichloromethane [(HPLC) grade] were purchased from Thermo Fisher Scientific (Loughborough, U.K.). Food-grade carbon dioxide was purchased from BOC Special Gases. Ammonium acetate was purchased from Sigma-Aldrich (Gillingham, U.K.). ACCUTRACE™ S10 fuel marker, the deuterated internal standard, ACCUTRACE™ S10- $d_{21}$  IS, and a variety of pre-dosed ACCUTRACE™ S10 fuel samples were supplied by Innospec, Ltd. (Ellesmere Port, U.K.). Commercial diesel fuel (ACCUTRACE™ S10 fuel marker free) was purchased from a Shell U.K. Ltd local forecourt.

## 6.6.2 Sample preparation

### 6.6.2.1 ACCUTRACE™ S10 stock solution

A total of 0.0100 g of ACCUTRACE™ S10 fuel marker was dissolved in dichloromethane (10 g) to give a 1000 mg/kg (1000 ppm). (Powder commonly used in experiments as it ensured sample preparation was consistent with IS). Alternatively 25 µL of 20% ACCUTRACE™ S10 solution (in aromatic solvent) was dissolved in dichloromethane to give a total volume of 5 mL, *i.e.*, standard solution of 1000 µL/L (1000 ppm). These solutions were then used as the nominal working solution and further diluted with Methanol.

Samples were prepared in methanol to allow for direct infusion ESI-MS to also be undertaken. No effect on chromatography or detection limits was observed when solutions prepared in dichloromethane used (data not shown). Methanol was also used preferentially where possible due to safety concerns around dichloromethane, however dichloromethane solutions were required when adding to fuel matrices due to the immiscibility of methanol in fuel.

### 6.6.2.2 Internal standard (ACCUTRACE™ S10-*d*<sub>21</sub>) stock solution

A total of 0.00100 g of ACCUTRACE™ S10-*d*<sub>21</sub> IS was dissolved in dichloromethane to give a total mass of 10 mL, *i.e.*, standard solution of 1000 mg/kg (1000 ppm). This solution was then used as the nominal working solution and further diluted with Methanol.

Solvent choice is also accredited to aforementioned reasons and dichloromethane can also be utilised as required.

### 6.6.2.3 Calibration solution

ACCUTRACE™ S10 fuel marker calibration standards were prepared containing nominally 1, 5, 10, 25, 50, 100, 250, 500, 1000, 2500, 5000 and 10000 ppb of ACCUTRACE™ S10 fuel marker using volumetric dilution of the working solution (1000 mg/kg or µL/L in dichloromethane) in Methanol for analysis by positive ion ESI UHPSFC-MS. ACCUTRACE™ S10 fuel marker and ACCUTRACE™ S10-*d*<sub>21</sub> Internal standard calibration standards were prepared containing nominally 1, 5, 10, 25, 50, 100, 250, 500, 1000, 2500, 5000 and 10000 ppb of ACCUTRACE™ S10 fuel marker and 500 ppb of S10-*d*<sub>21</sub> internal standard, both using volumetric dilution of the working solutions (1000 mg/kg or 1000 µL/L) in Methanol (and also dichloromethane for addition to fuel matrix) for analysis by positive ion ESI UHPSFC-MS.

#### 6.6.2.4 Real fuel samples dosed with ACCUTRACE™ S10 fuel marker

Six commercial samples of a variety of fuels dosed with ACCUTRACE™ S10 fuel marker were supplied by Innospec Ltd, and these samples were then doped with a known concentration (10 ppm (10  $\mu$ L of 1000 ppm solution in dichloromethane)) of internal standard ACCUTRACE™ S10- $d_{21}$  for analysis by positive ion ESI UHPSFC–MS.

#### 6.6.3 ACCUTRACE™ S10 fuel marker GC-MS method (undertaken in conjunction with Edward Wilmot) (modified Dow method)

All analyses were undertaken using a ThermoQuest Trace™ GC 2000 coupled to Finnigan trace MS quadrupole mass spectrometer. A non-polar RTX-5 fused silica capillary column (30 m x 0.25 mm i.d., 0.25  $\mu$ m film thickness) was used. The carrier gas was helium (He) with a flow rate of 1.2 mL/min and initially 10  $\mu$ L splitless injections were introduced into a split/splitless injector port at 240 °C. The temperature program used was 40 °C for 5 min, ramped at a rate of 15 °C/min to 240 °C, then ramped at a rate of 20 °C/min to 320 °C, and held at the final temperature for 6 min.

70 eV EI mass spectra were acquired with an ion source temperature of 200 °C. Full scan data were acquired,  $m/z$  20 to 558, at a scan rate 2 scans per second and a solvent delay of 5 minutes was used. Xcalibur® software (version 2.0) was used to record and process data and then the NIST 2014 Mass Spectral Library (version 2.2) was used to compare individual compounds.

SIR was used to detect the base peak and molecular ion: SIR  $m/z$  455, 476, 532, and 553 (ACCUTRACE™ S10 fuel marker base peak, ACCUTRACE™ S10- $d_{21}$  base peak, ACCUTRACE™ S10 fuel marker molecular ion, and ACCUTRACE™ S10- $d_{21}$  molecular ion, respectively); dwell time, 0.03 s; and mass span, 0.5  $m/z$  units.

#### 6.6.4 ACCUTRACE™ S10 fuel marker UHPSFC-MS methods

All analyses were undertaken using an ACQUITY UPC<sup>2</sup> system (Waters, Manchester, U.K.) coupled to a Waters SQD2 (Waters, Manchester, U.K.) single quadrupole mass spectrometer.

##### 6.6.4.1 Positive ion APPI UHPSFC-MS (full scan) (undertaken by John Langley and Julie Herniman)

Separations were performed using an ACQUITY UPC<sup>2</sup> (Waters, Manchester, U.K.) with a Waters HSS C18 SB packed column, 1.8  $\mu$ m particle size, 3  $\times$  100 mm. The column was held at 40 °C in a column oven, and 2.0  $\mu$ L of each sample was injected.  $scCO_2$  with methanol co-solvent used for separation at a flow rate of 1.5 mL/min. The  $scCO_2$  back pressure of the system was set to 150 bar. A gradient

elution was performed using the method in Table 6-5 and a 1 min isocratic pre-run (30% methanol) was used for column equilibration.

Table 6-5 - 3 minute gradient elution parameters (30-40%)

Time/min.	Solvent A (CO <sub>2</sub> )/%	Solvent B (methanol)/%	Curve
0.00	70	30	
1.00	60	40	6
2.30	60	40	6

Positive ion APPI mass spectra were recorded using a single quadrupole mass spectrometer (SQD2) and APPI ionisation source (Waters, Manchester, U.K.) with the following conditions: repeller voltage, 1.0 kV; cone voltage, 50 V; extractor, 3.0 V; source temperature, 150 °C; cone gas flow 1 L/h, probe temperature, 550 °C; desolvation gas flow, 1000 L/h (nitrogen); and acquisition and data processing achieved using MassLynx, version 4.1. Mass spectra were acquired between  $m/z$  100 and 1000 at a scan rate of 6.66 scans/s (scan time of 0.15 s). An internal solvent manager (ISM, Waters, Manchester, U.K.) was used to introduce the make-up solvent, toluene at a flow rate of 0.45 mL/min

#### 6.6.4.2 Positive ion ESI UHPSFC-MS (full scan and SIR)

Separations were performed using an ACQUITY UPC<sup>2</sup> (Waters, Manchester, U.K.) with a Waters HSS C18 SB packed column, 1.8 µm particle size, 3 × 100 mm. The column was held at 40 °C in a column oven, and 2.0 µL of each sample was injected. *sc*CO<sub>2</sub> with methanol (25 mM ammonium acetate) co-solvent used for separation at a flow rate of 1.5 mL/min. The *sc*CO<sub>2</sub> back pressure of the system was set to 150 bar. A gradient elution was performed using the method in Table 6-6 and a 2 min isocratic pre-run (2% methanol + 25 mM ammonium acetate) was used for column equilibration.

Table 6-6 - 6 minute gradient elution parameters (2%-5%-40%)

Time/min.	Solvent A (CO <sub>2</sub> )/%	Solvent B (methanol + 25 mM ammonium acetate)/%	Curve
0.00	98	2	
3.15	95	5	6
4.00	60	40	11
5.00	98	2	11
6.00	98	2	6

Positive ion ESI mass spectra were recorded using a single quadrupole mass spectrometer (SQD2) and ESCi multimode ionisation source (Waters, Manchester, U.K.) with the following conditions: capillary voltage, 3.5 kV; cone voltage, 20 V; extractor, 3.0 V; source temperature, 150 °C; cone gas flow 50 L/h, desolvation temperature, 350 °C; desolvation gas flow, 650 L/h (nitrogen); and acquisition and data processing achieved using MassLynx, version 4.1. Mass spectra were acquired between  $m/z$  120 and 1000 at a scan rate of 5 scans/s (scan time of 0.20 s). An internal solvent manager (ISM, Waters, Manchester, U.K.) was used to introduce the make-up solvent, methanol (50  $\mu$ M ammonium acetate), at a flow rate of 0.5 mL/min.

SIR was used to detect the ammoniated ACCUTRACE™ S10 fuel marker  $[M + NH_4]^+$  and ammoniated internal standard ACCUTRACE™ S10- $d_{21}$   $[M + NH_4]^+$ ,  $m/z$  550.8 and 571.9, respectively. All parameters were the same as the full-scan method, and a dwell time of 0.010 s was used.

### 6.6.5 Molecular modelling (undertaken by Maria Ashe (current PhD student in Langley Research group))

The three-dimensional structures, electrostatic potential maps, and geometry optimizations were performed using Spartan'14, version 1.1.8 (Wavefunction, Inc., Irvine, CA, U.S.A.)<sup>294</sup>. The full geometry optimization (calculation of equilibrium geometry at the ground state) was undertaken using Becke's three-parameter<sup>295</sup> Lee–Yang–Parr<sup>296</sup> hybrid density functional theory method with 6-31G\*\* basis set<sup>297</sup> (B3LYP 6-31G\*\*). The structures were optimized *in vacuo*. The surface maps were generated using the same level of theory as used for the optimized molecules.







## Chapter 7 Concluding remarks and future work

### 7.1 Concluding remarks

This research was focussed on the development and application of novel analytical approaches for the characterisation of components within deposits (fuel filters and IDIDs on fuel injector) and deposit and non-deposit forming fuels from the field, using multiple chromatography and mass spectrometry techniques, in the hope that comparing and contrasting the complimentary data will provide a greater understanding of the chemistry of the deposits and the diesel fuel more generally. Additionally, using these techniques to identify any components that are known to currently cause performance issues or are recognised deposit precursors and attempt to identify other deposit precursors that may be currently unrecognised species involved in deposit formation.

Polar column GC-MS affords detection of hydrocarbons and fatty acid methyl esters in diesels, with manual comparison of GC traces only identifying major and some minor differences but the SpectralWorks AnalyzerPro<sup>®</sup> approach, allows creation of compound libraries for each individual fuel and a percentage similarity between two diesels highlighting significant differences or similarities meaning that an automated approach allows rapid, more robust, quantified differentiation, reducing errors and does not require a trained analyst.

UHPSFC offers rapid separation and a diesel-compatible, hexane-like CO<sub>2</sub> mobile phase and was used in conjunction with positive ion electrospray ionisation mass spectrometry (positive ion ESI MS) to detect thermally labile and relatively polar compounds that are undetectable by GC-MS, while providing selectivity as the hydrocarbons in the diesels are not ionised. This means that a high throughput of diesel samples with minimal sample preparation can be achieved that allows differences and similarities to be determined and potential deposit forming compounds can be identified.

A screening method was successfully developed for a selection of recognised deposit forming compounds meaning that samples were characterised and compared with each other to further understand the composition from both deposit and non-deposit forming fuels.

Through development of the positive ion ESI UHPSFC-MS screening method, FAMEs, FAME oxidation products, MAGs and SGs were identified and further confirmed by molecular formulae from positive ion ESI FT-ICR MS. While development of negative ion ESI UHPSFC-MS afforded detection of FFAs further confirmed by molecular formulae from negative ion ESI FT-ICR MS.

## Chapter 7

A novel positive ion ESI UHPSFC-MS detection method for fatty acid sterol esters (FASEs) in biodiesel and mineral diesel blends (diesel/biodiesel) was developed as part of the screening method, believed to be unseen previously in mineral diesel blends. FASEs were fully characterised (in D#1) using positive ion ESI UHPSFC MS/MS QqQ as only observed by positive ion ESI UHPSFC-MS method as  $[M + NH_4]^+$  and  $[M + H - \text{Fatty acid}]^+$  respectively, and not seen by positive ion ESI FT-ICR MS.

These findings demonstrate these analytical techniques afforded detection of problematic compounds; both recognised deposit precursor components/group of components and other currently unrecognised species which may be involved in deposit formation, adding to the knowledge and understanding of the current deposit issues.

This screening methodology was applied to characterise diesel fuels, affording many similarities and differences to be seen within deposit and non-deposit forming diesel fuels from the field. However, this screening methodology and the individual methods within it have multiple applications, not exclusively for deposit issues.

The novel diesel fuels component screening methodology was utilised for the characterisation of fuel filters and a IDIDs on a fuel injector tip. Deposit sample preparation/removal is known to be challenging and methods were successfully developed for each deposit type. FAMEs, FAME oxidation, MAGs, FFAs, SGs, FASEs as well as PIB, PPG and additional additives were observed within fuel filter samples (both solvent extract and solid residue). Results from the IDID on the injector tip were indicative of “non commercial” low molecular weight PIBSIs used in DCAs in combination with possible metal carboxylate salt IDIDs or aged fuel IDIDs due to the presence of saturated fatty acids. This demonstrates the screening method can be utilised for both fuels and multiple deposits types from the FIE.

FASEs are currently an unrecognised deposit-forming compound, however they were also observed in a blocked fuel filter residue (SS5), suggesting further research into their deposit forming potential is required.

From the screening methodology, two sets of analysis protocol flow trees (diesels and deposits) were devised to assist analysts with characterisation of deposit forming components in fuels (diesels, biodiesels); IDIDs and fuel filter deposits, as well as fuels more generally. They link analytical techniques to compounds, aiding understanding and suggesting methodologies for analysis for an end user in industry. The analyst flow (diesel/deposit) analysis protocol tree affords guidance suggesting analytical approaches to be utilised for an unknown diesel/biodiesel/deposit

sample. The diesel/deposit flow analysis protocol tree informs thought processes to improve future understanding and characterisation of diesels/deposits.

Further advancement of the analysis method for JFTOT rod deposits and associated fuels, firstly to validate previously unexpected observation of adipate by Patel<sup>29</sup> and to optimise JFTOT rod sample preparation methodologies, known to be problematic, with solvent washing found to be preferable to scraping.

A better understanding of the deposit issue should aid and inform the following:

- Remediation chemistries for deposit issues
- Improved engine performance/reduced engine performance issues
- Fuel production
- Compounds removed/added to limit issues and/or improve performance
- Possible emissions from fuels improved (if chemistries further understood)

A modified GC-MS method (40 min) was utilised with legacy GC-MS instrumentation to detect and quantify ACCUTRACE™ S10 fuel marker at required quantitative level 2.5 ppm immediately following cleaning of the ion source and ACCUTRACE™ S10 fuel marker was unable to be detected at tank dilutions level. The sensitivity and performance of the instrument rapidly deteriorated due to repeat fuel injections that result in an ion source changes every 6 analyses and a limit of quantitation of ~2 ppm. Solutions such as modern 2D GC-MS systems, with the use of capillary flow Deans switch can be used to overcome these issues, however are not widely available in industry.

A novel, quick and reliable method was successfully developed on UHPSFC-MS to detect and quantify S10 fuel marker in fuel samples, with a limit of detection of 50 ppb (required quantitative level was 2.5 ppm) and a runtime of 8 minutes (~5 times faster than GC-MS). UHPSFC-MS affords little or no source cleaning issues and good compatibility with neat fuel injections containing S10. ACCUTRACE™ S10 fuel marker and ACCUTRACE™ S10-*d*<sub>21</sub> IS were successfully separated and resolved to a good standard using a developed UHPSFC-SIR method. Six fuel samples containing S10 fuel marker were also analysed and the concentration of ACCUTRACE™ S10 fuel marker successfully determined, with the addition of the internal standard to quantify S10 present.

Positive ion APPI was expected to be favoured due to aromaticity of ACCUTRACE™ S10 fuel marker structure and the lack of obvious basic sites present, however unexpected ionisation was observed by positive ion ESI. The complexity of the data was reduced due to the selectivity of positive ion ESI for detecting ACCUTRACE™ S10 fuel marker and ACCUTRACE™ S10-*d*<sub>21</sub> IS in doped fuels due to the lack of basic functional groups within base fuel components, meaning they are not ionised by ESI and not observed.

## Chapter 7

ACCUTRACE™ S10- $d_{21}$  IS should be regarded as a structural analogue rather than homologue/isotopologue due to unexpected chromatographic separation of ACCUTRACE™ S10 fuel marker and ACCUTRACE™ S10- $d_{21}$  IS, believed to be related to the high number of deuterium atoms within the ACCUTRACE™ S10- $d_{21}$  IS molecule.

This demonstrated an additional application of UHPSFC-MS for diesel fuels by the development of a quick and easy method for the detection and quantitation of the new fiscal fuel marker ACCUTRACE™ S10. This should assist the HMRC in their fight against fuel laundering as they report losses of £1.1 billion per annum at present, as well as limiting the damage to vehicles that results from the use of adulterated fuel.

## 7.2 Further work

To further improve the analysis of diesel/biodiesel fuels using these complementary analytical approaches, several areas of investigation are recommended.

Optimisation of all (both identifying components and component database comparison) SpectralWorks AnalyzerPro<sup>®</sup> parameters is required in order to get the best comparison possible. Additionally, an investigation into the proportional effects of different compounds within a fuel sample on percentage similarity obtained from SpectralWorks AnalyzerPro<sup>®</sup> software is required.

Brassicasterol glycoside should be added to the SGs method screen as it was found to be observed in rapeseed oil biodiesel in work by Bondioli *et al.*<sup>298</sup>.

Compounds of interest observed in the fuel filters should be further characterised using techniques such as MS/MS such as that undertaken for MAGs in the SS5 sample. Standards may also need to be analysed to fully verify assignments.

The screening methodologies should be utilised to analyse more deposit forming and non-deposit forming diesels from the field to examine a greater range of fuels with the profiles of the fuels investigated. To further improve analysis quantification should be undertaken using reference standards and certified reference materials where they exist. In addition, the screening methodologies should be utilised to analyse more deposits, particularly IDIDs on injector tips to observe a greater range of IDIDs. The data sets can then be compared and contrasted and used to build a library, adding to current understanding and knowledge of diesels/biodiesels, particularly their propensity to form deposits.

To achieve a more comprehensive picture of the issues arising currently, multiple engines with similar and different issues could be investigated. Samples from the entire FIE (the fuel, fuel filter and an injector tip) could be collected from each engine and analysed using the screening methodologies. The methodologies outlined within the deposit analysis protocol trees should be utilised to analyse the fuel, fuel filter and IDIDs on an injector tip from a problematic engine from the field to observe a full fuel flow through the FIE and the full picture of the IDID issue. The complimentary data sets acquired can then be compared and contrasted and see if links can be made.

Additional known deposit forming compounds<sup>28</sup> could be added to the screening methodologies. This might be achieved utilising the current analytical techniques but may also require development in a number of ways, depending on the compounds.

## Chapter 7

LLOD and LLOQ and SIR methods should be determined for each component in the screening methodology to determine the lowest level at which a component can be distinguished from being absent and provide confidence in the method.

Further development of the UHPSFC could be undertaken to see if additional compounds could be observed within samples. Such improvements could include different column chemistries, as well as varying modifier gradients *e.g.* elongated gradient to achieve greater separation of components.

Other mass spectrometry ionisation techniques should also be considered for analysis of fuels, deposits and associated samples including atmospheric pressure ionisation techniques such as APPI or other selective ionisation techniques to further develop the analytical approach for detection of a broader range of compounds *e.g.* non polar compounds and aromatics which ESI cannot, and APPI may provide improved data for some lipid species<sup>201, 225</sup>. Other techniques include ASAP (atmospheric solids analysis probe) or various surface mass spectrometry techniques to analyse deposits without sample prep, in-situ particularly if the sample is hard to remove from its location of origin.

Further compounds of interest (possible deposit forming compounds or others found to be of interest) or different analytical techniques to detect new compounds of interest that are added to the diesel fuels component screening method should be added to the analyst flow (diesel) analysis protocol tree and analyst flow (deposit) analysis protocol tree to further increase their potential as reference tools for unknown diesel/biodiesel and deposit analysis respectively.

In utilising the deposit analysis protocol trees for multiple different fuels, fuel filters and injector tips (IDIDs) the scope of the methodology will be assessed (and changes made as required) for many different deposit types and analysis methods.

The diesel and deposit analysis protocol trees could be trialled in industry (*i.e.* Innospec) with feedback collected to improve the usability and further develop the reference tool.

FASEs have not previously been identified as a known deposit-forming compound, although given their chemistry and other related known deposit forming compounds (FFAs and SGs) further research to investigate their deposit forming potential is recommended. FASEs have not previously been detected within mineral diesel blends (with biodiesel), however much research has been undertaken to characterise FASEs in vegetable oils and biodiesels. Therefore, further research to explore their presence in mineral diesel blends is recommended.



Sterols produced by the transesterification of FASEs are likely to be present after processing during production, this should be investigated and if found to be present should also be incorporated into the screening method.

Further investigation is required into the source of adipates on JFTOT rods including have adipates been observed in JFTOT rods following AVTUR testing.

Further work would need to be undertaken to explore the sample preparation methods further as only one set of JFTOT rods were provided meaning it was difficult to make a fair comparison of the two sample preparation methods. Ideally this work would be replicated in reverse with identical JFTOT rods (scraping followed by solvent washing) or ideally two sets of identical JFTOT rods acquired (scrape one set, solvent wash the other) for a direct fair comparison to be made of the data acquired.

Development of a (non-polar column) GC-MS SIR method for the detection of DEHA for trace analysis of adipates as it would result in improved sensitivity and selectivity

To further improve the UHPSFC-MS for the detection and quantitation of ACCUTRACE™ S10 fuel marker in low-duty fuels, several areas of investigation are recommended.

The use of tandem MS, particularly selective reaction monitoring (SRM), could be used to further improve LLOD and LLOQ, to ensure tank dilution levels at 25 ppb were obtained. This could be achieved using SRM for transitions from precursor ion of both ACCUTRACE™ S10 fuel marker and ACCUTRACE™ S10-*d*<sub>21</sub> IS to *m/z* 243 (trityl product ion).

The LLOD, LLOQ and ULOQ need to be determined exactly using a greater number of calibration standards within the regions of interest.

To work towards the UHPSFC-MS method being certified for use by Energy Institute or ASTM for the detection and quantitation of ACCUTRACE™ S10 fuel marker in low-duty fuels.

To further improve chromatographic separation of the two peaks, ACCUTRACE™ S10 fuel marker and ACCUTRACE™ S10-*d*<sub>21</sub> IS respectively, to aid peak area identification for quantitation.



## Appendix A Conferences, courses and seminars attended

### Conferences attended:

14th International Symposium on Hyphenated Techniques in Chromatography and Separation Technology (HTC-14), Ghent, Belgium, 27<sup>th</sup> - 29<sup>th</sup> January 2016.

37th British Mass Spectrometry Society (BMSS) Annual Meeting, Eastbourne, UK, 13<sup>th</sup> - 15<sup>th</sup> September, 2016.

Emerging Separation Technologies, Burlington House, London, UK, 30<sup>th</sup> March, 2014.

38th BMSS annual meeting, Manchester, UK, 5<sup>th</sup> - 7<sup>th</sup> September 2017. Poster presentation: "Analysis of diesel and components *via* GC-MS and UHPSFC-MS".

Petroanalysis conference, Energy Institute, London, UK, 17<sup>th</sup> November 2017. Poster presentation: "Analysis of diesel and components *via* GC-MS and UHPSFC-MS".

PEFTEC 2017, Antwerp, Belgium, 29<sup>th</sup> – 30<sup>th</sup> November 2017. Poster presentation: "Analysis of diesel and components *via* GC-MS and UHPSFC-MS".

### Courses attended:

(Ion mobility tutorial - Dr Mike Morris (Waters) 11<sup>th</sup> November 2015)

**Short course on Hyphenated Techniques in Supercritical Fluid Chromatography as part of HTC-14**, Ghent, Belgium, 26th January 2016.

**BMSS Introduction to Mass Spectrometry Short Course as part of 37th BMSS Annual Meeting**, Eastbourne, UK, 12<sup>th</sup> - 13<sup>th</sup> September, 2016.

### Seminars attended:

Dr Mike Morris (Waters) – "MS in medicine", 11<sup>th</sup> November 2015.

Prof Rob Beynon (University of Liverpool) – "Proteomics of Sex", 14<sup>th</sup> December 2016.

## Appendix A

Tom Lynch (BP) – “Fuel, Fun and Formula 1: “Using Analysis to Solve Problems in the Petroleum Industry”, 24<sup>th</sup> November 2017.

Waters Webinar series “Fundamentals of Mass Detection”, 30<sup>th</sup> August, 6<sup>th</sup> and 13<sup>th</sup> September 2018.

Prof Hiroaki Suga (Tokyo University) – “The RaPID way to discover bioactive macrocyclic peptides”, 10<sup>th</sup> October 2018





## Bibliography

1. Snape, I.; Harvey, P. M.; Ferguson, S. H.; Rayner, J. L.; Reville, A. T., Investigation of evaporation and biodegradation of fuel spills in Antarctica. I. A chemical approach using GC-FID. *Chemosphere* 2005, 61 (10), 1485-94.
2. Alberici, R. M.; Simas, R. C.; de Souza, V.; de Sá, G. F.; Daroda, R. J.; Eberlin, M. N., Analysis of fuels via easy ambient sonic-spray ionization mass spectrometry. *Anal. Chim. Acta* 2010, 659 (1–2), 15-22.
3. Barman, B. N.; Cebolla, V. L.; Membrado, L., Chromatographic techniques for petroleum and related products. *Crit. Rev. Anal. Chem.* 2000, 30 (2-3), 75-120.
4. Briker, Y.; Ring, Z.; Iacchelli, A.; McLean, N.; Rahimi, P. M.; Fairbridge, C.; Malhotra, R.; Coggiola, M. A.; Young, S. E., Diesel Fuel Analysis by GC-FIMS: Aromatics, n-Paraffins, and Isoparaffins. *Energy & Fuels* 2001, 15 (1), 23-37.
5. Johnson, K. J.; Rose-Pehrsson, S. L.; Morris, R. E., Monitoring Diesel Fuel Degradation by Gas Chromatography–Mass Spectroscopy and Chemometric Analysis. *Energy & Fuels* 2004, 18 (3), 844-850.
6. Cho, Y.; Islam, A.; Ahmed, A.; Kim, S., Application of comprehensive 2D GC-MS and APPI FT-ICR MS for more complete understanding of chemicals in diesel fuel. *Mass Spectrometry Letters* 2012, 3 (2), 43-46.
7. Thiébaud, D., Separations of petroleum products involving supercritical fluid chromatography. *J. Chromatogr. A* 2012, 1252, 177-188.
8. Li, W.; Malik, A.; Lee, M. L.; Jones, B. A.; Porter, N. L.; Richter, B. E., Group-Type Separation of Diesel Fuels Using Packed Capillary Column Supercritical Fluid Chromatography. *Anal. Chem.* 1995, 67 (3), 647-654.
9. Qian, K.; Diehl, J.; Dechert, G.; DiSanzo, F., The coupling of supercritical fluid chromatography and field ionization time-of-flight high-resolution mass spectrometry for rapid and quantitative analysis of petroleum middle distillates. *Eur. J. Mass Spectrom.* 2004, 10 (2), 187.
10. Rostad, C. E., Screening of Polar Components of Petroleum Products by Electrospray Ionization Mass Spectrometry. *Energy & Fuels* 2005, 19 (3), 992-997.
11. Hughey, C. A.; Hendrickson, C. L.; Rodgers, R. P.; Marshall, A. G., Elemental Composition Analysis of Processed and Unprocessed Diesel Fuel by Electrospray Ionization Fourier Transform Ion Cyclotron Resonance Mass Spectrometry. *Energy & Fuels* 2001, 15 (5), 1186-1193.
12. Rodgers, R.; Blumer, E. N.; Freitas, M. A.; Marshall, A. G., Complete Compositional Monitoring of the Weathering of Transportation Fuels Based on Elemental Compositions from Fourier Transform Ion Cyclotron Resonance Mass Spectrometry. *Environmental Science & Technology* 2000, 34 (9), 1671-1678.

## Bibliography

13. Tose, L. V.; Murgu, M.; Vaz, B. G.; Romão, W., Application of Atmospheric Solids Analysis Probe Mass Spectrometry (ASAP-MS) in Petroleomics: Analysis of Condensed Aromatics Standards, Crude Oil, and Paraffinic Fraction. *J. Am. Soc. Mass. Spectrom.* 2017, 28 (11), 2401-2407.
14. Wu, C.; Qian, K.; Walters, C. C.; Mennito, A., Application of atmospheric pressure ionization techniques and tandem mass spectrometry for the characterization of petroleum components. *Int. J. Mass spectrom.* 2015, 377 (Supplement C), 728-735.
15. Maire, F.; Neeson, K.; Denny, R.; McCullagh, M.; Lange, C.; Afonso, C.; Giusti, P., Identification of Ion Series Using Ion Mobility Mass Spectrometry: The Example of Alkyl-Benzothiophene and Alkyl-Dibenzothiophene Ions in Diesel Fuels. *Anal. Chem.* 2013, 85 (11), 5530-5534.
16. Evans, P.; Wolff-Briche, C.; Fairman, B., High accuracy analysis of low level sulfur in diesel fuel by isotope dilution high resolution ICP-MS, using silicon for mass bias correction of natural isotope ratios. *J. Anal. At. Spectrom.* 2001, 16 (9), 964-969.
17. Caumette, G.; Lienemann, C.-P.; Merdrignac, I.; Bouyssiere, B.; Lobinski, R., Element speciation analysis of petroleum and related materials. *J. Anal. At. Spectrom.* 2009, 24 (3), 263-276.
18. Harvey, S. D.; Jarman, K. H.; Moran, J. J.; Sorensen, C. M.; Wright, B. W., Characterization of diesel fuel by chemical separation combined with capillary gas chromatography (GC) isotope ratio mass spectrometry (IRMS). *Talanta* 2012, 99, 262-9.
19. Cody, R. B., Observation of Molecular Ions and Analysis of Nonpolar Compounds with the Direct Analysis in Real Time Ion Source. *Anal. Chem.* 2008, 81 (3), 1101-1107.
20. Manova, R. K.; Joshi, S.; Debrassi, A.; Bhairamadgi, N. S.; Roeven, E.; Gagnon, J.; Tahir, M. N.; Claassen, F. W.; Scheres, L. M.; Wennekes, T.; Schroen, K.; van Beek, T. A.; Zuilhof, H.; Nielen, M. W., Ambient surface analysis of organic monolayers using direct analysis in real time Orbitrap mass spectrometry. *Anal. Chem.* 2014, 86 (5), 2403-11.
21. Okumura, L. L.; Stradiotto, N. R., Simultaneous Determination of Quinoline and Pyridine Compounds in Gasoline and Diesel by Differential Pulse Voltammetry. *Electroanalysis* 2007, 19 (6), 709-716.
22. Edwards, J. C., A Review of Applications of NMR Spectroscopy in the Petroleum Industry. *Spectroscopic Analysis of Petroleum Products and Lubricants*, K Nadkami, ed. ASTM International 2011, 9, 423-472.
23. Diehl, B.; Randel, G., Analysis of biodiesel, diesel and gasoline by NMR spectroscopy – A quick and robust alternative to NIR and GC. *Lipid Technology* 2007, 19 (11), 258-260.
24. Breikreitz, M. C.; Raimundo Jr, I. M.; Rohwedder, J. J.; Pasquini, C.; Dantas Filho, H. A.; José, G. E.; Araújo, M. C., Determination of total sulfur in diesel fuel employing NIR spectroscopy and multivariate calibration. *Analyst* 2003, 128 (9), 1204-1207.
25. Santos Jr, V. O.; Oliveira, F. C. C.; Lima, D. G.; Petry, A. C.; Garcia, E.; Suarez, P. A. Z.; Rubim, J. C., A comparative study of diesel analysis by FTIR, FTNIR and FT-Raman spectroscopy using PLS and artificial neural network analysis. *Anal. Chim. Acta* 2005, 547 (2), 188-196.



26. Barker, J.; Langley, G. J.; Richards, P., Insights into Deposit Formation in High Pressure Diesel Fuel Injection Equipment. SAE International 2010, 2243, 1-21.
27. Trobaugh, C.; Burbrink, C.; Zha, Y.; Whitacre, S.; Corsi, C.; Blizard, N. Internal Diesel Injector Deposits: Theory and Investigations into Organic and Inorganic Based Deposits; SAE Technical Paper: 2013.
28. Berndt, S.; Schümann, U.; Sadlowski, T.; Buchholz, B., Development of a Laboratory Test for the Deposit Forming Tendency of Diesel Fuels. *ATZoffhighway worldwide* 2018, 11 (1), 50-55.
29. Barker, J.; Reid, J.; Smith, S. A.; Snape, C.; Scurr, D.; Langley, G.; Patel, K.; Carter, A.; Laphorn, C.; Pullen, F., The Application of New Approaches to the Analysis of Deposits from the Jet Fuel Thermal Oxidation Tester (JFTOT). *SAE International Journal of Fuels and Lubricants* 2017, 10 (2017-01-2293).
30. Barker, J.; Richard, P.; Snape, C.; Meredith, W., Diesel Injector Deposits-An Issue That Has Evolved with Engine Technology. 2011.
31. Barker, J.; Richards, P.; Scurr, D., Diesel deposits. *TAE international* 2013, 16 (1), 1.
32. Lau, K.; Junk, R.; Klingbeil, S.; Schümann, U.; Streibel, T., Analysis of Internal Common Rail Injector Deposits via Thermodesorption Photon Ionization Time of Flight Mass Spectrometry. *Energy & Fuels* 2015, 29 (9), 5625-5632.
33. Barker, J.; Snape, C.; Scurr, D., Information on the Aromatic Structure of Internal Diesel Injector Deposits From Time of Flight Secondary Ion Mass Spectrometry (ToF-SIMS). 2014.
34. Schwab, S.; Bennett, J.; Dell, D.; Galante-Fox, J.; Kulinoowski, A.; Miller, K., Internal injector deposits in high pressure common rail diesel engines. *SAE international* 2010, 3 (2), 865.
35. Quigley, R.; Barbour, R.; Fahey, E.; Arters, D.; Wetzl, J., A study of the internal diesel injector deposit phenomenon. *TAE international* 2010, 15 (01), 152.
36. Barker, J.; Reid, J.; Piggott, M.; Fay, M., The Characterisation of Diesel Internal Injector Deposits by Focused Ion-Beam Scanning Electron Microscopy (FIB-SEM), Transmission Electron Microscopy (TEM), Atomic Force Microscopy and Raman Spectroscopy. 2015, 2015-01-1826.
37. Barker, J.; Reid, J., Injector and Fuel System Deposits. In *10th International Colloquium Fuels Conventional and Future Energy for automobiles*, Technische Akademie Esslingen in Stuttgart/Ostfildern., 2015.
38. Barker, J.; Reid, J.; Snape, C.; Scurr, D.; Meredith, W., Spectroscopic Studies of Internal Injector Deposits (IDID) Resulting from the Use of Non-Commercial Low Molecular Weight Polyisobutylenesuccinimide (PIBSI). *SAE International Journal of Fuels and Lubricants* 2014, 7 (2014-01-2720), 762-770.
39. Barker, J.; Snape, C.; Scurr, D., A Novel Technique for Investigating the Characteristics and History of Deposits Formed Within High Pressure Fuel Injection Equipment. *SAE International* 2012, 5 (3), 1155-1164.

## Bibliography

40. Barker, J.; Richards, P.; Snape, C.; Meredith, W., A novel technique for investigating the nature and origins of deposits formed in high pressure fuel injection equipment. 2009.
41. Barker, J.; Richards, P.; Pinch, D.; Cheeseman, B., Temperature programmed oxidation as a technique for understanding diesel fuel system deposits. SAE international 2010, 3 (2), 85-99.
42. Speight, J. G., Handbook of Petroleum Product Analysis. 2002.
43. Chevron Diesel Fuels Technical Review; California, 2007.
44. Maugeri, L., Squeezing more oil from the ground. Scientific American 2009, 301 (4), 56-63.
45. Gary, J. H.; Handwerk, G. E., Petroleum refining : technology and economics. 4th ed.; M. Dekker: New York, 2001; p xii, 441 p.
46. Bauer, H.; Dietsche, K.; Jager, T.; Kimberley, W., Diesel-engine management: Systems and components. Third ed.; Robert Bosch GmbH: Germany, 2004.
47. Hart, L., A Simple Guide to Oil Refining. ExxonMobil, Ed. 2006.
48. Rood, D., A practical guide to the care, maintenance, and troubleshooting of capillary gas chromatographic systems. 2nd enl. and rev. ed.; Hüthig: Heidelberg, 1995; p 323.
49. Haddad, R.; Regiani, T.; Klitzke, C. F.; Sanvido, G. B.; Corilo, Y. E.; Augusti, D. V.; Pasa, V. M. D.; Pereira, R. C. C.; Romão, W.; Vaz, B. G.; Augusti, R.; Eberlin, M. N., Gasoline, Kerosene, and Diesel Fingerprinting via Polar Markers. Energy & Fuels 2012, 26 (6), 3542-3547.
50. American Society for Testing Materials, ASTM D975-11, Standard Specification for Diesel Fuel Oils. ASTM International: West Conshohocken, PA, 2011.
51. European Committee for Standardization, EN 590: 2013. Automotive Fuels Diesel Requirements and Test Methods. CEN Brussels, Belgium: 2013.
52. Barker, J.; Richards, P.; Goodwin, M.; Wooler, J., Influence of high injection pressure on diesel fuel stability: a study of resultant deposits. SAE international 2009, 1877 (1), 1.
53. Richards, P., Automotive Fuels Reference Book. 3 ed.; SAE International: Warrendale PA, 2014.
54. Asmus, A. F.; Wellington, B. F., Diesel engines and fuel systems. 1995.
55. Changes in Diesel Fuel The Service Technician's Guide to Compression Ignition Fuel Quality.
56. Suppes, G. J.; Rui, Y.; Rome, A. C.; Chen, Z., Cetane-Improver Analysis and Impact of Activation Energy on the Relative Performance of 2-Ethylhexyl Nitrate and Tetraethylene Glycol Dinitrate. Industrial & Engineering Chemistry Research 1997, 36 (10), 4397-4404.
57. Rezende, M. J.; Perruso, C. R.; Azevedo, D. d. A.; Pinto, A. C., Characterization of lubricity improver additive in diesel by gas chromatography–mass spectrometry. J. Chromatogr. A 2005, 1063 (1), 211-215.

58. Bubálik, M.; Beck, Á.; Baladincz, J.; Hancsók, J., Development of deposit control additives for diesel fuel. *Petroleum & Coal* 2009, 51 (3), 167-175.
59. Mortier, R. M.; Fox, M. F.; Orszulik, S. T., *Chemistry and technology of lubricants*. 3rd ed.; Springer: Dordrecht ; New York, 2010; p xiv, 560 p.
60. Groysman, A., *Corrosion in systems for storage and transportation of petroleum products and biofuels: identification, monitoring and solutions*. Springer Science & Business Media: 2014.
61. ATC Fuel Additives: Use and Benefit; 09/2013, 2013.
62. Passman, F., Microbial contamination and its control in fuels and fuel systems since 1980—a review. *International Biodeterioration & Biodegradation* 2013, 81, 88-104.
63. Botros, M. G. Cloud point depressants for middle distillate fuels. 6,143,043, 7/11/2000, 2002.
64. Elvers, B., *Ullmann's Energy, 3 Volume Set: Resources, Processes, Products*. John Wiley & Sons: 2015; Vol. 2.
65. United Nations. Statistical, D., *Glossary of environment statistics / Department for Economic and Social Information and Policy Analysis*. United Nations: New York, 1997.
66. Fuel Quality. [http://ec.europa.eu/clima/policies/transport/fuel/index\\_en.htm](http://ec.europa.eu/clima/policies/transport/fuel/index_en.htm) (accessed 13/11/2015).
67. Rodrigue, J.-P., *The Geography of Transport Systems* 4 ed.; Routledge: New York 2017.
68. Künzli, N.; Kaiser, R.; Medina, S.; Studnicka, M.; Chanel, O.; Filliger, P.; Herry, M.; Horak, F.; Puybonnieux-Textier, V.; Quénel, P.; Schneider, J.; Seethaler, R.; Vergnaud, J. C.; Sommer, H., Public-health impact of outdoor and traffic-related air pollution: a European assessment. *The Lancet* 2000, 356 (9232), 795-801.
69. SMMT European engine emission standards. <http://www.smmt.co.uk/industry-topics/environment/intro/european-engine-emission-standards/> (accessed 13/11/2015).
70. Vehicle Emissions Control. [https://en.wikipedia.org/wiki/Vehicle\\_emissions\\_control](https://en.wikipedia.org/wiki/Vehicle_emissions_control) (accessed 13/11/2015).
71. AA Euro Car Emission Standards. [https://www.theaa.com/motoring\\_advice/fuels-and-environment/euro-emissions-standards.html](https://www.theaa.com/motoring_advice/fuels-and-environment/euro-emissions-standards.html) (accessed 13/11/2015).
72. Miller, P.; Solomon, M., *A Brief History of Technology-Forcing Motor Vehicle Regulations*. 2009.
73. Fiebig, M.; Wiartalla, A.; Holderbaum, B.; Kiesow, S., Particulate emissions from diesel engines: correlation between engine technology and emissions. *Journal of Occupational Medicine and Toxicology (London, England)* 2014, 9, 6-6.

## Bibliography

74. Andersson, J.; Martini, G.; Mayer, A. In History and Future of Particle Number Legislation in Europe, 19th ETH-Conference on Combustion Generated Nanoparticles ETH Zentrum, Zürich, Switzerland, July 1st 2015; ETH Zentrum, Zürich, Switzerland, 2015.
75. RAC Euro 1 to Euro 6 – find out your vehicle's emissions standard. <https://www.rac.co.uk/drive/advice/emissions/euro-emissions-standards/> (accessed 21/02/2018).
76. Kassel, R.; Leonard, J. H. Ultrafine Particulate Matter and the Benefits of Reducing Particle Numbers in the United States; 2013.
77. Zanobetti, A.; Schwartz, J., The Effect of Fine and Coarse Particulate Air Pollution on Mortality: A National Analysis. *Environ. Health Perspect.* 2009, 117 (6), 898-903.
78. Williams, M.; Minjares, R., A technical summary of Euro 6/VI vehicle emission standards. ICCT International council on clean transportation 2016.
79. Barrett, S. R.; Speth, R. L.; Eastham, S. D.; Dedoussi, I. C.; Ashok, A.; Malina, R.; Keith, D. W., Impact of the Volkswagen emissions control defeat device on US public health. *Environmental Research Letters* 2015, 10 (11), 114005.
80. DieselNet Emission Standards. <https://www.dieselnet.com/standards/eu/ld.php> (accessed 26/02/2018).
81. United States Emission Standards. [https://en.wikipedia.org/wiki/United\\_States\\_emission\\_standards](https://en.wikipedia.org/wiki/United_States_emission_standards) (accessed 16/11/2015).
82. Cook, S.; Richards, P., Possible influence of high injection pressure on diesel fuel stability: a review and preliminary study. *SAE international* 2009, 01 (1878).
83. The Renewable Transport Fuels and Greenhouse Gas Emissions Regulations 2018 2018.
84. The Renewable Transport Fuel Obligations Order. In *Transport: Energy, Sustainable and Renewable Fuels*, 2007; Vol. 3072.
85. Barker, J., Langley, G., and Richards, P., Insights into deposit formation in high pressure diesel fuel injection equipment. *SAE Technical Papers* 2010, 2010-01-2243.
86. Jääskeläinen, H. Fuel Property Testing: Sulfur. [https://www.dieselnet.com/tech/fuel\\_diesel\\_sulfur.php#d7039](https://www.dieselnet.com/tech/fuel_diesel_sulfur.php#d7039) (accessed 16/11/2015).
87. Agarwal, A. K., Biofuels (alcohols and biodiesel) applications as fuels for internal combustion engines. *Prog. Energy Combust. Sci.* 2007, 33 (3), 233-271.
88. Mata, T. M.; Martins, A. A.; Caetano, N. S., Microalgae for biodiesel production and other applications: A review. *Renewable and Sustainable Energy Reviews* 2010, 14 (1), 217-232.
89. Demirbas, A., Progress and recent trends in biodiesel fuels. *Energy Convers. Manage.* 2009, 50 (1), 14-34.

90. Balat, M.; Balat, H., A critical review of bio-diesel as a vehicular fuel. *Energy Convers. Manage.* 2008, 49 (10), 2727-2741.
91. Atadashi, I. M.; Aroua, M. K.; Aziz, A. A., High quality biodiesel and its diesel engine application: A review. *Renewable and Sustainable Energy Reviews* 2010, 14 (7), 1999-2008.
92. Ratsameepakai, W. *Application of Separation Science and Mass Spectrometry to the Analysis of Fuels*. University of Southampton, Southampton, 2016.
93. Agarwal, A. K.; Das, L. M., Biodiesel Development and Characterization for Use as a Fuel in Compression Ignition Engines. *Journal of Engineering for Gas Turbines and Power* 2000, 123 (2), 440-447.
94. Phan, A. N.; Phan, T. M., Biodiesel production from waste cooking oils. *Fuel* 2008, 87 (17), 3490-3496.
95. Pinto, A. C.; Guarieiro, L. L. N.; Rezende, M. J. C.; Ribeiro, N. M.; Torres, E. A.; Lopes, W. A.; Pereira, P. A. D.; de Andrade, J. B., Biodiesel: An overview. *Journal of the Brazilian Chemical Society* 2005, 16 (6b), 1313-1330.
96. Wicking, C. C. *The Development and Application of Chromatography and Mass Spectrometry Techniques for the Analysis of Biodiesel and Fuel Related Compounds*. University of Southampton, Southampton, 2013.
97. Enweremadu, C. C.; Mbarawa, M. M., Technical aspects of production and analysis of biodiesel from used cooking oil—A review. *Renewable and Sustainable Energy Reviews* 2009, 13 (9), 2205-2224.
98. Smith, H.; Winfield, J.; Thompson, L., *The market for biodiesel production from used cooking oils and fats, oils and greases in London*. 2013.
99. *Water Industry Act 1991*. 1991.
100. Taylor, M., 'Total monster': fatberg blocks London sewage system. *The Guardian* 12/09/2017, 2017.
101. Lapuerta, M.; Rodríguez-Fernández, J.; Agudelo, J. R., Diesel particulate emissions from used cooking oil biodiesel. *Bioresour. Technol.* 2008, 99 (4), 731-740.
102. Toop, G.; Alberici, S.; Spoettle, M.; van Steen, H. *Trends in UCO market*; 2013.
103. Jeevahan, J.; Mageshwaran, G.; Joseph, G. B.; Raj, R. B. D.; Kannan, R. T., Various strategies for reducing Nox emissions of biodiesel fuel used in conventional diesel engines: A review. *Chem. Eng. Commun.* 2017, 204 (10), 1202-1223.
104. Liaquat, A. M.; Masjuki, H. H.; Kalam, M. A.; Fattah, I. M. R., Impact of biodiesel blend on injector deposit formation. *Energy* 2014, 72, 813-823.
105. Cody, R. B., Observation of molecular ions and analysis of nonpolar compounds with the direct analysis in real time ion source. *Anal. Chem.* 2009, 81 (3), 1101-7.

## Bibliography

106. Get mobile. <https://bhsagriculture.wikispaces.com/Get+Mobile> (accessed 26/11/2015).
107. Corkwell, K. Deposit Issues with Modern Diesel Engines.
108. Posada Sanchez, F.; Bandivadekar, A.; German, J., Estimated cost of emission reduction technologies for light-duty vehicles. The International Council on Clean Transportation. Washington DC (USA) 2012.
109. Denso Diesel Fuel Injectors Common Rail. <http://www.densoautoparts.com.au/products/diesel-fuel-injectors/commonrail.aspx> (accessed 25/11/2015).
110. Common Rail. [https://en.wikipedia.org/wiki/Common\\_rail](https://en.wikipedia.org/wiki/Common_rail) (accessed 26/11/2015).
111. What is Common Rail Direct Injection (CRD)? <http://alternativefuels.about.com/od/dieselbiodieselvehicles/a/diesellcrd.htm> (accessed 26/11/2015).
112. Dallmann, T.; Menon, A., Technology Pathways for Diesel Engines Used in Non-Road Vehicles and Equipment. International Council on Clean Transportation (ICCT): Washington, DC, USA 2016.
113. Posada, F.; Chambliss, S.; Blumberg, K., Costs of emission reduction technologies for heavy-duty diesel vehicles. ICCT White Paper 2016.
114. de Goede, S.; Barbour, R.; Velaers, A.; Sword, B.; Burton, D.; Mokheseng, K., The Effect of Near-Zero Aromatic Fuels on Internal Diesel Injector Deposit Test Methods. SAE International Journal of Fuels and Lubricants 2017, 10 (1), 163-183.
115. Edney, M. K.; Barker, J.; Reid, J.; Scurr, D. J.; Snape, C. E., Recent Advances in the Analysis of GDI and Diesel Fuel Injector Deposits. Fuel 2020, 272, 117682.
116. Schümann, U.; Berndt, S.; Cepelak, S.; Buchholz, B., Deposit Forming Tendency of Diesel Fuels in Injectors. ATZheavy duty worldwide 2020, 13 (2), 56-61.
117. Reid, J.; Cook, S.; Barker, J., Internal Injector Deposits From Sodium Sources. SAE International Journal of Fuels and Lubricants 2014, 7 (2014-01-1388), 436-444.
118. Fink, C.; Crusius, S.; Schümann, U.; Junk, R.; Harndorf, H. In Alteration of fuel properties at extreme conditions—Formation of deposits in common-rail injectors, 15. Internationales Stuttgarter Symposium, Springer: 2015; pp 1021-1032.
119. Barker, J.; Reid, J.; Smith, S. A.; Snape, C.; Scurr, D.; Piggott, M.; Fay, M.; Davies, A.; Parmenter, C.; Weston, N., Internal Injector Deposits (IDID). 2017.
120. Lacey, P.; Gail, S.; Kientz, J.; Benoist, G.; Downes, P.; Daveau, C., Fuel Quality and Diesel Injector Deposits. Journal of Fuels and Lubricants 2012, 5 (3), 182-195.
121. Urzędowska, W.; Stępień, Z., Prediction of threats caused by high FAME diesel fuel blend stability for engine injector operation. Fuel Process. Technol. 2016, 142, 403-410.

122. Arondel, M.; Rodeschini, H.; Lopes, M.; Dequenne, B., Fuel additives for reduction of internal diesel injectors deposits (IDID): A critical and priority route. SAE international 2012, 01 (1687).
123. Reid, J., Barker, J., Understanding Polyisobutylene Succinimides (PIBSI) and Internal Diesel Injector Deposits,. SAE Technical Paper 2013, 2013-01-2682.
124. Lubrizol Polyisobutylene Succinimides in Engine Oil. <https://www.lubrizol.com/CorporateResponsibility/ProductStewardship/PolyisobutyleneSuccinimides.html> (accessed 15/02/2016).
125. Corbett, P. J.; McIntosh, A. J.; Gee, M.; Hallett, J. P., Use of ionic liquids to minimize sodium induced internal diesel injector deposits (IDIDs). Molecular Systems Design & Engineering 2018, 3 (2), 397-407.
126. Schwab, S. D.; Fang, X. Fuel additives for treating internal deposits of fuel injectors. US009249769B1, 2016.
127. Simpson-Green, F.; Vaudrin, D. Method for cleaning deposits from an engine fuel delivery system. US008632638B2, 2014.
128. Joern, K.; Clayton, C. W.; Gee, M.; & Rimmer, J. Use of 2-ethylhexyl nitrate in combination with one or more detergents in a diesel fuel composition for the purpose of reducing internal diesel injector deposits (IDIDs) in a compression ignition combustion engine. 2017.
129. Panesar, A.; Martens, A.; Jansen, L.; Lal, S.; Ray, D.; Twilley, M. Development of a new Peugeot XUD9 10 hour cyclic test to evaluate the nozzle coking propensity of diesel fuels; 0148-7191; SAE Technical Paper: 2000.
130. Risberg, P. A.; Alfredsson, S., The Effect of Zinc and Other Metal Carboxylates on Nozzle Fouling. SAE International: 2016.
131. Ettre, L., Nomenclature for chromatography (IUPAC Recommendations 1993). Pure Appl. Chem. 1993, 65 (4), 819-872.
132. Ramsay, W., A Determination of the Amounts of Neon and Helium in Atmospheric Air. Proceedings of the Royal Society of London. Series A, Containing Papers of a Mathematical and Physical Character 1905, 76 (508), 111-114.
133. Tswett, M., Physikalisch-chemische Studien über das chlorophyll. Die Adsorptionen. Ber. Dtsch. Bot. Ges. 1906, 24 (316-323), 20.
134. McNair, H. M.; Miller, J. M.; Settle, F. A., Basic Gas Chromatography. Wiley: Hoboken, UNITED STATES, 2009.
135. Kirchner, J. G., Thin-Layer Chromatography—Yesterday, Today, and Tomorrow. J. Chromatogr. Sci. 1973, 11 (4), 180-183.
136. Martin, A. J.; Synge, R. L., A new form of chromatogram employing two liquid phases: A theory of chromatography. 2. Application to the micro-determination of the higher monoaminoacids in proteins. The Biochemical journal 1941, 35 (12), 1358-1368.

## Bibliography

137. Chromacademy Chromatographic parameters. [http://www.chromacademy.com/frameset-chromacademy.html?fChannel=0&fCourse=0&fSco=2&fPath=sco2/hplc\\_1\\_2\\_2.asp](http://www.chromacademy.com/frameset-chromacademy.html?fChannel=0&fCourse=0&fSco=2&fPath=sco2/hplc_1_2_2.asp) (accessed 16/03/2017).
138. Snyder, L. R., Column efficiency in liquid-solid adsorption chromatography. H.E.T.P. [height equivalent to a theoretical plate] values as a function of separation conditions. *Anal. Chem.* 1967, 39 (7), 698-704.
139. Van Deemter, J. J.; Zuiderweg, F.; Klinkenberg, A. v., Longitudinal diffusion and resistance to mass transfer as causes of nonideality in chromatography. *Chem. Eng. Sci.* 1956, 5 (6), 271-289.
140. Sparkman, O. D.; Penton, Z.; Kitson, F. G., *Gas chromatography and mass spectrometry: a practical guide.* Academic Press: 2011.
141. Chromacademy Van Deemter Plots. [http://www.chromacademy.com/frameset-chromacademy.html?fChannel=0&fCourse=0&fSco=104&fPath=sco104/fast\\_hplc\\_1\\_1\\_8.asp](http://www.chromacademy.com/frameset-chromacademy.html?fChannel=0&fCourse=0&fSco=104&fPath=sco104/fast_hplc_1_1_8.asp) (accessed 17/03/17).
142. Golay, M. J. E., Theory of Chromatography in Open and Coated Tubular Columns with Round and Rectangular Cross-sections. D. H Desty (Ed.), *Gas Chromatography* 1958, 36, 36-55.
143. James, A. T.; Martin, A. J. P., Gas-liquid partition chromatography: the separation and micro-estimation of volatile fatty acids from formic acid to dodecanoic acid. *Biochem. J* 1952, 50 (5), 679-690.
144. Chromacademy Optimising GC Temperature Programming. <http://www.chromacademy.com/chromatography-Optimising-GC-Temperature-Programming.html> (accessed 16/03/2017).
145. Chromacademy, GC - Theory and Instrumentation of GC- Gas Supply and Pressure Control - Quality of Gas Supply. In *GC - Theory and Instrumentation of GC*, Hinshaw, J. V., Ed. Chromacademy.
146. Vickers, A. K.; Decker, D.; Majors, R. E. The Art and Science of GC Capillary Column Production. <http://www.chromatographyonline.com/print/225950?page=full&id=&pageID=1&sk=&date=> (accessed 24/08/2018).
147. Gas Chromatography. <http://teaching.shu.ac.uk/hwb/chemistry/tutorials/chrom/gaschr.htm> (accessed 08/04/2016).
148. Chromacademy, GC - Theory and Instrumentation of GC- GC Columns. In *GC - Theory and Instrumentation of GC*, Hinshaw, J. V., Ed. Chromacademy.
149. Agilent Technologies HP-INNOWax. <https://www.agilent.com/en-us/products/gas-chromatography/gc-columns/capillary/hp-innowax#specifications> (accessed 19/04/2016).
150. Crawford Scientific Chromatography Technical Tips - Real Life GC Column Selection. <http://www.crawfordscientific.com/Chromatography-GC-Column-Selection-Principles.html> (accessed 19/04/2016).



151. Restek Corporation Rtx<sup>®</sup>-5 (G27) Columns (fused silica). <http://www.restek.com/catalog/view/134> (accessed 20/04/2016).
152. 12.4: Gas Chromatography. [https://chem.libretexts.org/Textbook\\_Maps/Analytical\\_Chemistry\\_Textbook\\_Maps/Map%3A\\_Analytical\\_Chemistry\\_2.0\\_\(Harvey\)/12\\_Chromatographic\\_and\\_Electrophoretic\\_Methods/12.4%3A\\_Gas\\_Chromatography](https://chem.libretexts.org/Textbook_Maps/Analytical_Chemistry_Textbook_Maps/Map%3A_Analytical_Chemistry_2.0_(Harvey)/12_Chromatographic_and_Electrophoretic_Methods/12.4%3A_Gas_Chromatography) (accessed 26/09/07).
153. Taylor, T. GC-MS Analysis I fundamentals of using gas chromatography with mass spectrometric detectors. [http://www.chromacademy.com/resolver-november2010\\_understanding\\_gcms\\_part\\_1.html](http://www.chromacademy.com/resolver-november2010_understanding_gcms_part_1.html) (accessed 12/04/2016).
154. Gere, D. R.; Board, R.; McManigill, D., Supercritical fluid chromatography with small particle diameter packed columns. *Anal. Chem.* 1982, 54 (4), 736-740.
155. Langley, G. J., Phase diagram of a pure substance. Shown temperature and pressure values are those of pure carbon dioxide. University of Southampton: Southampton.
156. Nováková, L.; Grand-Guillaume Perrenoud, A.; Francois, I.; West, C.; Lesellier, E.; Guillaume, D., Modern analytical supercritical fluid chromatography using columns packed with sub-2 $\mu$ m particles: A tutorial. *Anal. Chim. Acta* 2014, 824, 18-35.
157. Klesper, E.; Corwin, A. H.; Turner, D. A., High pressure gas chromatography above critical temperatures. *The Journal of Organic Chemistry* 1962, 27 (2), 700-701.
158. Berger, T. A. The Past, Present, and Future of Analytical Supercritical Fluid Chromatography. <https://www.chromatographytoday.com/article/supercritical-fluid-sfcgreen-chromatography/45/sfc-green-chemistry-group/the-past-present-and-future-of-analytical-supercritical-fluid-chromatography/1694> (accessed 28/08/2018).
159. Grand-Guillaume Perrenoud, A.; Veuthey, J.-L.; Guillaume, D., The use of columns packed with sub-2  $\mu$ m particles in supercritical fluid chromatography. *TrAC, Trends Anal. Chem.* 2014, 63, 44-54.
160. Beginner's Guide to Convergence Chromatography. [http://www.waters.com/waters/en\\_US/Beginner%27s-Guide-to-Convergence-Chromatography-3/nav.htm?cid=134941694&locale=/](http://www.waters.com/waters/en_US/Beginner%27s-Guide-to-Convergence-Chromatography-3/nav.htm?cid=134941694&locale=/) (accessed 28/08/2018).
161. Plachká, K.; Chrenková, L.; Douša, M.; Nováková, L., Development, validation and comparison of UHPSFC and UHPLC methods for the determination of agomelatine and its impurities. *J. Pharm. Biomed. Anal.* 2016, 125, 376-384.
162. Grand-Guillaume Perrenoud, A.; Veuthey, J.-L.; Guillaume, D., Comparison of ultra-high performance supercritical fluid chromatography and ultra-high performance liquid chromatography for the analysis of pharmaceutical compounds. *J. Chromatogr. A* 2012, 1266, 158-167.
163. Leere Øiestad, Å. M.; Berg, T.; Eliassen, E.; Wiklund, T.; Sand, K.; Leere Øiestad, E., Separation of isomers of new psychoactive substances and isotope-labeled amphetamines using UHPSFC-

## Bibliography

MS/MS and UHPLC-MS/MS. *Journal of Liquid Chromatography & Related Technologies* 2018, 41 (7), 391-400.

164. Lesellier, E.; West, C., The many faces of packed column supercritical fluid chromatography – A critical review. *J. Chromatogr. A* 2015, 1382, 2-46.

165. Waters, XSelect HPLC Columns.

166. Berger, T. A. *Supercritical Fluid Chromatography: Primer*; USA, 01/07/2015, 2015.

167. Chromacademy, *Supercritical Fluid Chromatography*. In *The Theory of HPLC*, Chromacademy, Ed. Chromacademy.

168. Ratsameepakai, W.; Herniman, J. M.; Jenkins, T. J.; Langley, G. J., Evaluation of Ultrahigh-Performance Supercritical Fluid Chromatography–Mass Spectrometry as an Alternative Approach for the Analysis of Fatty Acid Methyl Esters in Aviation Turbine Fuel. *Energy & Fuels* 2015, 29 (4), 2485-2492.

169. Smith, R. M., Supercritical fluids in separation science – the dreams, the reality and the future. *J. Chromatogr. A* 1999, 856 (1), 83-115.

170. ES Industries., *Basic SFC Primer Part I*. ES Industries., Ed.

171. Sparkman, O. D., *Mass Spec Desk Reference*. First ed.; Global View Publishing: 2000.

172. Hoffmann, E. d.; Stroobant, V., *Mass spectrometry : principles and applications*. 3rd ed.; J. Wiley: Chichester, West Sussex, England ; Hoboken, NJ, 2007; p xii, 489 p.

173. Watson, T.; Sparkman, D., *Introduction to Mass Spectrometry: Instrumentation, Applications and Strategies for Data Interpretations*. Fourth ed.; John Wiley & Sons, Ltd: Chichester, UK, 2007.

174. Murray, K. K.; Boyd, R. K.; Eberlin, M. N.; Langley, G. J.; Li, L.; Naito, Y., Definitions of terms relating to mass spectrometry (IUPAC Recommendations 2013). *Pure Appl. Chem.* 2013, 85 (7), 1515-1609.

175. Chromacademy, *Fundamental LC-MS Mass Analysers*.

176. Koppenaal, D. W.; Barinaga, C. J.; Denton, M. B.; Sperline, R. P.; Hieftje, G. M.; Schilling, G. D.; Andrade, F. J.; Barnes, J. H.; Iv, I. V., MS Detectors. *Anal. Chem.* 2005, 77 (21), 418 A-427 A.

177. Amster, I. J., Fourier Transform Mass Spectrometry. *J. Mass Spectrom.* 1996, 31 (12), 1325-1337.

178. Dempster, A. J., A new Method of Positive Ray Analysis. *Physical Review* 1918, 11 (4), 316-325.

179. Bleakney, W., A New Method of Positive Ray Analysis and Its Application to the Measurement of Ionization Potentials in Mercury Vapor. *Physical Review* 1929, 34 (1), 157-160.

180. Nier, A. O., A mass spectrometer for isotope and gas analysis. *Rev. Sci. Instrum.* 1947, 18 (6), 398-411.

181. Mass Spectrometry Tutorial - 2. Instrumentation. <http://tera.chem.ut.ee/~jpenchuk/documents/kursused/Mass-spec/fig1.jpg> (accessed 12/04/2016).
182. Mass Spectrometry Introduction. <http://www.chem.pitt.edu/facilities/mass-spectrometry/mass-spectrometry-introduction> (accessed 20/03/17).
183. Watson, J. T.; Sparkman, O. D., Electron Ionization. In *Introduction to Mass Spectrometry: Instrumentation, Applications, and Strategies for Data Interpretation*, Fourth ed.; John Wiley & Sons, Ltd: 2007; pp 315-448.
184. McLafferty, F. W.; Tureček, F.; Turecek, F., *Interpretation of mass spectra*. University science books: 1993.
185. Dole, M.; Mack, L. L.; Hines, R. L.; Mobley, R. C.; Ferguson, L. D.; Alice, M. B., Molecular beams of macroions. *The Journal of Chemical Physics* 1968, 49 (5), 2240-2249.
186. Fenn, J.; Mann, M.; Meng, C.; Wong, S.; Whitehouse, C., Electrospray ionization for mass spectrometry of large biomolecules. *Science* 1989, 246 (4926), 64-71.
187. Ho, C. S.; Lam, C. W. K.; Chan, M. H. M.; Cheung, R. C. K.; Law, L. K.; Lit, L. C. W.; Ng, K. F.; Suen, M. W. M.; Tai, H. L., *Electrospray Ionisation Mass Spectrometry: Principles and Clinical Applications*. *The Clinical Biochemist Reviews* 2003, 24 (1), 3-12.
188. Chromacademy, *Electrospray Ionisation - Theory*. In *Fundamental LC-MS*, Chromacademy, Ed. Chromacademy.
189. Banerjee, S.; Mazumdar, S., *Electrospray ionization mass spectrometry: a technique to access the information beyond the molecular weight of the analyte*. *International journal of analytical chemistry* 2012, 2012.
190. Gates, P. *High Performance Liquid Chromatography Mass Spectrometry (HPLC/MS)*. <http://www.bris.ac.uk/nerclsmsf/techniques/hplcms.html> (accessed 10/08/2016).
191. Rohner, T. C.; Lion, N.; Girault, H. H., Electrochemical and theoretical aspects of electrospray ionisation. *PCCP* 2004, 6 (12), 3056-3068.
192. Thomson, B.; Iribarne, J., Field induced ion evaporation from liquid surfaces at atmospheric pressure. *The Journal of Chemical Physics* 1979, 71 (11), 4451-4463.
193. Iribarne, J.; Thomson, B., On the evaporation of small ions from charged droplets. *The Journal of Chemical Physics* 1976, 64 (6), 2287-2294.
194. Gaskell, S. J., *Electrospray: principles and practice*. *J. Mass Spectrom.* 1997, 32 (7), 677-688.
195. Mallet, A. I.; Down, S., *Dictionary of mass spectrometry*. Wiley: Chichester ; Hoboken, NJ, 2009; p vii, 174 p.
196. Cech, N. B.; Enke, C. G., Practical implications of some recent studies in electrospray ionization fundamentals. *Mass Spectrom. Rev.* 2001, 20 (6), 362-387.

## Bibliography

197. Robb, D. B.; Covey, T. R.; Bruins, A. P., Atmospheric Pressure Photoionization: An Ionization Method for Liquid Chromatography–Mass Spectrometry. *Anal. Chem.* 2000, 72 (15), 3653-3659.
198. Raffaelli, A.; Saba, A., Atmospheric pressure photoionization mass spectrometry. *Mass Spectrom. Rev.* 2003, 22 (5), 318-331.
199. Kauppila, T. J.; Syage, J. A.; Benter, T., Recent developments in atmospheric pressure photoionization-mass spectrometry. *Mass Spectrom. Rev.* 2017, 36 (3), 423-449.
200. Gross, J. H., *Mass Spectrometry*. Springer: 2011.
201. Cai, S.-S.; Syage, J. A., Atmospheric pressure photoionization mass spectrometry for analysis of fatty acid and acylglycerol lipids. *J. Chromatogr. A* 2006, 1110 (1), 15-26.
202. Paul, W.; Steinwedel, H., Notizen: Ein neues Massenspektrometer ohne Magnetfeld. In *Zeitschrift für Naturforschung A*, 1953; Vol. 8, p 448.
203. Finnigan, R. E., Quadrupole mass spectrometers. *Anal. Chem.* 1994, 66 (19), 969A-975A.
204. Miller, P. E.; Denton, M. B., The quadrupole mass filter: basic operating concepts. *J. Chem. Educ.* 1986, 63 (7), 617.
205. Lawrence, E. O.; Edlefsen, N. E., *Science* 1930, 72, 378.
206. Comisarow, M. B.; Marshall, A. G., Fourier transform ion cyclotron resonance spectroscopy. *Chem. Phys. Lett.* 1974, 25 (2), 282-283.
207. Gates, P. Fourier-transform Ion Cyclotron Resonance Mass Spectrometry (FT-ICR-MS). <http://www.chm.bris.ac.uk/ms/fticrms.shtml> (accessed 08/09/218).
208. <https://jlab.chem.yale.edu/research/techniques/fourier-transform-ion-cyclotron-resonance-mass-spectrometry> (accessed 06\01\2019).
209. Mertens, T. Optimizing analysis of (modified) Fusarium mycotoxins in diverse samples from the brewing process. Universiteit Gent, 2016.
210. Cao, X.-L., Phthalate Esters in Foods: Sources, Occurrence, and Analytical Methods. *Comprehensive Reviews in Food Science and Food Safety* 2010, 9 (1), 21-43.
211. Patel, K. Analysis of internal diesel injector deposit formation by separation science and mass spectrometry. Doctoral Thesis, University of Southampton, Southampton, 2016.
212. American Society for Testing Materials, ASTM D8276 - 19, Standard Test Method for Hydrocarbon Types in Middle Distillates, including Biodiesel Blends by Gas Chromatography/Mass Spectrometry. 2019.
213. American Society for Testing Materials, ASTM E2997-16, Standard Test Method for Analysis of Biodiesel Products by Gas Chromatography-Mass Spectrometry, . ASTM International, West Conshohocken, PA,, 2016.

214. Energy Institute IP PM EU: Determination of ACCUTRACE™ S10 Fuel Marker in diesel fuel – Gas chromatography using heart-cut and refocusing technique. <https://publishing.energyinst.org/topics/fuel-quality-and-control/ip-test-methods/ip-pm-eudetermination-of-accutrace-s10-fuel-marker-in-diesel-fuel-gas-chromatography-using-heart-cut-and-refocusing-technique> (accessed 03/06/2018).
215. Tayari, S.; Abedi, R.; Tahvildari, K., Experimental investigation on fuel properties and engine characteristics of biodiesel produced from *Eruca sativa*. *SN Applied Sciences* 2019, 2 (1), 2.
216. Dolores, M.; Almena, C.; Esperilla, O. L.; Manzanero, F. M.; Duarte, Y. M.; Toscano, L. C. Q.; Wolf, G., Internal Diesel Injector Deposits: Sodium Carboxylates of C12 Succinic Acids and C16 and C18 Fatty Acids. *SAE Technical Paper Series* (2012-01-1969).
217. Gujar, A.; Anderson, T.; Cavagnino, D.; Patel, A., Comparative analysis of mass spectral matching for confident compound identification using the Advanced Electron Ionization source for GC-MS.
218. Major Fatty Acids in Some Oils and Fats Used or Tested as Alternative Diesel Fuels. In *The Biodiesel Handbook*, 2 ed.; Knothe, G. K., J.; Van Gerpen, J., Ed. AOCS Press 2010; p 462
219. AnalyzerPro. <http://www.spectralworks.com/products/analyzerpro/> (accessed 20/12/2016).
220. Ashraf-Khorassani, M.; Yang, J.; Rainville, P.; Jones, M. D.; Fountain, K. J.; Isaac, G.; Taylor, L. T., Ultrahigh performance supercritical fluid chromatography of lipophilic compounds with application to synthetic and commercial biodiesel. *J. Chromatogr. B* 2015, 983-984 (Supplement C), 94-100.
221. Johnson, D. W., Applications of Mass Spectrometric Techniques to the Analysis of Fuels and Lubricants. In *Mass Spectrometry*, InTech: 2017.
222. Zhan, D.; Fenn, J. B., Electrospray mass spectrometry of fossil fuels. *Int. J. Mass spectrom.* 2000, 194 (2–3), 197-208.
223. Smit, E.; Rüger, C. P.; Sklorz, M.; De Goede, S.; Zimmermann, R.; Rohwer, E. R., Investigating the Trace Polar Species Present in Diesel Using High-Resolution Mass Spectrometry and Selective Ionization Techniques. *Energy & Fuels* 2015, 29 (9), 5554-5562.
224. Catharino, R. R.; Milagre, H. M. S.; Saraiva, S. A.; Garcia, C. M.; Schuchardt, U.; Eberlin, M. N.; Augusti, R.; Pereira, R. C. L.; Guimarães, M. J. R.; de Sá, G. F.; Caixeiro, J. M. R.; de Souza, V., Biodiesel Typification and Quality Control by Direct Infusion Electrospray Ionization Mass Spectrometry Fingerprinting. *Energy & Fuels* 2007, 21 (6), 3698-3701.
225. Cai, S.-S.; Syage, J. A., Comparison of Atmospheric Pressure Photoionization, Atmospheric Pressure Chemical Ionization, and Electrospray Ionization Mass Spectrometry for Analysis of Lipids. *Anal. Chem.* 2006, 78 (4), 1191-1199.
226. Mo, S.; Dong, L.; Hurst, W. J.; van Breemen, R. B., Quantitative analysis of phytosterols in edible oils using APCI liquid chromatography-tandem mass spectrometry. *Lipids* 2013, 48 (9), 949-956.

## Bibliography

227. Barker, J., Cook, S., and Richards, P., Sodium Contamination of Diesel Fuel, its Interaction with Fuel Additives and the Resultant Effects on Filter Plugging and Injector Fouling. *SAE Int. J. Fuels Lubr.* 2013, 6 (3), 826-838.
228. Bannister, C. D.; Chuck, C. J.; Bounds, M.; Hawley, J. G., Oxidative Stability of Biodiesel Fuel. *Proceedings of the Institution of Mechanical Engineers, Part D: Journal of Automobile Engineering* 2011, 225 (1), 99-114.
229. Bondioli, P.; Gasparoli, A.; Lanzani, A.; Fedeli, E.; Veronese, S.; Sala, M., Storage stability of biodiesel. *Journal of the American Oil Chemists' Society* 1995, 72 (6), 699-702.
230. Waynick, J. A. *Characterization of biodiesel oxidation and oxidation products* CRC: 2005.
231. Basha, S. A.; Gopal, K. R.; Jebaraj, S., A review on biodiesel production, combustion, emissions and performance. *Renewable and Sustainable Energy Reviews* 2009, 13 (6-7), 1628-1634.
232. Alberici, R. M.; de Souza, V.; de Sá, G. F.; Morelli, S. R.; Eberlin, M. N.; Daroda, R. J., Used Frying Oil: A Proper Feedstock for Biodiesel Production? *BioEnergy Research* 2012, 5 (4), 1002-1008.
233. Kalo, P. J.; Ollilainen, V.; Rocha, J. M.; Malcata, F. X., Identification of molecular species of simple lipids by normal phase liquid chromatography–positive electrospray tandem mass spectrometry, and application of developed methods in comprehensive analysis of low erucic acid rapeseed oil lipids. *Int. J. Mass spectrom.* 2006, 254 (1), 106-121.
234. De Barros Bouchet, M. I.; Martin, J. M.; Forest, C.; le Mogne, T.; Mazarin, M.; Avila, J.; Asensio, M. C.; Fisher, G. L., Tribochemistry of unsaturated fatty acids as friction modifiers in (bio)diesel fuel. *RSC Advances* 2017, 7 (53), 33120-33131.
235. IUPAC., *Compendium of Chemical Terminology (the "Gold Book")*. 2nd ed.; McNaught, A. D.; Wilkinson, A.; Chalk, S. J., Eds. Blackwell Scientific Publications: Oxford, 1997.
236. Dunn, R. O., Effects of minor constituents on cold flow properties and performance of biodiesel. *Prog. Energy Combust. Sci.* 2009, 35 (6), 481-489.
237. Dunn, R. O., Effects of Monoacylglycerols on the Cold Flow Properties of Biodiesel. *JAOCS, Journal of the American Oil Chemists' Society* 2012, 89 (8), 1509.
238. Kortba, R., Bound by Determination. *Biodiesel Magazine* 2006, pp 42-50.
239. 6 - Fuel Properties. In *The Biodiesel Handbook (Second Edition)*, Knothe, G.; Krahl, J.; Van Gerpen, J., Eds. AOCS Press: 2010; pp 137-251.
240. Hirschegger, L.; Schober, S.; Mittelbach, M., Efficient and sensitive method for the quantification of saturated monoacylglycerols in biodiesel by gas chromatography–mass spectrometry. *Eur. J. Lipid Sci. Technol.* 2014, 116 (1), 89-96.
241. Hoed, V.; Zyaykina, N.; Greyt, W.; Maes, J.; Verhe, R.; Demeestere, K., Identification and Occurrence of Steryl glucosides in palm and soy biodiesel. *J. Am. Oil Chem. Soc.* 2008, 85 (1).

242. Lee, I.; Pfalzgraf, L. M.; Poppe, G. B.; Powers, E.; Haines, T., the Role of Sterol glucosides in filter plugging. *Biodiesel magazine* 2007, pp 105-112.
243. Camerlynck, S.; Chandler, J.; Hornby, B.; van Zuylen, I., FAME Filterability: Understanding and Solutions. *SAE Int. J. Fuels Lubr.* 2012, 5 (3), 968-976.
244. Oppliger, S.; Munger, L.; Nystroem, L., Rapid and highly accurate detection of sterol glucosides by ultraperformance liquid chromatography/quadrupole time of flight mass spectrometry. *J. Agric. Food. Chem.* 2014, 62 (4).
245. Wewer, V.; Dombink, I.; vom Dorp, K.; Dörmann, P., Quantification of sterol lipids in plants by quadrupole time-of-flight mass spectrometry. *J. Lipid Res.* 2011, 52 (5), 1039-1054.
246. Plank, C.; Lorbeer, E., On-line liquid chromatography—gas chromatography for the analysis of free and esterified sterols in vegetable oil methyl esters used as diesel fuel substitutes. *J. Chromatogr. A* 1994, 683 (1), 95-104.
247. Plank, C.; Lorbeer, E., Minor Components in Vegetable Oil Methyl Esters I: Sterols in Rape Seed Oil Methyl Ester. *Lipid / Fett* 1994, 96 (10), 379-386.
248. Verleyen, T.; Forcades, M.; Verhe, R.; Dewettinck, K.; Huyghebaert, A.; De Greyt, W., Analysis of free and esterified sterols in vegetable oils. *Journal of the American Oil Chemists' Society* 2002, 79 (2), 117-122.
249. Hailat, I.; Helleur, R., Identification of fatty acid sterol esters in margarine and corn using direct flow injection ESI-MSn ion trap-mass spectrometry. *Int. J. Mass spectrom.* 2014, 362, 24-31.
250. Feld, H.; Oberender, N., Characterization of damaging biodiesel deposits and biodiesel samples by infrared spectroscopy (ATR-FTIR) and mass spectrometry (TOF-SIMS). *SAE International Journal of Fuels and Lubricants* 2016, 9, 717+.
251. Solutions, D. F. Diesel Contamination - Stopping soft sticky stuff. <http://www.mycleandiesel.com/pages/SoftContaminants.aspx> (accessed 11/01/2019).
252. Harkins, W. D.; Brown, F., The determination of surface tension (free surface energy), and the weight of falling drops: The surface tension of water and benzene by the capillary height method. *J. Am. Chem. Soc.* 1919, 41 (4), 499-524.
253. Molea, A.; Visuian, P.; Barabás, I.; Suci, R.; Burnete, N. In *Key fuel properties and engine performances of diesel-ethanol blends, using tetrahydrofuran as surfactant additive*, IOP Conference Series: Materials Science and Engineering, IOP Publishing: 2017; p 012077.
254. American Society for Testing Materials, ASTM D3241-19b, Standard Test Method for Thermal Oxidation Stability of Aviation Turbine Fuels. ASTM International: West Conshohocken, PA, 2019.
255. Waynick, J. A., The Development and Use of Metal Deactivators in the Petroleum Industry: A Review. *Energy & Fuels* 2001, 15 (6), 1325-1340.
256. Jet Fuel Thermal Oxidation Test for Stability of Aviation Turbine Fuels (JFTOT). AmSpec, Ed. 2017.

## Bibliography

257. ASTM D3241, IP323. <http://www.adsystems-sa.com/img/instruments/dr10/methoddr10.jpg>.
258. Zhou, Q.; Gao, B.; Zhang, X.; Xu, Y.; Shi, H.; Yu, L., Chemical profiling of triacylglycerols and diacylglycerols in cow milk fat by ultra-performance convergence chromatography combined with a quadrupole time-of-flight mass spectrometry. *Food Chem.* 2014, 143 (0), 199-204.
259. Gil, J. H.; Hong, J. Y.; Jung, J. H.; Kim, K. J.; Hong, J., Structural determination of monoacylglycerols extracted from marine sponge by fast atom bombardment tandem mass spectrometry. *Rapid Commun. Mass Spectrom.* 2007, 21 (7), 1264-70.
260. Dunn, R. O.; Moser, B. R., Cold Weather Properties and Performance of Biodiesel. In *The Biodiesel Handbook*, 2nd ed.; Knothe, G.; Krahl, J.; van Gerpen, J., Eds. AOCS Press: 2010; pp 147-205.
261. Quigley, R.; Barbour R; D, B., An Investigation of Internal Diesel Injector Deposits  
Dynamometer Testing of Peugeot DW10 and DW10C Engines  
In 10th International Colloquium Fuels Conventional and Future Energy for automobiles, Technische Akademie Esslingen in Stuttgart/Ostfildern., 2015.
262. Inc., I. Dyes & Markers. (<http://www.innospecinc.com/our-markets/fuel-specialties/refinery-specialties/dyes-markers>) (accessed 04/04/2016).
263. Croud, V. B.; Marchant, C. A.; Maltas, P.; Hecht, L.; Douglas, R., Criminal removal of fuel markers by distillation. *Fuel Process. Technol.* 2016, 144, 341-347.
264. Puangmalee, S.; Petsom, A.; Thamyongkit, P., A porphyrin derivative from cardanol as a diesel fluorescent marker. *Dyes and Pigments* 2009, 82 (1), 26-30.
265. Samaras, V., Novel non-labile fuel markers. T.E. Laboratories Ltd.
266. Ocean Optics Authenticating Fuel From Plant to Pump. (<http://oceanoptics.com/authentication-fuel/>) (accessed 04/04/2016).
267. HM Treasury; HM Revenue & Customs; The Rt Hon Nicky Morgan MP New marker to tackle fuel fraud. (<https://www.gov.uk/government/news/new-marker-to-tackle-fuel-fraud>) (accessed 04/04/2016).
268. Fuel dyes. [https://en.wikipedia.org/wiki/Fuel\\_dyes](https://en.wikipedia.org/wiki/Fuel_dyes) (accessed 04/04/2016).
269. HCOTEG121520 - Marking: background: what markers are used? <http://www.hmrc.gov.uk/manuals/hcotegmanual/hcoteg121520.htm> (accessed 04/04/2016).
270. Energy Institute IP 298: Determination of quinizarin - Extraction spectrophotometric method. <http://publishing.energyinst.org/publication/ip-standard-test-methods/ip-298-determination-of-quinizarin-extraction-spectrophotometric-method> (accessed 04/04/2016).
271. Tucker, K.; Sawyer, R.; Stockwell, P., The Automatic Extraction, Identification and Determination of Quinizarin in Hydrocarbon Oils. *Analyst* 1970, 95 (1133), 730-737.



272. Figueira, A. C. B.; de Oliveira, K. T.; Serra, O. A., New porphyrins tailored as biodiesel fluorescent markers. *Dyes and Pigments* 2011, 91 (3), 383-388.
273. Henricsson, S.; Westerholm, R., Liquid chromatographic method for analysing the colour marker Solvent Yellow 124, N-ethyl-N-[2-(1-isobutoxyethoxy)ethyl](4-phenylazophenyl)amine, in diesel fuels. *J. Chromatogr. A* 1996, 723 (2), 395-398.
274. Orzel, J.; Daszykowski, M.; Grabowski, I.; Zaleszczyk, G.; Sznajder, M., Identifying the illegal removal from diesel oil of certain chemical markers that designate excise duty. *Fuel* 2014, 117, 224-229.
275. Romanini, D. C.; Trindade, M. A. G.; Zanoni, M. V. B., A simple electroanalytical method for the analysis of the dye solvent orange 7 in fuel ethanol. *Fuel* 2009, 88 (1), 105-109.
276. Trindade, M. A. G.; Ferreira, V. S.; Zanoni, M. V. B., A square-wave voltammetric method for analysing the colour marker quinizarine in petrol and diesel fuels. *Dyes and Pigments* 2007, 74 (3), 566-571.
277. Trindade, M. A. G.; Zanoni, M. V. B., Voltammetric sensing of the fuel dye marker Solvent Blue 14 by screen-printed electrodes. *Sensors and Actuators B: Chemical* 2009, 138 (1), 257-263.
278. John Crandall; Ned Roques; Spencer Parker; Joe Perron; Matt Holliday; Winniford, B., A Transportable micro and Fast GC for Chemical Markers in Adulterated Fuels. Company, T. D. C.; LLC, F. A. S. T., Eds. 2015.
279. May, E. M.; Hunt, D. C.; Holcombe, D. G., Communication. Method for the determination of the marker and dye in heavy fuel oils. *The Analyst* 1986, 111 (8), 993.
280. National Union of Farming New fuel marker dye from 1st April 2015. <http://www.nfuonline.com/business/inputs/new-fuel-marker-dye-from-1st-april-2015/> (accessed 04/04/2016).
281. Dow Chemical Company, ACCUTRACE™ Marking Solutions Fight Fuel Tax Evasion.
282. Malik, Y. Oil and fuel theft: The \$133 billion a year scandal. <https://www.oilandgasiq.com/default/news/oil-and-fuel-theft-the-133-billion-a-year-scandal> (accessed 04/07/2018).
283. Authentix Europol Confirms Link Between Organised Crime and Fuel Fraud. <https://authentix.com/blog/europol-confirms-link-between-organised-crime-and-fuel-fraud/> (accessed 04/07/2018).
284. Gras, R. L.; Luong, J. C.; Smith, W. E. Analytical method for detecting fuel markers. 2014.
285. Dow Chemical Company ACCUTRACE™ Marking Solutions Fight Fuel Tax Evasion. [http://msdssearch.dow.com/PublishedLiteratureDOWCOM/dh\\_092e/0901b8038092e4a8.pdf?file\\_path=ucon/pdfs/noreg/816-00112.pdf&fromPage=GetDoc](http://msdssearch.dow.com/PublishedLiteratureDOWCOM/dh_092e/0901b8038092e4a8.pdf?file_path=ucon/pdfs/noreg/816-00112.pdf&fromPage=GetDoc) (accessed 18/11/2016).
286. <http://forecourtretailer.com/> Independent Laboratory Ltd – The science of fuel traceability. <http://forecourtretailer.com/the-science-of-fuel-traceability/> (accessed 04/04/2016).

## Bibliography

287. Chambers, E. E.; Diehl, D. M. The Use of Stable-Isotope-Labeled (SIL) Internal Standards to Compensate for Matrix Effects: Key Considerations 2007.
288. Stokvis, E.; Rosing, H.; Beijnen, J. H., Stable isotopically labeled internal standards in quantitative bioanalysis using liquid chromatography/mass spectrometry: necessity or not? *Rapid Commun. Mass Spectrom.* 2005, 19 (3), 401-407.
289. Sandy, C. Fuel Marker Analysis in Diesel Fuel using 2D-GC/MS; 01/09/2015, 2015.
290. Dow Chemical Company ACCUTRACE™ S10 Fuel Marker in Lubricant Contaminated Diesel Fuel by Gas Chromatography/Mass Spectrometry; 28/05/2014, 2014.
291. Purcell, J. M.; Hendrickson, C. L.; Rodgers, R. P.; Marshall, A. G., Atmospheric pressure photoionization Fourier transform ion cyclotron resonance mass spectrometry for complex mixture analysis. *Anal. Chem.* 2006, 78 (16), 5906-5912.
292. Hayen, H.; Karst, U., Strategies for the liquid chromatographic–mass spectrometric analysis of non-polar compounds. *J. Chromatogr. A* 2003, 1000 (1), 549-565.
293. Langley, G. J.; Herniman, J.; Carter, A.; Wilmot, E.; Ashe, M.; Barker, J., Detection and Quantitation of ACCUTRACE S10, a New Fiscal Marker Used in Low-Duty Fuels, Using a Novel Ultrahigh-Performance Supercritical Fluid Chromatography–Mass Spectrometry Approach. *Energy & Fuels* 2018, 32 (10), 10580-10585.
294. Wavefunction Inc, Wavefunction Inc. Spartan'14. . Irvine, USA 2014.
295. Becke, A. D., Density-functional thermochemistry. III. The role of exact exchange. *The Journal of chemical physics* 1993, 98 (7), 5648-5652.
296. Lee, C.; Yang, W.; Parr, R. G., Development of the Colle-Salvetti correlation-energy formula into a functional of the electron density. *Physical review B* 1988, 37 (2), 785.
297. Huzinaga, S., Basis sets for molecular calculations. *Computer Physics Reports* 1985, 2 (6), 281-339.
298. Bondioli, P.; Cortesi, N.; Mariani, C., Identification and quantification of steryl glucosides in biodiesel. *Eur. J. Lipid Sci. Technol.* 2008, 110 (2), 120-126.

